

10383478

✓



EDINBURGH
UNIVERSITY
LIBRARY

Shelf Mark

Engineering library

EHSAN

Ph.D. 1997



30150

016431766

**A NEW TYPE OF MALONE ENGINE WITH
DIGITAL-DISPLACEMENT HYDRAULIC DRIVE**

Md. Ehsan

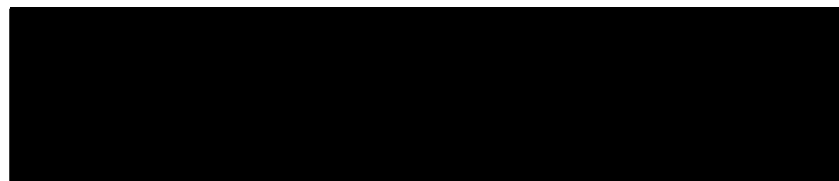
**A Thesis Submitted for the
Degree of Doctor of Philosophy**

University of Edinburgh

1997

Declaration

I certify that the work presented in this thesis,
except where credited to others, is my own.



ABSTRACT

Most Stirling engines operate on the principle of expansion and compression of a contained gaseous working fluid moving between two different temperature levels. Although Stirling engines have several advantages compared with other heat engines they face problems regarding sealing of working fluid (eg. hot hydrogen) and power control. Malone's modification to the Stirling design had water as a working fluid instead of gas. The engines needed to operate at high pressures and consequently gave high power densities. Unfortunately the work of Malone between 1920 and 1931, was scantily reported and has subsequently disappeared. The only significant interests in the Malone cycle have been for refrigeration and heat pumps.

The digital hydraulic drive, pioneered by Rampen and Salter, can be applied to produce piston motions for a low-speed heat engine and thus fits the Malone engine well. The digital-displacement pump-motor is a hybrid device, which combines reciprocating hydraulics with micro-processor control, creating a highly integrated machine capable of producing variable flow and power. Each cylinder has electronically controlled poppet valves, which are opened or closed by a timed pulse from a controller. This allows enabling or disabling of cylinders on a stroke-by-stroke basis, in any desired sequence. The same machine can be used both as pump or motor by controlling the valve actuation sequence. The advantages of this approach over conventional variable-swash hydraulic machines lie with both the response speed and the inherent energy efficiency.

Salter realised that combining the Stirling engine and digital hydraulic drive could lead to a new type of heat engine with some unique features. Using the digital hydraulic drive eliminates much of the mechanism and the conventional constraint of sinusoidal piston motion, allowing optimal control of the pressure-volume diagram of the engine cycle. The problem of sealing high pressure working fluid is eliminated as the sealing interface is transferred to the poppet valves and much cooler hydraulic oil. Salter also proposed a new concept of hot-end (expansion space) design for the Artemis-Malone engine which provides the uncommon combination of good thermal conductivity and high-temperature strength.

This thesis deals with the mathematical modelling of the Artemis-Malone engine and estimates the performance of the engine in operation. The modelling is carried out in two phases - static and time-domain. The static and dynamic models together form a design tool which is equivalent to a conventional second-order model. The static model deals with the design of different engine components, their functional limits and various subsystem losses at different power levels. The study estimates the performance of the engine and compares it with contemporary Diesels. The time-domain model, which is based on an isothermal model of the hot (expansion space) and cold-ends (compression space), investigates the effect of different relative motions of the moving components, on the engine cycle. The time-domain model incorporates simulation of the actual piston motion generated by the digital-displacement hydraulic drive. This allows the investigation of motion control and its effect on the pressure-volume diagram. It also allows several methods for controlling power to be tested. A final strategy has been suggested for instantaneous power control. The study concludes with the correlation and comparison of performance predicted by the static and the dynamic models.

ACKNOWLEDGEMENTS

I would like to thank the following people for their help throughout this work:

First and foremost my sincere thanks to W.H.S. Rampen, my supervisor, for his guidance and help throughout this project. Without his directions, inspiration and thought provoking comments, very little of this work would have been possible. Win has also been a very supportive friend during my stay in Scotland.

Next I would like to thank Professor S.H. Salter, my other supervisor, without whom the fundamental idea and motivation for the thesis would not have occurred. Part of the work presented in the thesis originated from him.

I thank all members of the Wave-power group and Artemis Intelligent Power Ltd, especially Jamie Taylor and John Almond, who offered help and advice at various occasions.

Finally but most importantly, thanks to my wife Ismat Ara (Shompa), who encouraged and selflessly supported me throughout this period. I also thank my parents for their support and encouragement.

The work of this thesis was supported by a scholarship from the Association of Commonwealth Universities (ACU).

To all, I offer my sincerest gratitude.

Md. Ehsan

June 1997

TABLE OF CONTENTS

CHAPTER-1 : Introduction	Page
1.1 Background of Stirling engines	1.1
1.2 Fundamentals of the Stirling cycle	1.3
1.3 Concept of Malone Engine	1.7
1.4 Concept of digital-displacement hydraulic drive	1.10
1.5 Combination of Malone cycle with digital-displacement hydraulic drive : The Artemis-Malone Engine	1.12
1.6 Overview of thesis structure	1.14
CHAPTER-2 : Literature Review	
2.1 Introduction	2.1
2.2 Modelling of Stirling engine cycles	2.1
2.3 Drive mechanisms used for power take-off in Stirling and Malone engines	2.6
2.4 Design and performance of digital-displacement pump-motors	2.8
CHAPTER-3 : Structure and operating principle of Artemis-Malone engine	
3.1 The main engine components	3.1
3.2 The thermodynamic pile	3.1
3.2.1 The hot-end	3.2
3.2.2 The cold-end	3.6
3.2.3 The regenerator	3.6
3.3 The hydraulic drive	3.8
3.4 Heat exchanger for recovering heat from exhaust gas	3.11
3.5 Control and ancillary drives	3.13
3.6 The sequences of the engine cycle	3.15

CHAPTER-4 : Design of the Artemis-Malone Engine

4.1.1	Background	4.1
4.1.2	Design procedures followed in the static-model	4.1
4.1.3	Brief discussion of the closed loops	4.4
4.1.4	Major equations used in the Mathcad model	4.9
4.2	Changes made to initial Mathcad model	4.20
4.3	Performance of the Artemis Malone Engine	4.25

CHAPTER-5 : Modelling of the hydraulic drive system

5.1	Introduction	5.1
5.2	Operating principle	5.1
5.3	Control techniques	5.4
5.3.1	Pressure control mode	5.6
5.3.2	Flow control mode	5.8
5.3.3	Ternary mode	5.9
5.4	Structure of the modelling of digital-displacement pump-motor	5.9
5.5	Simulation results of pump-motor models	5.13
5.6	Principle of using digital-displacement technique for achieving desired piston motion in the Artemis-Malone engine	5.18

CHAPTER-6 : Simulation of theoretical engine cycles in time domain

6.1	Concept of relative motions of different components	6.1
6.2	Mass of fluid in the regenerator	6.4
6.3	Effect of the relative motion profiles	6.7
6.4	Combination of motions resulting in different cycle-patterns	6.9
6.4.1	Piston-assisted pressure-rise and regenerator assisted pressure-fall cycle	6.10
6.4.2	Regenerator-assisted pressure-rise and pressure-fall cycle	6.13
6.4.3	Piston-assisted pressure-rise and pressure-fall cycle	6.16
6.5	Comparison and compatibility of different cycles	6.19
6.6	Thermal modelling of the hot-end	6.21

CHAPTER-7 : Simulation of real engine cycles

7.1	Modelling of more realistic cycles	7.1
7.2	Calculating imperfect motions for the regenerator	7.3
7.3	Piston motion generated by the pump-motor	7.11
7.4	The overall system	7.17

CHAPTER-8 : Control strategies for varying engine power

8.1	Methods of controlling the engine power	8.1
8.2	Comparison of different control strategies	8.4
8.2.1	Speed control	8.4
8.2.1	Regenerator stroke control	8.5
8.2.3	Controlling piston motion	8.12
8.2.4	Combined strategy	8.15

CHAPTER-9 : Continuous power control of the engine

9.1	Introduction	9.1
9.2.1	Power control by offsetting regenerator motion	9.1
9.2.2	Shifting between ternary-codes	9.7
9.2.3	Minimising power-lag in transition-cycle	9.11
9.2.4	Meeting variable power demand	9.15
9.3	Power control by offsetting and clipping regenerator motion	9.19
9.4	Power control by changing regenerator stroke	9.26
9.5	Comments on simulations with three strategies for power control	9.34

CHAPTER-10 : Comparison of static and dynamic simulation models

10.1	Introduction	10.1
10.2	Variable heat-flux through the full power design	10.2
10.3	Temperature gradient through the hot-end for variable heat flux (variable-frequency cycle)	10.4
10.4	Improving the static model using the time-domain model results	10.9
10.5	Incorporating variable pressure-level cycle in the static model	10.18
10.6	Performance of the engine in variable pressure-level cycles	10.20
10.7	Final engine specifications	10.27

CHAPTER-11 : Conclusion

11.1	Conclusions	11.1
11.2	Recommendations for future work	11.4

References		ref.1
-------------------	--	-------

Appendices

A.	Mathcad model for engine design.	a.1
B.	Time-domain simulation models.	b.1
C.	Ternary-codes for different power control strategies.	c.1
D.	Table for density of water and steam.	d.1
E.	Nusselt number for fully developed laminar flow through tubes of differing cross-sections.	e.1
F.	Information about J. F. Malone and about his works.	f.1

List of Tables

1.1 :	Advantages and disadvantages of Stirling Engines.	1.6
3.1 :	Limiting Chemical Composition (%) of Inconel 625.	3.4
4.1 :	Specifications of an Artemis-Malone engine-design at full power.	4.28
4.2 :	Subsystem loss calculations.	4.31
4.3 :	Comparison of performance of the Artemis-Malone engine with some Diesel engines.	4.32
9.1 :	Engine parameters and power ranges (Power control by offsetting).	9.3
9.2 :	Engine parameters and power ranges (Power control by clipping).	9.20
9.3 :	Engine parameters and power ranges (Power control by changing regenerator stroke).	9.28
10.1:	Correction factors for non-linearity of pressure variation used for speed calculations in the static model for variable-pressure engine cycles.	10.18
10.2:	Results from time domain model, used in the static variable-pressure model.	10.19
10.3:	Specifications of the Artemis-Malone engine-design for full power.	10.27
10.4:	Control of power.	10.30

List of Figures

- | | | |
|-------|---|------|
| 1.1 : | P-V and T-S diagrams of a Carnot cycle with four sequential processes. | 1.4 |
| 1.2 : | P-V and T-S diagrams of Ideal Stirling cycle. | 1.4 |
| 1.3 : | General arrangement and operating sequence of a Malone engine with liquid working fluid. | 1.9 |
| 3.1 : | Schematic sectional view of a module of the Artemis-Malone engine. | 3.3 |
| 3.2 : | Illustration of the pumping and motoring action of the flexible piston and the digital-displacement hydraulic drive. | 3.9 |
| 3.3 : | Sectional view of the heat exchanger for recovering heat from the combustion gases leaving the hot-end, into the incoming air. | 3.12 |
| 3.4 : | Operating cycle and sequences of regenerator and flexible piston motions of the Artemis-Malone engine, for a piston assisted pressure rise and regenerator assisted pressure fall cycle. | 3.16 |
| 4.1 : | Flow chart showing the inter-related closed-loops of the Mathcad model used for the design of the Artemis-Malone engine. | 4.3 |
| 4.2 : | Temperature drops across different components of thermal resistance as heat passes through the hot-end and the cold-end structure. | 4.6 |
| 4.3 : | Temperature distribution against maximum normal stress along the radial thickness of the Inconel disks and comparative values with data for 2000, 10000 a 100000 hour rupture life for Inconel 625. | 4.8 |
| 4.4 : | Under steady state heat flow the total heat added in the burner equals the heat passed through the hot end and various heat losses. | 4.8 |
| 4.5 : | Effect of changing fin dimensions and spacing on surface area and convective heat transfer co-efficient at flame to fin interface. | 4.23 |
| 4.6 : | Stages of hot-end design modifications, sectional views of one side are shown only (three cases). | 4.26 |
| 5.1 : | Cylinder head arrangement of a digital-displacement pump-motor. | 5.3 |
| 5.2 : | Valve actuation sequence of motoring cycle. | 5.3 |
| 5.3 : | Nature of flow from a reciprocating cylinder at different speeds. | 5.5 |

5.4:	Flow from a multi-cylinder pump.	5.5
5.5 :	Simulation Programme Flow-Chart for Pump/Motor Model.	5.11
5.6 :	Superimposed flow of multiple cylinders enabled according to respective decisions, 10 cylinder pump shifting from 100% - 75% flow capacity at 1800 rpm.	5.12
5.7 :	Pump response at 10% to 90% step rise of flow demand at a constant speed (pressure-control mode).	5.14
5.8 :	Pump response to 17% speed change, while the flow demand remains constant (pressure-control mode).	5.15
5.9 :	Pump response at 20% to 80% step rise of flow demand, at a constant speed (Flow-Control Mode).	5.16
5.10 :	Pump response at 80% to 20% step fall of flow demand, 10 cylinder pump running at 1800 rpm (Flow-Control Mode).	5.16
5.11 :	10 cylinder Pump-Motor following a variable demand curve, at 1800 rpm (Flow-Control Mode).	5.17
5.12 :	Schematic presentation of the arrangement of digital-displacement hydraulic drive for generating piston motion.	5.19
5.13 :	Typical enabling decision, pump-motor flow and resulting piston motion curve trying to match a desired motion.	5.20
6.1 :	Component of masses in the system.	6.3
6.2 :	Variation of fluid mass inside the regenerator with pressure.	6.3
6.3a :	Consideration of linear and an arbitrary non-linear temperature distributions of fluid inside the regenerator.	6.5
6.3b:	Variation of fluid mass inside the regenerator for linear and non-linear temperature gradients of 425 to 100 °C.	6.5
6.4 :	Simulation programme flow-chart for determining cycle pressure.	6.6
6.5 :	Motion of regenerator and desired piston motion resulting in the cyclic pressure variation (piston assisted pressure-rise and regenerator assisted pressure-fall cycle).	6.11
6.6 :	P-V diagram of the cycle (do)	6.12
6.7 :	Variation of different mass components with cycle pressure, while the total-mass remains the same (do).	6.12

6.8 :	Motion of regenerator and desired piston motion resulting in the cyclic pressure variation.(regenerator assisted pressure-rise and pressure-fall cycle).	6.14
6.9 :	P-V diagram of the cycle (do).	6.15
6.10 :	Variation of different mass components with cycle pressure, while the total-mass remains the same (do).	6.15
6.11 :	Motion of regenerator and desired piston motion resulting in the cyclic pressure variation (piston assisted pressure-rise and pressure-fall cycle).	6.17
6.12 :	P-V Diagram of the cycle (do).	6.18
6.13 :	Variation of different mass components with cycle pressure, while the total-mass remains the same (do).	6.18
6.14 :	Comparative presentation of P-V diagrams and piston motions (3 cycles).	6.20
6.15 :	Predicted variation of temperature of the hot-end fluid and heat flow through the hot-end, as the mass of fluid inside the hot-end changes through the cycle.	6.23
7.1 :	Simulation programme flow-chart for calculation of realistic engine cycle.	7.1
7.2 :	Regenerator actuation options.	7.4
7.3 :	Acceleration requirements for a modified triangular regenerator motion profile.	7.6
7.4 :	Schematic drawing of a probable regenerator-displacer drive system.	7.7
7.5 :	Desired piston motion for sinusoidal regenerator motion and the P-V diagram of the resulting engine cycle.	7.9
7.6 :	Schematic drawing of a probable regenerator drive system providing a sinusoidal regenerator motion.	7.10
7.7a :	Flow chart of different types of feedback control loops tested.	7.12
7.7b :	Desired piston motion and those generated by the pump-motor with and without additional feedback loops on the decision making algorithms.	7.12
7.8 :	Piston motion generated by the pump-motor following an analogue demand signal having additional feed-back control (modified triangular regenerator motion).	7.14

7.9 :	Piston motion generated by the pump-motor following an analogue demand signal with additional feed-back control (sinusoidal regenerator motion).	7.15
7.10 :	Piston motion generated by the pump-motor following a ternary pattern and the resulting full-power engine cycle for sinusoidal regenerator motion.	7.16
7.11 :	Schematic of a proposed overall system for transferring energy from the hot-flame gases to the wheels.	7.18
8.1 :	(Speed Control) Piston motion generated by the pump-motor, when it is still running at high speed, while the engine speed is reduced to half.	8.6
8.2 :	(Stroke Control) Piston motion generated by the pump-motor still running at high speed, while the amplitude of regenerator motion is reduced to half.	8.7
8.3 :	Effect of decreasing the regenerator stroke by 10%, while the piston motion following a ternary pattern remains unchanged.	8.10
8.4 :	Effect of offsetting the regenerator motion towards the cold-end without changing its stroke length, while the piston motion (following a ternary pattern) remains unchanged.	8.11
8.5 :	Effect of offsetting piston motion away from its TDC as the ternary pattern followed is changed, while the regenerator motion remains unchanged.	8.14
8.6 :	Offsetting the regenerator motion towards the cold-end, though the drive cylinder motion is the same.	8.17
8.7 :	Changing the profile of the regenerator motion, though the drive cylinder motion is the same.	8.19
8.8 :	Effect of offsetting the regenerator motion towards the cold-end along with clipping of the stroke at the cold-end, while the piston motion remains unchanged.	8.20
8.9 :	Changing the regenerator stroke for finer control of power.	8.22
9.1 :	Change of power-zones and offsetting requirements, with changes in power demand (offsetting method).	9.4
9.2a :	Variation of cycle pressures for piston motion of different power-zones.	9.5

9.2b :	Variation of piston motion for different power-zones.	9.5
9.3 :	Pressure-volume diagrams of the engine cycle at different power-zones.	9.6
9.4 :	Pressure variation within the cycle with regenerator and piston motion	9.8
9.5 :	Cycle response to maximum step change of power zone shifts between zone 0 and zone 5.	9.10
9.6 :	Cycle response to maximum step change of power zone shifts between zone 0 and zone 5.	9.12
9.7a :	Cycle response to maximum step change of power zone shifts between zone 0 and zone 5.	9.13
9.7b :	Changes made to the ternary-code applied to the transition cycle.	9.14
9.8 :	Cycle changes as the power demand varies within a power zone.	9.16
9.9 :	Engine cycle following variable demand from the user, where power is calculated in a cycle-by-cycle basis.	9.17
9.10 :	Power output from the engine under a power-zone hunting situation.	9.18
9.11 :	Change of power zones and offsetting requirements, with changes in power demand (offsetting and clipping method).	9.21
9.12a:	Variation of cycle pressures for power zone one compared to the previous strategy, as the ternary-code is changed.	9.23
9.12b:	Variation of piston motion as the ternary-code is changed for power-zone one.	9.23
9.13 :	Pressure-volume diagrams of the engine cycle at different power zones.	9.24
9.14 :	Cycle changes as the demand increases and passes through a power-zone change.	9.25
9.15 :	Change of power-zones and stroke requirements, with changes in power demand (variable regenerator stroke method)	9.29
9.16a:	Variation of cycle pressures for piston motion at different power-zones.	9.30
9.16b:	Variation of piston motion for different power-zones.	9.30
9.17 :	Pressure-volume diagrams of the engine cycle at different power-zones.	9.31
9.18 :	Cycle response to step change of power from zone-0 to zone-5 and then returning to zone-1.	9.32
9.19 :	Cycle changes as the user demand decreases and passes through a power-zone change.	9.33

- 10.1 : The shifting of the temperature-stress curve as the heat flux decreases. 10.5
The flame-fin root temperature is maintained by changing the proportion of cooling air.
- 10.2 : Shifting of the temperature-stress curve as the heat flux decreases, 10.7
with fixed hot-end steam temperature. The flame-fin root temperature is maintained by changing the proportion of cooling air.
- 10.3 : Performance of the Artemis-Malone engine as a function of heat flux 10.8
with hot-end steam temperature maintained at the full-power level.
- 10.4 : Shifting of the temperature-stress curve as the heat flux decreases, 10.10
with mid-wall temperature at the hot-end being maintained.
- 10.5 : Performance of the Artemis-Malone engine as a function of heat flux 10.11
with mid-wall temperature of hot-end maintained at the full-power level.
- 10.6 : Changes of air-ratios made at different heat flow rates to maintain 10.12
desired temperatures.
- 10.7 : Corrected engine speeds (cyclic frequency) for different heat flow rates. 10.15
- 10.8 : Calculation of positive (motoring) and negative (pumping) work in the 10.16
Mathcad model.
- 10.9 : Consequence of reducing regenerator spinning speed at lower heat fluxes. 10.21
- 10.10: Over-heating of the hot-end metal can be avoided in a variable pressure 10.23
level cycle, by controlling the spinning speed of the regenerator.
- 10.11: Performance estimates of Artemis-Malone engine, following the 10.24
variable pressure-level cycle.
- 10.12: The shifting of the temperature-stress curve as the heat flow decreases, 10.25
in variable-pressure cycle.
- 10.13: Comparative results of variable-pressure and variable-frequency 10.26
cycles for various heat flow rates.

CHAPTER - 1

Introduction

1.1 Background of Stirling engines

Stirling machines are heat engines which operate on the principle of compression and expansion of working fluid at different temperature levels. They incorporate a regenerator, a form of heat exchanger (acting as a thermodynamic sponge) alternately accepting and rejecting heat to and from a working fluid and thus recycling a major fraction of the energy flow from one cycle to the next. The flow of working fluid is controlled by volume changes, so that there is a net conversion of heat energy to work and vice versa. Because of the use of the regenerator, Stirling machines can have very high thermal efficiencies. Stirling machines have been used as heat engines as well as refrigerators or heat pumps.

The original Stirling engine was invented in 1815 by Robert Stirling in Scotland. It was not until 1850, that McQuorne Rankine explained the thermodynamics of a Stirling cycle following the enunciation of the principle of mechanical equivalent of heat by James Joule. Throughout the 19th century early Stirling engines, more usually termed as hot air engines, were made and used in the thousands. These early engines were used for various applications, most common being the generation of power for pumping water and the driving of small machinery. These were generally big, heavy and slow-running machines with limited heat transfer capabilities which suffered from low maximum temperatures. However these were preferred in many cases to the contemporary reciprocating steam engines of small capacity, which had relatively large accessories (eg. boilers and condenser). With the development of internal combustion engine in late 19th century, the air engines lost their market and by the time of first world war hot-air engine production had virtually ceased worldwide.

Research on Stirling engines was revived in late 1930's by Philips Electric company in Netherlands¹. Though they initially aimed to build small electric generators, they soon proceeded to larger engines and cryocoolers. By 1948 Philips had a V4 engine (11 kW) running. Because of the quiet operation and favourable torque characteristics Stirling engines were well suited to ships and submarines. Philips focused much on developing such engines, specially the 149 kW four cylinder 'boxer' engine. Under a license agreement with Philips, Stirling research was carried on by General motors from 1958-1970. The GM programme was very extensive and involved a wide range of engines. At GM there was progressive development on Stirling engine research. Towards the end of the programme their effort was principally concentrated on a four cylinder bus engine. Unfortunately the GM Stirling programme came to an abrupt end, mostly due to a loss of will in the GM management. The Ford motor company picked up the GM licence with Philips but the Ford programme was never as extensive as GM. Ford and Philips initially developed a 135 kW double acting Siemens-Stirling engine for the Ford Torino sedan. After the energy crisis created by the rise in fuel costs imposed by OPEC, 'Energy Research and Development Administration (ERDA)' of US government also partly sponsored the Ford project for a 67 kW car engine. The combined team was making good progress, when the programme was suddenly cancelled in early 1980's in face of recession in the automotive industry. Ford's decision to discontinue the programme influenced the Philips management, who in turn decided to stop their Stirling programme and disbanded the Stirling research and development team. Since then relatively small programs have been carried out by small companies formed by people involved in the major research projects mentioned before. These are currently active both in Stirling engines and refrigeration. Presently an automotive Stirling engine (ASE) project is carried out by a joint effort of several US agencies (Ernst, 1993) aimed to transfer European Stirling engine technology to US in a form suitable for the end user. More detailed information of research works on Stirling technology are available from several references (Walker et al. 1994; Walker, 1980; West, 1983; West, 1986; Hargreaves, 1991).

¹ Most of the historical information on Stirling engine research were gathered from 'Stirling Engines' by G. Walker, 1980 and 'The Stirling Alternatives' by G. Walker et al. 1994.

1.2 Fundamentals of the Stirling cycle

Before examining the Stirling cycle, it is worth reviewing the Carnot cycle - which indicates the theoretical maximum thermal efficiency of a heat engine. Figure 1.1 shows the P-V and T-S diagrams as well as the four sequential processes of the Carnot cycle. The maximum thermal efficiency is given as: $\eta_{th} = (T_{max} - T_{min}) / T_{max}$. This is the highest possible value of thermal efficiency between two temperature levels and is attained when all the heat transfer to and from the system occurs at the constant temperatures of T_{max} and T_{min} . In practice it is not possible to construct Carnot cycle engines. The major problems are :

- There are no materials which are perfectly insulating or conducting, which are required for the isothermal processes.
- Friction and leakage losses occur as the pistons slide in the cylinder.
- In the P-V diagrams the slope of Isothermal and Isentropic processes are so similar for a gas that the area of the P-V diagram becomes negligibly small unless very large pressure difference or very long piston strokes are used.

The ideal Stirling cycle is similar to Carnot cycle in most respects. The main difference is that the two isentropic processes (compression and expansion) are replaced by constant volume processes as in figure 1.2. The simple arrangement of a cylinder containing two opposed pistons, with a regenerator in between them is used. Although in practice a variety of arrangements may be employed, the main processes are the same. If the heat transferred in process 2-3 in figure 1.2 has the same magnitude as in the process 4-1, then only heat transfer between the engine and the surrounding is the heat supplied at T_{max} and the heat rejected at T_{min} . Hence in principle the Stirling cycle should have the same thermal efficiency as the Carnot cycle. The advantage of the Stirling cycle over the Carnot cycle lies in the replacement of the two isentropic processes by constant volume processes, which greatly increases the area of the P-V diagram, giving more work from the same hardware. Hence it is not necessary to resort to impractically high pressures and/or swept volumes (as needed in Carnot cycle) to obtain reasonable amount of work. Figure 1.2 also shows relative position of a Carnot

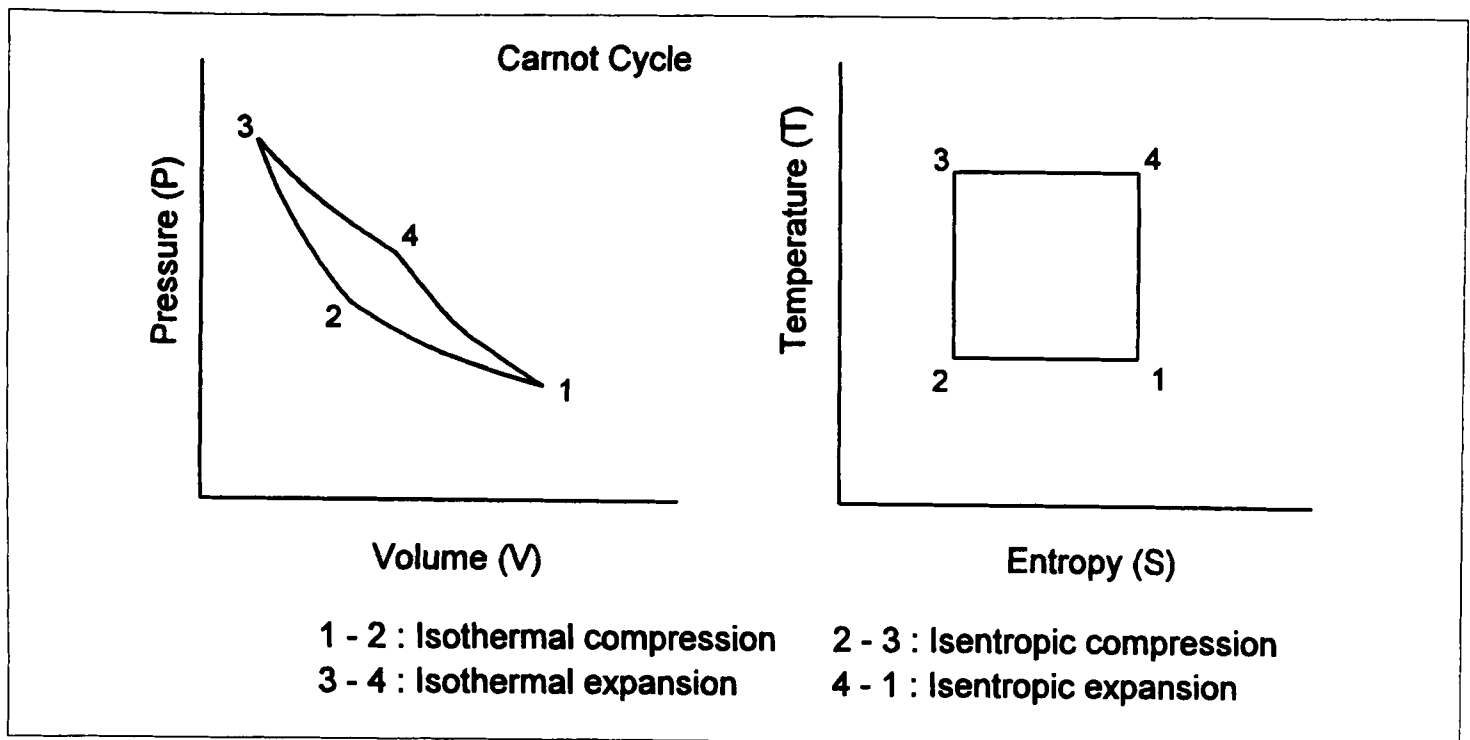


Figure 1.1 : P-V and T-S diagrams of a Carnot cycle with four sequential processes.

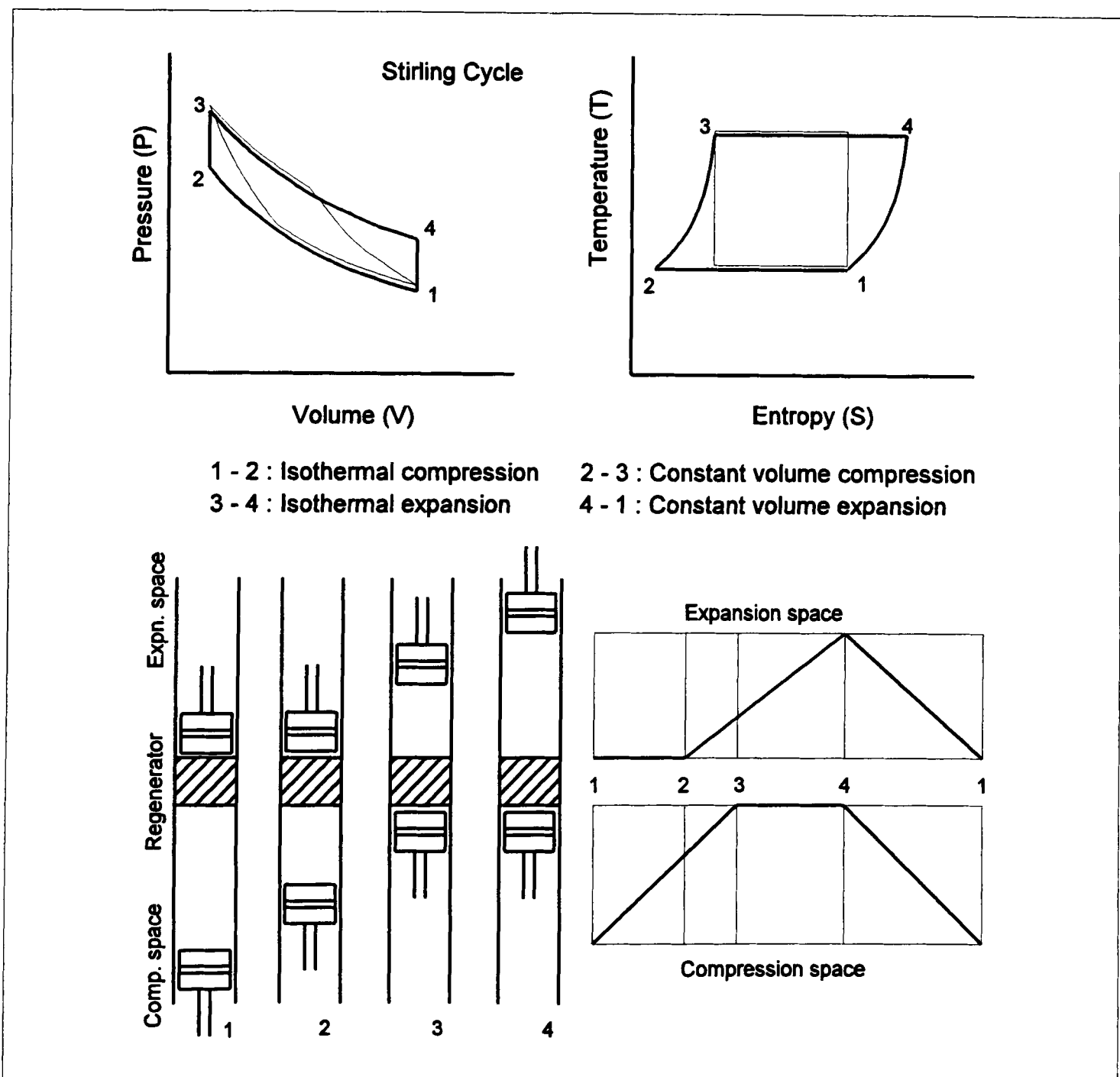


Figure 1.2 : P-V and T-S diagrams of Ideal Stirling cycle. The thin lines show the corresponding diagrams of a Carnot cycle with common ranges of temperature, pressure and volumes. Cycles are slightly offset for clarity. Time-displacement for compression and expansion spaces are shown below. *Source : The Stirling Alternatives, 1994*

cycle (thin line) compared to the Stirling one, with common values of maximum and minimum temperature, pressure and volumes. The area enclosed in both plots are larger than the Carnot cycle, indicating greater work done per cycle.

Though theoretically very promising, in practice the efficiency achieved by Stirling engines are limited by several constraints.

- The regenerator makes the Stirling process inherently more efficient. On the other hand the maximum temperature attained (T_{\max}) for a Stirling cycle is limited by the metallurgical limit of construction materials used, as they have to suffer continuous exposure to this temperature over a long period of time. The maximum temperatures attained in internal combustion engines are several fold higher than Stirling machines, yet they can be constructed with common materials like cast iron, as the maximum temperature is localised, attained only momentarily and the does not reach the wall.
- The non-continuous motions of the pistons of the Stirling cycle are difficult to produce. Continuous sinusoidal motion causes loss of the P-V diagram area and results into lower efficiencies.
- Limited heat transfer in the heating and cooling sections, aerodynamic flow losses and heat losses to the surroundings in all the three modes (ie. conduction, convection and radiation) reduce the efficiency attained by a practical Stirling cycle.

Table 1.1 shows the major advantages and disadvantages of Stirling engines. Stirling engines, being external combustion in nature, can use any type of fuel. The combustion is continuous type rather than explosive as in IC engines. This generally results quieter engine operation and vastly lower pollutant emissions. Stirling engines generally are two stroke cycle, having much smaller cyclic torque variation compared to four stroke IC engines which facilitates engine balancing and reduces lubricant consumption. The combustion products of Stirling engines do not come into contact with the moving parts which leads to lower wear rates. Thermal efficiencies of Stirling engines remain more or less the same over a wide range of loads, giving flat part-load characteristics (this is

also true for diesel engines). The availability of large number of cycle control parameters allows a variety of design approaches and wide range of engine structures.

TABLE 1.1 : Advantages and disadvantages of Stirling engines.

ADVANTAGES	DISADVANTAGES
Multi fuel Capability	Manufacturing Costs
Quiet Operation	Seal Reliability
Flat Part-load Characteristics	Radiator size
Low Pollutant Emissions	Complex Control Systems
Low Cyclic torque Variation	
Low Lubricant Consumption	
Low Internal Wear Rates	
Variety in Design	

Source : The Stirling Alternatives (Walker et al. 1994)

Though having all these advantages, Stirling engines also have some disadvantages which are sufficiently important to make Stirling engine uncompetitive with present internal combustion engines, except in very specific circumstances.

- Higher manufacturing cost compared to present IC engines. This is one of the primary disadvantage of producing Stirling engines in large numbers. The increased cost arises from the need to use special materials, like high temperature alloys, for the hot parts. Increased size and cost of heat-exchangers and radiators adds to this disadvantage. On the other hand Stirling engines have to work with upper temperature limits, much lower than those of IC engines, which ultimately reduces the inherent efficiency advantage of Stirling engines (although exhaust out of IC engines may have higher temperature).
- Sealing has been a major problem in Stirling engines for a long time. Seals are needed to contain the working fluid as well as to prevent the ingress of lubricant into the cylinder. The sealing problem is exacerbated in Stirling engines using light gases like helium or hydrogen (hot hydrogen can pass through mild steel),

which are necessary to attain high power density (eg. 60 kW /litre displacement or above). Use of such light gases in high speed and highly pressurised Stirling engines pose difficult sealing problems and the seals need to be maintained even when the engine is not running. It demands seals which - effectively contain high pressure, preferably non-lubricated, requiring low maintenance, easily replaceable and maintain low friction characteristics even when operating at high speed and elevated temperature. These problems have not been completely solved yet, despite very large development spending by Ford, General motors and Philips. Though some seal designs have shown better performance, they still lack a reliable and repeatable manufacturing process.

- Control systems for Stirling engines are generally more complicated, requiring more expensive mechanisms, compared to those in other common heat engines. Due to the presence of thermal inertia, a varying fuel flow rate does not provide rapid control of engine output. Supplementary control systems (eg. pressure or stroke control) are often used to attain rapid response of the engine to load changes.

1.3 Concept of the Malone engine

Liquids can also be used as working media for heat engines, although the practitioners of this method are few (Swift, 1989). Liquids actually have large thermal expansion coefficients over a large temperature range (about $0.7 T_{crit}$ to T_{crit} , where T_{crit} = Critical temperature), even compared to gas. For example water expands at a rate about 1/10th of air a room temperature, 1/2 that of a gas at 175°C, same at 260°C and twice as much at 315°C. Liquid engines need to operate at high pressures, to attain such high temperatures, without boiling. In these ranges of temperature and pressure, termed as the 'Dense phase', the distinction between gaseous steam and liquid water vanishes as the densities become similar. The specific heat capacity of liquids is vastly higher than those of gases, while the compressibility remains low. These characteristics allow the use of very compact heat-exchangers with low pumping power. As temperature changes resulting from adiabatic processes are relatively small for liquids, liquid engines need to use Stirling type regenerative or recuperative cycles. Liquid engines

in all ways conform to the definition of Stirling engines, but use a liquid working fluid instead of a gas. Such closed cycle regenerative engines with liquid fluids are called Malone engines, in honour of John Malone, who invented them.

John Fox Jennings Malone was born in England in 1880². He ended his formal education by 1898 and later served the merchant marine for 14 years. Leaving the merchant marine, Malone found the Sentinel Instrument company and later, the Fox instrument company and began experimenting with liquid engines in the 1920s, in Newcastle-Upon-Tyne. Malone built and tested three liquid engines between 1924-1931. As far as it is known, Malone presented only one account of his work to the Royal Society of Arts in 1931. Malone in his paper claimed 27% indicated efficiency (compared to about 13% efficiency of contemporary steam engines). The paper contained photographs of two large two-cylinder vertical machines and a smaller single-cylinder horizontal engine. They operated at low speeds of 24 - 250 rpm. High pressures were used, which varied from a low value of nearly 70 bar to a maximum of 275 bar. Malone's engines used supercritical water as the working fluid. In addition to water he also experimented with oils, liquid carbon-dioxide and mercury and concluded that he had found water to be best (Malone, 1931).

Figure 1.3 shows the general arrangement and operating sequence of a Malone engine. The heart of his engine, which he called the "thermodynamic pile" (or "TD pile" in abbreviation), contained the regenerative displacer (or regenerator) and the working fluid. The power piston, equipped with pressure seals, was placed in another tube in parallel to the TD pile. The regenerator displaced the water back and forth between the hot-end and cold-end heat exchangers, alternatively heating and cooling it. This heating and cooling caused pressure changes, because of the large thermal expansion and small compressibility (ie. high bulk modulus) of water. The movement of the piston compressed or expanded the working fluid. Because of the phasing between the regenerator and piston (each moved by a crank), the overall effect at the piston was

² Source : 'John Malone and liquid engines' by G.W Swift, Scientific America September 1992.

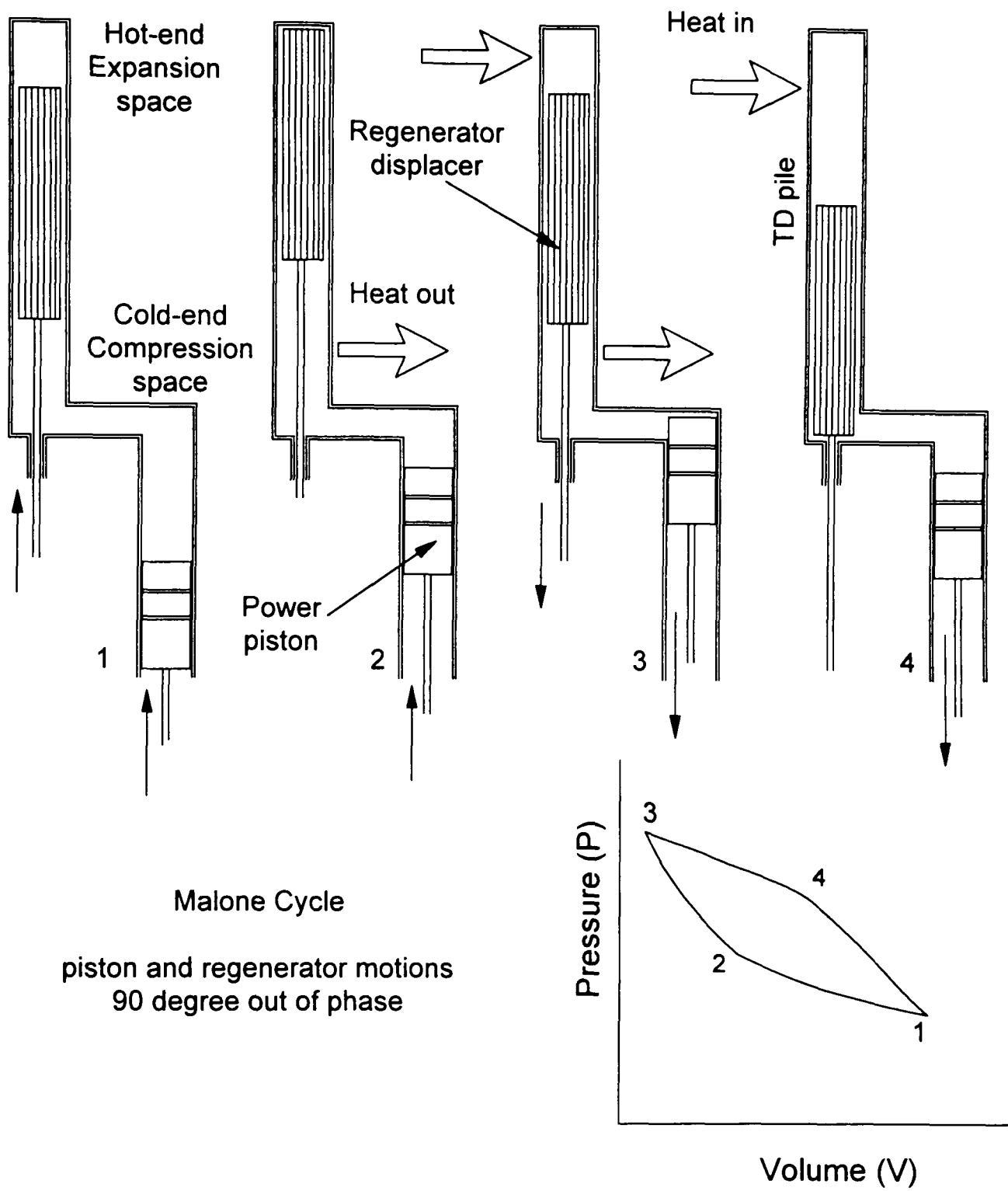


Figure 1.3 : General arrangement and operating sequence of a Malone engine with liquid working fluid (after Malone 1931). The regenerator also acts as the displacer moving fluid between the hot-end and the cold-end. The piston displacement changes the pressure of the fluid.

expansion at high pressure and compression at low pressure, so that net work was done by water on the power piston and ultimately transferred to a rotating shaft. Malone's engine enjoyed several immediate advantages over the air engines which preceded them:

- The supercritical water allowed very high cycle pressures to be used (up to 800 Bar or 12,000 psi), which produced very large amounts of work per stroke (Walker, 1980).
- The cold water formed the hydraulic link between his TD piles and the power piston. This gave no sealing difficulties, even with conventional gland materials available at that time.
- Water returned to atmospheric pressure as the engine was turned off. This made the engine much less liable to idle leakage loss compared to engines using pressurized gas.
- The working fluid in the TD piles had heat transfer capabilities, substantially better than that of gases. This allowed better heat transfer and higher power densities could be attained.

Unfortunately, Malone fell victim to the depression and the increasing dominance of petrol and diesel engines - themselves spurred on by the improving economics of liquid fuel use. By late 1931 John Malone was bankrupt and the liquid engine development came to an abrupt halt.

1.4 Concept of digital-displacement hydraulic drive

The digital-displacement pump-motor is a hybrid device, which combines reciprocating hydraulics with micro-processor control, creating a highly integrated machine capable of producing variable flow and power. These are hydraulic machines developed by W.H.S Rampen and S.H. Salter, at the University of Edinburgh (Rampen, 1992). The digital-displacement pump and the pump-motor were patented in 1990 and 1991 respectively, although the work originated in the early 1980s in connection with wave power research. High pressure hydraulics were considered to be the only feasible

method, to convert the immense torque and low velocities of wave power converters (eg. the Salter Duck), into a uniform high-speed input required for electric power generation. The wave power research was later virtually stopped, but the digital-displacement technology emerged as a product of it.

The technology (Rampen et al. 1991, 1994) is based on conventional hydraulic piston machines but with actively controlled poppet valves. Each cylinder has electronically controlled inlet and outlet poppet valves (with actuators), which are opened or closed by a properly timed electric pulse from a micro-processor controller. This allows enabling or disabling of cylinders, by actuating the small electro-magnetic latches on a stroke-by-stroke basis, giving any desired sequence. For noise reasons, only an entire cylinder displacement could be enabled or left disabled. From its resemblance to digital logic (0/1), the name 'Digital-Displacement' evolved. The same machine can be used both as pump or motor, by controlling the valve actuation sequence. The novelty of the design lies in the precise timing of the valve actuation. As the valves are actuated at times in the cycle when there is almost no pressure difference across them, the actuators can be small and use little power. A small accumulator is connected to the pump-motor to provide time-averaging of the flow pulsation created by discrete number of cylinder enabling, leading to an essentially smooth flow output.

The advantages of the digital-displacement machine over conventional variable-swash hydraulic machines lie with both the response speed and inherent energy efficiency. The compatibility with micro-processors allows the use of advanced control logic. This machine is capable of attaining either full or zero output from any starting condition, in less than a single shaft revolution. As disabled cylinders are not pressurised, losses are reduced in comparison with swash-plate machines leading to higher efficiency, especially at part load. The cylinders may be arranged in axial or radial configuration. The radial configuration allows (due to force balancing) multi-banking of up to eight separate pump-motor units on a common shaft. An arrangement of more than one radial pump-motor banks on a common shaft can be used as a summing junction for torque and power.

A relevant arrangement of a hydraulic drive would be a hydraulic ram being coupled to a digital displacement pump-motor. This would allow the hydraulic ram to be moved in almost any arbitrary way, as long as a large number of pump-motor cylinders are available during the motion of the ram. A pump-motor running at a speed much faster than the frequency of ram motion or physically having a large number of cylinders, can increase control over the motion profile of the ram. Although in practice there are limitations to the maximum speed of the pump-motor shaft and number of cylinders in the pump-motor structural configuration. Using a similar arrangement in a heat engine meant arbitrary piston motions could be achieved, breaking the constraints of conventional sinusoidal piston motions. This allows the manipulation of piston motions and the optimal control of pressure-volume diagrams, for achieving greater outputs from thermodynamic cycles. Though the scope of implementing this technology in internal combustion engines is limited due to the high operating engine speeds, it may have great prospect for Stirling or Malone engines which generally operate at much lower speeds.

1.5 Combination of Malone cycle with digital-displacement hydraulic drive : The Artemis-Malone engine

A combination of the digital displacement hydraulic drive and the Stirling cycle could lead to a new form of heat engine, this was realised by S. H. Salter. W.H.S Rampen pioneered the idea for using the digital drive in a Malone engine, instead of a Stirling. He found that, with their low speed and high-torque cycles, the digital hydraulic drive could be used most effectively in Malone engines. Together they decided to move ahead with such an engine design, through their R&D company, Artemis Intelligent Power Ltd. The proposed engine was termed as 'Artemis-Malone Engine'. The new engine has several additional features which may make it possible to overcome some of the major problems of Stirling engines. These mainly include the following, which are elaborated in the following chapters.

- The leakage problem is reduced in Malone engines compared to Stirling engines by choosing a working fluid which condenses (eg. water) when the engine is not working. The leakage problem can be further reduced by using a hydraulic drive rather than a conventional piston. In the Artemis-Malone engine a flexible separator membrane is used to isolate water in the TD pile and oil in the hydraulic circuit. This ensures complete sealing of the working fluid. There still may be need of seals in hydraulic machines but the problem is shifted from hot water to much cooler oil, while the poppets of the pump-motor have been demonstrated to have very good sealing capability.
- The digital-displacement hydraulic drive allows the creation of arbitrary piston motion which is independent of the regenerator (displacer) motion. This ends the limitation of constraining the motions to sinusoidal form and phase angle, as in conventional cranks. This gives much greater opportunity to shape and extend the area of P-V diagram produced by the engine and make better utilisation of the thermodynamic cycle.
- The thermal resistance of hot-end (expansion space) wall needs to be low for good heat transfer. However it does need to be sufficiently thick and strong to withstand high internal pressure for a long time at elevated temperatures. But the metals which have good high-temperature strength, are generally very poor thermal conductors. This problem was solved by having a composite hot-end structure composed of metals with high thermal conductivity and high-temperature strength. The hot-end was made from a laminated stack of alternate copper (highly conductive) and Inconel 625 (an alloy with high-temperature strength) washers, diffusion bonded (or vacuum brazed) together. The inner and outer radial dimensions of copper disks were chosen such that they extend as integral inner and outer fins, enhancing the heat transfers at the flame-fin (at outside) and steam-fin (inside) interfaces. The heat transfer at the steam-fin interface was further enhanced by swirling the fluid inside the hot-end.

1.6 Overview of thesis structure

This thesis mainly deals with the various aspects of the design of Artemis-Malone engine, control techniques for its operation and estimates its performance using static and dynamic (time-domain) models. Chapter three explains the structure and operating principle of the engine. Chapter four presents the static model of the engine, which mainly deals with design of engine components. Chapter five describes time domain modelling of digital-displacement pump-motors. Chapter six describes dynamic models of theoretical engine cycles while chapter seven incorporates realistic regenerator motions and piston motions generated by the pump-motor for more realistic cycle models. Chapter eight investigates different control strategies for controlling engine power. Chapter nine presents the simulation results of different power-control strategies for continuous control over varying load cycles. Chapter ten returns to the static model and using information from the time domain simulation, updates it to allow a comparison of performance results from the static and dynamic approaches.

CHAPTER - 2

Literature Review

2.1 Introduction

In this chapter a general review is made of some of the previously published works which are related to this thesis. The review could be divided into three sections which cover the fields of :

- (i) Modelling of Stirling engine cycles.
- (ii) Drive mechanisms used for power take-off in Stirling and Malone engines.
- (iii) Design and performance of digital-displacement pump-motors.

2.2 Modelling of Stirling engine cycles

A number of techniques for modelling Stirling cycles are used in practice, with varying levels of detail and computational complexity. A comprehensive comparison of different simulation models was given by Taylor (1984). The conventional simulation models are divided into three categories - first, second and third order models.

First-order models :

The first-order models are improved forms of ideal cycle analysis. Analysis by Schmidt is the classical example of this type (Schmidt, 1871). The analysis is based on continuous motions of the pistons and isothermal conditions at the compression and expansion spaces. Schmidt analysis had a closed (implicit) form of solution, which is a significant advantage when compared to some higher-level analyses (Walker et al. 1994). The Schmidt analysis is considered to be highly idealised and the results optimistic, although it is still solely used for some predictive models (Isshiki, 1992). The Schmidt cycle has been examined and expanded in detail in many of the recent Stirling texts (Walker, 1980; Reader and Hooper, 1983; West, 1986; Urieli and

Berchowitz, 1984) and is used as the basis of many second-order simulation models. The major development following Schmidt came in 1960, with the *limited heat-transfer theory* by Theodor Finkelstein (Finkelstein, 1960). This theory allowed the heat transfer between contents and cylinder walls, during compression or expansion, to take values in between the two extreme cases of isothermal or adiabatic processes. Finkelstein's model did not have a closed solution and involved the solution of different simultaneous partial differential equations. According to this model the conditions in the regenerator were still considered isothermal, while conditions in the cylinders could be adiabatic. For such a cycle the theoretical cycle efficiency became a function, not only of temperature, but also of other parameters (eg. swept volume, phase, dead-volume etc.). The model still retained all other assumptions of Schmidt model and hence is also considered idealized. Walker and Khan (Walker and Khan, 1965) investigated variation of different design parameters on the performance of adiabatic Stirling cycles. Significant work using the adiabatic approach, were presented by others (Qvale and Smith, 1969; Lee, 1976; West 1986; Chen and West, 1987).

Second-order models :

The most widely used design method followed by Stirling analysts is one in which the results of a first-order analysis (isothermal or adiabatic) are corrected by the incorporation of various losses arising in real engines. This technique, known as decoupled second-order analysis, was pioneered by Joseph Smith at MIT in 1960. The losses were grouped into mechanical and thermal losses and could be static or dynamic in nature. Each of the losses were considered to occur independently of the others. The predictions of the second order analysis could be fairly representative ($\pm 10-20\%$) of test-bed results (Walter et al. 1990).

Decoupled second-order simulation models, using an isothermal approach, were actively pursued and fully enumerated by William Martini (Martini, 1982; 1983). He developed mini and personal computer programs for Stirling engines and made these available to the interested market. After Martini's death, further developments were carried out to generalise these programs for most known types and configurations of

Stirling engine (Weiss et al. 1986; Srinivasan et al. 1985; Walker et al. 1990). Separate versions of user-friendly programs were developed by Marvin Weiss at University of Calgary for both Stirling engines and coolers (eg. MARWIESS, CRYOWEISS). Later another program (MULTIWEISS) was developed for application to multiple expansion Stirling engines (Walker et al. 1992). These programs are easy to use but assume that user is able to make realistic parameter choices for the Stirling machine.

Second-order simulation models, using an adiabatic approach, were developed by the Stirling research group at Royal Naval Engineering College (Reader and Hooper, 1983; Sylvestre, 1987) and by Berchowitz (Berchowitz, 1878; 1986). The only modelling work carried out for the Malone cycle, was by Swift (1989), who also used this approach. The model takes detail account of various losses in adiabatic cycle, but is limited to sinusoidal motions. The model is applied for a heat-pump, which also reveals the advantage of using liquid in a Malone heat-pump cycle, compared to gas. This paper also points out, how liquids are actually thermodynamically complex and active, contrary to common conception. Adiabatic simulations have also been reported to be used by Philips in their research on Stirling cycles, although little of that has been published (Walker, 1980).

Third-order models :

Third-order computer simulation refers to highest analytic level of Stirling cycle simulations. The third-order models attempt to take into account all thermo-fluid processes occurring in a Stirling engine. Working processes inside the engine involve unsteady fluid motion, with varying flow areas, in the presence of friction and heat-transfer. The equations defining the processes are not unique and are covered in classical gas-dynamics studies. At this level of analysis all three conservation laws - mass, energy and momentum - are used to produce a set of governing differential equations . These equations could be solved by *Nodal-analysis* or by the *Method of characteristics* (Taylor, 1984). The two techniques differ in the co-ordinate system chosen. The most comprehensive review of different numerical solution techniques is given by Organ (1992).

Nodal-analysis of Stirling engines was pioneered by Finkelstein (1975). For nodal analysis the engine needs to be specified as to exact dimensions, materials and fluid choice. The engine volume is then divided into a number of small cells or node elements. Inside each cell properties are considered to be uniform. Two methods are used for defining this cell framework. With the Eulerian nodal frame, the working space is divided into volumes fixed with respect to axial space co-ordinates (Urieli, 1984). However some disagree with the validity of this technique (Rix, 1988; Organ, 1992). They argue, that the Eulerian-grid is incompatible with the moving boundaries formed by the pistons. The grid also creates artificial smoothing of pressures and temperature discontinuities within the working fluid as it move through the reference framework. The other approach uses a Lagrangian grid system where cells always encompass a fixed mass of working fluid, thus the reference move with the working fluid (Rix, 1988). On the other hand Eulerian grid simulations have been defended by Bauwens (1993). However in both cases the differential equations of the conservation laws are developed and generally converted to one-dimensional finite difference equations and applied to each cell in turn. These equations are integrated with respect to time, provided that all the cell properties are known at some initial point of the engine cycle. The common procedure for solution is to start with some initial arbitrary conditions (in most cases an isothermal Schmidt cycle-type is used) and then to proceed through several engine cycles until quasi-steady state is achieved (time marching solution). This is reached when the instantaneous values of pressure, temperature and mass distribution are not significantly different from preceding cycles (Walker, 1980).

In the method of characteristics the frame of reference is the particle path. To simplify the manipulation of the equations in the computer, the particle trajectories are mapped on to a grid fixed in time and space. This method of characteristics provides a detailed understanding of the gas-dynamics within the Stirling engine but ideally would need parallel processing computers (Reader and Hooper, 1983). David Gedeon has developed a globally-implicit-finite-difference (GLIMPS) method to solve the gas-dynamics equations simultaneously over the full-cycle period, instead of customary time marching solution (Gedeon, 1986). It is intended to meet the need for a fast-running simulation using a minimal number of nodes in the computational grid. His work have

been extensively used in NASA free-piston program and has been calibrated against experimental data (Glen and Tew, 1992).

Although third order models provide more realistic approximations of the engine cycle, the predictions are often engine-specific and need to be calibrated against test-bed results. Generally third-order modelling requires long computation times, 40 -200 times longer compared to second-order models (Walker et al. 1990) with higher-performance computer hardware. Often convergence factors are used to force reduction of the convergence-time and some controversies still exist between the preferred choice of nodal frame-work (Rix, 1988).

Choice of simulation model :

The choice of the simulation model to be used depends to a great extent on the desired degree of accuracy of results, simulation run speed, the stage of the engine-development and the availability of computer hardware. At the present stage of development of the Artemis-Malone engine, a second-order decoupled model using an isothermal approach is chosen as the simulation technique to be adopted. Although simulations in the alternative adiabatic approach should be more realistic as compared to isothermal cycles, in practice these performance predictions were reported to be conservative (Walker et al. 1990). At this stage the model will be developed for the engine concerned rather than a generalised one, this allows more specific detailing (eg. design optimisation). Such a second-order model will be fast to use, could be developed using available software on personal computers, but is expected to be fairly representative in its predictions.

2.3 Drive mechanisms used for power take-off in Stirling and Malone engines

The literature review regarding Stirling-Malone cycles presented here is limited to the drive mechanisms used, which is the most significant change proposed with the Artemis-Malone engine.

A comprehensive review of different mechanical arrangements used for piston and regenerator motions is given by Walker (1980). The most common arrangement used for converting work done by the working fluid into mechanical work is the conventional piston-crank arrangement. This is used extensively in internal combustion engines and also was used by John Malone (1931) in his liquid engines. This mechanism is very simple and cheap to make in large scale. However with this arrangement, as forces are transmitted between the piston and crankshaft, appreciable side forces are exerted. This pushes the piston against the cylinder wall, which may cause increased wear of piston seal as well as the cylinder wall. This problem is increased in the case of Stirling engines, which tend to use non-lubricated seals. Lubricating seals are not desirable for Stirling engines because oil vapours dispersed from the seal gets trapped in the fine passages of the regenerator matrix and may get carbonized. Leaking of lubricating oil even may lead to auto-ignition if air is used as the working fluid. The problem is greatly reduced in a crank-connecting rod-crosshead assembly, where a slider arrangement is incorporated in between the piston and the crank. This increases the size of the arrangement and makes it more difficult to balance dynamically at high speeds.

A review of the problems of using these arrangements were made by Reader (1983). Organ (1992) has also dealt with kinematics of Stirling engine drive mechanisms. To remove the side forces on the piston, the rhombic drive was developed by Rolf Meijer (1959) in the Philips Stirling engine programme. A similar kinematic arrangement was invented by Lanchester in 1893. The rhombic drive consists of two counter-rotating meshing gears and a twin link arrangement. This allows perfectly balanced reciprocal motion of the piston and the displacer, with no side forces acting on them. The Rhombic drive needs to be fabricated with precision in order to achieve good

mechanical efficiency and requires a large number of bearings, which increases the production cost. A number of different drive mechanisms were developed, eg. Ross Yoke mechanism (Ross, 1979), Wood linkage (Wood, 1978) and swash-plate drive (Mattavi et al. 1969). However all of these gave sinusoidal or near sinusoidal motion profiles of the piston and regenerator with a fixed phase difference. Hence all of these mechanisms are constrained by a sinusoidal relation of the moving elements.

There have been attempts to free the piston motion from the sinusoidal constraints. The free-piston engine or liquid-piston engines are of this type. In free-piston engines the fluid forces move the piston and there is no linkage connecting to the piston to constrain its motion. The displacer is connected to a power piston through a gas reservoir. Power could be taken off in electric, hydraulic or mechanical means (Beale et al. 1973). Advantages of free-piston engines are simplicity, hermetic sealing, low cost, self-starting and long life. The problems with free piston engines are :- difficulty in maintaining the piston position and its centering in the cylinder for consecutive cycles (ie. stopping drifting). Additional active flow control systems may be needed to repeat thermodynamic cycles. It should be noted that liquid-piston engines are different from engines which use liquid working media. Liquid-piston engines have the power piston and the displacer piston both made of liquids, generally water. In fluidyne design of liquid piston engines (West, 1983), a U-tube contains the displacer in the form of a water column oscillating to move gas (ie. the working media) between the hot-end and cold-end through a regenerator. Expansion and contraction of the gases causes the power piston (which is also another liquid column) to move and produce work. Displacer motion is achieved using an asymmetric-jet-stream effect of water from the power piston. These engines have may have limited applications in stationary low power systems.

There also have been attempts to replace conventional drive mechanisms of Stirling engines with hydraulic drives. In the Stirling engine designed at Reading university (Dunn et al. 1975), the power piston was replaced by an isolator membrane in the form of a hydraulic bag. Hydraulic oil was pumped in and out of the hydraulic bag, creating the same effect as power piston on the gaseous working media. The variation of

volume of oil in the bag was controlled by a swash-plate hydraulic drive. Unfortunately there was a problem with leakage of oil across the seals of the hydraulic plunger of the swash-plate drive, although the isolator membrane provided sealing of the working fluid.

2.4 Design and performance of digital-displacement pump-motors

The digital-displacement technology, as far as known, is a novel one. Although the use of poppet valves in hydraulic machines are not new. The patent searches which were carried out during the development of the digital displacement machines, revealed a number of active valve hardware and systems for mechanically off-loading pumping cylinders (Moller, 1957; Craig, 1992; Miller, 1987). Nothing was revealed which anticipated the ideas nor dealt with the problems of the digital-displacement technique. The adaptability of this technique, which was initially developed as a pump, into motoring operation makes the concept unique.

The details of the development of the digital displacement pump is described in the Ph.D work of Rampen (1992). This describes the working principle and algorithms implemented by the controller. Details of the design of electro-magnetic latches include a finite element analysis of the magnetic latch circuit. Fluid flow losses and forces acting on disabled poppets were predicted and compared with experimental results. Experiments were carried out with a number of poppet valve shapes, leading to the choice of an ellipsoidal (mushroom shape) one for the poppets. Controller design and hardware implementation were addressed and finally the pump performances are compared to predictions made using a pump model written in Basic language. The literature review part of the thesis also provides more detailed references to other papers on comparable technologies.

A number of papers have been published regarding computer simulations and experimental results of pump-motor performance, though the work has been only concentrated at Edinburgh University. Prototypes of a six cylinder axial piston pump (1990), single cylinder pump-motor (1994) and six-cylinder axial pump-motor (1996)

were built by Rampen at Edinburgh. The performance of a digital hydraulic pump for constant-pressure-control was presented at Bath (Rampen et al. 1991). This paper shows the results for maintaining a constant pressure level under variable hydraulic load, by controlling the flow from the pump. A paper covering the predicted and measured frequency response of the a digital hydraulic pump subjected to a oscillatory load flow were presented at Bath the following year (Rampen and Salter, 1992). Here the peak pressure deviations from the set level were presented as surface plots against loading frequency and pump flow (in terms of capacity). The controller senses the change in demand, computes the decision algorithm and then implements the valve actuation, this finite time lag causes the pressure deviation from the set value. Results showed a broad resonant peak which corresponded to 180 degree phase shift from the reference time of the pressure control algorithm. The motoring cycle was presented first at Bath (Rampen et al. 1994). This included the operating principle and experimental results of the performance of a single cylinder pump-motor, which demonstrated satisfactory operation of the machine in motoring. Salter (Salter et al. 1993) estimated the transmission efficiency of a digital hydraulic drive. Taking all possible loss components in the pump-motors into account, the result showed more than 90% mechanical throughput efficiency.

Combining a number of multi-cylinder pump-motors (each one called a bank) with radial piston configuration, along a common shaft with multi-eccentrics, allowed the creation of a common junction for torque and power (Salter and Rampen, 1993). Such arrangements were termed as *Wedding-Cake* machines. The paper describes the working principle of the machines along with several special design features (eg. big-end bearing). The present state of development of Wedding-Cake digital hydraulic pump/motor is presented by Rampen (Rampen et al. 1995). The paper has three major sections. These include fatigue testing of the polymer poppets (up to 10^9 cycles), which showed the capability of using poppets for long term operation (approximately 11,000 hours of continuous operation). Annular shaped valves (ie. ring type) were developed for the poppets compared to ellipsoidal (mushroom-shaped) ones used at present. This involved flow analysis in the valve using finite element package (Ansys-Flotran) with the final shape being gradually developed through an iteration procedure. Results

predicted a large reduction of the fluid forces acting on the disabled annular valve and a reduction of pressure drop compared to the present shape. The last section described experimental results of the performance of the big-end bearings, which confirmed that the idling losses of these bearings can be kept low. These modifications should be included in later designs of wedding-cake machines.

Each bank of the wedding-cake machine may be providing fluid to an individual service with its own distinct cylinder enabling sequence. Controllers for each bank could work independently. The use of two or more pump-motor banks in the wedding-cake with suitable accumulator devices can as a whole run as an energy storage and isolating device. The author described the simulation results of a two-bank wedding cake machine working as hydraulic transmission for a wave power converter (Ehsan, et al. 1995). The first bank converts energy from the waves into hydraulic fluid (working only as a motor). The second bank acts as a pump or motor and transfers energy into and out of a gas accumulator as required. As a result a uniform power output is available from the shaft (running at nearly fixed speed), despite non-uniform energy input from sea-waves. The technique is equally effective in the reverse sense (Ehsan et al. 1996). It was shown that a two-bank Wedding-Cake arrangement can be used to satisfy a non-uniform power demand from a small input source giving uniform power. In this case the first bank works as a pump-motor transferring energy to and from an accumulator, while the second bank acts as pump only. The simulation results for the performance of a pump-motor running with variable shaft speed were also presented in this paper.

CHAPTER - 3

Structure and Operating Principle of Artemis-Malone Engine

3.1 The main engine components

The structure and operation of the Artemis-Malone engine can be described in terms of its major components. These could be grouped as :

1. Thermodynamic pile :
 - (a) Hot-end.
 - (b) Cold-end.
 - (c) Regenerator.
2. Hydraulic drive.
3. Heat exchanger for exhaust heat recovery.
4. Controls and Ancillary drives.

3.2 The thermodynamic pile

The thermodynamic pile (or TD pile) which contains the working fluid, consists of the hot-end, a separator tube with a regenerator-displacer inside and the cold-end. The hot-end transfers heat from an external flame into the working fluid inside the TD pile. The regenerator heats up and cools down the working fluid alternatively and transfers heat from one cycle to the successive one. This recycling of heat plays a very significant role in the performance of Stirling cycles and its rate may be several fold that of the heat intake rate through the hot-end. The cold-end transfers the heat (which has not been converted to work) to the cooling-water sink. The thermodynamic pile generally has a long slender aspect ratio, which assists in heat transfer across the wall and reduces conduction losses.

3.2.1 The hot-end

The hot-end is a pressure vessel which can withstand high internal pressure, while also possessing good thermal conductivity to transfer heat from the hot combustion gases into the working fluid. Unfortunately these two properties are not possessed by a metal both commercially available and economic to use. Copper has very good thermal conductivity but is very weak at high temperature and prone to oxidation. On the other hand stainless steel and nickel based alloys like Inconel (mainly an alloy of chromium and nickel, details of composition is given in table 3.1) have good high-temperature strength but poor thermal conductivity. A design has been suggested by S.H. Salter to build the hot-end of the TD pile with a stack of alternately placed copper plates and Inconel washers, which are diffusion bonded together.

Diffusion bonding (also called vacuum brazing) is a method in which carefully cleaned metal parts with close fitting surfaces plated with a thin coat of copper or nickel are clamped together. The assembly is placed in a vacuum or inert atmosphere and heated to about 1100°C and left for 15 minutes. The metals at the contact surfaces diffuse into one another and form a very neat, strong bond with no need for flux. Using nickel coating can result in joints that can be used at temperatures up to 800°C (Schwartz, 1995). In the present design copper was chosen for its high thermal conductivity and Inconel 625, the composition of which is shown in table 3.1 (Inco Alloy International, 1985), was chosen for its high-temperature strength. Figure 3.1 shows a sectional view of the TD pile with the hot-end. The reference positions shown for regenerator and piston motions should be noted, as they are later used throughout the thesis, to describe piston and regenerator motions. The inner and outer dimensions of the copper plates or washers are chosen so that they create extended fin surfaces at the inside and outside of the composite-wall, formed by the bonded copper-Inconel disks. The design of the composite wall has two important features :

- The layers of copper and Inconel act like parallel resistances against heat flow from the flames coming into the working fluid. The thermal resistance of copper layers is much smaller compared to that of the Inconel layer (copper is

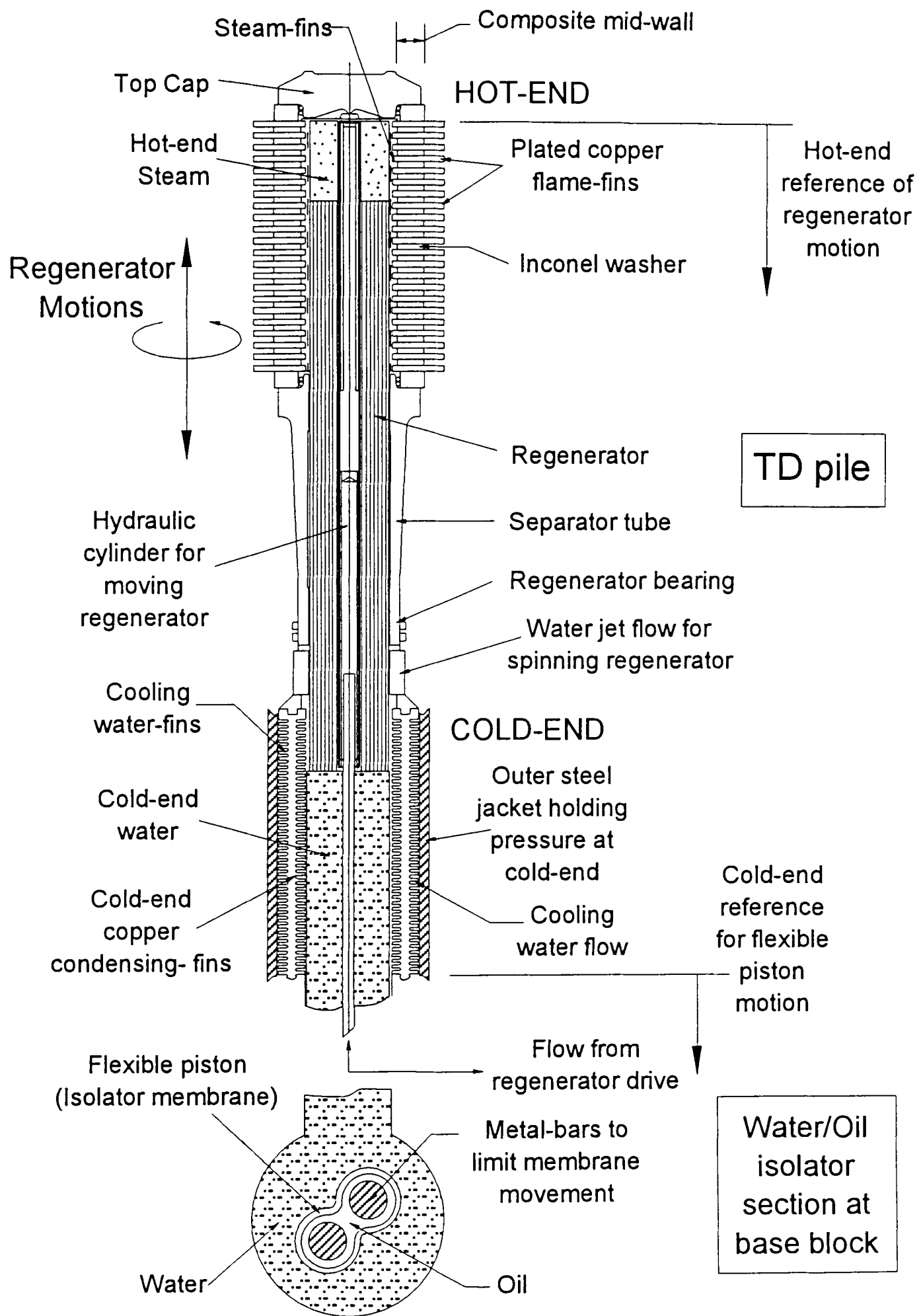


Figure 3.1 : Schematic sectional view of a module of the Artemis-Malone engine. The figure shows the TD pile and the water-oil isolator section of the hydraulic drive at the base block of the engine.

at least 20 times more conductive), as a result the equivalent thermal resistance is vastly reduced compared to Inconel, although greater than copper alone. The proportion of copper and Inconel thicknesses determine the level of equivalent thermal resistance of the composite-wall. The choice of this ratio is limited by the number of copper-Inconel surfaces necessary to maintain low shear stress levels at the brazing interfaces.

- At temperatures above 900°C copper has almost no strength and melts at 1065°C. Hence at elevated temperature there is little chance that copper would resist any stress (Henderson et al. 1971). In the design of the copper-Inconel stack, the Inconel is assumed to take the entire stress. Forces acting across the thickness of the copper disk, due to fluid pressure, are transmitted into the Inconel through the brazed interfaces. Compared to the copper area directly exposed to fluid pressure, the area of the brazed surfaces is much greater (each copper disk has two brazing surfaces). This largely reduces the stresses in both the copper and copper-Inconel interfaces.

TABLE 3.1 : Limiting Chemical Composition (%) of Inconel 625

Nickel	58.0 min.	Manganese	0.50 max.
Chromium	20.0 - 23.0	Silicon	0.50 max.
Iron	5.0 max.	Phosphorus	0.015 max.
Molybdenum	8.0 - 10.0	Sulphur	0.015 max.
Columbium and Tantalum	3.15 - 4.15	Aluminum	0.40 max.
		Titanium	0.40 max.
Carbon	0.1 max.	Cobalt	1.0 max.

There are two metallurgical constraints imposed by the hot-end design. The hottest zone of the hot-end structure will be the outer edges (or fin-tips) of the external flame-fins facing the combustion gases. The temperature of the fin-tips should not exceed the safe limit for copper (which was considered to be below 750°C), to avoid any fin

deformation. As the engine is of external combustion type, the outer fins are exposed to combustion gases. For operating at this high temperature the hot-end metal, especially copper, needs to be protected against corrosion due to oxidation. Nickel plating or coating of the hot-end metal may be used for protection against oxidation. The lack of fresh supply of oxygen inside the TD pile and relatively lower temperature make the oxidation problem at the inner surface of the hot-end less difficult. The second, but never the less important, thermal limit is imposed by the creep behaviour of Inconel, which takes the entire pressure stress. The stresses in Inconel disks are distributed in the radial direction with the highest level at the inner edge (eg. like a thick walled cylinder subjected to internal pressure). The temperature distribution is almost linear, increasing towards the outer edge. Combining these two gives stress distribution along the temperature scale. This curve needs to be compared to rupture stress-temperature curves of Inconel (Inco Alloy International, 1985) for different operational life times (eg. 2000 hr, 10000 hr etc.). The relative position of the design stress-temperature distribution compared to the creep curves, dictates the expected life of the hot-end. This has been described in detail in chapter four and chapter ten.

The heat transfer at both the outer flame-fins and inner steam-fins depends on the fin surface area, fin-efficiency, velocity and physical properties of the fluid flowing past and the geometry of the flow path. Although some of these parameters are inter-related, they can be manipulated sufficiently within practical limits to get the desired heat passing into the hot-end with an acceptable temperature distribution in the hot-end metals. On the outer side, the main consideration for the heat transfer is to control temperature drop at the flame-to-fin interface, which ensures maximum use of the highest allowable fin temperature, while keeping below the safe limit. The heat transfer at the steam-fin interface can be considerably improved by spinning the regenerator inside the hot-end. Jets of water pumped from the cold-end may impinge tangentially on the regenerator surface near the cold-end, to make it spin about its longitudinal axis (like a Pelton-wheel impeller). The spinning of the regenerator creates turbulent flow condition at the steam-fin interface which significantly enhances the heat transfer rate at the interface. A thin tube with longitudinal slits may be placed in between the outer surface of the regenerator and the edge of the inner fins, to act as an impeller and

provide the swirling effect, irrespective of the axial position of the regenerator in the TD pile. The thin slitted tube is placed such that it touches the outer surface of the regenerator, which locates it radially but which still allows relative axial motion of the regenerator, like a spline.

3.2.2 The cold-end

The cold-end transfers the fraction of the heat arriving from the hot-end, which has not been converted to work, into the cooling-water sink. It consists of a copper tube with internal and external fins. Heat is transferred from the condensing working fluid by the condensing-fins, through the wall and rejected to the cold water circulated around the cooling water-fins. The finned copper section is too weak to take the internal pressure and so is contained by a closely fitted stainless steel tube. The cooling water is circulated through the gaps between the steel jacket and the water fins. The heat transfer at the condensing-fins is much better compared to the hot-end because of the much higher fluid densities, but swirling the fluid will improve it further.

3.2.3 The regenerator

The regenerator-displacer, hence referred to as the regenerator, oscillates between the hot and cold-ends and is a very important component of Stirling-Malone cycle engines. It acts like a thermodynamic sponge and transfers a large part of the heat rejected from one cycle into the next one and is mainly responsible for the potentially higher thermal efficiencies of these cycles. In moving between the two ends, the regenerator displaces fluid as well as transferring heat to-and-from the fluid passing through it. As the regenerator moves from the cold towards the hot-end, the steam at the hot-end is displaced into the regenerator, condensed and released to the cold-end. This steam cools down to the cold-end temperature as the regenerator absorbs heat and its temperature rises. Conversely when the regenerator moves from the hot towards the cold-end, it displaces cold-end water and heats it before it emerges at the hot-end. The energy flow in the regenerator may be several times higher (eg. 430%) than the cyclical energy input from the combustion gases at the hot-end (Walker, 1980).

The regenerator in each thermodynamic pile consists of a stainless steel tube about one millimetre smaller in diameter than the inside of the copper steam-fins and having a length several times its diameter (giving a slender aspect ratio). The length of the regenerator tube equals that of the hot-end fin block and the separator section with the cold-end. Inside the outer regenerator tube are permeable, heat storing elements as have been used in Stirling engines. These could be sintered stainless steel - balls, rolls of fine wire mesh or of spiral wound thin shim. Stainless steel shims may be passed through rollers to give it a pattern of dimples or bumps, to define the gap between the layers of the spiral and the porosity of the regenerator (Swift, 1989). Some small holes through the shim may relieve any radial pressure difference across the regenerator. The fluids at two ends are at very different temperature levels, so the regenerator will experience a large temperature gradient across it. This results in different levels of thermal expansion at either end. To improve the fitting of the regenerator bearings at each end of the separator tube, the outer surface of the regenerator could be ground to a taper so that it becomes parallel when it is at the middle of the expected range of temperature gradient (suggested by S.H.Salter).

The regenerator has two axes of motion which occur simultaneously. The main mode is the reciprocation in the axial direction, while the other is a rotational motion of the regenerator about its axis. Two separate drive mechanisms are needed to generate these.

For the axial motion, sufficient force is needed to drive the permeable regenerator between the two ends, against the pressure difference generated by its resistance to fluid flow. A small hollow plunger is fitted inside the core of the regenerator body, around which the metal shim is coiled. Fluid flowing in or out of this actuator volume causes the regenerator to move. The entrance of the hydraulic line into the regenerator core needs a seal with spherical freedom, so that it does not interfere with the spinning of the regenerator. The cold-end water can be used as the fluid of the regenerator hydraulic drive. This has the advantage of reducing the sealing problem and the actuation power needed to drive the regenerator as compared with external drive means. The regenerator drive system is considered in greater detail in chapter seven. The pressure of the

working fluid in the TD pile allows single-sided operation. This means the area difference between the two end faces of the regenerator always creates a biasing force pushing the regenerator towards the cold-end (acting like a spring) and the hydraulic system only needs to move fluid from the cold-end to the hot-end. As the regenerator motion affects the thermodynamic cycle significantly, the actuator drive needs to be either continuously controlled or predictable in its motion.

3.3 The hydraulic drive

The hydraulic drive is a unique feature of the Artemis-Malone engine. Instead of having a conventional piston mechanism (with all its sealing problems), a digital displacement pump-motor and a flexible elastomeric isolator diaphragm is used to form the hydraulic drive. Digital-displacement pump-motors are reciprocating hydraulic machines with actively controlled poppet valves. These valves can be closed by sending a pulse from a micro-processor controller, for enabling individual cylinder flows. The general features of the pump-motor have been mentioned in chapter one and will be described in detail in chapter five. The base manifold block of the Artemis Malone engine contains longitudinal galleries. In case of a multi-module engine, half of the thermal modules are connected to each gallery. Figure 3.1 includes a sectional view of the base manifold block of the engine. Each gallery contains two metal bars running its full length. A long elastomeric tube is placed inside each gallery, such that it contains the two metal bars inside it. The elastomeric tube or membrane is termed the 'flexible piston', as its effect on the working fluid is similar to a piston, when it inflates or contracts. The flexible piston also isolates the working fluid (ie. water) and the hydraulic oil, effectively removing the sealing problem from the TD pile. The inner wall of the elastomeric tube touches the outer curvature surfaces of the bars. The two bars provide a shape-former onto which the elastomeric tube can collapse in order to limit the deforming stresses and ensure a very long fatigue life. The inside of the elastomeric tube is connected to the digital-displacement pump-motor hydraulic unit. While the outer side of the elastomeric tube is in contact with the water of the cold-end.

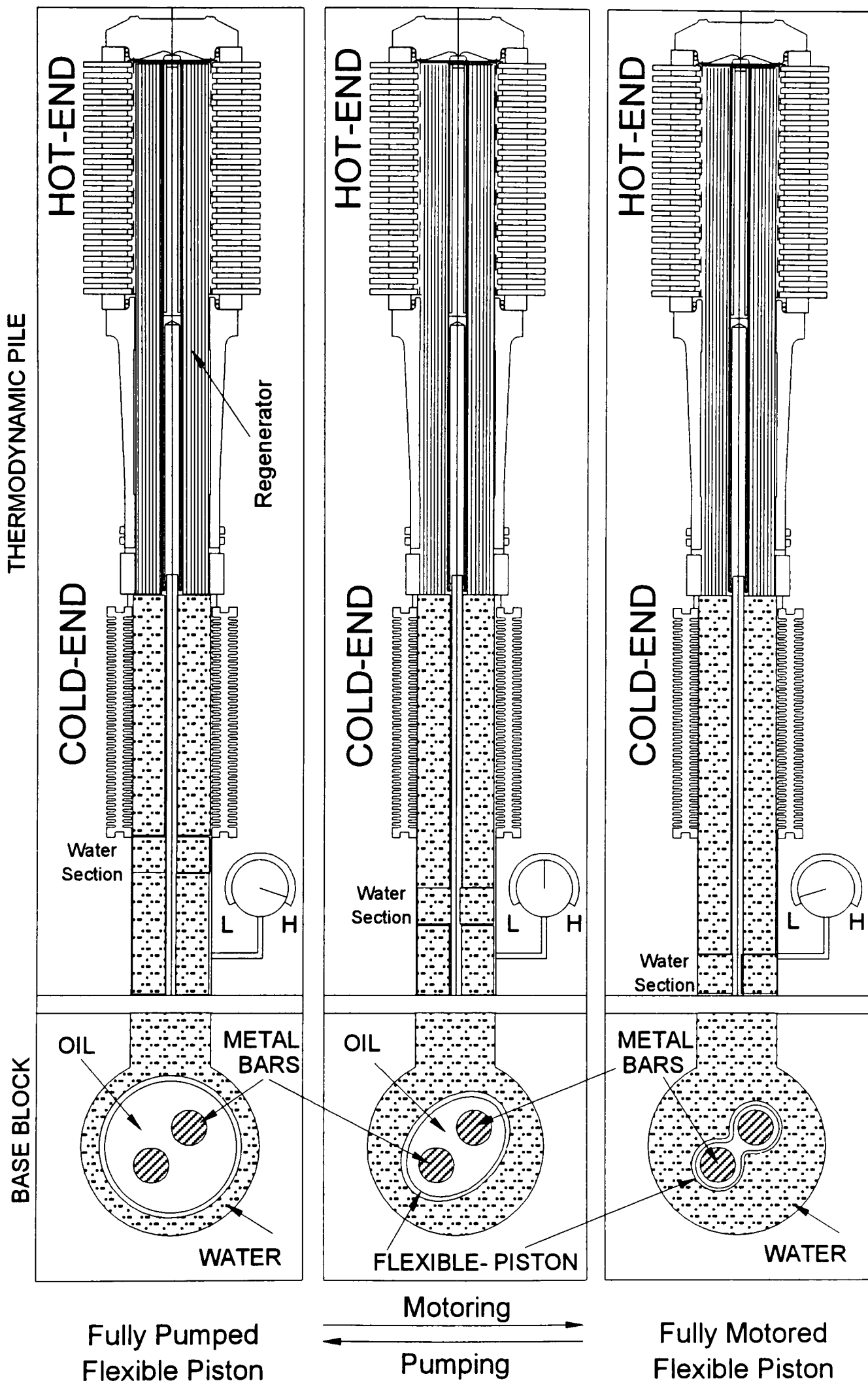


Figure 3.2 : Illustration of the pumping and motoring action of the flexible piston and the digital displacement hydraulic drive. As the oil is pumped inside the flexible tube inflates and the system pressure rises (like the pumping action of a piston, work is done on the fluid). The tube contracts as oil is motored out of the flexible tube and pressure falls as, work is done by the fluid.

Any desired flow-level (within the maximum capacity) can be attained by the pump-motor by changing the enabling rate of cylinders and fluid can be moved bi-directionally in and out of the flexible piston. Thus the TD pile volume can be varied following almost any arbitrary signal, to affect the thermodynamic cycle. This is illustrated in figure 3.2 as the flexible piston is inflated or contracted to fully pumped and fully motored states, while the regenerator does not move. The pressure gauge indicates the change of cycle pressure. The power stroke of the TD pile forces water out of cold-end of the working volume while the hydraulic drive unit is signalled to motor. During a pumping stroke the hydraulic unit is signalled to pump, returning water into the TD pile.

In summary the digital-displacement hydraulic drive gives three major advantages :

- The isolation of the working fluid from the hydraulic oil, almost entirely removes the sealing problem from the hot-end. Instead the sealing is transferred at the pump-motor, where the poppet valves (with proper choice of shape and material) provide excellent sealing of oil at a much lower temperature.
- In the hydraulic drive, working volume of a pump-motor cylinder is used many times per thermodynamic cycle. This allows generating almost any arbitrary piston motion (inflating or contracting), independent of the regenerator positions. Hence the two moving parts are free from the constraints of conventional sinusoidal motion and fixed phase difference. This gives much wider opportunity of achieving arbitrary piston motion profiles enabling the manipulation of the P-V diagrams to optimize the thermodynamic cycle.
- Use of the hydraulic drive eliminates conventional piston, connecting rod, crank shaft and the control mechanism.

3.4 Heat exchanger for recovering heat from exhaust gas

There is a fundamental difference between the exhaust heat from an internal combustion engine and that of a Stirling or Malone engine. The exhaust gas from the IC engine carries a major part of the heat rejected in the process of converting heat to work (the other major portion of the heat is rejected to the cooling water). On the other hand, in the case of the external combustion Stirling or Malone engine, the heat in the hot combustion gases leaving the hot-end does not get into the working fluid at all. The temperature of the combustion gases leaving the hot-end needs to be at a temperature sufficiently higher than the fins, to allow heat transfer into the hot-end. Hence a significant amount of heat remains in the outgoing combustion gases which is too precious to be discharged to the atmosphere.

In modern Stirling engines, much of this heat in the outgoing gases is recovered by warming the incoming air flow. This reduces the fuel requirement for raising the temperature of the combustion products and so improves the thermal efficiency. A simple contra-flow heat exchanger could be made by wrapping two layers of thin stainless steel shim (about 0.25 mm thick) in a spiral of several layers round the fin block and the burner assembly. Figure 3.3 shows the top view of such an arrangement. The double spiral provides the paths for a contra-flow heat exchanger with large surface area. Adjustable baffles may be used inside to control the flow distribution of gases on to the hot-end. The gaps between sheets can be maintained by using dimples or spacers. A trade-off exists between the blower power, space requirement and heat recovery. Hence the heat exchanger design needs to be optimised for - flow passage length, flow passage area and blower power requirement.

3.5 Control and ancillary drives

There are several control loops to be maintained for the operation of the Artemis-Malone engine, some of which are inter-related. The flame temperature is controlled by the proportion of air and fuel involved in the combustion. The flame temperature and the regenerator swirling speed control the fluid temperature inside the hot-end. The

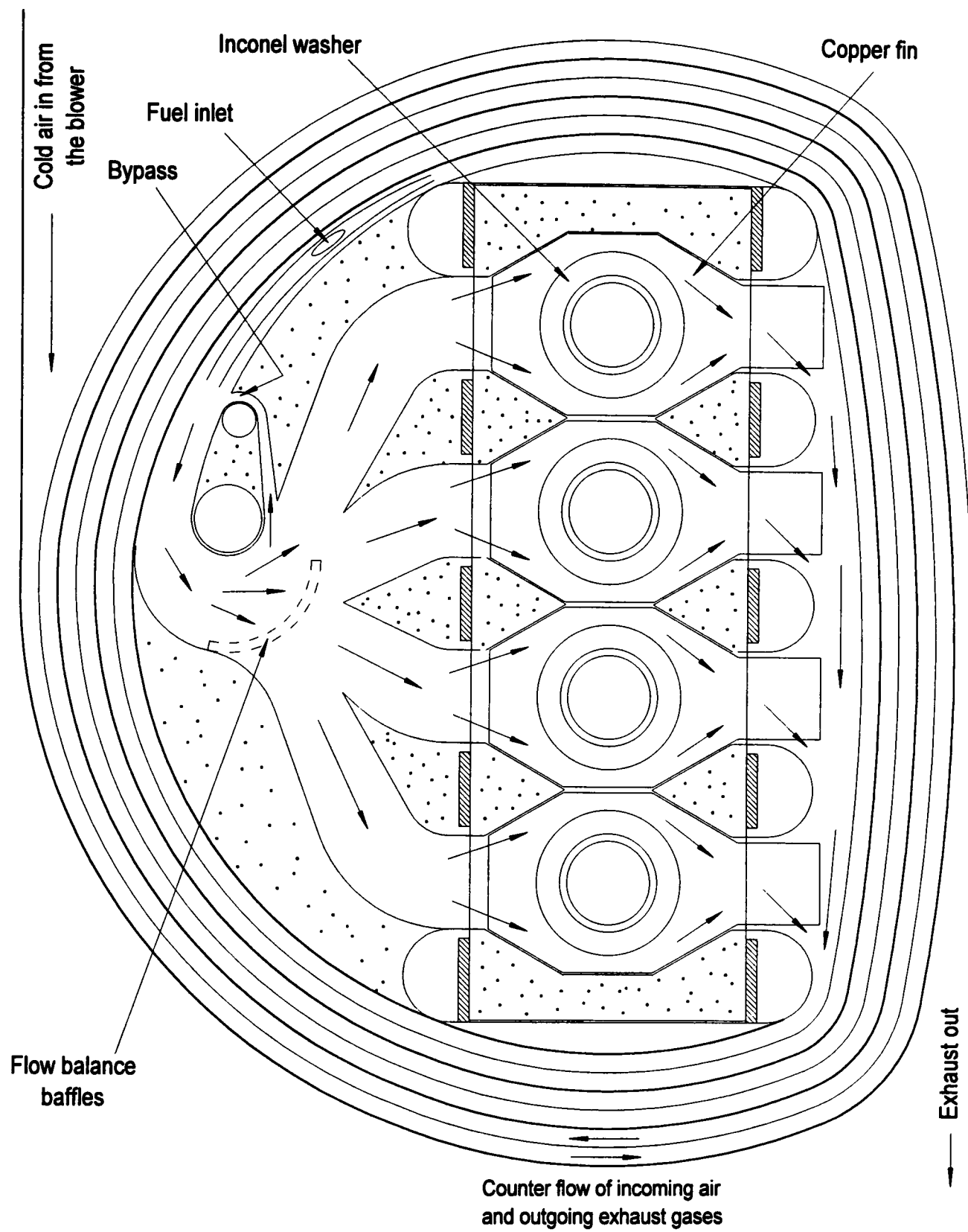


Figure 3.3 : Sectional view of the heat exchanger for recovering heat from the combustion gases leaving the hot-end, into the incoming air. The double spiral provides path for a counter flow heat-exchanger. This surrounds the burner section and the hot-ends of the TD piles.
Drawing : By S.H.Salter.

piston motion is generated by the oil flow controlled by the pump-motor. In most of the control loops a drive system is also involved. The objectives of the control loops may also vary under different circumstances in order to optimise power, efficiency or engine life. Electronic controls and processors are now advanced enough to cope with these requirements and can employ complex algorithms and rules for real-time control. The main control loops can be stated as :

- Burner fuel flow rate, which is proportional to the power demanded, is regulated by a control loop which responds to the hot-end metal temperatures. For pumping gaseous or liquid fuel, modern gas heating systems or fuel injection systems used in IC engines may be used. The fuel flow rate is controlled as the hot-end temperature sensors find the metal temperatures are either getting too high or too low. At different power levels (ie. fuel burning rates), the air flow rate needs to be adjusted to control the flame temperature and that of the hot-end metals downstream. The aim is to keep the hot-end metal temperatures at their highest safe limits, irrespective of the fuel burning rate. The proportion of air flow rate compared to fuel, can be varied using a look-up table for different heat flow rates. The air flow variation required also depends on the location at the hot-end (eg. outer fin edge, mid wall or hot-end steam) where a desired temperature-level is to be maintained (for different fuel burning rates) and the look-up table should be prepared accordingly. Thermocouple or other temperature sensing devices may be used to monitor the temperatures of different parts of the hot-end.
- The reciprocating motion of the regenerator is crucial to the control of the P-V diagram. Since the Artemis-Malone engine does not have a drive shaft, the frequency of the regenerator motion dictates the engine cycle frequency. The reciprocating motion of the regenerator is driven by a separate hydraulic drive which may use the cold-end water as the working fluid. A feed-back control loop ensures the regenerator is following the desired motion. The spinning of the regenerator about its axis, which provides enhanced heat transfer at the inner fin surfaces at both ends, is generated by water jets impinging tangentially on its surface. A small centrifugal pump may be fed water from the cold-end to

drive this system. The centrifugal pump speed could be varied to control the heat transfer at the steam-fin interface inside the hot-end.

- The pump-motor has its own controller to make decisions for enabling and disabling the cylinders, according to a demand, which ultimately creates the piston motion. Enabling can be made in both the pumping or motoring sense, according to the requirement. These decisions could be made to follow a desired piston motion, computed (on board) by monitoring the system pressure and the regenerator motion. Otherwise it could be following a pre-set sequence of cylinder enabling depending on the power demand, with the sequence changed to adapt to different power levels. The pump-motor shaft needs to be running at a speed much higher compared to the regenerator. This results in large number of cylinders being available during one regenerator cycle, allowing the required piston motion to be tailored. For the latter control approach the piston and regenerator motion cycles need to be synchronised for each regenerator cycle.
- The temperature at the cold-end can be controlled as the flow rate of the circulating water around it. Although the effect of controlling the cold-end temperature on the engine cycle, is relatively small (Reader and Barnes, 1988). A small centrifugal pump is used to circulate the water around the cold-end, which will give up its heat to the atmosphere through a radiator.
- A system is needed to drive an alternator, to charge up a battery which may deal with the electrical needs of various accessories. The alternator could be coupled to the pump-motor shaft. A pump-motor running at a fixed speed throughout the power range, would provide an excellent drive for efficient running of alternators, which present IC engines lack. Any power control strategy, which allows fixed pump-motor speed, would be preferred from this point.

3.6 The sequences of the engine cycle

The shape of an engine cycle diagram can be substantially altered by controlling the motion of the moving parts (ie. the regenerator and the piston). The motions are decided on a cycle-by-cycle basis, hence the moving parts only need to come to the same reference point at the end of each cycle. Figure 3.4 shows the motion sequences of a piston-assisted pressure rise and regenerator-assisted pressure fall cycle and the pressure-volume diagram generated.

The Malone cycle is a two stroke cycle. During the power stroke the regenerator moves from the hot-end to the cold-end and the piston is motored, transferring energy to the hydraulic oil. In the return stroke the regenerator returns back to the hot-end, but the piston goes through three different motion patterns and finally returns back to its cold-end reference at the end of the cycle. The cycle description starts from point 1, with the regenerator and the piston at their reference positions at hot-end and cold-end (as referred in figure 3.1). The system pressure is at the high-level and the flexible piston is fully inflated. Hot-end and cold-end fluid temperatures are intended to be maintained as constant throughout the cycle. The effect of inflating or contracting the flexible piston is illustrated by the equivalent movement of a water section. From 1 - 2 the regenerator moves towards the cold-end and the piston is also motored accordingly (ie. moved away from the cold-end reference) to maintain the high-pressure-level. At state 2 the regenerator ends its motion towards the cold-end and the flexible piston is fully motored, forming itself around the bars inside the manifold. During this process water from the cold-end passes through the regenerator, which heats it before it emerges into the hot-end. Heat also passes in through the hot-end which allows the fluid emerging from the regenerator to attain the hot-end temperature.

In the process 2 - 3, the regenerator starts moving back to towards hot-end. The piston remains stationary (ie. no oil is pumped in), allowing the cycle pressure to drop. This process is only continued until the cycle pressure reaches the desired lower level of cycle. From 3 - 4, as the regenerator finishes its return motion and moves back to its hot-end reference, the piston is pumped accordingly (ie. moved along with it towards

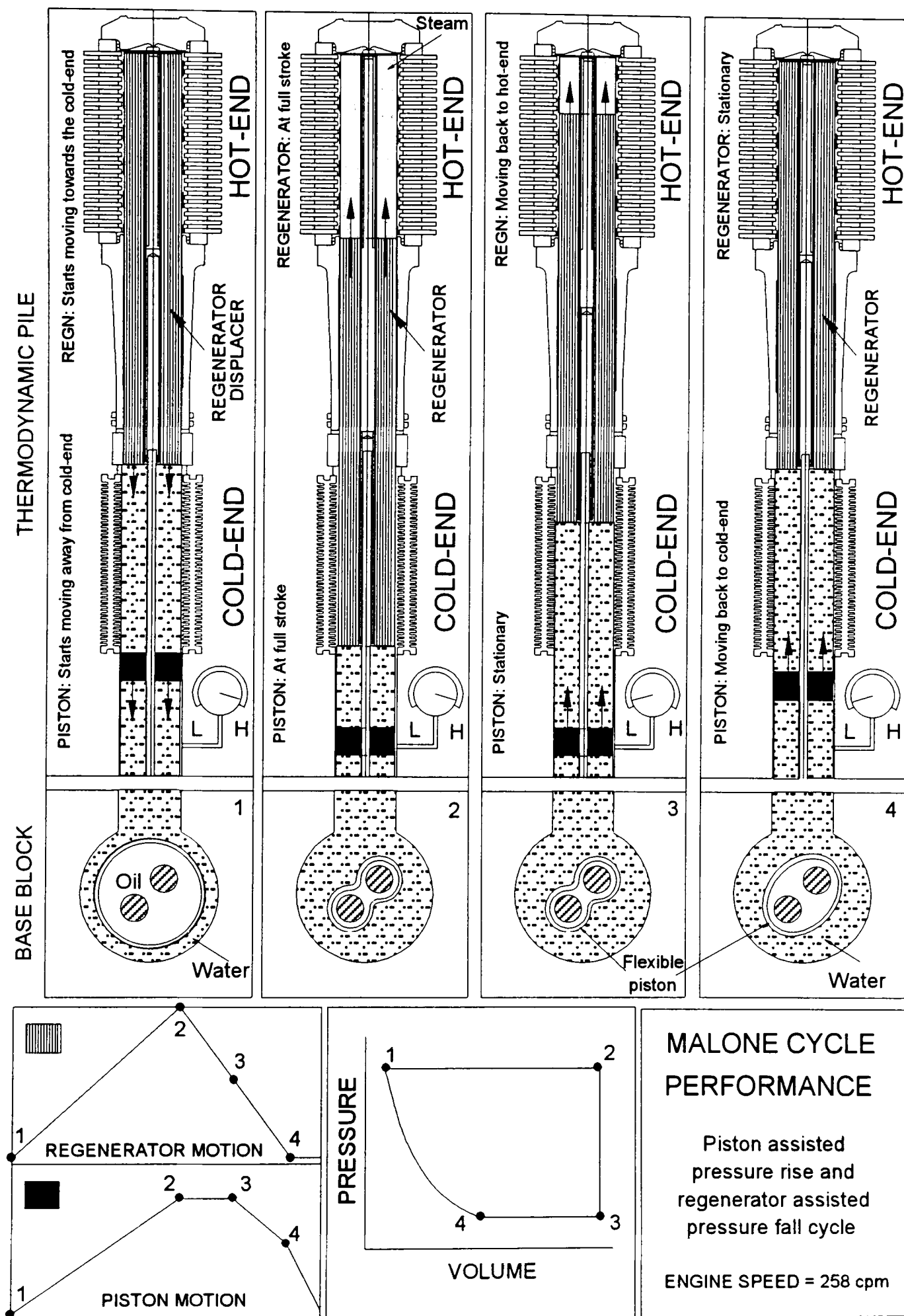


Figure 3.4 : Operating cycle and sequences of regenerator and flexible piston motions of the Artemis-Malone engine, for a piston assisted pressure rise and regenerator assisted pressure fall cycle.

the cold-end reference) to maintain the low-level-pressure. During the entire return stroke of the regenerator, fluid is moved from the hot-end through the regenerator, back to the cold-end. During this process the fluid is cooled down as heat is absorbed by the regenerator. From 3-4 the regenerator remains stationary, while the piston is inflated back to its original shape in order to restart the cycle. This raises the system pressure back to the high level. The work needed to compress the low pressure liquid to high pressure is much less compared to the work done by the working fluid in the power stroke, producing net useful power from the cycle.

CHAPTER - 4

Design of the Artemis-Malone Engine

4.1.1 Background

The preliminary static model of the Artemis-Malone engine was developed using mathematical software (Mathcad, 1995), by S.H. Salter. This has become a large document, which contains the many equations needed for designing different engine components and presents related results, based on a large number of engine parameters. The aim was to develop a fast-running PC based modelling tool for estimating performance of the engine. The model provided initial approximation of the engine cycle, allowing fast optimization of the main design parameters. For investigating further details of the cycle a time domain model would be needed. In the process of verifying this Mathcad model, some major changes were made. These changes were considered to be sufficiently important, to present these as a part of the thesis. The dimensions and engine parameters produced by the static model were used in the time domain modelling of the thermodynamic cycle of an engine module in the following chapters. The contents of this chapter are divided into three parts. The first part explains how the present Mathcad model works, the second discusses the major modifications introduced into the model and the third part shows some performance results of the Artemis-Malone engine.

4.1.2. Design procedure followed in the static-model

The design procedure starts with a set of desired engine parameters and group of numerical factors relating dimensions of different engine components including the heat-exchanger. In the Mathcad-model these are incorporated as given inputs which are active throughout the programme. The main parameters include the following :

- Heat flux passing through the hot-end
- Maximum allowable cycle pressure
- Maximum allowable metal stress
- Number of modules and the spacing between them
- Porosity of regenerator and a group of factors defining some of its motion limits
- Desired hot-end and cold-end fluid temperatures
- Chosen temperatures of hot-air exiting from and cooled-gas entering into the heat-exchanger.
- A group of numerical factors relating dimensions of different engine components and accessories.

In addition to these main input parameters, a large number of equations are provided for calculating further details of individual sections of the engine. Many of these successive calculations are interrelated and some of them cannot be correctly carried out without some of the down-stream values. For example - the temperature reached by the hot-end steam, as the heat flows through the composite metal wall depends on the total thermal impedance on the way, while the thermal impedance at the steam-inner fin interface depends on the steam temperature itself. These require iterative close-loop solutions for some of the design parameters.

In the modified model there are five such closed-loops, some of which are inter-dependent. A design solution is considered to be converging when the guessed or chosen values in all of the loops match their calculated ones. The numerical complexity of solving all these closed-loops simultaneously was avoided, using a human interface in the Mathcad model. The designer himself works as the iterative mechanism, for the closed-loop solution as he changes the different numerical factors until all the loop solutions converges. In addition to solving the closed-loops the design also needs to meet certain limit specifications eg. engine life, exhaust temperature etc. The design also needs to be optimised for maximum efficiency and the best possible power-to-weight ratio. This iterative process is made easier for the designer, by including a control panel at the end of the programme. This allows the user to easily modify engine parameters and numerical factors, as well as to monitor their effect on the design,

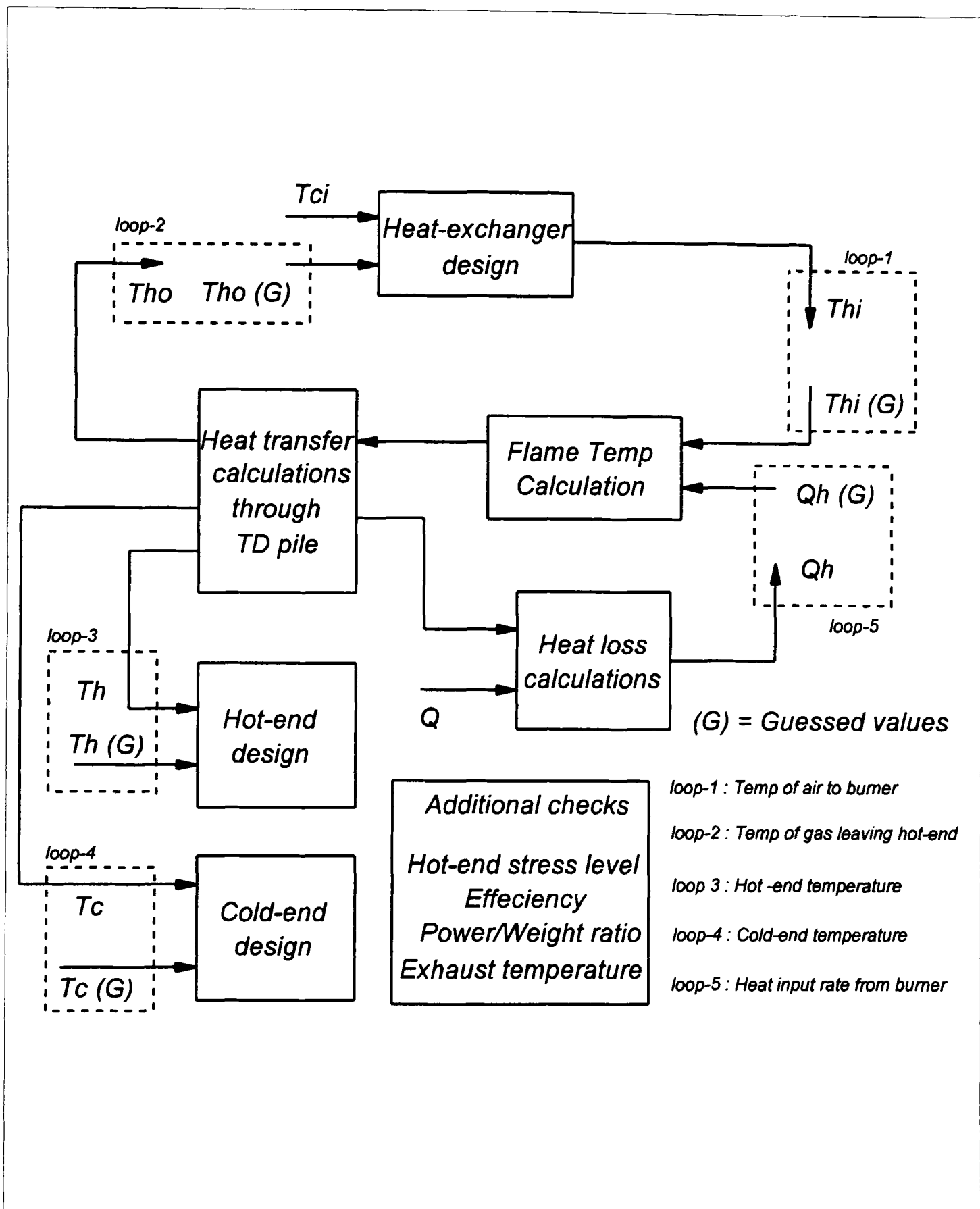


Figure 4.1 : Flow chart showing the interrelated closed-loops of the Mathcad model used for the design of the Artemis-Malone engine. In addition to solutions converging at all the close loops, a good design also takes into account - the stress level of Inconel at the hot-end, overall efficiency and power-to-weight ratio of the engine and exhaust temperature to atmosphere.

without going to the detailed level of the model. The final version of the Mathcad model is included in appendix A.

4.1.3 Brief discussion of the closed-loops

Figure 4.1 shows a flow chart of the closed-loops used in the Mathcad model and the main additional check-list. A short description of each of these closed-loops, some of which are interrelated, are given below (notations used are similar to those in the model given in appendix A) :

Loop-1 : Temperature of pre-heated air entering the burner

This loop involves the heat exchanger design. Downstream from the heat exchanger in the burner section, the hot gas temperature (T_F) is calculated as the fuel burns. This depends on the temperature of the incoming air out of the heat-exchanger and mass flow rate of air (which depends on whether excess air is used for cooling), as well as the rate of burning the fuel and the heating value of the fuel itself. The flue gas temperature is calculated on the basis of a guessed exit-air temperature from the heat exchanger (T_{hi}). The heat exchanger design parameters (eg. gap between plates, plate width, number of raps etc.) were altered to ensure that the air temperature coming out matched the guessed value. The heat-exchanger design is based on the temperature of inlet fresh-air (T_{ci}), and a guessed value for hot-gases leaving the hot-end flame-fins (T_{ho}). This guessed value of gases leaving the hot flame-finblock itself is solved in another loop.

Loop-2 : Temperature of gases leaving the hot-end

The second loop involves the hot-end design and heat transfer through it. A temperature was guessed for the gases leaving the hot-end for the heat-exchanger design (T_{ho}). Using heat balance equation this loop ensures that, after giving up the required heat at the hot-end, the temperature of the outgoing gases match the initial guess. This loop also checks that the temperature of the outgoing gases are comfortably higher than the hottest parts of the flame-fins (eg. leading edges), while the highest metal

temperature (T_{fo}) is within the operational limit of the fin material. A check is also made so that the temperature of exhaust gases, released to the atmosphere, is not too high.

Loop-3 : Temperature of hot-end steam

Under steady state condition the temperature drop across composite metal structure is equal to the product of the heat flow rate and the thermal resistance on its way. For a given flue gas temperature (T_f) and desired heat flow rate (Q) the thermal resistance of the hot-end metal structure determines the temperature of the fluid inside the hot-end (T_{st}). Figure 4.2 shows a schematic presentation of the temperature drop across the hot-end and the thermal resistances. The total thermal resistance on the way into the TD pile can be lumped into three major groups. These are :

- The flame-to-fin resistance on the outer fins, where the heat transfer is mainly convective (Z_{ff} Flame fin impedance).
- The thermal resistance of the composite wall of copper-Inconel, where heat is transferred by conduction (Z_{hw} Hot-wall impedance).
- The fin-to-steam resistance on the inner fins, for convective heat transfer (Z_{sf} Steam fin impedance).

The first and the third components are dependent on the fluid temperature and pressure, as well as the type of flow (eg. laminar or turbulent) and the geometry of the flow cross-section. So, even for a particular high-level of cycle pressure, an initial choice of the steam temperature (T_{st}) is needed to calculate the impedance of the steam-fin inside. In this third loop the hot-end design is manipulated (eg. by changing wall thickness and fin-density and dimensions) to make sure that the steam temperature inside the hot-end matches the initial guess. The hot-end steam temperature effects the Carnot efficiency of the engine very significantly.

For the hot-end design the radial stress distribution in the Inconel is also plotted against the temperature distribution in radial direction, to investigate the creep strength of the design. This curve is compared to rupture stress vs. temperature curves for Inconel 625 for different service lives. These curves were calculated by S.H. Salter from stress-

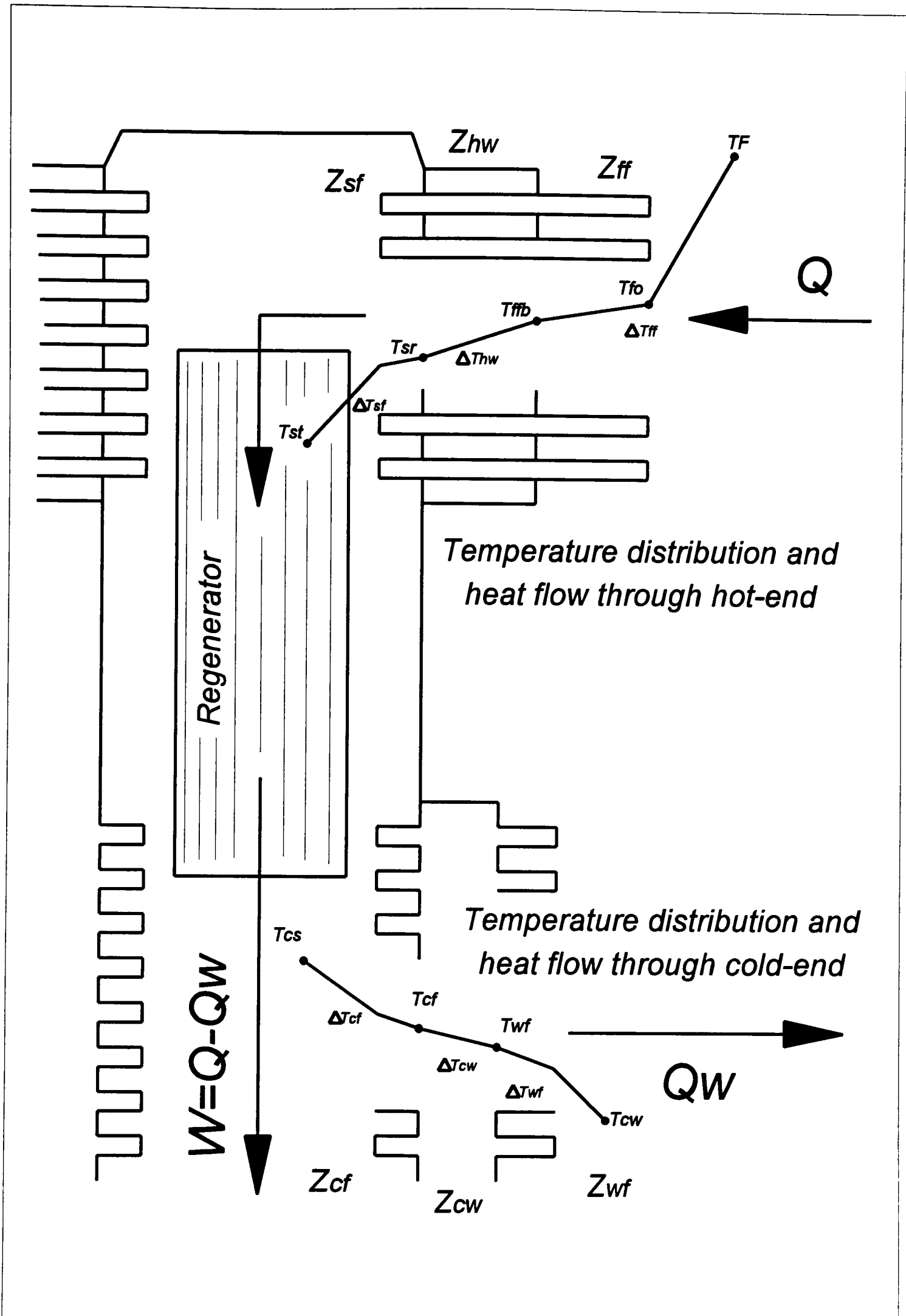


Figure 4.2 : Temperature drops across different components of thermal resistance as heat passes through the hot-end and the cold-end structure. Heat converted to work (W) is calculated from carnot efficiency and rest of the heat rejected to the sink is calculated as $Q_w = Q(1 - \eta_{th})$.

rupture life data for Inconel 625 (Inco Alloy International, 1985). In figure 4.3 the thick curve shows the radial stress distribution against the temperature (temperature increases radially outwards) and the dotted lines, the rupture stresses against temperature for different service lives. It is interesting to note that the solid curve shifts its position diagonally in the figure as the radial thickness of the Inconel stack is changed. With increased thickness the stress level comes down, but due to increased wall thermal resistance the temperature distribution is stretched, pushing the curve to the right. This curve gives an estimation of the operation life of the hot-end under creep.

Loop-4 : Temperature of cold-end water

For calculating the heat transfer through the cold-end, into the cooling water, again a chosen temperature for the cold-end water (T_{cs}) is needed. Figure 4.2 shows the temperature drops at major thermal impedances, as heat is rejected to through the cold-end. Similar to the hot-end the resistance to heat flow can be divided in to three parts:

- The water-to-fin resistance on the inner fins, where the heat transfer is mainly convective (Z_{cf} Condensing fin impedance).
- The thermal resistance of the copper wall, where heat is transferred by conduction (Z_{cw} Cold-wall impedance).
- The fin-to-cooling water resistance on the outer fins, for convective heat transfer (Z_{wf} Water fin impedance).

This loop ensures that the heat flow and the thermal impedances make the cold-end water temperature match the guessed value. The cold-end design is modified (eg. changing the fin dimensions, wall-thickness, fin density etc.) to achieve this. The heat passing through the cold-end (Q_w) is calculated from the heat flow into the hot-end and the theoretical Carnot efficiency (η_{th}), which is defined as :

$$\eta_{th} = \frac{(T_{st} - T_{cs})}{T_{st}}$$

T_{st} = Temperature of hot-end steam.

T_{cs} = Temperature of condensing steam.

Final efficiency (η_f) is calculated as :

$$\eta_f = \frac{(\text{Power output from thermo dynamic cycle} - \text{losses in different ancillary drives})}{(\text{Total heat input rate})}$$

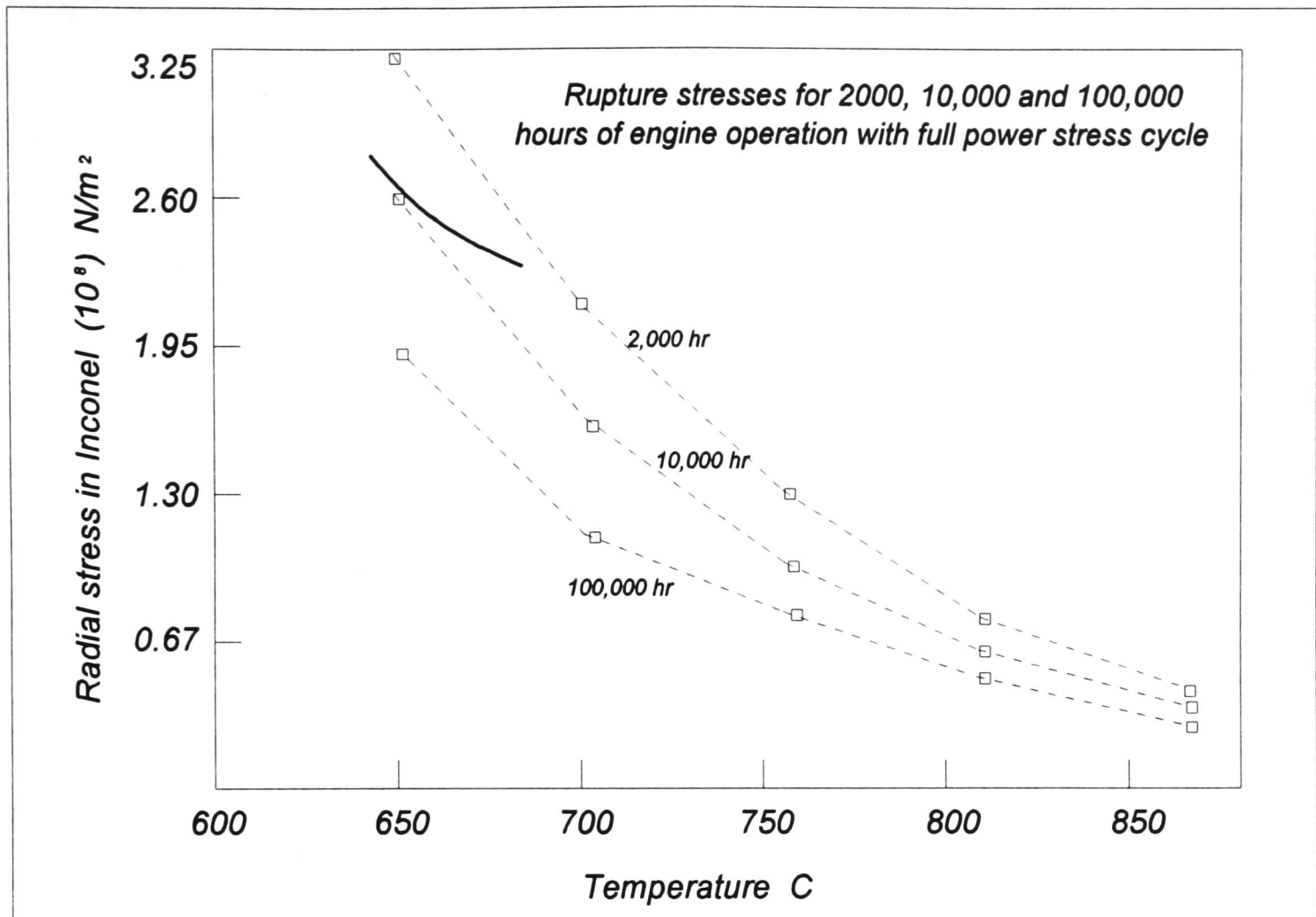


Figure 4.3 : Temperature distribution against maximum normal stress along the radial thickness of the Inconel disks and comparative values with data for 2000, 10,000 and 100,000 hour rupture life for Inconel 625.

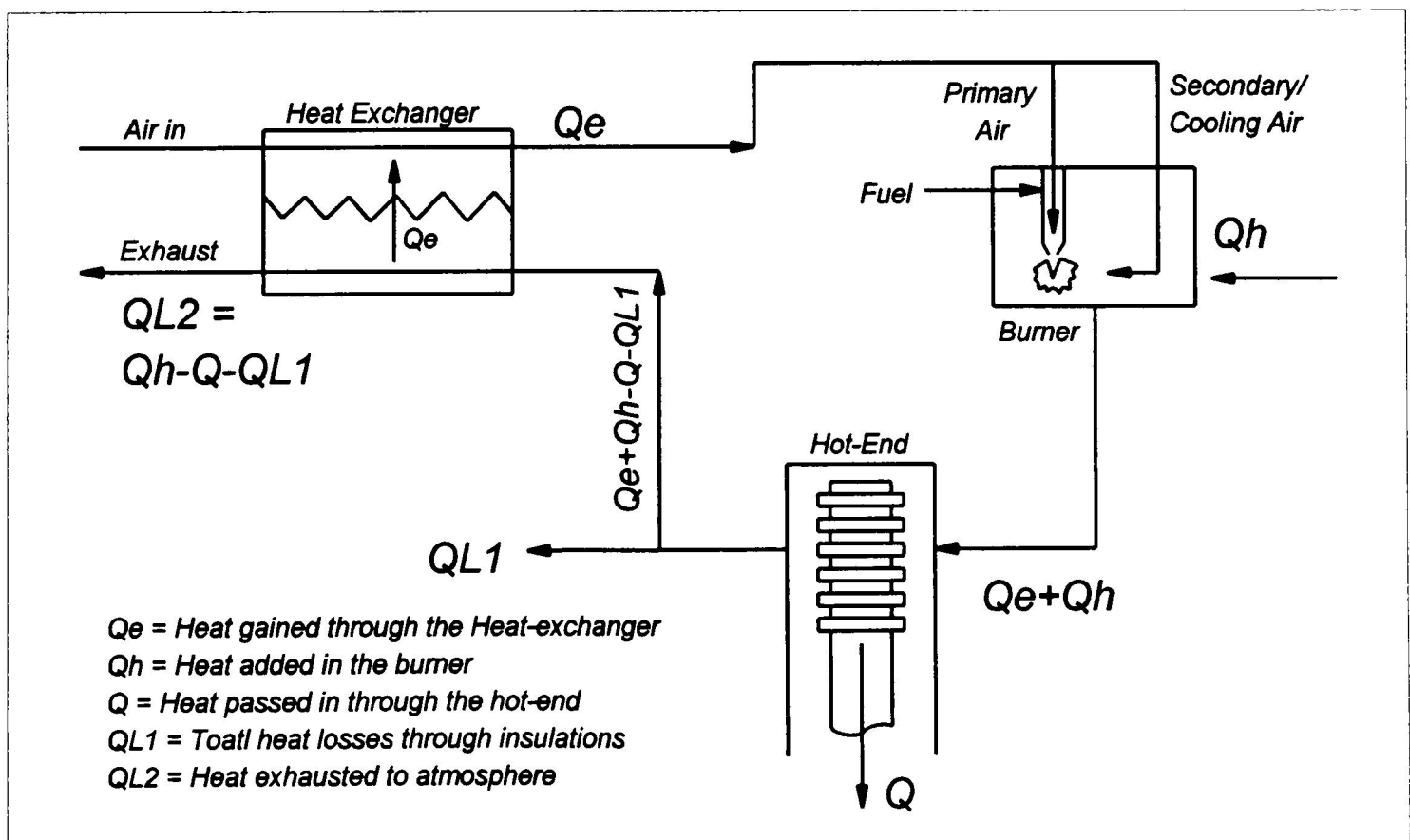


Figure 4.4 : Under steady state heat flow the total heat added in the burner equals the heat passed through the hot-end and various heat losses. The heat-exchanger recirculates some heat within the system.

Loop-5 : Total heat input to the system

The total heat input needed for running the engine at a desired level is ultimately supplied by the combustion of fuel in the burner. This loop calculates the various heat losses, as well as heat passing into the hot-end and sums up them to give the total required fuel consumption. Figure 4.4 shows a schematic presentation of the heat flows across the system. The incoming air (which is in excess of the stoichiometric ratio required for the fuel) gains heat through the heat-exchanger (Q_e) and as a result, this heat is recirculated within the system. Part of the pre-heated air is sent into the burner for burning the fuel, while the other part bypasses it to provide secondary air to bring down the flame temperature. The need for secondary air is explained in more detail later. Under steady state, the heat input required from the burner (Q_h) equals the sum of the heat flux passing through the hot-end (Q), heat in the exhausting gases (QL_2) and heat losses to the surrounding through the insulation (QL_1).

4.1.4 Major equations used in the Mathcad model

The major equations used for modelling the Artemis-Malone engine are shown below. These are grouped according to the engine component they represent or similarity of functions. Similar denotations are used as in the Mathcad model.

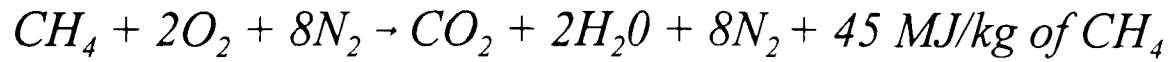
Burner section :

The required fuel flow rate is calculated as :

$$Mm = \frac{Q_h}{HV} = \frac{Q \cdot LF}{HV}$$

Where, Mm = Mass flow-rate of fuel per module.
 Q_h = Heat generation rate per module as the fuel burns in the burner.
 Q = Desired heat flux through each module.
 LF = Heat loss factor, takes account of heat flows other than that through the TD pile.
 HV = Heating value of fuel (lower value used).

The combustion equation (with natural gas as fuel) in the burner can be presented as :



The mass flow rate of gas (air and fuel) per module was calculated from the ratio of the molecular weights

$$MG = Mm \frac{(16+(2 \times 32+8 \times 28)) \cdot AR}{16}$$

where, $AR =$ Air-ratio, defines proportion of excess air-flow, used to reduce flame temperature.

Temperature of the flame can be defined as :

$$T_{Fl} = T_{ih} + \frac{Mm \cdot HV}{MG \cdot C_g} \quad \text{Average flame temperature}$$

$$T_F = (T_{Fl} + T_{oh})/2$$

where, $C_g =$ Average specific heat of the gas.

$T_{oh} =$ Temperature of gases leaving the hot-end

Heat exchanger :

The heat transfer rate across a heat-exchanger can be expressed as :

$$q = \varepsilon \cdot C_{min} (T_{oh} - T_{ic})$$

where,

$$C_{min} = MG \cdot NM \cdot C_g$$

$T_{ic} =$ Temperature of cold air entering the heat -exchanger.

$NM =$ Number of modules (TD pile) in the engine.

$\varepsilon =$ Effectiveness of the heat-exchanger, which is the ratio of actual and the maximum possible heat transfer across it.

The effectiveness (ε) of the heat-exchanger is widely defined (Incropera et al. 1990) with the non-dimensional parameter NTU (number of transfer units). For a concentric tube counter-flow heat-exchanger ε relates as,

$$\varepsilon = \frac{1 - \exp[-NTU(1 - C_r)]}{1 - C_r \cdot \exp[-NTU(1 - C_r)]} \quad C_r = \text{Ratio of the heat capacity (mass flow rate times specific heat) rates of the hot and the cold fluid.}$$

The temperature of pre-heated air coming out and hot-gases entering the heat-exchanger are chosen initially. Their values are recalculated to ensure the closed loops are satisfied.

$$T_{ih} = T_{ic} + \frac{q}{MG.NM.C_g}$$

$$T_{oh} = T_{F1} - \frac{Q}{MG.C_g}$$

$$\text{and } T_{oc} = T_{ic} + \frac{Wha}{MG.NM.C_g}$$

where, $Wha = (1-\epsilon).C_{min}.(T_{oh} - T_{io}) = \text{heat lost with the exhaust gases.}$

$Q = \text{Heat flux passing through each module (TD pile).}$

$T_{oc} = \text{Temperature of exhaust gases to atmosphere.}$

The pressure drop (ΔP_{ex}) for blowing the air across the heat-exchanger is :

$$\Delta P_{ex} = \left(\frac{4.f_c.\rho.V_{ex}^2.Lex}{D_{hmex}.2} \right)$$

$$\text{where } f_c = \left(4.\log \frac{Rnoex}{(4.53.\log(Rnoex) - 3.82)} \right)^{-2}$$

$f_c = \text{Friction coefficient for flow in a non-circular passage.}$

$V_{ex} = \text{Average gas velocity in the heat-exchanger passage.}$

$Rnoex = \text{Average Reynolds number in the passage.}$

$D_{hmex} = \text{Hydraulic diameter of the flow-section in the heat-exchanger.}$

A simplistic noise prediction calculation (Goodwall, 1980) was based on the assumption that gases blowing through the heat-exchanger is the primary source of noise. The predicted noise level in decibel (dB) was calculated as :

$$dB = 60.\log(Vex) + 20.\log(dex) + 20.\log\left(\frac{Toc+273}{Tic+273}\right) - 4$$

where, $Tic = \text{Temperature of cold air entering the heat-exchanger.}$

$dex = \text{Equivalent diameter of the exhaust flow area at outlet.}$

The hot-end :

The heat transfer through the hot-end is modelled as a series of thermal impedances and temperature drops as explained in the hot-end temperature loop and illustrated in figure 4.2. The total thermal resistance in the hot-end can be expressed as :

$$Z_{hot-end} = Z_{ff} + Z_{hw} + Z_{sf}$$

Thermal resistance at both the flame-fin and the steam-fin interface depends on the velocity and properties of fluid, geometry of the flow path, fin area and efficiency of the fins. For both the flame-fin (outer) and steam-fin (inner) the thermal impedance can be formulated in the same way. For the flame fins :

$$Z_{ff} = \frac{1}{A_{ff} \cdot H_{ff} \cdot \eta_{ff}} \quad \text{and} \quad Q = A_{ff} \cdot H_{ff} \cdot \eta_{ff} \cdot \Delta T_{ff}$$

Where, A_{ff} = Surface area of the flame-fins.

H_{ff} = Convective heat transfer coefficient.

η_{ff} = Fin-efficiency of flame-fins.

ΔT_{ff} = Temperature drop from the flame to fin-root.

Fin area is calculated from the dimensions and number of the fins etc. The efficiency is calculated from the simplified equation for active tip fins :

$$\eta_{ff} = \frac{\tanh \left[\sqrt{\frac{2 \cdot H_{ff}}{\lambda \cdot nf \cdot t_{cu}}} \cdot \left(L_{ff} + \frac{t_{cu} \cdot nf}{2} \right) \right]}{\sqrt{\frac{2 \cdot H_{ff}}{\lambda \cdot nf \cdot t_{cu}}} \cdot \left(L_{ff} + \frac{t_{cu} \cdot nf}{2} \right)}$$

where, λ = Thermal conductivity of the fin-material (eg. copper).

nf = No. of adjacent fins joined together (valid only for flame fins).

L_{ff} = Radial length of flame-fins.

t_{cu} = Thickness of copper disks.

The fin-base (T_{ffb}) and fin-tip (T_{ffo}) temperatures for the flame-fin is calculated as :

$$T_{ffb} = T_F - Q.Z_{ff}$$

$$T_{ffo} = T_F - (T_F - T_{ffb}) \cdot \left[\frac{1}{\cosh(m.L_{ff})} + \frac{H_{tff}}{m.\lambda} \cdot \sinh.m.L_{ff} \right]$$

The convective heat transfer coefficient was calculated from empirical equations depending on laminar or turbulent flows. For laminar flows, eg. for the flame-fins :

$$H_{tff} = \frac{C.ka}{D_{hmf}}$$

where, $ka =$ Thermal conductivity of the fluid.

$D_{hmf} =$ Hydraulic mean diameter of the gap between the fins.

$C =$ This is a constant, the value of which depends on the aspect ratio of the area of the flow section (see appendix E for detail).

For turbulent flow (eg. at the steam-fin interface) it can be calculated from Nusselt number (Nsu) as :

$$H_{tff} = \frac{Nsu.ka}{D_{hmf}} \quad \text{and} \quad Nus = 0.023.Rnos^{0.8}.Pr^{0.333}$$

Using Gnielinski's equation gives more accurate values for Nusselt numbers

$$Nsu = \frac{(f/8)(Rnos - 1000).Pr}{1 + 12.7(f/8)^{0.5}(Pr^{0.666} - 1)}$$

where, $f =$ friction factor.

and $Pr = (\mu.C_p/k) =$ Prandlt number of the fluid.

Heat transfer coefficients for the fins were calculated in a similar way. Both the steam-fins at the hot-end and the condensing-fins at the cold-end actually only transfer significant amounts of heat during a fraction of the cycle. The average heat transfer coefficient values are calculated as :

For the steam fins inside hot-end, $H_{tfs} = H_{tfs} \cdot ftRhc$

For condensing fins inside cold-end, $H_{tfc} = H_{tfc} \cdot (1 - ftRhc)$

where, $ftRhc =$ Fraction of the cycle for which the regenerator moves from the hot-end to the cold-end.

The central wall section of the hot-end, which is a composite structure of copper and Inconel disks was modelled as two thermal impedances working in parallel

$$Z_{w_{cu}} = \frac{\ln\left(\frac{D_{io}}{D_{ii}}\right)}{2 \cdot \pi \cdot \lambda_{cu} \cdot N_{ff} \cdot t_{cu}} \quad Z_{w_{inc}} = \frac{\ln\left(\frac{D_{io}}{D_{ii}}\right)}{2 \cdot \pi \cdot \lambda_{inc} \cdot N_{ff} \cdot t_{inc}}$$

where, $D_{io} =$ Outer diameter of Inconel disks.

$D_{ii} =$ Inner diameter of Inconel disks.

$N_{ff} =$ Number of flame fins.

The total thermal resistance of the parallel combination making up the hot wall is :

$$Z_{hw} = \frac{1}{\left(\frac{1}{Z_{w_{cu}}} + \frac{1}{Z_{w_{inc}}}\right)}$$

For steady state, thermal resistance and temperature drops are related as below, similar relations are true for the cold-end as well.

$$Q = \frac{\Delta T_{hot-end}}{Z_{hot-end}} = \frac{\Delta T_{ff}}{Z_{ff}} = \frac{\Delta T_{hw}}{Z_{hw}} = \frac{\Delta T_{sf}}{Z_{sf}}$$

The mid-section temperature of the composite wall (T_{mw}) is calculated as the average of the fin-base temperatures of the flame-fins and the steam-fins.

The stress in the hot-end structure due to internal fluid pressure is mainly resisted by the Inconel disks. The force acting on the copper disks are considered to be transferred to the Inconel disks through the copper-Inconel brazing interfaces. The normal stresses

in the Inconel ring, at a radius r , in radial (σ_r) and tangential (σ_t) direction can be expressed as :

$$\sigma_r = PH \cdot \frac{\frac{t_{inc} + t_{cu}}{4} \cdot \frac{D_{ii}^2}{4} \left[\frac{D_{io}^2}{r^2} \right]}{\frac{D_{io}^2}{4} - \frac{D_{ii}^2}{4}} \cdot \left[1 - \frac{D_{io}^2}{r^2} \right] \quad \sigma_t = PH \cdot \frac{\frac{t_{inc} + t_{cu}}{4} \cdot \frac{D_{ii}^2}{4} \left[\frac{D_{io}^2}{4} \right]}{\frac{D_{io}^2}{4} - \frac{D_{ii}^2}{4}} \cdot \left[1 + \frac{D_{io}^2}{r^2} \right]$$

where, $PH =$ High-level of fluid pressure in the TD pile.
 D_{ii} and $D_{io} =$ Inner and outer diameter of the Inconel disk.
 t_{cu} and $t_{inc} =$ Thickness of Inconel and copper disk.

The stresses vary across the radial length and are generally higher at the inner edge, though opposing in nature. The tangential stress was higher compared to the radial one and needed to be lower than the allowable stress level for Inconel.

The shear stress at the copper-Inconel brazes interface can be calculated as :

$$\sigma_s = \frac{PH \cdot \pi \cdot D_{ii} \cdot t_{cu}}{\frac{\pi}{4} \cdot (D_{io}^2 - D_{ii}^2) \cdot 2}$$

The stress level from shear strain due to pressure force or differential thermal expansion of copper and Inconel was found to be much smaller, as compared to the tensile stress.

The hot-wall temperature distribution at any radius (r) along the radial length was found as :

$$T_r = T_{ffb} + \Delta T_{hw} \frac{\ln\left(\frac{2 \cdot r}{D_{io}}\right)}{\ln\left(\frac{D_{io}}{D_{ii}}\right)}$$

The stress and temperature distribution across the hot-wall radius were combined to plot stress distribution across the temperature range of the composite hot-wall. This curve

was compared with calculated stress vs. temperature curve of Inconel 625 for different rupture lives, to estimate the life of the hot-end design.

The pressure drop in the combustion gases through the fin block (ΔP_p) can be calculated as :

$$\Delta P_p = \frac{VGC}{\left(\frac{N_{ff}}{nf}\right)} \cdot \frac{12 \cdot \mu_g \cdot D_f}{\left(D_f - \frac{D_{io}}{2}\right) \cdot (t_{inc} \cdot nf)^3}$$

where, $VGC =$ Volume flow rate of gases passing across the flame-fins.

$D_f =$ Outer diameter of flame fins.

$\mu_g =$ Viscosity of the gas.

The total pumping power needed to blow the gases across the flame-fin blocks and two way trip through the heat exchanger can be summed as :

$$P_{expu} = (2 \cdot V_{cld} \cdot \Delta P_{ex} + VGC \cdot \Delta P_p) \cdot NM$$

where, $V_{cld} =$ Volume flow rate of air at the cold air inlet.

$VGC =$ Volume flow rate of gas through the copper flame fin section.

Regenerator :

The regenerator moves between the hot-end and the cold-ends each held at different temperature levels. The fluid temperature and, hence, properties vary across the length of the regenerator. A linear temperature gradient of the fluid is assumed in the regenerator. For modelling, the regenerator length is split into a number of segments (NLR) of equal lengths. The average temperature (TL) of each is calculated as :

$$\text{For } i=1 \dots NLR \quad TL_i = TC + \frac{i-0.5}{NLR} \cdot (TH - TC)$$

where, TH and TC are the choice of hot-end and cold-end fluid temperatures.

The motion of the regenerator is limited by the following parameters :

Lfb = Length of flame-fin block = Regenerator stroke.

$ftRm$ = Fraction of cycle time the regenerator is moving in either direction.

$ftRhc$ = Fraction of cycle-time the regenerator is moving from hot-end to the cold-end.

Fluid passes through the regenerator as it moves between the hot and cold-ends. The mass flow rate of fluid passing through the regenerator are considered to be equal in all the segments, although the mass flow rates at which fluid passes through the regenerator may be different during the two directions of its motion (depending on $ftRhc$).

The pressure drop based on laminar flow, across the i th segment or layer (ΔPhc_i) as the regenerator moves from the hot-end to the cold-end is calculated as following :

$$\Delta Phc_i = \frac{\dot{q}_i \cdot 12 \cdot \mu_i \cdot LL}{LuwR \cdot tRg^3}$$

where, q_i = Volume flow rate of fluid in the segment (depends on temperature).

μ_i = Viscosity of the liquid in the segment (depends on temperature).

LL = Length of each segment.

$LuwR$ = Unwrapped length of the regenerator shim.

tRg = Gap between wrapping layers of the shim.

The drive force for moving from the hot to cold-side is $FRhc = \sum \Delta Phc \cdot (A_{ro} + A_{rb})$

A_{ro} and A_{rb} are the open and blocked areas of the regenerator section. The force acting on the other direction of motion (ie. cold-to-hot) $FRch$ was calculated in a similar way.

The regenerator drive power for the whole engine is,

$$PowRhc = FRhc \cdot \frac{Lfb}{tRhc} \cdot NM \quad PowRch = FRch \cdot \frac{Lfb}{tRch} \cdot NM$$

The mean regenerator drive power :

$$PowRM = \frac{PowRhc \cdot ftRm \cdot ftRhc + PowRch \cdot ftRm \cdot (1 - ftRhc)}{2}$$

where, $PowRhc$ = Power requirement to drive the regenerator from hot to cold-end.

$PowRch$ = Power requirement to drive the regenerator from cold to hot-end.

$tRhc$ and $tRch$ are time required for regenerator motion between two ends.

The amount of heat recirculated by the regenerator between successive cycles and the corresponding temperature change in metallic mass of the regenerator is estimated as:

$$\Delta E = (Enw_H - Enw_C) \cdot \Delta MH$$

$$\text{and } \Delta TR = \frac{\Delta E}{MR \cdot C_{Regn}}$$

where, ΔE = Change of internal energy stored in regenerator metal, per stroke.

Enw_H = Internal energy of hot-end steam, per unit mass.

Enw_C = Internal energy of cold-end water, per unit mass.

ΔMH = Increase in fluid mass at hot-end.

ΔTR = Cyclic temperature variation of regenerator (assuming uniform distribution).

MR = Mass of regenerator metal.

C_{Regn} = Specific heat of regenerator metal.

The power required to spin the regenerator can be calculated from the shear torque (τ) and the spinning speed (ω). Calculations are similar for both-ends, with fluid density varying mainly. Mean power to rotate the regenerator (swirling loss) at the cold-end :

$$PowsWC = (\tau \cdot \omega/2) \cdot NM$$

$$\text{and } \tau = \{(\rho/2) \cdot V_{sew}^2 \cdot A_{cf} \cdot f_{ccw} \cdot (D/2)\}$$

V_{sew} = Swirling velocity near the fins.

A_{cf} = Surface area of the condensing fins.

D = Bore of the TD pile.

f_{ccw} = Estimated friction coefficient at the condensing fins.

Cycle calculations and efficiencies

The Carnot efficiency (η_{th}) is based on the hot-end and cold-end fluid temperatures. It should be noted when all the closed-loops agree, $TH = T_{st}$ and $TC = T_{cs}$.

$$\eta_{th} = \frac{TH - TC}{TH + 273}$$

Heat rejected to the cooling water sink at the cold-end $Q_w = Q(1 - \eta_{th})$

The volume flow rate of water needed through the cooling jacket around the cold-end is:

$$VW = \frac{Q_w \cdot NM}{(T_{wf} - T_{cw}) \cdot 4184 \cdot 1000}$$

where, T_{cw} and T_{wf} = Temperatures of cooling water at inlet and exit.

The power required to circulate the water, $Powc = VW \cdot (\Sigma \Delta Ph)$

where, $\Sigma \Delta Ph$ = Summation of pressure drops in the water jacket and piping.

The indicated power (without ancillary losses taken in to account) of the engine is :

$$Pow = \eta_{th} \cdot Q \cdot NM$$

Work done each cycle can be found by summing the positive (motoring) and negative (pumping) work. Work done by one thermal module in one stroke

$$W1 = VI2 \cdot PH \quad \text{where, } VI2 = (\Delta MC - \Delta MH) / \rho_{chp}$$

ΔMC = Decrease in fluid mass at cold-end.

ΔMH = Increase in fluid mass at hot-end.

ρ_{chp} = Density of cold-end fluid at high pressure.

$VI2$ = Flow out to the isolator (flexible piston).

Work on the fluid to raise the pressure in the pumping stroke (assuming linear pressure-rise),

$$W2 = VC3 \cdot (PH + PL) / 2 \quad \text{where, } VC3 = (\Delta M_{hot-end} + \Delta M_{Regenerator}) / \rho_{clp}$$

where, $\Delta M_{hot-end}$ = Increase dead-space fluid mass is hot-end, as the pressure is raised.

$\Delta M_{Regenerator}$ = Increase in regenerator fluid-mass as the pressure is raised.

PH and PL = High and low-levels of pressure for the cycle.

VC3 = Volume of extra mass needed to be pumped into the regenerator and hot-end dead space to raise the pressure level from PL to PH.

Net work from one cycle of the whole engine, $W_{eng} = (W1 - W2).NM$

The engine speed (rpm) needed to produce the calculated indicated power output is :

$$Engrpm = (Pow.60)/W_{eng}$$

Final thermal efficiency is calculated as :

$$\eta_f = \frac{Pow - Powl}{(Q.NM + QW)}$$

where, $Pow - Powl = Pow_{act} = \text{Actual power output from the engine.}$

$Powl = \text{Summation of all ancillary drive losses.}$

$$= Pow_{RM} + P_{expu} + Pow_{swH} + Pow_{swC} + Pow_c$$

$QW = \text{Heat loss with exhaust + estimation of loss to surroundings.}$

4.2 Changes made to the initial Mathcad model

The major changes made to Salter's Mathcad model can be grouped under four headings, some details of them are discussed below.

- (a) Re-designing the flame fins.
- (b) Introduction of secondary or cooling air.
- (c) Total heat balance.
- (d) Radial stress calculation of the Inconel disks.

(a) Re-designing of the flame-fins :

In the original design the flame fins, ie. the fins on the outer-side of the hot-end, were found to be too densely spaced (eg. 103 fins in a length of 116 mm, 55 kW design). This gave rise to two problems - the pumping power requirement to force the air flow through the closely spaced flame fins was a considerable fraction of the output (about 6%). The other problem was the flame to external flame fin impedance was very small

compared to the other components of total impedance. This resulted in only a small temperature drop in the interface as the heat passed through it, which caused the flame fin temperature to be higher than the safe limit (for copper fins 750°C was considered to be safe) which would lead to a melt down of the flame-fins. It was realised that the flame-fin design needed reconsidering. The impedance of the flame-fin interface (Z_{ff}) and the heat flow rate (Q) was defined as :

$$Z_{ff} = \frac{1}{A_{ff} \cdot H_{ff} \cdot \eta_{ff}} \quad \text{and} \quad Q = A_{ff} \cdot H_{ff} \cdot \eta_{ff} \cdot \Delta T_{ff}$$

Where,
 A_{ff} = Surface area of the flame-fins
 H_{ff} = Convective heat transfer coefficient
 η_{ff} = Fin-efficiency of flame-fins
 ΔT_{ff} = Temperature drop from the flame to fin-root

Hence the same heat flow can be maintained with different composition of :- fin surface area, convective heat transfer coefficient, fin-efficiency and temperature of the flame. Careful consideration will reveal that these factors are interrelated and variations are limited to a great extent by the hot-end design requirement.

As copper is used as the fin material (for its high conductivity and fast response to thermal changes) the fin efficiency does not vary much until the fins get very long radially. This is not be desirable in terms of the space requirement of the engine. Temperature of the flame coming out of the burner, depends little on the hot-end design. The only controllable parameters are the surface area and the heat transfer coefficient. Hence it is desired to have a smaller area and/or lower heat transfer coefficient to produce a large temperature drop across the flame-fin interface. The extent to which both of these parameters can be varied, is also limited by the structure. The ratio between highly conductive copper and far less conductive (about 25:1 ratio) Inconel needed to be maintained to have low thermal resistance through the composite hot-wall. The thickness of the copper fins could not be increased as this would increase the stress in copper. Increasing the mean diameter of the composite wall to reduce flame-fin area is also not helpful, as for a desired module height or displacement volume this would reduce the length to diameter aspect ratio, which affects heat transfer undesirably by increasing conduction losses (Walker, 1980). The surface area of the flame-fins could

be reduced by decreasing the fin outer diameter. This is also helpful in terms of surface heat transfer coefficient as its value decreases with reduced aspect ratio of the flow area (Incropera et al. 1990) as shown in figure 4.5. This is only true as long as the flow in the fin channels remain laminar, which was the case initially. As the flow area decreases the flow become turbulent, causing the heat transfer coefficient to rise. Hence area reduction with reduced fin-outer diameter only increases the thermal impedance until the flow becomes turbulent. Area reduction of the fin can also be achieved by brazing or stamping two or more fins together. Combining more than two adjacent fins could give rise to contact resistance problems and might be more complicated in production. Area reduction also has the advantage of reduced length/width aspect ratio (as the gap between fins are doubled with joining of two fins), which also reduces heat transfer coefficient. The concept of combining adjacent fins and its effect on convective heat transfer coefficient is shown in figure 4.5. Area reduction by stamping and reducing outer fin diameter was tested together to enhance the thermal impedance. Unfortunately the two techniques did not bring the desired reduction of fin surface area and convective heat transfer coefficient, ie. increase the thermal impedance enough to drop the fin temperature within safe limits for copper as well as transfer the desired rate of heat flow. None of the fin configurations (even considering no fins) produced desired combination of fin-area and convective heat transfer coefficient, to achieve desired temperature drop (to protect the metal) and to transfer heat through the hot-end at the desired rate. So methods of reducing the temperature-drop requirement by decreasing flame temperature, as used in gas turbines and some Stirling engines, needed investigation.

(b) Introduction of excess air for cooling :

In order to reduce the flame temperature (which is above 2000°C normally), excess air was passed through the burner, which also helped to cool the burner itself. In the final design air flow was about twice the stoichiometric ratio of air flow needed for complete combustion of the fuel. This ratio may be different at different heat inputs (ie. desired power levels). Reduction of the flame temperature also decreases the NO_x formation (Walker et al. 1994), a major smog producing pollutant. Excess air has been used in

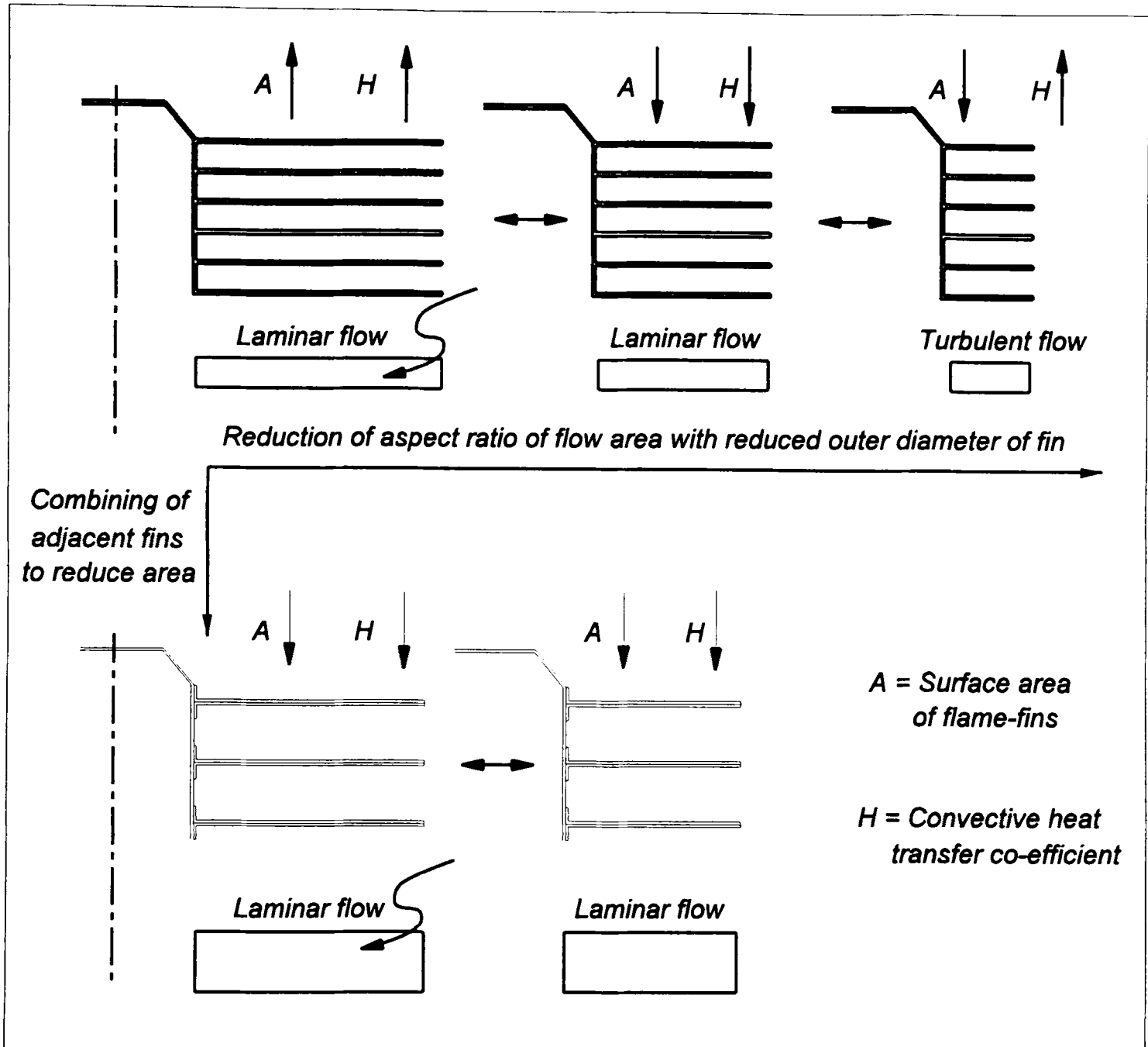


Figure 4.5 : Effect of changing fin dimensions and spacing on surface area and convective heat transfer coefficient at flame to fin interface. Reducing the outer diameter of the fins reduces fin-area but reduction of heat transfer coefficient is only achieved until the flow becomes turbulent, as flow velocity rises. Joining adjacent fins reduce fin-area and heat transfer coefficient. The aspect ratio of length to width (spacing) also has significant effect on the flow, as it changes the hydraulic diameter of flow section. A longer length to space ratio increases the convective heat transfer coefficient for laminar flow.

other Stirling engine designs (Kitzner, 1980; Anon, 1979). The penalty is extra pumping power for passing this increased flow through the system, which includes resistance to flow at the fin blocks, double length trip through the heat exchanger and other frictional losses. Heat exhausted to the atmosphere also would increase. At this point the possibility of recirculating a part of the mass for cooling purpose could be a possible solution. There was two problems associated with such recirculation.

- One is that an additional small pumping mechanism would be needed to return part of the gas back to upstream. Need of the extra blower may be avoided by having expanding area flow-path along with a recirculating channel, at the cost of some additional flow resistance. It is then difficult to control the amount of recirculation flow according to the engine requirement.
- The main blower is placed at the main air intake where the temperature is low, but it is difficult to maintain a blower at the temperature of gases entering the heat-exchanger. Further downstream in the heat-exchanger the temperature will be less, but the pressure difference the blower needed to overcome would increase.

For these reason at this stage of the engine design, a single air flow path and a single blower at the inlet for controlling the air flow was considered.

Another point to be noted is that the temperature of the gases leaving the hot-end must be comfortably higher than the highest fin temperature, to allow steady heat transfer. This is also reflected in the temperature of pre-heated air coming out of the heat-exchanger. For stoichiometric air flow this causes the flame temperature to rise to very high levels.

(c) Total heat balance :

For maintaining a steady state of heat transfer the total heat input to the system should match the total heat output leaving the system. All the input is coming from the burner

and part of the heat is being recirculated within the system, as the outgoing gases preheat the incoming gases in the heat-exchanger. The heat flowing out of the system includes heat transferred through the hot-end (part of which is converted to useful work while the rest is rejected to the sink), heat losses through insulation in various flow paths and heat exhausted to the air. Hence the burner must supply heat passing through the hot-end as well as the heat losses. This was incorporated into the fuel requirement as an additional loss factor (LF) in the Mathcad model.

(d) Redesigning of the hot-end for strength :

For creep-calculation of the Inconel structure (along the radial thickness), the normal stresses were calculated for both tangential direction and radial direction. The maximum of these two were compared against the rupture strength data for Inconel 625. The acting shear stress was not taken as the basis of comparison as it was much less (factor of hundreds) due to the composite design of the hot-end, which increases the shear area vastly. Another suggestion was made (by W.H.S Rampen) that a thin Inconel tubing (seal-tube) be incorporated into the hot end design. This would remove stress from copper and ensure that there will not be any leakage from the hot-end due to creep failure of the hot copper fins. Figure 4.6 c shows how the Inconel tube would be placed in the hot-end composite structure. The Inconel tube is supported by the Inconel washers outside, against internal pressure. For present design and cycle pressure (400 bar) a tube thickness of less than a quarter of a millimetre is adequate. The addition of seal-tube tubing creates some additional thermal resistance and temperature drop (about 25°C at full power). Incorporating a seal-tube in the design assumes that very good contact exists between the meeting surfaces after the vacuum brazing is done. Any gap in between may cause large thermal resistance to heat flow. The provision of both a variable thickness seal-tube and air-gap was incorporated into the Mathcad model.

4.3 Performance of the Artemis Malone engine

Table 4.1 shows the main design features of an engine optimized for full-power (about 55 kW). The design features are calculated using the modified Mathcad Model and by

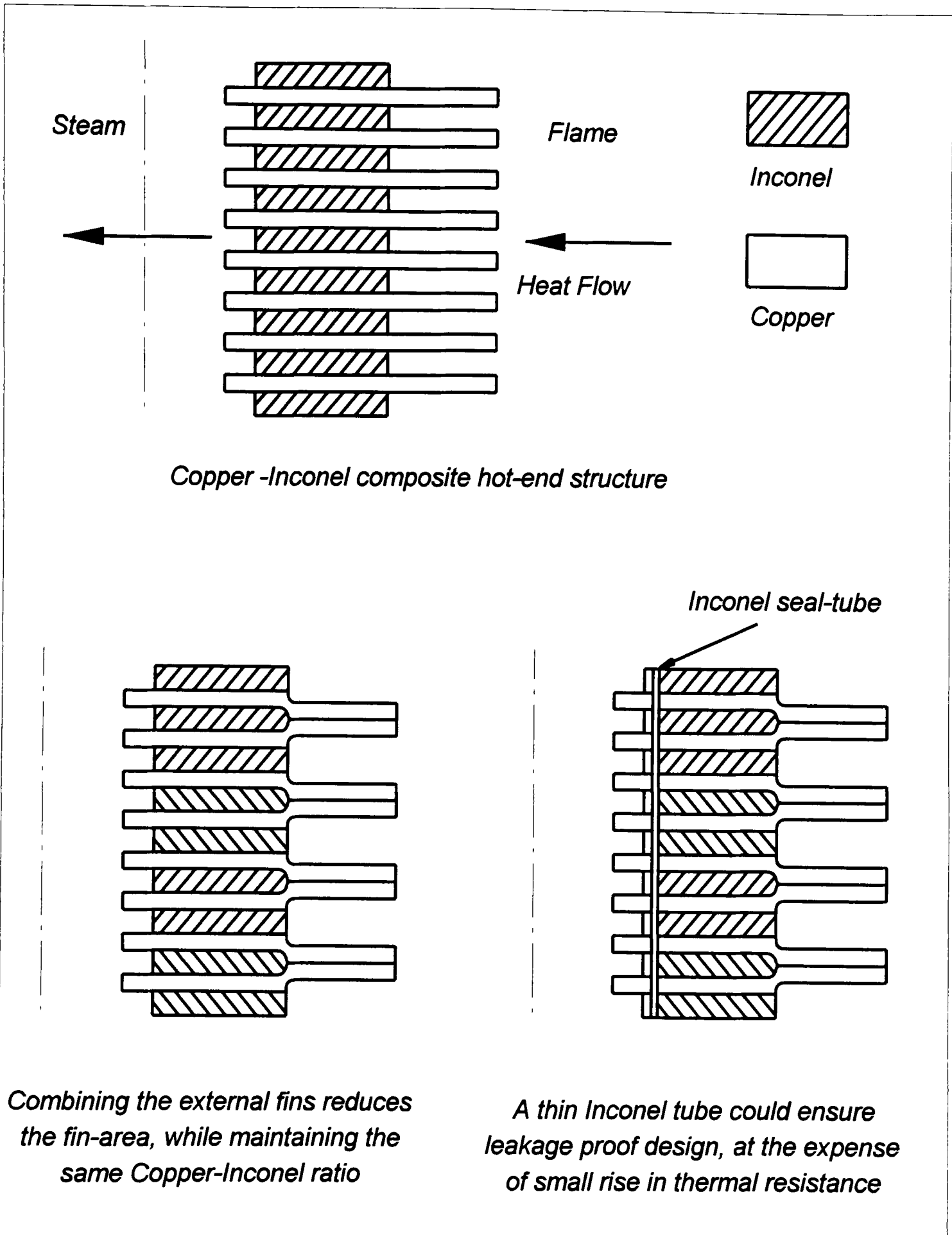


Figure 4.6 : Stages of hot-end design modifications, sectional views of one side are shown only.

- (a) Composite structure of copper and Inconel washers, providing low thermal resistance to heat flow as well as withstanding internal pressure at elevated temperature.
- (b) Stamping of two adjacent flame fins to reduce surface area and convective heat transfer coefficient.
- (c) Introduction of an Inconel seal-tube, takes stress off copper and ensures a leak-proof design although the thermal resistance of the hot-end increases a little (26°C more temperature drop at full power).

iterative process of converging the solutions of all the closed-loops mentioned in the first section of the chapter. The results presented correspond to a full power cycle. The thermodynamic cycle used in the model consists of four parts :

- (i) The cycle pressure is raised to a specified high-level as the piston ends its motion towards the cold-end, while the regenerator stays at the hot-end.
- (ii) Regenerator moves from the hot-end to the cold-end, while the piston is moved away from the cold-end accordingly, to maintain the high pressure of the cycle.
- (iii) The pressure is allowed to fall to a specified low-level as the regenerator starts its motion back towards the hot-end, by keeping the piston stationary.
- (iv) The piston is moved accordingly as the regenerator finishes the remainder of its return stroke to the hot-end, to maintain the low-level pressure.

It should be noted here that the Mathcad model only specifies the regenerator motion, which includes stroke length and fractions of the cycle through which it moves between the hot-end to the cold-end. It calculates an estimate for piston stroke, but gives little information about motion profiles. The thermodynamic cycles are discussed in greater detail in chapter six.

Various parameters and numerical factors affect the design of the engine in different ways. Some of these are listed below :

- In general the temperature drops across the hot-end and cold-end structures vary directly with the heat flux passing through them. This needs consideration for designing hot and cold-ends for different power requirements, as well as varying the heat flux (ie. the power output) through a certain engine design.
- The bore factor, along with the number of modules and their spacing, affects the engine design in terms of overall dimensions of the TD pile, which has large effect on the power-to-weight ratio of the engine.
- The outer Inconel diameter affects the stress capacity of the hot-end most significantly. Increasing the outer diameter of Inconel disks reduces the metal stress and should improve the hot-end creep life. This also increases the

TABLE 4.1 : Specifications of an Artemis-Malone engine-design at full power

Engine Design Parameters

Number of modules (TD piles)	4
Module spacing	84 mm
Desired full-load output power	55 kW
Maximum allowable cycle pressure	400 bar
Minimum desired cycle pressure	10 bar
Maximum allowable metal stress	$3 \times 10^8 \text{ N/m}^2$
Heat flux/Module	27 kW
Hot-end temperature	550 °C
Cold-end temperature	95 °C

Main results for full power cycle

Full power output	56.1 kW
Carnot efficiency Hot-end at 549°C and cold-end at 95°C	55.2 %
Final efficiency (considering heat losses and power for ancillary drives)	50.4 %
Heat input rate	111.56 kW
Excess air requirement	105%
Engine speed/Module	221 cycles/min
Module bore	40 mm
Overall height	552 mm
Overall length	621 mm

Heat-exchanger design

Air temperatures	Entering from the atmosphere Entering into the burner section	25 °C 738 °C
Gas temperatures	Entering the heat-exchanger from hot-end Exhausted to the atmosphere	770 °C 59 °C
Number of double wraps in the heat-exchanger		10
Gap between wrapping sheets		14.25 mm
Height of wrapping sheets		224 mm

Table 4.1 continuing

Hot-end design

Number of Copper/Inconel disks per Module		66			
Copper disk dimensions	Outer diameter	84 mm			
	Inner diameter	40 mm			
	Thickness	0.7 mm			
Inconel disk dimensions	Outer diameter	60 mm			
	Inner diameter	48 mm			
	Thickness	1 mm			
Flame fins	Number	66			
	Radial length	12 mm			
Steam fins	Number	66			
	Radial length	4 mm			
Temperature distribution °C					
Avg. Flame	Flame-fin tip	Flame-fin root	Mid-wall	Steam-fin root	Steam
1240	716	684	658	631	549

Cold-end design

Condensing fins/ Water-fins	Number	58		
	Radial length	4 mm		
	Thickness	1 mm		
Copper wall thickness between inner and outer copper-fins		4 mm		
Cooling water temperature	Water in	55 °C		
	Water out	77 °C		
	Flow rate	0.6 l/sec		
Temperature distribution °C		Condensing steam	Condensing-fin root	Water-fin tip
		95	84	77

Regenerator design

Regenerator dimensions	Outer diameter	38.25 mm
	Core diameter	11 mm
	Length	240 mm
Stroke length		116 mm
Solidity of regenerator material		60 %
Spinning speed		2335 rpm
Heat recirculation rate	per cycle	31.4 kJ
	Compared to heat input	447%
Cyclic temperature rise (full power)		61 °C

temperature drop in the wall, which requires the temperature of the outer-edge of the wall to be raised, in order to maintain the steam temperature in the hot-end. As a result the solid curve in figure 4.3 moves down (lower stress) as well as being stretched to the right (wall temperature increase). Changing the dimensions of Inconel disks affects the fin areas in the flame and steam side as well as the aspect ratio of the flow path created by the fins. These ultimately change the thermal impedances at the interfaces.

- The thickness of copper and Inconel disks dictate the number of fins in a TD pile. The thickness as well as the inner and outer diameter of the copper sections, determine the geometry and control the thermal impedances at the interfaces (eg. gas-metal, steam-metal etc.)
- The addition of excess air causes the average flame temperature to be lowered, this is reflected in lower metal temperatures at the hot-end. It also allows increase of the thermal mass needed to transfer the heat into the hot-end. Higher hot-end temperature levels may be desirable in terms of efficiency but is limited by the maximum safe temperatures for materials. Blowing extra air requires extra power, but allows the flame-fins to operate within their safe limits.
- The heat-exchanger design governs how effectively heat of the outgoing gases can be recovered back into the incoming air. This affects the overall thermal efficiency as well as the temperature at which the heated air enters into the burner section, thus affecting the flame temperature. Reducing the gap between heat exchanger plates or increasing the flow path length leads to better heat recovery and less heat lost at the exhaust. It also increases the pressure drop along the flow path which increases the power requirement of the blower. For highest efficiency a compromise between the two must be made.

Table 4.2 shows the main subsystem losses accounted in the design and comparative presentation of the losses. For the full power design about 43% of the heat supplied to the engine is rejected at the cooling water flowing around the cold-end. About 3% is lost due to convective heat losses to the surrounding air through the insulation and the exhaust. Among the subsystem drive losses the blower is most significant and the main part of blower losses occurs in flowing the fluid through the heat-exchanger. Total

TABLE 4.2 : SUBSYSTEM LOSS CALCULATIONS

$$P_{act} = P_{ideal} - P_{regndslp} - P_{blower} - P_{cooling\ water} - P_{swirling}$$

Loss calculations in design for 55 kW engine running at full power :

1. Power loss for regenerator motion = 0.644 kW

Where, $P_{owRM} = (P_{hc.ftRm.ftRhc} + P_{ch.ftRm.(1-ftRhc)})/2$

$$ftRm = 0.92 \quad ftRhc = 0.576$$

2. Power loss for blower = Loss for blowing gas through fin-block

+ Losses for flow through heat exchanger.

$$W_{expu} = (VGC.dp_{finblock} + 2.V_{gas}.dp_{exchanger}).(No. of modules)$$

$$W_{expu} = 0.14 + 1.44 = 1.571 \text{ kW}$$

3. Power loss for circulating cooling water = 0.012 kW

$$\text{Flow rate} = 0.6 \text{ l/sec}$$

4. Swirling losses = Power_{Swirl Hotend} + Power_{Swirl Coldend}

$$= 0.124 + 0.313 = 0.437 \text{ kW}$$

With, Swirl Velocity = 4.89 m/s and swirl speed of 2334 rpm.

Losses occurring in	Before considering drive losses (kW)	With 25% additional drive losses (kW)	Losses in terms of percentage of		
			Q _{in} %	P _{ideal} %	P _{out} %
Regn-dspl Motion	0.644	0.804	0.72	1.3	1.4
Blower	1.571	1.963	1.76	3.3	3.57
Cooling water	0.012	0.015	0.01	0.02	0.03
Swirling	0.437	0.546	0.49	0.92	1

Waste heat :

$$\text{Heat wasted to cooling water} = 4 \cdot (1 - 0.552) \cdot 27 = 48.38 \text{ kW (43.4\% of } Q_{in} \text{)}$$

$$\text{Heat lost through exhaust} = 3.2 \text{ kW (2.9\% of } Q_{in} \text{)}$$

$$\text{Heat losses through insulation} = 0.22 \text{ kW (0.2\% of } Q_{in} \text{)}$$

**TABLE 4.3 : COMPARISON OF THE ARTEMIS-MALONE ENGINE
WITH SOME DIESEL ENGINES**

	KUBOTA Super-03 Series Diesel Engine Model F2803-E	PERKINS SERIES 1000 Diesel Engine Model 1004-4	ARTEMIS- MALONE ENGINE
Max Power (kW)	43	65	56
Engine Speed (rpm/cpm)	2800	2600	221
Number of Cylinders/Modules	5	4	4
Bore × Stroke (mm)	87 × 97.4	100 × 127	40 × 116
Dry Weight (kg)	223	338	173 [□]
Brake Specific Fuel Consumption (g/kWh)	236	215	161
Efficiency % at Maximum Power	33%	--	50%
Max Efficiency η %	36% at 26 kW	39%	51% at 23 kW †
Power to Weight Ratio (W/kg)	191	193 (260)* * For turbo-charged after-cooled version	328
Displacement (cc)	2746	4000	532
Exhaust Emissions :			‡
Total HC	0.4	1.2	0.02
NO_x	9.6	13	0.21
CO	2.68	3.2	0.07
Pm (Particulates) (g/kWh)	0.55	0.6	0.01
Noise	Noisy	Noisy	Quiet

□ Typical weights of accessories like - blower, alternator, starter motor, pumps, casings and heat-exchanger are included.

† This value is quoted from results of part-load performance presented in chapter 10.

‡ Values are calculated from typical domestic gas furnace data (Campbell, 1986).

NB. Data for Diesel engines are collected from brochures provided by the manufacturers.

drive losses account for less than 4% of the heat input. Mechanical power for blowing the air and gas, moving the regenerator axially, circulating the cooling water around the cold-end and swirling losses in spinning the regenerator was taken into account.

Table 4.3 shows the comparative performance of the engine with two modern diesel engines of similar power ratings. The Artemis-Malone engine performance predictions shows advantages over the diesel engine in terms of efficiency (over 10%, absolute) and power-to-weight ratio (about 1.5 times). The cycle frequency of the Malone engine (as it physically does not have any crank shaft) is much slower compared to the diesel engines speeds, which indicates much higher torque output (with less cyclic variation). The displacement volume is a fraction of that of diesel engines, giving high power-density (typical of high-pressure hydraulics). The exhaust emission calculations were based on typical domestic gas furnace data (Campbell, 1986), which demonstrates the relatively clean combustion of Stirling engines in general. Noise prediction at the exhaust is only based on the air flowing through the spirally coiled heat-exchanger and may be simplistic.

CHAPTER - 5

Modelling of the Hydraulic Drive System

5.1 Introduction

Most hydraulic system loads need variable flow for their proper operation. Conventionally this can be achieved in three ways. One is through flow control valves which alter the flow at the expense of energy loss. Variable swash-plate axial-piston machines are frequently employed for hydrostatic drives where energy becomes a consideration. Less commonly, a fixed displacement pump can be driven by a variable speed prime-mover. This chapter describes a fourth method: the digital-displacement technique (Rampen et al. 1990; 1991; 1994) which provides yet another way of controllably transferring energy between mechanical and fluid power.

The advantages of the digital-displacement machine over conventional variable-swash hydraulic machines lie with both the response speed and inherent energy efficiency. Their compatibility with micro-processors allow the use of advanced control logic. Full or zero output can be attained from any starting condition, in less than a single shaft revolution. As disabled cylinders are not pressurised, losses are lower in comparison with swash-plate machines leading to higher efficiency, especially at part-load.

5.2 Operating principle

The operating principles of digital-displacement pump-motors are described in previous works by Rampen and Salter (Rampen et al. 1990; 1994; 1995). The basic structure of a digital-displacement machine is similar to the conventional reciprocating machine, with poppet valves connecting to the low and high-pressure manifolds of each cylinder. But, instead of being self-acting, each of the poppet valves is equipped with an electro-magnetic actuator. The valves are operated by a micro-controller at precise times, near the ends of the stroke, in order to establish fluid connection between the moving piston

and the appropriate manifold. This control allows cylinders to behave in any of three ways, they can pump or motor - adding or subtracting fluid from the high pressure manifold - or they can be disabled. The function of each cylinder can be changed at each end of each stroke. As the valves are actuated at times in the cycle when there is almost no pressure difference across them, the actuators can be compact and use little power. Either permanent magnets or springs are used to maintain the disabled poppets at default positions. A micro-controller controls the valves from its output port via a bank of power semiconductors. Figure 5.1 shows the cylinder head arrangement of a single cylinder digital-displacement pump-motor (Rampen et al. 1994).

When digital-displacement control is used, a decision is made as each cylinder approaches either end of its stroke. The controller considers the state of the system and takes a decision either to enable it to either pump or motor or else to disable it. The valve actuation sequence is different for pumping and motoring. The pumping cycle starts with an intake stroke and with the low pressure valve open. If a cylinder is to be enabled, the controller closes the intake valve just prior to bottom-dead-centre (BDC) with the result that the contents are pumped into the high-pressure manifold over the next half shaft revolution. As the piston rises the pressure is increased until it reaches the level of the high-pressure side, opening the high-pressure valve. A disabling decision leaves the inlet valve open so that the delivery manifold does not receive any fluid from the decision cylinder over the same period and the fluid is returned to the low-pressure manifold.

Figure 5.2 shows a schematic representation of a motoring cycle (Rampen et al. 1994). To enable a cylinder for motoring, the controller closes the low-pressure valve shortly before the piston reaches top-dead-centre (TDC). Once the valve is closed, the cylinder pressure rises to equal to that of the high-pressure manifold by the time the piston reaches TDC. The high-pressure valve can then be opened and latched. The piston is then propelled by the fluid pressure towards BDC. In a similar fashion to the TDC valve-sequence, the high-pressure valve is closed prior to BDC such that the residual piston stroke can de-pressurise the cylinder and allow the low-pressure valve to be re-opened. The fluid can then be exhausted through the low-pressure valve into the low-

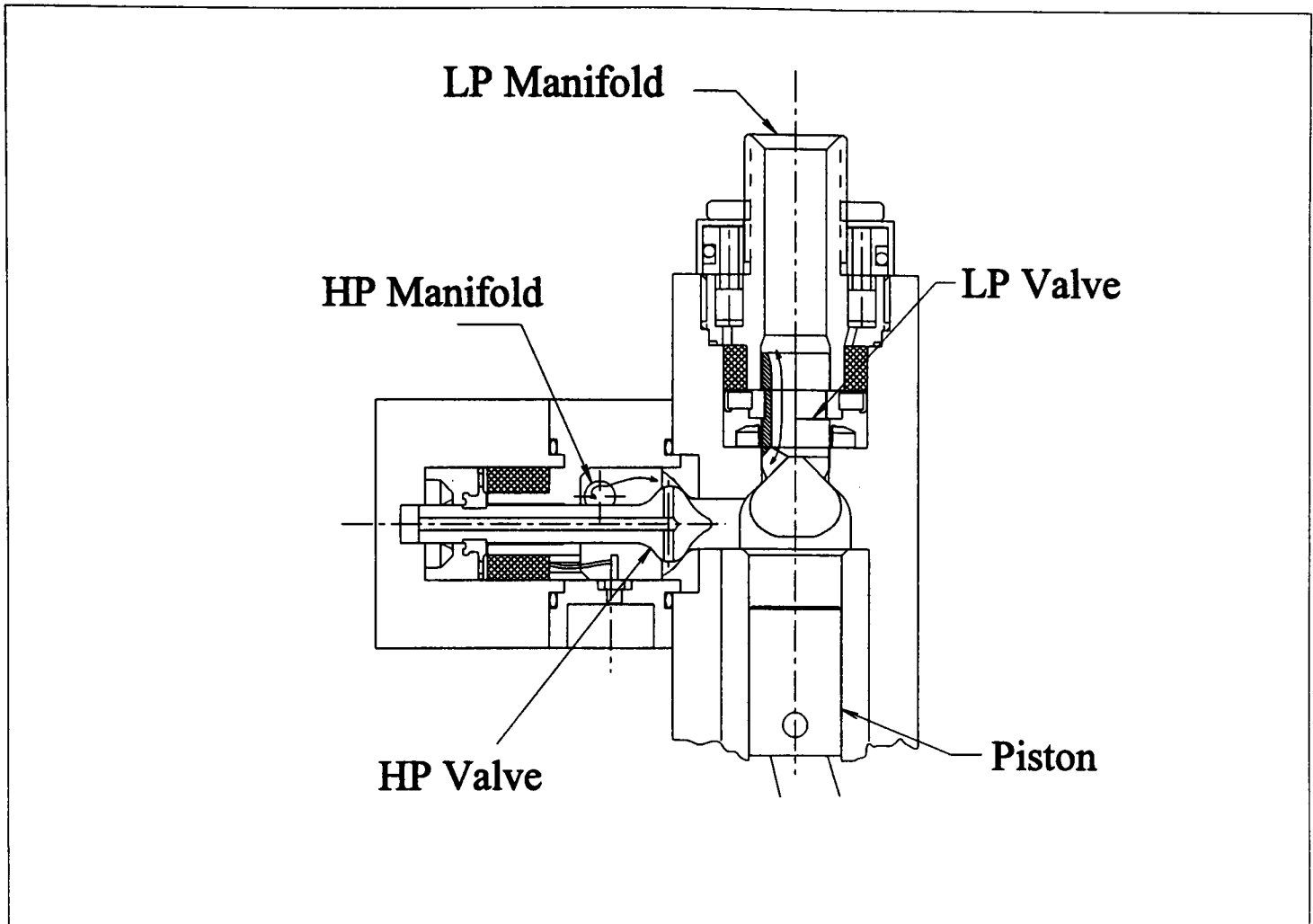


Figure 5.1 : Cylinder head arrangement of a digital- displacement pump-motor
Courtesy : Artemis Intelligent Power Ltd, UK

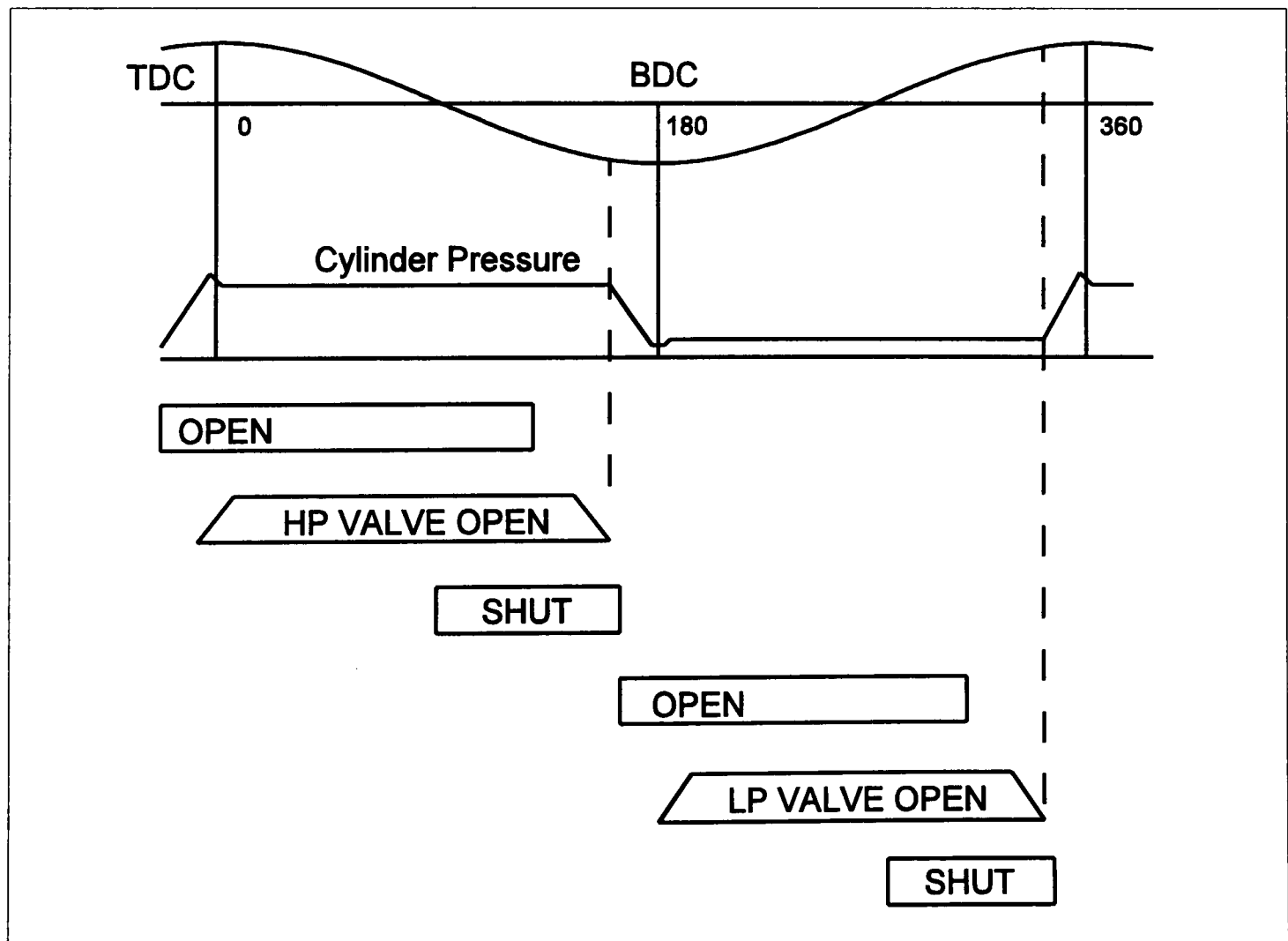


Figure 5.2 : Valve actuation sequence of motoring cycle
Original drawing by S.H.Salter

pressure manifold. The controller can switch between motoring, pumping or nulling operations as required by simply changing the valve actuation sequence.

5.3 Control techniques

Before going into the details of the control techniques it is helpful to have a look into the flow out of a multi-cylinder reciprocating pump. Figure 5.3 shows the sinusoidal flow pattern out of a single cylinder. With the reduction of pump speed the maximum flow velocity reduces, while the time span of flow increases, keeping the total volume of flow discharged constant to one cylinder's displacement. The volume of a cylinder discharge can be calculated as :

$$Total\ Volume\ Discharged = \frac{V}{2} \int_0^{\pi} \cos(\theta) d\theta$$

where, $\theta = (Angular\ speed\ of\ shaft \times Time) - Phase\ angle$

$V = Cylinder\ volume$

Figure 5.4 shows the in-phase cylinder flows out of a multi-cylinder pump and their combined effect.

Two basic algorithms may be used by the controller to make enabling decisions. These are either pressure or flow-control modes. Alternatively, in the case of a cyclic load-demand, the enabling pattern can be pre-set into a sequence of decisions. All these methods share two key characteristics. The first is that there is a quantisation error, due to the selection of entire cylinders, which must be carried forward by a displacement accounting technique. The pressure ripple associated with this flow variation is minimised by putting a small accumulator near the delivery valves, which smooths the output, in effect adding a low-pass filter after the pump-motor. The second characteristic is the delay of response following a decision. An enabled cylinder influences the output for a half shaft revolution after the valve actuation occurs. This delay error is resolved by including a look-ahead time (or shaft angle), where the decision cylinder is making a substantial contribution to the pump-motor's output. The

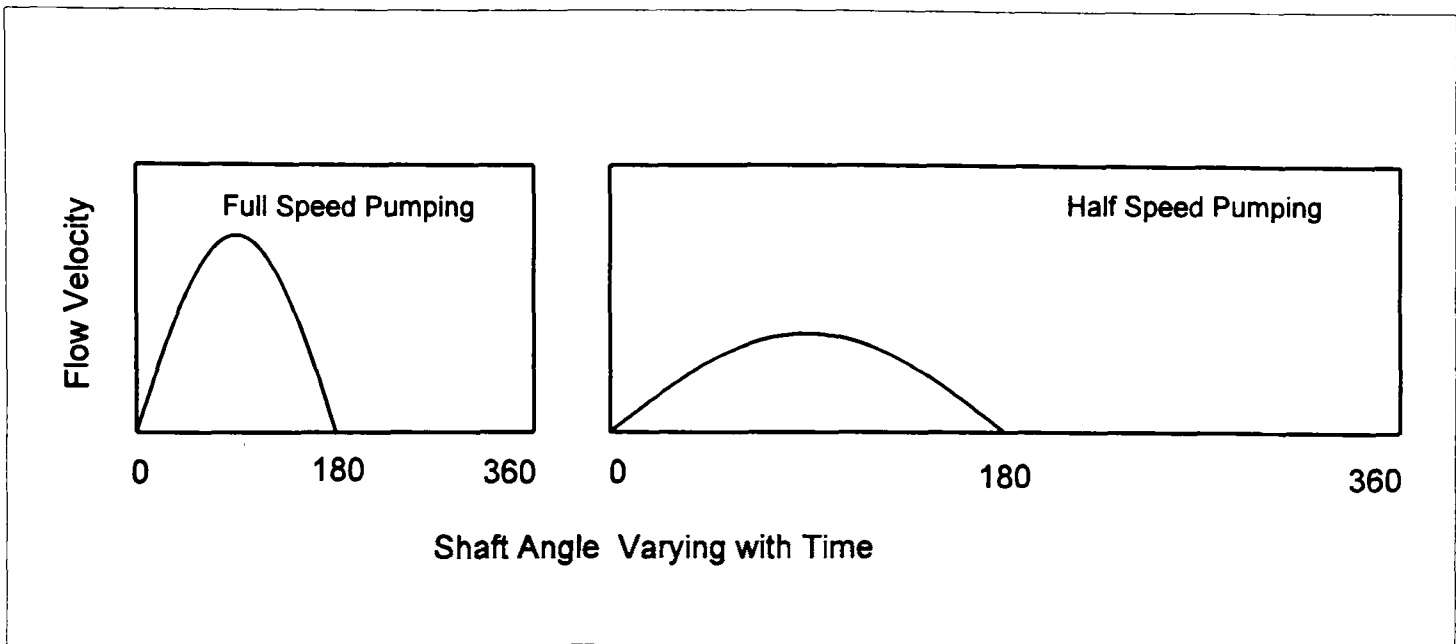


Figure 5.3 : Nature of flow from a reciprocating cylinder at different speeds.

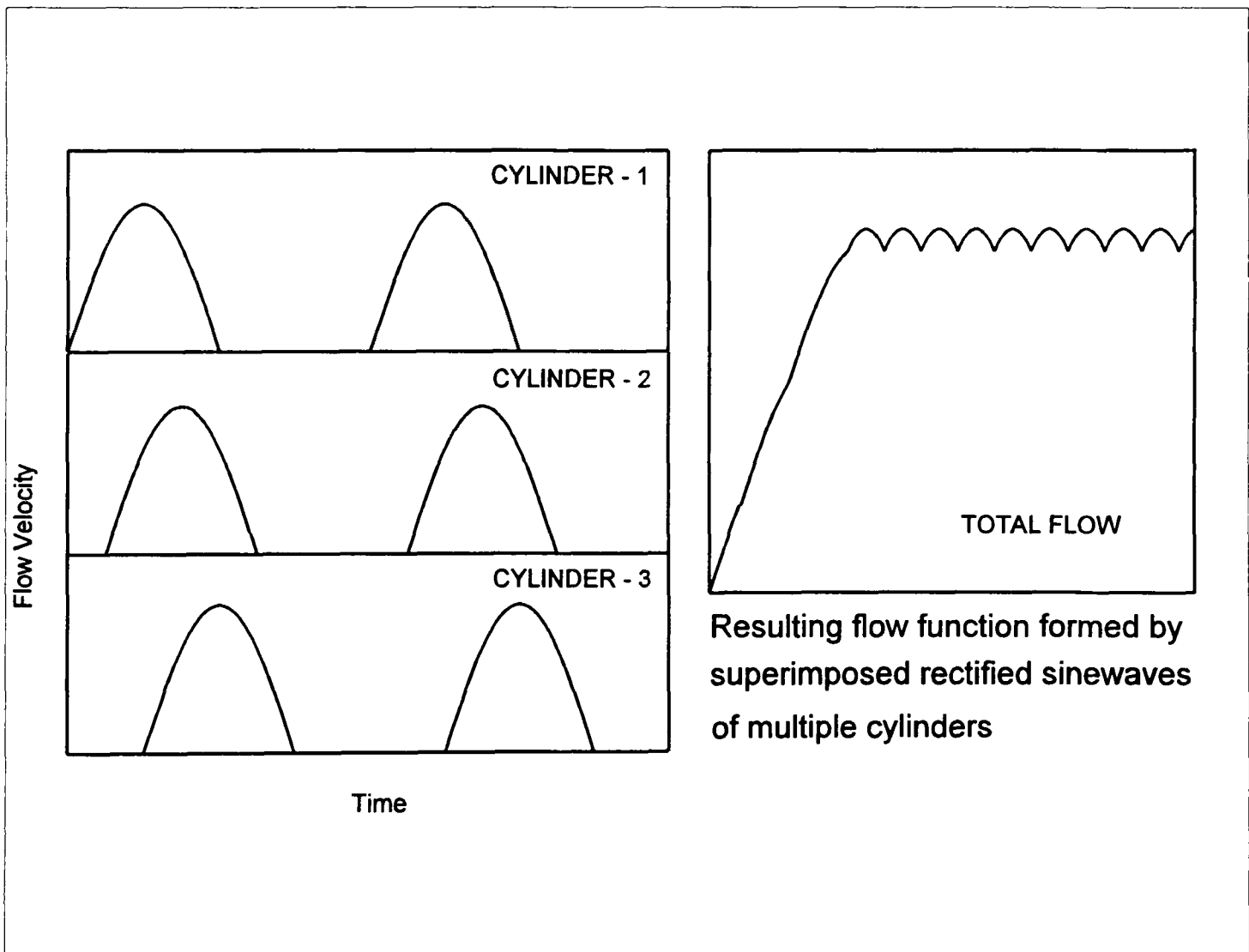


Figure 5.4: Flow from a multi-cylinder pump.

look-ahead angle is defined at a point where one uncommitted cylinder's worth of displacement has contributed to the output, as described by previous work done on pump modelling by Rampen (1992).

This can be calculated from the equation :

$$2 = \sum_{i=1}^{ip(n/2)} (\cos(0) - \cos(m))$$

where, n = number of cylinders
 $\phi = 2\pi/n$ (ip = integer part)
 $m = (\psi - i.\phi)$ but $0 \leq m \leq \pi$
 ψ = Look-ahead Angle

Number of Cylinders	Look-ahead Angle (rad)
2	3.141
5	2.199
6	2.094
9	1.863
10	1.810

5.3.1 Pressure control mode

The pressure-control mode maintains a demand pressure at the pump discharge under variable flow conditions (Rampen et al. 1991). A small linear accumulator, of known compliance, is incorporated into the discharge system both to smooth output and to allow the controller to convert pressure error, from a transducer signal input to the controller, into displacement error. Accumulator size can be chosen so that the half cylinder accumulation error results in an acceptable pressure deviation from the set level. One limitation of simulating the flow in pressure-control mode is that the load characteristic of the system down-stream also has to be defined in order to predict the pressure of the next time-step. This is a problem faced only in the simulation, as the pressure does not need to be found by solving close-loop relations in real systems. It can be known simply by using a transducer. For this simulation a variable orifice has been used for convenience, though in practice the method has been shown to work for a variety of reactive loads. If all the known displacements during the previous time interval can be summed then the load flow during that interval can be inferred. The volume of fluid pumped or motored S_p can be calculated for the interval preceding decision k :

$$S_p = \frac{V}{2} \sum_{i=1}^{ip(n/2)+1} D_{k-i} ((\cos(i-1)\phi) - \cos(i\phi))$$

where, V = cylinder volume

D = decision value

n = number of cylinders

$\phi = 2\pi/n$ (ip = integer part)

The displacement out of the accumulator S_a can be calculated from the pressure difference between the current and the previous decisions.

$$S_a = C_1(p_k - p_{k-1})$$

where, C_1 = accumulator constant (linear type)

p = system pressure

(this equation depends on the type of accumulator used)

The load flow Q_s can be found by summing the two :

$$Q_s = \frac{S_p + S_a}{t}$$

where, t = interval time between decisions

The algorithm now changes its time reference point and considers the projected flow in the time interval between the actual time and the look-ahead time. The displacement of already committed cylinders S_c is calculated as :

$$S_c = \frac{V}{2} \sum_{i=1}^{ip(n/2)} D_{k-i} ((\cos(i\phi) - \cos(i\phi + \psi)))$$

where, ψ = look-ahead angle

The accumulator displacement S_o is then set to bring it back to zero error position. The load displacement S_s is calculated from load flow :

$$S_o = C_1(p_{set} - p_k)$$

$$S_s = Q_s \frac{\psi}{\omega}$$

where, ω = rotational velocity

Finally the decision D_k for a look-ahead cylinder is :

$$D_k = \frac{(S_s - S_o - S_c)}{V_d} \quad \text{where: } V_d = \frac{V}{2} (\cos(0) - \cos(\psi))$$

Flow from an orifice (load) Q_s can be defined as :

$$Q_s = C_2 A \sqrt{P}$$

where, $C_2 = \sqrt{2/\rho} C_D$
 A = orifice area
 ρ = fluid density
 C_D = coefficient of discharge

Hence, the equation for pressure can be written as:

$$0 = C_1(p_k - p_{k-1}) - \frac{C_2 t A}{2} (\sqrt{p_k} + \sqrt{p_{k-1}}) + S_p$$

where, p_k is unknown

5.3.2 Flow control mode

The flow-control algorithm tries to minimise the accumulated displacement error over the history of the pump, following the variations in load demands. Although it is essentially open loop, pressure feedback can be employed to suppress low frequency resonances while driving reactive loads. This has been demonstrated in the laboratory and is implemented by a term representing the difference between the averaged and instantaneous pressure. The accumulator acts like a flow-averaging device at the delivery, but its performance is affected by the pressure created by the load response.

The decision D_k for a current cylinder is computed as :

$$D_k = \frac{(S_s - S_c - e - C_1(p_k - p_{avg}))}{V_d}$$

where, $V_d = \frac{V}{2} (\cos(0) - \cos(\psi))$

S_s = flow demanded over look-ahead period

S_c = displacement coming from already committed
cylinders during the look-ahead time

e = cumulative error resulting from previous decisions

p_{avg} = A running average of pressure of last five decisions

ψ = look-ahead angle

5.3.3 Ternary mode

Here the decision making process is off loaded from the controller, instead it reads decisions from a ternary code or table (composed of +1,-1 and 0 entries) and repeats the sequence of enabling (pumping/motoring) or disabling cylinders. This mode is advantageous when the same set of operations are repeated. In cases where rapid changes in demand are expected, it is difficult for the control algorithm to foresee them and ternary mode could be especially useful. The ternary code table can be tuned to meet any requirement of the repeating operation. Hence this mode of operation can be robust (perfect repeatability of cycles) but flexible to load requirement (as the code can be changed) at the same time. Operation in ternary mode is open-loop, but pressure feedback could also be employed.

5.4 Structure of the modelling of digital-displacement pump-motor

The computer model of digital displacement pump-motor simulates the flow through it on a millisecond-by-millisecond basis. This provides an excellent tool to allow the testing of different cylinder enabling strategies and their effects on the flow. Programmes for six and ten cylinder machines were developed, but they can be easily modified to allow for different cylinder numbers. The same programme can simulate pumping as well as motoring, with both fixed or time-varying shaft speed. A dynamic graphical simulation package "SYSTEM BUILD" has been used for the modelling, which is a part of the family "MATRIXx Version 4.1". The whole programme acts like a collection of sub-programmes superimposed in different layers. There is a well defined degree of hierarchy between different layers and sub-layers. Different

subsystems can have the same, different or conditionally different time steps as is required. These non-linear and conditional time relationships are automatically computed, allowing the simulation to work under variable shaft speed, where the shaft speed acts like the master clock for all sub-programmes of the pump-motor simulation. The programme blocks can be divided in to five groups:

- (i) **The parameter blocks** - These constitute the basic structure of the multi-cylinder pump-motor, definition of cylinder sizes, phase relationships, look-ahead angles and the shaft speed (which may be fixed or a varying time series of any pattern). These blocks are sampled at regular time intervals, during simulation.
- (ii) **The load-demand blocks** - These define the demand signals of load. This may be a fixed load, a varying time series of flow-demand or expressed as a percentage of flow capacity at a particular speed.
- (iii) **The Sequential Trigger generating blocks** - These create signals each time a cylinder reaches the top-dead-centre (TDC) or the bottom-dead-centre (BDC), which acts like the trigger of the programme. These are generated proportionally with the rise or fall of shaft speed. Other sub-programmes and signal holding blocks are activated (which again may be conditional), depending on these signals. These trigger generating blocks are sampled at high frequency (eg. one tenth of a millisecond) to reach high precision on the timing of triggering signals.
- (iv) **The decision making blocks** - These blocks are activated at the instance of each sequential trigger signal. The algorithms make a decision regarding the following cylinder - whether to enable (pump or motor) or disable (null) it. Different types of algorithms: flow-control, pressure-control or ternary-code table can be used, according to choice. The decisions regarding pumping, nulling or motoring give signals of +1, 0 or -1 value. These decisions are incorporated with the sequential trigger signals and passed to the "decision implementing blocks".
- (v) **The decision implementing blocks** - These convert the series of decisions into corresponding flow of cylinders, hence generating the flow function through the pump-motor. Some of these blocks act as memory, holding the decision of respective cylinders for the next half-shaft revolution. While the others convert the decisions into physical fluid flow through the corresponding cylinders. Flow of overlapping cylinders are superimposed resulting in the total flow function. To achieve a precise output flow function, these blocks are sampled continuously.

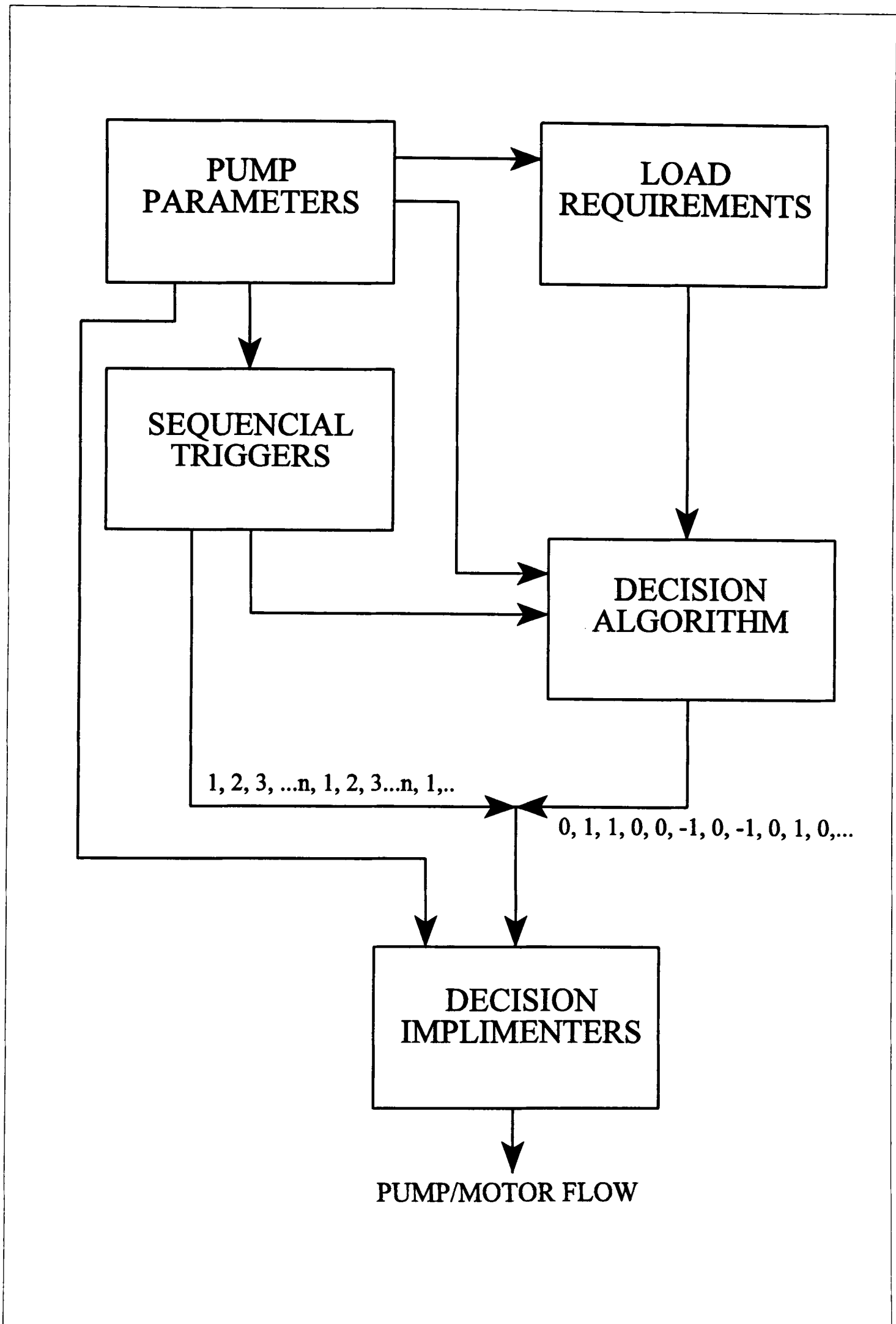


Figure 5.5 : Simulation Programme Flow-Chart for Pump-Motor Model.

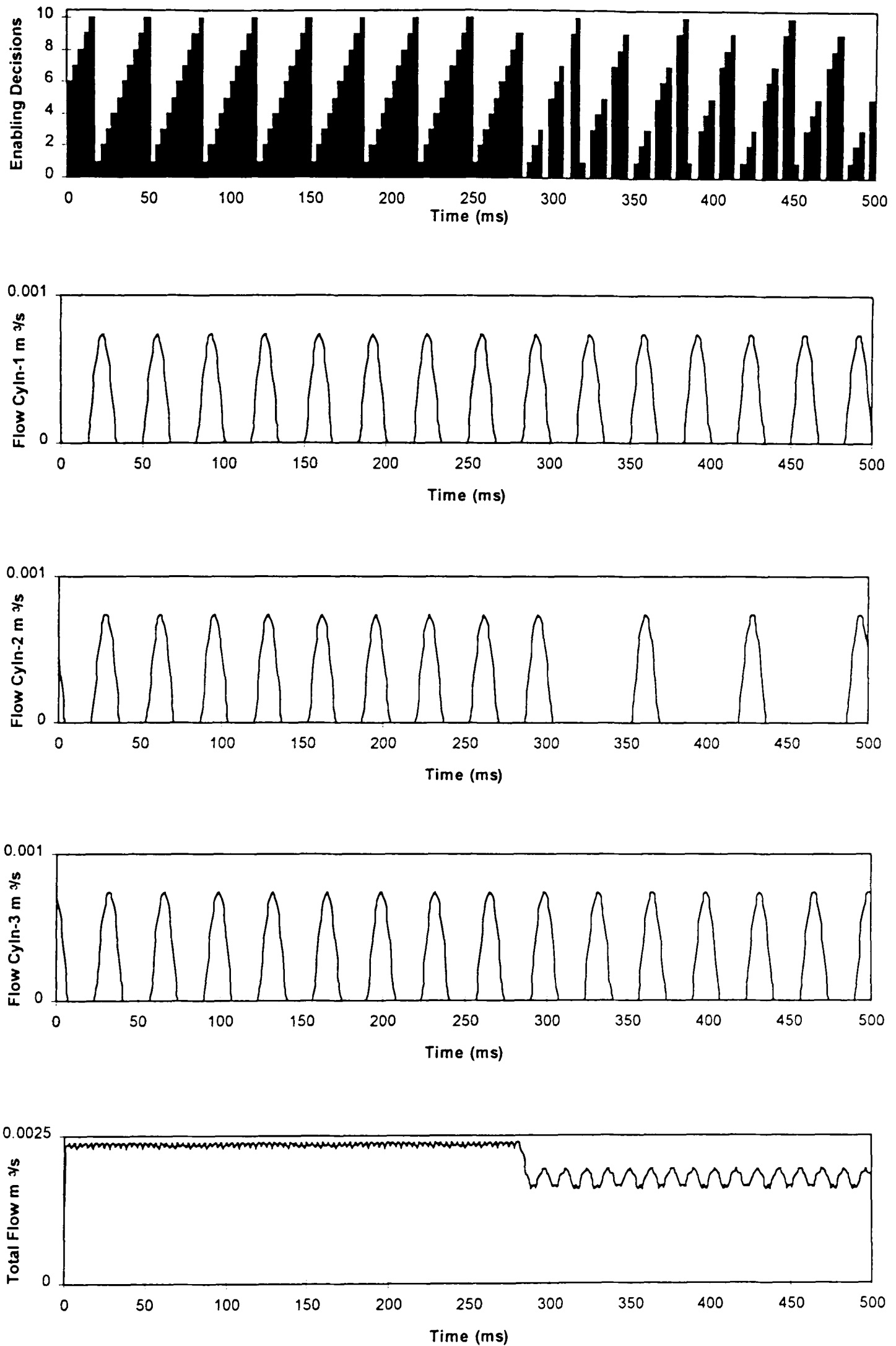


Figure 5.6 : Superimposed flow of multiple cylinders enabled according to respective decisions, 10 cylinder pump shifting from 100% - 75% flow capacity at 1800 rpm. The change in cylinder enabling pattern is noticeable.

Figure 5.5 shows the flow chart of the programmes. One of the major difficulties faced in developing a pump-motor model capable of operating at variable speeds, was found to be small time mismatches (which may be 1-3 times the high-frequency sampling intervals) among outputs coming out of different sub-programmes. Such mismatches had significant adverse effect on the corresponding interaction of some of the sub-programmes, especially between the decision making and the decision implementing sub-programmes. These were dealt with incorporation of proper time delays, synchronising the output of all the sub-programmes. Another difficulty arose as sampling frequency of sub-programmes with different time rates, could not be set in terms of time as they would need to change with varying shaft speeds. The same applied for timing requirements of data holding blocks. This problem was overcome by constructing the sequential-trigger generating sub-programme mentioned above. All the sub-programmes (activation of some of which may be conditional) are triggered by this, instead of fixed time intervals.

Figure 5.6 shows the generation of decisions and the resulting flow of a multi-cylinder pump. The change in decision enabling pattern is noticeable in the top graph as the flow demand drops. Instead of enabling every available cylinder (100%), every one in four available cylinders are kept disabled (for 75%) to meet the flow demand. The detailed programmes for a 10-cylinder digital-displacement pump-motor are presented in appendix B.

5.5 Simulation results of pump-motor models

Figure 5.7 shows the results of a digital-displacement pump with an initial demand of 10% which is then step increased to 90%. A six cylinder pump, of 25mm bore \times 16mm stroke (MacTaggart-Scott radial piston pump), running at 1800 rpm, was used for the model. The accumulator is designed to provide one cylinder volume of displacement on either side for $\pm 10\%$ variation from the set pressure of 200 bar. The step change models an abrupt increase of load orifice area. There is a lag between the step change and the response of the pump, during which flow in or out of the accumulator dominates. Within 30 milliseconds the pump has adjusted to the changed demand.

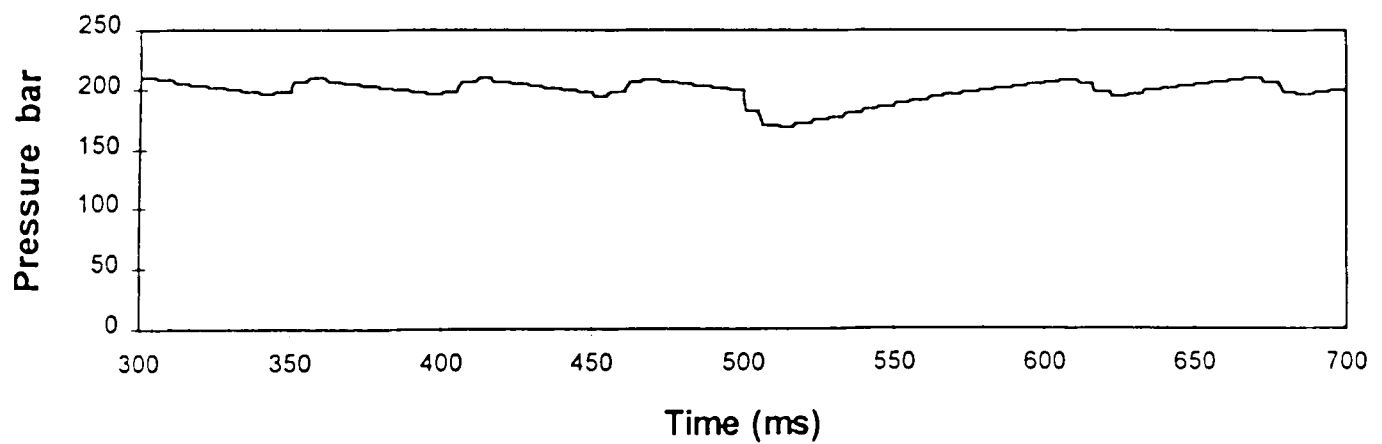
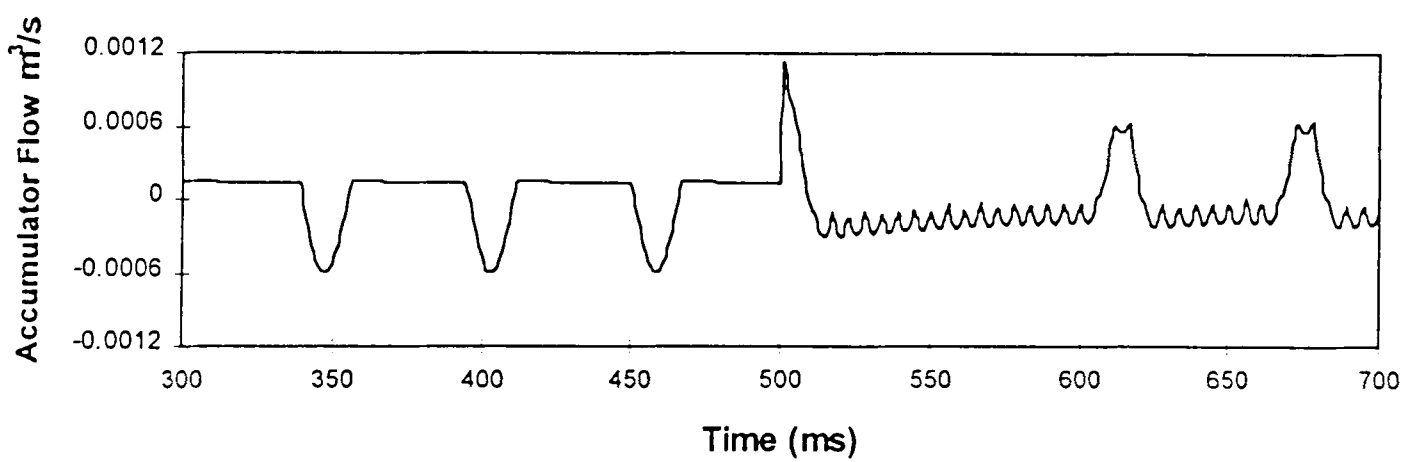
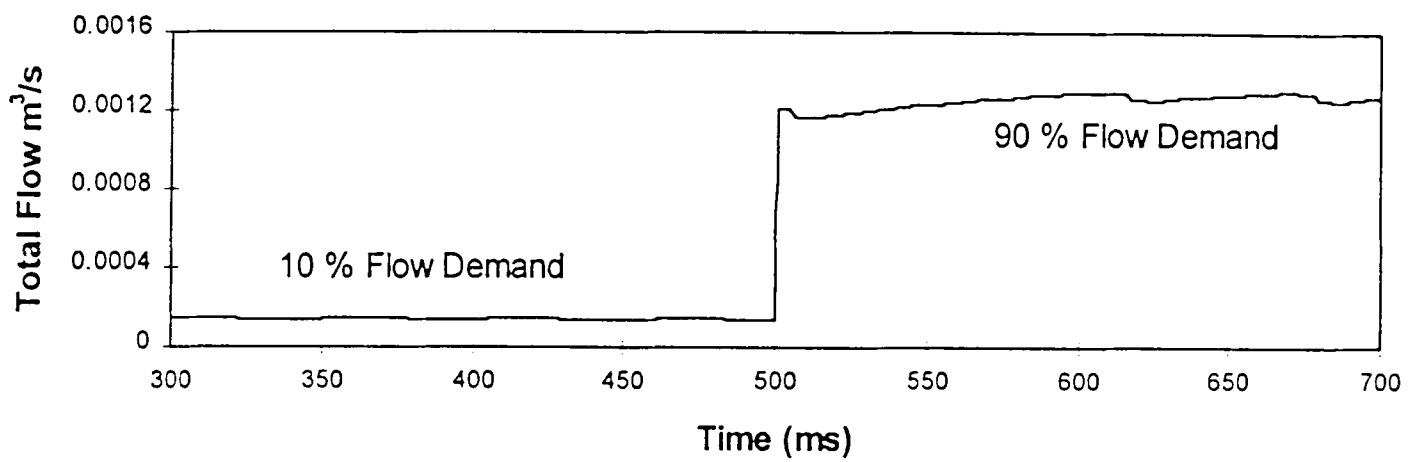
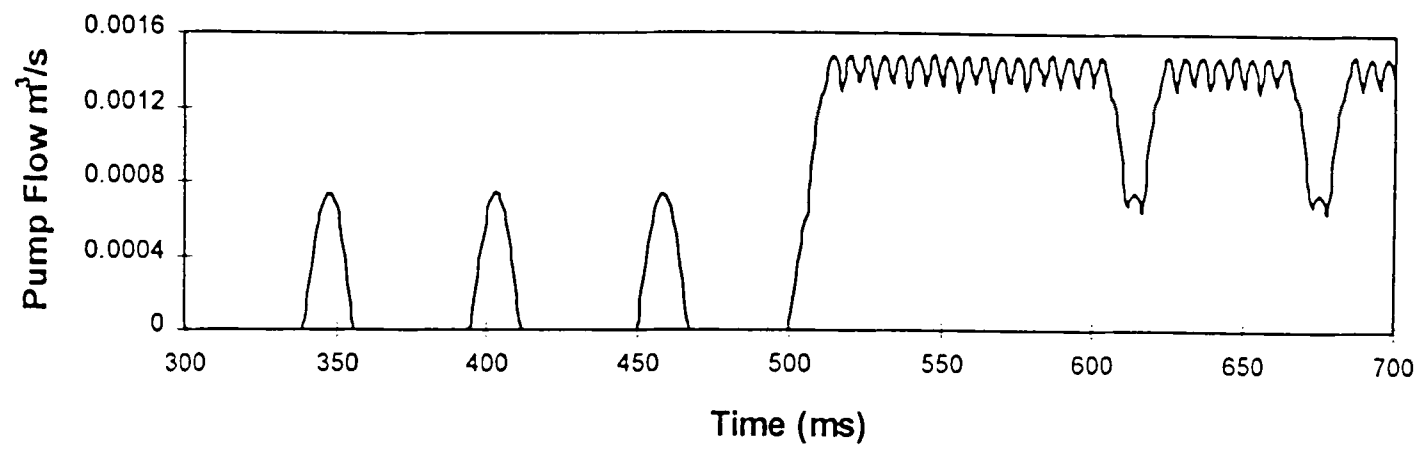


Figure 5.7 : Pump response at 10% to 90% step rise of flow demand at a constant speed (pressure-control mode)

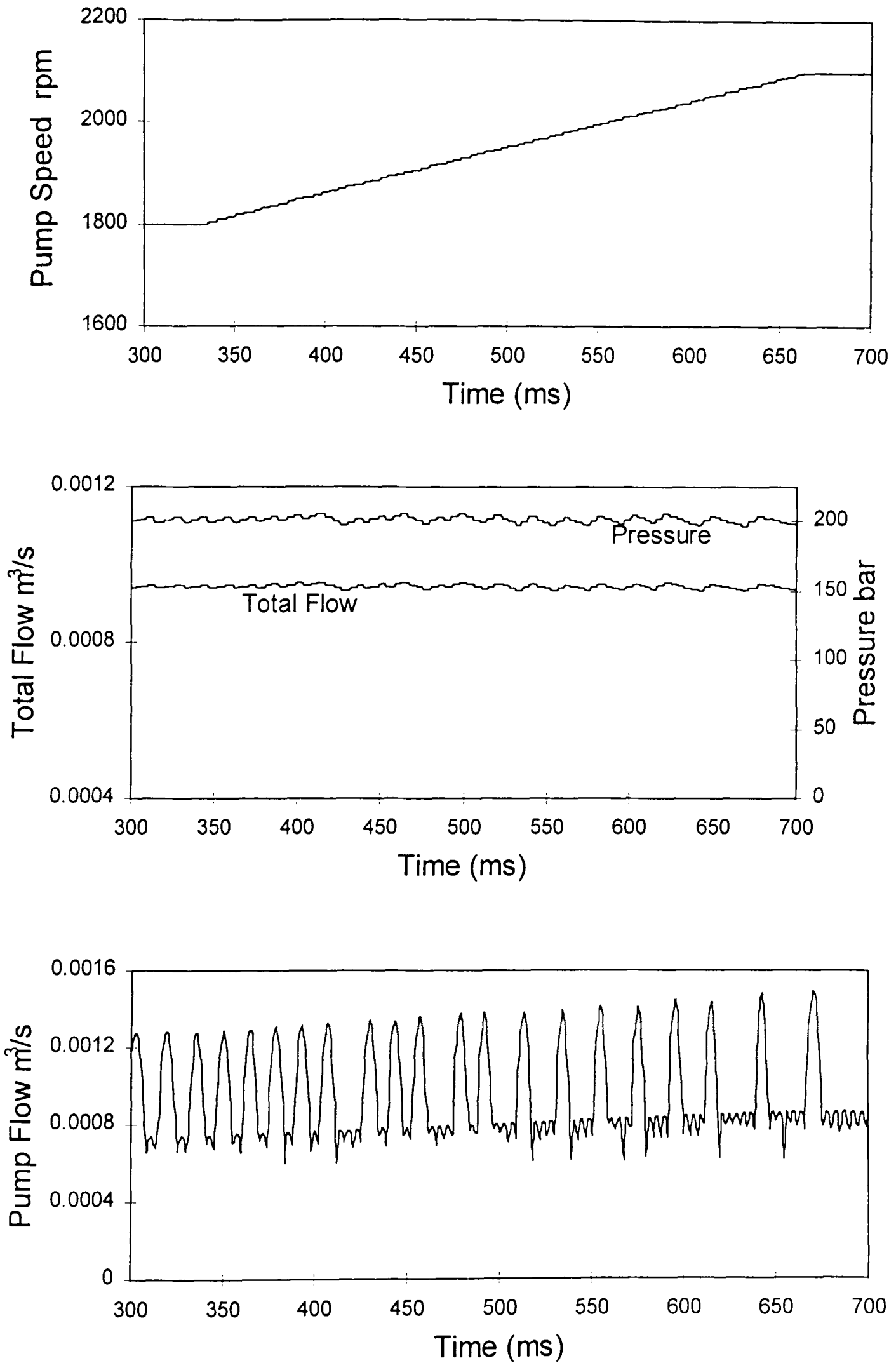


Figure 5.8 : Pump response to 17% speed change, while the flow demand remains constant (pressure-control mode)

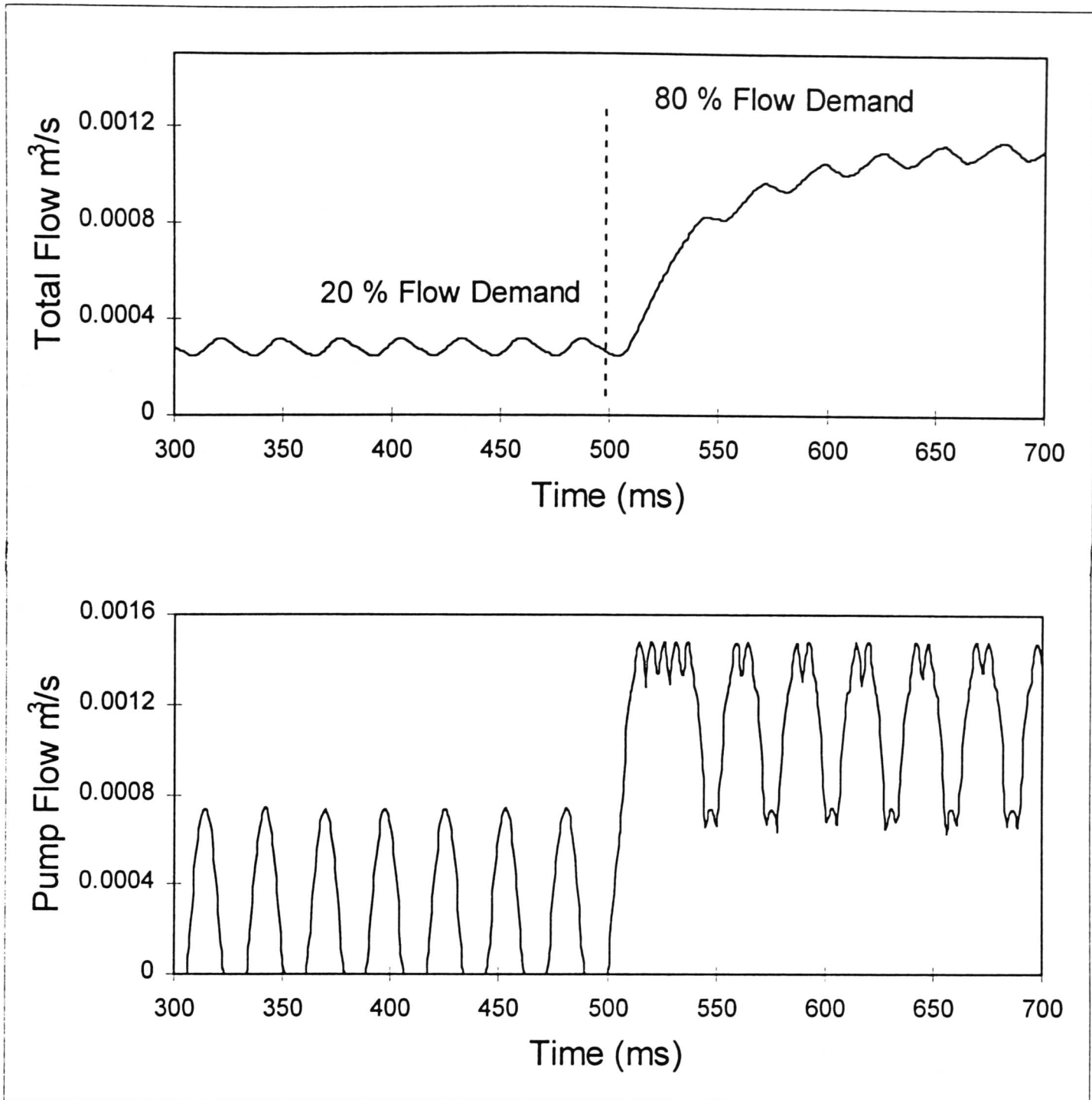


Figure 5.9 : Pump response at 20% to 80% step rise of flow demand, at a constant speed (Flow-Control Mode).

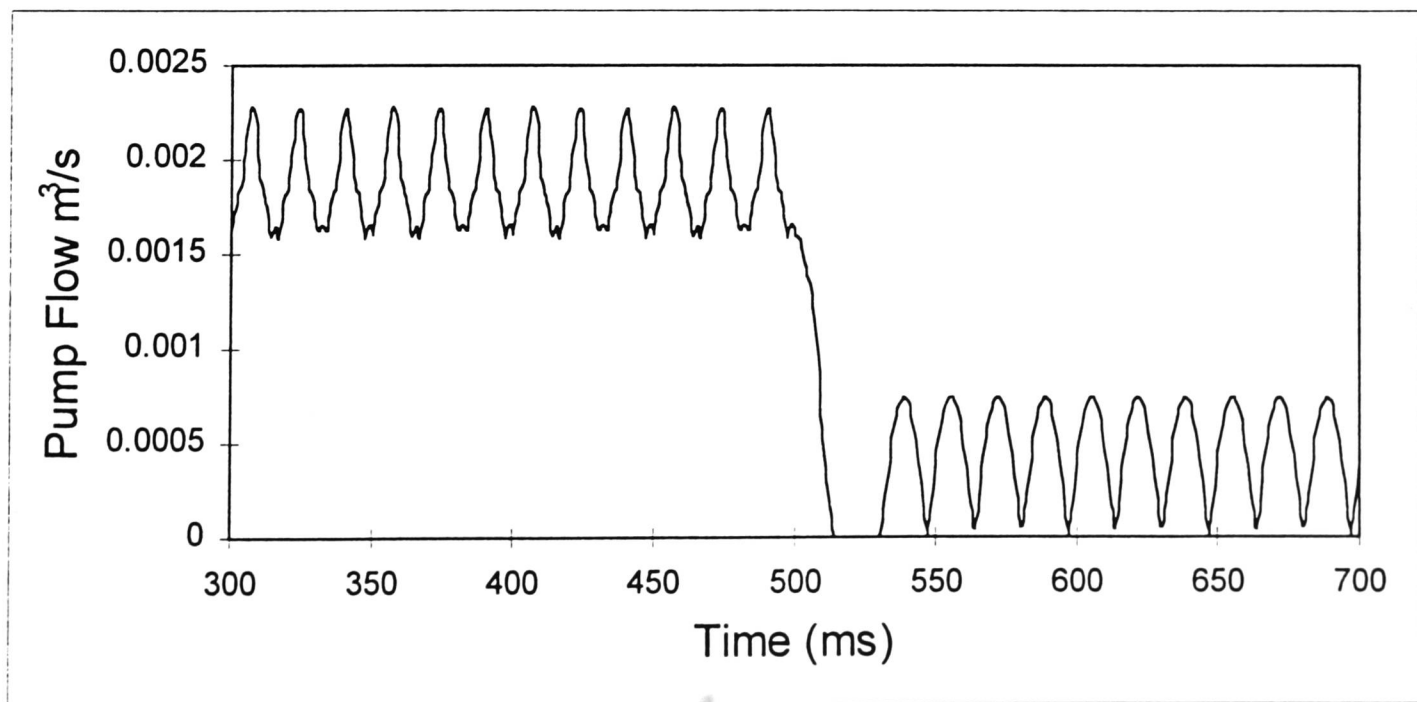


Figure 5.10 : Pump response at 80% to 20% step fall of flow demand, 10 cylinder pump running at 1800 rpm (Flow-Control Mode).

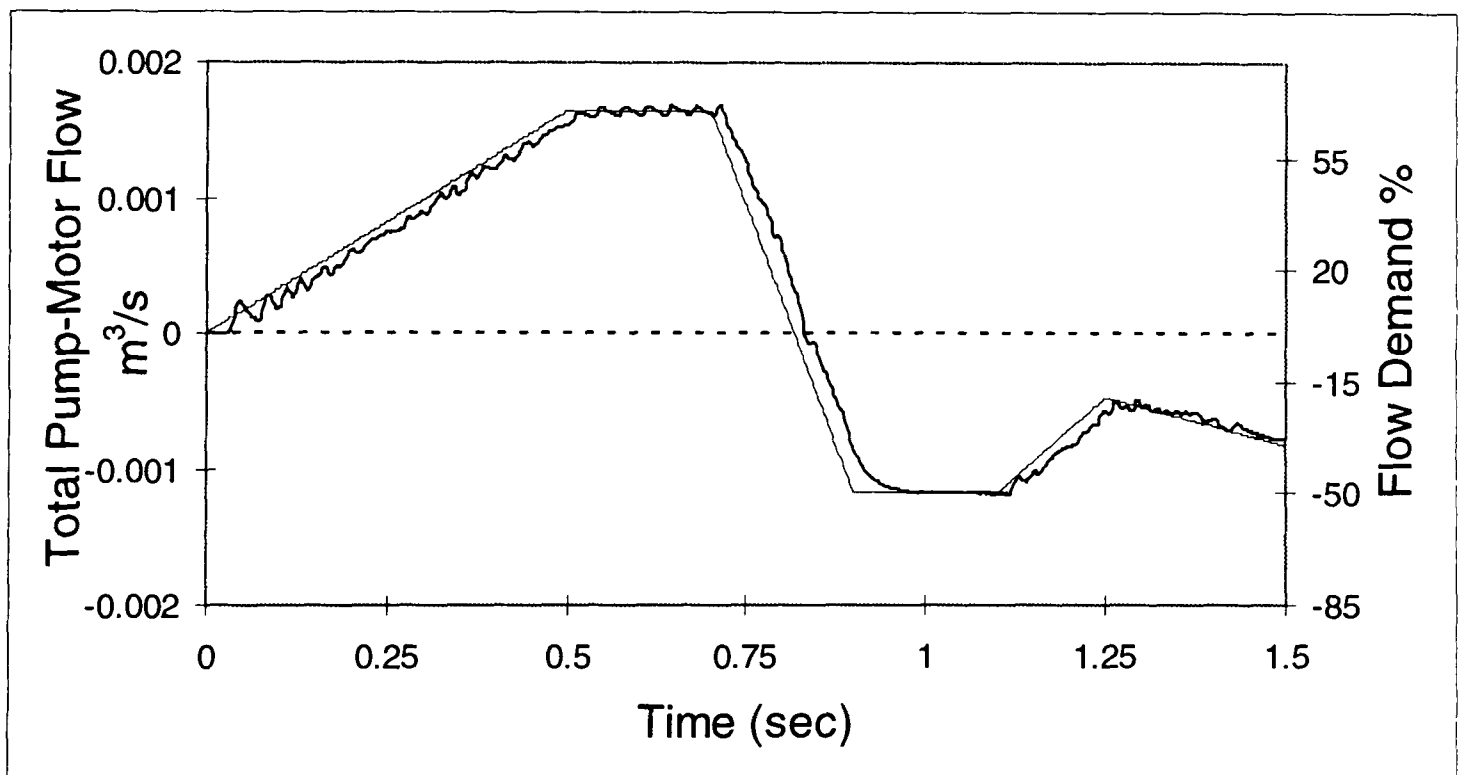
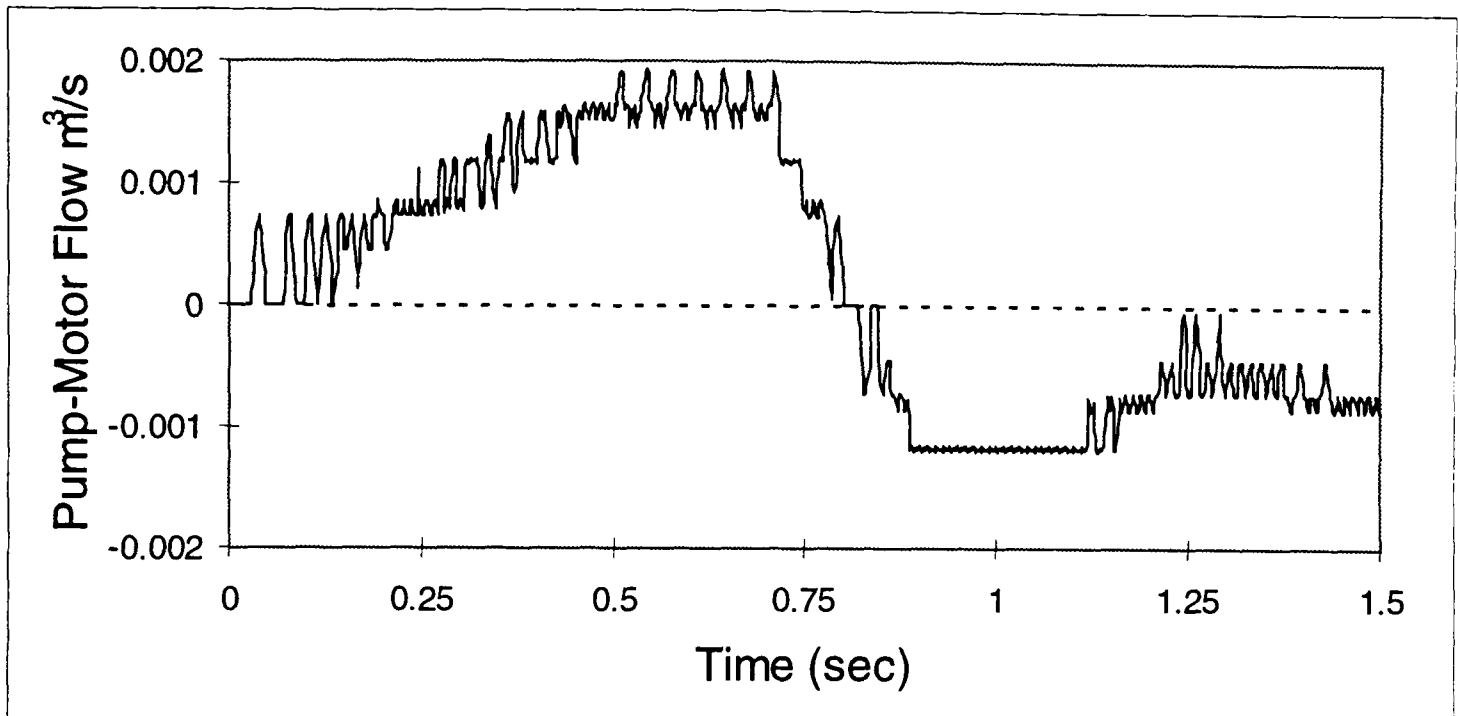


Figure 5.11 : 10 cylinder Pump-Motor following a variable demand curve, at 1800 rpm (Flow-Control Mode)

Figure 5.8 shows the pump response to a speed change from 1800 rpm to 2100 rpm, over a time of 0.33 sec. All other pump parameters are unchanged. At higher speed the time for each cylinder stroke is reduced, which is compensated by higher flow velocities as the displaced volume per cylinder is the same. To maintain the flow demand cylinder enabling becomes less frequent at higher speed, as can be seen in the spacing between the peaks.

Figure 5.9 shows the response of a pump under flow-control, having an initial demand of 20% which is then step increased to 80%. The same six cylinder pump, running at 1800 rpm and driving a constant pressure resistive load, was used for the model. The accumulator was considered as a moving averaging device for flow. The flow ripple can be reduced by increasing the number of cylinders as well as the speed. Figure 5.10 shows the pump flow with a 10 cylinder machine, having same cylinder-size, at 1800 rpm. Figure 5.11 shows the 10 cylinder pump-motor following a variation of positive (pumping) and negative (motoring) flow demands, while running at 1800 rpm.

Unlike conventional machines, banks of radial pump-motors can be combined along a common shaft and used as a summing junction of both torque and power, whilst providing isolation between services. One or more accumulators may be used in conjunction with some of these services, allowing the storage of power in the system. The radial configuration provides good force balancing and gives an optimal layout for the mechanical components like valves and bearings. Two examples (of opposite nature), showing application of this technique have been published (Ehsan et al. 1995; 1996).

5.6 Principle of using the digital-displacement technique for achieving desired piston motion in the Artemis-Malone engine

In most of the reciprocating heat engines the piston motion is generated through crank-slider arrangement and hence is inherently nearly sinusoidal in nature. The phase relationship between different moving parts are subjected to a fixed pattern as all motions are interrelated in a fixed way. The use of digital-displacement pump-motor

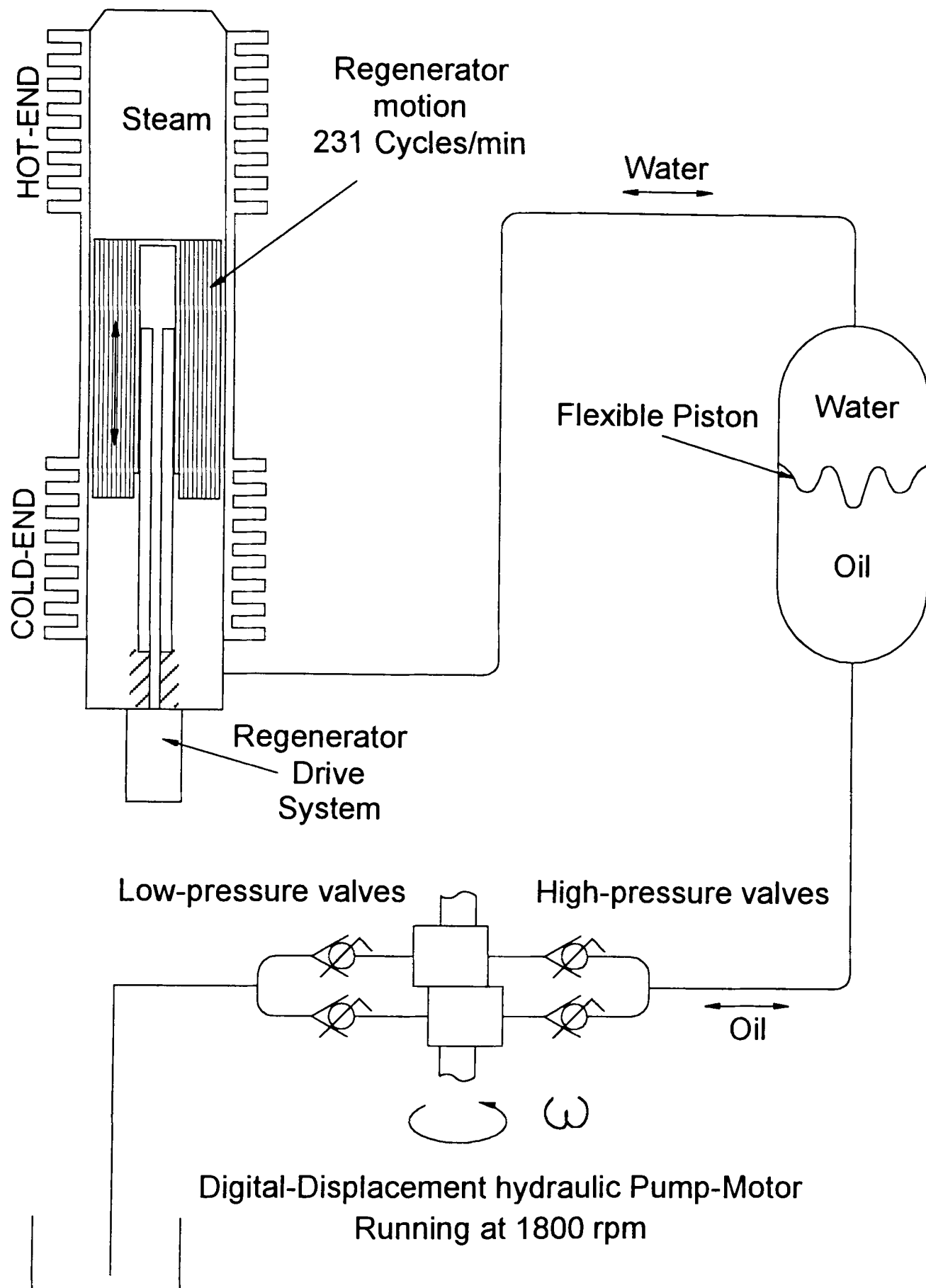


Figure 5.12 : Schematic presentation of the arrangement of digital-displacement hydraulic drive for generating piston motion in an Artemis-Malone module.

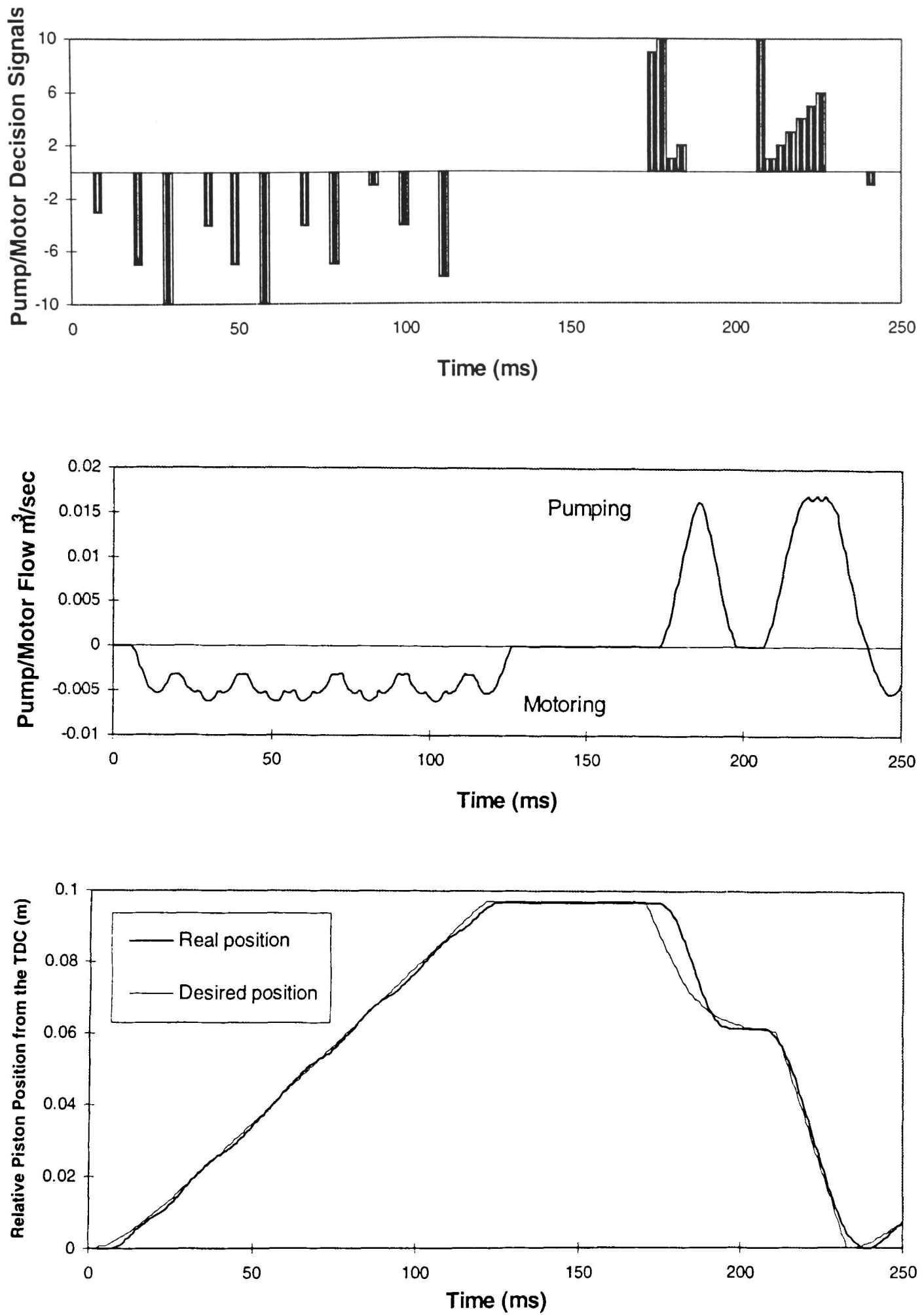


Figure 5.13 : Typical enabling decision, pump-motor flow and resulting piston motion curve trying to match a desired motion.

as a hydraulic drive overcomes these limitations and allows independent motions of different profiles and phase relationships. To generate any smooth piston motion a sufficiently large number of pumping or motoring cylinders must be available during one cycle of piston motion. This can be achieved by running the pump-motor at a much faster speed compared to piston and while also having greater cylinder numbers in the pump-motor.

Figure 5.12 shows the working principle of the flexible piston arrangement with the thermodynamic pile of a Malone module. As described in chapter three, the power stroke of a thermal module forces water out of cold-end of the working volume and the hydraulic drive unit is signalled to motor. This causes the contraction of the flexible tube, forcing oil out through the hydraulic motor. On the other hand during a pumping stroke the hydraulic unit is signalled to pump, putting oil into the elastomeric tube (flexible piston). This causes it to inflate, forcing more water into the thermodynamic pile, raising the pressure. Figure 5.13 shows a typical piston motion curve generated by the digital-displacement hydraulic drive. The pumping and motoring decision signals are assigned such that, the piston motion resulting from the pump-motor flow tries to match a desired piston motion curve. A limitation of the piston motion curve is that it is generated from the resolution of one cylinder volume as only an entire cylinder can be pumped or motored.

CHAPTER 6

Simulation of Theoretical Engine Cycles in the Time Domain

6.1 Concept of relative motions of different components

The static model of the Artemis-Malone engines provides an estimate of component dimensions, performance and functional limits, but it provides little information about the relative motions of regenerator-displacer and the flexible-piston of the hydraulic drive. These relative motions mainly control the system pressure and hence the type of thermodynamic cycle the engine will produce. Modelling of the motions of the two reciprocating elements and the resulting engine cycles is necessary to study and develop control strategies for the engine. This chapter describes the time-domain modelling of an engine with features estimated by the MathCad model in chapter four. The dynamic simulation package (MATRIXx) employed for the pump-motor modelling was also used for the time domain simulations of engine cycles.

The time-domain model is based on a number of assumptions, some of which originate from the static model described in chapter four. These include :

- (i) For a steady cycle a certain rate of heat passes from the combustion gases into the thermodynamic pile. A part of the heat is converted to useful work and the rest is rejected to the cooling water sink.
- (ii) At any instant of the cycle, the temperature inside the hot-end and the cold-end are maintained at nearly constant levels T_H and T_C .
- (iii) Fluid passes in between the hot-end and cold-end spaces through the regenerator-displacer as it is moved. At any instant during the cycle a fixed temperature gradient is maintained by the fluid inside the regenerator-displacer.
- (iv) The density of cold water connecting the TD pile and the flexible piston (separator membrane) varies very little with pressure and hence has insignificant

effect on the variation of cycle pressure. Hence its effect can be neglected for calculating cycle pressure variations.

- (v) At any instant during the cycle the total mass of fluid inside the thermodynamic pile, to the flexible piston (ie. the combined hot-end, cold-end and the regenerator-fluid mass) remains constant.
- (v) The pressure drop across the regenerator-displacer is negligible (less than 3 bar).

Figure 6.1 shows a schematic drawing of the mass components. Henceforth the term regenerator will be referred to the regenerator-displacer (or regn. in abbreviation) for convenience. The reference locations of the TD pile used to show the regenerator and piston motions in figure 6.1 are followed later (same as in figure 3.1). The total fluid mass inside the sealed system can be divided into three components. The fluid mass present inside the hot-end (M_{hot}) has two components, one of which is a dead volume. This does not vary throughout the cycle (eg, space in between steam-fins and clearance volumes in the inner side of the hot-end). The other part of hot-mass is contributed from the space created as the regenerator-displacer moves. Similarly, the fluid making up the cold-mass (M_{cold}) also has swept and dead volume components. The swept volume varies as the regenerator and the flexible piston are moved. The remaining mass component is that of the fluid inside the porous regenerator (M_{regn}). As the fluid temperatures inside the two ends and the hence the gradient through the regenerator is considered to remain unchanged throughout the cycle, the mass of each component is a function of system pressure, while the sum of them remains constant. As the total mass of the different components is constant at any point of the cycle, the new system pressure can be solved as the regenerator and/or the flexible piston moves. An implicit closed algebraic loop solver was needed to calculate the new system pressure. This was done using the "Stiff System Solver" of the simulation software, which is mainly based on Newton-Raphson iteration method (Petzold, 1983). In general the relative contribution of hot-mass and regenerator-fluid-mass compared to the total, increases with higher system pressure.

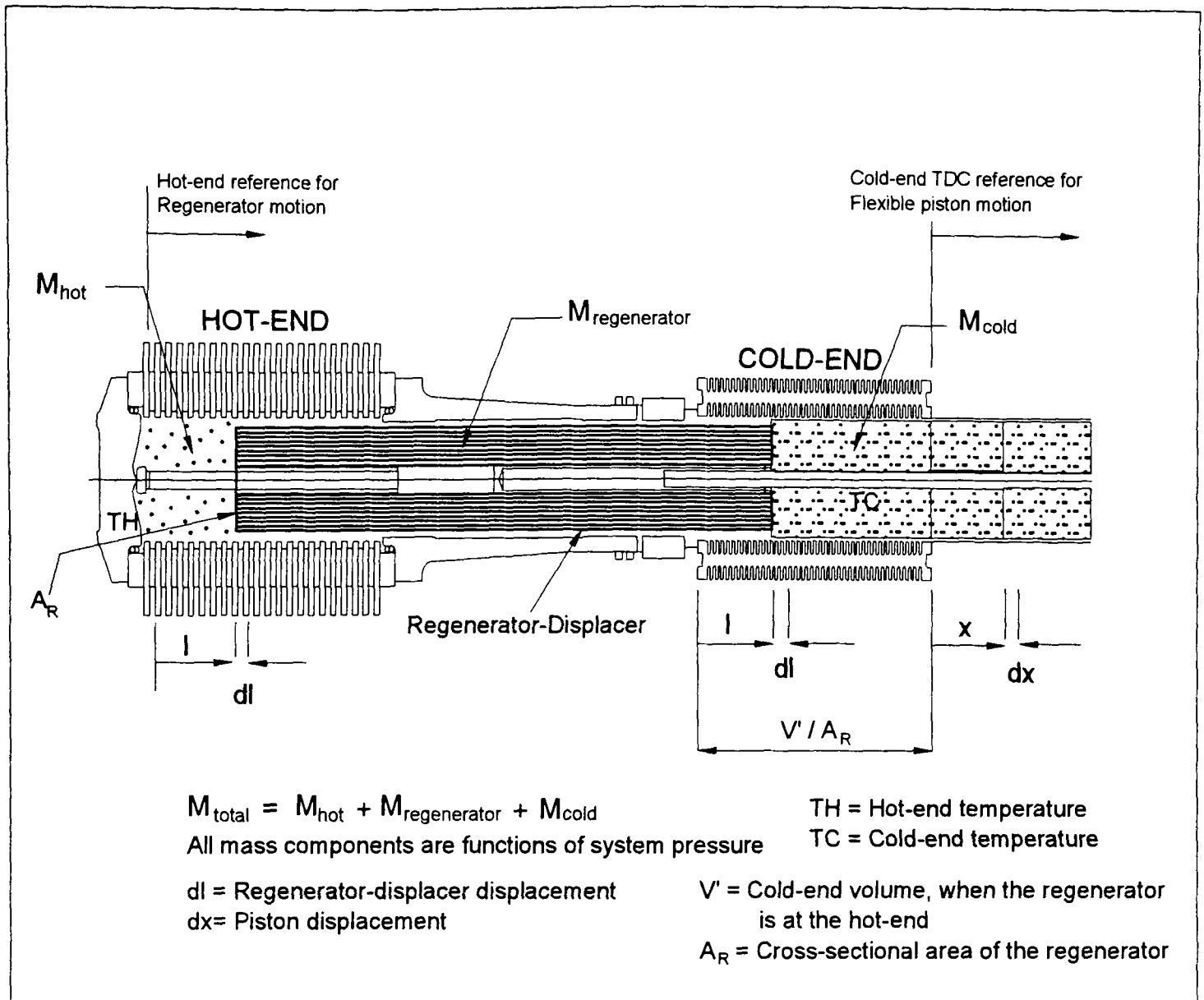


Figure 6.1 : Component of masses in the system

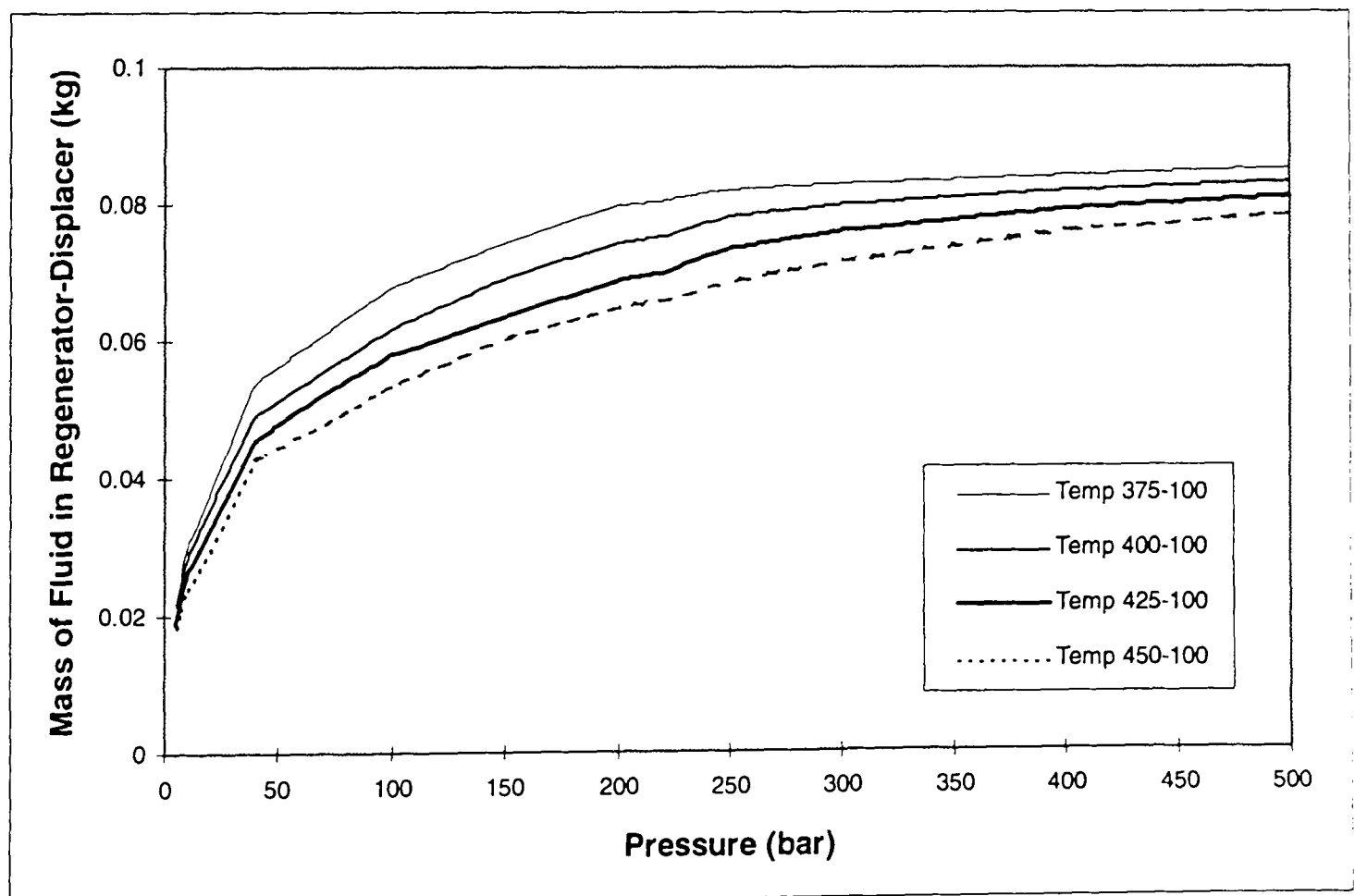


Figure 6.2 : Variation of fluid mass inside the regenerator with pressure. Linear temperature gradients of fluid considered are 450,425,400 and 375°C to 100°C.

6.2 Mass of fluid in the regenerator

To solve the closed loop for system pressure with each new position of the regenerator and piston, a method to calculate the fluid mass inside the regenerator is needed. The mass of fluid inside the regenerator is a function of the temperature distribution of the fluid across it and the system pressure. Calculations relating to the fluid inside the regenerator are difficult because of the large temperature gradient and consequent change of conditions or phases along its length. To complicate matters these may be continuously changing as the regenerator moves between the two ends. In the modelling of the flow through the regenerator constant fluid temperatures are assumed at each end with a fixed temperature gradient of the fluid through the regenerator length. The regenerator is considered to be composed of a number of small disc-like elements perpendicular to the axis of translational motion. So the summation of the fluid masses of all these small sections, each held at a particular temperature, provides a good approximation of the entire fluid mass. Figure 6.2 shows the variation of fluid mass inside the regenerator with pressure, as different levels of temperature gradient are maintained across it. It is difficult to find the exact nature of this temperature gradient and it may be varying through a cycle as the pressure changes. A sensitivity study for linear and an arbitrary non-linear considerations of temperature gradient as in figure 6.3 shows that the variation of regenerator fluid mass for different profiles of temperature gradient is small compared to the total mass (less than 4%) and hence does not change the engine cycle significantly. The arbitrary non-linear distribution is chosen on the assumption of phase changes in the central segments of the regenerator, decreasing the gradient at the middle.

Figure 6.4 shows a flow chart of the programmes used for calculating the cycle pressure. Temperatures at the hot and cold-ends, temperature distribution of the fluid inside the regenerator and cycle pressure provide fluid densities at each different section from a steam-property look-up table. The regenerator and piston motions and the density information are used for calculating the mass components. The desired regenerator motion is defined (as a signal generation block), while the corresponding piston motions are calculated using boolean logic as shown later (section 6.3 - 6.4). The

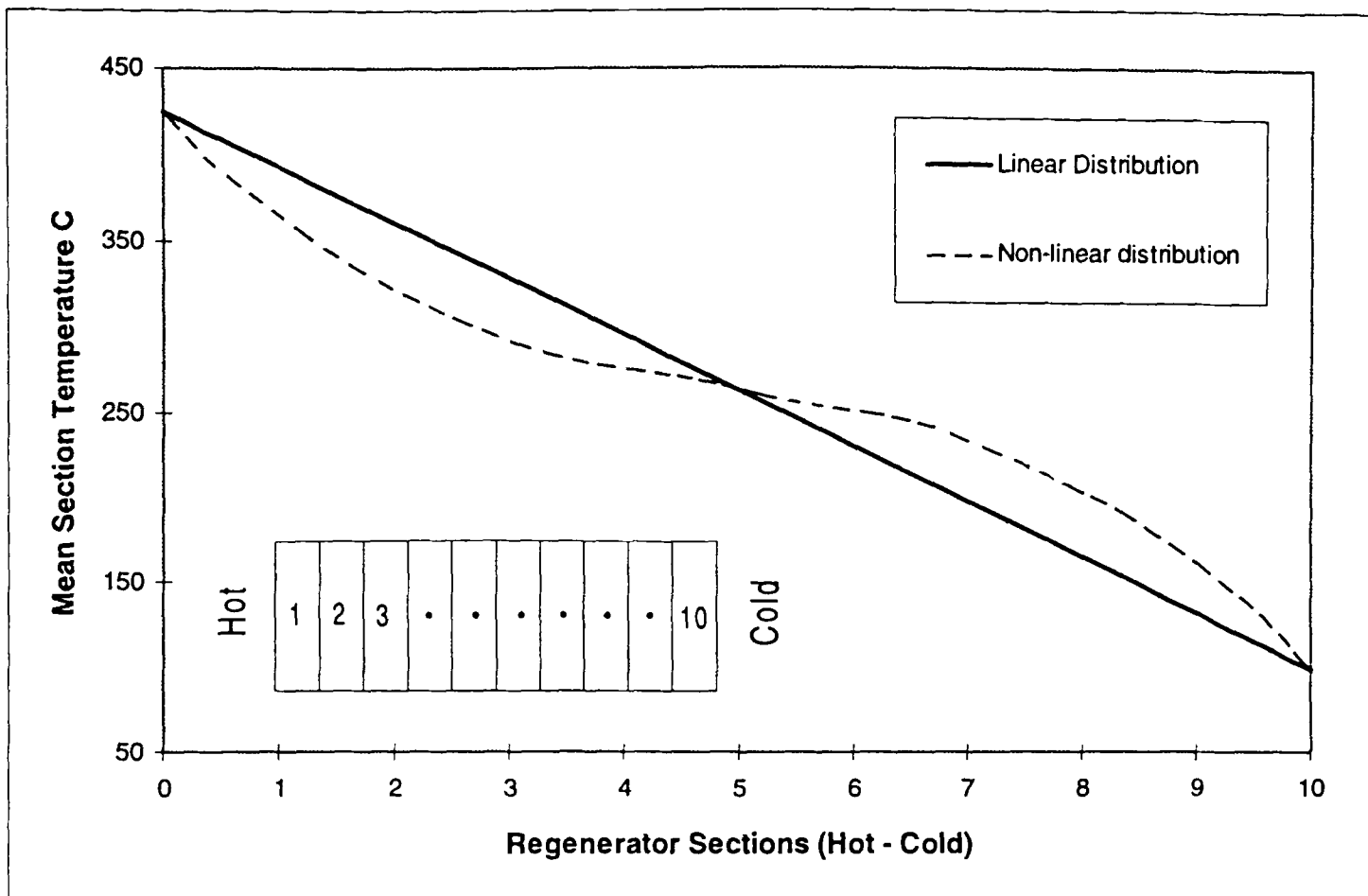


Figure 6.3a : Consideration of linear and an arbitrary non-linear temperature distributions of fluid inside the regenerator.

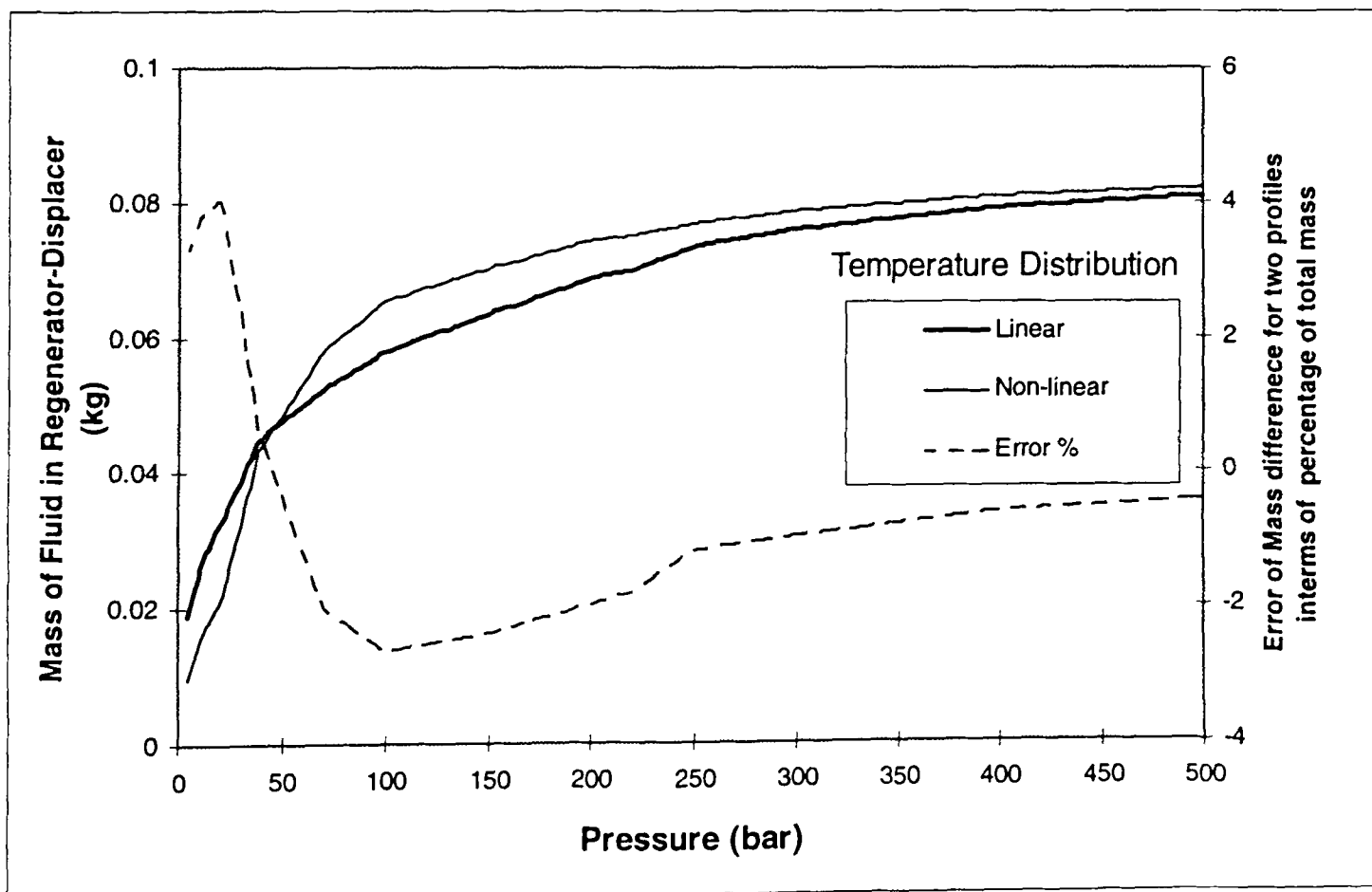


Figure 6.3b : Variation of fluid mass inside the regenerator for linear and non-linear (as shown in figure 6.3a) temperature gradients of 425 to 100 °C. Variation of fluid-mass inside the regenerator for different profiles of temperature gradient is small compared to the total mass.

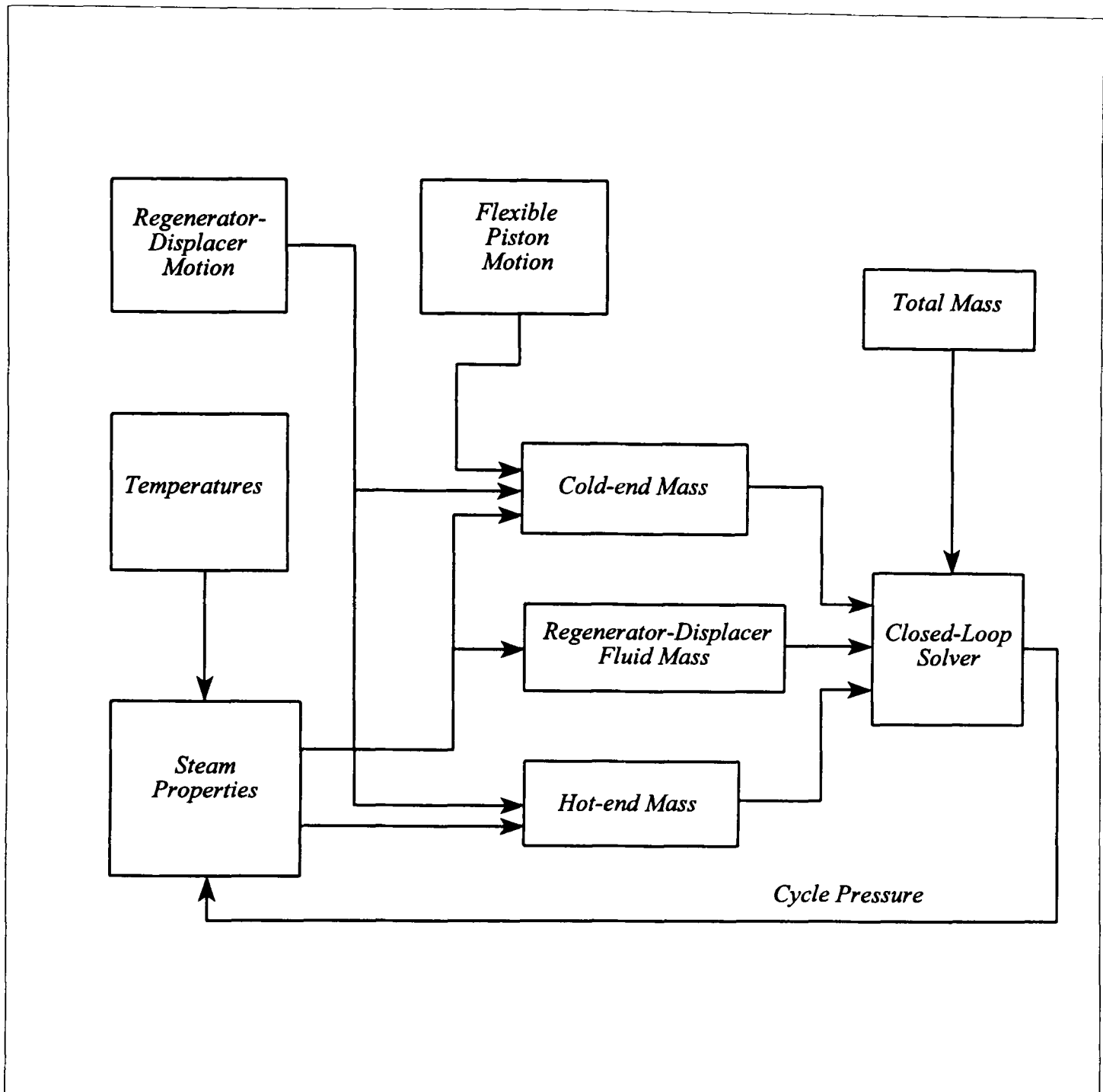


Figure 6.4 : Simulation programme flow-chart for determining cycle pressure.

cycle pressure needed to be solved using a closed-loop solver. The main problems found in developing the programme was the proper initialization of the cycle pressure value at the starting of the closed-loop solution. Activation of some data holding blocks for the first run of the simulations finally solved this problem. The Stiff-system-solver proved to be robust in general, although in some cases the relative tolerance and the maximum iteration numbers needed to be altered to get converging solutions.

6.3 Effect of the relative motion profiles on system pressure

The relative motions of the regenerator and the flexible piston control the pressure generation and hence the pattern of the engine cycle. In general the relative motions can be grouped into three categories :

- (i) When only the regenerator is moving, pressure rises as it moves from the hot-end reference (figure 3.1 and 6.1) towards the cold-end and vice-versa, while the piston is stationary.
- (ii) When only the flexible piston is moving, pressure rises as the piston moves towards the cold-end reference (ie. the flexible membrane is inflated) and vice-versa, while the regenerator is stationary.
- (iii) If the regenerator is moving from the hot-end towards the cold-end and the flexible piston is contracting, then there is a certain ratio between these two motions where the pressure remains constant. The value of this ratio depends on the pressure level which is being maintained.
- (iv) A combination of opposite motions, eg. the regenerator moving towards the cold-end and the flexible membrane also inflating can cause a more rapid rise in pressure and vice-versa.

An expression of the particular ratio of the two motions can be deduced easily. Referring back to figure 6.1, where the summation of all mass components are shown, we may write :

$$M_{total} = M_{hot} + M_{regn} + M_{cold}$$

Where all the mass components are functions of pressure as the temperatures are considered to be held constant.

For any particular position of the regenerator and flexible piston this can be further defined as:

$$M_{total} = (V_{dh} + A_R \cdot l) \cdot \rho_h + M_{regn} + (V_{dc} + V' + A_R \cdot (x-l)) \cdot \rho_c$$

Where,

V_{dh} = Dead volume at the hot-end.

V_{ch} = Dead volume at the cold-end.

ρ_h = Fluid density at hot-end.

ρ_c = Fluid density at cold-end.

A_R = Cross-sectional area of the regenerator.

V' = Cold-end volume, when the regenerator is at the hot-end.

l = Regenerator position from the hot-end reference.

x = Piston position from the cold-end reference.

For a very small change in position (dl) of the regenerator, a corresponding change in piston position (dx) keeps the system pressure the same. As the cycle pressure and the temperature-gradient across the regenerator fluid are unchanged, the mass component inside the regenerator also remains the same. So the expression can be rewritten as:

$$M_{total} = (V_{dh} + A_R \cdot (l + dl)) \cdot \rho_h + M_{regn} + (V_{dc} + V' + A_R \cdot (x - l + dx - dl)) \cdot \rho_c$$

Where, dl = Change in regenerator position.

dx = Change in piston position.

Hence the relation between the two motions to maintain a pressure is :

$$dx = dl.K \quad \text{Where, } K = \frac{\rho_c - \rho_h}{\rho_c}$$

We can name this ratio (K) as the "*pressure-maintenance ratio*". As the densities depend on the pressure, hence the value of "*pressure-maintenance ratio*" may be different depending on the pressure level to be maintained.

6.4 Combination of motions resulting in different cycle-patterns

The combination of different motion sequences of the regenerator and the flexible piston can result in several patterns of engine cycle. The cycles can be divided into three categories, which can be listed as :

- (1) Piston-assisted pressure-rise and regenerator assisted pressure-fall cycle.
- (2) Regenerator-assisted pressure-rise and pressure-fall cycle.
- (3) Piston-assisted pressure-rise and pressure-fall cycle.

Cycles developed from theoretical motions are described in this section. In all cases the cycle simulation starts with the regenerator at the hot-end reference commencing its motion towards the cold-end, while the flexible piston is at the top-dead-centre (TDC) reference. In all of the descriptions the denotations PH and PL refers to the high-pressure and low-pressure levels chosen for the cycle, which eventually is set by the hot-end design.

6.4.1 Piston-assisted pressure-rise and regenerator assisted pressure-fall cycle

Here the system is at the higher limit of pressure, when the cycle begins. The relative motions can be divided into several zones:

- (a) If system pressure is rising above the desired upper limit of pressure ($P > P_H$).
and if the regenerator is moving from the hot-end towards the cold-end ($dl > 0$).
then the piston is moved (motored) at "*pressure-maintenance ratio*" relative to the regenerator motion ($dx = K \cdot dl$), to maintain a constant pressure.
- (b) If system pressure is in between the desired upper and lower limits of pressure ($P_H \geq P \geq P_L$).
and if the regenerator is moving from the cold-end towards the hot-end ($dl < 0$).
then the piston is kept stationary ($dx = 0$), allowing the pressure to fall.
- (c) If system pressure is falling below the desired lower limit of pressure ($P < P_L$).
and if the regenerator is moving from the cold-end towards the hot-end ($dl < 0$).
then the piston is moved (pumped) at "*pressure-maintenance ratio*" relative to the regenerator motion ($dx = K \cdot dl$), allowing the pressure to be maintained.
- (d) If the regenerator is stationary ($dl = 0$)
and if the piston is not back to the reference at the starting of the cycle.
then the piston is moved at a fixed velocity (pumped at a fixed rate), so that the piston is brought back to the starting reference at the end of the cycle, resulting in the pressure to be raised to the upper limit again.

Figures 6.5 -6.7 show the relative motions, the P-V diagram and variation of mass components through the cycle. The cycle is designed for about 14-15 kW indicated power output per module, giving 55 kW for an engine with four modules.

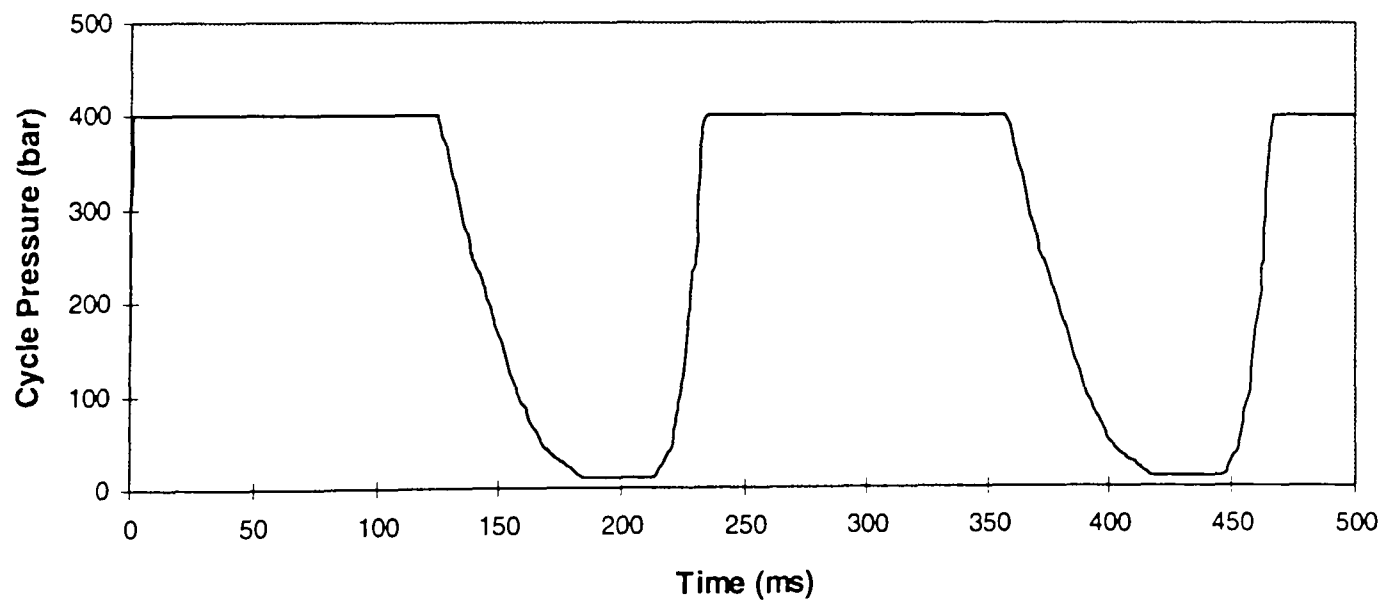
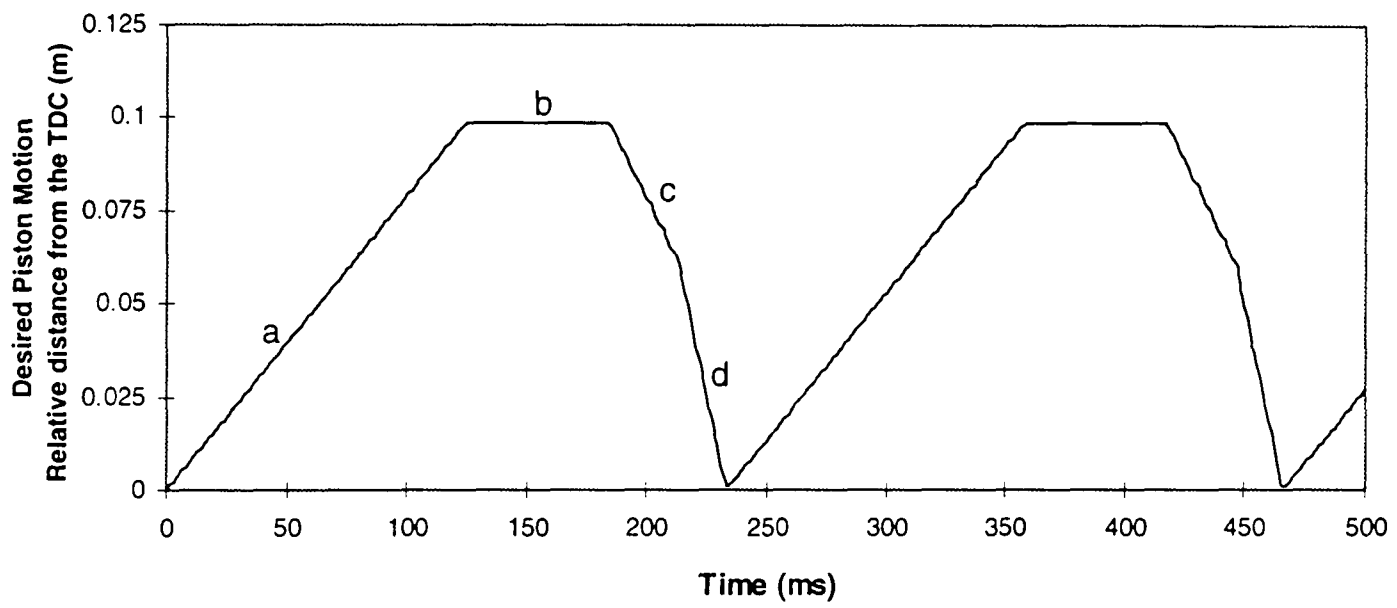
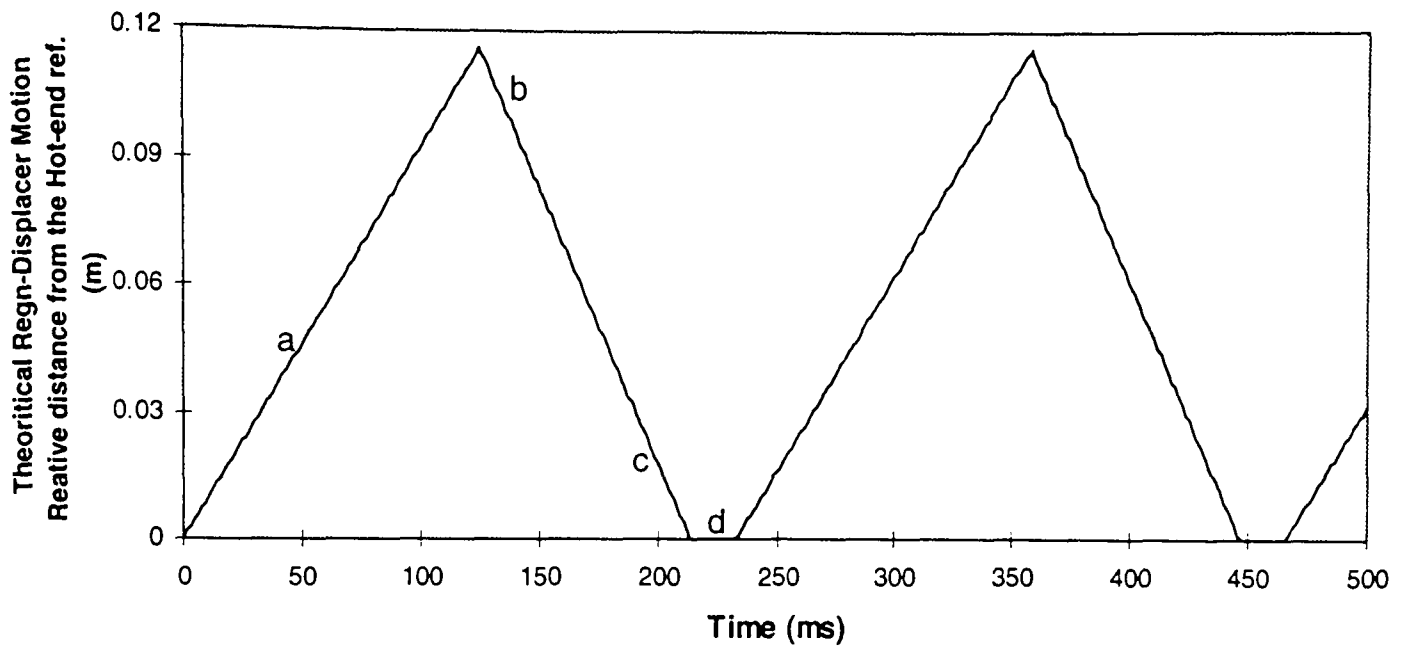


Figure 6.5 : Motion of regenerator and desired piston motion resulting in the cyclic pressure variation.

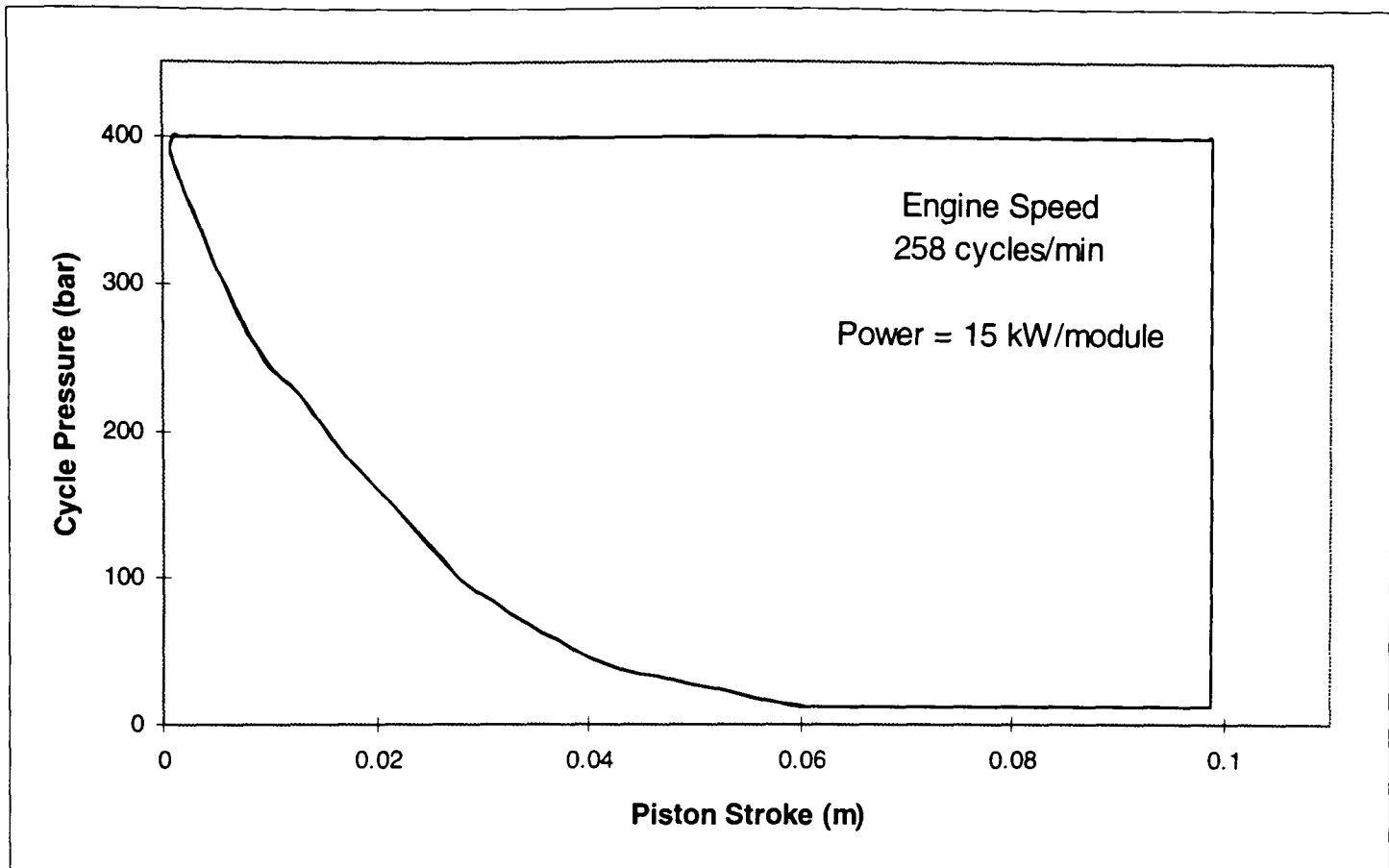


Figure 6.6 : P-V diagram of the cycle (piston assisted pressure rise and regenerator assisted pressure fall).

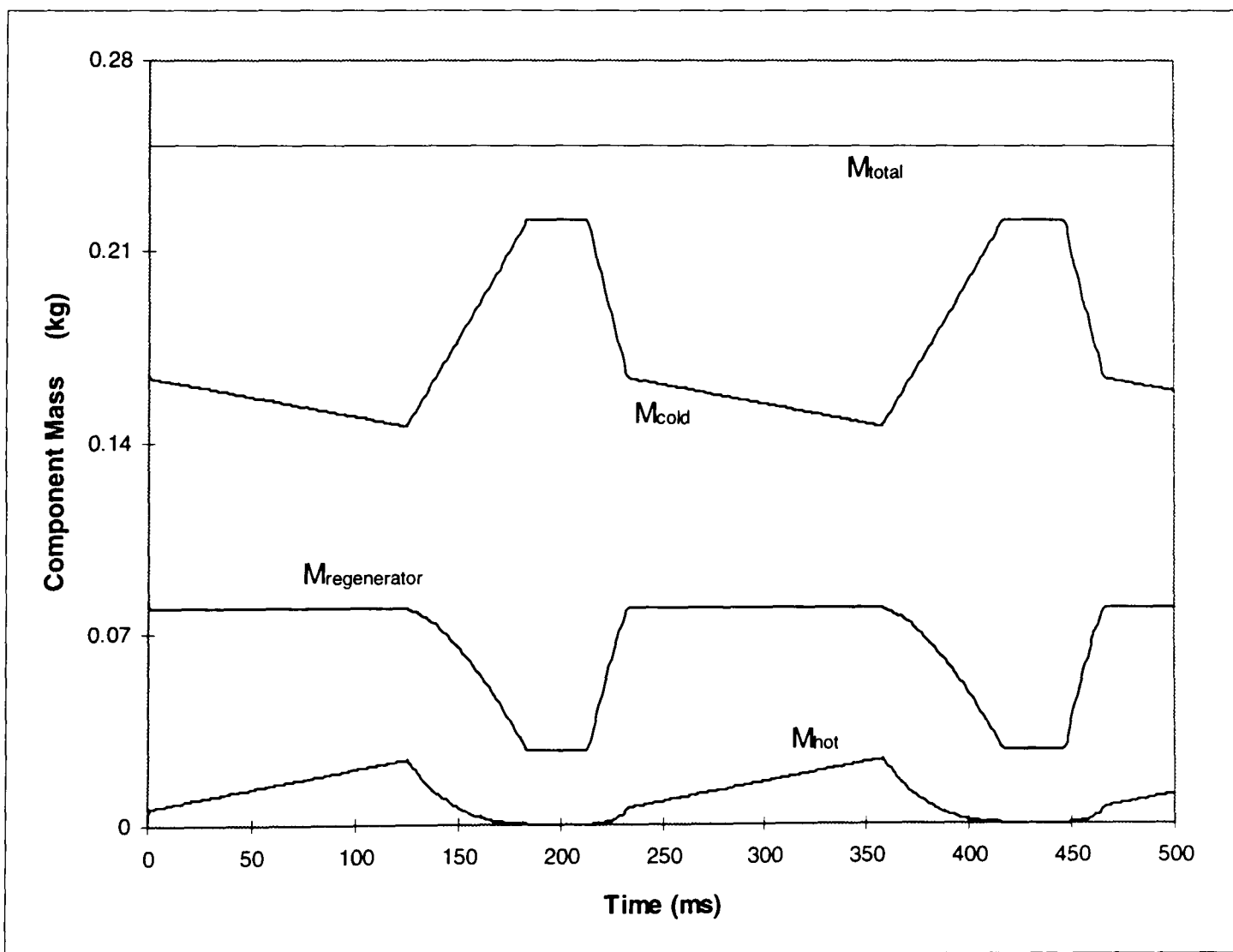


Figure 6.7 : Variation of different mass components with cycle pressure, while the total-mass remains the same.

6.4.2 Regenerator-assisted pressure-rise and pressure-fall cycle

Here the system is at the lower limit of pressure, when the cycle begins. The relative motions can be divided into several zones:

- (a)** If system pressure is within the upper and lower limit of pressure ($P_H \geq P \geq P_L$).
and if the regenerator is moving from the hot-end towards the cold-end ($dl > 0$).
then the piston is kept stationary ($dx = 0$), allowing the pressure to rise up to the desired upper limit.
- (b)** If system pressure is rising above the desired upper limit of pressure ($P > P_H$).
and if the regenerator is moving from the hot-end towards the cold-end ($dl > 0$).
then piston is moved (motored) at "*pressure-maintenance ratio*" relative to the regenerator motion ($dx = K \cdot dl$), allowing the pressure to remain constant.
- (c)** If system pressure is within the upper and lower limits of pressure ($P_H \geq P \geq P_L$).
and if the regenerator is moving from the cold-end towards the hot-end ($dl < 0$).
then the piston is kept stationary ($dx = 0$), allowing the pressure to fall to the desired lower limit.
- (d)** If system pressure is falling below the desired lower limit of pressure ($P < P_L$).
and if the regenerator is moving from the cold-end towards the hot-end ($dl > 0$).
then piston is moved (pumped) at "*pressure-maintenance ratio*" relative to the regenerator motion ($dx = K \cdot dl$), allowing the pressure to remain at lower limit.

The results show a large drop in indicated power, relative to the previous cycle. This is caused by using a part of the stroke, when the regenerator moves from the hot-end to the cold-end, to raise the pressure. This reduces the effective length of the power stroke and hence the net work done in each cycle. Offsetting of the desired piston motion relative to the range through which it was moving for the previous cycle should also be noted. Figures 6.8 -6.10 show the relative motions, P-V diagram and variation of mass components throughout the cycle.

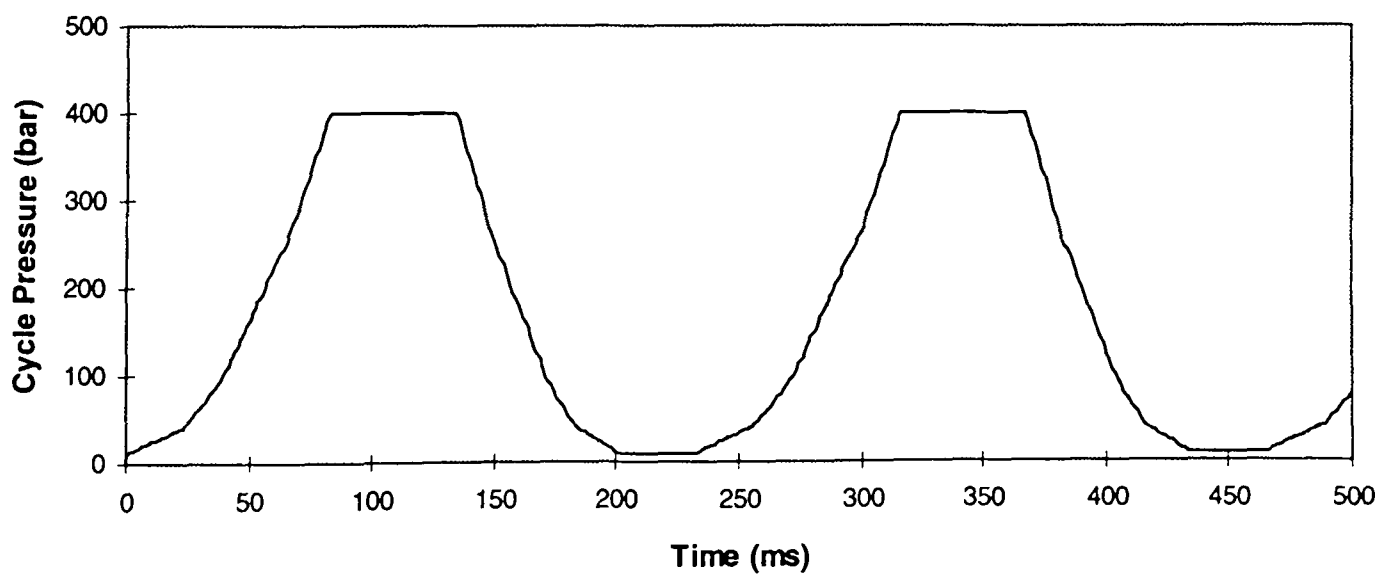
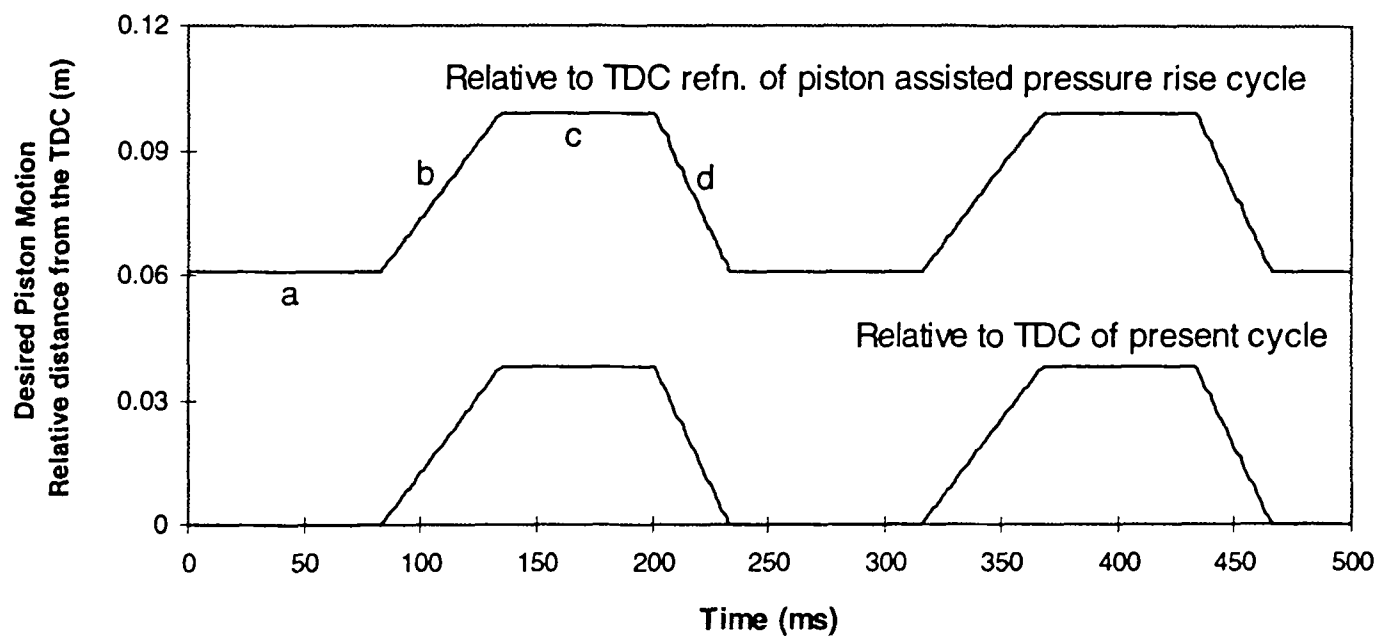
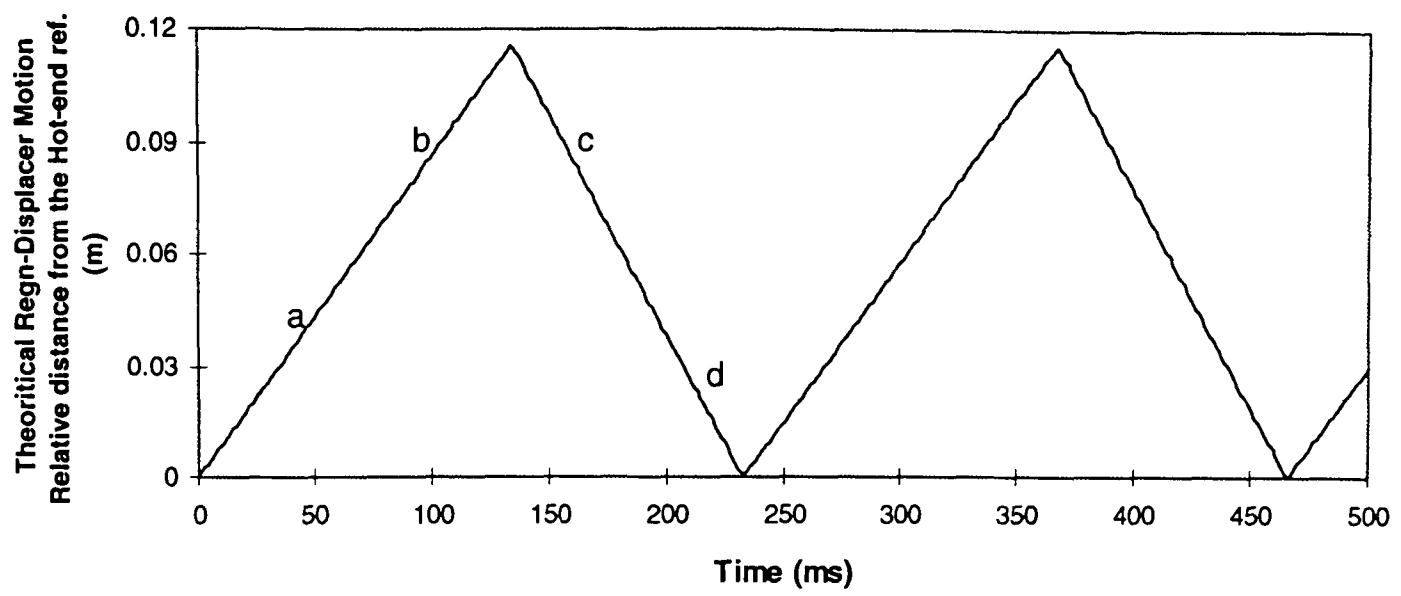


Figure 6.8 : Motion of regenerator and desired piston motion resulting in the cyclic pressure variation.

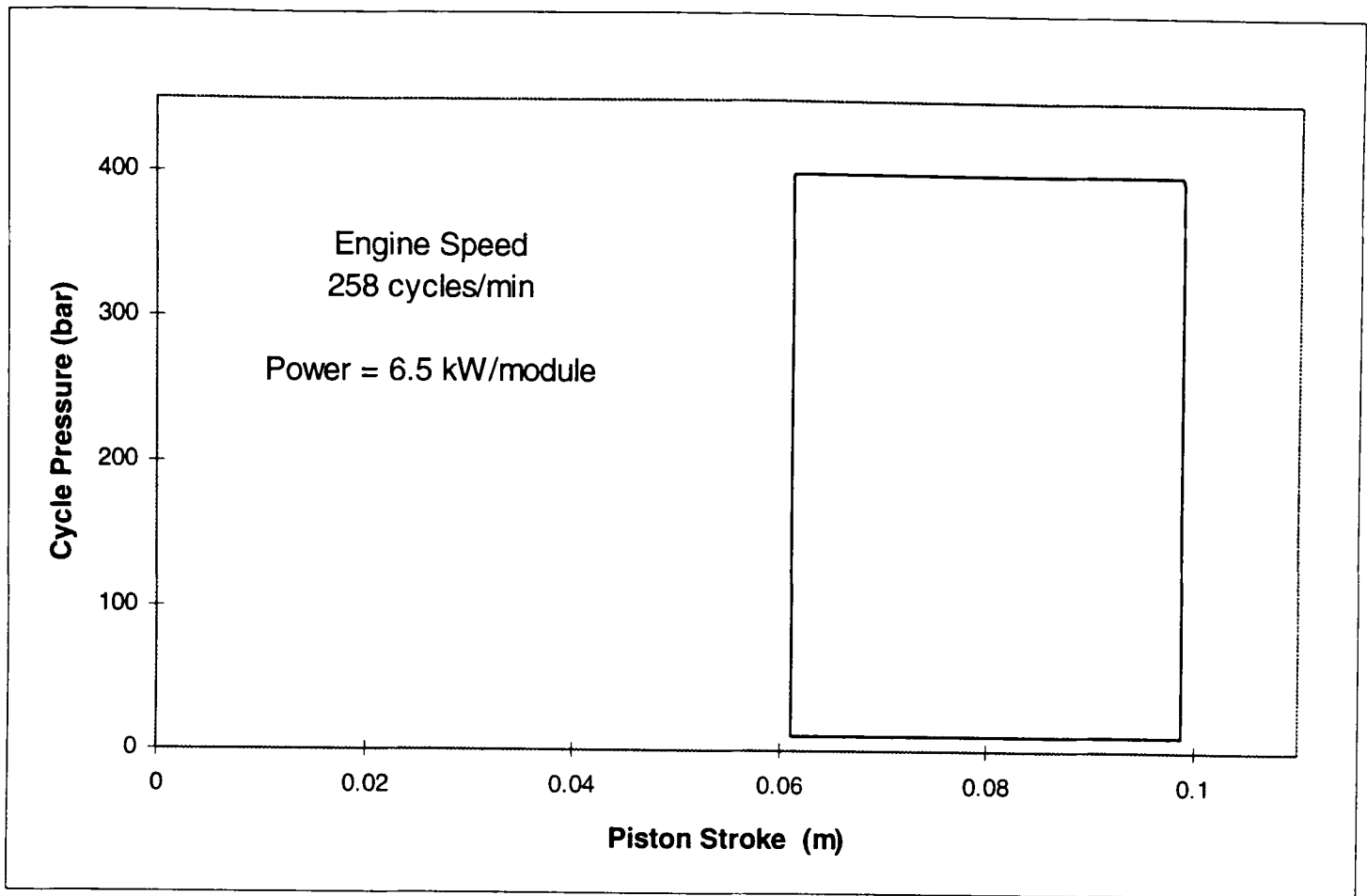


Figure 6.9 : P-V diagram of the cycle (regenerator assisted pressure rise and fall).

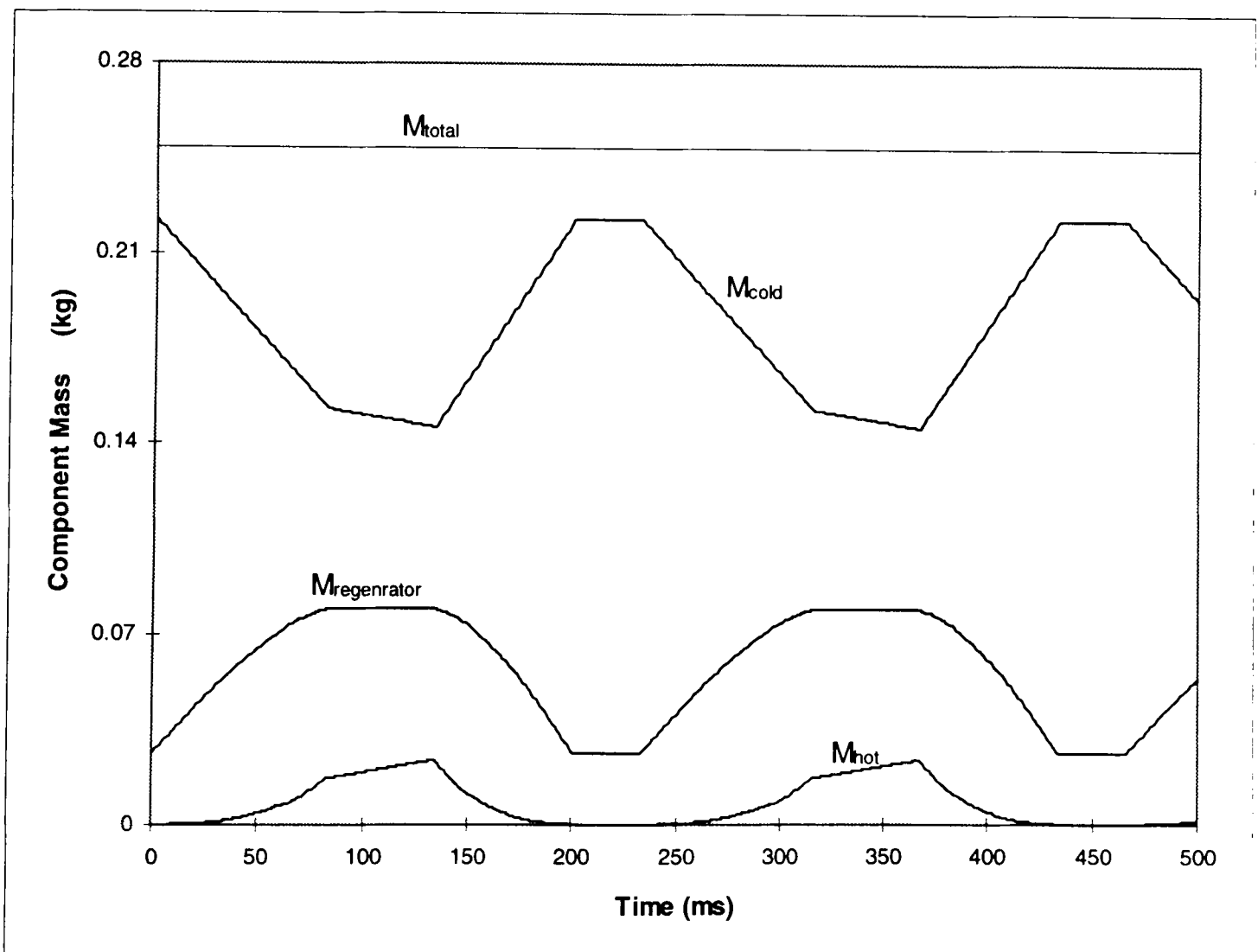


Figure 6.10 : Variation of different mass components with cycle pressure, while the total-mass remains the same.

6.4.3 Piston-assisted pressure-rise and pressure-fall cycle

Here the system is at the higher limit of pressure, when the cycle begins. The relative motions can be divided into several zones:

- (a)** If system pressure rises above the desired upper limit of pressure ($P > P_H$).
and if the regenerator is moving from the hot-end towards the cold-end ($dl > 0$).
then the piston is moved (motored) at "*pressure-maintenance ratio*" relative to the regenerator motion ($dx = K \cdot dl$), to keep the pressure constant.
- (b)** If system pressure is in between the upper and lower limits of pressure ($P_H \geq P \geq P_L$).
and if the piston position is above a certain specified value.
and if the regenerator is moving from the hot-end towards the cold-end ($dl > 0$).
then the piston is moved at a fixed velocity (motored at a fixed rate), faster than the previous motion in "*pressure-maintenance ratio*". Allowing the pressure to fall to a specified level as the regenerator stops in the cold-end.
- (c)** If system pressure is within the upper and lower limits of pressure ($P_H \geq P \geq P_L$).
and if the regenerator is moving from the cold-end towards the hot-end ($dl < 0$).
then the piston is kept stationary ($dx = 0$), allowing the pressure to fall to lower limit.
- (d)** If system pressure is falling below the desired lower limit of pressure ($P < P_L$).
and if the regenerator is moving from the cold-end towards the hot-end ($dl < 0$).
then the piston is moved (pumped) at "*pressure-maintenance ratio*" relative to the regenerator motion ($dx = K \cdot dl$), keeping pressure at the lower band of the cycle.
- (e)** If the regenerator is stationary ($dl = 0$).
and if the piston is not back to the reference at the start of the cycle.
then the piston is moved at a fixed velocity (pumped at a fixed rate), so that the piston is returned to the starting reference at the end of the cycle, causing the pressure to be raised to the higher limit once again.

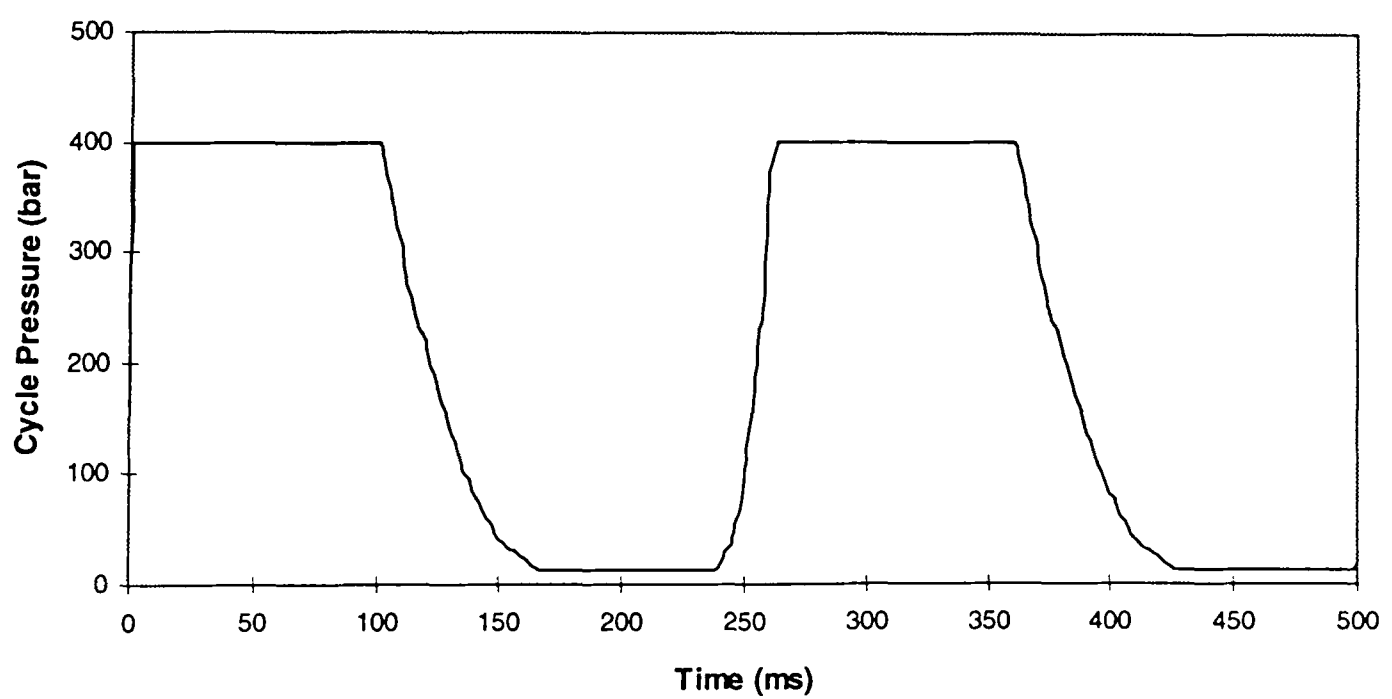
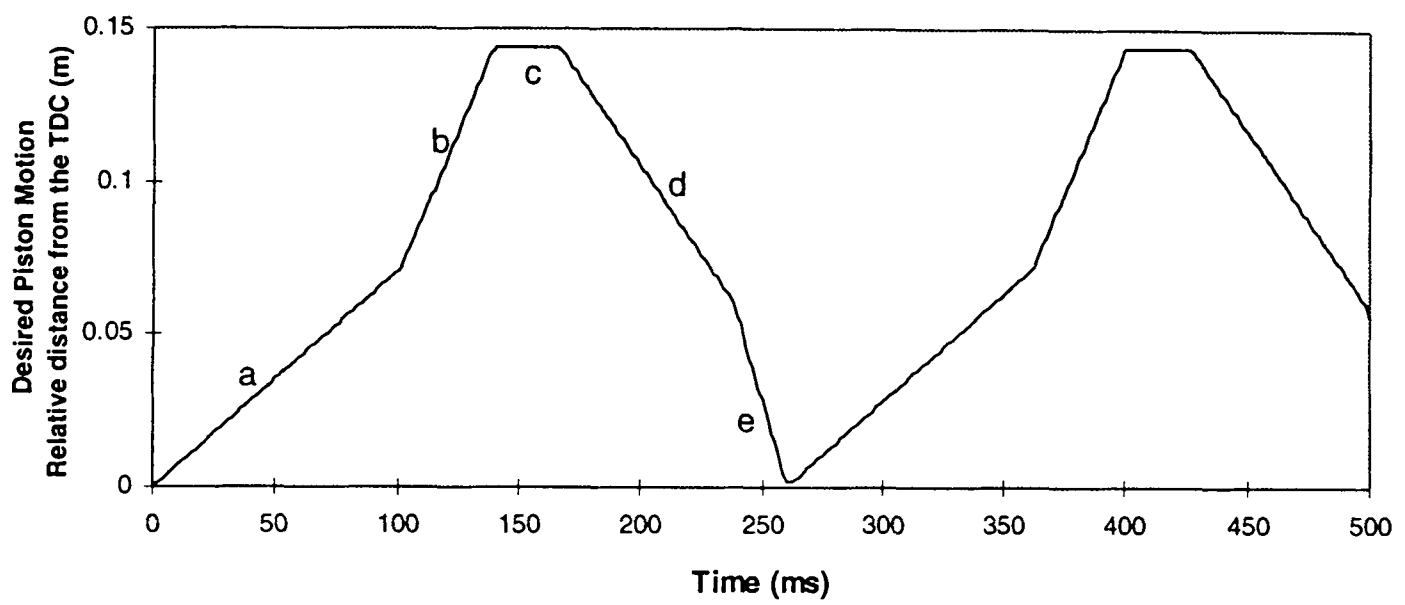
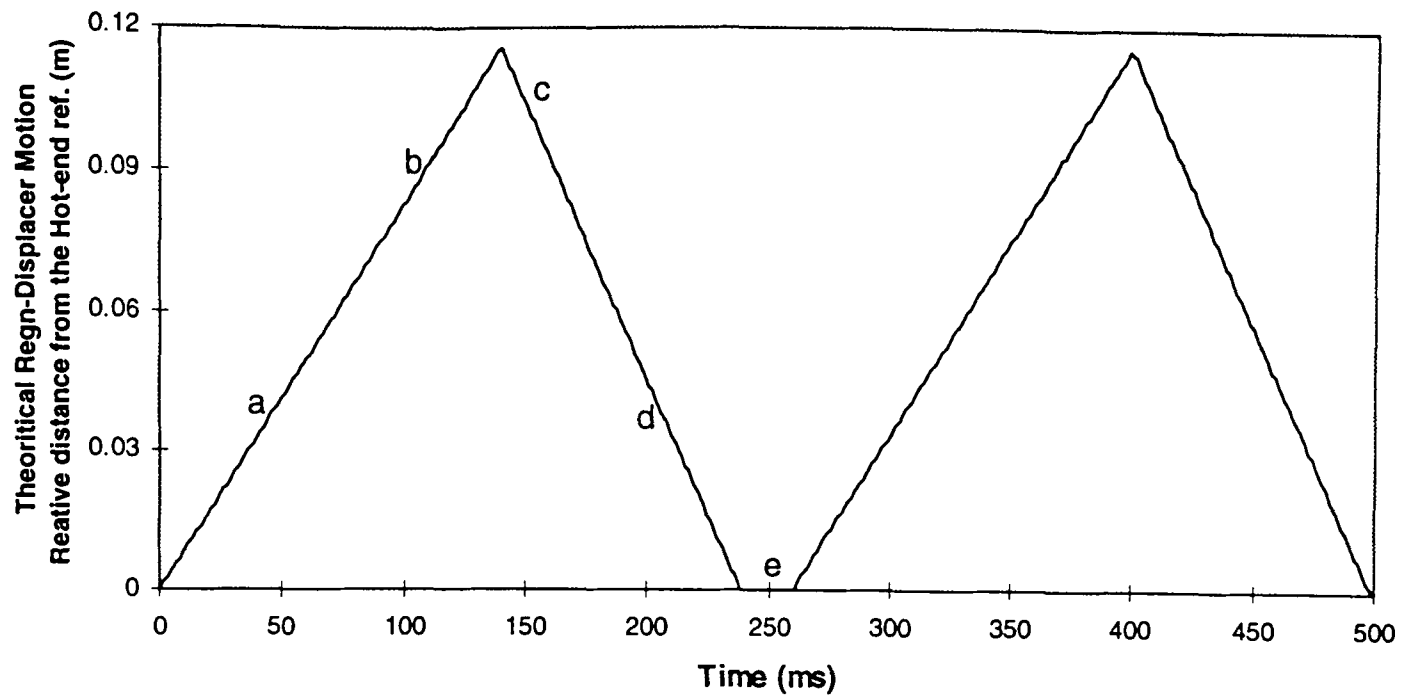


Figure 6.11 : Motion of regenerator and desired piston motion resulting in the cyclic pressure variation.

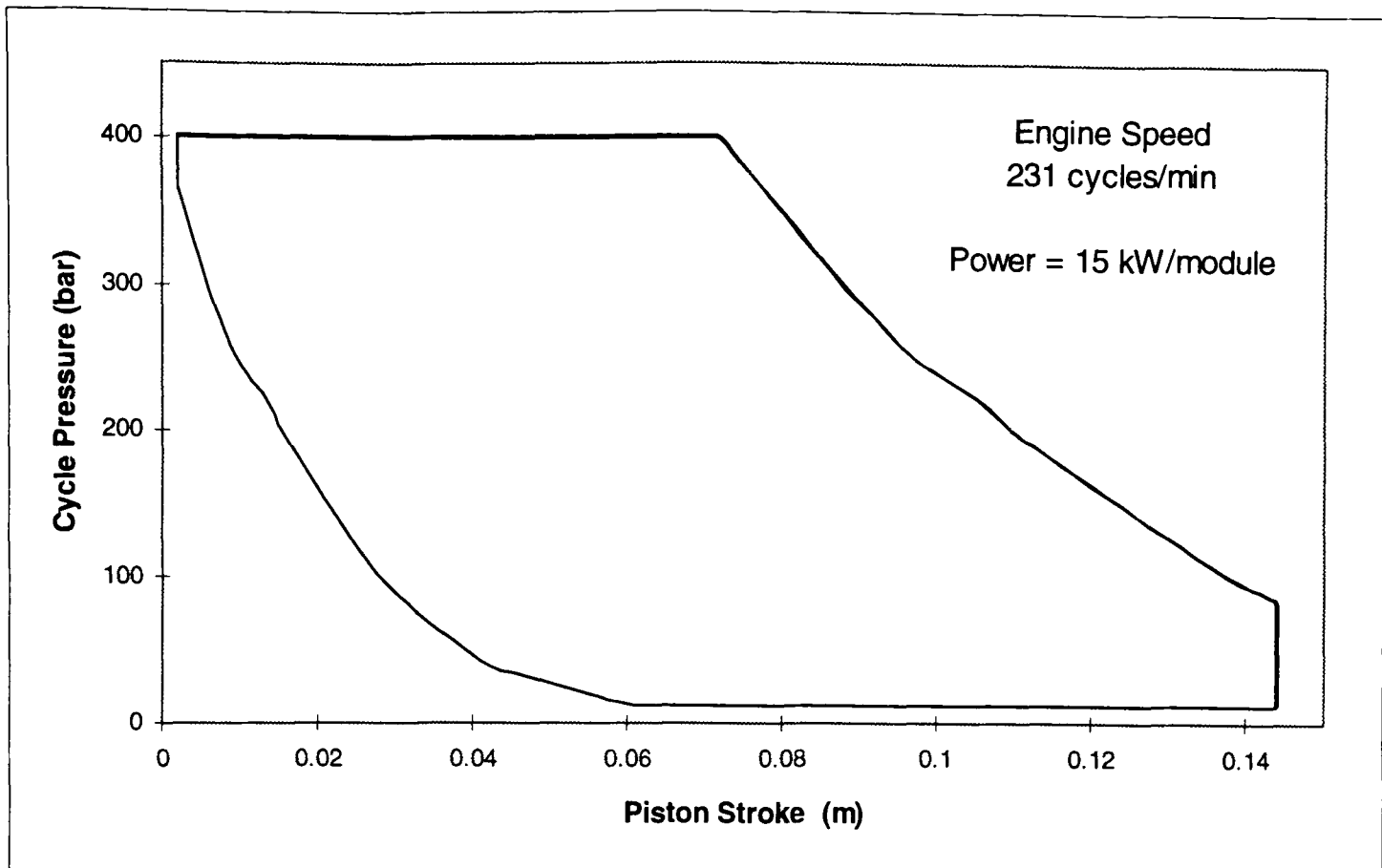


Figure 6.12 : P-V diagram of the cycle (piston assisted pressure rise and fall).

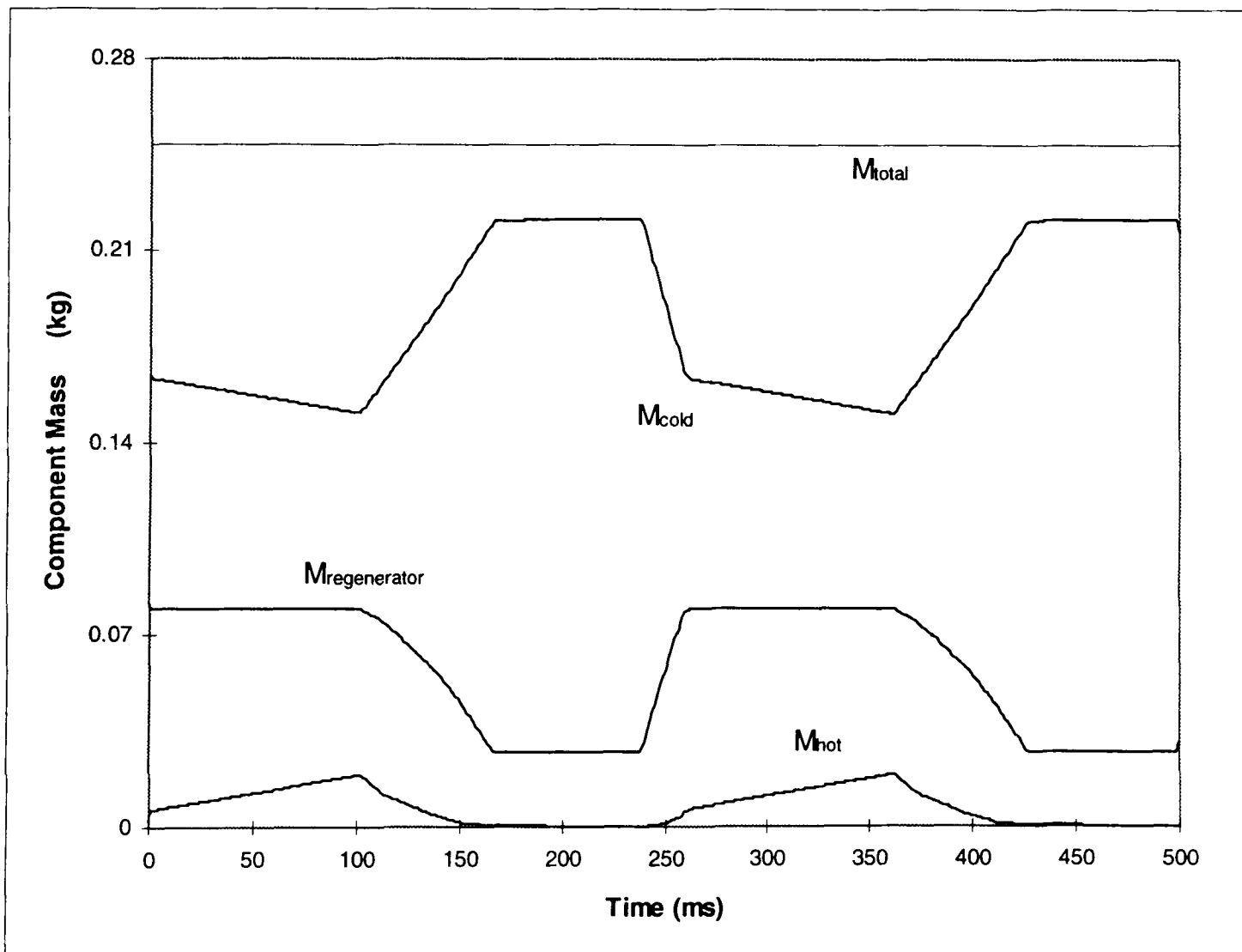


Figure 6.13 : Variation of different mass components with cycle pressure, while the total-mass remains the same.

Figures 6.11 - 6.13 show the relative motions, P-V diagram and variation of mass components throughout the cycle. It could be noted that there are two different motoring rates by the piston as the regenerator moves towards the cold-end. If additional motoring is done during the same time span, the overall area of the P-V diagram and consequently the power output is increased. Given that the TD pile is limited by its heat transfer capabilities, this allows the engine to run slower, for the same power output.

6.5 Comparison and compatibility of different cycles

Each of the three theoretical cycle patterns investigated in this chapter has advantages and disadvantages. In the piston-assisted pressure-rise cycle (Cycle-1), pumping by the hydraulic unit is used to raise the pressure to the higher level, while the regenerator is kept at the hot-end. A result of this is that a high pressure is maintained through out the entire power stroke, when the regenerator moves from the hot-end to the cold-end and the piston is moved away from its TDC reference accordingly (ie. the hydraulic unit motoring). On the other hand for the regenerator-assisted pressure-rise cycle (Cycle-2), no pumping is done by the pump-motor to raise the pressure. Instead the pressure rises as the regenerator is moved towards the cold-end while the flexible piston is left stationary. Less power is needed to raise the pressure but part of the regenerator motion from hot-end to cold-end is lost in this process, effectively reducing the power stroke. Hence the area of the P-V diagram reduces and for the same engine cycle frequency (which is actually the frequency of the regenerator motion), only about 45% of the piston-assisted cycle power output is achievable. Though this is not very encouraging in terms of power output, it opens a way of effectively reducing the power output to nearly the half by simply controlling the way the flexible piston is inflating or contracting. This can be easily implemented by changing the enabling signals to the pump-motor. It should be noted that when the same sealed system is changing between the two cycles, there is an offset between the two piston motions to maintain the conservation of the total mass. One limitation of the first two cycles is that the regenerator starts moving back towards the hot-end, while the system pressure is at the higher level. This means that in the case of an area-differential between the two end

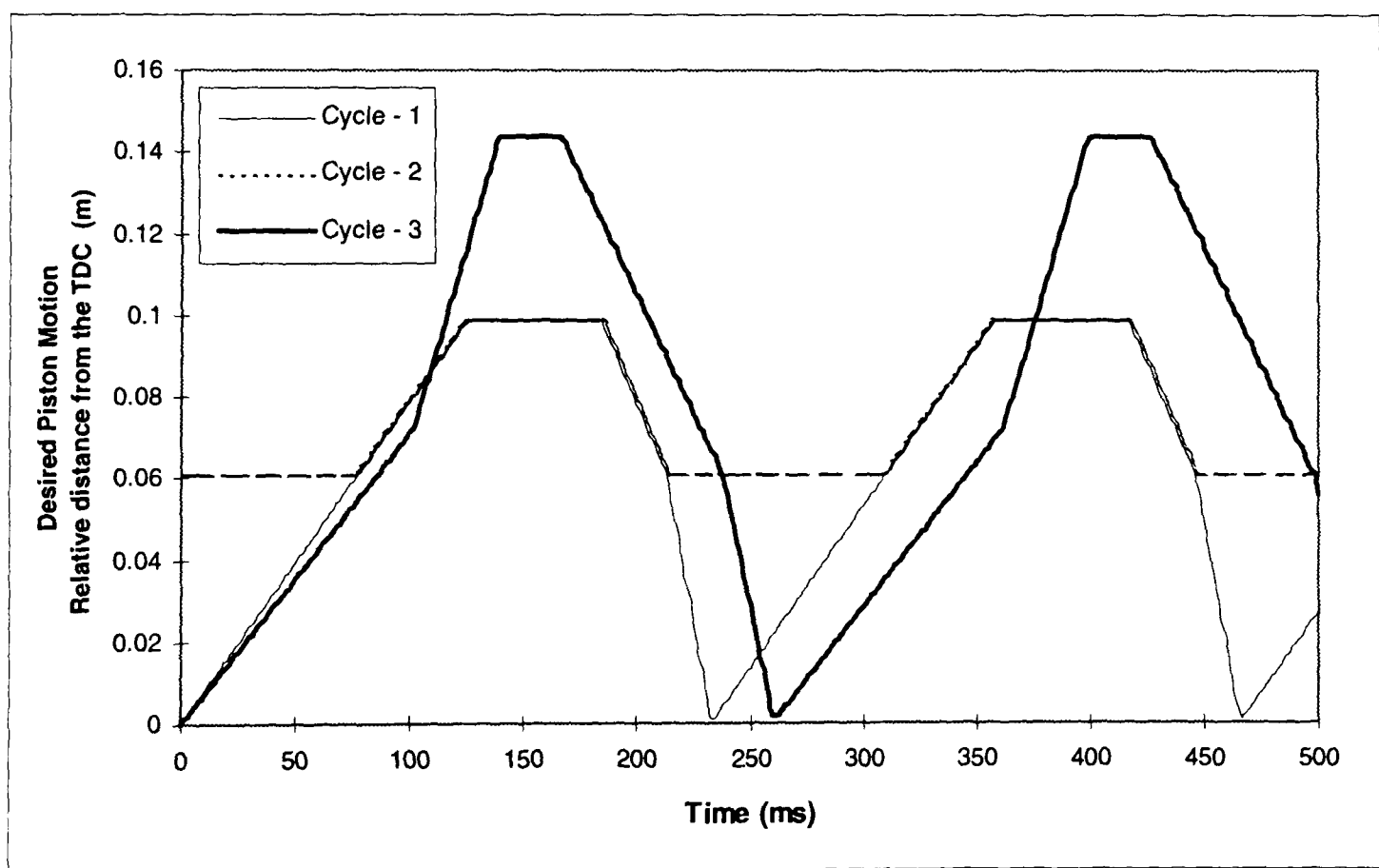
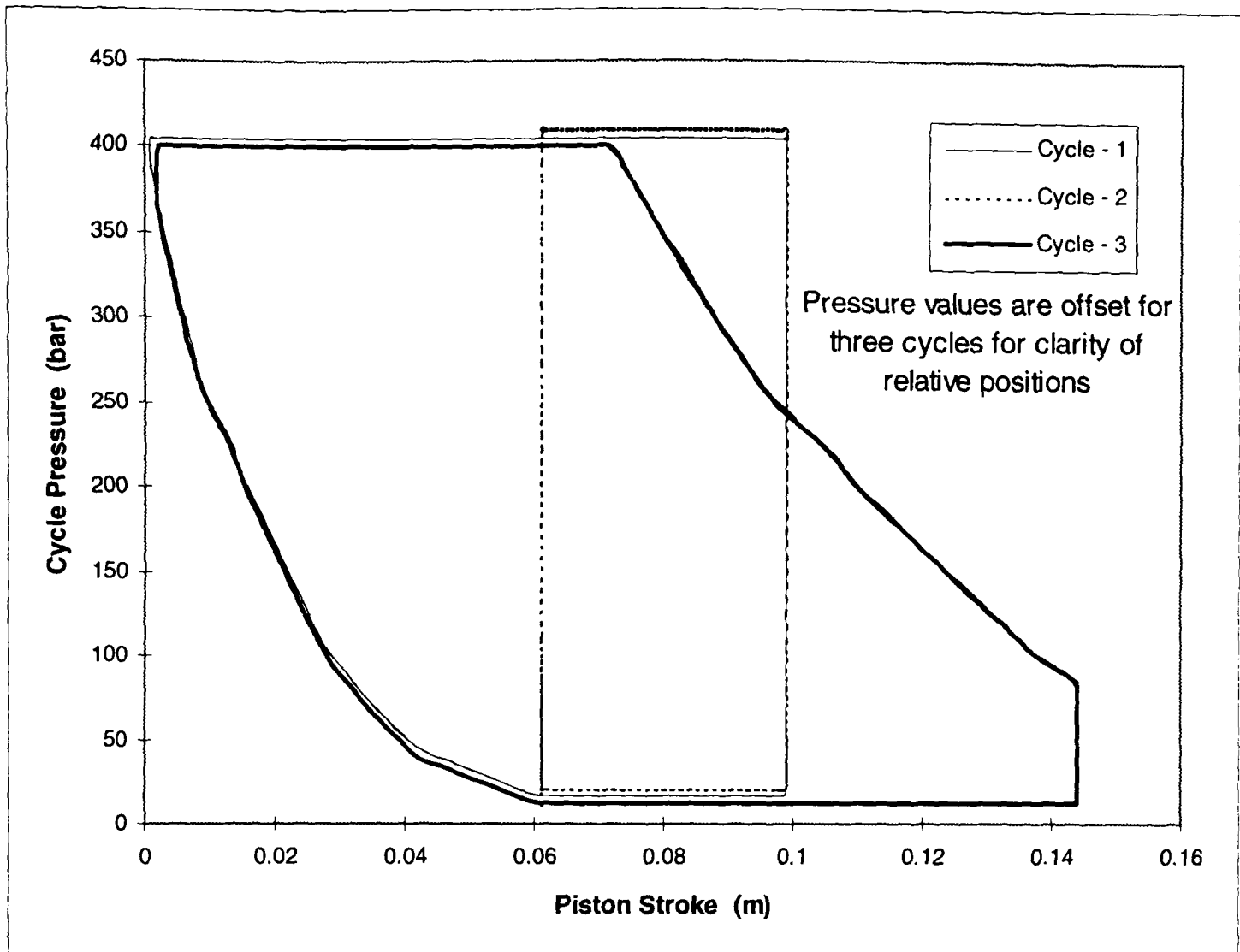


Figure 6.14 : Comparative presentation of P-V diagrams and piston motions

Cycle-1: Piston-assisted pressure-rise and regenerator-assisted pressure-fall

Cycle-2: Regenerator-assisted pressure-rise and pressure-fall

Cycle-3: Piston-assisted pressure-rise and pressure-fall cycle

Note : Regenerator motion profiles are same in all cases.

faces of the regenerator and the regenerator-drive referenced to atmospheric pressure, the force needed to start the motion will be large. This will increase the capacity requirements of the regenerator drive, though the force needed to move the regenerator will start to drop quickly as the system pressure falls (with the regenerator moving towards the cold-end). In case of the piston-assisted pressure-fall cycle (Cycle-3), after the piston reaches a certain position it is motored at a rate faster than the "*pressure-maintenance ratio*" allowing the pressure to drop below a certain level, by the time the regenerator reaches the cold-end. This reference position and the higher rate of motoring (though it needs to be within the capacity of the pump-motor) determines the level to which the pressure will drop at the end of the regenerator motion from hot-end to the cold-end. This lowest cycle pressure reached at the end of the regenerator stroke towards the cold-end in turn depends on the highest pressure level available in the regenerator-drive system. Figure 6.14 shows the comparative positions of the P-V diagrams and the piston motions of the three cycles. All cycles are based on the same regenerator motion profile, making the prospect of seamless switching between the cycles possible. Area of the P-V diagram the for cycle-3 (piston-assisted pressure-rise and pressure-fall) is larger compared to that of cycle-1 (piston-assisted pressure-rise and regenerator assisted pressure-fall cycle). As a result cycle-3 can run slower compared to the first cycle, to produce the 14-15 kW indicated power per module. The flexible piston also has different ranges of motion for the three cycles.

6.6 Thermal modelling of the hot-end

Modelling the thermal variations inside the hot-end is quite complicated due to the inter-dependency of various parameters. The heat-transfer occurring from the steam-fins at the inner side of the hot-end is a function of a number of interrelated parameters resulting in the need for closed-loop solvers. These include the change of steam volume at hot-end (which is dictated by the regenerator position), the change of system pressure (which is a function of relative motions of the regenerator and the flexible piston), the resulting change in mass of gases at the hot-end, the variation of temperature of the hot-end mass and the change of thermal resistance at the steam-fins. Part way through the cycle relatively cooler masses are entering the hot-end increasing

the hot-mass as the regenerator moves towards the cold-end or the hydraulic unit is pumped rapidly . In other parts of the cycle the amount of hot-mass decreases as the regenerator moves towards the hot-end. So the rate of heat flow through the hot-end will vary throughout each cycle. There also exists a thermal inertia at the hot end which comprises of the thermal capacitance of the hot-end metal and the hot-end gases. The rate at which the temperature of hot-end mass varies depends on the ratio of these two. Hence the steady flow of heat through the hot-end (as used in the MathCad model) may be described more precisely as a quasi-steady state of heat flow with variations at the same frequency of the thermodynamic cycle (ie, the frequency of regenerator motion). Unless the variation is matched with the engine cycle, the hot end temperature would either be gradually rising or falling.

The purpose of this investigation is to determine to what degree the hot-end temperature and the heat flow through it may vary during each cycle. Averaged value of convective heat transfer coefficient over the cycle were used as described in the MathCad model (chapter four). The model used simplifications based on the following assumptions :

- (i) The hot-end and its contents increase in temperature as the mass of hot-end gasses decrease.
- (ii) The hot-end and its contents decrease in temperature as the mass of hot-end gases increase.
- (iii) The temperature of all hot-end gases are same, regardless the regenerator position.
- (iv) Heat loss by conduction through the separator piece is negligible.

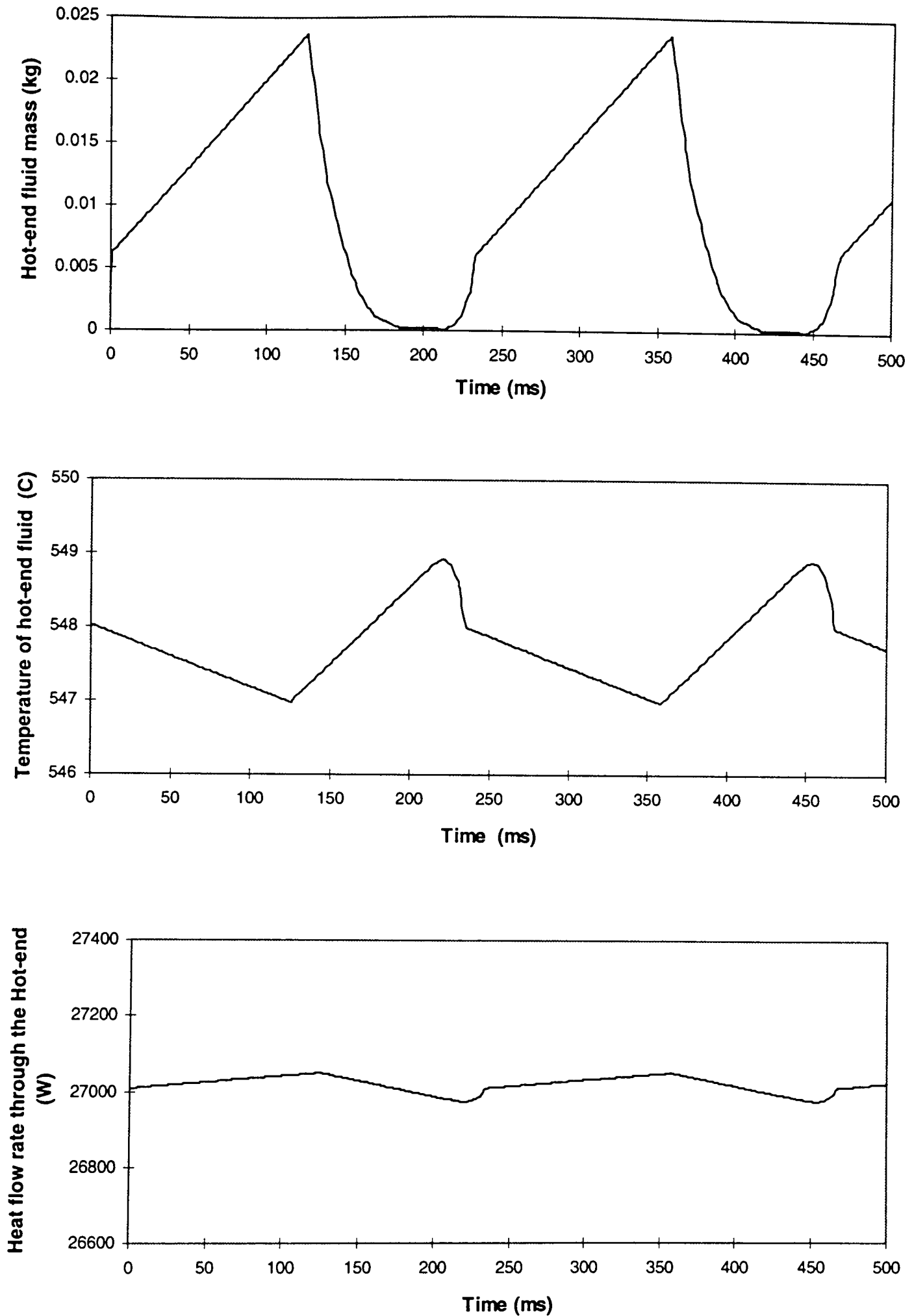


Figure 6.15 : Predicted variation of temperature of the hot-end fluid and heat flow through the hot-end, as the mass of fluid inside the hot-end changes through the cycle.

For the simplified thermal model the new temperature of the hot-end mass at the end of a small time interval can be calculated from the heat balance equation. For the part of the cycle when the fluid mass inside the hot-end is increasing,

$$MC(T-T_L) + m_L C_{hg}(T-T_L) + (m-m_L)C_{hg}(T-T_{in}) = Q.\Delta t$$

Where,

Δt = Time steps for simulation calculations (typically 1 millisecond).

T = Temperature of hot-end masses at the end of present time interval.

T_L = Temperature of hot-end masses at the end of last time interval.

T_{in} = Temperature of fluid entering into the hot-end through the regenerator.

m = Mass of hot-end gases at the end of present time step.

m_L = Mass of hot-end gases at the end of last time step.

C_{hg} = Specific heat of hot-end gases, considered to be unchanged with temp.

Q = Heat flow rate through the hot-end at the end of last time step.

$MC = \sum MC = (M_{cu} C_{cu} + M_{inc} C_{inc})$, is the sum of the products of the mass and respective specific heats of materials constructing the hot-end (eg, copper and Inconel).

Similarly for other parts of the cycle when the hot-end mass is either decreasing or remaining unchanged, the temperature at the end of present time step can be calculated from the equation :

$$MC(T-T_L) + m C_{hg}(T-T_L) = Q.\Delta t$$

Figure 6.15 shows the variations of hot-end temperature and heat flow passing through the hot-end for piston-assisted pressure rise and regenerator assisted pressure-fall cycle as in figure 6.5. Results show that the variations are small (within $\pm 2^\circ\text{C}$), which suggests that considering the hot-end fluid temperature to be constant through out the cycle would not significantly affect the cycle simulation. This thermal modelling also allows testing of the estimated temperature (from static model) at which the fluid enters the hot-end from the regenerator, as it affects the temperature at which the hot-end fluid mass is held.

CHAPTER - 7

Simulation of Real Engine Cycles

7.1 Modelling of more realistic cycles

The cycles modelled so far are simplified in the sense that they have evolved from theoretical motions of the two principal moving parts. In practice the regenerator is driven by an imperfect hydraulic system and the flexible membrane inflates or contracts dependent on the flow of oil going into or out of it from the pump-motor at a resolution of one cylinder volume - giving a quantisation error. Hence, even in the case of proper heat transfer and system temperatures being maintained, the generation of these theoretical cycles depends on the ability of the drive systems to approximate the theoretical motions. In this chapter more realistic motions are incorporated into the model for the regenerator and the flexible piston, so that realistic cycles may be evaluated.

Figure 7.1 shows the flow chart of this engine modelling procedure. The programmes (modified from those described in chapter six) used for simulating real engine cycles can be divided into three major components. The first simulates imperfect motions of the regenerator, computes the corresponding desired piston motion required to generate a particular pattern of cycle and inputs this as a demand signal to the pump-motor model. The second stage activates the pump-motor model which attempts to follow the demanded piston motion (subjected to quantisation and delay errors) and returns the actual generated piston motion to the engine model. The third stage re-calculates the engine cycle produced with the realistic regenerator motion and the piston motion from the pump-motor.

Dividing the computational load into these three phases made the model run faster, as well as making it easier to initialise and left it less prone to non-convergence of implicit solutions. However it was essential to ensure that the regenerator cycle and piston

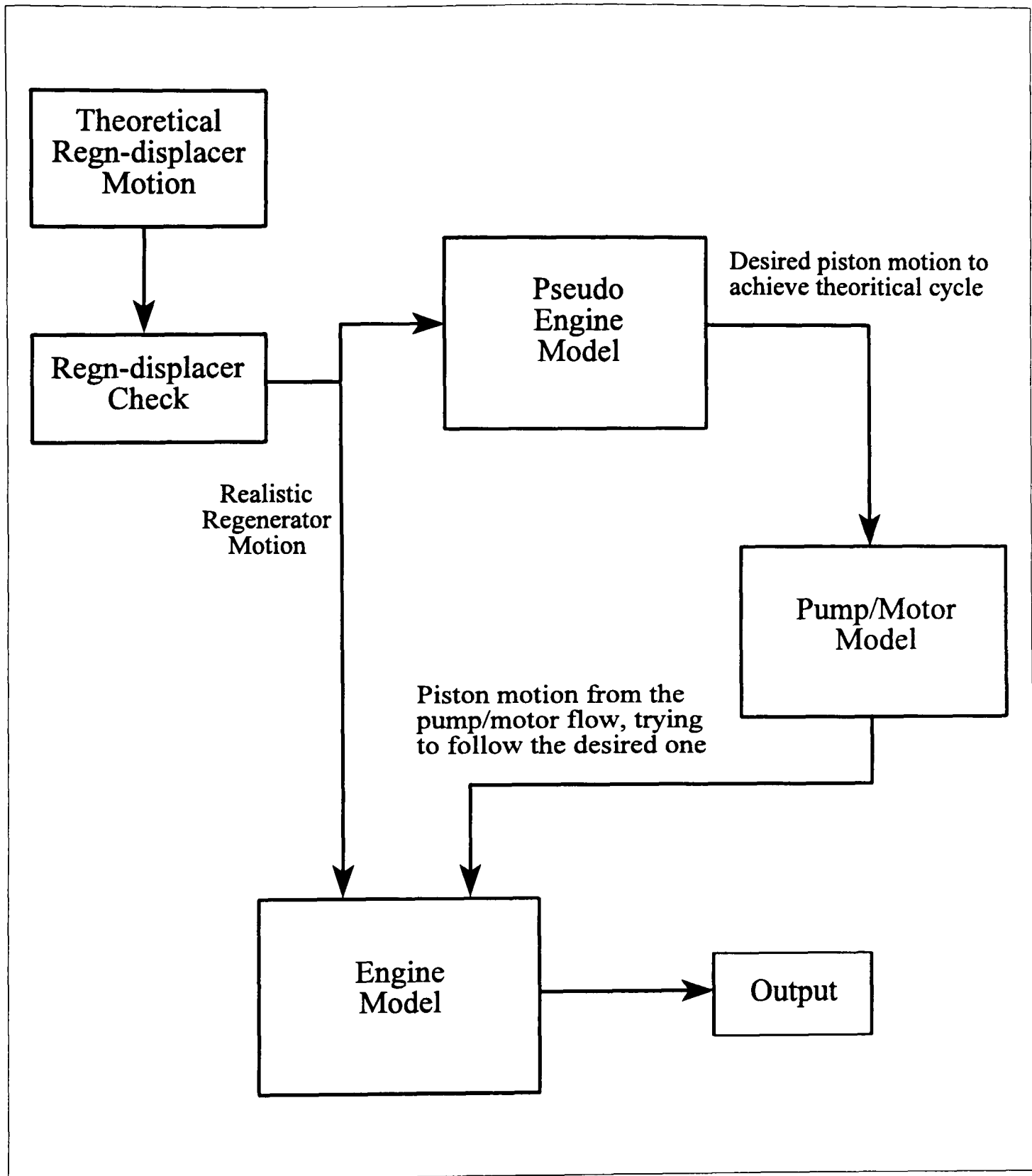


Figure 7.1 : Simulation programme flow-chart for calculation of realistic engine cycle.

cycle, generated from the pump-motor model, are precisely matched in time. Even apparently small discrepancies were found to cause gradual shifts of the pressure-volume diagram generated in a number of successive cycles.

In this chapter the simulation of regenerator motion is discussed first, followed by modelling of piston motion and finally these two are incorporated together to produce realistic engine cycles. The full power cycles are discussed here, while the part load cycles are discussed in the next chapter.

7.2 Calculating imperfect motions for the regenerator

Before investigating motions achievable by the hydraulic drive we can look at the different available ways for driving the regenerator. Each has some advantages and some limitations. The final choice needs to be made from the results of experimental studies.

Fundamentally there can be two types of regenerator actuation, single-sided and double-acting. Figure 7.2 (a) & (b) shows a schematic presentation of the two cases. The advantage of a double acting ram is that the force acting on the porous regenerator as it moves is only due to the viscous drag of fluid passing through it. This is small in magnitude and does not vary much with system pressure. The disadvantages are that a double-acting drive cylinder is needed to move the regenerator in both directions. The seal at the hot side, experiencing high temperature, is extremely difficult to maintain. But this can be reduced to a great extent by a double acting drive piston arrangement having the seal inside the regenerator rather than at the hot end as in figure 7.2a.

The single sided regenerator drive has a pressure bias due to the unequal areas of the actuator, so that a force always acts on the regenerator trying to push it towards the cold-end. The magnitude of this biasing force depends on the cycle pressure as well as the area difference between the two faces. Hence the drive system of the regenerator only needs to push it towards the hot-end since it automatically returns when it is allowed to move back to the cold-end. A seal needs to be maintained but the task is

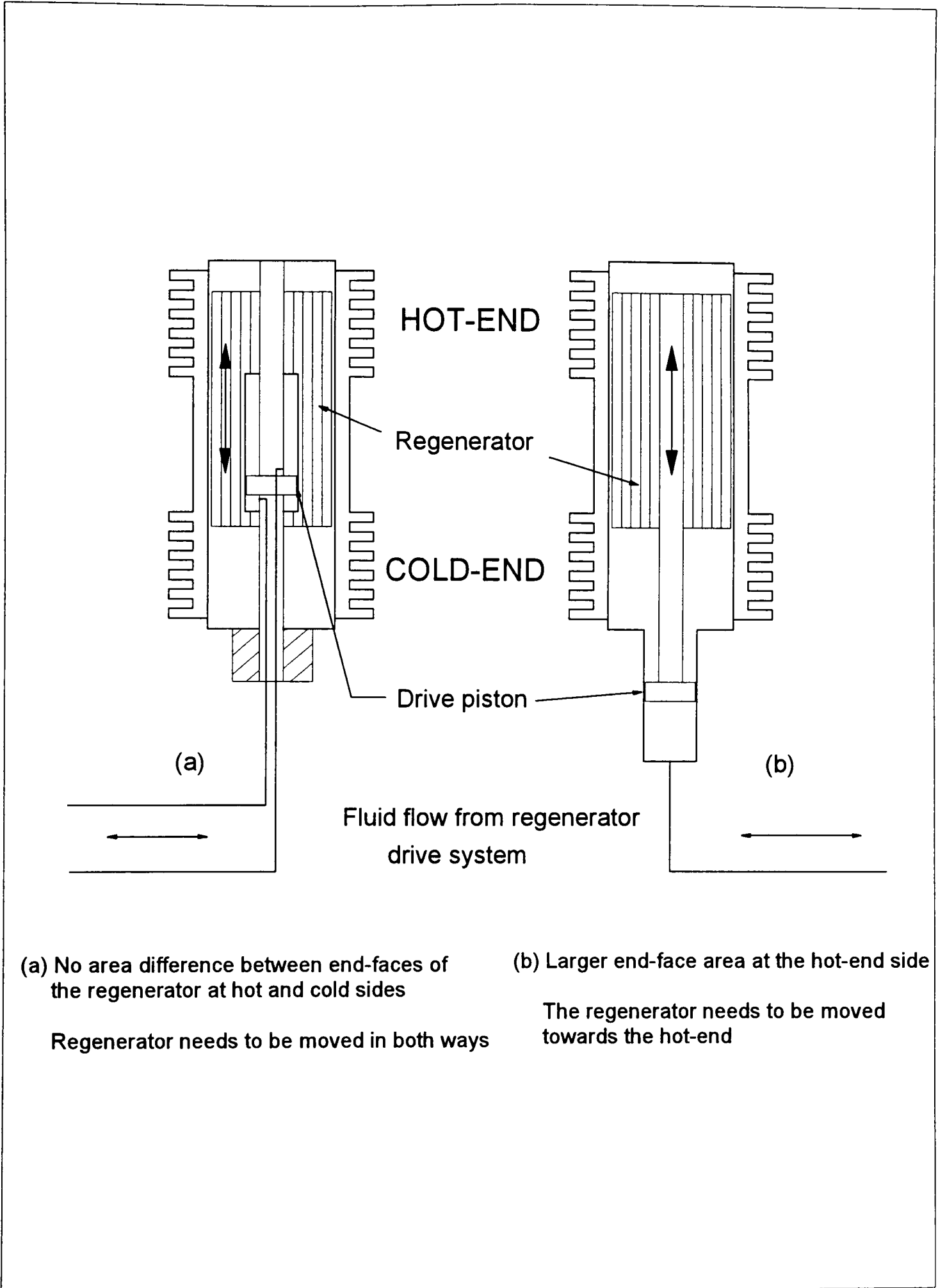


Figure 7.2 : Regenerator actuation options.

much easier at the cold-end, as the temperature is low. This system is also more compact compared to the previous case and the drive system only has to do work for a part of the engine cycle.

The limitation of the second case is that the drive system must be able to develop sufficient pressure to start the motion of regenerator towards the hot-end, working against the cycle pressure. This requirement is effectively decreased if the engine cycle is chosen such that the cycle pressure reduces to a low level by the time the regenerator finishes its motion towards the cold-end (as shown in figures 6.11,6.12 and 7.5). Once the regenerator starts moving towards the hot-end, the cycle pressure begins to drop, hence reducing the force due to area differential against which the regenerator drive system has to work. Another way of reducing the power requirement of the regenerator drive (which can be used for both double acting and single sided regenerator) is to use the cold-end water, which is already at the system pressure, as its working fluid. From these considerations the single sided actuator configuration with area difference between two faces seemed to be the more attractive and practical one.

The theoretical regenerator displacement curves suggested in chapter six have triangular or trapezoidal wave forms. This requires almost instantaneous velocity changes, which in turn demand extremely high accelerations. In practice the maximum driving force and hence acceleration imparted on the regenerator is limited by the pressure rating of the hydraulic drive system. The real motions achieved would be much smoother with gradual changes in velocity and acceleration limits. Figure 7.3 shows such a modified triangular regenerator motion cycle which may be achievable by a drive system. With a drive piston area of 7.5 mm in diameter and drive system pressure of 100 bar and regenerator mass of about 1 kg, the acceleration limit is above 400m/s^2 . In the simulation, the modified regenerator motion curves were generated by the combination of an integration and a differentiation block using different time intervals while checking the acceleration requirements.

Figure 7.4 shows a schematic presentation of a possible hydraulic drive system for the motion of the regenerator using gear pumps. The electric motor driving the regenerator

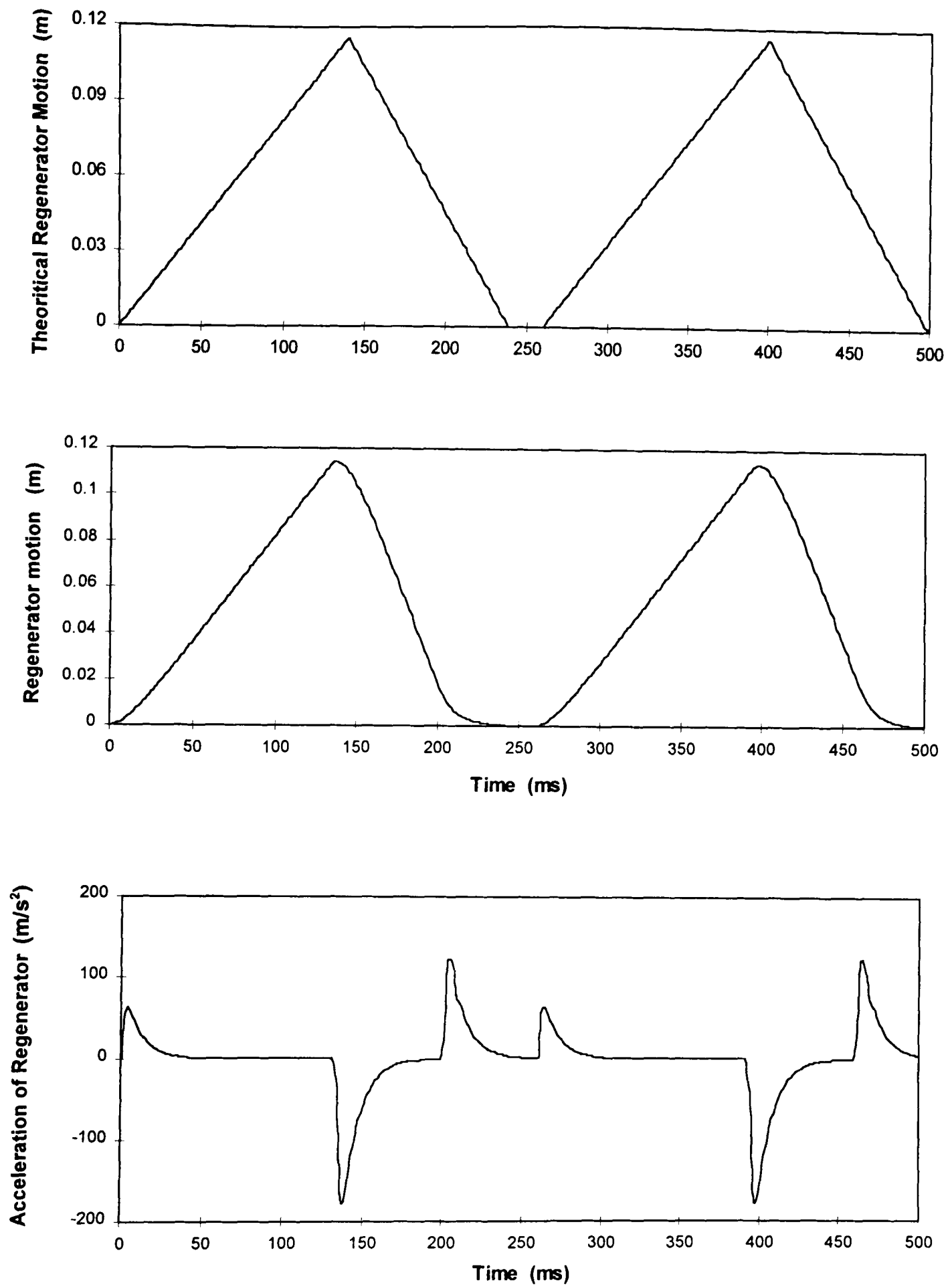


Figure 7.3 : Acceleration requirements for a modified regenerator motion profile. Curves at the top show the theoretical and modified regenerator motions.

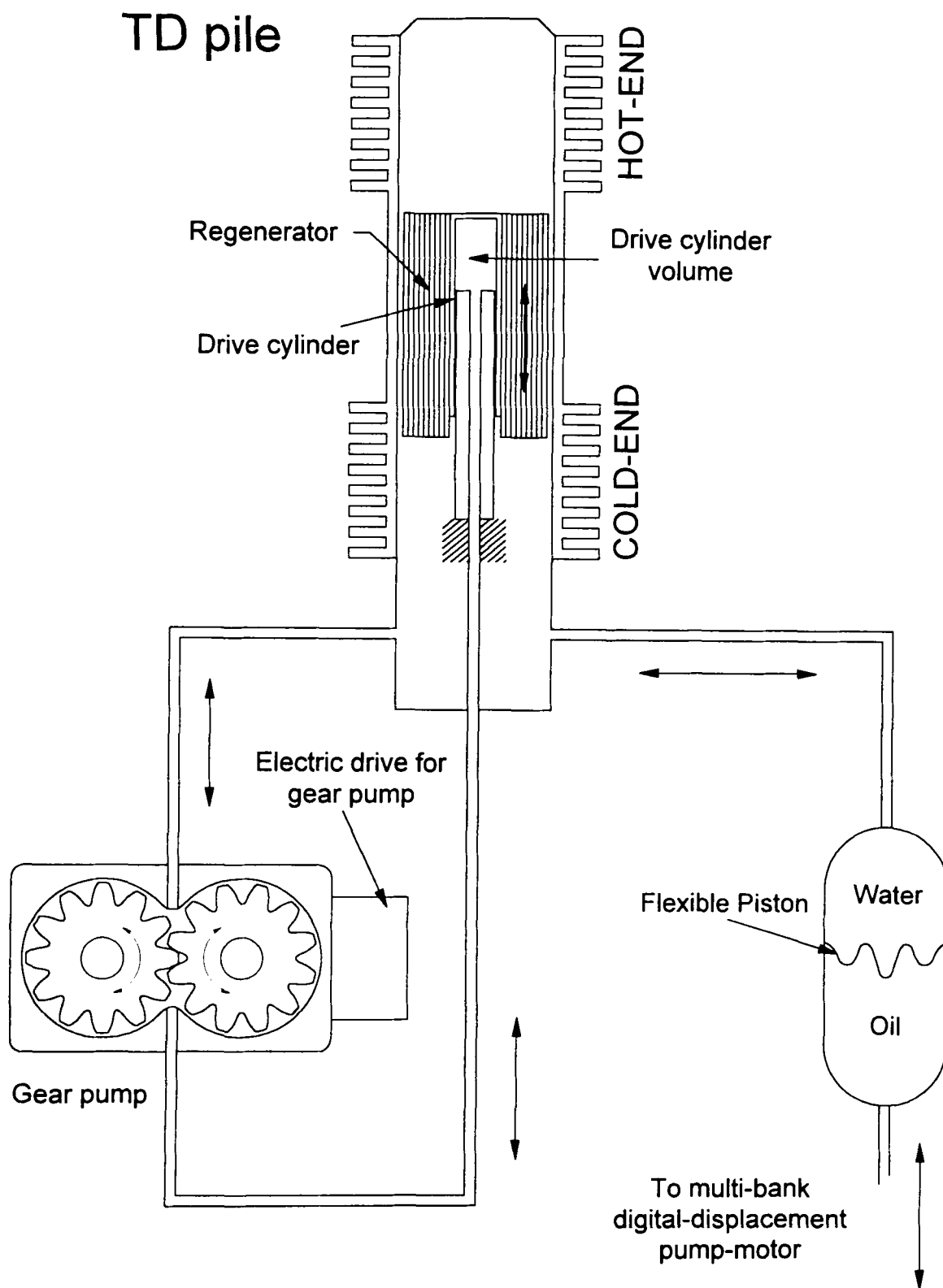


Figure 7.4 : Schematic drawing of a probable regenerator drive system

follows a demand signal to control the regenerator motion. During the power stroke the regenerator moves towards the cold-end due to the pressure-force generated from the difference of exposed area of the end-faces, producing positive power from the regenerator drive. Conversely work needs to be done by the drive to move the regenerator towards the hot-end. An accumulator could be incorporated into the regenerator drive system to conserve some the energy gained in the power stroke to be used to move the regenerator in the other way. But this adds the complexity of controlling the pre-charge pressure of the accumulator accurately, with variation of cycle pressure-level. Conserving the gain as kinetic energy in the drive-shaft could be more easily achieved.

An alternative is to use a simple sinusoidal regenerator motion, which is much easier to achieve and to control the complicated motion profile entirely from the flexible-piston driven by the digital-displacement pump-motor. The pump-motor is capable of generating arbitrary piston motions, which can lead to similar pressure-volume (P-V) diagrams as generated using trapezoidal or triangular motion from the regenerator. Figure 7.5 shows the motion required by the flexible piston with sinusoidal regenerator motion. This desired motion allows the generation of a P-V diagram very similar to that with the triangular motion of the regenerator (figure 6.12). Figure 7.6 shows the schematic drawing of a possible drive system for sinusoidal regenerator motion. The drive-shaft of the regenerator pump is geared down (about 8:1 ratio), so that large number of pump-motor cylinders are available during each regenerator cycle (ie. engine cycle). This allows finer control of the piston motion generated by the pump-motor and ultimately of the area and shape of the P-V diagram. An eccentric on the drive-shaft causes the plunger to move in a sinusoidal pattern. This motion is transmitted to the water in the regenerator drive-cylinder, placed inside the regenerator, across an isolator membrane. Dwell period is provided in the cycle, so that possible leakages of water across the drive cylinder seal or oil plunger can be refilled at the end of each cycle. During the regenerator stroke towards the cold-end (ie. the power-stroke) positive torque is transmitted to the drive-shaft from the plunger. Conversely the drive shaft has to move the regenerator against the system pressure on its way towards the hot-end. As explained in chapter six, the piston motion can be modified to reduce the cycle pressure

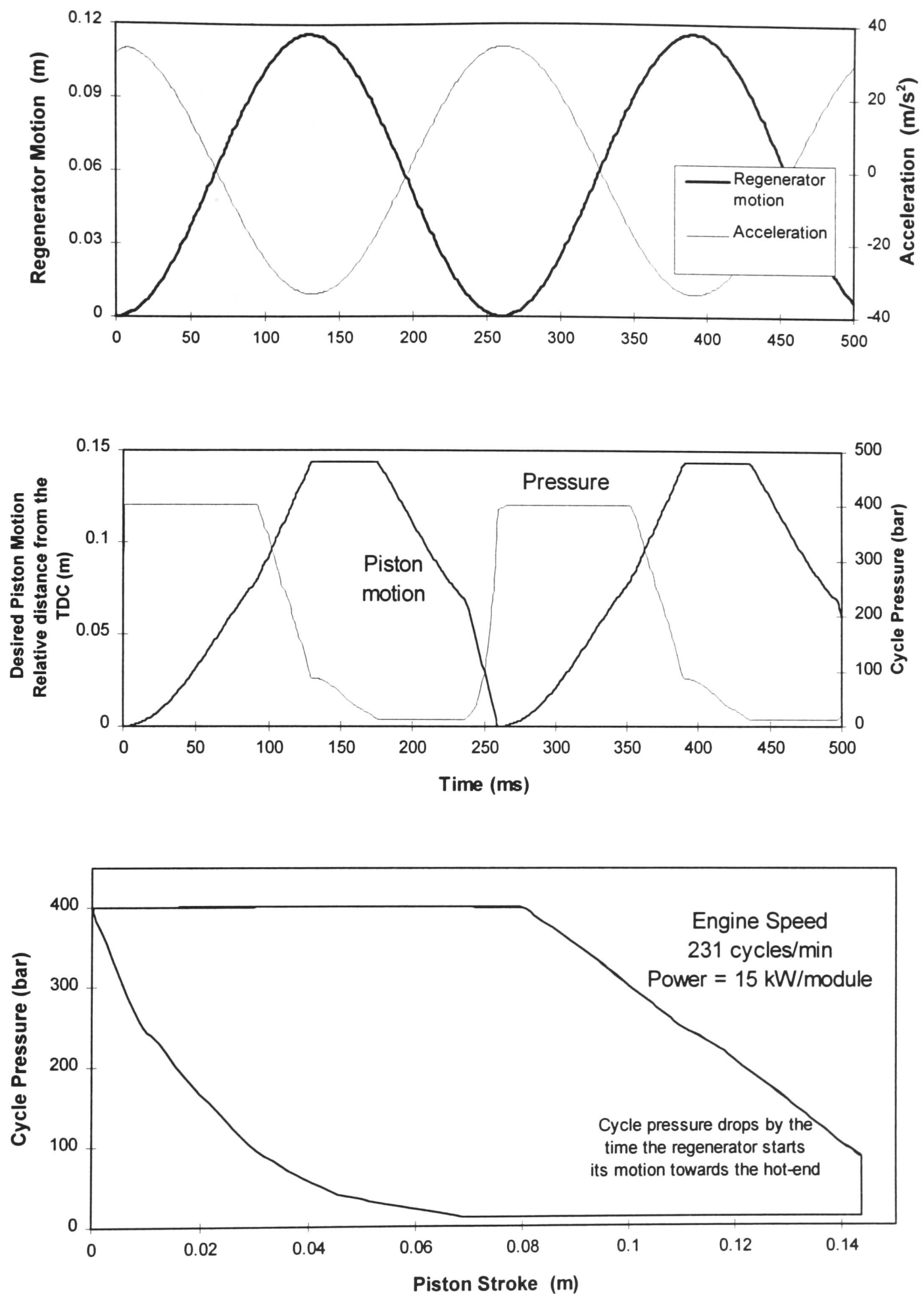


Figure 7.5 : Desired piston motion for sinusoidal regenerator motion and the P-V diagram of the resulting engine cycle. Power output is equivalent to the cycle with triangular regenerator motion.

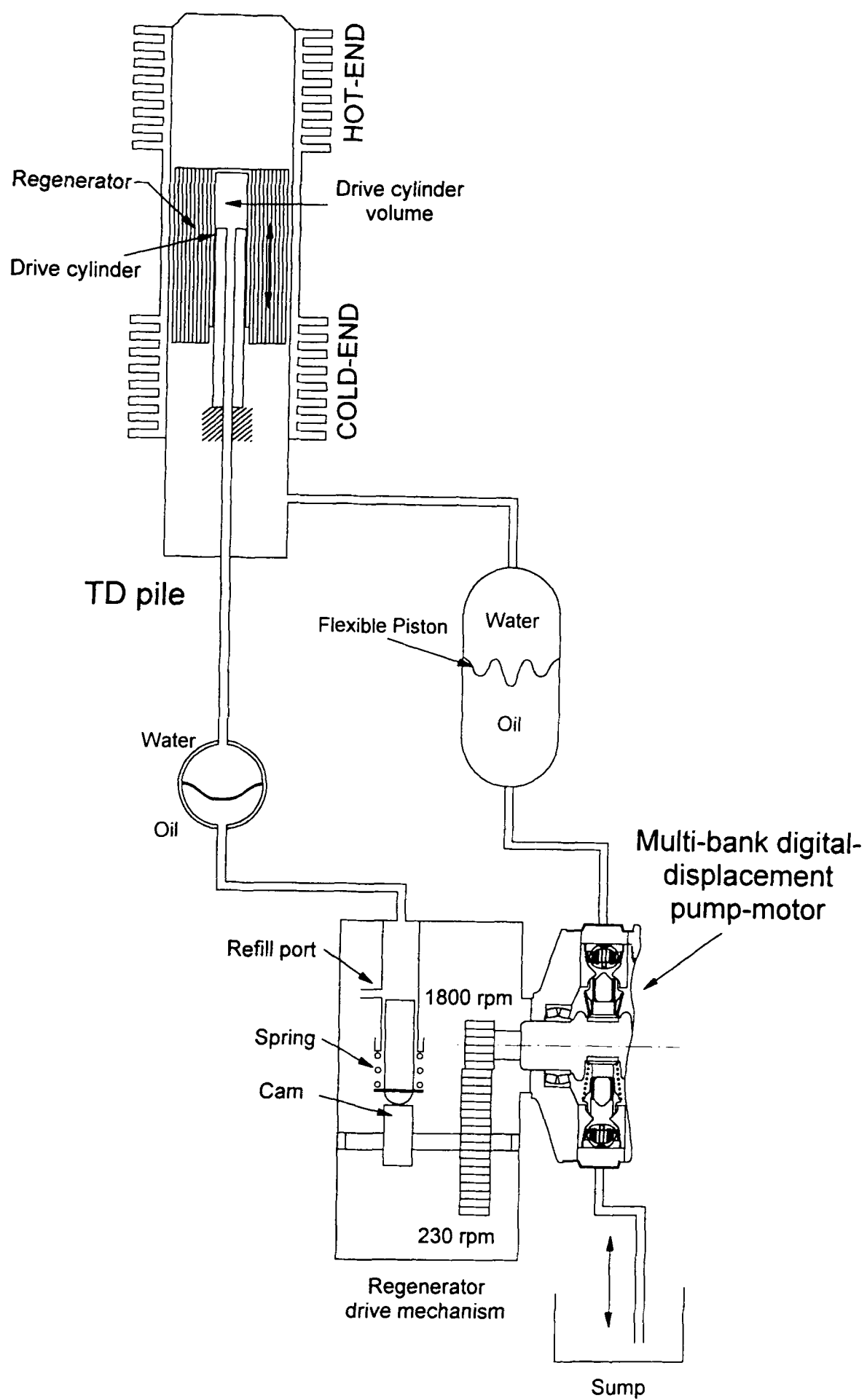


Figure 7.6 : Schematic drawing of a probable regenerator drive system providing a sinusoidal regenerator motion.

to a lower level, by the time the regenerator starts its motion back towards the hot-end (piston assisted pressure-rise and pressure-fall cycle).

7.3 Piston motion generated by the pump-motor

The other motion needed to be incorporated to simulate a realistic cycle is that of the flexible piston as generated from the pump-motor flow. As shown in figure 7.1 the required piston motion derived from the theoretical engine model is fed into the pump-motor programme which has already been described in chapter five. To achieve the desired motion, the velocity of the piston should be proportional to the enabled capacity of the pump-motor running at a constant speed under a flow-control mode. The simulations showed that attempts by the controller to follow an analogue signal of desired piston velocity and displacements were limited by the prediction time needed by the algorithm, especially at the corner points of the motion profile. This was due to very fast changes of demand signal, which the algorithm could not predict, resulting in lag in response to follow it accurately.

Additional feedback control loops were needed to get piston displacements following an analogue demand close to the desired curve. Flow charts of the nature of feed-back loops tested with flow-control algorithms are shown in figure 7.7a. Errors compared to the desired piston motion could be fed back to change the decision from flow-control algorithm or could be used to modify the input demand signal. Figure 7.7b shows the effect of using a feedback loop, which effectively controls over-shoots and under-shoots in the generated piston motion. Figure 7.8 and 7.9 shows the piston motions generated by the pump-motor, with feedback control, for modified-triangular and sinusoidal regenerator motions and the resulting engine cycles.

However application of feedback control had some limitations. Although piston motions could be repeated through the same approximate range, it became very difficult to ensure that they were enabled exactly in the same sequence for repeating cycles. This is reflected in the imperfect super-imposition of the repeating cycles in the P-V diagrams of figure 7.8 and 7.9. This might be due to the quantization error of the pump-

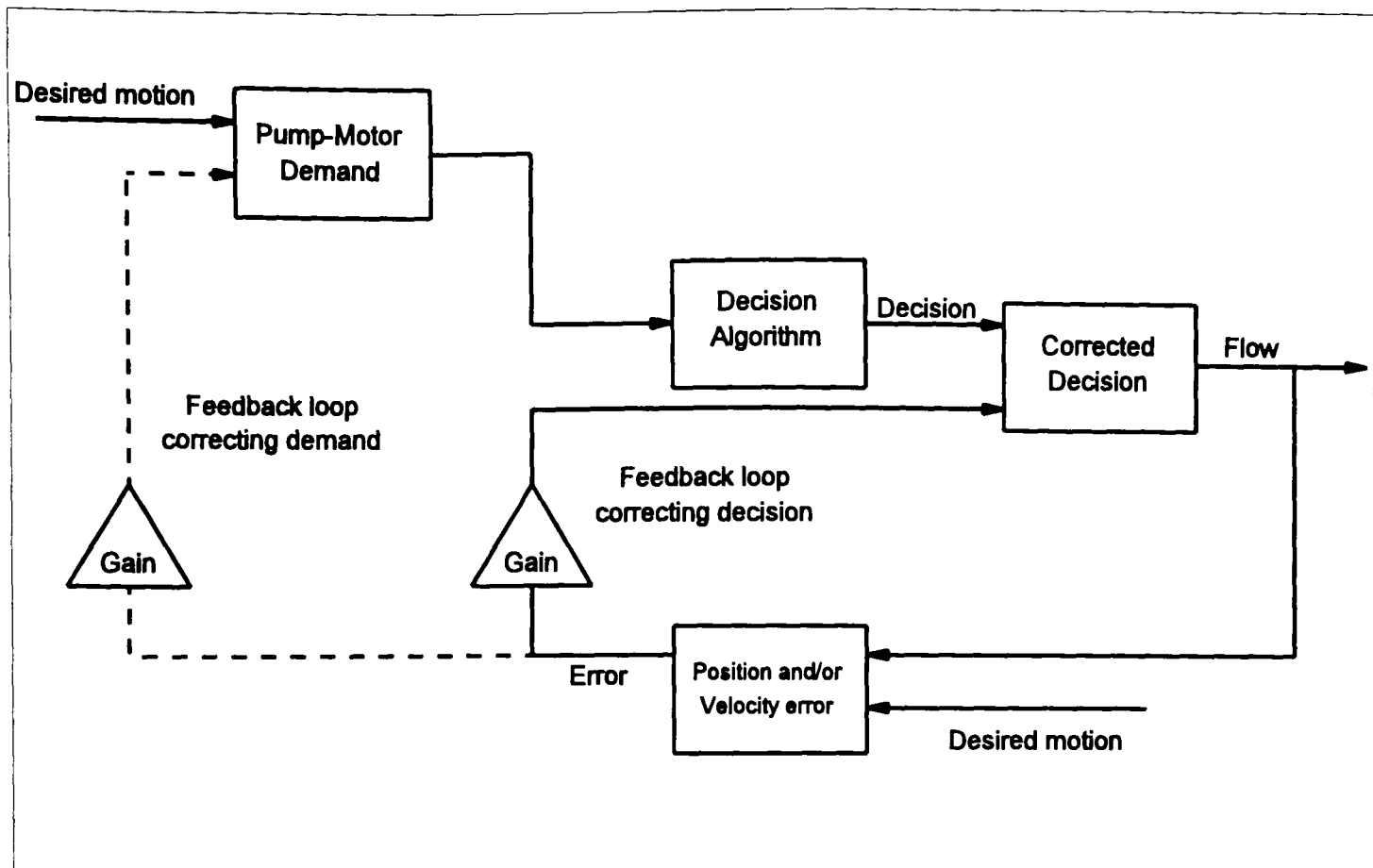


Figure 7.7a : Flow chart of different types of feedback control loops tested. Errors relative to the desired motion may be fed back to change the decision itself or to modify the demand profile, in order to follow the desired motion.

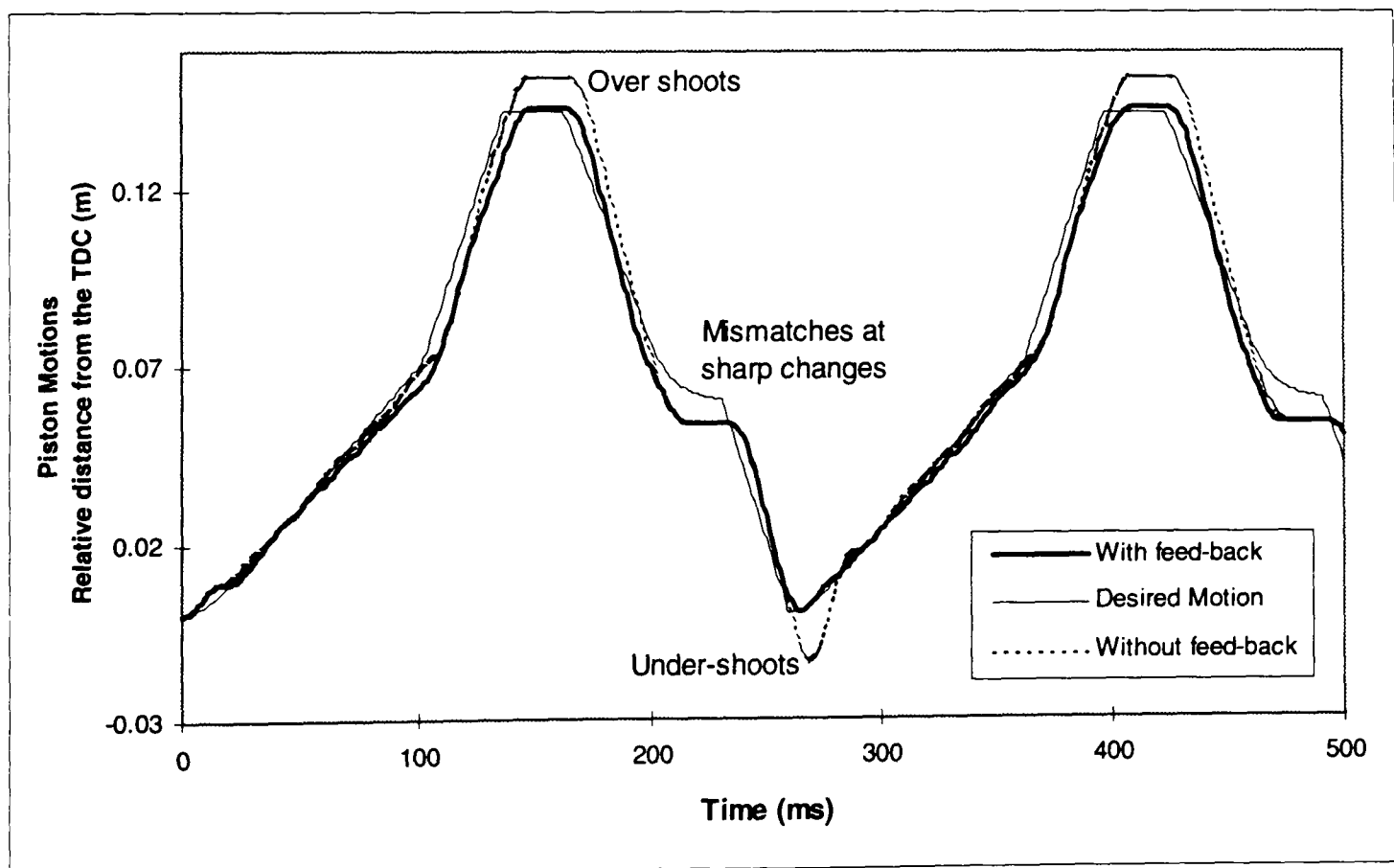


Figure 7.7b : Desired piston motion and those generated by the pump-motor with and without additional feedback loops on the decision making algorithms. Desired piston motion, corresponding to triangular regenerator motion, is followed by the pump-motor. Application of feedback loops reduces over-shoot and under-shoot to great extent, though it can not follow sharp-changes closely and ensure perfect repetition of piston cycles.

motor or the sensitivity of the additional feedback control-loop. The consequence of deviations from desired piston motions depends on, at which part of the cycle it is taking place. Misjudgment of one cylinder volume may cause undesired pressure-fluctuation which may result in a high-pressure spike or lead to cavitation at low-pressures. It is also difficult to make the feedback loops equally effective for different ranges and patterns of piston motions. The gain values and the algorithm used for feedback control needed to be changed to get close match for different desired piston motions and was difficult to generalise.

Under these circumstances using the ternary-mode of cylinder enabling appeared to be a convenient alternative. The ternary-code could be pre-tuned to follow the desired piston motion with much greater accuracy and repeatability. A ternary-code which is a sequence of enabling (pumping or motoring) and disabling decisions of pump-motor cylinders was followed by the controller, in a cycle-by-cycle basis. The enabling pattern generated by the flow-control algorithm could be used as a basis for the ternary-code, which could then be tuned to accurately match the desired motion. With fixed regenerator and pump-motor speeds (or fixed speed-ratio), the number of available cylinders during each engine cycle remains the same, allowing cyclic implementation of a ternary-code. In the model this was achieved by incorporating a look-up table and modifying the sequential trigger block (chapter five). The modified block provided cyclic numbering to the sequential triggers, using which decisions were read from the look-up table by the controller. The number of ternary patterns to be used, depends on the power-control strategy employed by the engine, which is discussed in the following two chapters. The use of ternary-code provided fixed piston motion independent of the regenerator, allowing a study of the changes in the engine cycle resulting from modulation of the regenerator motion. Additional decisions for limit conditions or safety reasons could be employed which override decisions from the ternary-table, under such circumstances. Figure 7.10 shows the piston motion generated from a ternary-pattern and the resulting engine cycle. The enabling (motoring or pumping) sequence shows the generation of the piston motion by the digital-displacement hydraulic drive. Using the ternary-mode allows the piston motion to follow the demand more closely as well as repeat consequent cycles.

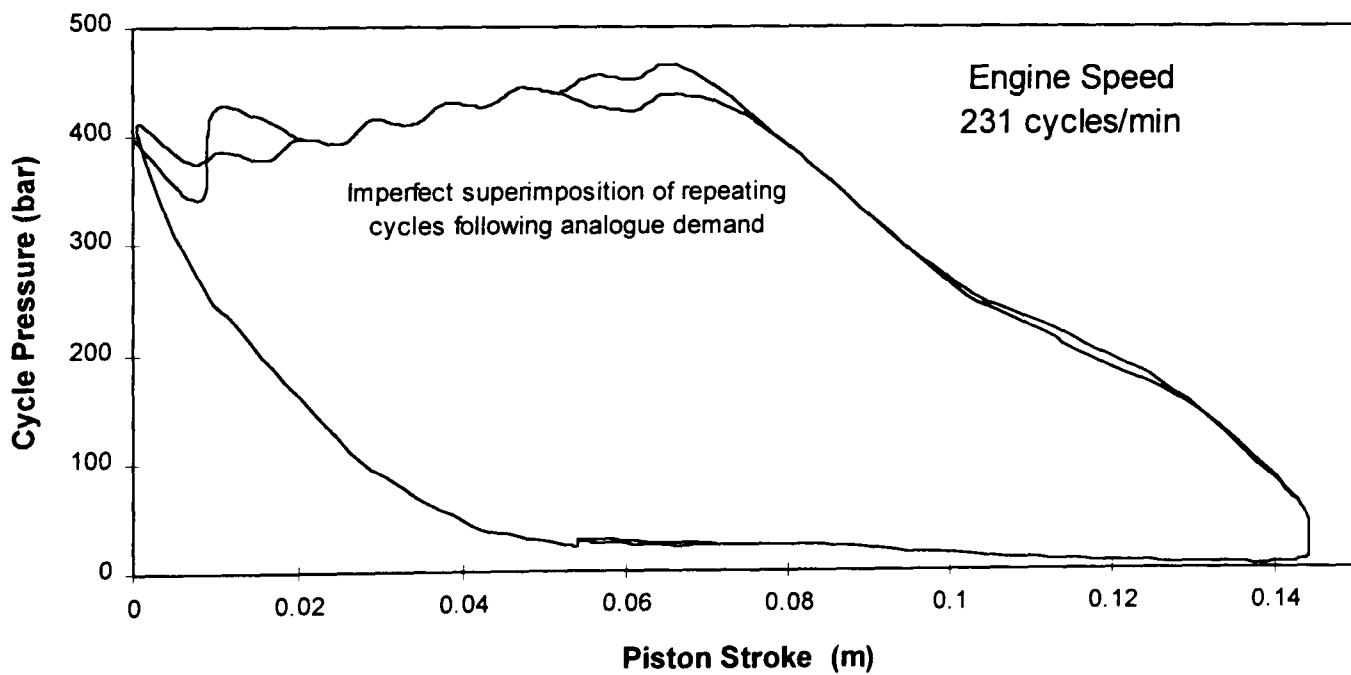
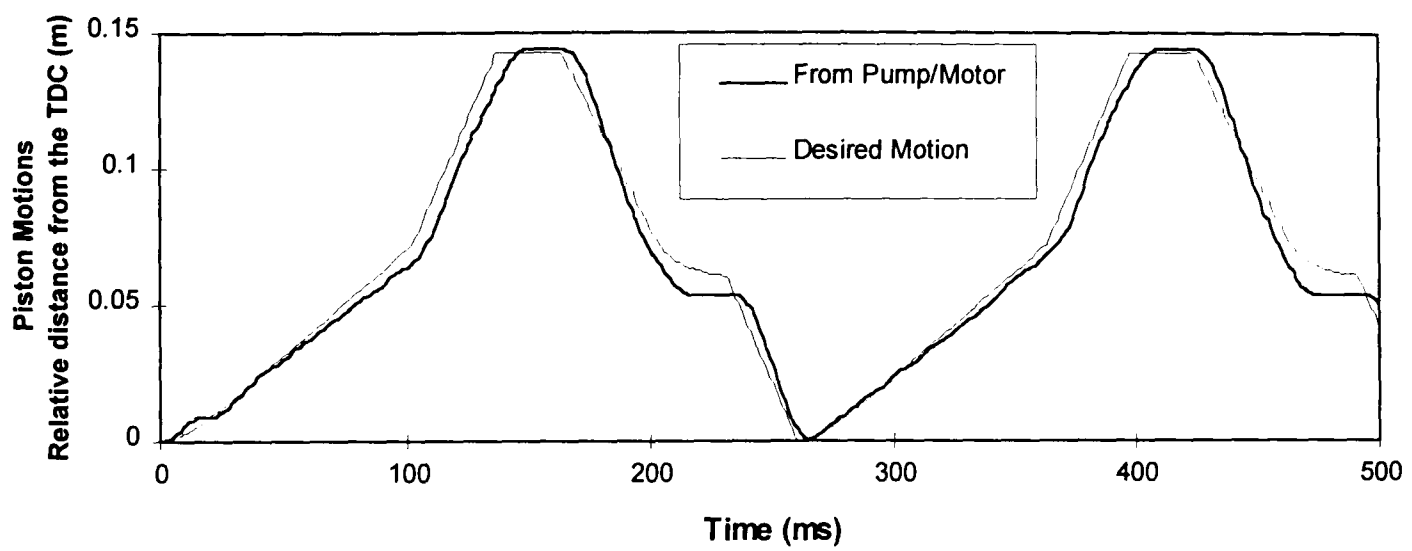
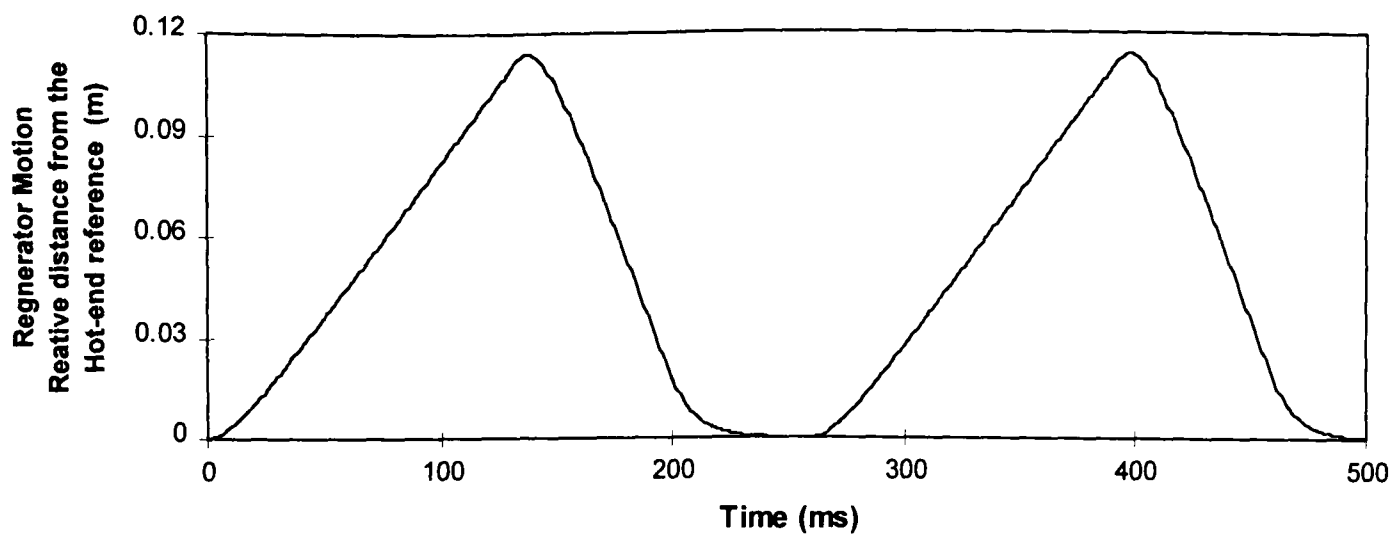


Figure 7.8 : Piston motion generated by the pump-motor following an analogue demand signal having additional feed-back control. The resulting engine cycle with smooth triangular regenerator motion is shown below. Repeating cycles do not superimpose perfectly.

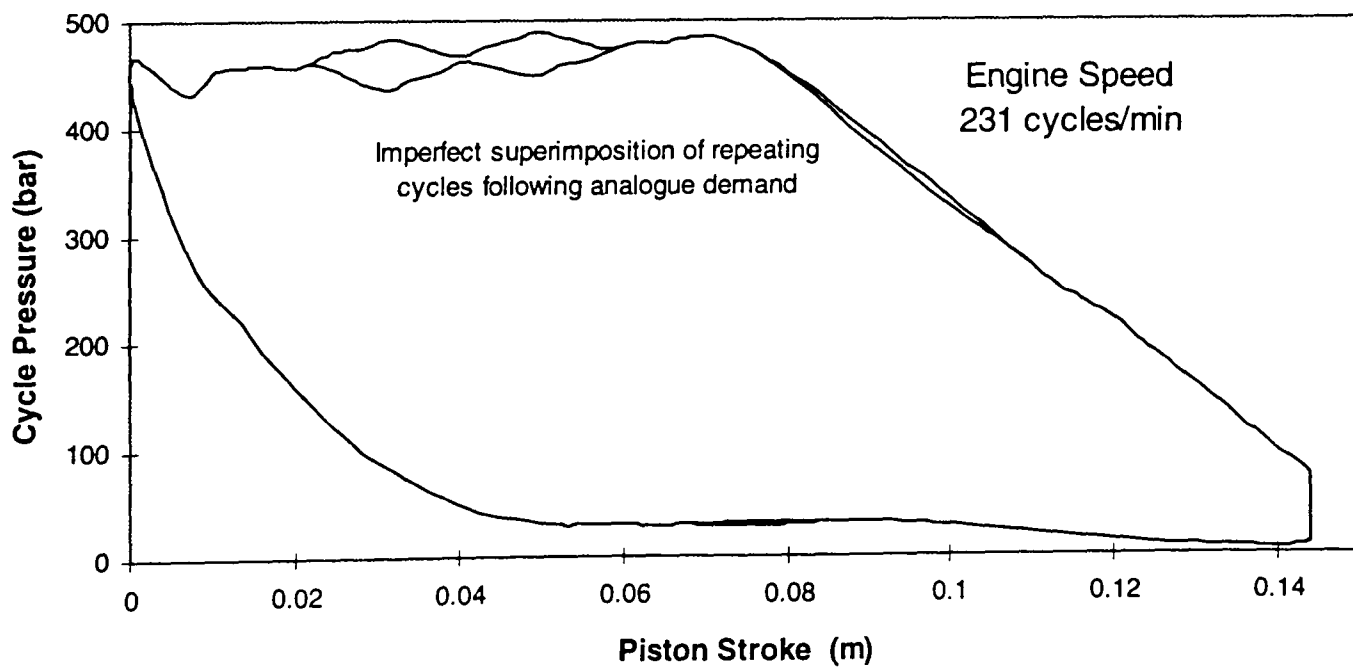
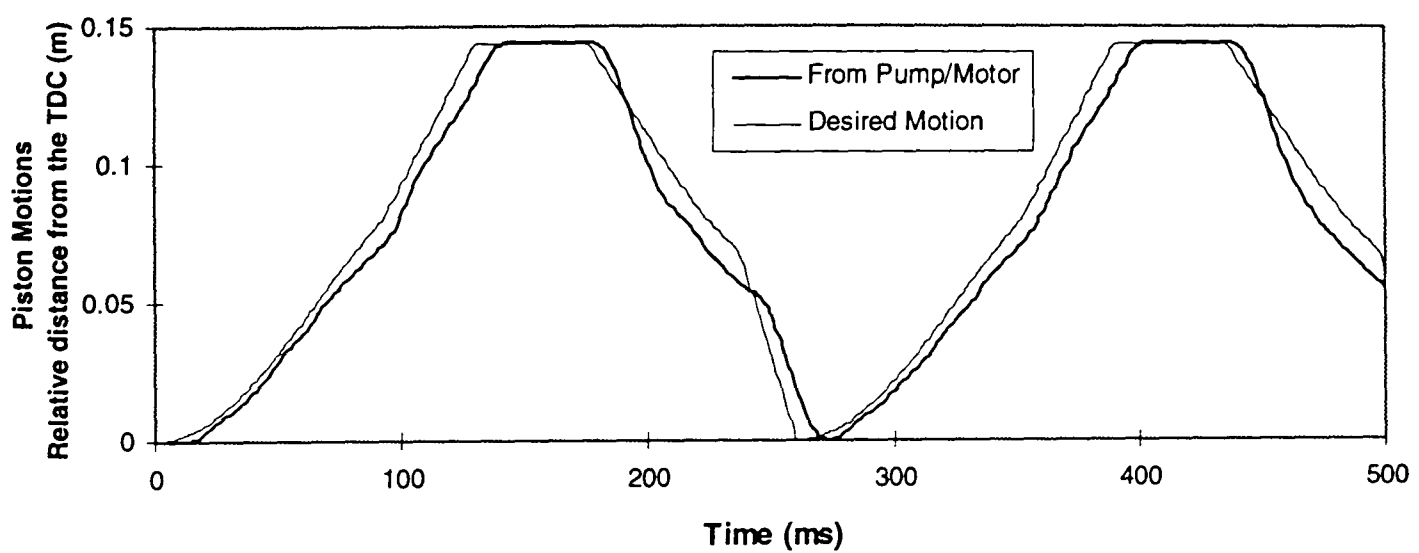
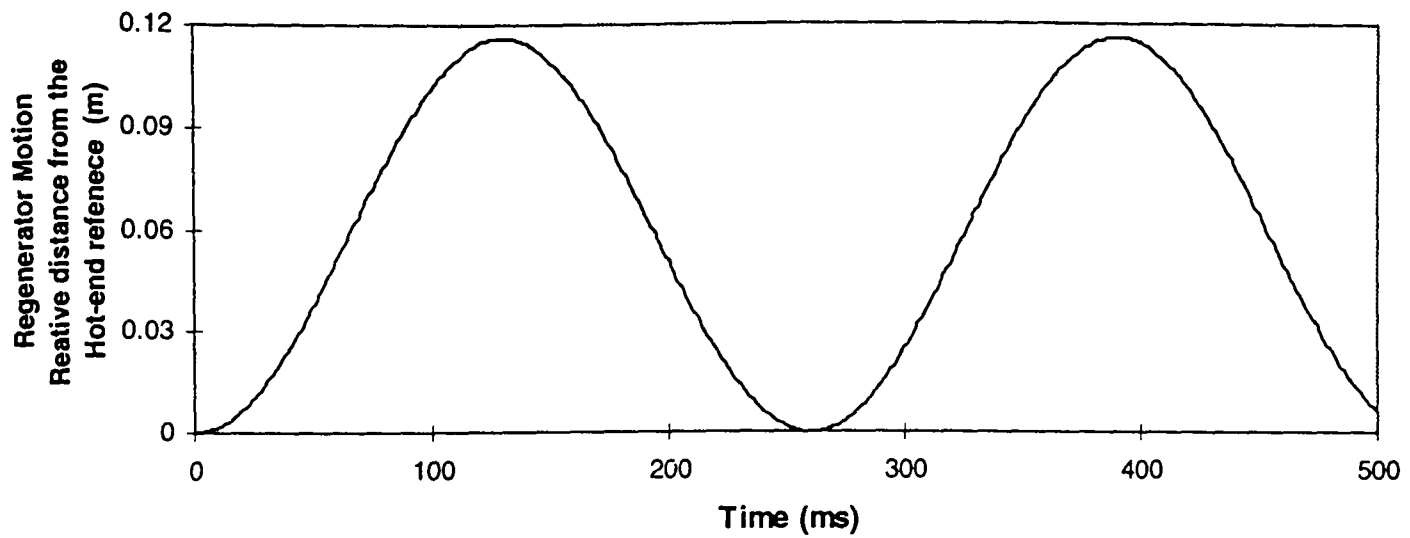


Figure 7.9 : Piston motion generated by the pump-motor following an analogue demand signal with additional feed-back control. The resulting engine cycle with sinusoidal regenerator motion is shown. Repeating cycles do not superimpose perfectly.

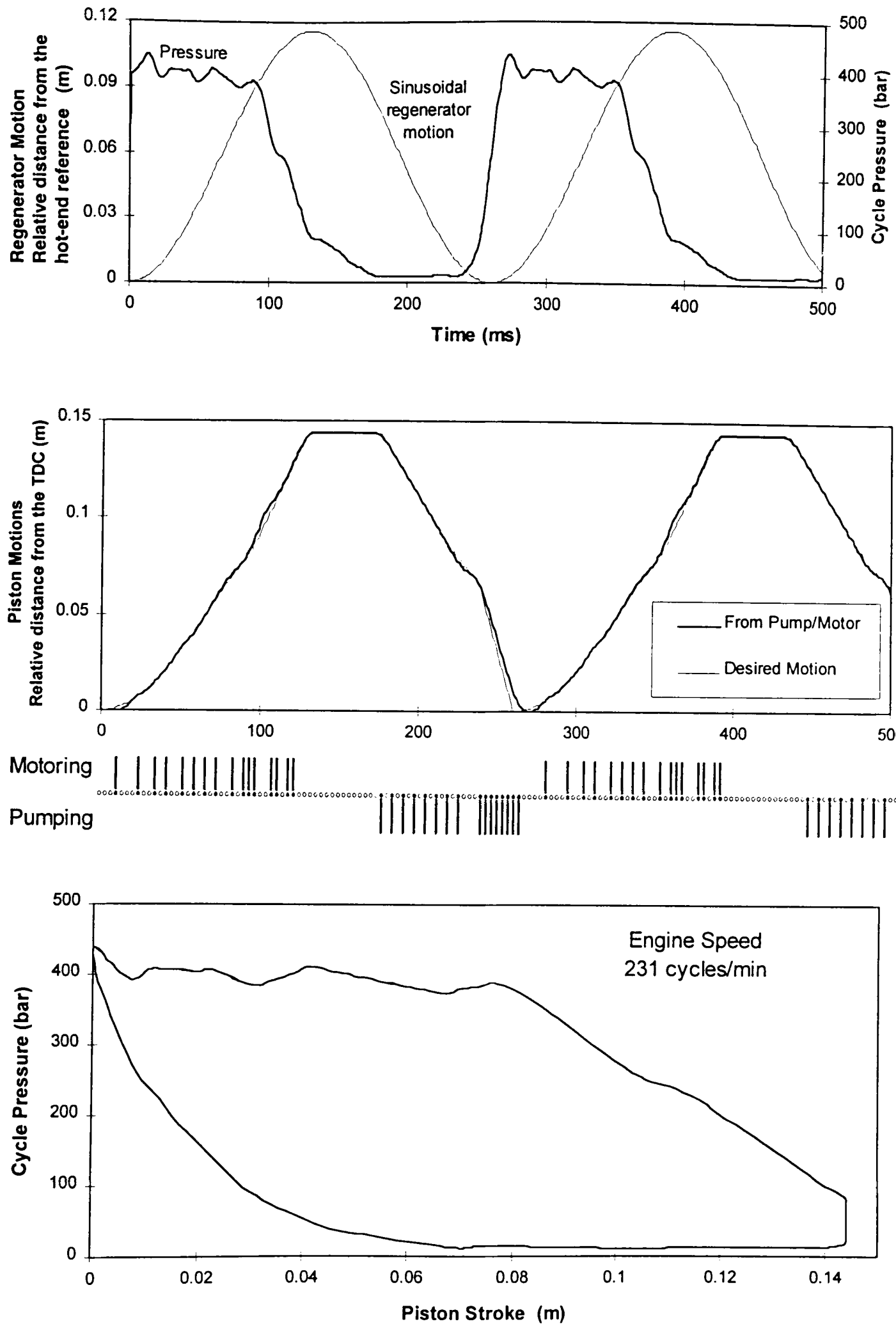


Figure 7.10 : Piston motion generated by the pump-motor following a ternary pattern and the resulting full-power engine cycle for sinusoidal regenerator motion. Following a pre-tuned cyclic enabling sequence by the pump-motor makes the piston follow sharp changes in desired profile. A total of 78 cylinders are available during one piston cycle.

7.4 The overall system

As practical regenerator motions and piston motions generated by the pump-motor have been included into the model, it is useful to have an overall view of the entire system from the TD piles up to the wheels (ie. the load). Figure 7.11 gives a schematic presentation of the entire system. The main components are the TD piles, the multi-bank digital-displacement pump-motor, flexible pistons, regenerator drive mechanisms, wheel motors and a gas-accumulator.

Both hydraulic power take-off from the TD piles and transmission of the power up to the wheels (or other loads) are performed by multiple banks of the pump-motors. One bank may be connected to each half of the TD piles allowing them to work anti-phase. Each of these banks pump water into the TD piles, via the oil-water interface of the flexible piston, during the compression-stroke. Conversely they motor high-pressure fluid out during the power-stroke, giving net positive torque at the pump-motor shaft. Other banks of the pump-motor use this torque to transfer hydraulic oil into the digital wheel motors to get desired mechanical power output. The advantage of using the digital-hydraulic transmission through to the wheels is that of continuously-variable transmission and thus the elimination of the conventional gear box. An additional pump-motor bank could be used for transferring energy in and out of a gas accumulator. This could provide energy needed during starting the engine as well as store energy as the vehicle rolls down-hill or brakes.

The regenerator motion is generated from a drive mechanism, which runs at a fixed speed ratio to the pump-motor shaft. The regenerator-drives work as explained earlier and techniques for controlling regenerator motions are discussed in more details in the next chapter. Auxiliary drives (eg. alternators) may be mounted on the pump-motor shaft which could take advantage as a constant speed drive.

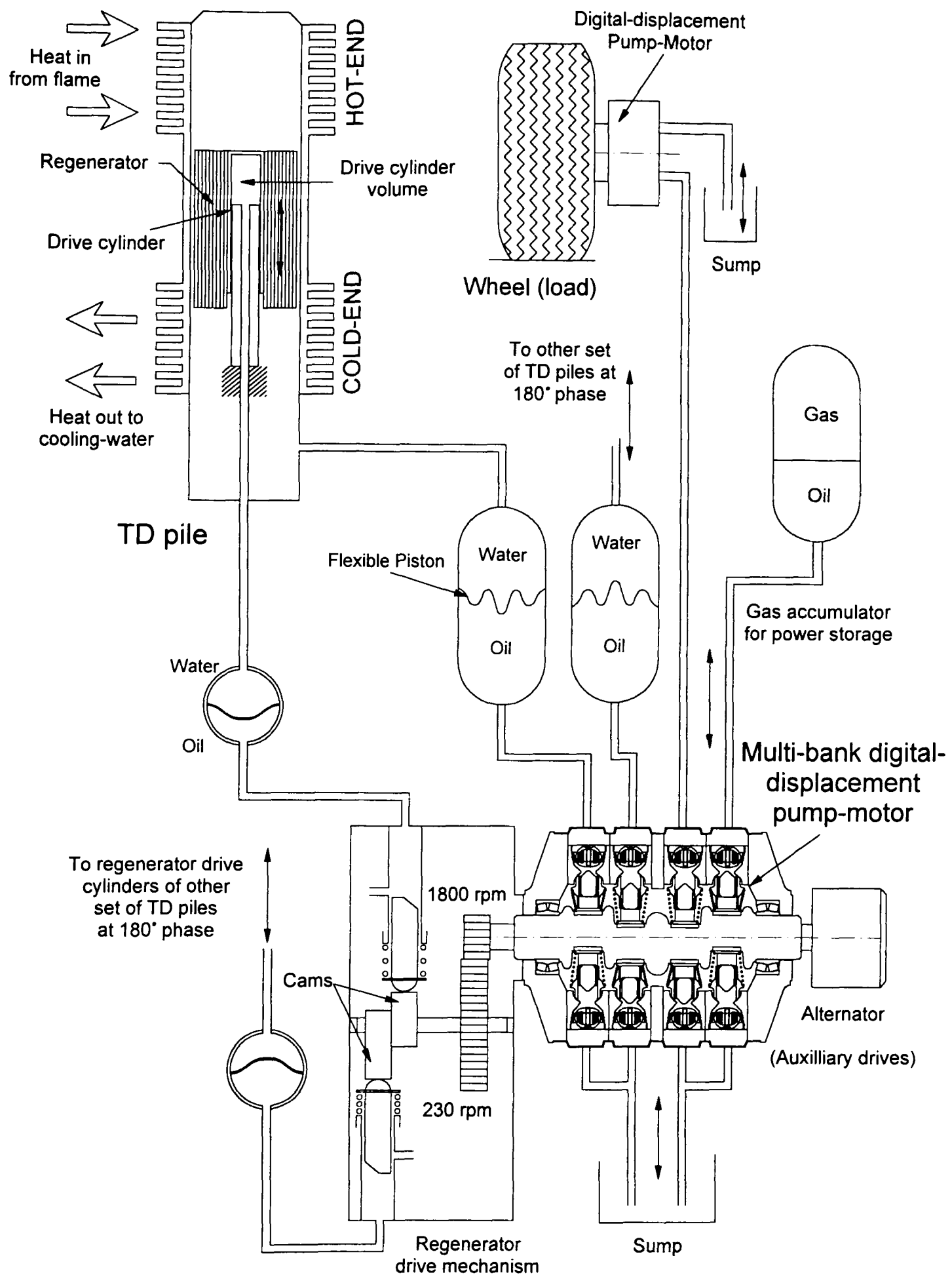


Figure 7.11 : Schematic of a proposed overall system for transferring energy from the hot-flame gases to the wheels. TD piles are divided into two groups at 180° phase to each other and are connected to individual pump-motor banks and regenerator drive mechanisms.

CHAPTER - 8

Control Strategies for Varying Engine Power Levels

8.1 Methods of controlling the engine power

Up to this point only full power engine cycles have been discussed. In practice an engine may need to meet different types of load-demands eg. driving an automobile at different speeds, load-requirements when going up-hill or down-hill, driving synchronous generators, pumping fluids etc. The load may have variable torque or variable speed requirements or both. The different techniques available (Walker et al. 1994) for controlling the power output of a Stirling or Malone cycle and their preferred applications in Artemis-Malone engine can be briefly described as follows:

- (i) **Temperature modulation:** The power output rises with increase in hot-end (expansion space) temperature or with decrease in cold-end (compression space) temperatures. Hot-end temperature can be controlled by changing fuel and/or air flow to the burner while the cold-end temperature can be controlled by the coolant flow. Reducing the hot-end temperature reduces the Carnot efficiency significantly, leading to lower engine efficiencies at part load. For example with hot-end and cold-end temperatures of 550 and 100°C the Carnot efficiency is about 55%, but it reduces to 40% as the hot-end temperature drops to 350°C. Controlling the hot-end temperature would need a high response fuel-control system. But large thermal inertias at the hot-end create a problem for fast response to temperature changes and the metallurgical limits of hot-end metal temperatures need to be considered with. Control of cold-end temperature has a relatively low effect on power output (Reader and Barnes, 1988). In many Stirling engine designs the hot-end temperature is held steady at all operating conditions (Walker, 1980). The design limits of the Artemis-Malone engine are based on the maintenance of fixed temperatures at both the hot-end and cold-ends. Hence the option of varying hot-end temperature is not considered as a primary way of controlling power.

- (ii) **Phase control:** Changing the phase relationship between two reciprocating components affects the pressure-volume diagram and hence the power output. The power output of a conventional Stirling engine as a function of phase angle is sinusoidal in form (Walker, 1980). In the Artemis-Malone engine this option has much greater flexibility as the motions are not linked by a fixed mechanism. The phase control can be effected by changing or shifting the pump-motor enabling decisions.
- (iii) **Speed control:** The power output of the engine increases at higher speeds, though at a progressively diminishing rate in practice, due to the increasing significance of friction losses, thermal saturation of regenerator matrix and decreased effectiveness of heat exchanger. Speed control is used in some Stirling engines (eg. United Stirling 1977, Philips 1971), but is more common in Stirling refrigerators (Walker et al. 1994). The Artemis-Malone engine could use a constant P-V (pressure-volume) diagram or work per cycle, while changing the cyclical frequency for power control (variable-frequency control). With changed engine speed (ie. frequency of regenerator motion) the frequency of piston motion also needs to be changed. The speed control may be done in two ways - using a fixed speed-ratio between the pump-motor and the regenerator drive or using a variable speed-ratio such that the pump-motor runs at a constant speed independently of the varying engine speed. The second option has the advantage of providing a fixed speed shaft at all engine power levels, which is very attractive for driving many auxiliary systems. In both cases the pump-motor tries to follow the desired piston motion according to the regenerator cycle.
- (iv) **Stroke control:** Variation of the stroke lengths of one or both of the reciprocating motions can be an effective way of controlling the pressure level and power. This method is applicable to free-piston or free-displacer machines but not to conventional engines with crank drive mechanisms. Regenerator stroke variation was used by John Malone (1930) as the principal mode of power control. In the 'Thermoelectron Tidal Generator Engine' designed for artificial hearts (Watelets et al. 1976), power control was achieved by varying piston stroke. In the case of

the Artemis-Malone engine this includes stroke control for both the regenerator drive motion and the flexible piston driven by the pump-motor. In both cases stroke control may involve changing the amplitude or offsetting the motion or both. The effect of offsetting motions are somewhat analogous to dead volume control. In all cases the engine and the pump-motor run at fixed speed, while pump-motor tries to follow either a desired piston motion corresponding to the regenerator motion or a desired pre-fixed motion independent of that of the regenerator.

- (v) **Pressure level control:** Variation in the mean pressure level of the working fluid is one of the most widely used control system for power regulation in Stirling engines (eg. Philips 1959). An increase or decrease in the pressure level of the working fluid in the engine can be achieved by adding or decreasing the mass content inside the thermodynamic pile. Due to the complexity of having additional systems for charging mass in and out of the hot-end (where the fluid volume changes with pressure) in a controlled and continuous way and the sealing problems associated with it, this was not considered for the hot-end of the Artemis-Malone engine. On the other hand, at the cold-end (where liquid volume changes little with pressure), shifting of the flexible piston effectively changes the mass of fluid in the regenerator and the hot-end, thus changing system pressure. Another method of cycle pressure modulation can be achieved by controlling the dead-volume. Dead volume can be defined as the part of the working space not swept by either of the reciprocating elements. It should be noted that dead spaces at the hot-end and the cold-end differ in compressibility and hence their effect on system pressure. For example cold-end water at 100°C has a bulk modulus of about 2 GPa, while hot-end steam at 550°C has a value of 0.04GPa and is therefore 50 times more compressible. Hence the effect of changing the dead-volume at the hot-end is more significant on system pressure. For the same reason liquid beyond the cold-end always acts as a dead-volume, but has very little effect on system pressure. Conventionally dead-volume control is done by making an adjustable reservoir space available to the working volume. In the Artemis-Malone engine this can alternatively be done by offsetting either of the

piston or regenerator motion. In case of the flexible piston at the cold-end this is effectively the same as changing the fluid mass in the regenerator and the hot-end by shifting piston motion.

A combination of these techniques may also be used for power control over the entire working range of an engine.

8.2 Comparison of different control strategies

A more careful inspection of the control methods appropriate for the Artemis-Malone engine would reveal their advantages and limitations.

8.2.1 Speed control

Speed control has the advantage that the engine mechanisms repeat through the same cycle motion with only the frequency changing the power. This means that the reciprocating motions can be well tuned to create the desired P-V cycle. A ternary pattern (which allows a desired motion to be followed more closely) can be used effectively for the flexible piston drive only when the pump-motor speed is linked to the engine speed, keeping the speed-ratio constant. This is necessary because the same number of pump-motor cylinders need to be available during one cycle period of the engine to generate the tuned piston motion, independent of cycle frequency. Alternatively the pump-motor (running at a fixed speed) may maintain variable speed-ratios with the engine and follow an analogue demand signal. With the pump-motor operation kept fixed at high speed, the enabling of pump-motor cylinders has to be made less frequently (as with fixed speed the flow output of each cylinder remains the same) to match the slower piston motion. This is reflected in a more abrupt piston motion which causes larger pressure ripples in the thermodynamic cycle (especially at the higher pressure level), as shown in figure 8.1 where the engine speed is reduced to half and with the pump-motor following an analogue demand signal. Cylinder enabling sequences are not exactly the same for consecutive cycles when the pump-motor controller follows an analogue signal and this results in imperfect superimposition of cycles in the P-V diagram (figure 8.1). The effect is worse at lower engine speeds.

As the P-V diagram has approximately the same area at any power level the engine always has to go through same amplitude of pressure variation (from 400 bar to 10 bar approximately) in each cycle. The creep rate, and hence the life of the pressure vessel, is a higher-order function of the pressure it has to sustain (Greenfield, 1972). The relation can be represented by the equation : $\epsilon = K\sigma^n$ where ϵ is the strain rate, σ is the stress and K and n are constants of the material. For many metals and alloys value of n ranges from three to five. This means that if the stress is doubled creep strain rates will usually increase somewhere between 8 and 32 times, hence reducing the engine life correspondingly.

8.2.2 Regenerator stroke control

In this approach the speeds of the engine and the pump motor are kept constant. This ensures that always the same number of pump-motor cylinders are available during each engine cycle (which allows the use of ternary patterns) and, also, that a fixed speed is available for auxiliary drives. As the stroke length of the regenerator is reduced to half, the desired amplitude of piston motion is also reduced correspondingly in an attempt to maintain the same pattern of pressure-volume diagram. But with fixed pump-motor speed, fewer enabled cylinders are needed (as the flow output of each cylinder of the pump-motor remains the same) which again makes the motion more abrupt and results in larger pressure ripples in the thermodynamic cycle (specially when trying to maintain the higher pressure level), as shown in figure 8.2 when the regenerator stroke is reduced to half and the pump-motor follows an analogue demand signal. Following a ternary sequence will give similar results, although the number of ternary codes available for achieving different regenerator stroke lengths will be much limited. The pressure pulses increase in magnitude as the regenerator stroke is reduced. Results shown in figure 8.1 and 8.2 indicate that with a fixed pump-motor speed, if every change in regenerator motion (in stroke-length or frequency) needs to be followed by a corresponding change in piston motion generated by the pump-motor (in order to maintain the same pattern of the P-V diagram), the resulting effects on the engine cycle may not be always desirable. In such situations an alternative control approach of using a pre-tuned piston motion seemed to be attractive. The existence of a pre-tuned but fixed piston motion

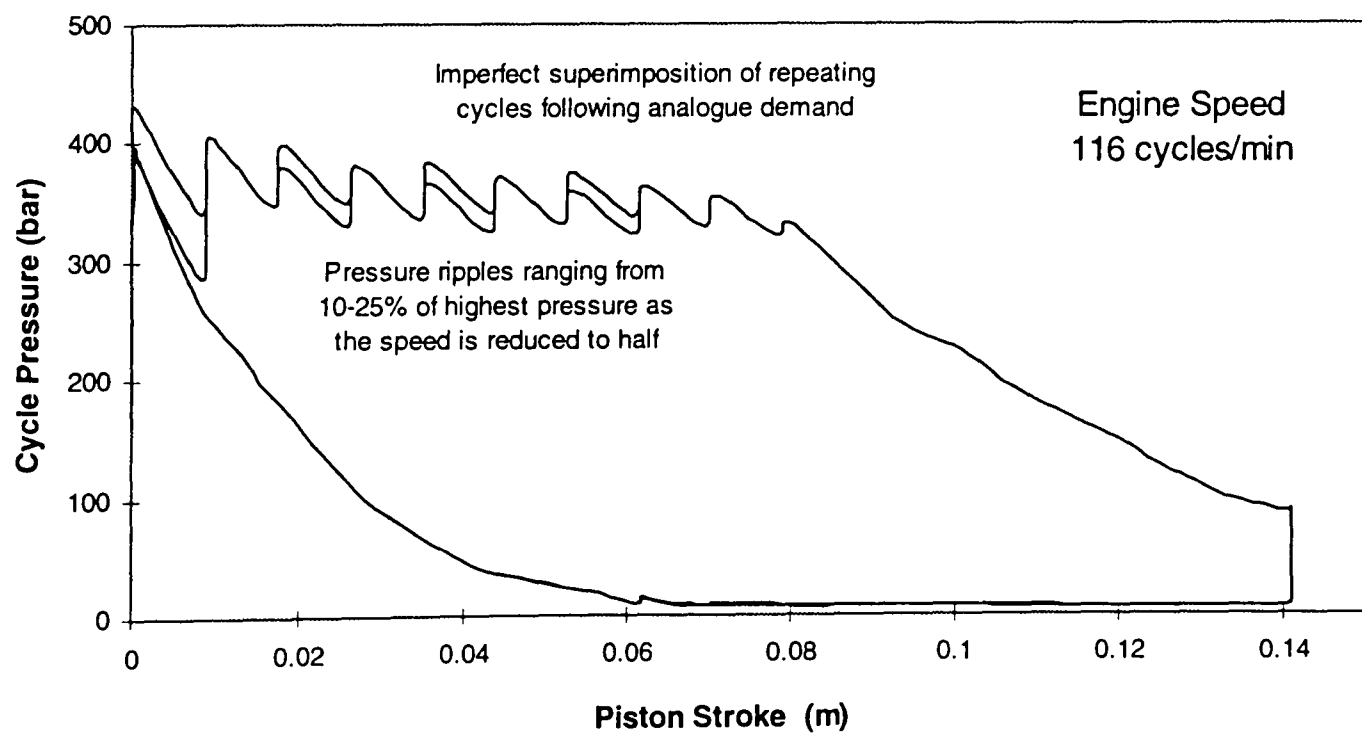
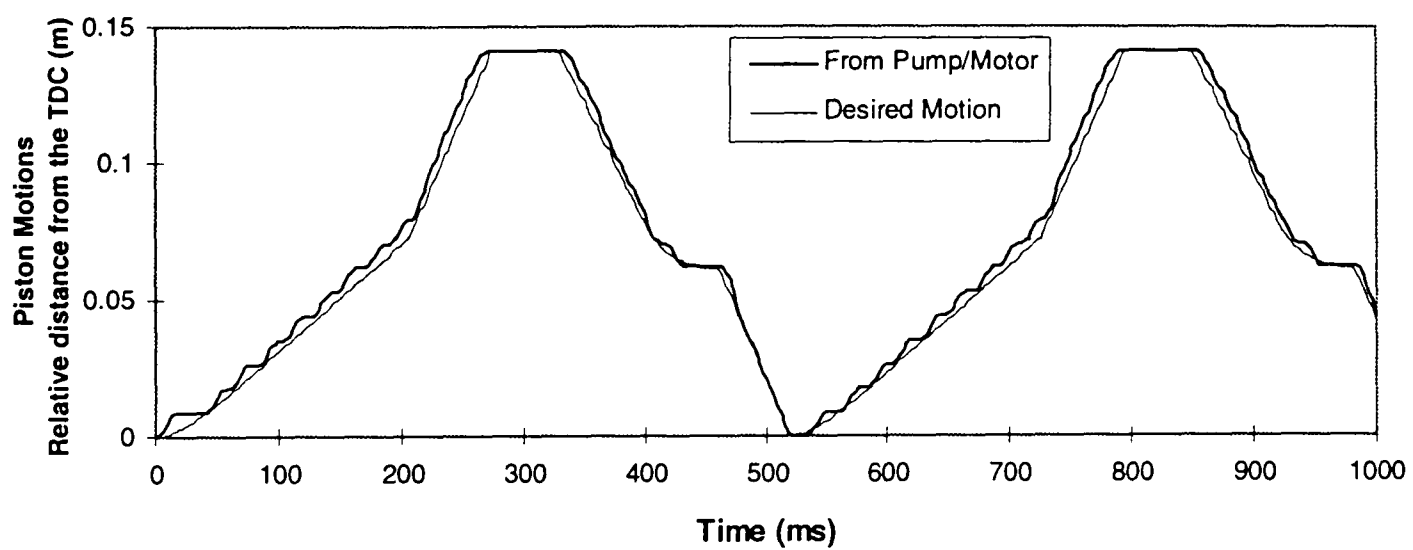
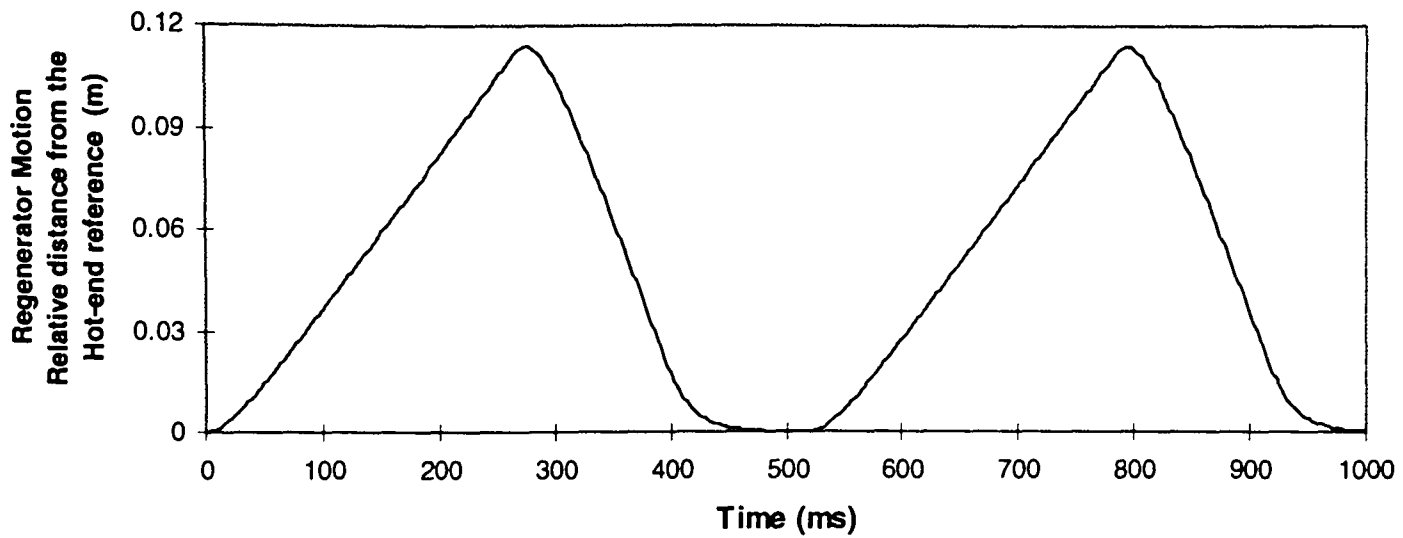


Figure 8.1 : (Speed Control) Piston motion generated by the pump-motor, when it is still running at high speed, while the engine speed is reduced to half. The resulting cycle shows large pressure ripples (10-25% of the desired high-pressure level).

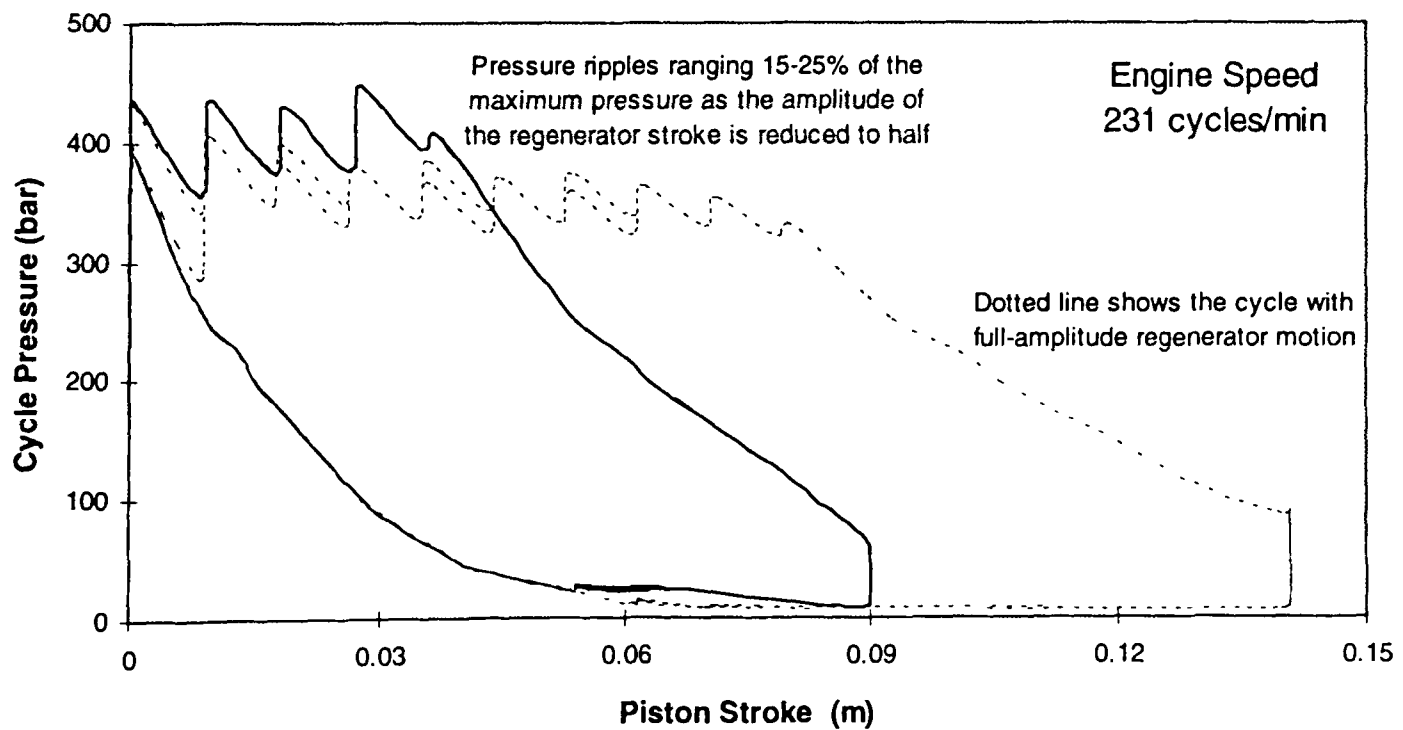
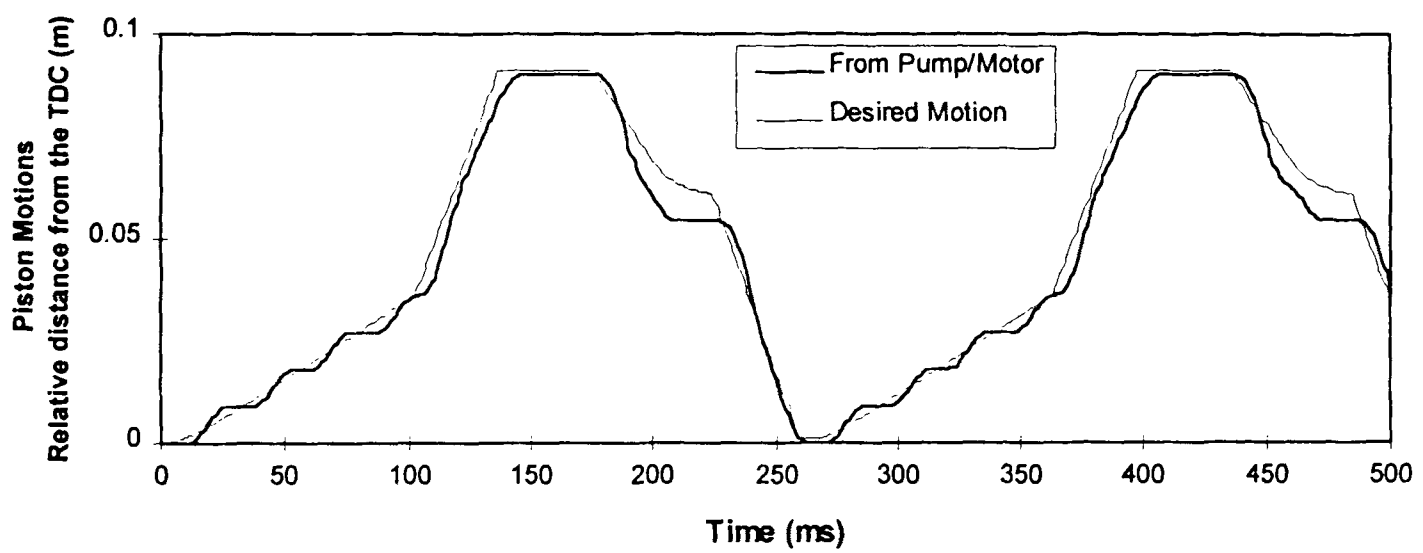
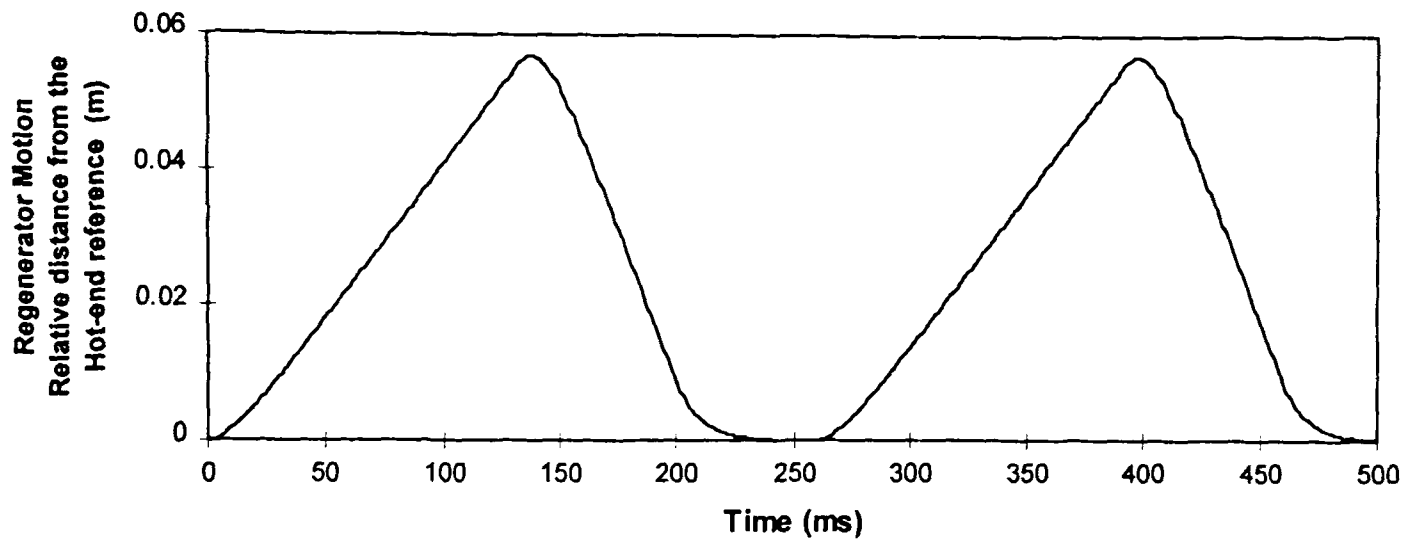


Figure 8.2 : (Stroke Control) Piston motion generated by the pump-motor still running at high speed, while the amplitude of regenerator motion is reduced to half. The resulting cycle has larger pressure ripples. The dotted line shows the cycle for full stroke regenerator motion.

allows the effects of changed regenerator motion on the resulting cycle to be studied, independent of the piston motion.

Once it was decided that the engine and the pump-motor speeds would be kept constant, thus allowing the use of pre-tuned ternary cylinder enabling codes, the prospects of controlling the regenerator motion for regulating the power over the entire working range of the engine was reinvestigated. The two main aspects were to examine the effect of changing the regenerator stroke length and to offset the full stroke motion towards the cold-end on the thermodynamic cycle, while the piston motion remained unchanged. Simulations were carried out using a sinusoidal regenerator motion instead of a triangular motion, as it demanded less abrupt changes in regenerator velocity and was easier to achieve in practice.

Varying regenerator stroke lengths:

Figure 8.3 shows the effect of varying the stroke of the regenerator motion on the engine cycle, while the piston motion is unchanged. With the regenerator stroke reduced, the piston also needs to move at a slower rate in order to maintain the cycle pressure as the regenerator moves towards the cold-end in the power stroke. But, as the piston motion remains unchanged, it continues to move at a rate relatively faster than that needed to hold the cycle pressure. This results in a gradual drop of pressure as the regenerator moves from the hot-end to the cold-end. The changes do not occur at an equal rate at different pressure levels. The pressure drop is higher at higher pressures. During the other part of the cycle, when the regenerator and the piston move back to their initial positions, the effect on the cycle pressure is less, as can be seen from the low pressure levels of the cycles in figure 8.3. As a result, with decreased regenerator stroke, the area of the P-V diagram decreases and consequently produces less power.

If the power modulation throughout the entire working range is done by controlling the regenerator stroke alone, the thermodynamic pile would experience large-amplitude pressure-variations in each cycle (as it passes through the highest and lowest levels of pressure) which would have adverse effects on the engine life.

Varying offset of regenerator motion:

Figure 8.4 shows the effect of changing the working range (offsetting) of the regenerator motion with a fixed stroke, while the piston is following a fixed pattern of motion. Offsetting the regenerator motion is equivalent to controlling the dead volume at the hot-end, although keeping the total mass of fluid in the thermodynamic pile unchanged. The offsetting of a fixed stroke regenerator motion may be done by using a biasing cylinder which shifts the entire range of motion. With the regenerator moved towards the cold-end and the piston stationary or if the regenerator motion is offset towards the cold-end but the piston motion is kept constant, the fluid mass at the cold-end decreases. As the temperatures of the hot-end and cold-end fluids are considered to be constant, the system pressure rises to conserve the mass balance. The effect is not the same at different pressure levels, with the rise being greater at higher pressures. Hence offsetting the regenerator motion towards the cold-end does not merely shift the position of the pressure-volume diagram in pressure axis, it changes the enclosed area and hence the cycle power. It should be noticed that reducing the stroke of the regenerator decreases the pressure and the cycle power, while offsetting the fixed stroke regenerator motion towards the cold-end raises the pressure and increases it. The drive mechanisms needed for changing the stroke amplitude and for offsetting the stroke of the regenerator may have different degrees of complexity.

This technique of offsetting can be used for continuously varying power over a limited range but is not suitable if used alone for controlling the entire working range. For such a case the piston and fixed stroke regenerator motion (without any offset) needs to be set for a low-power thermodynamic cycle (eg. 10% of full power) . The power will rise as the regenerator motion is offset towards the cold-end. But with the peak pressure rise, the high line in the P-V diagram following the power stroke becomes inclined as seen in figure 8.4. As a result, the peak-pressure-requirement to produce full-power from the low-power cycle (by offsetting regenerator motion) exceeds the design pressure limits of the hot-end.

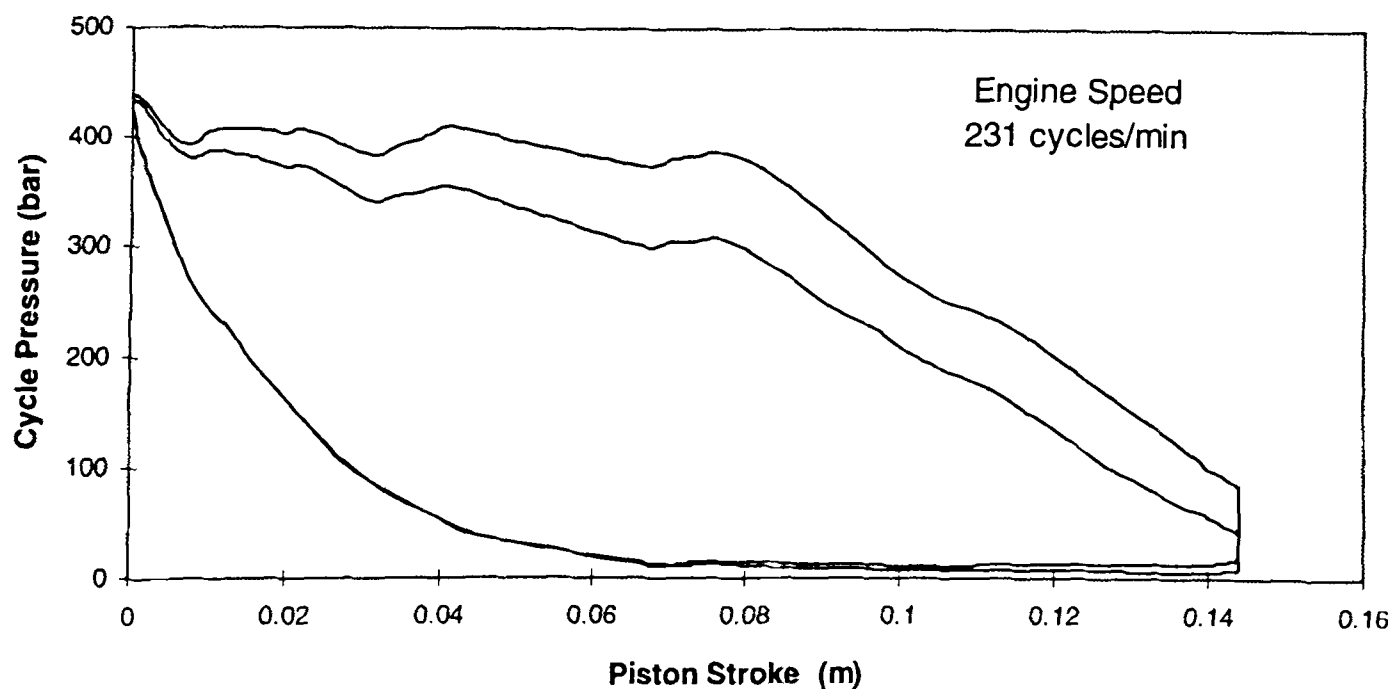
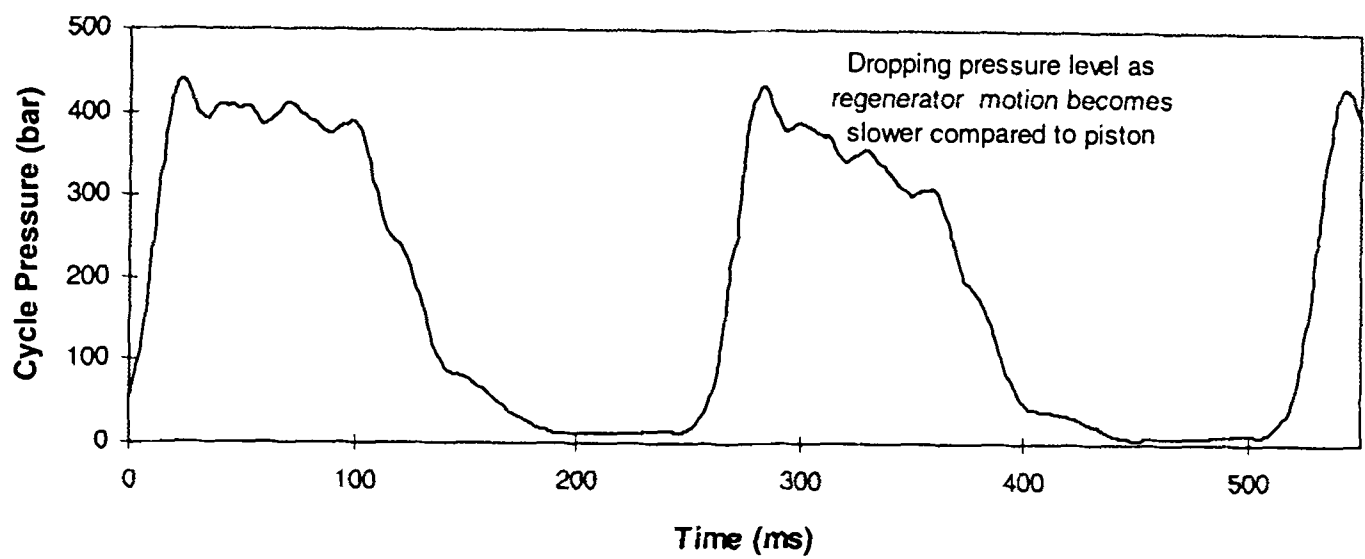
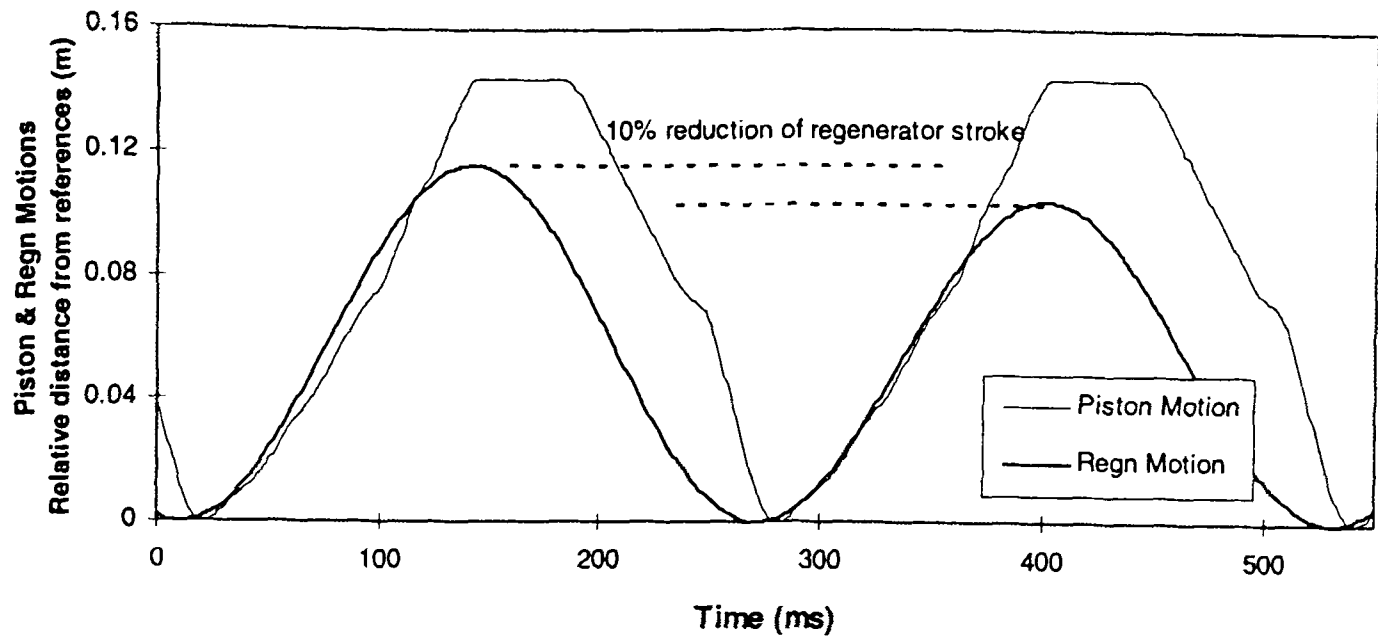


Figure 8.3 : Effect of decreasing the regenerator stroke by 10%, while the piston motion following a ternary pattern remains unchanged. Cycle pressure gradually falls as the regenerator is now moving at lower velocity compared to the piston motion. Power output is reduced by 23% compared with full power.

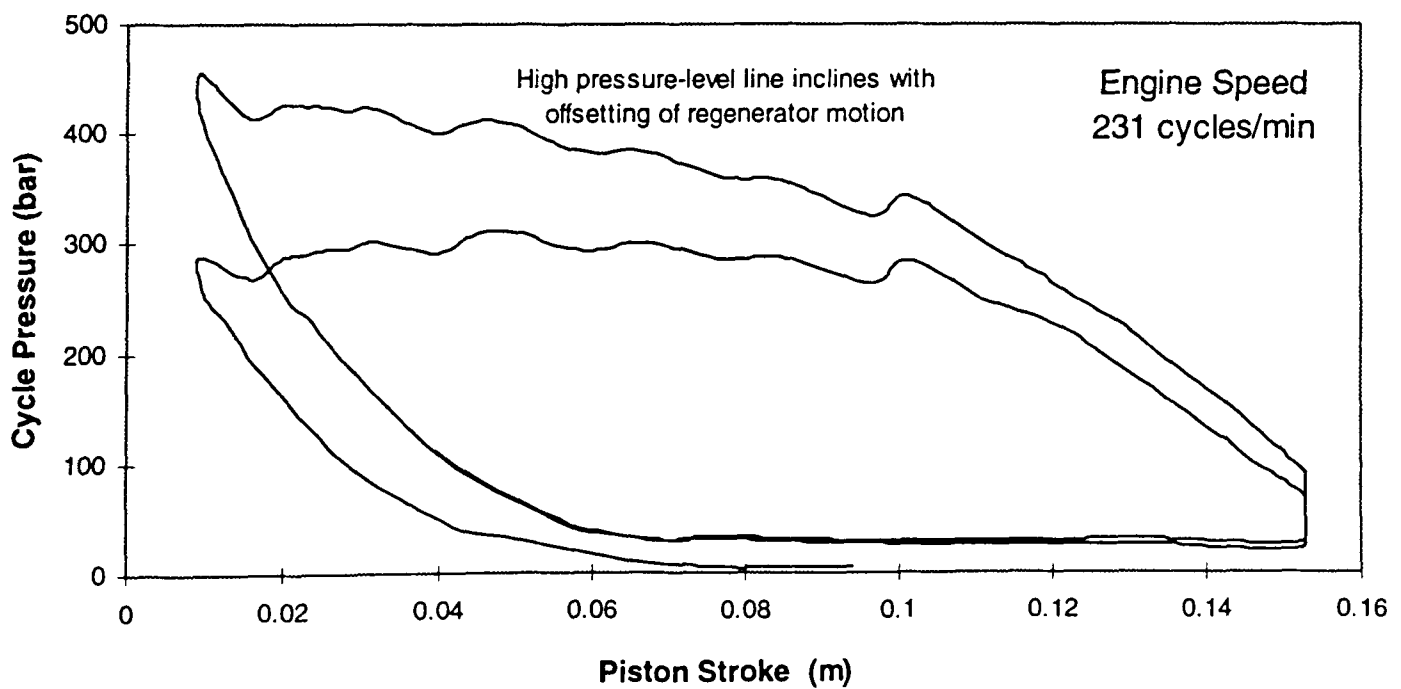
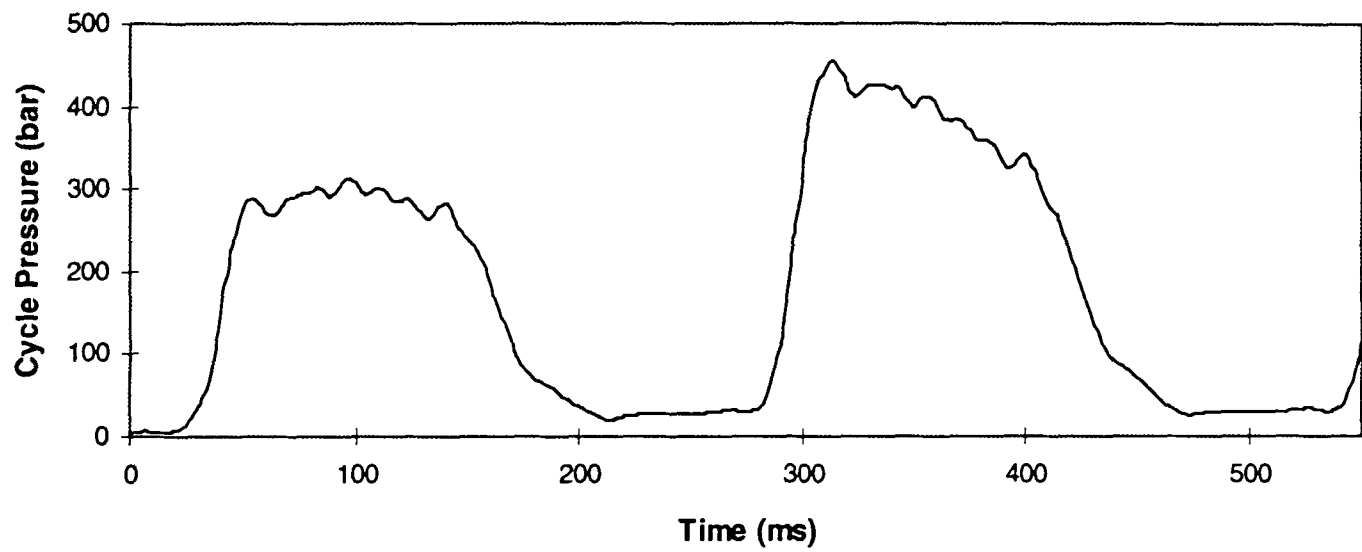
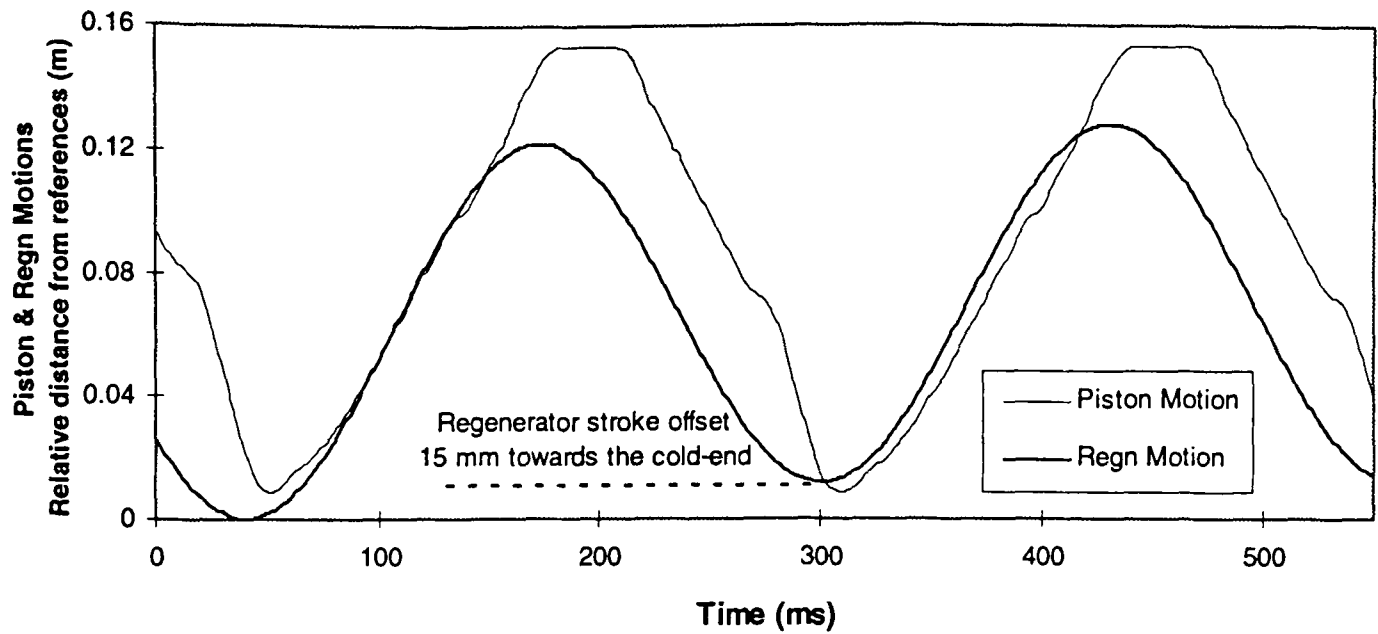


Figure 8.4 : The effect of offsetting the regenerator motion towards the cold-end without changing its stroke length, while the piston motion (following a ternary pattern) remains unchanged. Cycle pressure rises with the offsetting resulting in 32% rise in power output.

8.2.3 Controlling piston motion

Another effective way of controlling the output power may be to control the pressure level of the engine cycle by offsetting the piston motion, keeping the regenerator motion fixed. Here also the engine and the pump-motor speed is considered to be fixed. For each offset of piston motion the pump-motor follows a table of ternary code. Each adjacent piston motion profile is offset by one cylinder volume of the pump-motor. This depends on the desired P-V diagram shape of the resulting thermodynamic cycle. At the beginning of each thermodynamic cycle (ie. when the regenerator starts its stroke from the hot-end to the cold-end), the controller identifies the appropriate ternary-code and executes that enabling sequence throughout the cycle. With increased offsetting (without changing the stroke) the piston moves in a range further away from the TDC reference. As the piston motion is offset from the TDC reference (with or without changing the amplitude) the fluid mass at the cold-end increases and, for constant end temperatures, the peak pressure level of the cycle reduces to conserve the mass, resulting in a power reduction. The limitation of controlling the engine power level by offsetting the piston motion lies in the quantisation error of the pump-motor. It is only possible to offset the piston motion by increments of one or multiple cylinder volumes. This gives rise only to a finite number of pressures levels (eg. five to six, depending on the cylinder volume) which allows for only the same number of output levels. This technique is the most effective way discussed so far for ranging the output power and gaining crude-control of engine output. The advantages include :

- The peak pressure level of the cycle varies proportionally with power, so the TD pile only has to withstand high pressure for full load.
- The reduced stress level and creep rate extends engine life.
- The engine goes through smaller pressure-swings through cycles at part load leading to less noise.
- Fixed pump-motor and engine speeds can be used.
- The offsetting of piston motion does not need any additional hardware since it can be achieved by incorporating one or more extra pumping or motoring cylinders in the enabling sequence of the pump-motor.

For a fixed regenerator motion the piston motions could be set for a number of ternary patterns (eg. in the model the entire working range was divided in to six pressure levels and power zones, each corresponding to a ternary pattern of piston motion). Each shifted piston motion was offset from the other by one cylinder volume of the pump-motor. Figure 8.5 shows transition of thermodynamic cycle with piston motions shifting away from the TDC by one cylinder volume of the pump-motor, resulting in reduced cycle pressure and power.

The technique of offsetting the piston motion using the pump-motor has all the advantages mentioned above for crude-power-control. It unfortunately has shortcomings as a method for fine-power-control, due to quantisation. There can be two possibilities for controlling engine power to any desirable level, using this method alone.

One method might use a very large number of ternary patterns - trying to manipulate ternary patterns for each of the six power levels to have a very large number of variations of P-V diagrams ranging from the present power level to the next offset one. Any rearrangement of a ternary sequence needs to ensure a number of constraints as follows:

- The piston needs to come back to the same position at the end of each cycle hence the number of pumping and motoring cylinders per cycle has to be same.
- The maximum and minimum pressure throughout a cycle should not exceed the permitted pressure range.
- It is desirable that the high pressure is maintained with minimum ripple as the regenerator moves towards the cold-end and sharp pressure fluctuations should be avoided.

All these constraints make the variability of the ternary set far too restricted to make the necessary variety of P-V diagrams to sweep each power range.

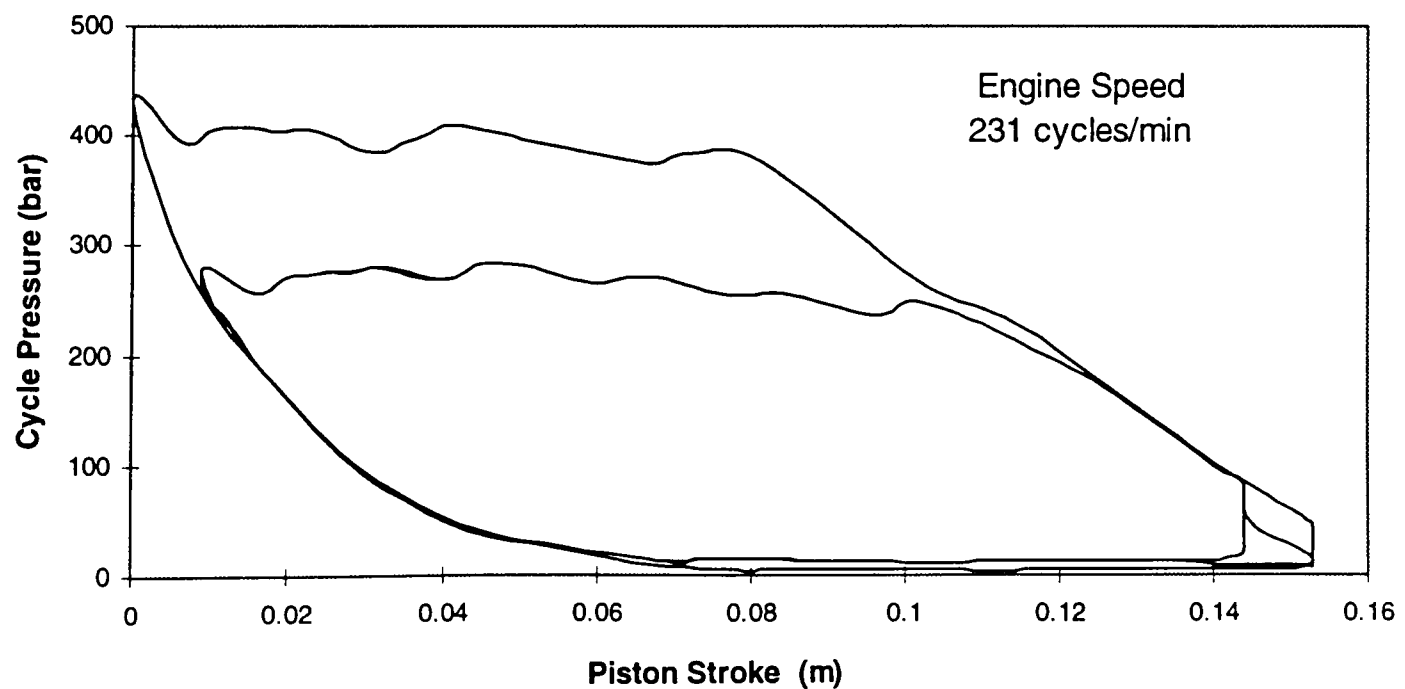
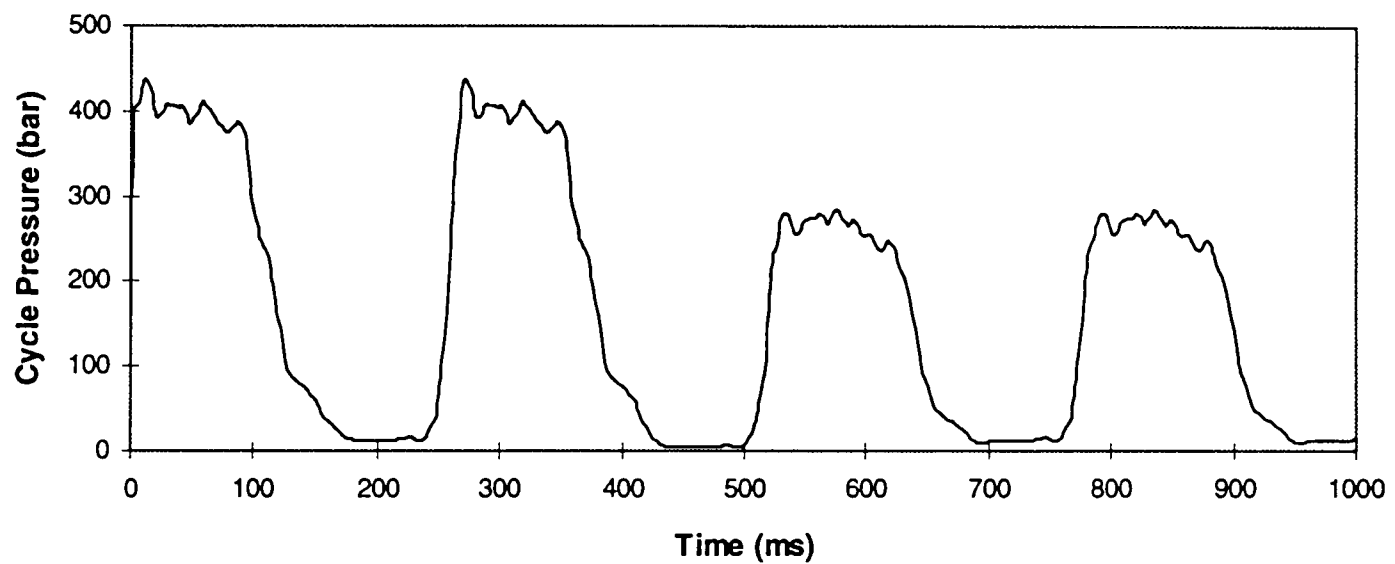
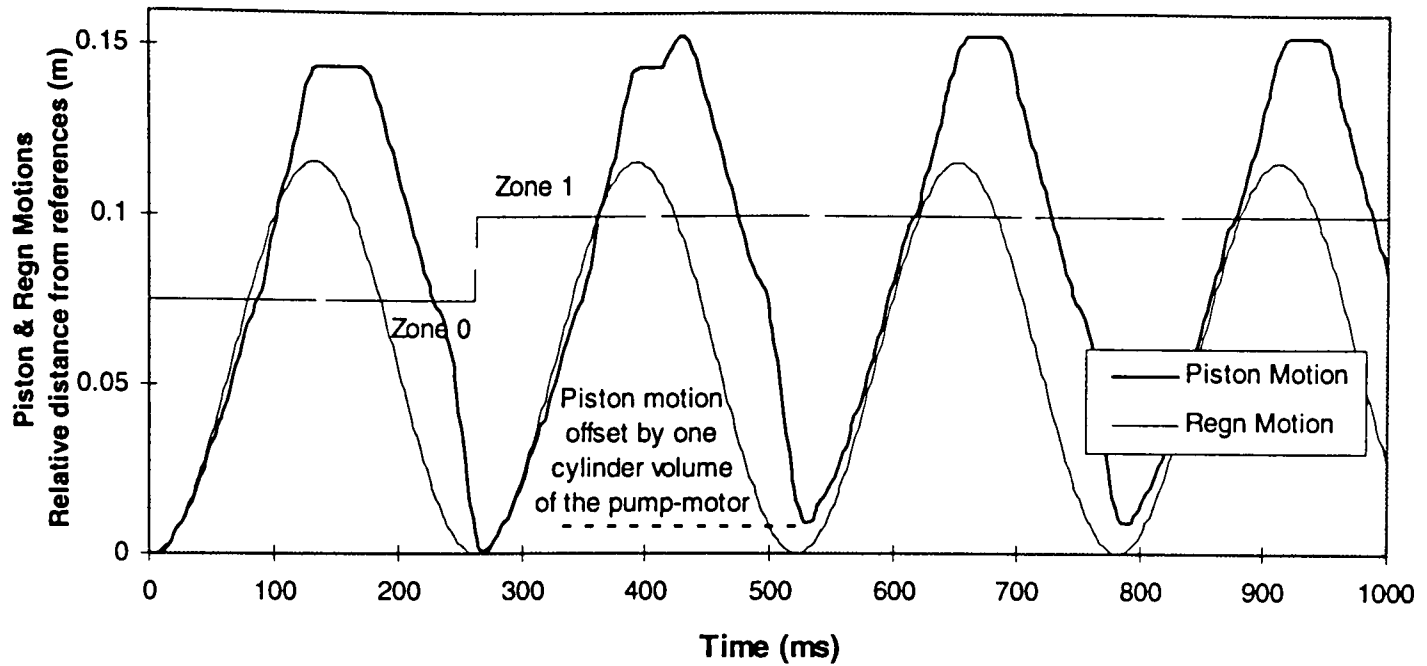


Figure 8.5 : The effect of offsetting piston motion away from its TDC as the ternary pattern followed is changed, while the regenerator motion remains unchanged. As the piston range moves further away from its TDC, cycle-pressure falls resulting in 33% reduction in power.

The other suggestion (by W.H.S Rampen) was to avoid fine control of the power altogether by time averaging the output of different power levels achieved by crude control through a power storage device (eg. a gas accumulator) in the transmission line. But this has the disadvantage that the piston motion will be offsetting very frequently causing almost all cycles to be *transition cycles* (cycle in which the piston motion is offset). In the transition cycles, due to an ongoing change of piston motion, the power output from the engine has a larger discrepancy from the demand. This problem of power mismatch in transition cycles will be described in more detail in the next chapter. This technique also has the inherent limitation that an instantaneous power demand is followed at a resolution of the power difference between adjacent thermodynamic cycles (piston motion generated by two adjacent ternary-code). This may lead to a quantisation problem in terms of power. So, on the whole, power-control by offsetting pre-tuned piston motions was found to be more suitable for achieving crude control of power over the entire working range.

8.2.4 Combined strategy

Results of the different control strategies discussed so far show that some disadvantages are associated with each of them if they are used as the only power control technique for the entire working range of the engine. This suggests that it may be advantageous to use a combination of control strategies to cover the entire power range.

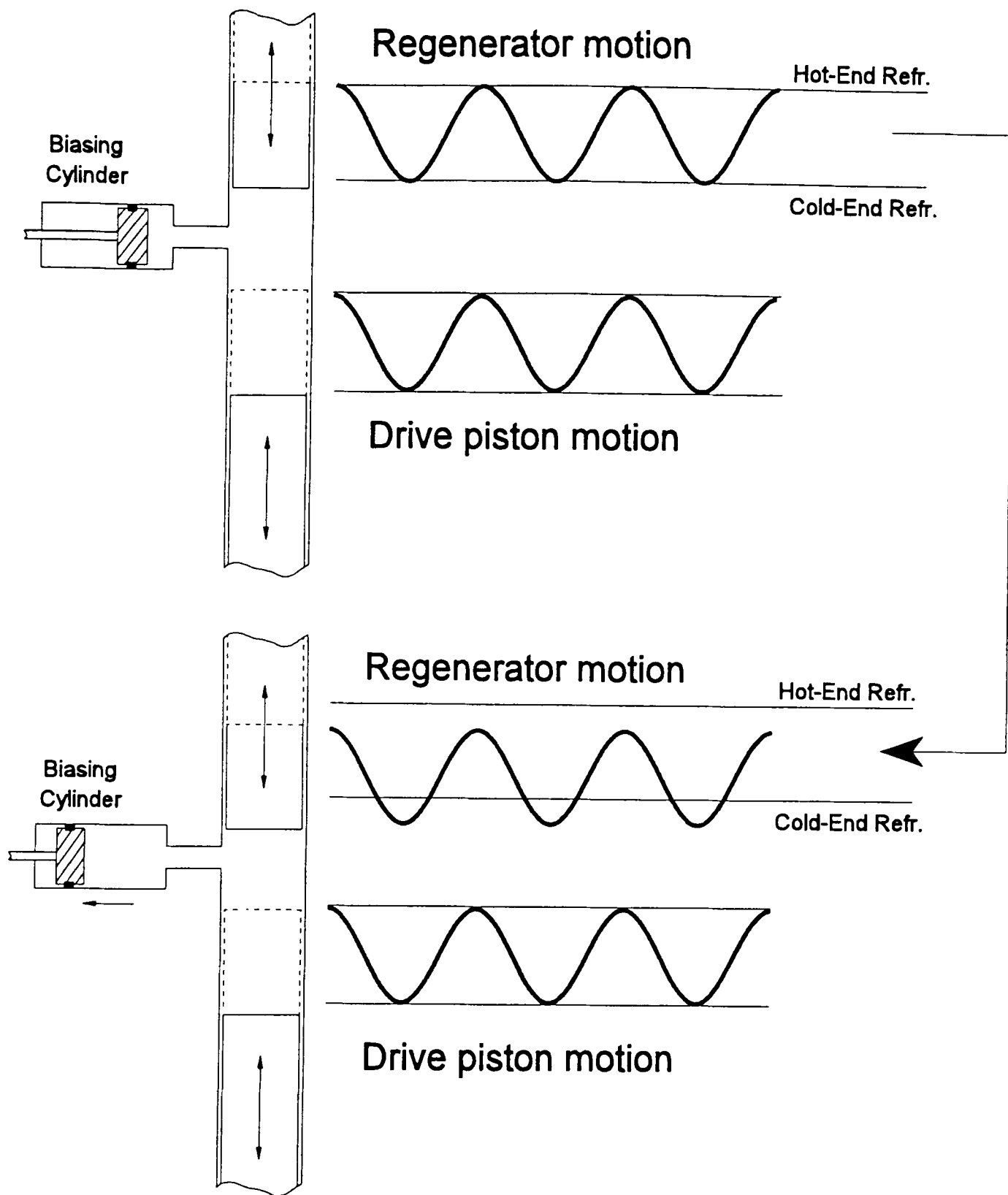
Once the choice for coarse-power-control was made using the option of offsetting the piston motion, different techniques were investigated to achieve finer control on output power in between two adjacent power levels. Simulation of different combinations of the main strategies and their further variations were carried out. These were intended for controlling both the regenerator and piston motions to achieve full power output variability from the engine. Finally three control strategies were proposed instead of a single one, as the simulation results for each looked promising. For each method the same technique of offsetting the piston motion is used for coarse power control. So the common strategy for all the three methods can be given as :

- The total power range of the engine is divided into several suitable power-zones.
- The engine (ie. regenerator cycle) and the pump-motor always run at fixed speeds maintaining a fixed speed-ratio. Hence for each engine cycle a fixed number of cylinders are available at the pump-motor to control the flexible piston motion.
- The enabling sequence to be followed by the pump-motor is updated at the beginning of each regenerator cycle. For each power-zone, the pump-motor repeatedly follows a set of ternary-code for enabling and disabling cylinders, independent of the nature of regenerator motion.
- Each successive set of code results in a piston motion in a step further away from the TDC by one cylinder volume. As soon as the power demand changes zones, the pump-motor enabling is shifted to the ternary-code of the corresponding zone. Ternary-codes can be selected or tuned corresponding to the requirements of the fine-control-method, chosen in the combined control method, which may be different for the three methods.

All three methods use regenerator motion control, though the way the regenerator motion is varied is different for each. These are described as follows:

(1) Fine control by offsetting :

In this strategy the fine control of power in between adjacent power levels is done by offsetting the regenerator motion towards the cold-end. The regenerator always moves between the hot-end and the cold-end in a sinusoidal motion with a fixed stroke. In the model regenerator motion control was achieved by offsetting the output from the sinusoidal motion generator block. In practice a separate fine controlled motion biasing system (eg. a biasing cylinder) can be used for offsetting the regenerator motion towards the cold-end. A schematic drawing of such a system is shown in figure 8.6. As the amount of liquid inside the biasing cylinder is increased, the regenerator motion is offset towards the cold-end. Offsetting the regenerator motion causes the peak cycle pressure to rise and hence the power output. At zero offset of the regenerator motion in each zone the piston motion causes engine power to be equal to the lowest power demanded in that power-zone. With increasing demand level, the regenerator motion



As the volume of liquid taken in the biasing cylinder increases the regenerator motion is offset towards the cold-end. This causes rise in cycle pressure and hence the power output.

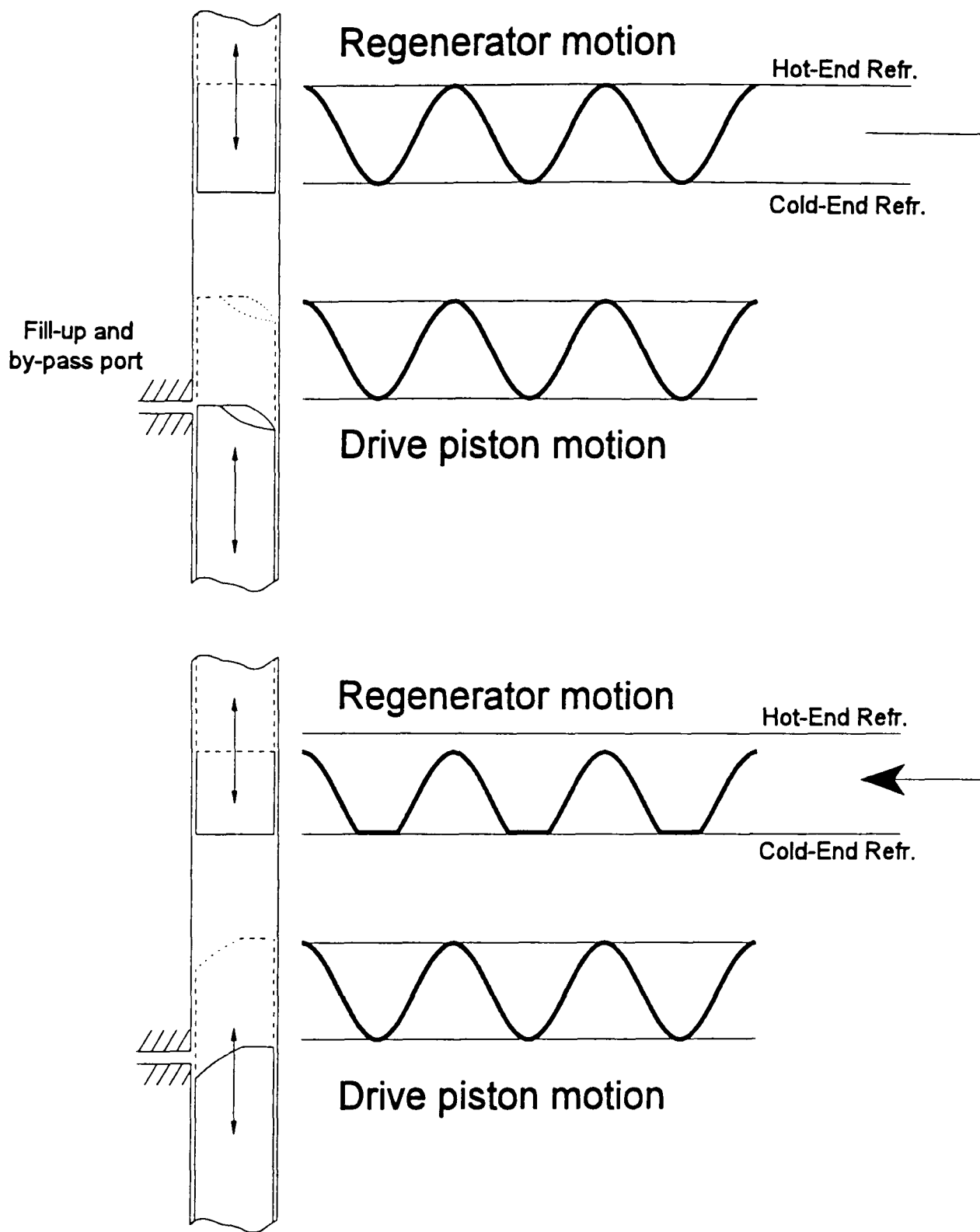
Offsetting regenerator motion towards the cold-end

Figure 8.6 : Offsetting the regenerator motion towards the cold-end, though the drive cylinder motion is the same. Changing the volume of liquid inside the biasing cylinder changes the position of the regenerator motion relative to the hot-end reference. Increasing the volume of biasing cylinder liquid causes the regenerator motion to be offset towards the cold-end while the stroke length remains the same.

is increasingly offset towards the cold-end to meet the requirement. This is only continued until the demand reaches the lower limit of the power-zone above. The controller then shifts the piston motion ternary-code and the regenerator offsetting is brought back to zero. For further increase in demand the whole process is repeated, while the reverse happens as the demand from the user falls. Examples of such transitions will be described in the next chapter.

(2) Fine control by offsetting and clipping:

The second plan also uses offsetting of the regenerator motion towards the cold-end for fine control of power but in a different way such that the regenerator motion is offset as well as clipped at the cold-end. Instead of changing the position of a fixed stroke regenerator motion as in the previous strategy, an inclined top drive piston and a port can be used to offset as well as clip the regenerator motion at the cold-end. In the model this was achieved by offsetting the output from the sinusoidal regenerator-motion generator block as well as conditioning it through a limiting-filter. Figure 8.7 shows a schematic drawing of the mechanism, which acts in a way similar to the flow control mechanism used in mechanical pumps of diesel injectors. The port is used for refilling and bypassing fluid in and out of the regenerator drive cylinder. The regenerator is always biased towards the cold-end under any positive system pressure due to area differential of the end faces of the regenerator. Instead of being flat, the top of the drive piston has an inclined face. For full stroke, the port is almost always closed, hence sinusoidal motion of the drive cylinder is transmitted to the regenerator. When the rotational position of the plunger is changed, the inclined face is brought to the port such that part of the drive cylinder's stroke towards the hot-end is lost (as the regenerator only starts the move after the port is closed). Clipping the regenerator motion towards the cold-end causes the regenerator to move in a range further away from the hot-end reference, causing the peak-pressure to rise (for the same reason as was explained with stroke control). Figure 8.8 shows the clipped motion of the regenerator and the resulting engine cycle. The rate of increase is less than offsetting, as in the previous method, because part of the regenerator stroke is lost due to the clipping at the cold-end. For each power-zone, without any clipping of regenerator motion, piston motion causes engine power to be equal to the



Closure of the hole is delayed by rotating the plunger through an angle, clipping the regenerator motion at the cold-end. This causes the power output to rise.

Offsetting and Clipping regenerator motion towards the cold-end

Figure 8.7 : Changing the profile of the regenerator motion, though the drive cylinder motion is the same. Changing the rotational position of the inclined top drive piston causes a delay in the closure of the port during upward stroke. This causes the regenerator motion to be offset as well as clipped at the cold-end.

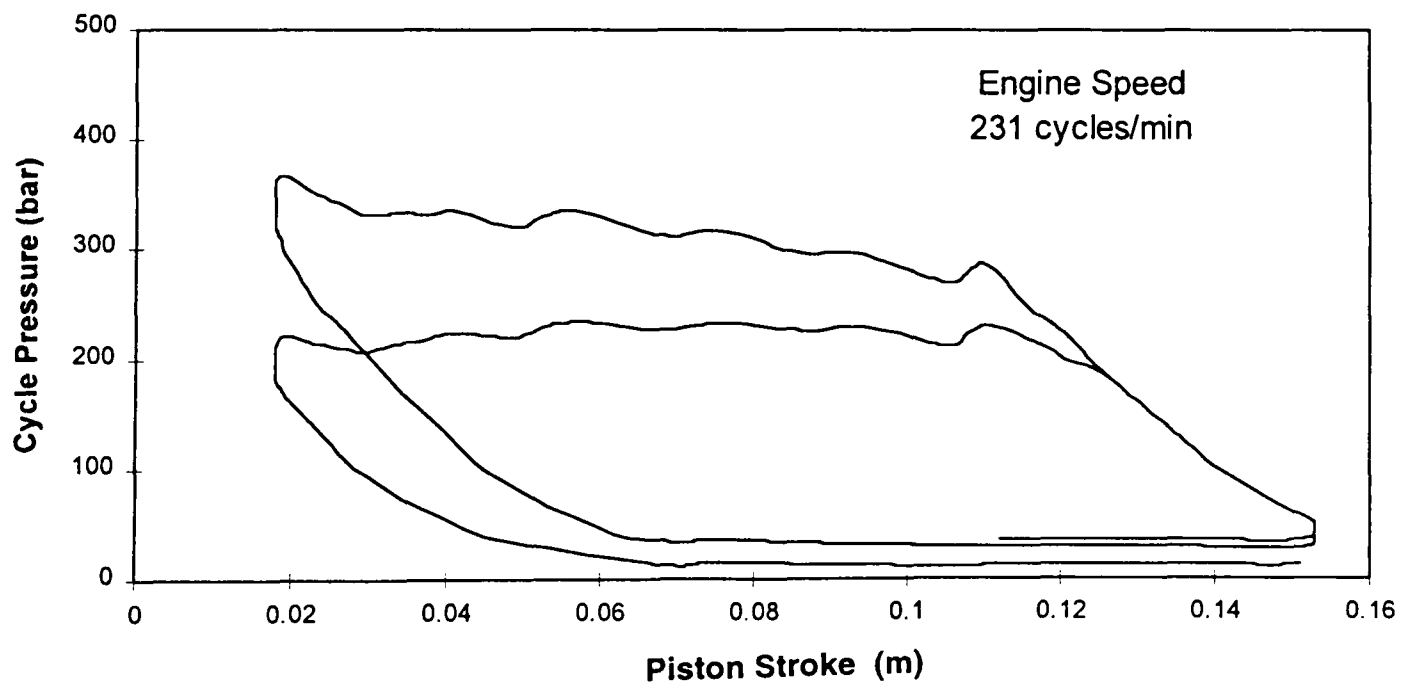
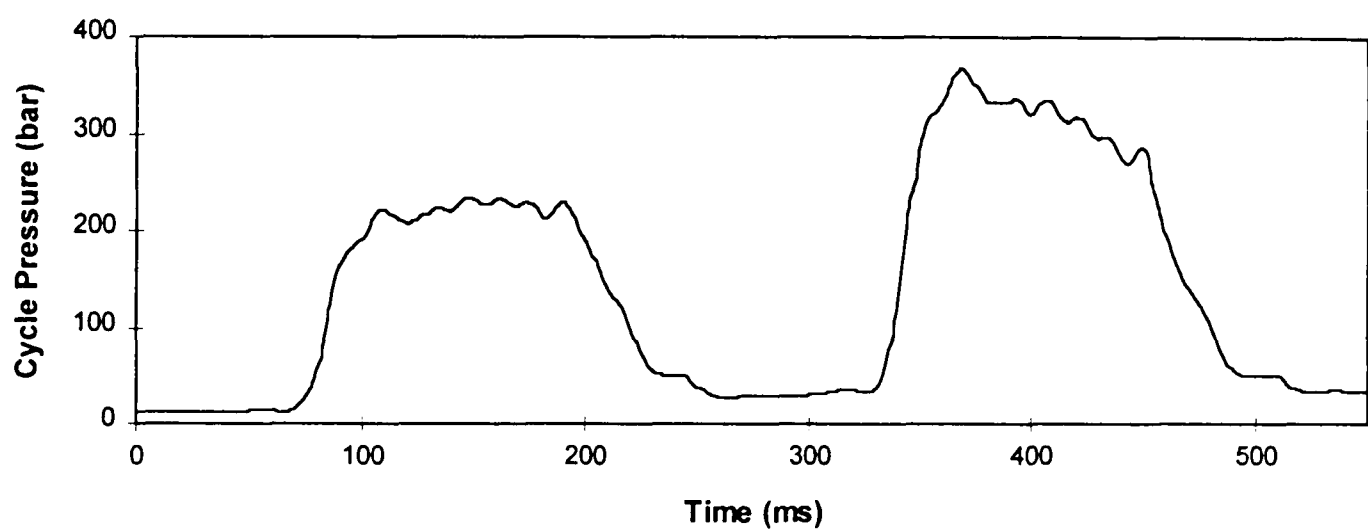
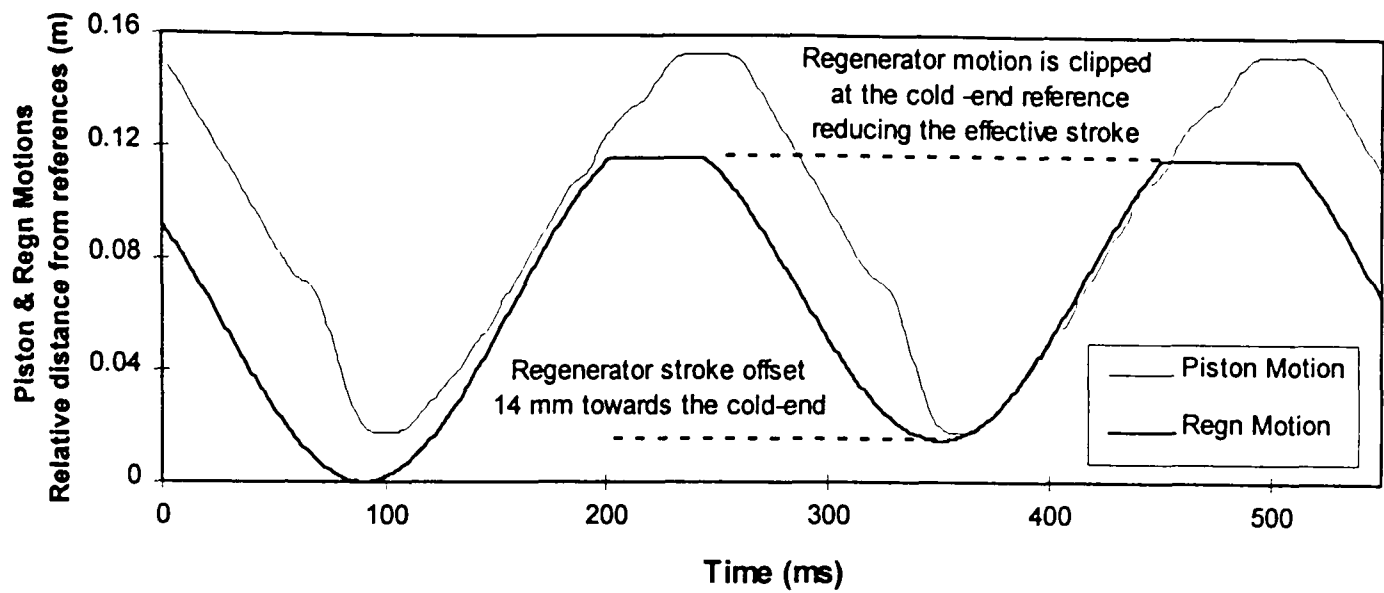


Figure 8.8 : The effect of offsetting the regenerator motion towards the cold-end along with clipping of the stroke at the cold-end, while the piston motion (following a ternary pattern) remains unchanged. Cycle pressure rises with the offsetting resulting to 20% higher power output, but due to reduction of effective stroke of the regenerator (by clipping) more offsetting is needed compared to the previous method.

lowest-power demanded in that power-zone. With increasing demand, the regenerator motion is increasingly offset as well as clipped near the cold-end to meet the requirement. This can only be continued until the demand reaches the lower limit of the next power-zone above. Then the piston motion shifts ternary-code and the regenerator clipping is stopped by resetting the angular position of the drive piston. For further increase in demand the whole process is repeated, while the reverse happens as the demand decreases.

(3) Fine control by changing stroke:

In this method the regenerator moves in between the hot-end and the cold-end following the desired motion profile. In the model, variation in regenerator strokes were achieved by changing the gain value of the regenerator-motion generating block. Figure 8.9 shows a schematic presentation of a probable mechanism where the stroke of the sinusoidal regenerator motion is varied. Varying the swash-plate angle changes the regenerator stroke, while a biasing cylinder keeps the motion still referenced to the hot-end. In the final design different arrangements (eg. using gear-pumps as shown in chapter seven) might be used for changing the regenerator stroke. Reducing the amplitude (stroke) of the regenerator motion from its hot-end reference, causes the peak cycle pressure to fall (as explained in the stroke control section before) and hence the power output. With the full stroke of the regenerator motion at each zone the piston motion causes engine power to be equal to the highest power of that power-zone. It should be noted that lowest power of each zone was obtained at full regenerator stroke in the two previous methods. With reduced demand, the stroke of the regenerator motion is decreased to match the requirement. But this is only continued until the demand reaches the upper limit of the power-zone below. Then the piston motion shifts ternary-code and the regenerator motion is brought back to full stroke. For further decrease in demand the whole process is repeated, while the reverse happens as the demand rises.

Each of these control methods or strategies were considered in detail and the simulation results described in the following chapter.

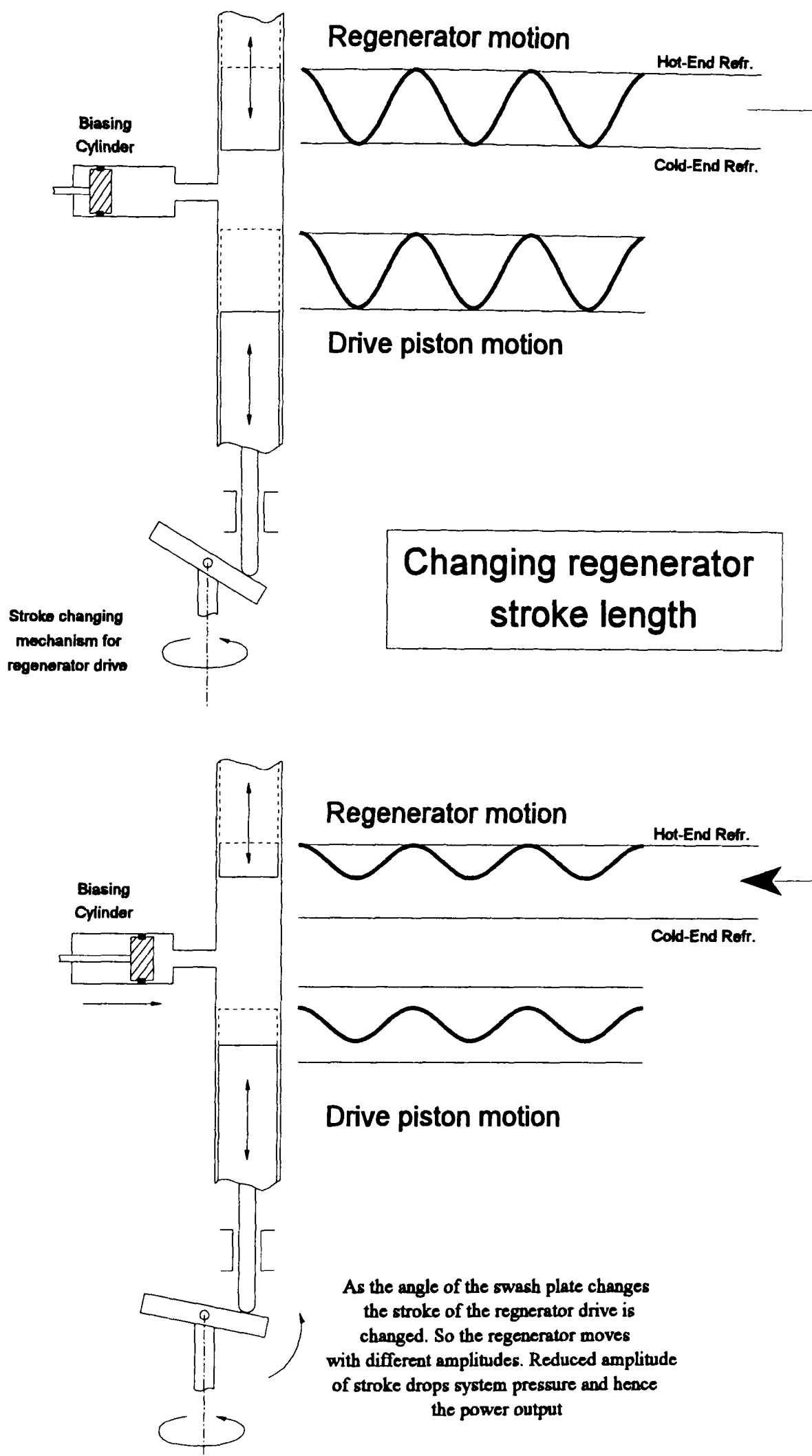


Figure 8.9 : Changing the regenerator stroke for finer control of power. A mechanism eg. a swash plate arrangement may be used to change the stroke as the swash-angle is varied. Though different in amplitude the changed motion is still similar (ie. sinusoidal in this case) and starts from the hot-end reference.

CHAPTER 9

Continuous Power Control of the Engine

9.1 Introduction

In the previous chapter three strategies have been suggested for instantaneous power control of the Artemis-Malone engine. Each strategy consists of a combination of methods for coarse and fine-control of power. For all of the three cases, alteration of cycle pressure-levels by offsetting the piston motion is used for coarse-control of power. Three prospective methods for fine-control of power were suggested, though all involve modulation of regenerator motion. Possible mechanical arrangements for achieving these regenerator motions have also been described. At this stage simulations were carried out for each of these combined power-control strategies, to investigate their capabilities to meet instantaneous power demand. Detailed results are presented for one of the combined strategies and the differences in engine cycles generated from the other two are emphasised. As the same coarse power-control technique was used for each case, the combined strategies are named after the method used for fine-control of power.

9.2.1 Power control by offsetting regenerator motion

For the target Artemis-Malone engine power-demand ranged from 1.8-15.1 kW per TD pile, giving a total full-power output of about 55 kW with four TD piles. The crude control power range was divided into 6 power zones, for each of which a pre-tuned ternary-code was set which the pump-motor, and consequently the flexible piston, would follow. Both the engine and the pump-motor ran at fixed speeds maintaining a ratio such that a fixed integer number of pump-motor cylinders are available during one engine cycle (78 cylinders with the present speed ratio). For each successive zone the piston advanced one cylinder volume further away from the TDC reference of piston motion. This lowers the peak pressure developed in the cycle and, hence, the power output from the engine. Additional features in the control algorithm which adjust the

ternary-mode allowed seamless transition between different ternary-codes which ultimately changed the range of piston motion.

The progressive offsetting of the regenerator motion towards the cold-end was used for fine control of power within each zone. It was assumed that the regenerator always followed a sinusoidal motion of fixed stroke. As the entire range of motion of the regenerator is offset towards the cold-end, the system pressure rises. The rise in pressure is more significant in the high pressure parts of the engine cycle so the pressure-volume diagram is not merely shifted up in pressure scale, rather the area inside the pressure-volume curve increases, which results in more power.

The choice of ranges for the different power levels were made so that, offsetting of the regenerator motion to the same magnitude (which was found to be about 12 mm) is necessary to cover each of the power zones. In the present choice each cylinder volume of the pump-motor is about 9.5 cc, which is equivalent to a piston motion of about 9 mm in the thermodynamic pile. A small biasing fluid cylinder (as shown in chapter eight) is needed to push the entire motion range of the regenerator towards the cold-end. The flow control system of the biasing cylinder needs to have good frequency response and in the present model it is expected to be capable of offsetting the regenerator motion by 12 mm within an engine cycle period (about 260 ms), which is about 50 mm/sec. Table 9.1 shows the details of the cycle parameters and the power-zones chosen. Figure 9.1 shows the shifts and changes in power-zones and regenerator offsetting needed throughout the working range of the engine. Figure 9.2a and 9.2b show the variation of pressure cycles and the shifting of the flexible piston away from the TDC reference at the cold-end in successive power zones. For all of the cycles the regenerator is moving sinusoidally without being offset towards the cold-end. Figure 9.3 show the pressure-volume diagrams of each power zone. The darker curve shows the engine cycle at the lower power level of the power zone with regenerator motion without any offset. The lighter curve shows the same but at the higher power level of the zone with full offset of regenerator motion.

TABLE 9.1 : Engine parameters and power ranges

(Power control by offsetting regenerator motion)

Power range/module	1.8 - 15.1 kW
Thermodynamic pile bore	40 mm
Regenerator stroke	116 mm
Engine/Regenerator cycle speed	231 cycles/min
Pump-Motor speed	1800 rpm
No. of cylinders in the pump-motor	10
Pump-motor cylinder volume	9.5 cc (approx)
Piston motion equivalent to one cylinder displacement	9 mm (approx)
No. of pump-motor cylinders available in each engine cycle	78

Power Zone	Pressure Level bar	Cylinder displacement pumped in or motored out	Piston motion range using ternary code mm	Regenerator motion offset needed mm	Power range kW
0	400	16	0 - 144	0	15.1
1	275	16	9-153	0-12	10.8-15.1
2	200	15	18-153	0-12	8.1-10.8
3	150	15	27-162	0-12	5.7-8.1
4	100	15	36-171	0-12	3.3-5.7
5	50	14	45-171	0-12	1.8-3.3

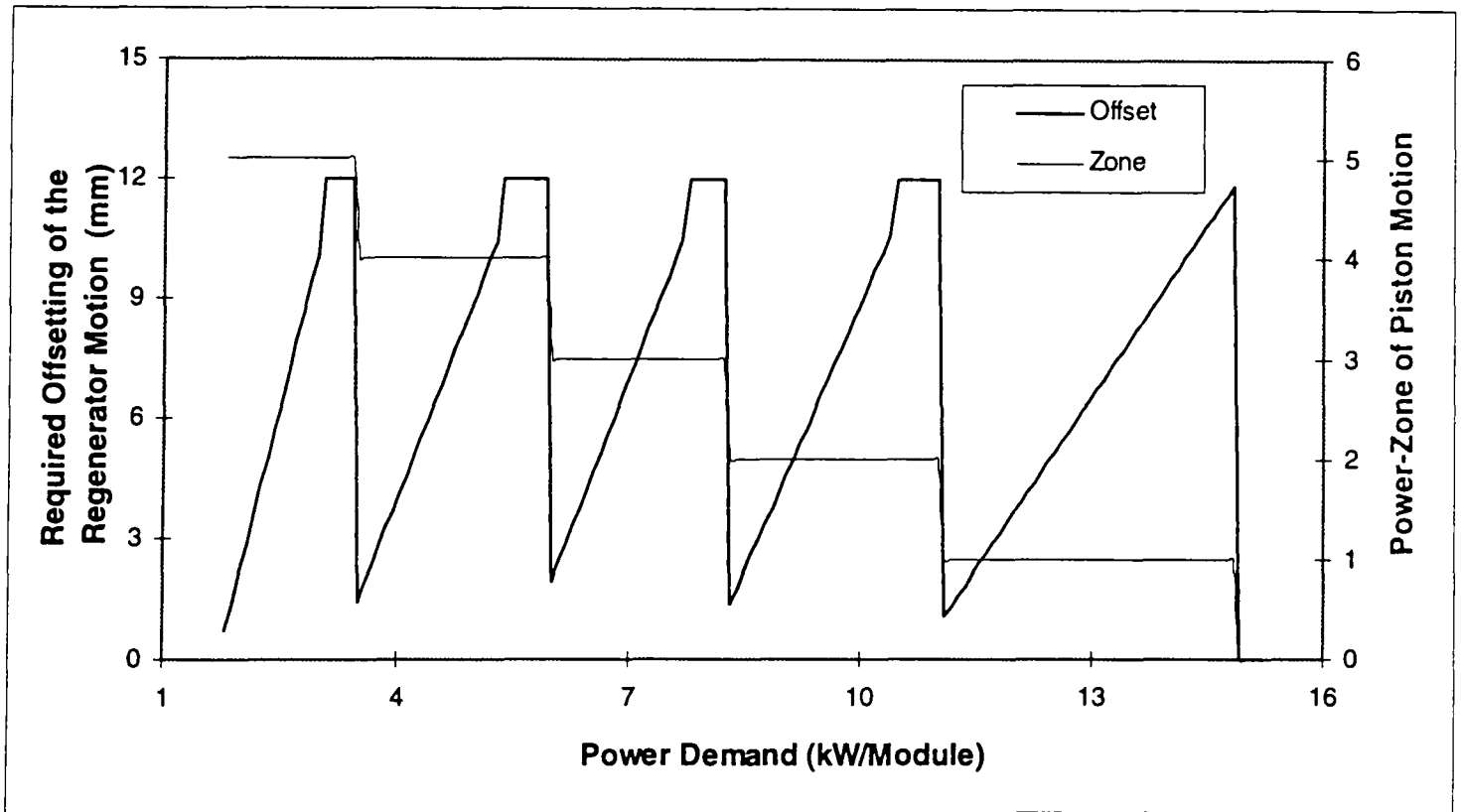
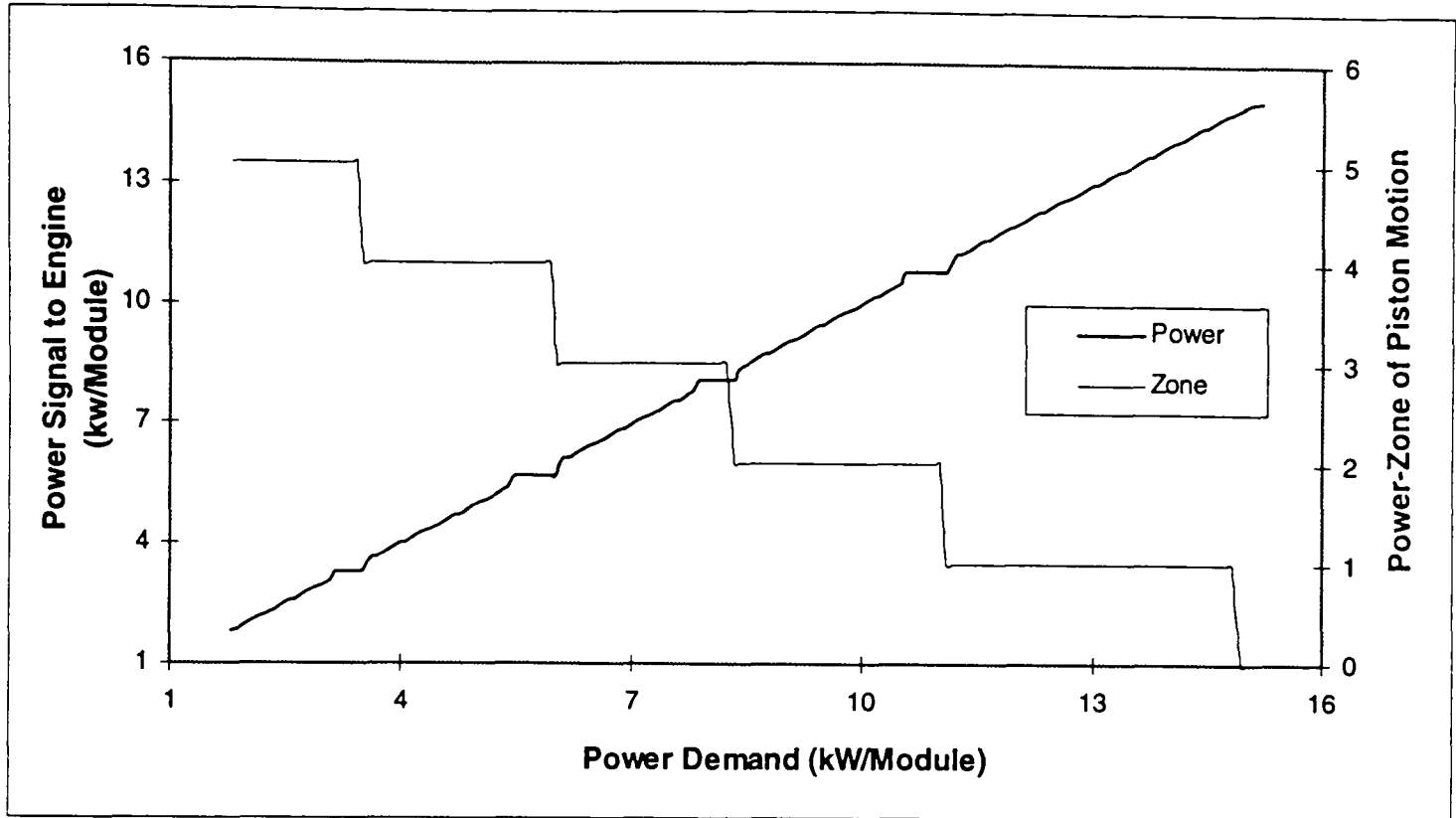


Figure 9.1 : Change of power-zones and offsetting requirements with changes in power demand. At the transition between zones the demand signal is filtered to avoid hunting across zone boundaries.

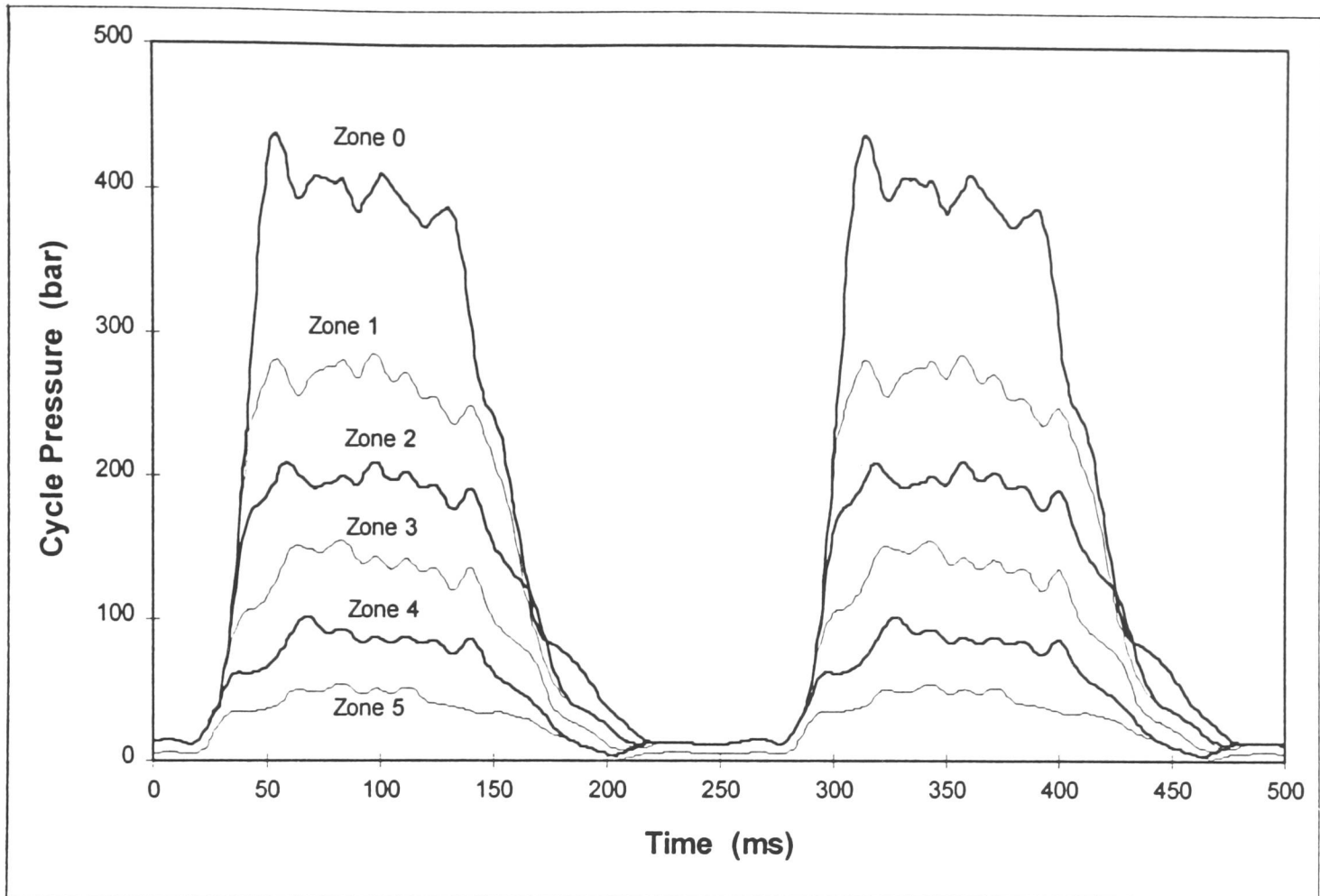


Figure 9.2a : Variation of cycle pressures for piston motion of different power-zones. For each successive zones the piston advances further from its TDC reference, resulting in lower cycle pressure.

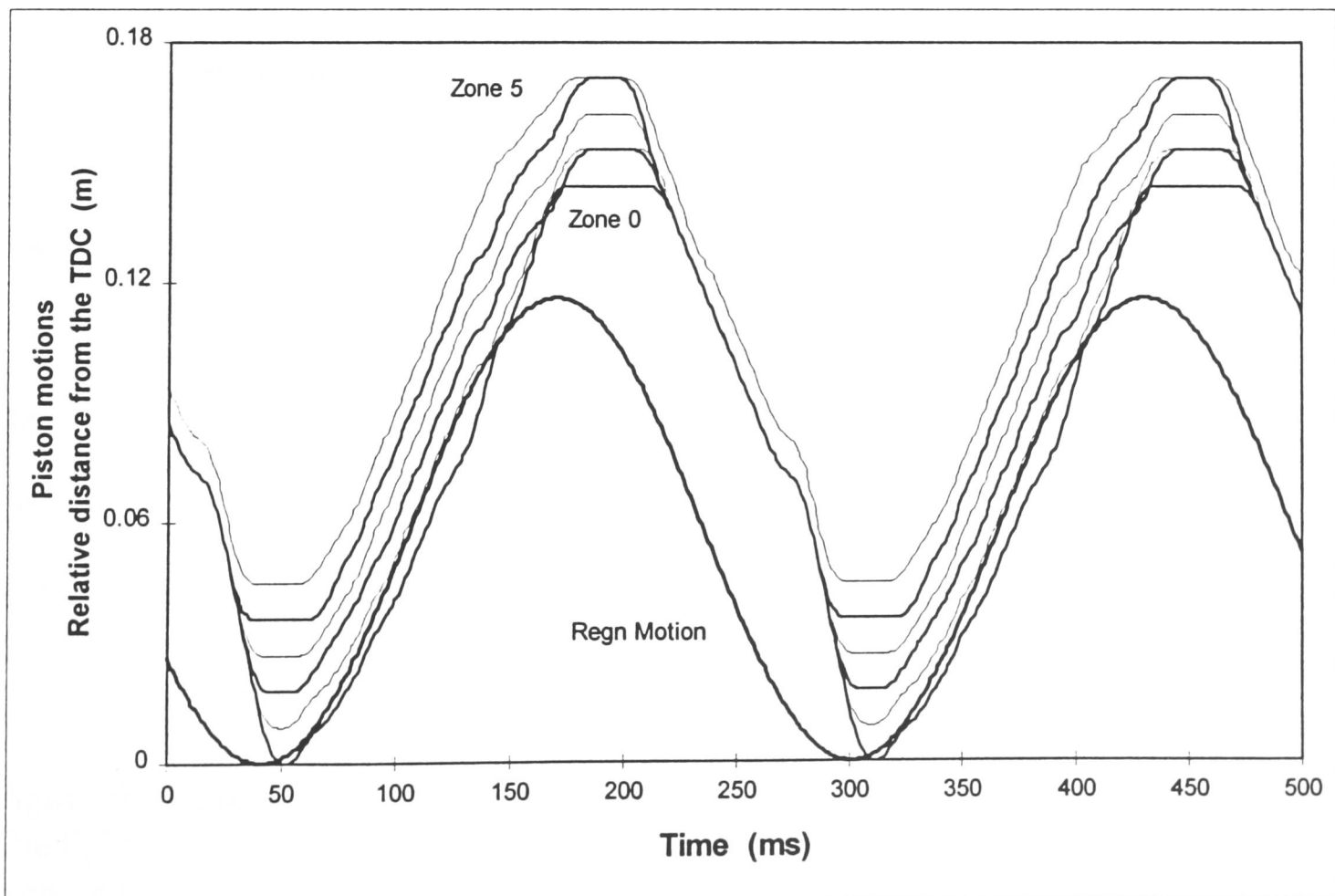


Figure 9.2b : Variation of piston motion for different power-zones. For each successive zones the piston advances further from TDC reference, while the regenerator motion is unchanged.

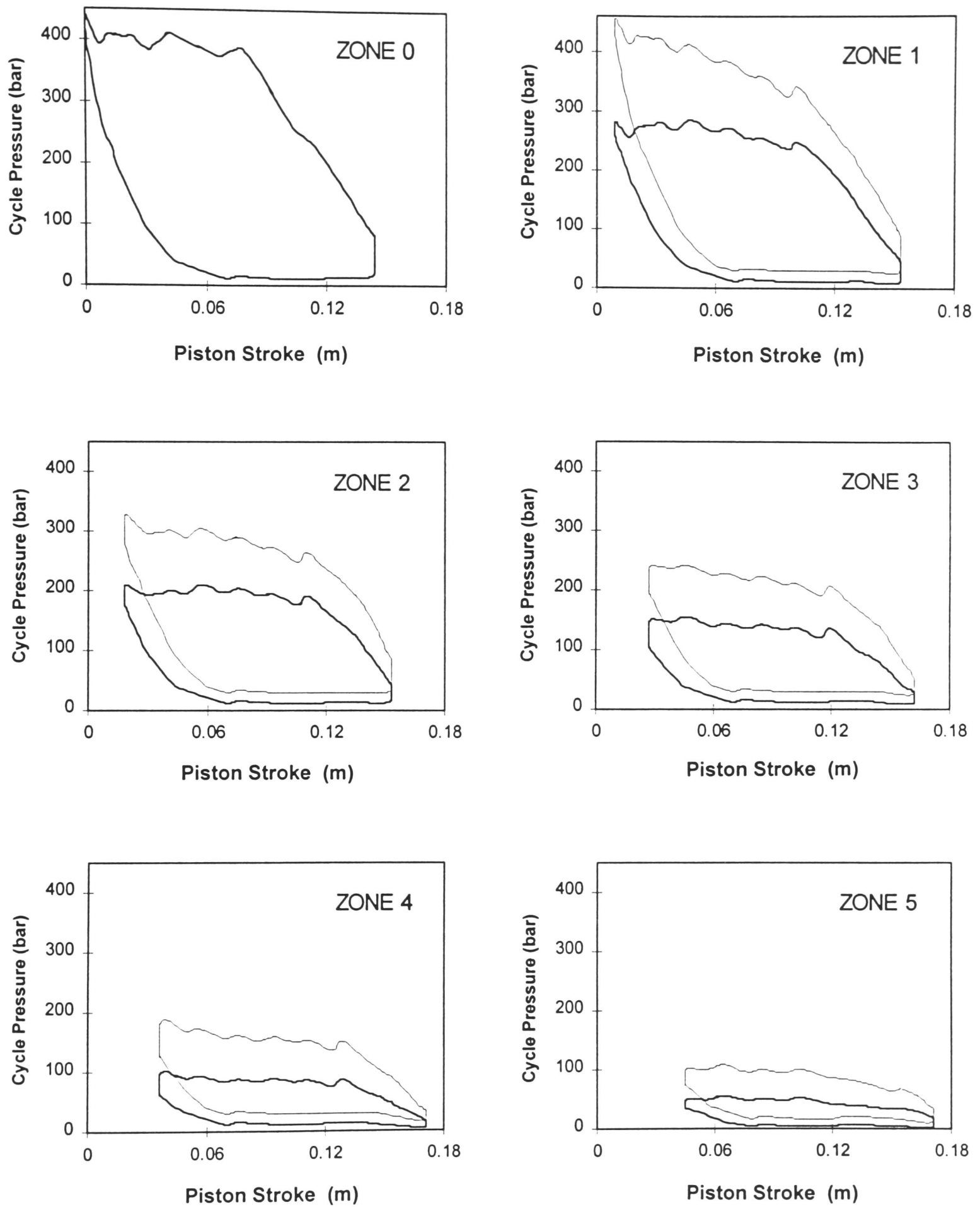


Figure 9.3 : Pressure-volume diagrams of the engine cycle at different power-zones. The lighter curves show the cycles when the regenerator motion is offset towards the cold-end. With the offsetting the pressure rise is more prominent at higher pressures resulting in greater enclosed area and hence power. Within each zone the piston follows a pre-determined motion, according to the ternary-code.

9.2.2 Shifting between ternary-codes

For each of the cycles shown in figure 9.2 and 9.3 the pump-motor follows the ternary-code of the corresponding power zone. Tables of ternary-codes used by the pump-motor are given in appendix - C. These contain +1 indicating a motoring decision, -1 indicating a pumping decision and 0 for doing neither (nulling). The chosen cycle reference starts from the regenerator at its hot-end reference and the piston at its TDC reference at the cold-end. As shown in figure 9.4, the ternary-code can be divided into three main regions, the motoring-zone, the nulling-zone and the pumping-zone. Motoring decisions are located at the beginning (motoring-zone) and pumping decisions (pumping-zone) are located at the end of the ternary-code, while successive disabled decisions lie in between them (nulling-zone). The pumping-zone could again be subdivided into - low-speed and high-speed pumping-zone. Cycle pressure is maintained at desired low-level during low-speed pumping, while the cycle pressure rises rapidly as the piston is brought back to starting position by high-speed pumping. The 78 decisions in the code correspond to 78 cylinders available during one cycle of the regenerator motion (ie. the engine cycle). The same pump-motor cylinder (eg. cylinder one) does not need to be available at the beginning of each engine cycle since the decisions are executed for the next available 78 cylinders in each cycle. For each power zone the ternary-codes are pre-tuned for the best match of the desired piston motion at the lowest power level of that zone. As long as the power demanded is within the present zone the pattern of piston motion does not change, though the regenerator motion may be offset to different degrees according to the demand.

Once the ternary-codes were set for different zones, the smooth shifting between the different ternary-codes of each power-zone needed consideration. The cycle, during which the controller senses the need to change the power-zone and acts accordingly, can be termed a *transition-cycle*. The transition from one ternary pattern to another can be achieved by replacing one or more extra pumping or motoring decisions on the transition cycle ternary sequence, as required.

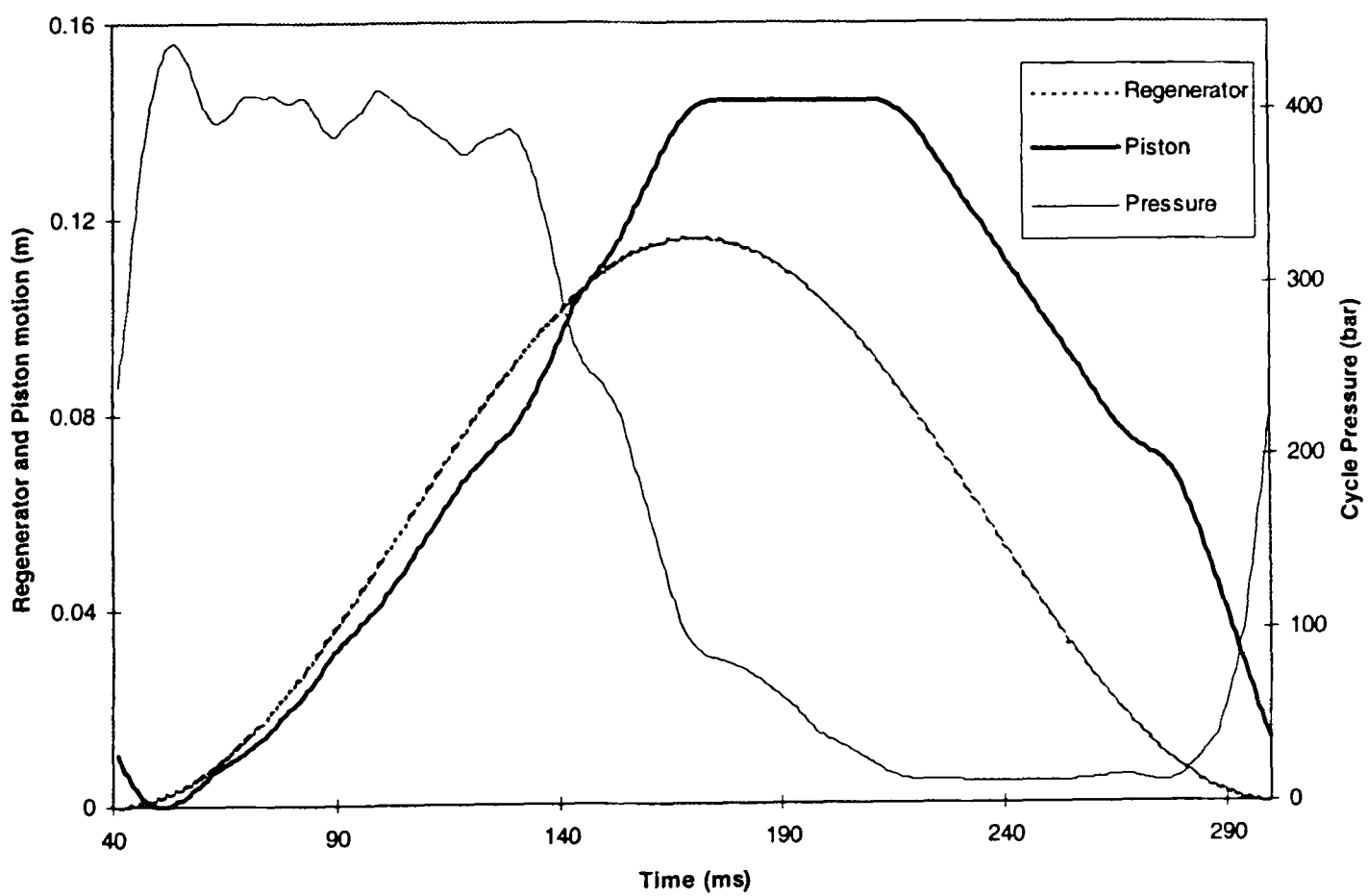
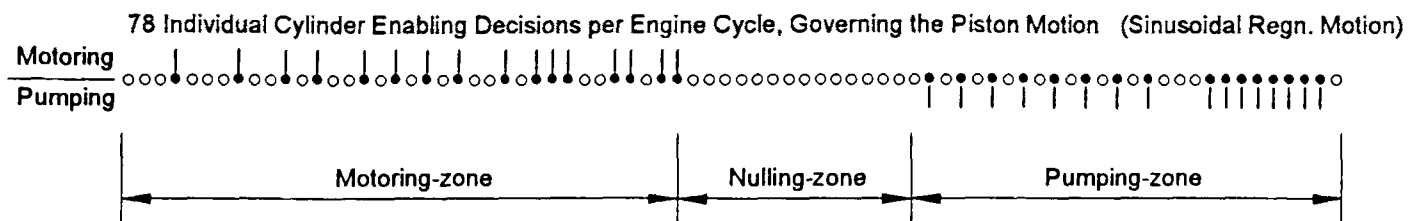


Figure 9.4 : Pressure variation within the cycle with regenerator and piston motion. At the top enabling sequence (ternary-code) is shown for 78 cylinders available during one cycle. The ternary-code is composed of motoring, nulling and pumping-zones according to the type of decision.

The region in the ternary-code, where the decisions for offsetting the piston motion are replaced, regulates the consequence on the transition-cycle, though this does not affect successive cycles, until another transition arrives. Each extra motoring decision (1) must replace a nulling decision (0) or a pumping decision (-1) to be effective, while a replaced pumping decision (-1) can be effective only if it replaces a nulling (0) or motoring decision (1). The obvious location seems to be the nulling-zone in the middle of the code, where the piston is not moving. The result is that a transition-cycle with extra motoring, causes the piston to move further away and cause the lower overall cycle pressure to fall. On its way back it does not come back to the TDC reference. A transition-cycle with extra pumping which starts earlier causes the low pressure-level of the cycle to rise and increases the pumping work. The piston then returns closer to the TDC reference and will carry on from the new reference in the following cycles. The transition cycles for extreme step changes are shown in figure 9.5, where the demand requires step changes from zone zero to zone five and then back again. The calculation of power is made on a cycle-by-cycle basis as only one module is considered. At the end of motoring in the transition-cycle, when the piston is required to drive five additional motoring cylinders, the system pressure goes undesirably low (which may lead to cavitation). On the other hand during the transition cycle from zone-five to zone-zero (low to higher power) the pumping starts earlier, raising the lower pressure level of the cycle. This results in a net power decrease during the transition cycle which is opposite to the desired change.

One solution of this problem could be to set the lower limit of pressure high enough to avoid cavitation, but this would lead to a higher upper limit of cycle pressure (which would affect the vessel design considerations) or give less power. An alternative approach may be to place the offsetting decisions for the transition at other parts of the ternary-code. Instead of these decisions being placed in the nulling-zone, they are placed at the end part of the pumping-zone of the code. In this case, when extra cylinders are motored to shift power zones the piston is allowed to move away from the cold-end reference as before. On its way back the inserted motoring decisions neutralize some of the pumping decisions and offset the piston motion. Conversely additional pumping decisions inserted at the end of pumping-zone moves the piston

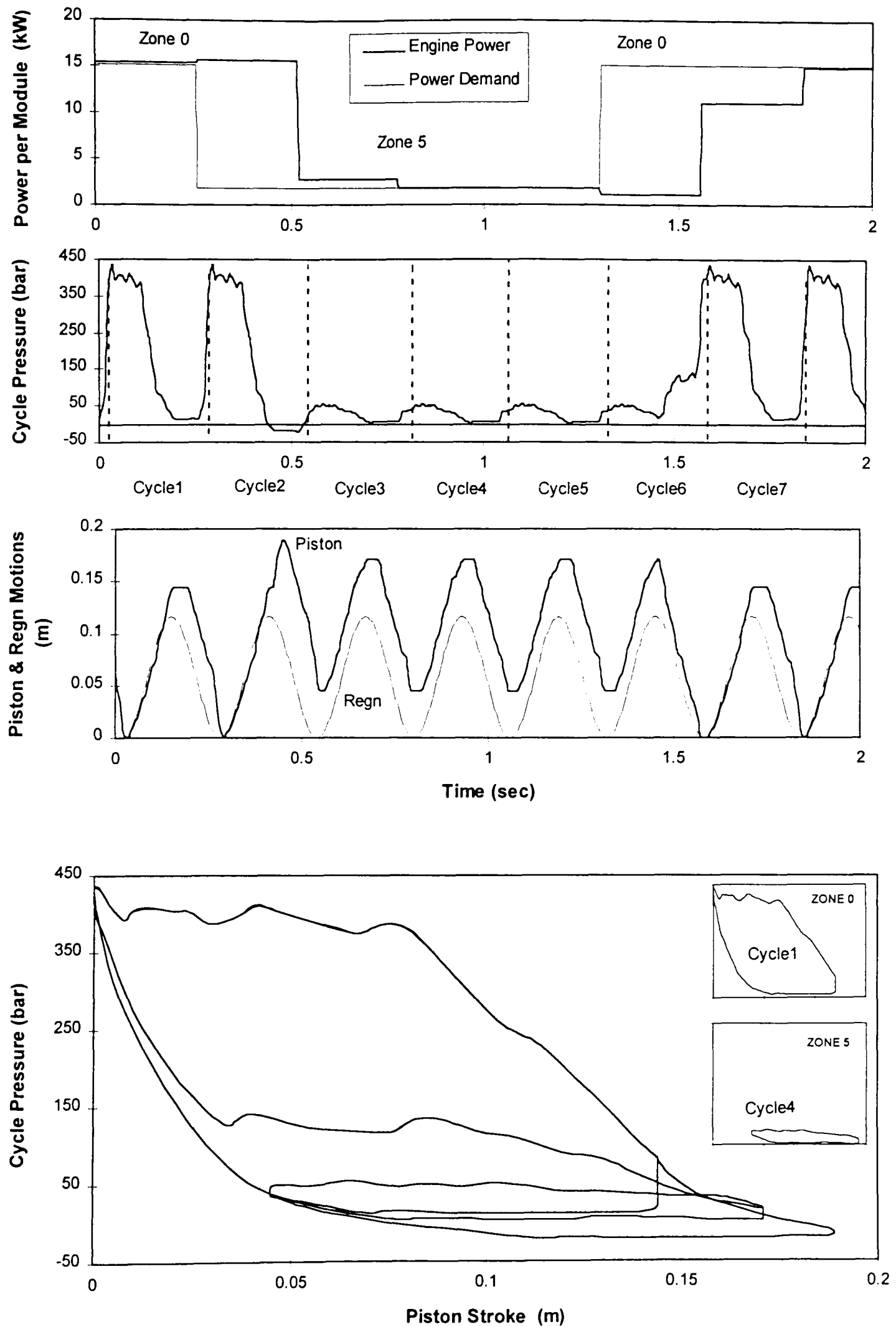


Figure 9.5 : Cycle response to maximum step change of power zone shifts between zone 0 and zone 5. Decisions to offset piston motion are inserted at the nulling-zone of the ternary-code, resulting in undesirable pressure changes in the transition cycles. Inserts show the cycles for zone-5 and zone-0. Sinusoidal regenerator motion is unchanged.

back towards the TDC reference at the cold-end. It is worth noting that replacing pumping decisions at the end part of the pumping-zone of the ternary-code only becomes effective if they are replacing nulling (0) decisions (or transferred to the next available nulling decision). Figure 9.6 shows the resulting cycle, where the undesired fall and rises of pressures are avoided during transition from one zone to the other.

One limitation still exists: on a cycle by cycle basis, the power change in the transition cycle lags by one cycle period from the demand. The lag is of constant duration but the magnitude of error becomes maximum when shifting between the highest (zone 0) and lowest (zone 5) power-zones. The placement of extra pumping or motoring decisions in the ternary-code, needed to offset piston motion and shift power-zones, are also given in appendix C.

9.2.3 Minimising power-lag in transition-cycles

The discrepancy between demanded and generated power in the transition cycles could be reduced to great extent by placing equal numbers of extra pumping and motoring decisions (in addition to the ones placed for offsetting piston motion) during the transition cycles to distort it in a desired pattern. The aim is to reduce the peak-cycle pressure in the downward (in terms of power) transition-cycle and increase it in an ascending transition-cycle. For a downward transition some extra cylinders are motored at the beginning of the cycle to reduce the peak cycle-pressure although same number of cylinders are pumped in at the end of the motoring-zone so that the change does not affect the lower pressure level of the cycle nor the piston position at the end of the transition cycle. For an ascending transition extra cylinders are pumped first and then motored later to give an increase in the peak pressure level. The number of cylinders pumped in and motored out depends on the scale to which change in cycle pressure is required and hence is greater for larger changes of power levels. A set of replacing decisions to distort transition cycles for power zone shifts is also included in appendix C. Figure 9.7a shows the resulting cycles for extreme step changes of power (ie. between power-zone zero and five) when transition cycle distortion is activated. The error is decreased by about 40% for the extreme case (shifting five zones) and nearly eliminated when shifting by one or

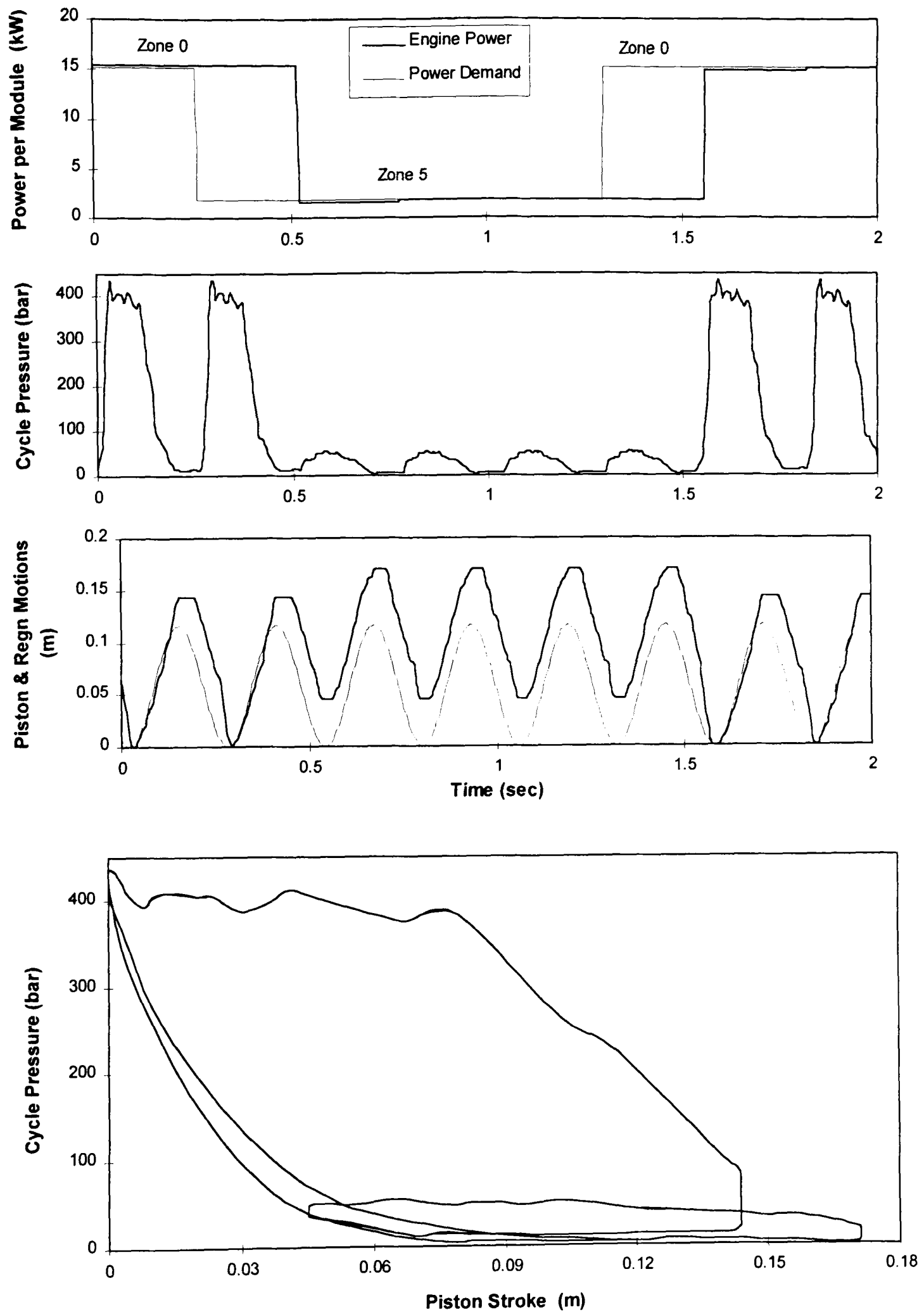


Figure 9.6 : Cycle response to maximum step change of power zone shifts between zone 0 and zone 5. Decision replacement is done at the end of pumping region of the ternary-code resulting in removal of undesirable pressure changes in the transition cycles. Response still lags by a cycle period to demand. Regenerator motion is kept unchanged.

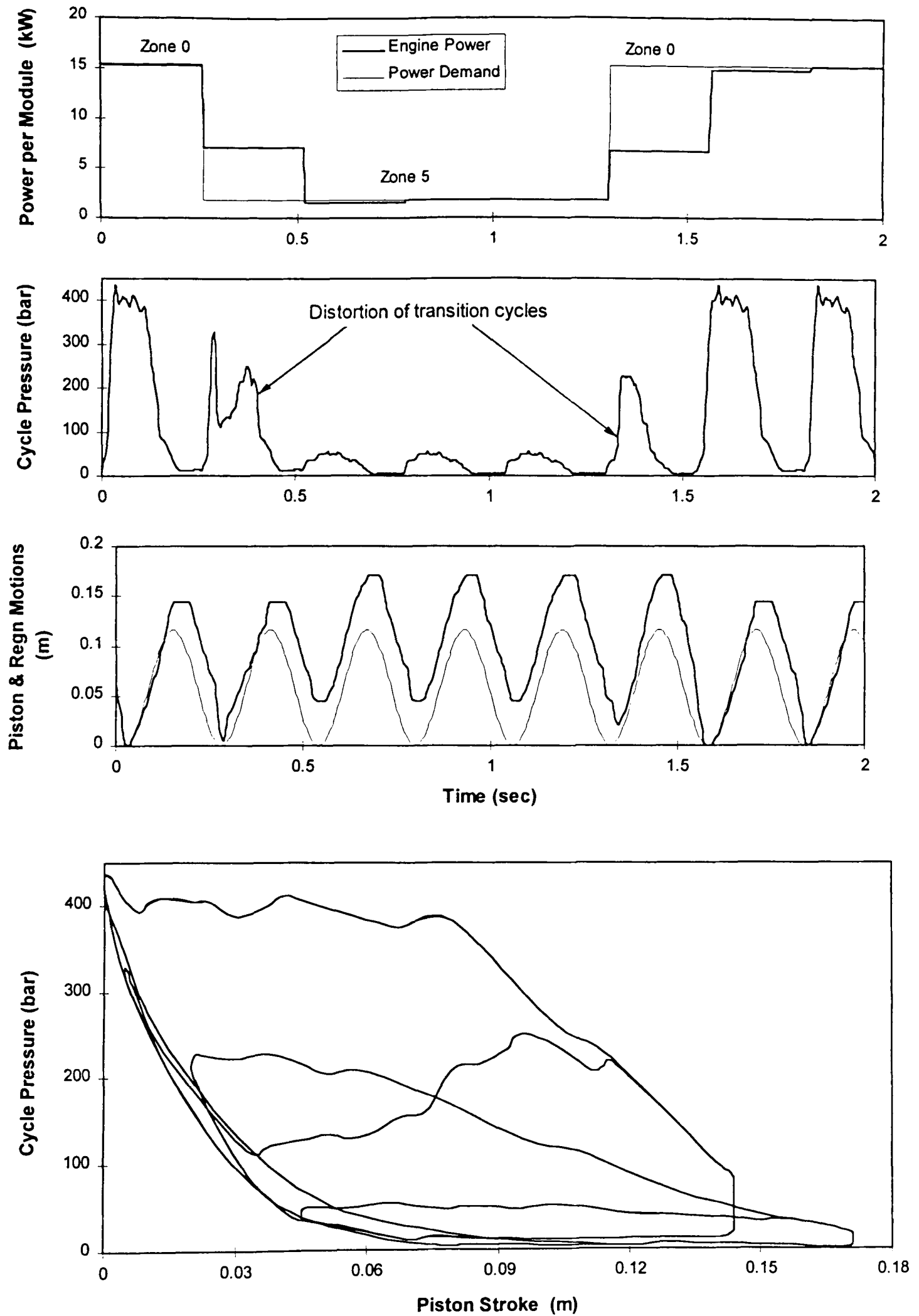


Figure 9.7a : Cycle response to maximum step change of power zone shifts between zone 0 and zone 5. Replacing decisions at the end of pumping region of the ternary-code and distortion of the transition-cycle improves cycle response at the transitions.

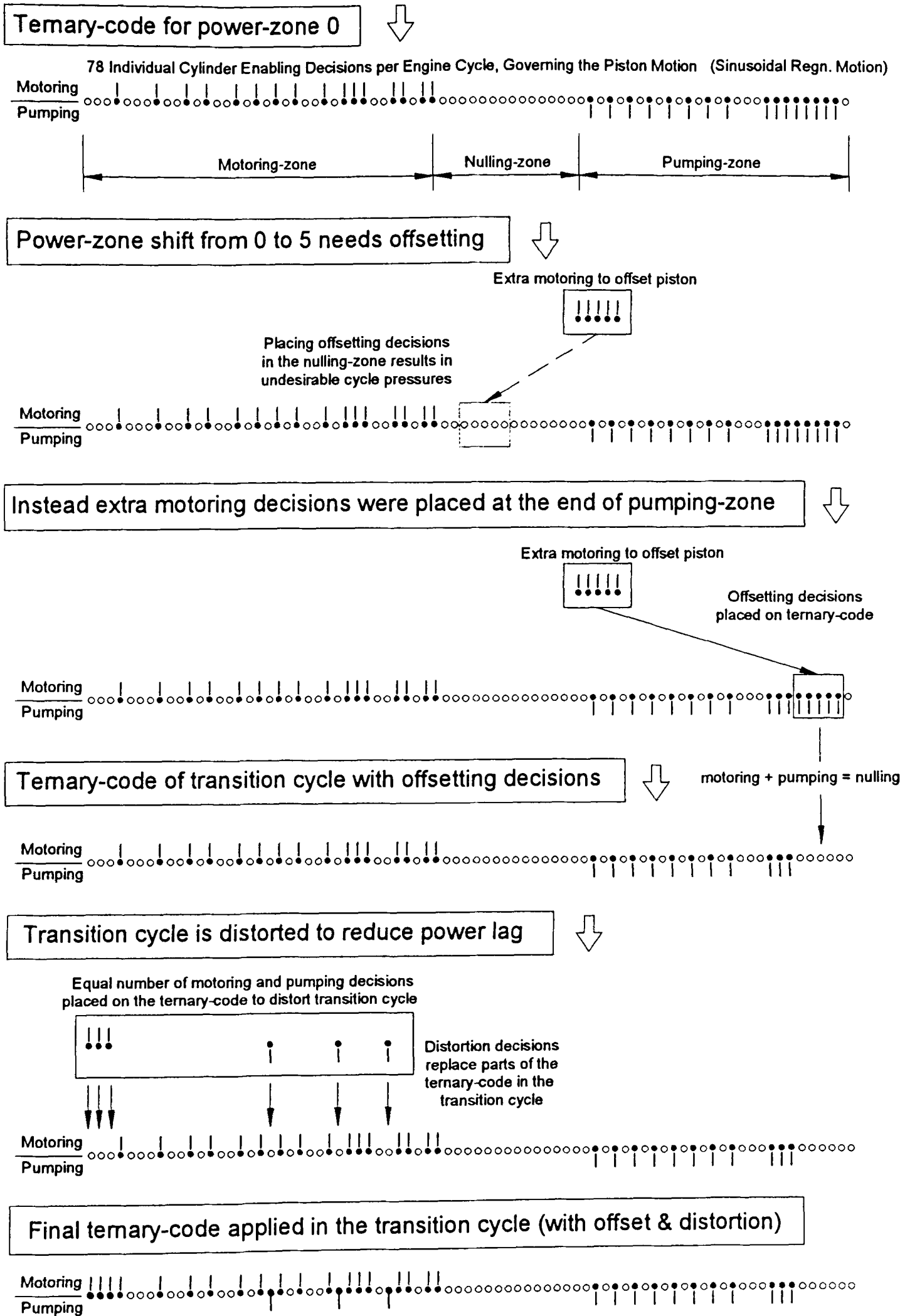


Figure 9.7b : Changes made to the ternary-code applied to the transition cycle. Extra motoring is incorporated as the power demand is decreased from zone-0 to zone-5, to offset the piston motion. Decision replacements are made at the end of the pumping-zone, to avoid undesirable cycle pressures. Distortion decisions are incorporated in the motoring-zone of the code to reduce error between power demanded and generated, in the transition-cycle.

two power-zones. In the modelling these decision replacements in the ternary-code, both for offsetting piston motion and manipulating transition-cycles, were achieved through replacement look-up tables. The controller implemented these parts of the ternary-code only for the corresponding transition-cycles. Figure 9.7b shows the final ternary-code applied to a transition-cycle, where offsetting and distortion decisions change parts of the original code.

9.2.4 Meeting variable power demands

The ternary-codes were tuned to range the power-zones such that same amount (about 12 mm) of offsetting of the regenerator motion was needed to change the power output from the lowest to the highest level within each power-zone. Figure 9.8 shows how the variation of power demand is met within a power zone. The offsetting of the regenerator motion is changed on a cycle-by-cycle basis with demand, while the piston motion remains unchanged. It should be noted that, with the present design, the offset requirement is set at the beginning of each engine cycle and the offset drive takes some time to reach the desired position at the beginning of each cycle, as shown in figure 9.8.

Figure 9.9 shows the engine following an arbitrary varying demand. All the control parameters - power demand, zone and offsetting the regenerator stroke etc. are set at the beginning of each cycle. As soon as the demand requires a power zone change the piston motion range is offset accordingly as shown in the piston motion curve. Within each power zone the regenerator motion is offset accordingly to exactly meet the demand. The cycle pressure, in general, varies with the power requirement with exception of the transition cycles, where cycle distortions are activated to reduce the error between demand and output power. The power curve shows that the error between demand and response generated during the transition cycles, is almost eliminated using the distortion technique.

Figure 9.10 shows a zone-hunting situation where the demand is constantly varying between power zone one and two though changing little in magnitude. To avoid repeating zone shifts under such conditions, dead-band filters are provided in the

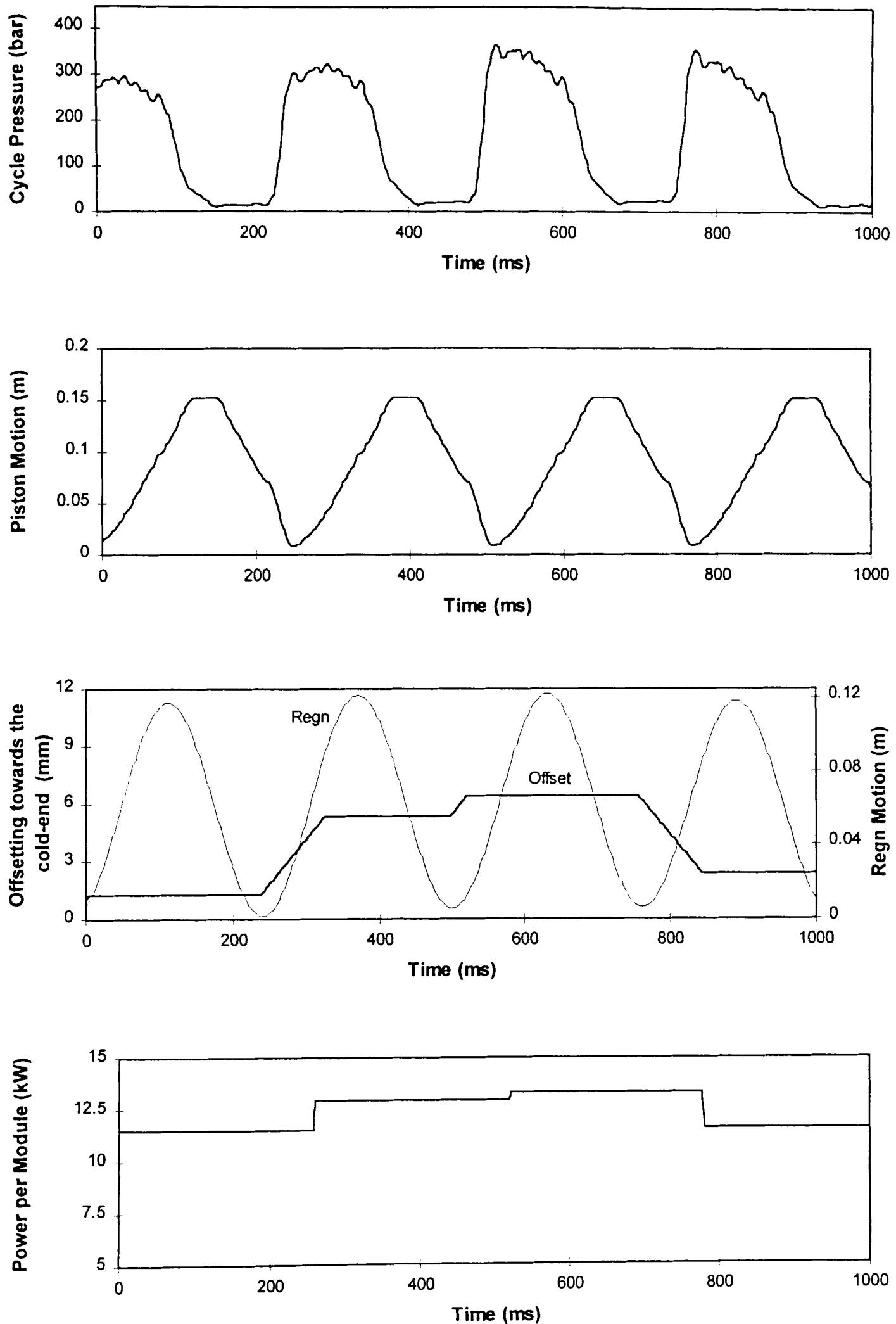


Figure 9.8 : Cycle changes as the power demand varies within a power zone. The cycle pressure varies with the demand as the offsetting of the regenerator motion varies accordingly. For each cycle a finite time is needed to reset the regenerator to the desired position. The piston motion remains unchanged.

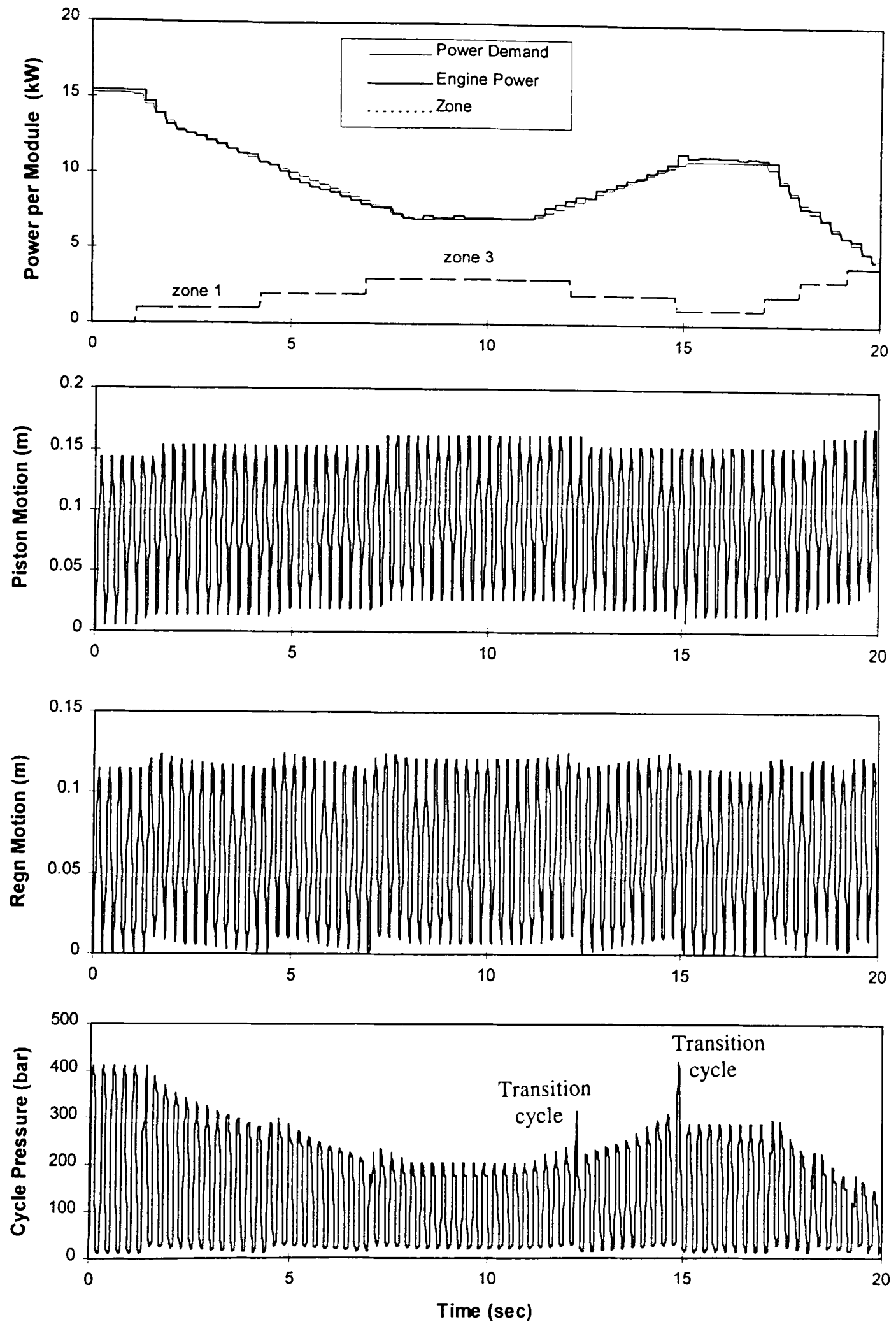


Figure 9.9 : Engine cycle following variable demand from the user, where power is calculated in a cycle-by-cycle basis. Peak pressure of the cycle varies with power demand, as the piston and regenerator motions are changed accordingly. Exceptions are the transition cycles, where the cycle is distorted to reduce discrepancy between power generation and demand.

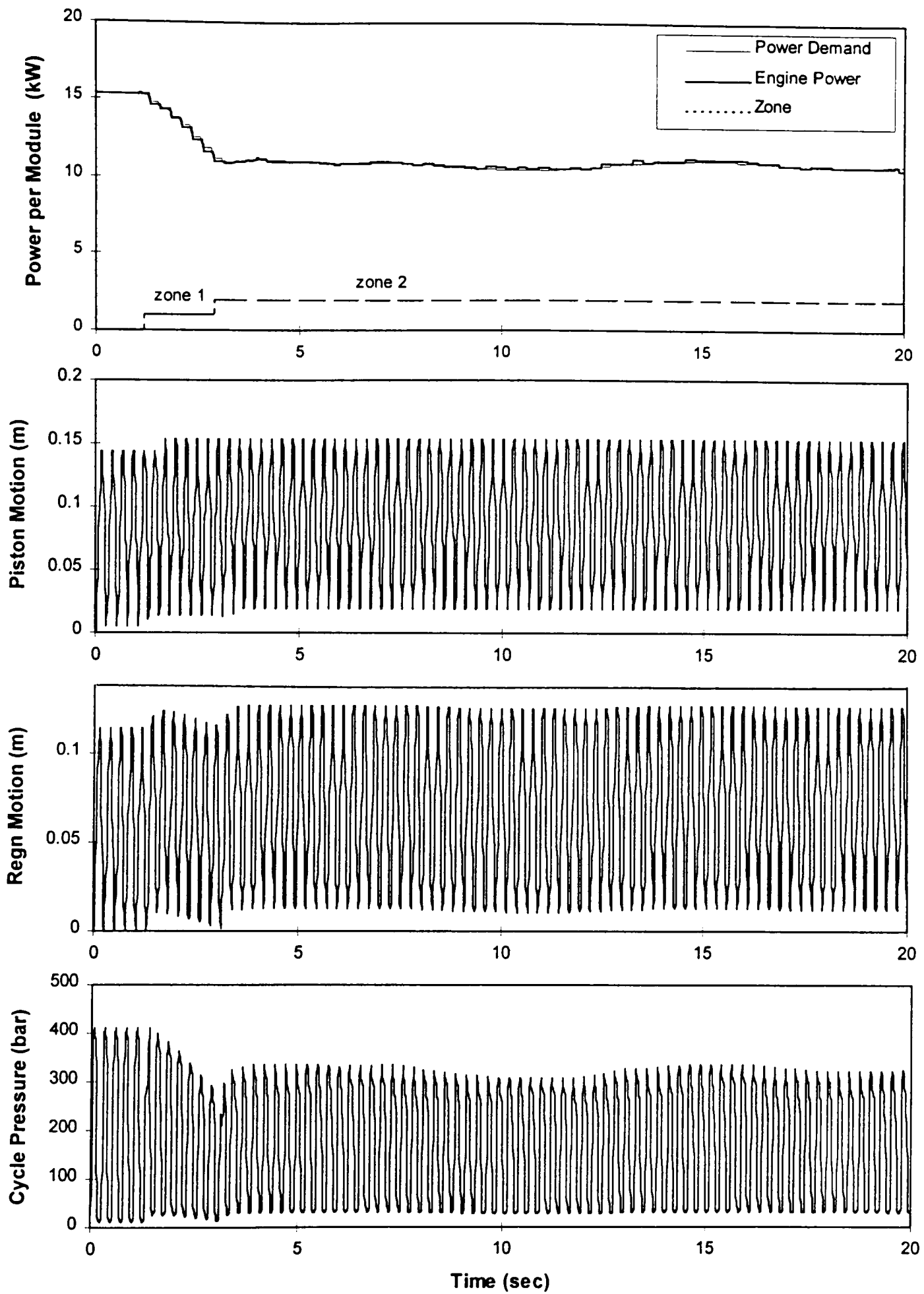


Figure 9.10 : Power output from the engine under a power-zone hunting situation. In addition to having filters in the control-algorithm for the transition zone, allowing variations in the offset amplitude can be useful.

control algorithm so that zone shift only occurs when the demand changes enough to justify it. The regenerator motion curve shows that the variations in power demand within the filter band can be followed more closely by having modifications (corresponding to these variations) incorporated into the offsetting requirements of the regenerator motion. Modification of the offsetting range of regenerator motions may also be used in order to cross-over zone boundaries and to avoid problem of zone-hunting.

9.3 Power control by offsetting and clipping regenerator motion

This strategy differs from the previous one in the way the regenerator motion is controlled. Instead of offsetting the entire motion range of the regenerator using an additional biasing cylinder, the regenerator motion is clipped at the cold-end. It should be noted that clipping at the cold-end both offsets the motion and reduces the effective stroke, while stroke length remains fixed with the offsetting-method. For this a mechanism as described in section 8.3d of the last chapter could be used, where the regenerator drive cylinder has a 'bypass and filling port' and the drive cylinder has an inclined top face. Changing the rotational position of the inclined piston allows control of the timing at which the filling port closes which effectively clips the regenerator motion at the cold-end. This mechanism is more compact and could be easier to control compared to the one used in offsetting-method. As the regenerator motion is offset and clipped at the cold-end, the increase in P-V area is less compared to the previous method for equivalent offsetting. This occurs as a part of the regenerator stroke is lost during clipping (ie. when the regenerator remains at the cold-end) and with the piston moving the cycle pressure falls. To move up from one power-zone to the next a larger offsetting towards the cold-end (up to 18 mm) is needed, compared with the offsetting-method.

The same set of ternary-code could be used for piston motion as in the offsetting method, though with one exception. As a result of larger offsetting, the peak pressure developed during a cycle also increases as compared to offsetting-method. This is not a very big problem for piston motion of zone two or higher (ie. towards lower power),

TABLE 9.2 : Engine parameters and power ranges
(Power control by offsetting and clipping regenerator motion)

Power range/module	1.8 - 15.1 kW
Thermodynamic pile bore	40 mm
Regenerator stroke	(116 - offset) mm
Engine/Regenerator cycle speed	231 cycles/min
Pump-Motor speed	1800 rpm
No. of cylinders in the pump-motor	10
Pump-motor cylinder volume	9.5 cc (approx)
Piston motion equivalent to one cylinder displacement	9 mm (approx)
No. of pump-motor cylinders available in each engine cycle	78

Power Zone	Pressure Level bar	Cylinder displacement pumped in or motored out	Piston motion range using ternary-code mm	Regenerator motion offset needed mm	Power range kW
0	400	16	0 - 144	0	15.1
1	300	16	9-153	0-11	11.6-15.1
2	200	15	18-153	0-18	8.1-11.6
3	150	15	27-162	0-14	5.7-8.1
4	100	15	36-171	0-12	3.3-5.7
5	50	14	45-171	0-13	1.8-3.3

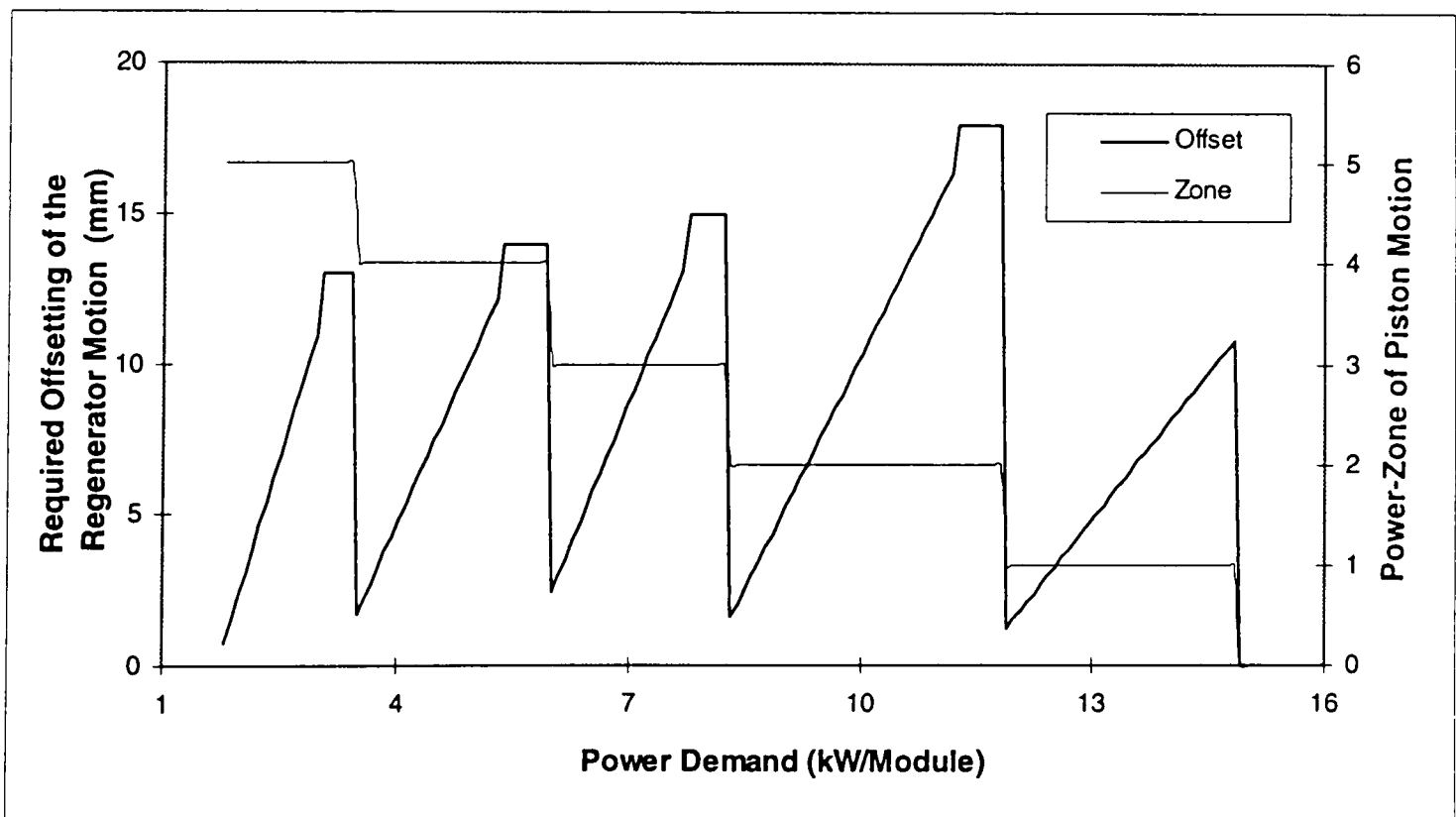
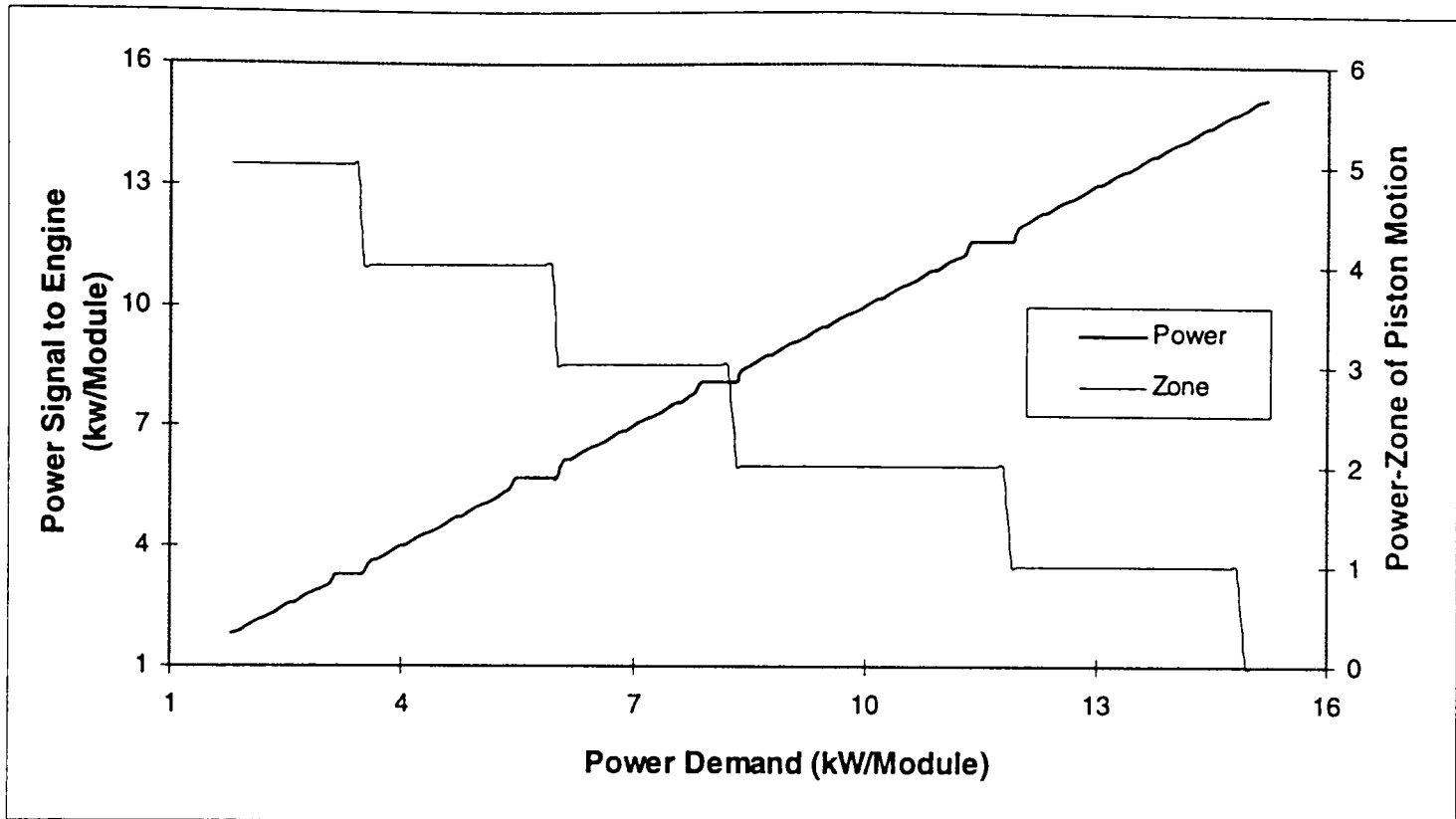


Figure 9.11 : Change of power zones and offsetting requirements, with changes in power demand. At the transition between zones the demand signal is filtered to avoid hunting across zone boundaries.

because the peak pressure developed due to required offsetting of the regenerator (to take the power up to the lower-level of the power-zone above) does not exceed the design limits of the TD pile. But in the case of zone one, the power range and the ternary-code need to be modified in order to keep peak pressures within design limits of the hot-end. Table 9.2 shows the cycle parameters and power zones chosen for the offsetting and clipping method. Figure 9.11 shows the ranges of different power zones and regenerator offsetting and clipping needed throughout the working range of the engine. It should be noted that the power rating of zone-one has been changed, as compared to table 9.1, in order to limit the offsetting, hence the peak-pressure requirement to cover the range. The regenerator offsets needed were generally larger. Tables of the ternary-codes and replacing decisions used for shifting power-zones and distortion of the transition cycles are included in appendix C.

Figure 9.12a and 9.12b show the variation of cycle pressure and flexible piston motion for zone-one, with sinusoidal regenerator motions without either offsetting or clipping. The figures also show the differences, resulting from different ternary-codes used for zone-one, in the two strategies. The cycle pressure is relatively lower at the initial part of regenerator motion towards the cold-end. This limits the peak pressure rise when the regenerator motion is offset and clipped as reflected in the P-V diagram of zone-one in figure 9.13. As the same ternary-codes are used for other power-zones, the variation of cycle pressure and piston motion are identical to results (figure 9.2a & 9.2b) for the previous strategy. Figure 9.13 shows the P-V diagrams at each power level. The darker lines show the engine cycle at the lower power level at each zone with full stroke regenerator motion without any offsetting or clipping towards the cold-end. Lighter curves show the engine cycle at the higher power level of the respective zone with full offsetting and clipping of regenerator motion at the cold-end. Compared to figure 9.3, for all zones the slope of the pressure changes are steeper, due to increased offsetting.

Figure 9.14 shows the change of engine cycle as the power demand rises up into the power-zone above. As long as the demand is within zone three, with increased demand, the regenerator motion is offset further towards the cold-end, resulting an increased clipping time at the cold end. As the demand rises enough to make a transition to the

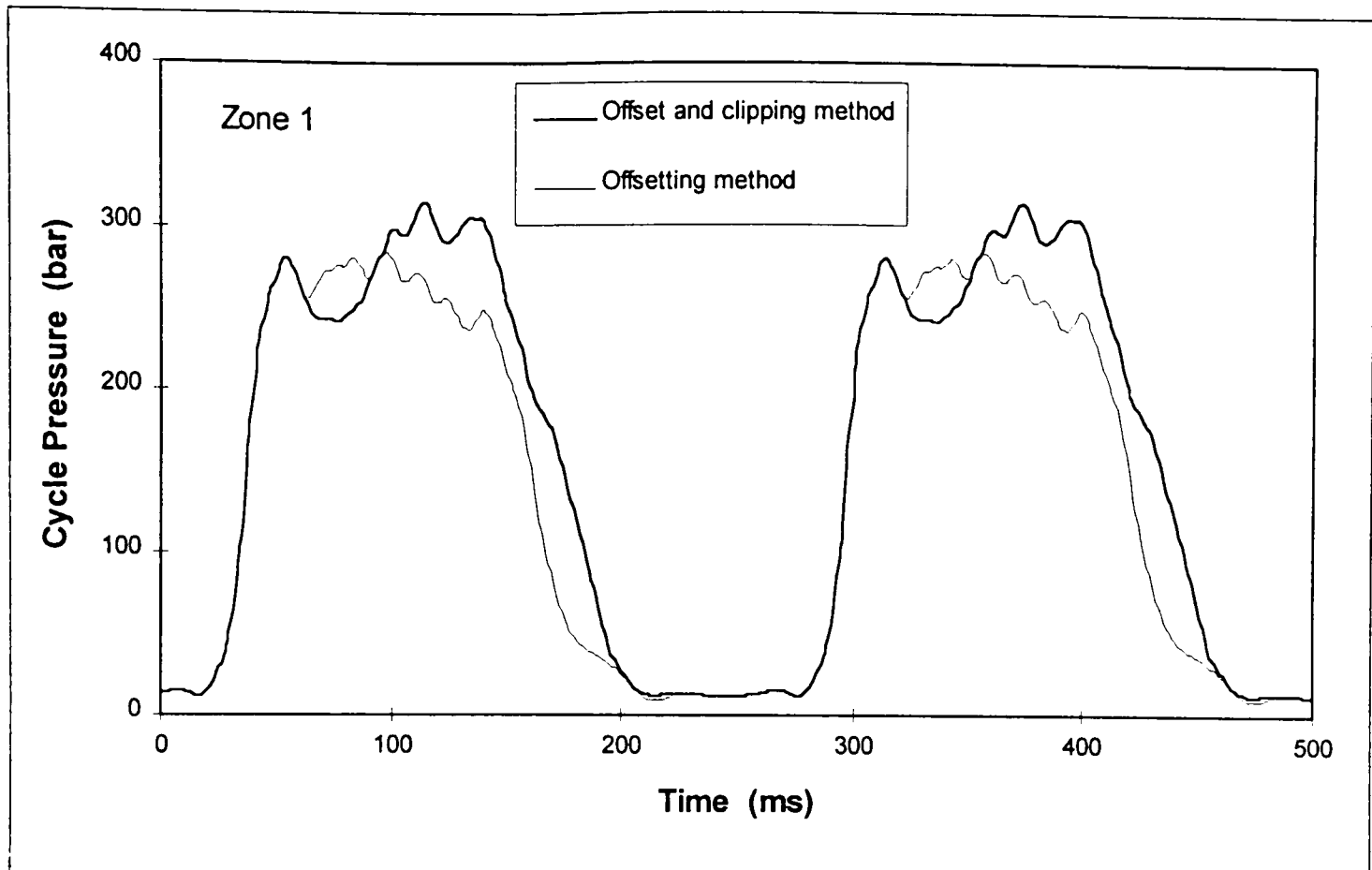


Figure 9.12a : Variation of cycle pressures for power zone one compared to the previous strategy, as the ternary-code is changed. Pressures are kept relatively low at the beginning of regenerator motion towards the cold-end. This limits peak pressure as offsetting and clipping is applied to increase cycle power.

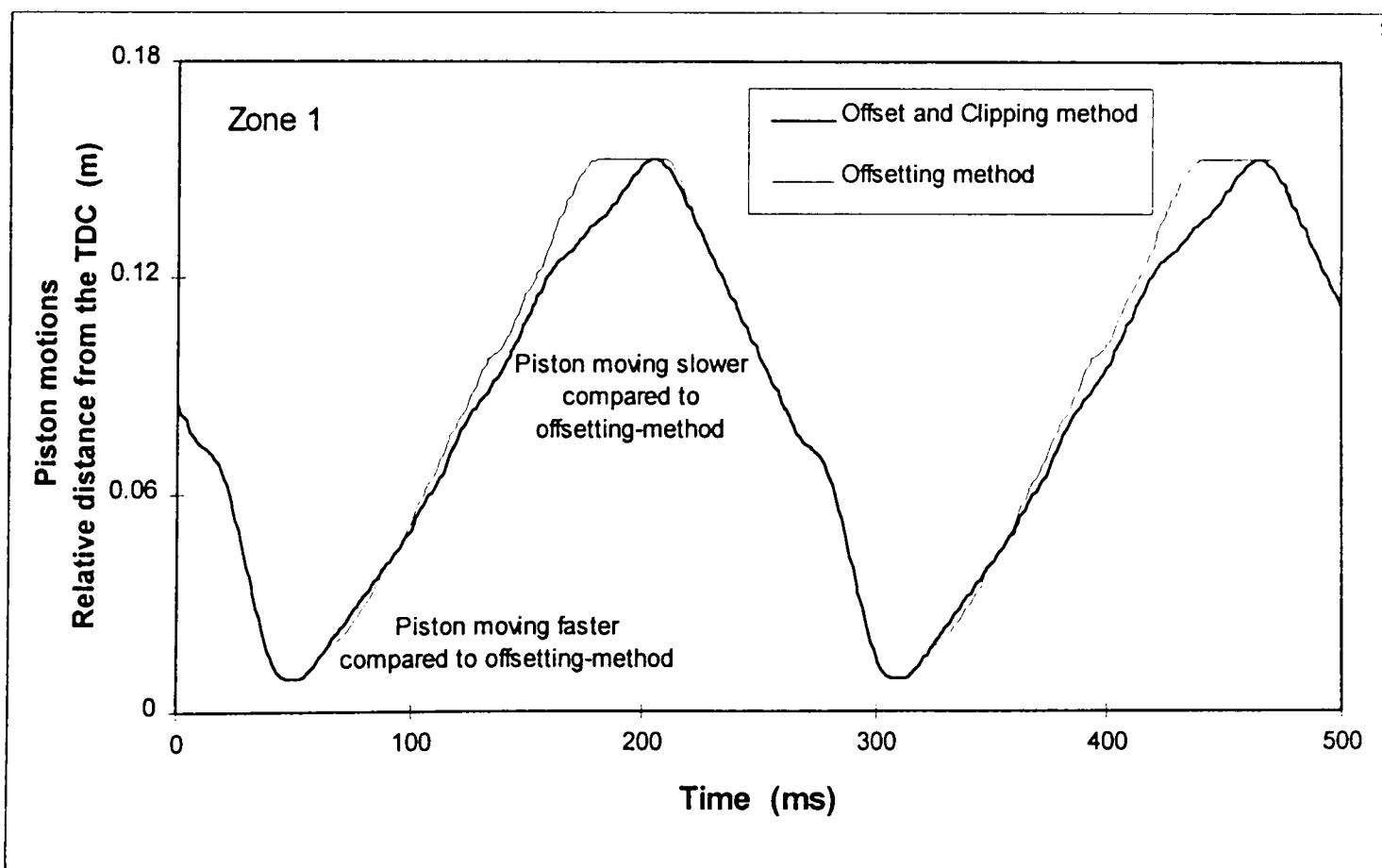


Figure 9.12b : Variation of piston motion as the ternary-code is changed for power-zone one. At the beginning of regenerator stroke the piston is moved faster in the second method, while later it is moved at a slower rate. This results in the variation of cycle pressure as shown above. In both cases full stroke sinusoidal regenerator motion without either offsetting or clipping are used.

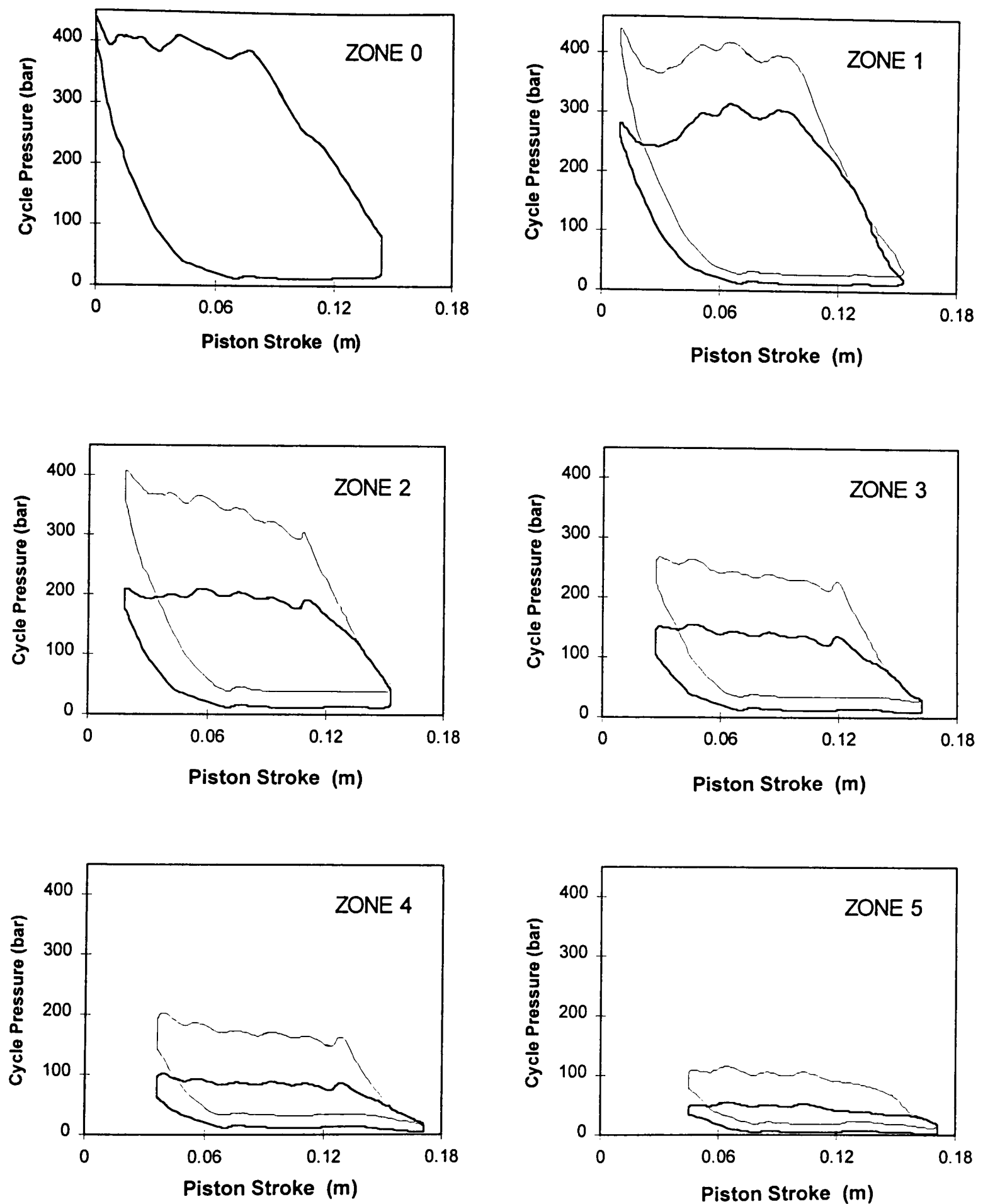


Figure 9.13 : Pressure-volume diagrams of the engine cycle at different power zones. Lighter curves show the cycles when the regenerator motion is offset and clipped at the cold-end. With offsetting the pressure rise is more prominent at higher pressures resulting in greater enclosed area and hence power. Within each zone the piston follows a pre-determined motion, according to the ternary-code.

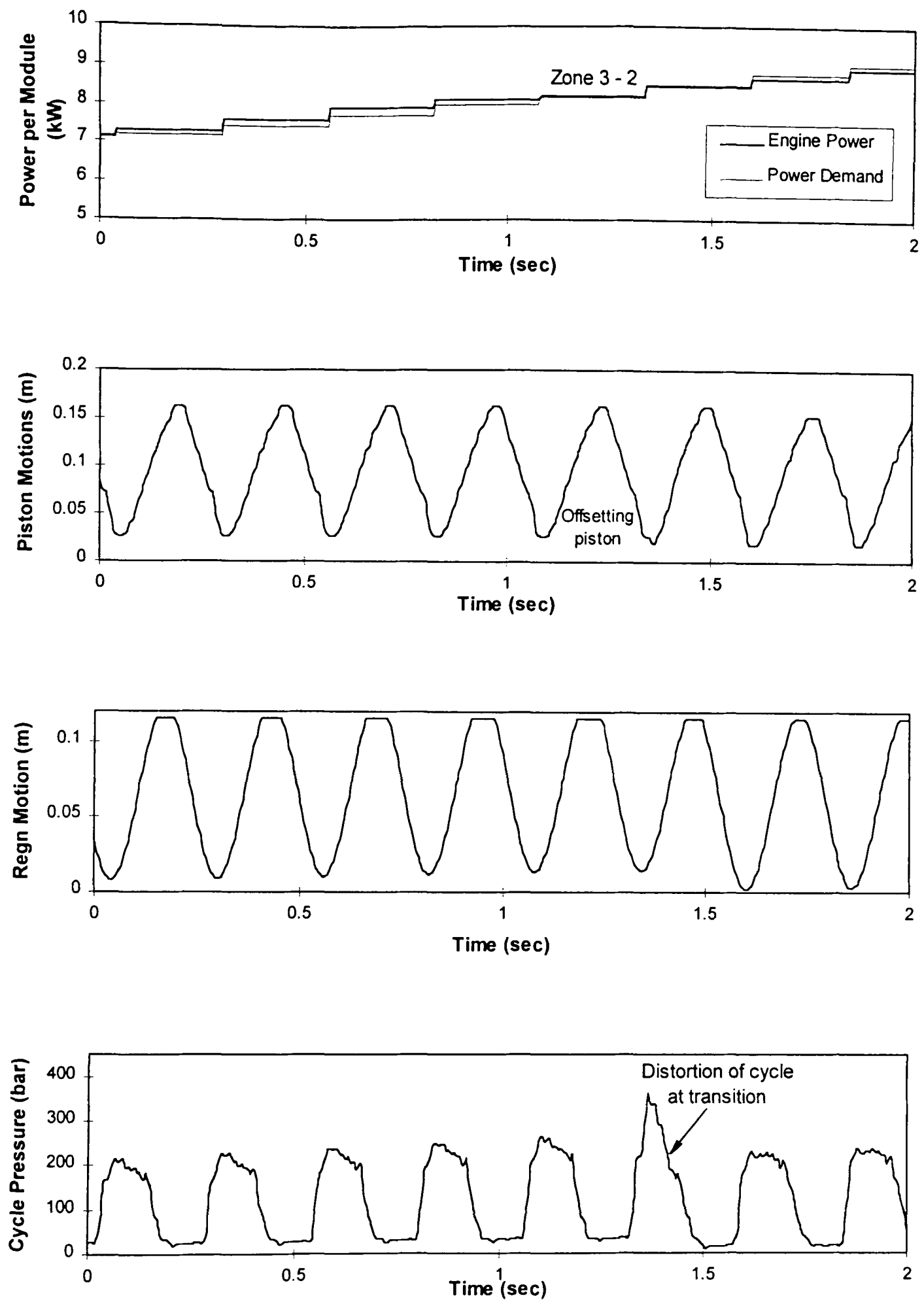


Figure 9.14 : Cycle changes as the demand increases and passes through a power-zone change. Within a power-zone the regenerator motion is offset further towards the cold-end increasing the clipping time. In the transition cycle, the piston motion is reset to a new range and replacing decisions to distort the transition cycle are activated to keep the power output close to the demand during transition.

power-zone above, the piston motion is offset to towards the TDC reference. Decisions for cycle distortion are also activated in order to reduce the power error during transition. After the transition cycle, the flexible piston is shifted to the motion corresponding to zone two and remains unchanged until any further change of power-zones. The offsetting and clipping of the regenerator motion is changed accordingly to meet the varying power demand within zone two.

Similar results were found for simulations of long operating periods (eg. 20 sec) with variable power demands and also for hunting conditions, as shown in figure 9.9 and 9.10, hence presentation of these results are not repeated.

9.4 Power control by changing regenerator stroke

In this strategy the fine control on power is achieved by changing the stroke length of the regenerator, instead of offsetting or clipping. Hence the pattern of the regenerator motion remains same (always coming back to same hot-end reference), while the amplitude of motion is changed. This strategy differs from the last two - in the way cycle pressure varies with changes in the regenerator stroke. In both of the last two methods, the cycle power increases as the regenerator motion is offset or clipped towards the cold-end. In this strategy the regenerator motion is always referenced to the hot-end and changing the stroke varies the distance it travels towards the cold-end. Unlike the other two, as the regeneration motion is modulated from full-stroke (ie. the stroke is reduced), the power generated decreases. As the cyclic frequency of the regenerator motion remains unchanged, with reduced stroke the regenerator velocity decreases while piston motion is unchanged. As a result the high pressure-level gradually drops as the regenerator moves towards the cold-end. Conversely, when the regenerator returns to the hot-end piston motion causes the low pressure-level to gradually rise. More prominent changes at higher pressures decrease the area of the pressure-volume diagram with reduced regenerator stroke with proportional effect on power output.

Another noticeable difference between this strategy and the last two is that, without any change, the regenerator moves at full stroke and the power output is equal to the upper limit of each power zone (lower limit for the two previous methods). Reducing regenerator stroke decreases the power generated to the lower-limit of the power-zone. Sinusoidal or triangular regenerator motion with limited acceleration (as shown in chapter seven) could be used. Results are presented in this section with triangular regenerator motion.

The choice of range of different coarse power-zones was governed by the desire to keep the stroke length variation of the regenerator the same across the different power-zones (100-85 % of the full stroke). This consideration and different type of regenerator motion results in ternary-codes different from those used in the last two methods. Table 9.3 shows the cycle parameters and the ranges of different power zones. Regenerator strokes are defined as percentage of full stroke. Figure 9.15 shows the shifts between different power zones and the fraction of full-stroke regenerator motion needed throughout the power range.

Figure 9.16a and 9.16b shows the variation of pressure cycles and the shifting of the flexible piston away from the TDC reference at the cold-end with successive power-zones. The piston motions and pressure variations are different from those of the two other methods, as the ternary-codes are different and triangular regenerator motion is used. When the regenerator moves towards the cold-end, the piston motion has two distinct slopes which maintain and then reduce the cycle pressure respectively. This change in slope will be less prominent for a sinusoidal regenerator motion. Figure 9.17 shows the P-V diagrams for each power-zone. The darker curves show the engine cycle with full regenerator stroke, at the higher power level of the zone. The lighter curves show the cycle with power reduced to the lower level of the zone, with reduced regenerator stroke. The table of ternary-codes corresponding to the triangular motion of the regenerator at different power-zones is given in appendix C.

Figure 9.18 shows the transition of the cycle corresponding to step changes of power demand from zone-zero to zone-five before returning to zone-one. The offsetting of

TABLE 9.3 : Engine parameters and power ranges

(Power control by changing regenerator stroke)

Power range/module	1.8 - 15.1 kW
Thermodynamic pile bore	40 mm
Regenerator stroke	116×(fract.) mm
Engine/Regenerator cycle speed	231 cycles/min
Pump-Motor speed	1800 rpm
No. of cylinders in the pump-motor	10
Pump-motor cylinder volume	9.5 cc (approx)
Piston motion equivalent to one cylinder displacement	9 mm (approx)
No. of pump-motor cylinders available in each engine cycle	78

Power Zone	Pressure Level bar	Cylinder displacement pumped in or motored out	Piston motion range using ternary-code mm	Regenerator motion range fraction of full stroke	Power range kW
0	400	16	0 - 144	100-87 %	15.1-10.8
1	300	16	9-153	100-88 %	10.8-8
2	200	16	18-162	100-88 %	8-6
3	150	15	27-162	100-85 %	6-3.5
4	100	14	36-162	100-85 %	3.5-1.9
5	50	13	45-162	100	1.9

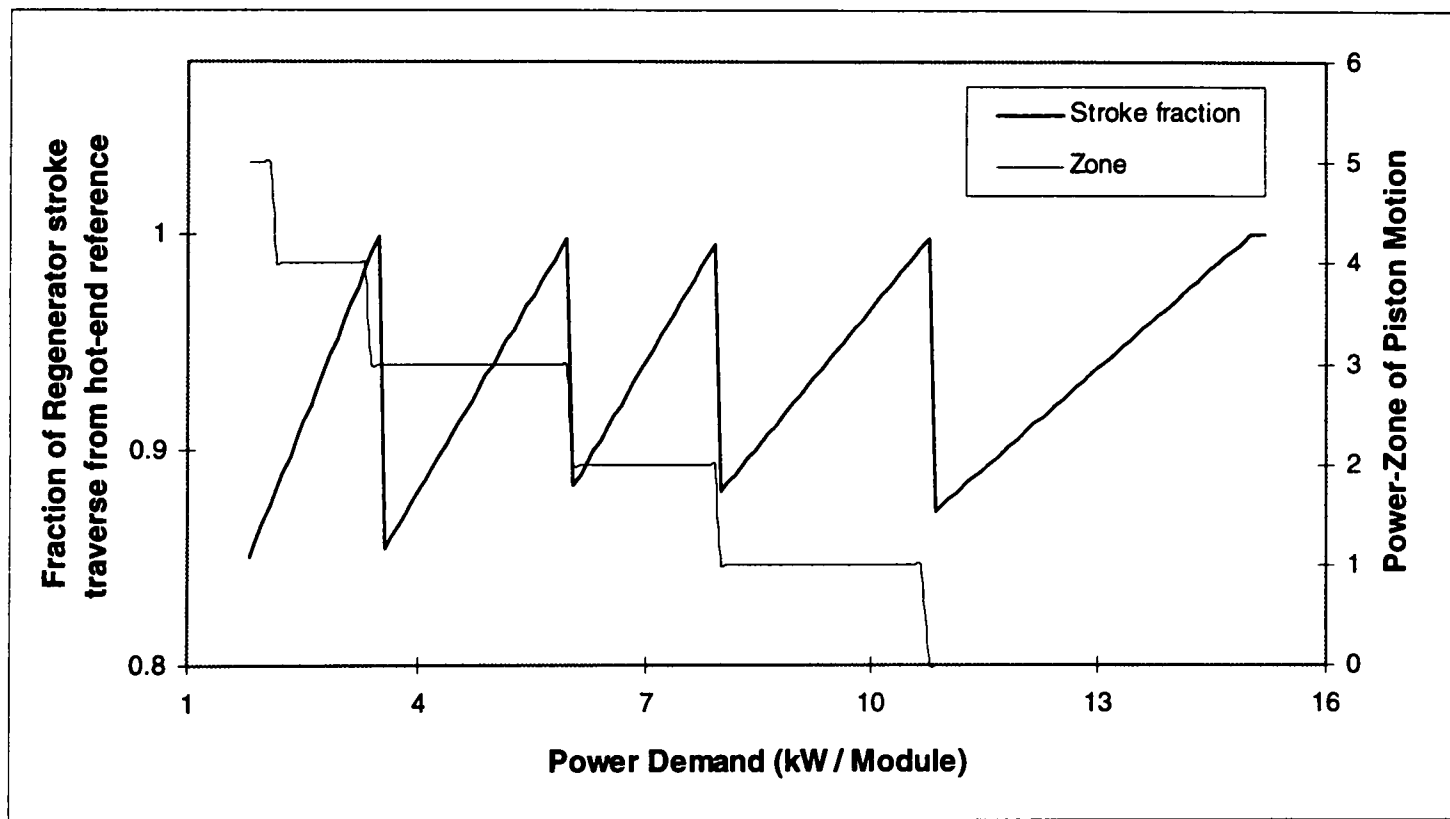
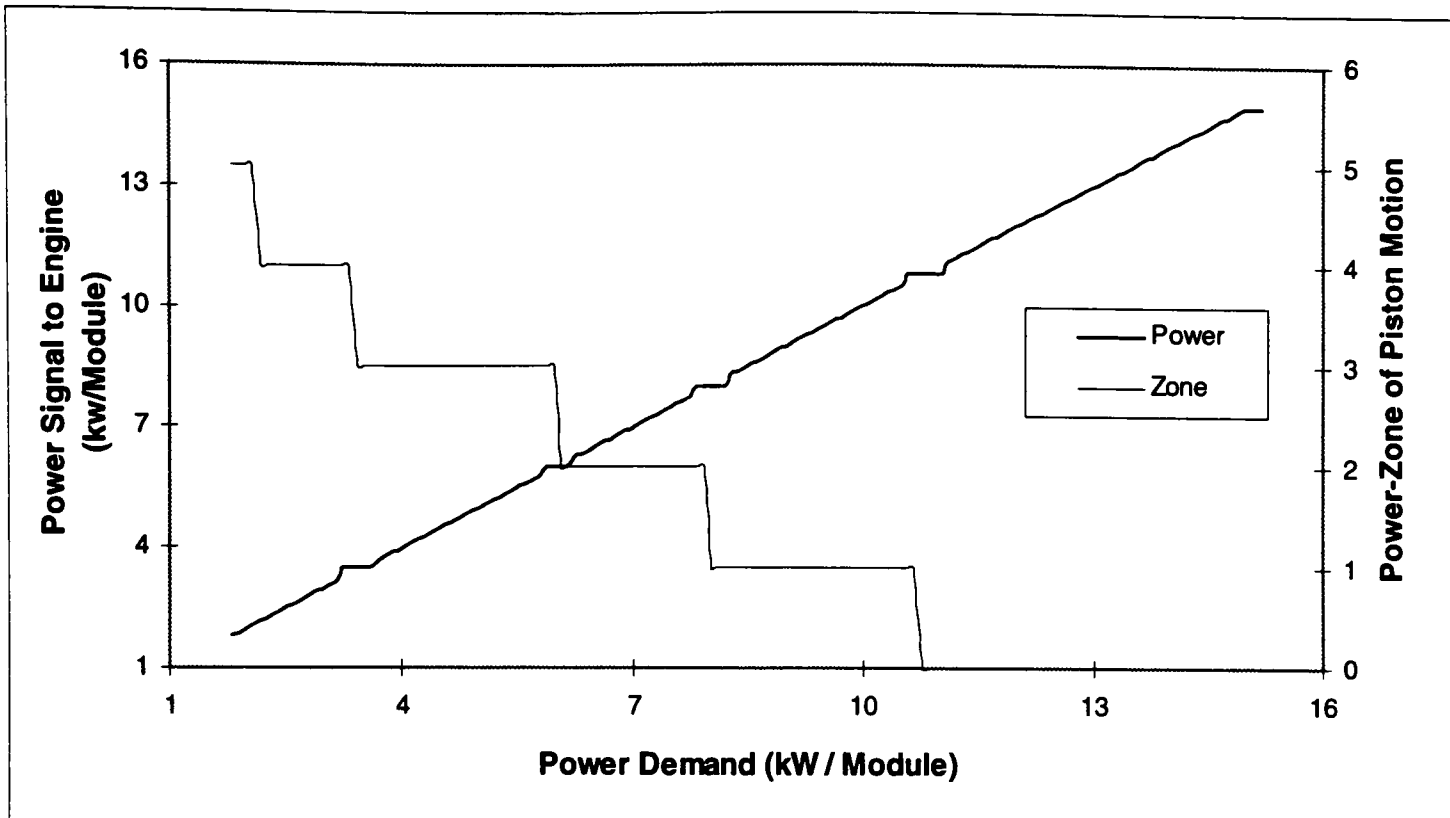


Figure 9.15 : Change of power-zones and stroke requirements, with changes in power demand. At the transition between zones demand signal is filtered to avoid zone hunting situation across the boundaries.

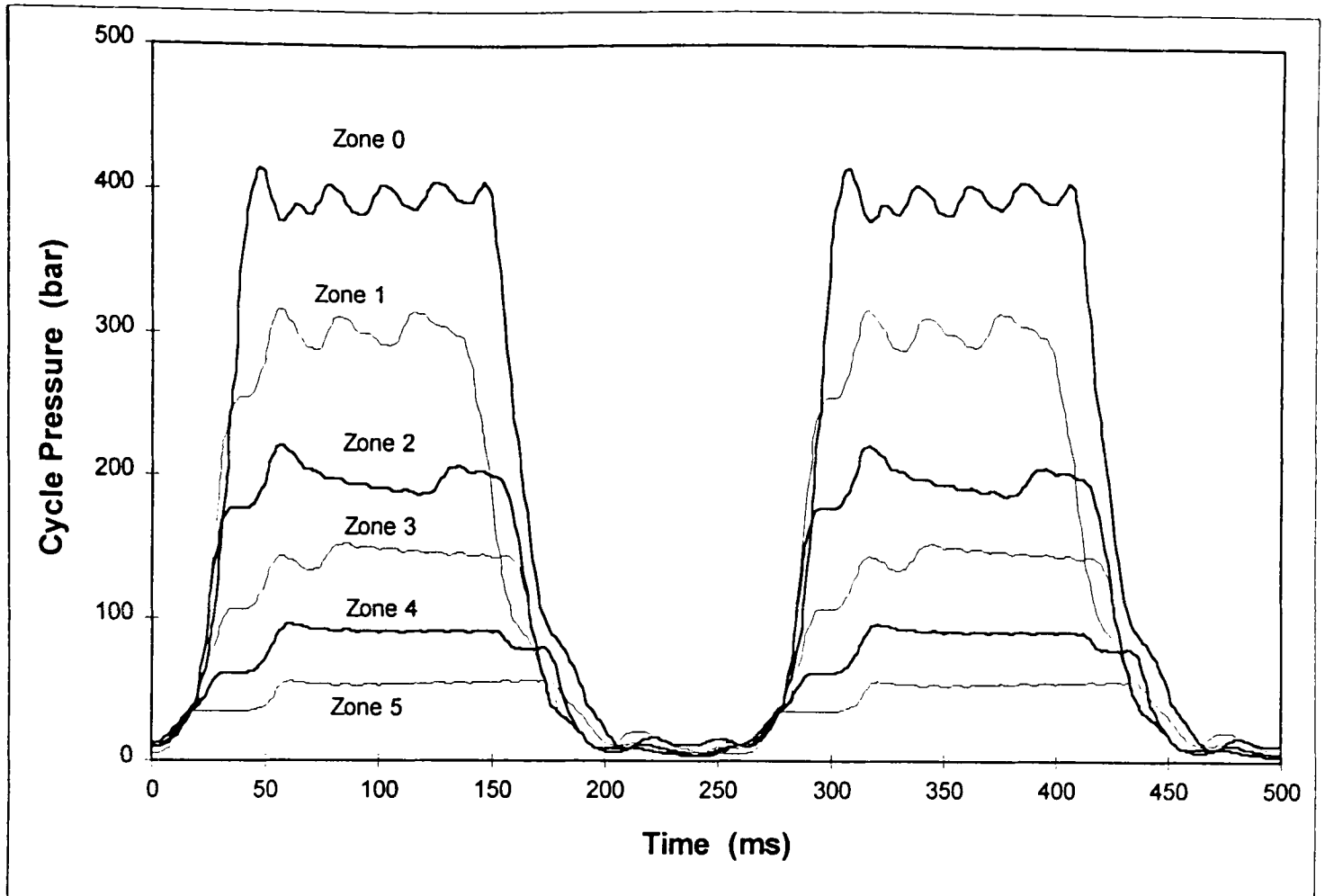


Figure 9.16a : Variation of cycle pressures for piston motion at different power-zones. For each successive zones the piston advances further away from its TDC, resulting in lower cycle pressure.

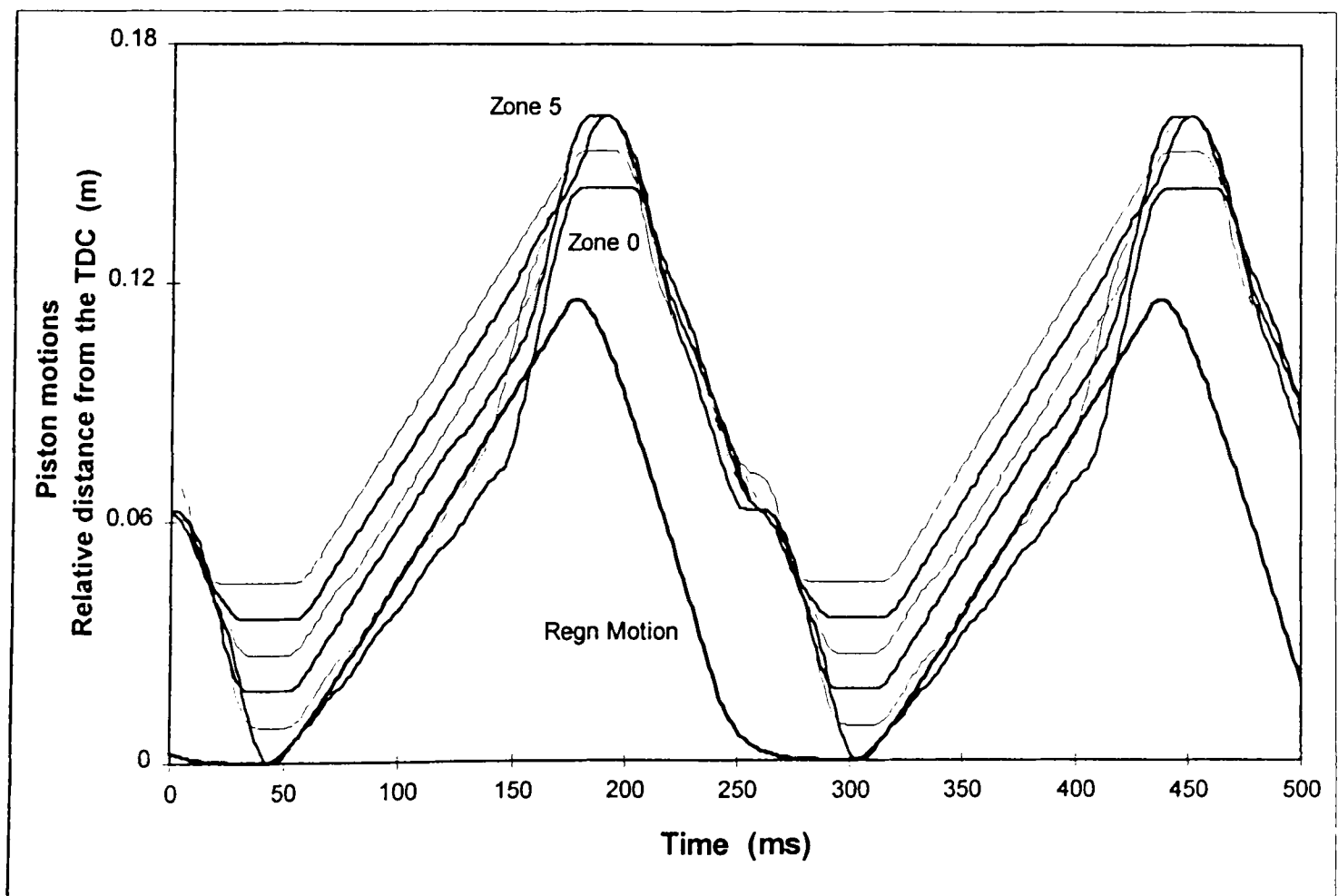


Figure 9.16b : Variation of piston motion for different power-zones. For each successive zones the piston plays further from the TDC, while the triangular regenerator motion is unchanged.

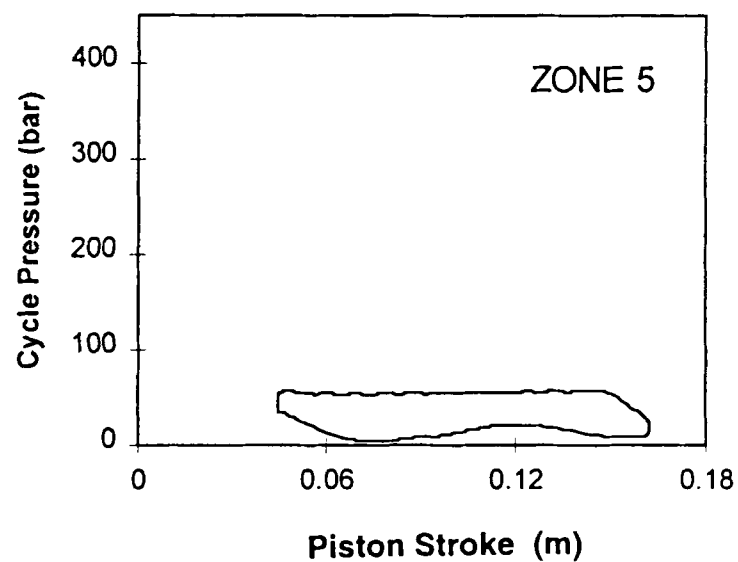
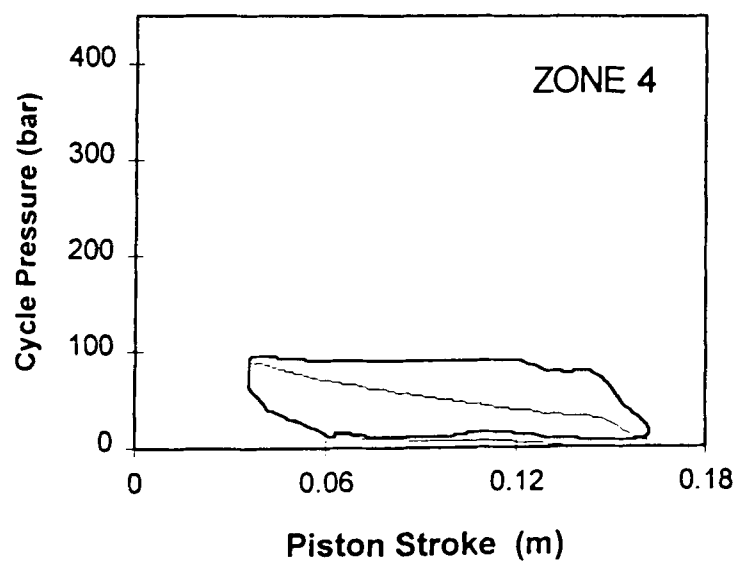
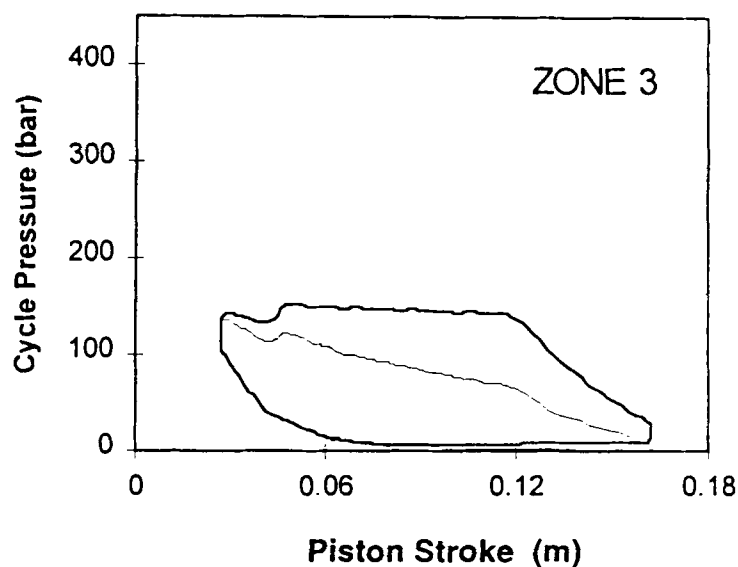
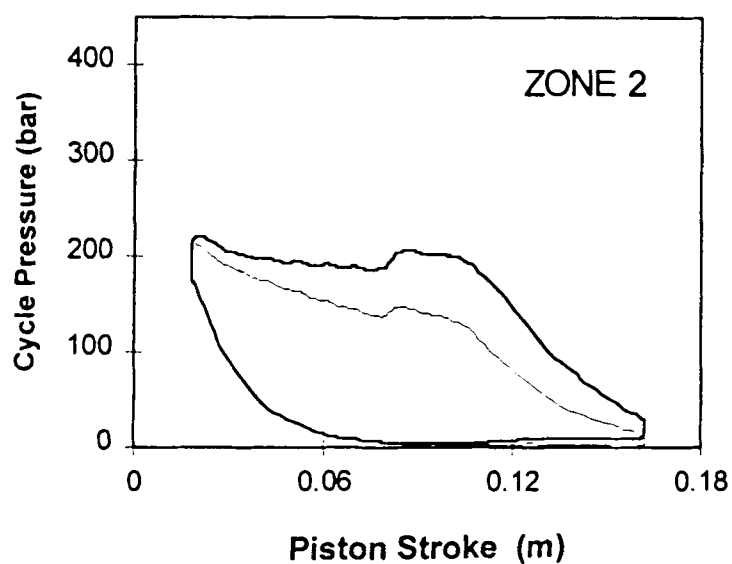
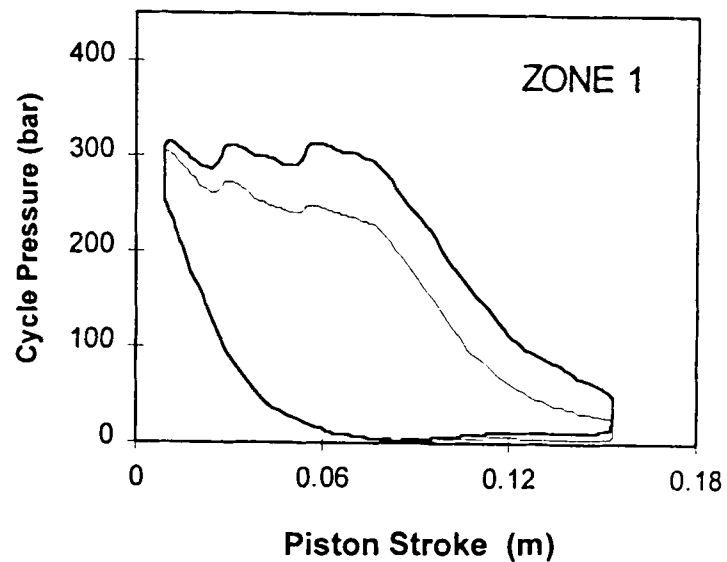
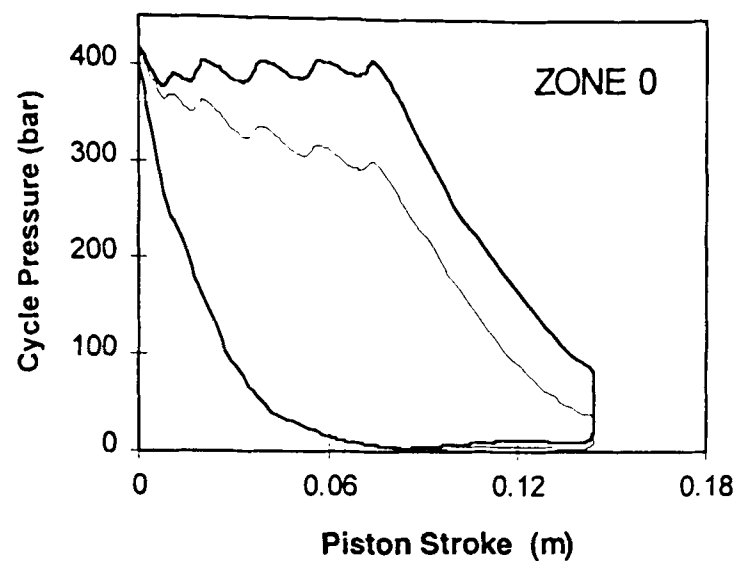


Figure 9.17 : Pressure-volume diagrams of the engine cycle at different power zones. Lighter curves show the cycles when the regenerator stroke length is reduced, though similar in nature of the full stroke motion. With reduced regenerator stroke the pressure fall is more prominent at higher pressures resulting in reduced enclosed area and hence power. Within each zone the piston follows a pre-determined motion, according to the ternary-code.

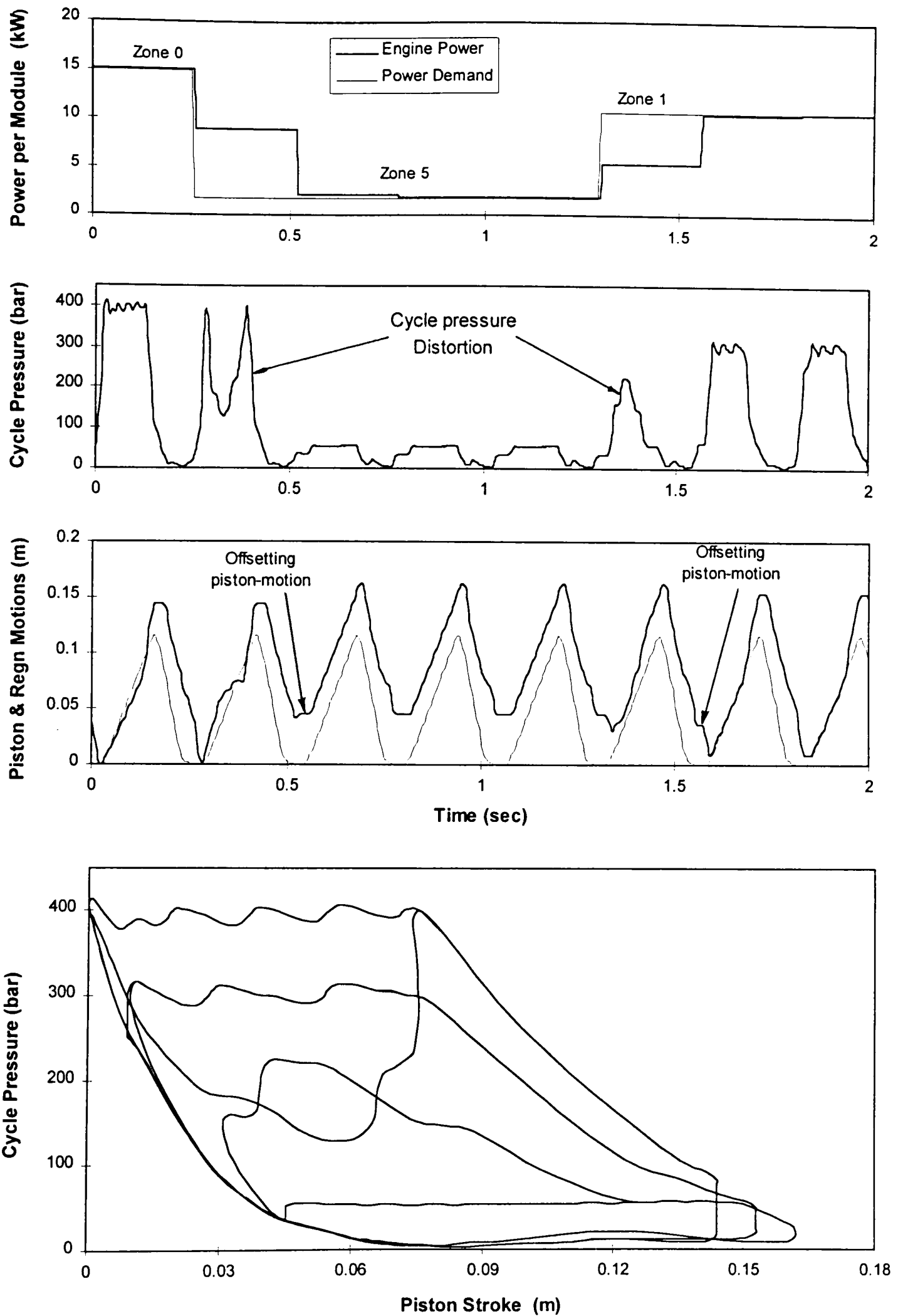


Figure 9.18 : Cycle response to step change of power from zone-0 to zone-5 and then returning to zone-1. Additional superimposition to distort transition cycle to improve cycle response to step changes of power.

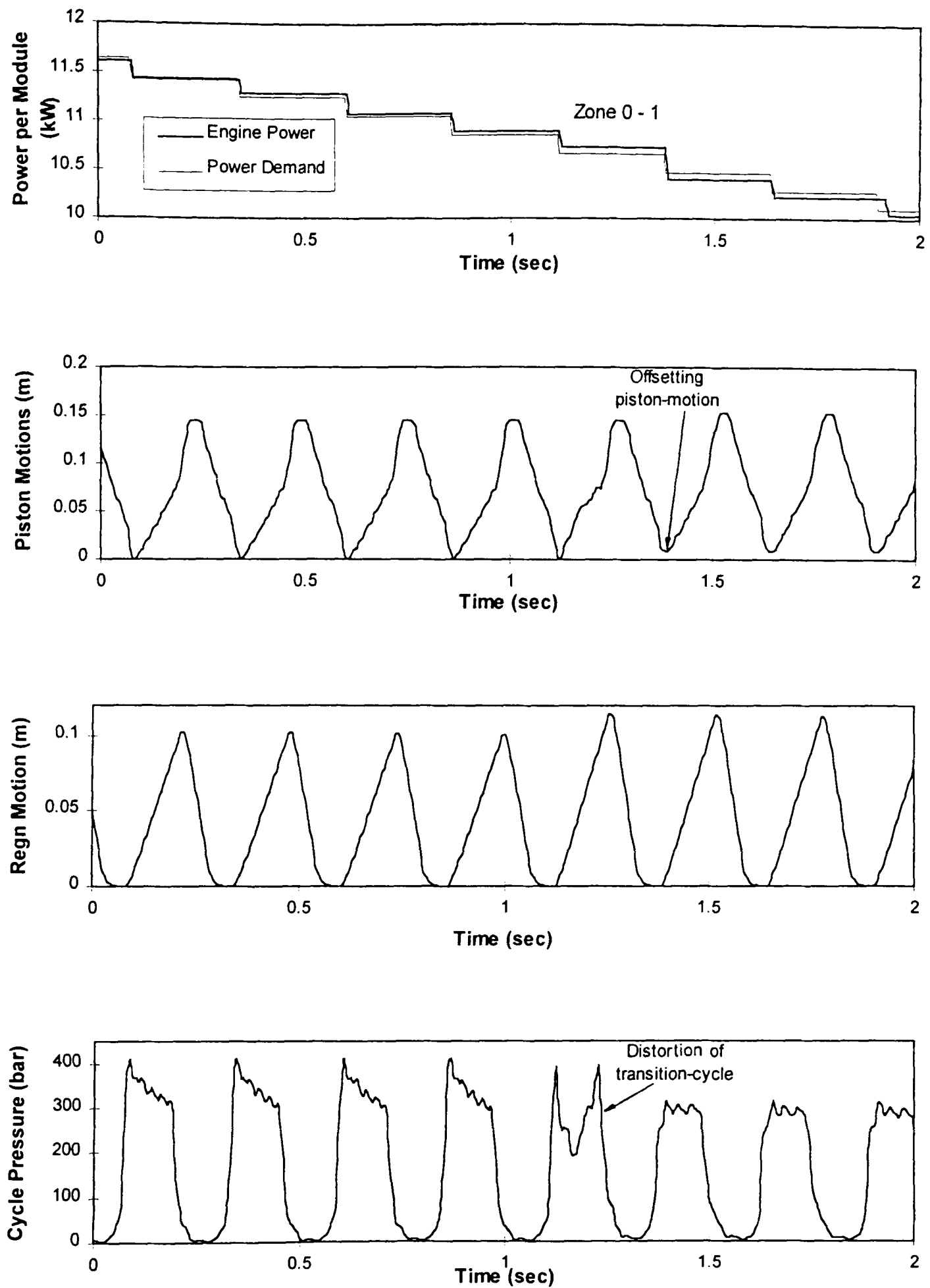


Figure 9.19 : Cycle changes as the user demand decreases and passes through a power zone change. Within a power zone the regenerator motion is adjusted by changing stroke length to follow the power demand, though starting from and ending at the same hot-end reference. In the transition cycle the piston motion is reset to new range and superimposing decisions to distort the transition cycle is activated to keep the power output close to the demand during transition.

piston motion corresponding to the shifting of power-zones is made in a similar way as in the other two plans by replacing additional pumping or motoring decisions, into the ternary-code. The decision replacing technique for cycle distortion is applied to minimise differences in the power output and demand in the *transition-cycle*. The effect is exhibited in the pressure trace of figure 9.18.

Figure 9.19 shows the cycle response, as power demand decreases passing through a power-zone shift. As long as the demand is within zone-zero the piston motion corresponds to the ternary-code of the same zone. The fine-control of power is done by changing the regenerator stroke, while the motions still start from and end at the hot-end reference. As the demand shifts from zone-zero to zone-one, the piston motion is offset for the next zone and the regenerator motion is reset at full stroke. Once within zone-one the regenerator stroke is again changed according to the demand.

9.5 Comments on the simulations with three strategies for power-control

In this chapter simulation results are presented for three strategies of total power-control, as laid out in chapter eight. In general each of the three strategies were found to be capable of meeting the instantaneous power demand. The mechanisms required to achieved the desired modulation of regenerator motion may finally dictate which of these is implemented in practice. The offsetting of piston motion, for coarse power-control, was achieved by replacing extra pumping or motoring decisions in the ternary-code at transition-cycle. Some error between power demanded and generated by the engine occurs at the transition cycles, while the piston motion is being offset. Some additional replacement of decisions in the ternary-code were used to distort the pressure variation in the transition cycle in a pre-determined way. This technique eliminated the power-error for transitions between adjacent power-zones and reduced it significantly for the largest zone-shifts. The presence of a hydraulic buffer or inertia between the engine and the load may further minimise the effect of any error.

CHAPTER - 10

Comparison of Static and Dynamic Simulation Models

10.1 Introduction

In this chapter the results of the static and dynamic models are compared. For this all aspects of the two models need to be examined and initial assumptions brought in to agreement. The engine cycle used in the static model, described in chapter 3 and 4, is a *variable-frequency cycle*. The cyclic frequency is changed to vary the power output, while each cycle always executes the same pressure variations. On the other hand, as described in chapters six through nine, the time domain modelling revealed that a *variable-pressure cycle* would be the preferred control method. In this approach the TD pile cyclic pressure-level is altered to vary the power output, while the cyclic frequency remains nearly constant. The time domain model estimates the indicated power, while the static model calculates overall efficiency (the reasons are restated in section 10.5). In this chapter modifications are introduced to the static model so that it can be adapted for the *variable-pressure cycle* to estimate cycle efficiencies for different power outputs, using this approach.

First, in order to compare the performance estimates of two models throughout the power range, performances of the static model are investigated (section 10.2 and 10.3) for different power outputs, using *variable-frequency* control. In section 10.4 limitations of the estimates made by the static model are considered. Using results from the dynamic model with the same type of cycle (ie. *variable-frequency*), corrections, based of the estimates of the static model are proposed. Modifications are then introduced to the static model to allow *variable-pressure* control, using information gained from the time domain model. In section 10.5 engine performance for the power-range are estimated with *variable-pressure* control and a comparison is made with the *variable-frequency* method.

10.2 Variable heat-flux through the full power design (variable-frequency control)

The design of the engine, using the static (Mathcad) model in chapter four, was optimized for full power, although it could be carried out for any power level. In practice most engines would spend much of their time at part-load and therefore will have constantly varying heat flow rates through the TD pile. At this stage the performance of the engine, designed with the aid of the static model for full power stresses and temperatures, was evaluated for different heat flow rates. With lower heat flows, there are generally smaller temperature drops across the various thermal impedances of the TD pile. This may not be equally true for all thermal resistances as some of them may vary significantly as temperature changes. For a fuel burning with stoichiometric air-fuel ratio, the flame temperature varies very little (less than a few percent) at any fuel burning rate. Given that the flame temperature remains the same, while the temperature drop across the sum of thermal resistances is reduced, the temperature levels in the TD pile through to the hot-end steam must rise. This is also true if a fixed proportion of excess air is always maintained compared with stoichiometric air requirements.

This problem of overall hot-end temperature rise can be resolved by increasing the excess air-ratio in an inverse proportion to the heat flux. It should be noted that increasing excess air-ratio with reduced fuel burning rate, does not necessarily mean quantitatively increasing the gas flow rate through the system and the mass flow rate of combustion products may even reduce. For simulating different heat flow rates, the following changes were found :

- Decreasing the temperature of the pre-heated air entering the burner, as well as the gases leaving the hot-end, reduces the temperature level of the gases and metal in hot-end. Both temperatures need to be changed in synchrony for the loops to converge, as the heat-exchanger design is already fixed at this stage. The rise or fall of these two temperatures was found to have only a small effect on the temperature at which the gases are exhausted to the surroundings. Hence

the choice of these temperatures can be used as a general tool for offsetting flame temperature and temperatures inside the hot-end, to achieve desired temperature levels.

- Altering the hot-end and cold-end temperatures change the Carnot efficiency and ultimately the thermal efficiency. Changes in the hot-end temperature affects the efficiencies much more significantly compared to what can be achieved with the potential cold-end variation.
- Changing the heat-loss factor (LF in chapter four, which is used to balance the heat supplied at the burner with the sum of the heat flux through the hot-end and the heat losses to surroundings), mainly effects the temperature at which the gas leaves the hot-end. It subsequently alters the temperature of pre-heated air coming out of the heat-exchanger as well as the exhaust out of the engine, but on a much smaller scale compared to previously. The effect on the flame temperature is also small. The heat balance loop was considered to have converged once the supplied heat to the burner nearly agreed with the sum of the heat flowing through the hot-end along with the losses to the surroundings (eg. within 100 watts).
- Altering the excess air-ratio (AR in chapter four, defined as the ratio of actual mass flow rate of air to the stoichiometric mass flow rate of air) mainly affects the flame temperature which in turn alters the metal and fluid temperatures inside the hot-end. The effects are much less significant on the temperature of the gases leaving the hot-end and downstream in the heat-exchanger, as the increase in mass flow rate compensates for the temperature change. Though increased excess air-ratio reduces the flame and metal temperatures, it increases the power consumption of the blower as well as the heat loss at the exhaust.
- At each different heat flow rate (ie. power level), a number of solutions may satisfy all the closed-loops. The solutions presented here represent those optimised to gain maximum efficiency.

10.3 Temperature gradient through the hot-end for variable heat flux (variable-frequency cycle)

The choice of the excess air-ratio, required at lower heat flows, depends on the desired temperature distribution in the TD pile and the location where the temperature is desired to be maintained. For different heat flows (ie. at part loads) studies were made with :

- (i) Fixed flame-fin root temperature.
 - (ii) Fixed hot-end steam temperature.
 - (iii) Fixed mid-wall temperature for hot-end.
- (i) In the first method, the excess air-ratio and other parameters are changed so that, for different heat flows the flame-fin root temperature (ie. temperature of the outer edge of the composite wall) remains the same as the full power one (about 685°C). In the Mathcad-model this is done by achieving similar flame-fin root temperatures (T_{fb} , by iteration), while in practice it would require temperature sensors (eg. a thermocouple) at the base of flame-fins. With decreased heat flux the temperature drop through the composite wall (which is the product of the thermal impedance and the heat flow rate) falls and the temperature of the inner edge of the composite wall rises. For any particular heat flux, the hot-end goes through the same cyclic pressure variation, as only the cyclic frequency varies and the composite wall is always stressed to nearly the same degree. This causes the curves of stress-temperature to rotate clockwise, pivoting about the flame-fin root temperature with decreasing heat flow, as shown in figure 10.1. It should be noted that the temperature scale also represents radial locations on the fin in outwards direction. This causes the stress distribution curve to exceed the safe stress for 2000 hrs rupture life line of Inconel 625 (Inco Alloy International, 1985), at 10 kW (37% of the full rating) heat flux per module. This choice of hot-end metal temperature distribution will result in lower engine life at part load, when less heat flux would be passed through the hot-end.
- (ii) The problem of reduced engine life (ie. the hot-end) at part-load could be overcome by maintaining a fixed steam temperature inside the hot-end. In this

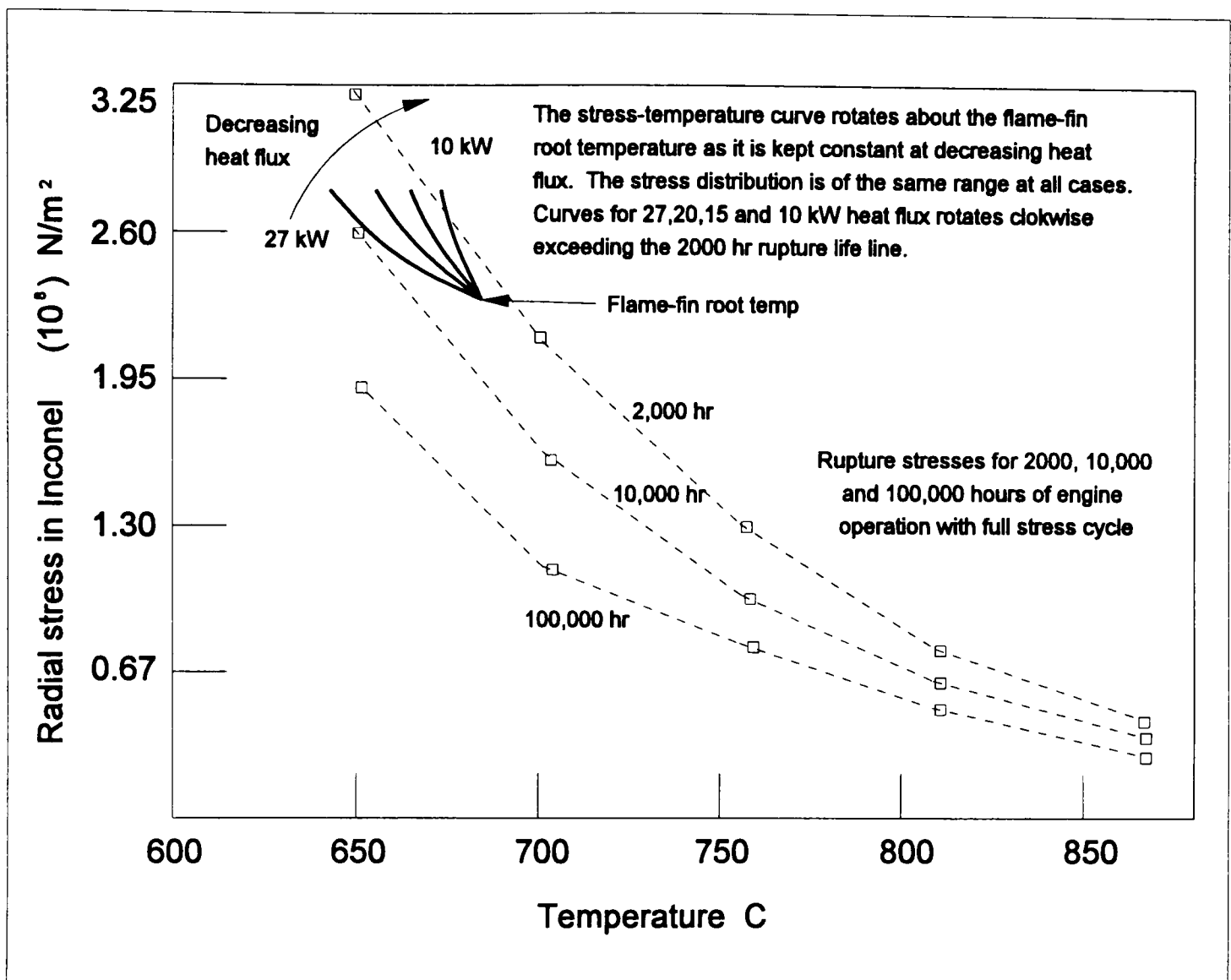


Figure 10.1 : The shifting of the temperature-stress curve as the heat flux decreases. The flame-fin root temperature is maintained by changing the proportion of cooling air. The hot-wall stresses are the same as the cycle goes through same type of pressure variation for any heat flux. This causes the curve to rotate clockwise, crossing the 2000 hour rupture life line of Inconel 625 at about one third of the full-power heat flux.

Source : Rupture stress curves for different service lives were calculated by S.H.Salter using data from Inco Alloy International 1985.

NB. This drawing is not exactly to scale.

approach the design hot-end steam temperature is maintained for different heat flow rates. This was achieved by controlling the excess air-ratio, heat-loss factor as well as the temperature levels at which the gas leaves the hot-end and pre-heated air enters the burner. In the model this was done by having the same choice of desired hot-end steam temperature (T_H), while in practice this requires a sensor monitoring the steam temperature and sending this information back to the blower and burner controllers. As the steam temperature is intended to be maintained, the reduced temperature drops at lower heat flow rates cause the metal temperatures to be lower and, thus, requires the surrounding flame temperature also to be lower correspondingly. This reduction in the temperature of the hot-end metal shifts the stress-temperature line to the left, ensuring much longer hot-end life at part loads, as illustrated in figure 10.2.

Figure 10.3 shows some engine performance curves resulting for this approach. At reduced heat flux the mid-wall temperature of the hot-end decreases. The temperature of condensate at the cold-end also decreases, but by a smaller amount. The changes in the cold-end temperatures improve the Carnot efficiency slightly (less than 3%), while the final engine efficiency is maintained across the range at around the full power value, down to approximately one third power. Below that the frictional and heat losses become dominant and rapidly decrease the efficiency.

The required thermodynamic cycle frequency shows a linear relationship with heat flow. The advantage of this approach (ie. sensing the hot-end steam temperature), is that the design ensures a safe life at any heat flow level the almost constant hot and cold-end fluid temperatures make the design of the regenerator and the other components inside the TD pile much easier. The limitation of this approach is that the hot strength of the hot-end metals is only fully utilized at full power, since the hot-end metal temperatures will be reduced for lower heat flow rates. Conversely this would extend the hot-end life.

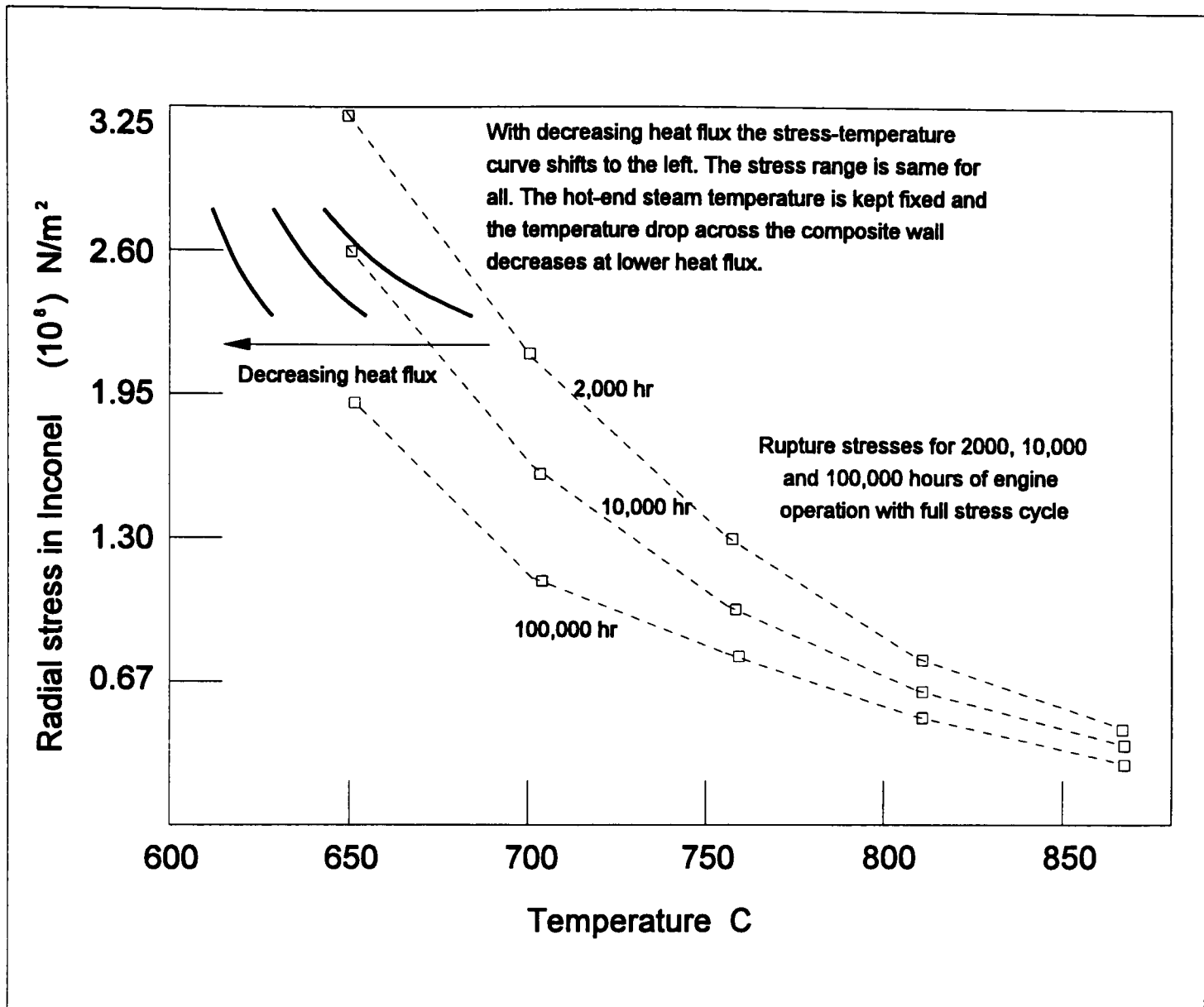


Figure 10.2 : Shifting of the temperature-stress curve as the heat flux decreases, with fixed hot-end steam temperature. The flame-fin root temperature is maintained by changing the proportion of cooling air. The hot-wall temperatures decrease at lower heat flux. The range of hot-wall stresses remain the same, which cause the curves to gradually move to the left with decreased heat flux.

NB. This drawing is not exactly to scale.

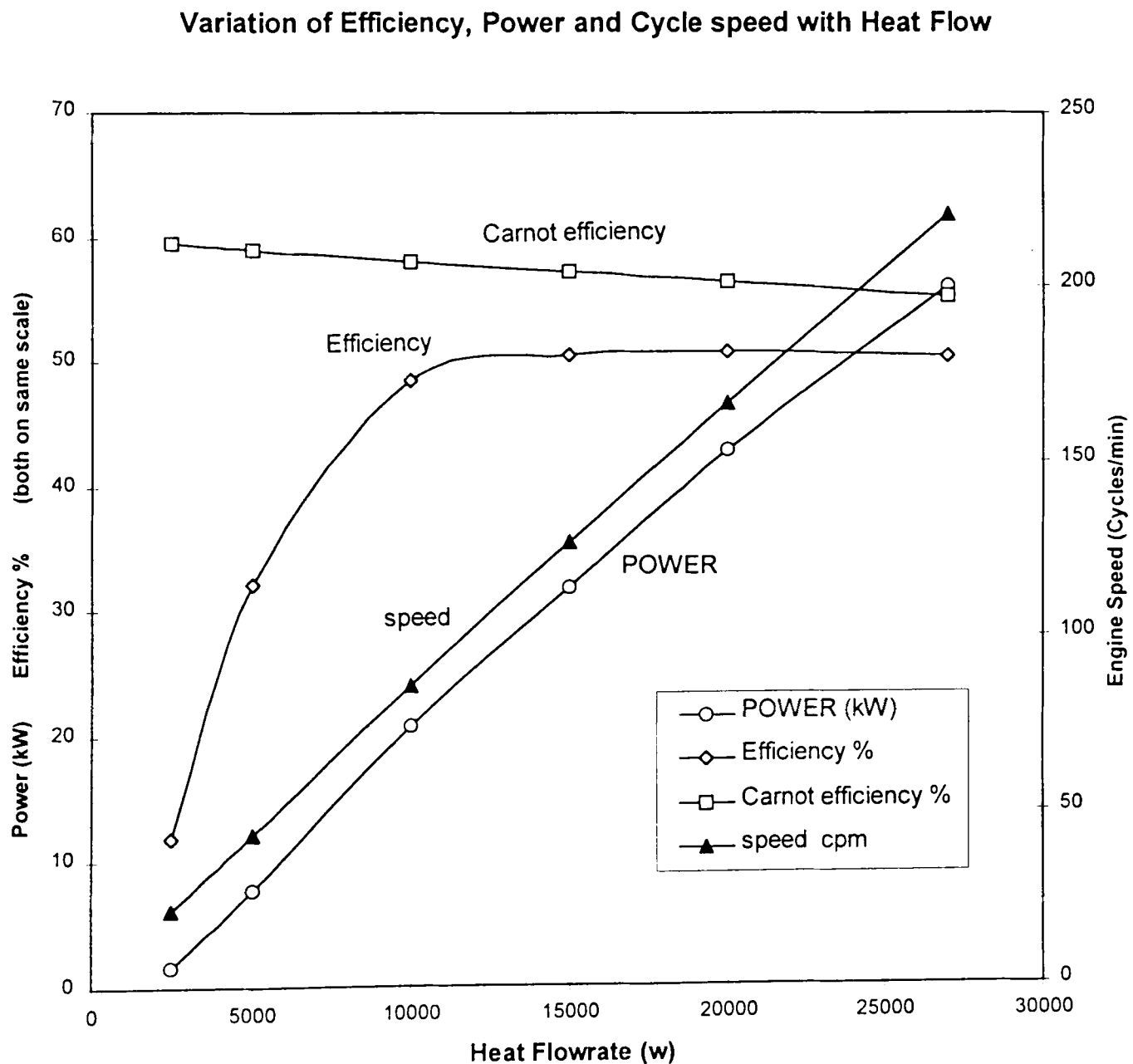
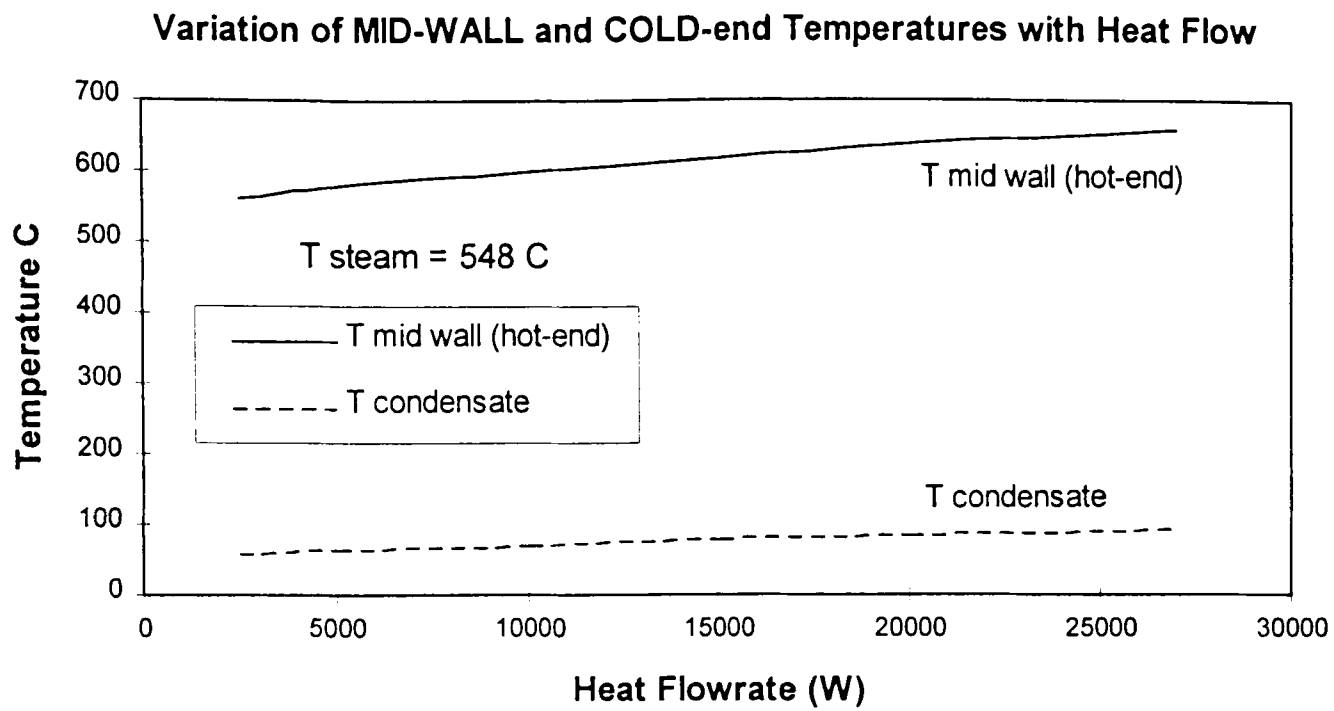


Figure 10.3 : Performance of the Artemis-Malone engine as a function of heat flux with hot-end steam temperature maintained at the full-power level. The small rise in Carnot efficiency is caused by the reduction in cold-end temperature heat flows. High final efficiency is maintained down to about 1/3rd level of full-power heat flux.

(iii) Another approach may be to maintain the temperature of the composite wall, at any arbitrary location along its radial length, at a constant temperature, independent of heat flow rate. The mid-wall temperature was considered to be a good choice as the reference, because it reduced the highest metal temperature at the outer edge, while also increasing the hot-end steam temperature, as heat flow reduced. The solid stress-temperature curve rotates clockwise, pivoting about the mid-wall temperature with decreased heat flux, as shown in figure 10.4. Figure 10.5 shows the engine performance at different heat flows using this approach. At lower heat flows, the increased temperature difference between the hot-end and cold-end fluids increase the Carnot efficiency giving up to 8% improvement compared to the previous approach. This also increases the overall efficiency by some about 2% (at the peak value). The engine speed and power curves are similar to those of figure 10.2. This third approach lies somewhat in between the other two. It makes better utilization of the hot-strength of the metals in the hot-end, while ensuring safe engine life across the power range. Figure 10.6 shows the variation of the air-ratio and the total mass flow rate of gas (combustant and cooling air), in the last two approaches. Less cooling air is required for the mid-wall monitored design than for the steam monitored one (ranging from 2%-6%) which accounts for a decreased blower power and thus a contribution to improved efficiency. It should be noted that the increase in air-ratio does not necessarily increase the total mass flow rate, despite the air needed for stoichiometric burning of the gas decreasing for lower heat flows.

10.4 Improving the static model using the time domain model results

A particular cycle pattern is described in the Mathcad model, where every cycle goes through similar pressure variations irrespective of the power requirement and the required cyclic frequency is calculated from the amount of net work available in each thermodynamic cycle. When compared to the time domain model (MatrixX) it had two main limitations :

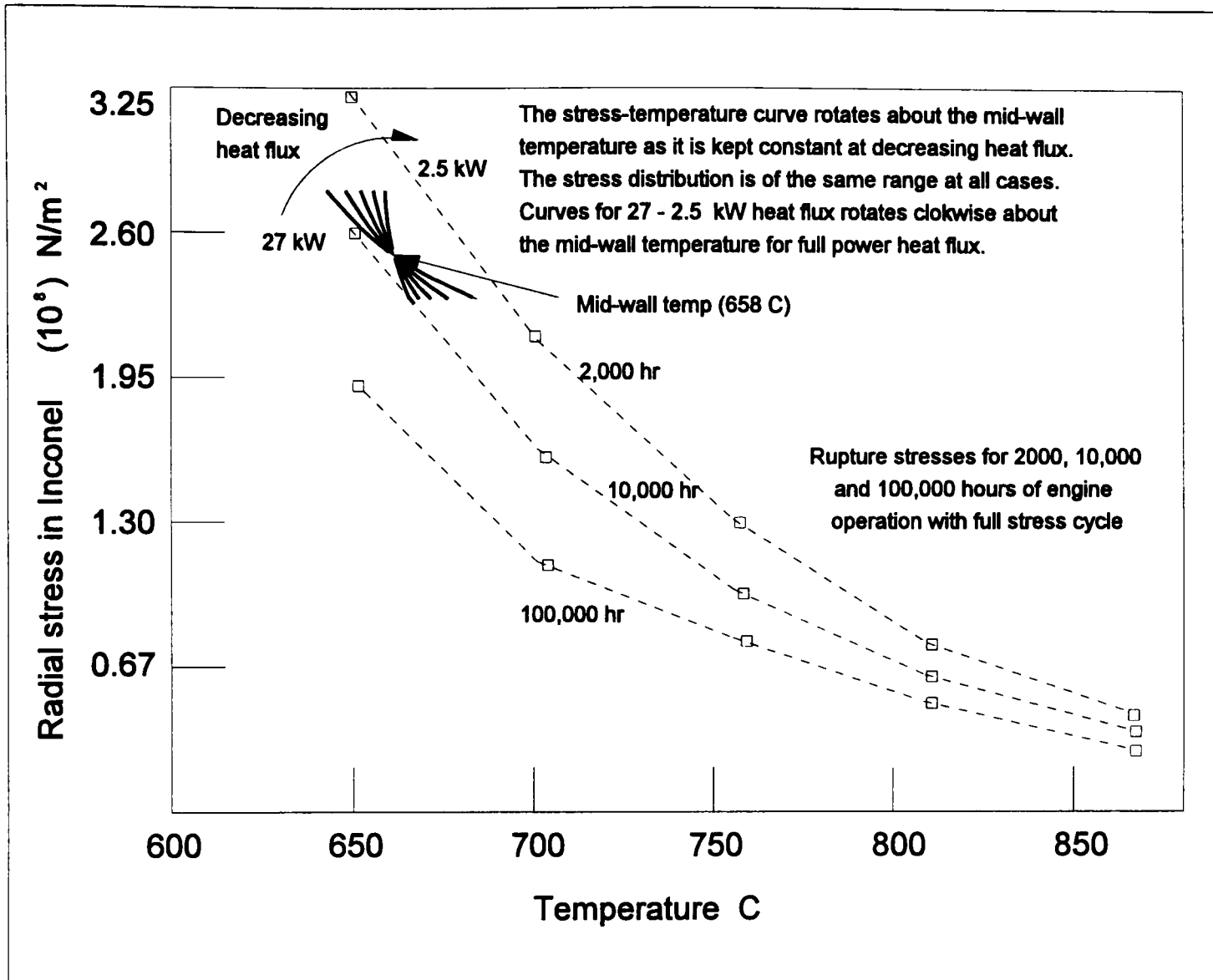


Figure 10.4 : Shifting of the temperature-stress curve as the heat flux decreases, with mid-wall temperature at the hot-end being maintained. This is done by changing the proportion of cooling air. The hot-wall stresses being the same, the stress-temperature curve rotates clockwise with reduced heat flow. As the temperature drop across the hot-wall reduces, the hot-end design remains safe at part-load.

NB. This drawing is not exactly to scale.

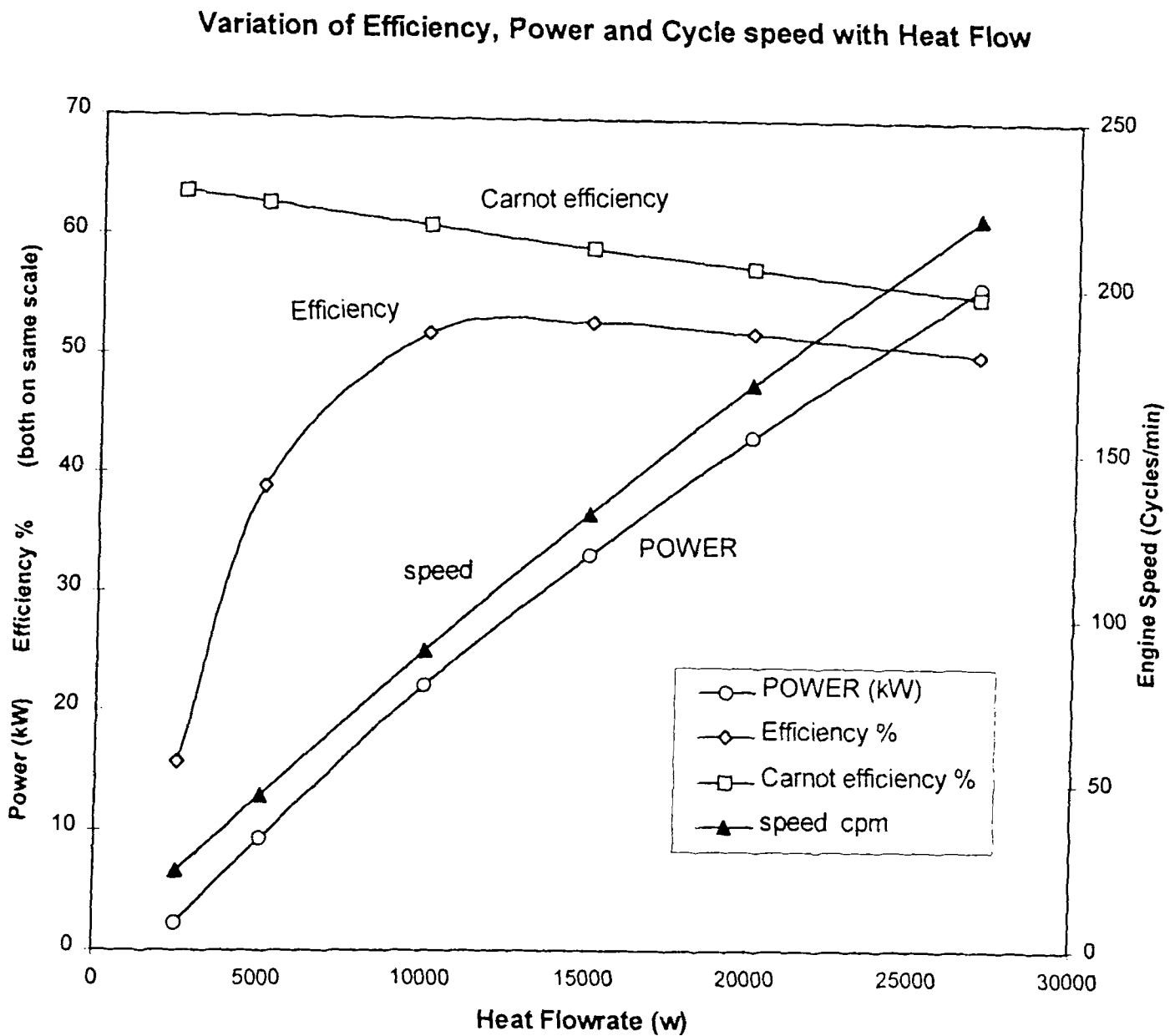
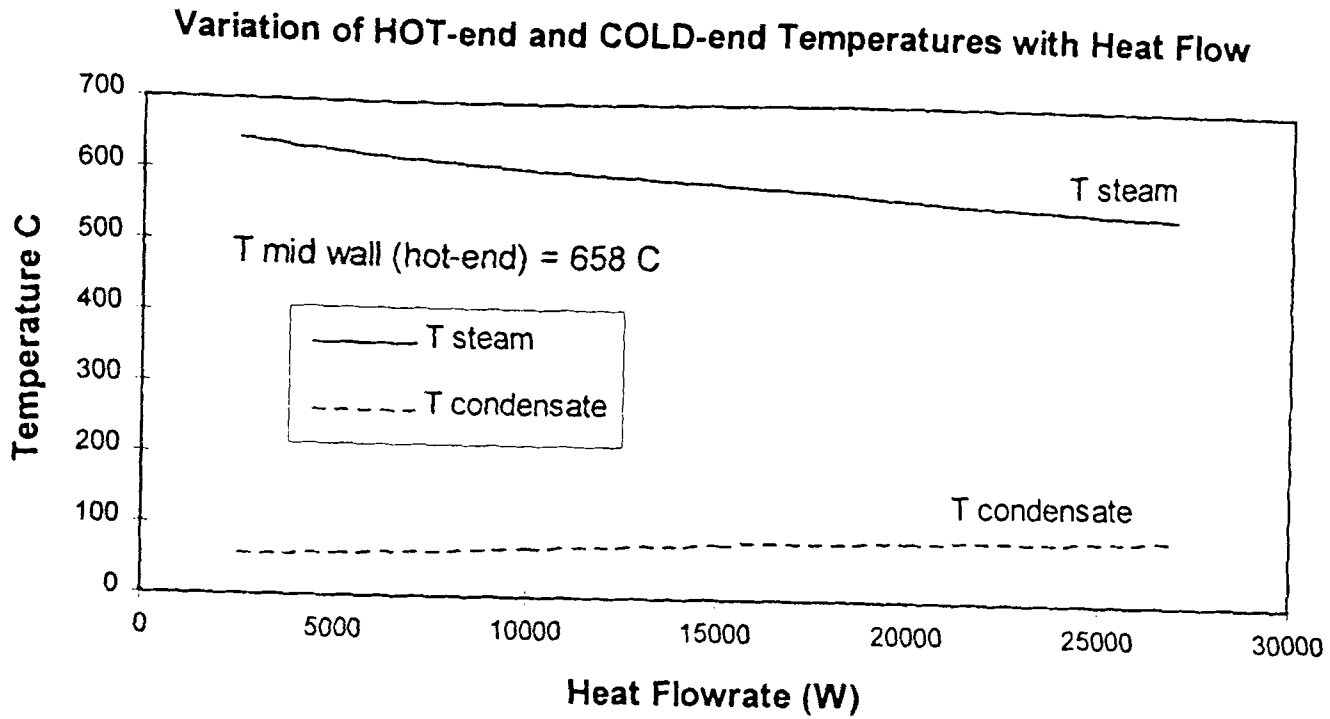


Figure 10.5 : Performance of the Artemis-Malone engine as a function of heat flux with mid-wall temperature of hot-end maintained at the full-power level. The rise in Carnot efficiency is mainly due to higher hot-end steam temperatures. High final efficiency is maintained down to about 1/3 level of full-power heat flux. As in figure 10.3, speed requirement maintains nearly linear relationship with heat flux.

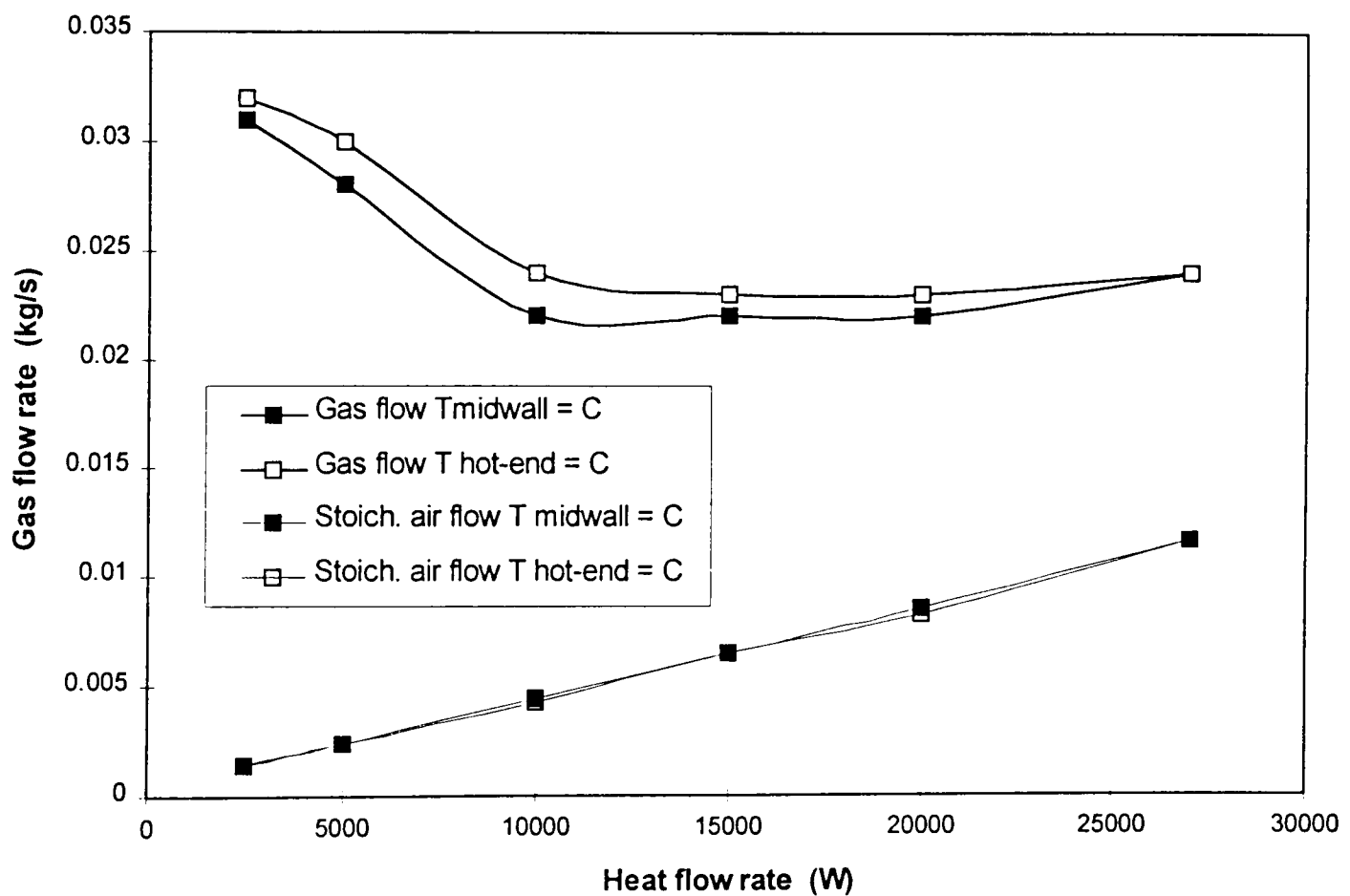
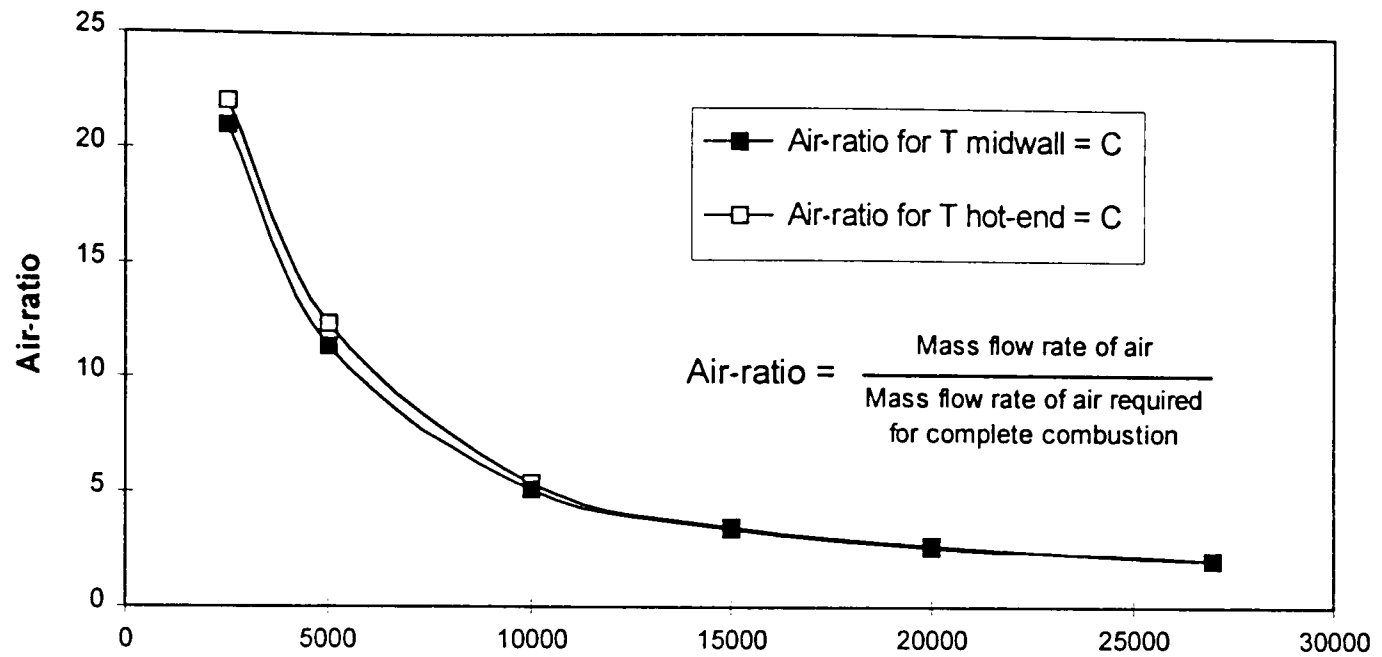


Figure 10.6 : Changes of air-ratios made at different heat flow rates to maintain desired temperatures. Curves are shown for maintaining constant steam and mid-wall temperatures at the hot-end. Increase in air ratio does not necessarily mean increase in mass flow rate. The stoichiometric air flow needed for combustion, decreases with lower heat flows (ie. decreased fuel burning rates).

- In the Mathcad model, for calculating the positive (motoring) and negative (pumping) work in each thermodynamic cycle, the variation of the fluid mass inside the regenerator was not taken into account. For the particular cycle pattern, and the assumptions taken for the model, this was reasonable for calculating the positive work (motoring), as the cycle pressure and temperatures are considered to be constant when the regenerator moves from the hot-end to the cold-end during the power stroke. On the other hand, the fluid mass in the regenerator increases as the pressure rises during the pumping stroke. The dynamic model showed the fluid mass inside the regenerator increasing by nearly a factor of four, as the pressure was raised from 10 bar to 400 bar (based on similar hot-end and cold-end temperatures). Hence the change of fluid mass inside the regenerator (which is the major part), as well as the change of mass in the dead volume at the hot-end (which was considered in the Mathcad model) should be taken into account for calculating the pumping work.
- The Mathcad model only considers linear motions of the moving parts and assumes linear variations of changing pressure. It is unable to predict non-linear variations of cycle pressure with regenerator and piston motions. These pressure variations may rise from :-
 - (i) Non-linear motions required of the regenerator and piston.
 - (ii) Imperfections of the motion achieved by these components.
 - (iii) Nonlinear variations of fluid properties with pressure.

At this stage the simplistic assumptions of the Mathcad model could be corrected through the use of results from the time-domain modelling of the equivalent cycle. The variation of regenerator fluid mass was incorporated into the pumping work. This resulted in a rise in estimated pumping work and consequently less net work done in each cycle. As a result the cyclic frequency requirement needed to be increased to meet the power requirement. As the variation of regenerator fluid-mass was incorporated in the static model, the cyclic frequency requirement was found to be nearly 30% higher than the initial estimates at various heat fluxes. Results from the static and dynamic models, both with hot-end steam temperature maintained (for all heat flows), were used

for comparison. A discrepancy still remains between the two models regarding the cyclic frequency requirements (eg. 289 and 259 cycles/min from corrected static and dynamic models for full engine power), although it can be explained from the non-linearity of the pressure variations.

Unfortunately the non-linearity of pressure variation could not be incorporated into the Mathcad model directly. Instead it could be included as a numerical factor to match the corrected cyclic frequency from the static and the time domain model. During the pumping action, in the static model, the cycle pressure is assumed to be rising linearly with linear piston motion, while the time domain model showed the pressure rise was not exactly linear. This is illustrated in figure 10.8. This difference of the nature of pressure variations caused a discrepancy in the work-done per cycle, calculated in the static and dynamic models. The assumption of linear pressure variation caused an over-estimation the engine speed (or under-estimation of the P-V diagram area) requirement for attaining desired full power. This discrepancy was resolved in the static model using a correction factor for non-linear pressure variation. This factor can be defined as the ratio of the areas of P-V diagram (ie. work done per cycle) calculated without (static model) and with consideration (time-domain model) of the non-linear variation of cycle pressure. For the present design and cycle type (ie. variable-frequency) and parameter choice, this factor (ie. the area ratio) was found to be about 0.9. This ultimately results in the discrepancy between predicted required engine speeds to generate full power by the two models. Inclusion of these two corrections (ie. regenerator-fluid mass and non-linearity in pressure variation) allows the results for static and dynamic model to agree for a variable-frequency engine cycle, reducing the final correction factor on the speed estimation of the static model to be 1.18. Figure 10.7 shows the different cycle speeds resulting from the static model with and without the corrections incorporated. The increased speed also raised frictional losses and thus caused a 1-2% decrease in overall efficiency at different heat flow rates. The value of the correction factor for non-linearity in pressure distribution is greatly dependent on the shape of the P-V diagram of individual cycles, which in turn depends on the piston motion generated by the pump-motor as well as the cycle pressure variations. Hence it is very difficult to generalise it. It's value will approach one, as the pressure rise or

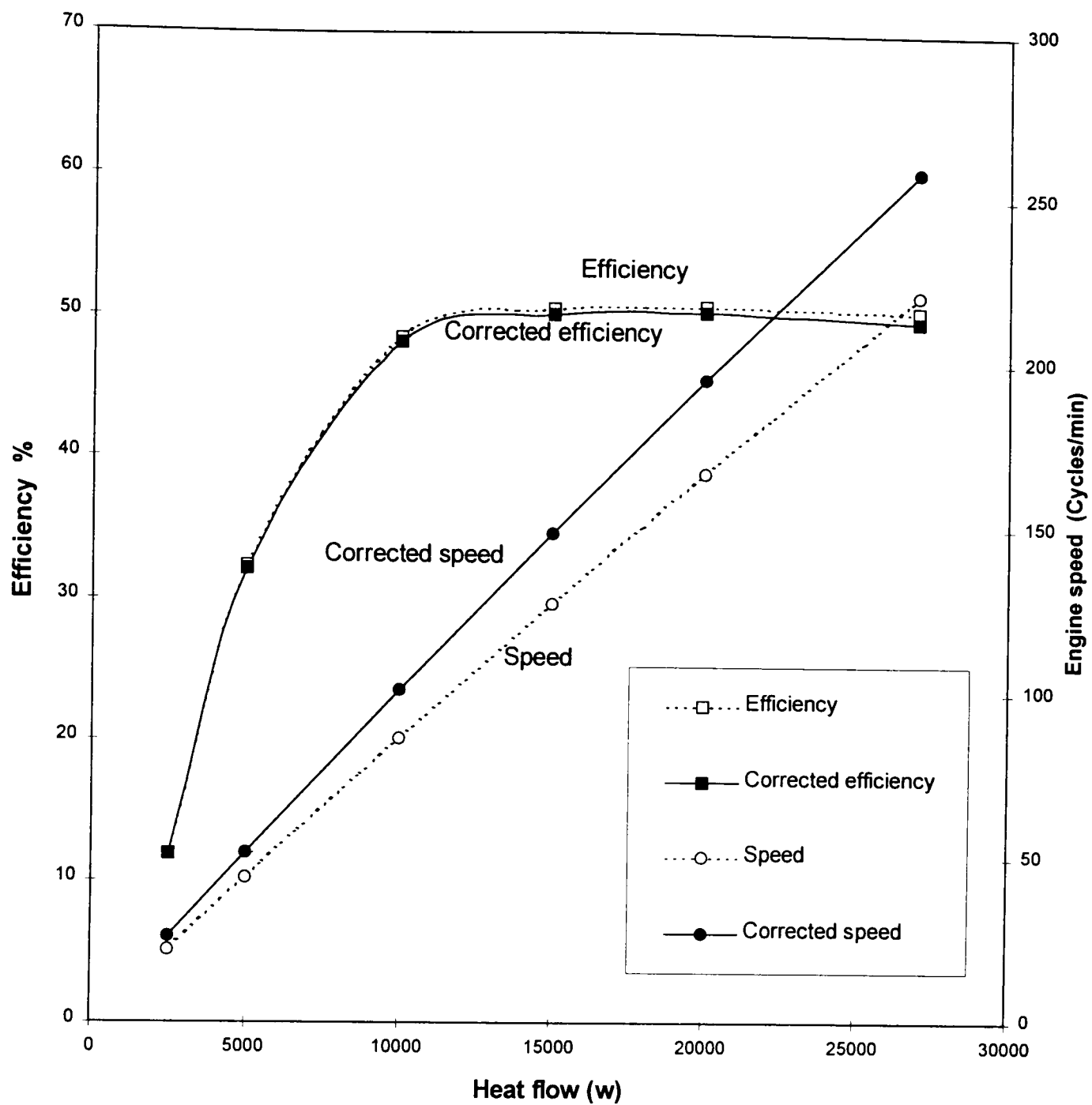


Figure 10.7 : Corrected engine speeds (cyclic frequency) for different heat flow rates. Incorporating the change of regenerator fluid mass and non-linearity of pressure variation raises the speed requirement estimation, calculated from the static model, by 18% (factor of 1.18). The increased speed causes the efficiency to decrease slightly.

$$\text{Net work done per cycle} = W_{A \text{ motor}} + W_{B \text{ motor}} - W_{\text{pump}}$$

$$W_{A \text{ motor}} = (PH).(\text{Piston stroke A}).(\text{Piston area})$$

$$W_{B \text{ motor}} = 1/2.(\text{Piston stroke B}).(PH + P_{\text{expansion}}).(\text{Piston area})$$

$$W_{\text{pump}} = 1/2.(PH + PL).(VL)$$

$$\text{where, } VL = (\Delta M_{\text{dead}} + \Delta M_{\text{regenerator}}) / \rho_{\text{cold-end}}$$

PH = High level of cycle pressure

PL = Low level of cycle pressure

$P_{\text{expansion}}$ = Pressure reached as the regenerator ends moving towards the cold-end

ΔM_{dead} = Increase in hot-end dead volume mass as pressure rises from PL to PH

$\Delta M_{\text{regenerator}}$ = Increase in regenerator fluid mass as pressure rises from PL to PH

$\rho_{\text{cold-end}}$ = Density of liquid at the cold-end (varies little with pressure)

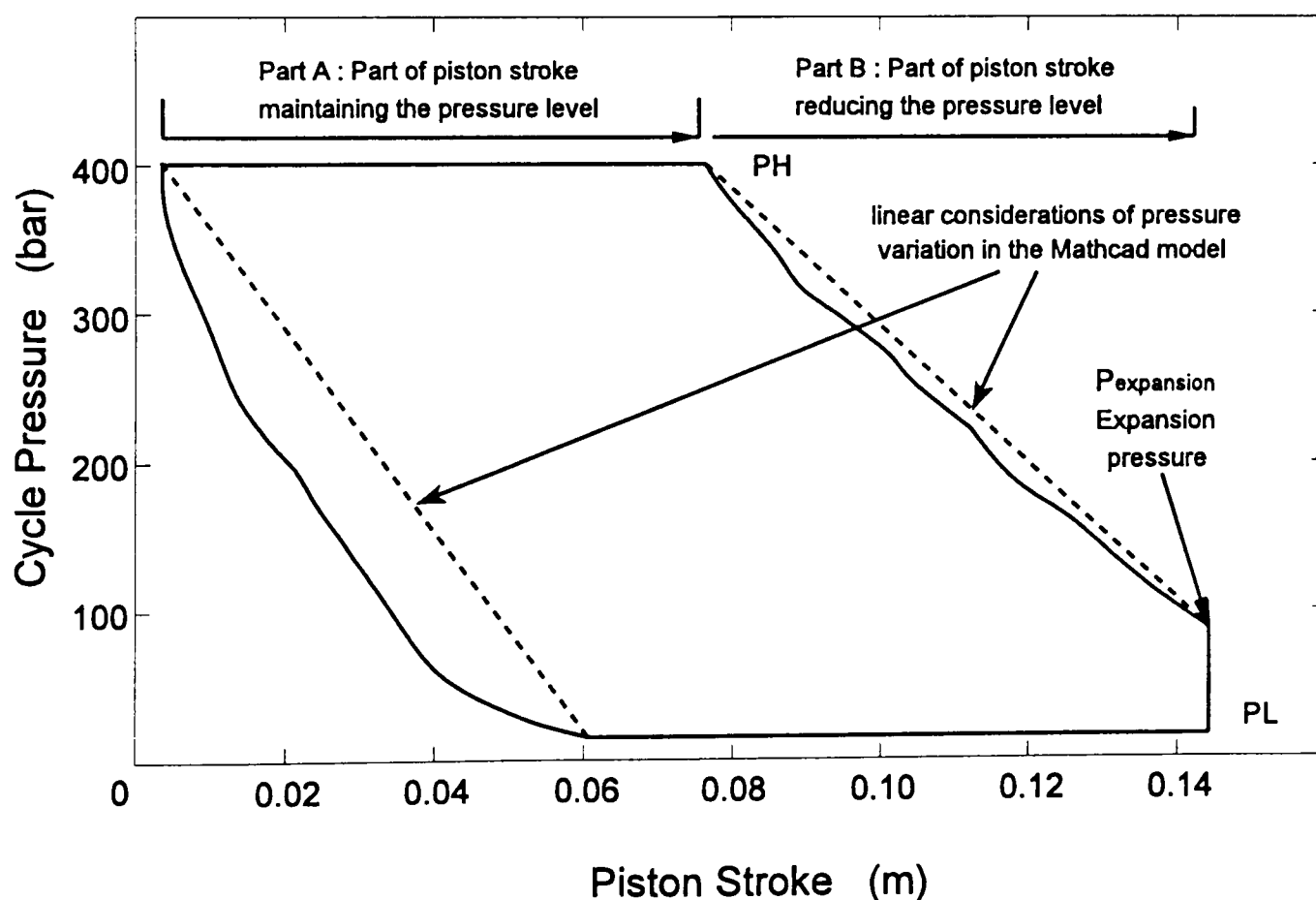


Figure 10.8 : Calculation of positive (motoring) and negative (pumping) work in the Mathcad model. For each case work-done is calculated as the product of piston stroke, piston area and pressure. For a piston assisted pressure fall cycle the power stroke of the piston is divided into two parts. In part A the cycle pressure is maintained, while at part B the piston is motored further to reduce the cycle pressure. For calculating the work done an estimation of the expansion pressure is needed.

fall becomes close to a linear function of piston motion. The estimation of the correction factors for variable-pressure cycles are considered in the next paragraph.

Studies of the time domain model revealed (chapter six) that a greater amount of net work per cycle could be achieved by allowing the piston to motor further as the regenerator returns towards the hot-end. This is reflected in larger enclosed area in the P-V diagram as was described in detail in chapter six (piston assisted pressure rise and fall cycle). This would allow the same power to be achieved at lower cyclic frequencies and a consequent rise in efficiency. The Mathcad model needed some modifications to incorporate these cycles. This was done in a simplistic way by changing the equations for calculating positive work in each cycle. The calculation of positive work is illustrated in figure 10.8. The piston motion in the power stroke is divided into two parts. In the first part (marked A) the piston motors to maintain the cycle pressure as the regenerator moves towards the cold-end. Piston motion in part A is similar to that already in use in the Mathcad model. In part B of the power stroke, the piston is motored at a faster rate to reduce the cycle pressure. The reduced cycle pressure reached at the end of the regenerator motion towards the cold-end is termed as *expansion-pressure*. Results from the time domain model provide values for both parts of the piston motion as well as the expansion-pressure. Linear considerations for pressure rise and fall was used to calculate work-done in each cycle. For the piston assisted pressure rise and fall cycle, the calculation of net work could be formulated as shown in the previous page above figure 10.8.

The effect of non-linearity of pressure changes on the area of the P-V diagram was found to be reduced in the piston assisted pressure rise and fall cycle. The errors due to linear consideration of pressure-rise and pressure-fall sections compensate each other to some extent, as shown in figure 10.8. As the exact numerical value would be different for individual cycles, a set of values were sought for the working pressure range, which could be used with the variable-pressure cycles. Table 10.1 shows the value of the correction factors (for taking account of non-linearity of pressure variations) for variable-pressure cycles for different power levels. Interpolated values could be used for power levels in between.

Table 10.1 : Correction factors for non-linearity of pressure variation used for speed calculations in the static model for variable-pressure engine cycles.

Indicated Power level (Engine with four TD piles) kW	High level of cycle pressure bar	Correction factor
60	400	0.98
46.3	275	0.98
32.4	200	0.96
23.2	150	1.03
13.2	100	1.05
7.3	50	1.04

For a full power cycle, the speed requirement was found to be 233 cycles/min compared to 259 cycle/min from the former cycle (piston assisted pressure rise and regenerator assisted pressure fall cycle) used in the Mathcad model. This results in an improvement in efficiency from 49.7% to 50.3%, at full power (56 kW). The speed requirements from the static model (after considering corrections for variation of regenerator fluid-mass and non-linearity of pressure variations agreed within $\pm 2\%$ of the speed requirement estimated from MatrixX (231 cycles/min). Most probably these small discrepancies result from the values of the correction factors used for the linear approximation for pressure variations.

10.5 Incorporating variable pressure-level cycle in the static model

The original Mathcad model uses a cycle in which the cyclic frequency changes with power requirement (variable frequency cycle) where the P-V diagram is essentially identical, irrespective of the power requirement. As explained in chapter eight, a fixed speed pump-motor generating the piston motion has difficulty in maintaining similar pressure-volume diagrams at reduced cyclic frequencies. The imperfections in piston motion give rise to large pressure ripples in the cycle. Having cycle pressure varied

with power requirement decreases the stresses and will improve the life of the thermodynamic pile significantly. These considerations lead to the strategy of changing the cycle pressure according to the power requirement. The pressure level is altered by offsetting the piston motion, with the pump-motor running at a constant speed. Studies of these cycles were carried out using the time domain model in MatrixX, as described in chapters eight and nine.

Most of the limitations of the MatrixX model are stated in the assumptions described at the beginning of chapter six, some of which are inherited from the Mathcad model. The time-domain model mainly deals with what is happening inside the TD pile as the moving parts change their position with time. The present model does not include blocks or sub-programmes for modelling what happens outside the TD pile eg. heat-exchanger, burner and heat transfer across the fins etc. Hence, though detailed P-V diagrams and indicated power could be obtained from the MatrixX model, it lacked the ability to calculate power losses and final efficiencies. It could be done in MatrixX, but this would have meant repeating all the detailed loss calculations, which have little to do with the time-domain. The Mathcad model is a more appropriate, faster and easier way to carry out these calculations. At this stage the efficiencies of the variable pressure-level cycles (modelled in time domain) were estimated using the Mathcad model. The data shown in table 10.1, generated from the time domain modelling were introduced into the Mathcad model after it was modified to accept it, as shown in figure 10.8.

TABLE 10.2 : Results from time domain model, used in the static variable-pressure model.

Results are obtained for,	low level of cycle pressure = 10 bar
	Hot-end temperature = 550 °C
	Cold-end temperature = 95 °C
and	dimensions of the present design

continued...

High-level of cycle pressure (bar)	Change in regenerator mass as the pressure changes between high and low levels (kg)	Piston stroke Part A* (mm)	Piston stroke Part B* (mm)	Range of piston motion from cold-end reference (mm)	Expansion Pressure* (bar)
400	0.0447	73	71	0 - 144	80
275	0.0385	91	53	9 - 153	50
200	0.0339	94	41	18 - 153	40
150	0.0281	93	42	27 - 162	30
100	0.0239	94	41	36 - 171	20
50	0.0172	97	29	45 - 171	20

* Values were approximated ($\pm 5\%$) from the graphs.

10.6 Performance of the engine in variable pressure-level cycles

Study of the performance of Artemis-Malone engine, using the time domain data in the Mathcad model produced some interesting findings. In the Mathcad model the speed at which the regenerator spins, while it moves inside the TD pile, was made a linear function of the heat flow passing through the hot-end (on top of a base value). This was done in order to achieve better heat-transfer at the steam-fins for higher heat flux while reducing the swirling losses at lower heat flow rates. The technique is effective for the variable frequency cycles as the cycle pressures remain the same at different power levels. On the other hand, if the cycle pressure reduces with reduced heat flow, the steam density decreases. This causes increased thermal resistance in the steam-fin interface. If the spinning speed is decreased at reduced heat flux, this enhances the thermal resistance further by making the flow less turbulent (reflected in the decreasing Reynolds number). As this happens, the advantage of spinning the regenerator, in terms of heat transfer, diminishes. In order to maintain a fixed hot-end steam temperature for reduced heat fluxes, the entire hot-end needs to be elevated in temperature by reducing the proportion of cooling air. This causes the hot-end metal temperatures (especially copper) to exceed the safe limits. This is illustrated in figure 10.9 where the spinning speed of the regenerator is decreased at lower heat flux. The copper flame-fin

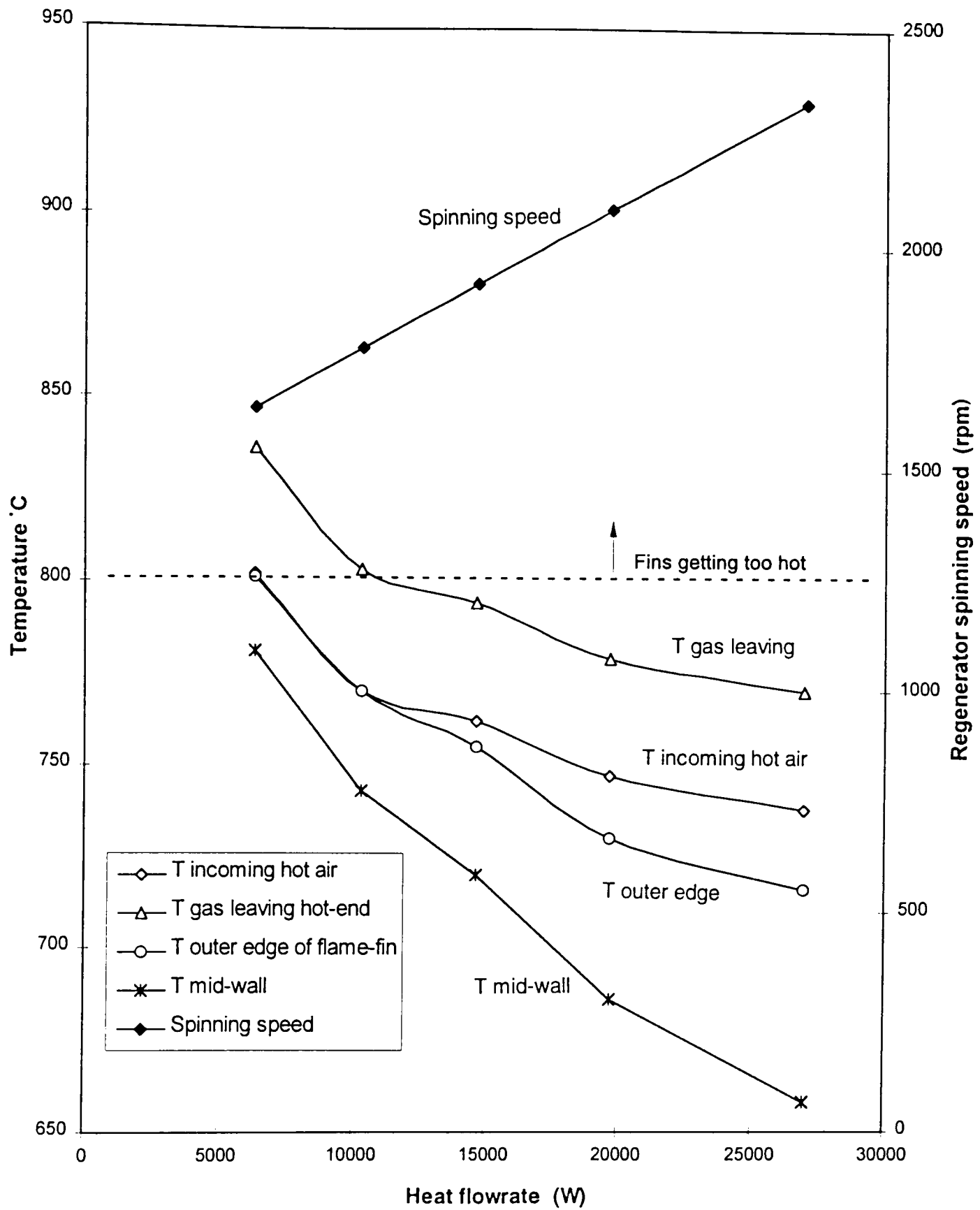


Figure 10.9 : The consequence of reducing regenerator spinning speed at lower heat fluxes. In order to maintain constant hot-end steam temperature, all gas and hot-end metal temperatures needed to be elevated to compensate increased temperature drop at the steam-fin interface. The temperatures of gas entering the heat-exchanger and hot-air entering the burner section also increases. This causes the metal, especially the copper flame-fin to become too hot.

temperatures exceed 800°C , by the time the heat flux is reduced to about a quarter of the full-power rate, which is not desirable.

For the varying pressure-level cycle this could be avoided by either, keeping the spinning speed of the regenerator constant, or by increasing it, with reduced heat flow rate. This reduces the rise of thermal impedance at the steam-fin interface at lower power levels, as is shown in figure 10.10. A constant spinning speed was maintained until the heat flux was reduced to about one quarter of the full-power value where upon it was increased. This allowed the temperature drop at the steam-fin interface to be controlled and the thermal impedances at the flame-fin interface (laminar flow) and composite wall to vary little with different heat flows. It also permitted the maintenance of nearly constant temperatures for the gases both leaving the hot-end and entering the burner, across the power range. The fin-tip temperature was kept below 750°C which was considered to be safe. The spinning speed needed to be increased at very low heat fluxes to control these temperatures.

Figure 10.11 shows the estimated performance of the Artemis-Malone engine, following variable pressure-level cycles and maintaining the hot-end steam temperature. It showed similar pattern of variation of efficiency (both Carnot and final) and power, compared to a variable cyclic frequency and fixed pressure-level cycle (as modeled before). The shifting of the stress-temperature curve in the variable-pressure cycle is shown in Figure 10.12. The reduced heat flow causes the stress-temperature curves to shift downwards. Figure 10.13 shows comparative results of two types of engine cycles with variable heat flux. The predicted speed in the variable pressure-level cycle was not exactly fixed at a speed as in the time domain model (about 231 cycles/min), but varied through a small range (225-240 cpm). In all probability this variation was caused by inaccuracies in the approximation of expansion-pressures and piston strokes. The cycle speed and regenerator spinning speed are higher for the variable pressure-level cycles at part loads compared to variable-frequency ones. This may lead to increased frictional losses, though these are counteracted by the reduced density of the hot-end fluids. After inclusion of these effects the final efficiency curves are of very similar form for both types of cycles (figure 10.13). Hence it can be concluded that there are no performance

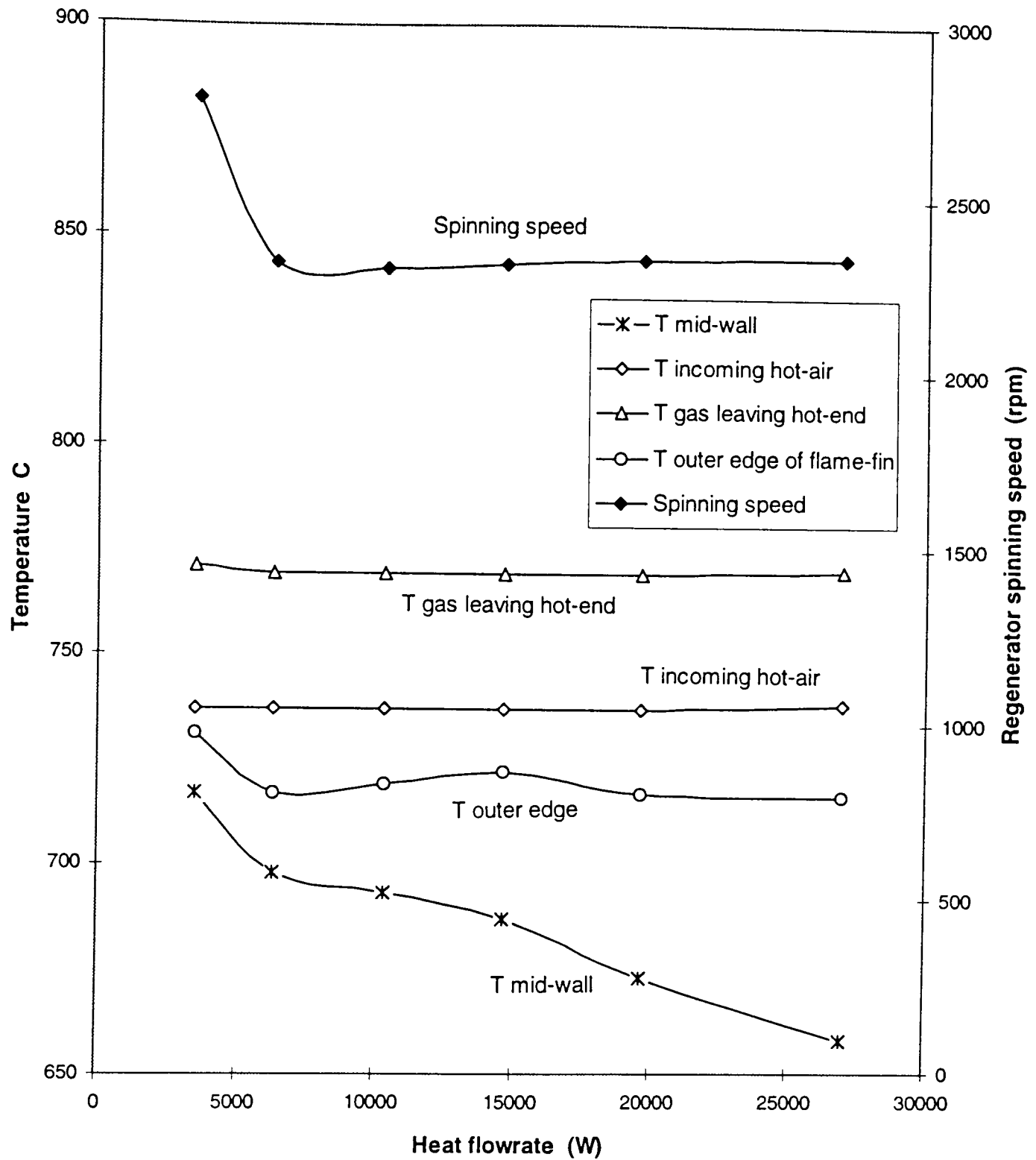


Figure 10.10 : Over-heating of the hot-end metal can be avoided in a variable pressure level cycle, by controlling the spinning speed of the regenerator. Increased spinning speed at lower pressures compensates for the decrease in fluid density and keeps the flow turbulent. Nearly constant gas temperature at the inlet of the heat-exchanger and the pre-heated air entering the burner can be maintained throughout the heat flux range.

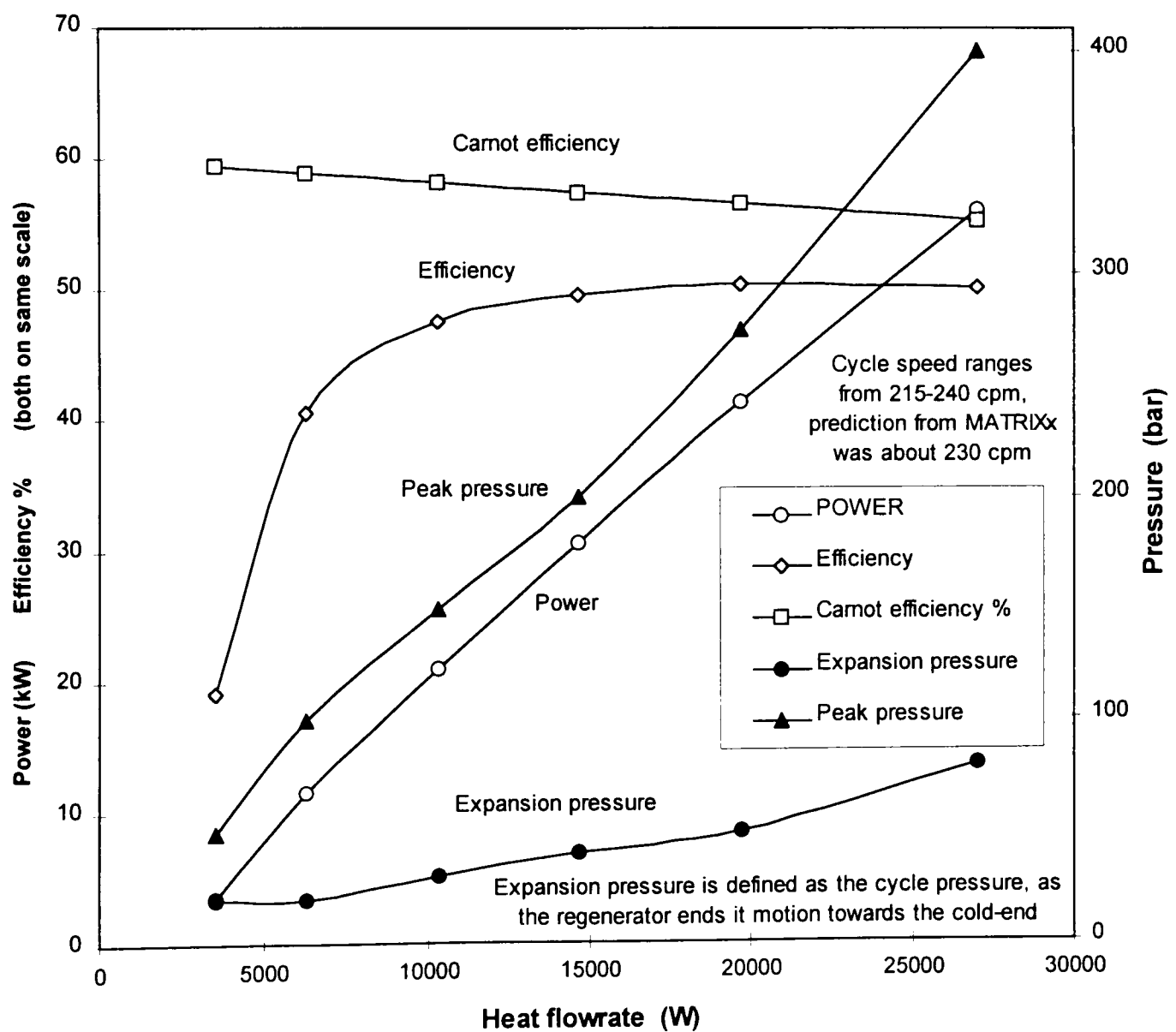
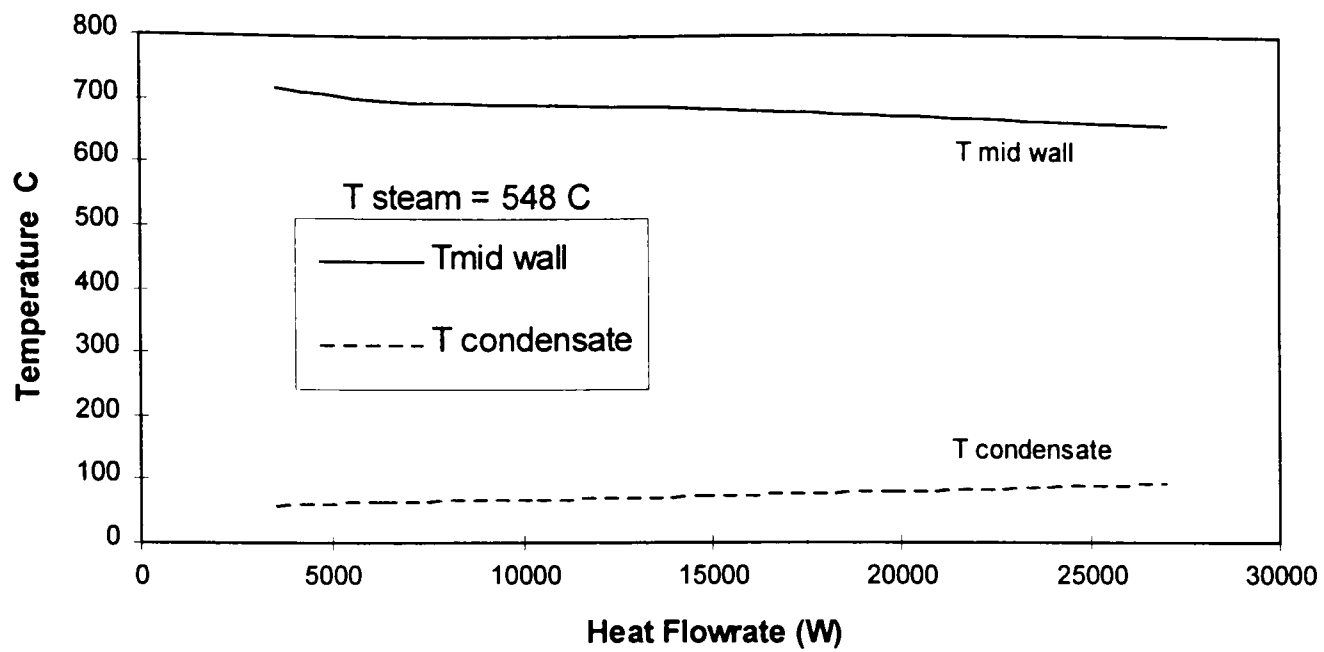


Figure 10.11 : Performance estimates of Artemis-Malone engine, following the variable pressure-level cycle. Results are similar to those obtained by the variable frequency cycle. Pressure levels and expansion pressures were approximated from P-V diagrams obtained by the time domain modelling of the thermodynamic cycles.

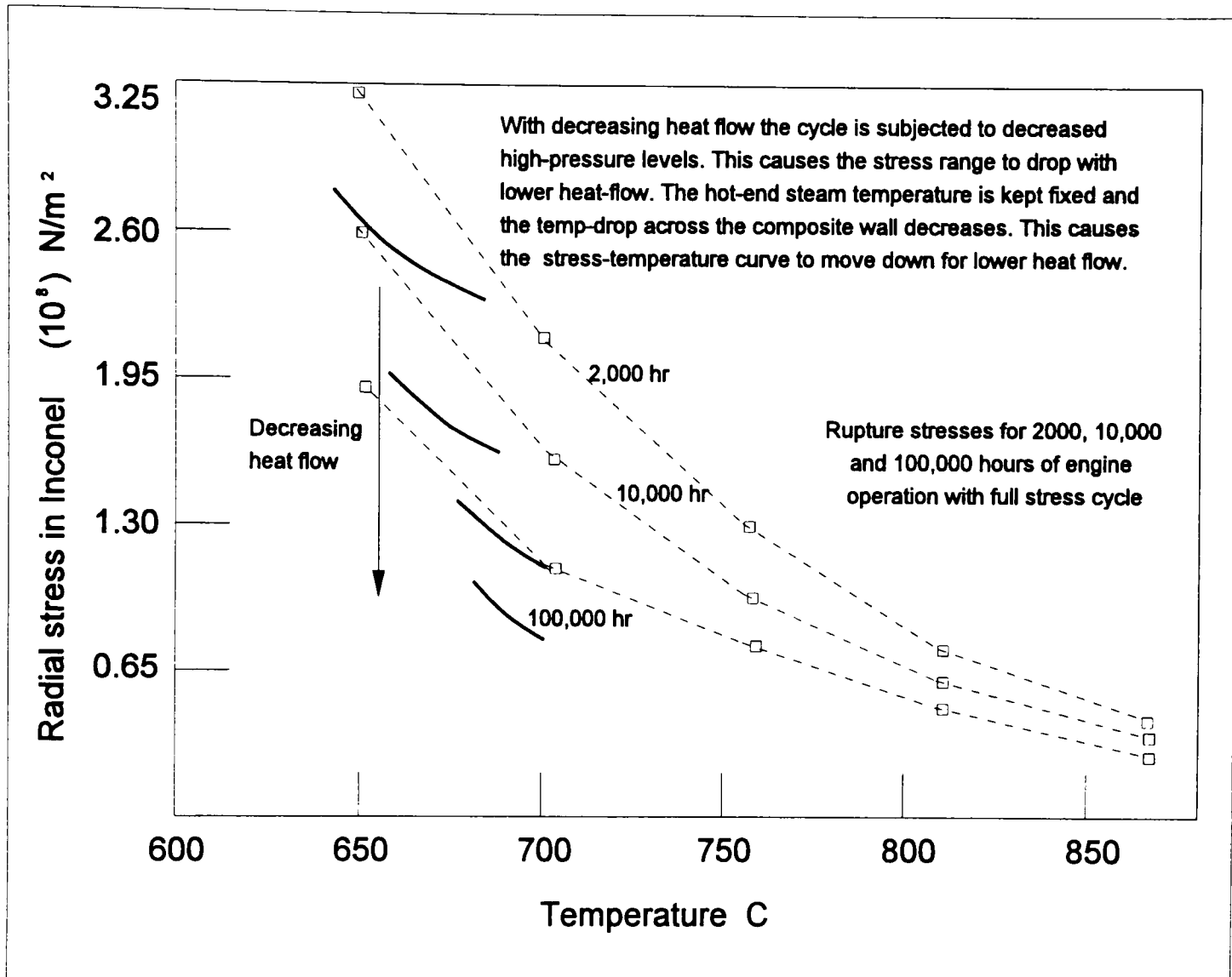


Figure 10.12 : The shifting of the temperature-stress curve as the heat flow decreases, in variable-pressure cycle. With reduced heat flow the high-level of cycle pressure is reduced, decreasing hot-wall stresses. The hot-end steam temperature is maintained controlling the air flow rate, while the temperature drop across the wall decreases with lower heat flux. This causes the stress-temperature curve to shift down, improving engine life at lower heat flow rates. Curves are shown for 27, 19.7, 14.9 and 10.2 kW heat flow rates per TD pile, with peak cycle pressures of 400, 275, 200 and 150 bars respectively.

NB. This drawing is not exactly to scale.

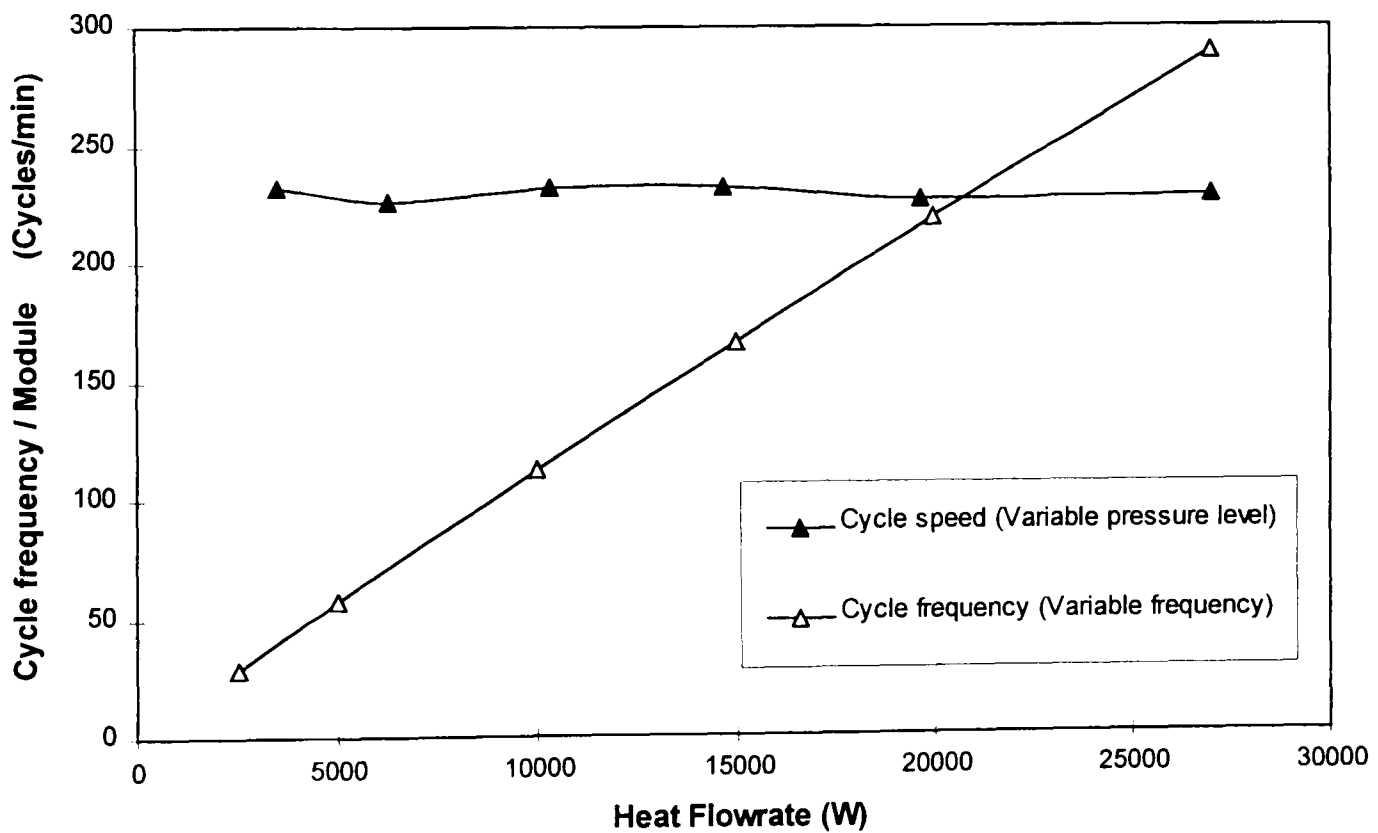
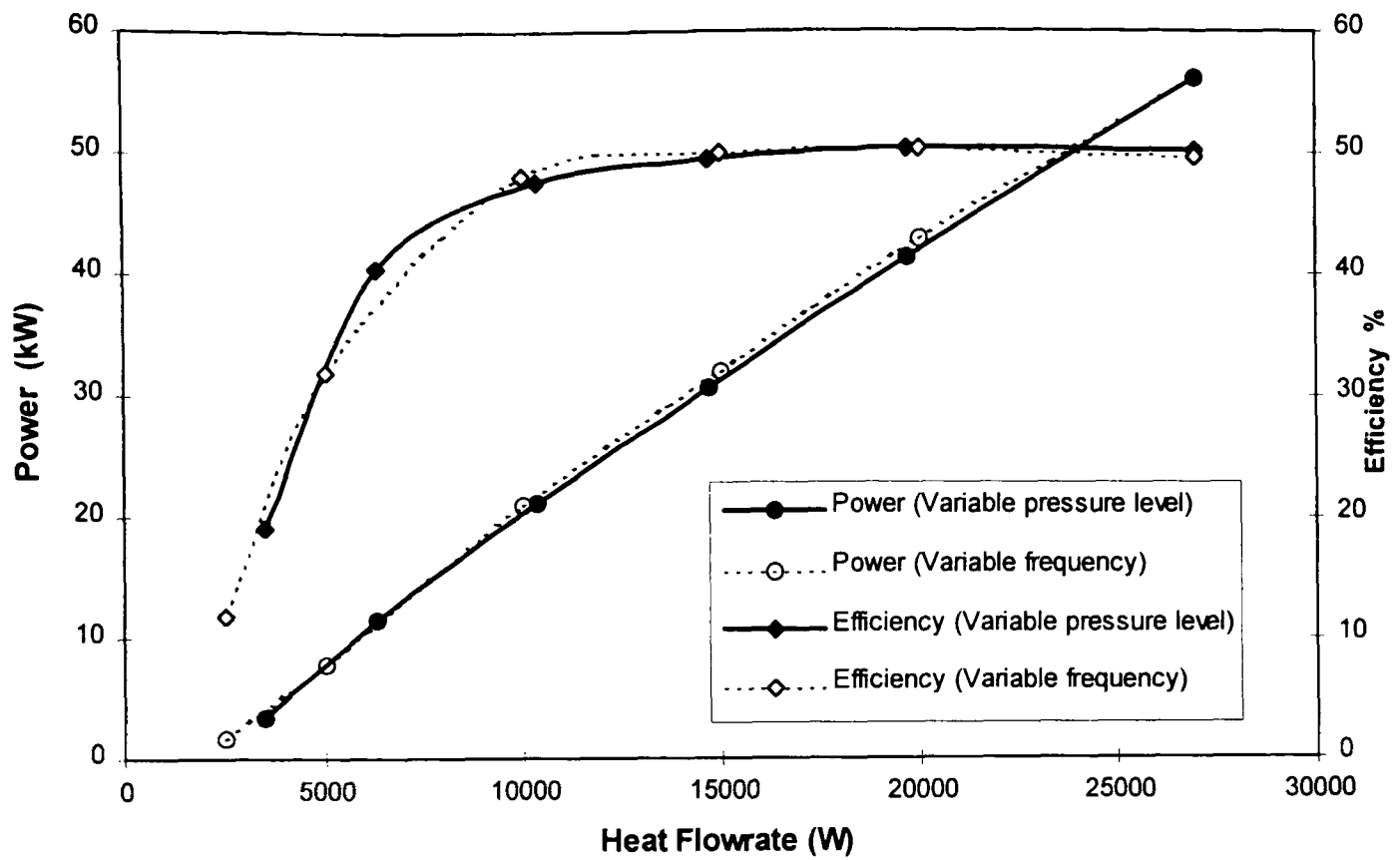


Figure 10.13 : Comparative results of variable-pressure and variable-frequency cycles for various heat flow rates. Nearly identical efficiency curves indicate similar performances can be achieved with both techniques, while the variable-pressure cycle has several design advantages over the other. The cycle speed varies linearly in the variable-frequency cycle as linear function of heat flux, while the cycle speed varies little with heat flux in the variable-pressure cycle.

penalties particular to the variable pressure-level cycle, which has additional advantages (eg. engine-life, noise, fixed shaft speed, controllability of the pump-motor etc.), compared to the variable frequency cycle. Engine life in applications where power varies a lot eg. cars, could be massively extended (eg. from 3000 hrs to 30,000 hrs). This in turn can be taken advantage of though the reduction of TD pile wall thickness, which allows higher hot-end steam temperatures leading to higher thermal efficiencies and better power-to-weight ratio.

10.7 Final engine specifications

In the previous chapters variations of different engine parameters and power control techniques have been investigated. These are summarised in tabular form as the final specifications of the Artemis-Malone engine.

TABLE 10.3 : Specifications of the Artemis-Malone engine-design for full power

Engine Design Parameters

Number of modules (TD piles)	4
Module spacing	84 mm
Nominal full-load output power	55 kW
Maximum allowable cycle pressure	400 bar
Minimum permissible cycle pressure	10 bar
Maximum allowable metal stress at hot-end	$3 \times 10^8 \text{ N/m}^2$
Heat flux/Module	27 kW
Hot-end fluid temperature	550 °C
Cold-end fluid temperature	95 °C

Contd...

Main results for full power cycle

Full power output	56.1 kW
Efficiency	0.497
Carnot efficiency (Hot-end at 549°C and cold-end at 95°C)	55.2 %
Heat input rate	111 kW
Excess air requirement	105%
Engine speed/Module	231 cycles/min
Module bore	40 mm
Overall height	552 mm
Overall length	621 mm
Power-to-weight-ratio (including various accessories, table 4.1)	328 W/kg

Heat-exchanger design

Air temperatures (a) Ambient atmospheric	25 °C
(b) Entering into the burner section	738 °C
Exhaust gas (a) Entering the heat-exchanger from hot-end	770 °C
temperatures (b) Exhausted to the atmosphere	59 °C
Heat lost with the exhaust (full power) As % of heat input	3 %
Number of double wraps in the contra-flow heat-exchanger	10
Width of flow passage	14.25 mm
Height of flow passage	224 mm
Average temperature of air in the heat-exchanger	450 °C
Reynolds number of flow at mid-section	31600
Heat recirculation rate As % of Heat input	61 %
Average convective heat transfer coefficient inside	128 W/m ² -°K

Cold-end design

Condensing fins/ Water-fins	Number Radial length Thickness	58 4 mm 1 mm
Copper wall thickness between inner and outer copper-fins		4 mm
Heat lost to cooling water (full power) Relative to heat input		44 %

Cold-end design continuing...

Cooling water temperature	Water in	55 °C	
	Water out	77 °C	
	Flow rate	0.6 l/sec	
Temperature distribution °C	Condensing steam	Condensing-fin root	Water-fin tip
	95	84	77

Hot-end design

Number of Copper/Inconel disks per Module	66				
Copper disk dimensions	Outer diameter Inner diameter Thickness	84 mm 40 mm 0.7 mm			
Inconel disk dimensions	Outer diameter Inner diameter Thickness	60 mm 48 mm 1 mm			
Flame fins (Effective number as two adjacent fins are joined)	Number Radial length	66 33 12 mm			
Steam fins	Number Radial length	66 4 mm			
Temperature distribution °C					
Avg. Flame	Flame-fin tip	Flame-fin root	Mid-wall	Steam-fin root	Steam
1240	716	684	658	631	549

Regenerator design

Regenerator dimensions	Outer diameter Core diameter Length	38.25 mm 11 mm 240 mm
Stroke length		116 mm
Solidity of regenerator material		60 %
Spinning speed		2335 rpm
Total regenerator displacement/cycle		533 cc
Heat recirculation rate	per cycle	31.4 kJ
	Compared to heat input	447%
Cyclic temperature rise (full power)		61 °C

TABLE 10.4 : Control of power

<p>Crude power control</p>	<p>Crude power-control is achieved by offsetting the piston motion. This is done by pumping or motoring extra cylinders of hydraulic oil into or out of the flexible membrane. Power range in between each offset position are called power-zones. Piston motion is generated as the pump-motor follows a pre-tuned ternary look-up table of cylinder enabling, for each respective power-zone. Piston motion requirements are updated in a cycle-by-cycle basis.</p>
<p>Fine power control</p>	<p>Fine power-control, in between adjacent power zones, is achieved by offsetting and clipping* the regenerator motion towards the cold-end. This is done using an arrangement similar to the flow control mechanism used for mechanical diesel injector pumps. This combines offsetting the regenerator motion towards the cold-end with stroke control. Water at the cold-end is used in the regenerator drive. A variable dwell period in the drive mechanism clips the regenerator motion at the cold-end and allow time to replenish any fluid leakage in the drive system. Regenerator motion requirements are also updated in a cycle-by-cycle basis.</p>

* Two alternative regenerator motions could also be used.

Contd...

Piston and Regenerator motions throughout the power range

Power range/TD pile	1.8 - 15.1 kW
Regenerator stroke	(116 - offset) mm
Engine/Regenerator cyclic speed	231 cycles/min
Pump-Motor speed	1800 rpm
No. of cylinders in the pump-motor	10
Pump-motor cylinder volume	9.5 cc (approx)
Piston motion equivalent to one cylinder displacement	9 mm (approx)
No. of pump-motor cylinders available in each engine cycle	78

Power Zone	Pressure Level bar	Cylinder volumes pumped in or motored out	Piston motion range using ternary-code mm	Regenerator motion offset needed mm	Power range kW
0	400	16	0 - 144	0	15.1
1	300	16	9-153	0-11	11.6-15.1
2	200	15	18-153	0-18	8.1-11.6
3	150	15	27-162	0-14	5.7-8.1
4	100	15	36-171	0-12	3.3-5.7
5	50	14	45-171	0-13	1.8-3.3

Contd...

**Variation of different engine parameters with increased power demand
(variable-pressure control with hot-end steam temperature maintained)**

(Results are shown graphically in figure 10.10 - 10.12)

Engine parameter	Range of change
Heat flow rate through the TD piles	14 - 108 kW
Fuel flow rate	0.4 - 2.48 g/s
Air-ratio (Air flow rate/ Stoichiometric air flow rate)	15 - 2.05
Flow rate of products of combustion (including cooling air)	114 - 99 g/s
Temperature of pre-heated air entering burner	736 - 738 °C
Temperature of hot gas leaving the flame-fins	772 - 770 °C
Exhaust temperature	60 - 58 °C
Maximum hot-end fin temperature	732 - 716 °C
Maximum stress in the hot-end wall	37 - 296 MPa
Hot-end steam temperature*	547 - 549 °C
Regenerator cycle frequency	230 ± 3 cycles/min
Regenerator spinning speed	2800 - 2300 rpm
Pump-Motor speed	1800 ± 25 rpm
Cooling water flow rate	0.12 - 0.6 l/s
Maximum cycle pressure	50 - 400 bar
Indicated power output	8 - 60 kW
Power losses	5 - 4 kW
Thermal efficiency	19 - 50 %

* Maintaining mid-wall temperature of the hot-end also could be used.

CHAPTER 11

Conclusions and Recommendations

11.1 Conclusions

The main results of the work are subdivided and listed as follows :

1. Engine modelling :

- (a) A mathematical model of the Artemis-Malone engine has been developed, using a combined static and dynamic approach. The time domain model is a first-order model using an isothermal approach which predicts the indicated cycle power. The model is capable of incorporating arbitrary motions for the regenerator and piston, as might be generated by the digital-displacement pump-motor. The various engine losses (both internal and external to the TD pile) are calculated using the static model over the full range of power. Combination of the two models provides the equivalent of a conventional second-order model.
- (b) The static modelling allows optimising the dimensions of the engine components, at maximum power output using a set of desired engine parameters. It also calculates various parasitic losses and the final engine efficiencies. The static model is developed using PC based mathematical software. This provides high computational speeds allowing fast optimization of the engine design. The indicated power predictions of the static model are simplistic, as it does not include the effects of cyclic pressure variations and the motion profiles of the piston and the regenerator.
- (c) The dynamic (time-domain) model, based on an isothermal analysis, provides implicit solution of the cyclic variation of the pressure in small time steps (eg. 1 millisecond). This allows investigation of different motion profiles of the

moving parts and their consequent effect on the overall engine cycle. The dynamic model is developed using a work-station based time-domain simulation software (PC version is available now) and the computational speed is much slower compared to the static model. This is used for more detailed investigation of the engine cycle, estimated by the static model. The dynamic modelling incorporates simulation of accurate piston motions generated by the pump-motor (ie. the digital hydraulic drive) and hence provides realistic predictions of indicator diagram of the engine cycle. It also provides more detailed model of fluid mass movement in and out of the porous regenerator during the cycle. The prediction of indicated power is fed back to the static model to recalculate the engine performance, improving the predictions.

2. Engine design :

- (a)** The two main novel features of the engine design were the special composite structure of the hot-end and the elimination of the sealing problem through the use of the flexible isolator-piston and digital hydraulics. The bi-metallic composite design of the hot-end wall provides a combination of good thermal conductivity and high temperature strength, which does not exist in a single commercially available metal. This allows the creation of a hot-end which transfers heat into the working fluid with a limited temperature drop.
- (b)** The flexible piston provides isolation of the working fluid (water) and the hydraulic oil. The use of the hydraulic drive system gives several advantages over conventional mechanical arrangements. These include :
 - (i)** Removal of the sealing from hot-end working fluid to oil in the hydraulic pump-motor at a much cooler temperature.
 - (ii)** The digital hydraulic drive allows almost any arbitrary piston motion, releasing the engine from the conventional constraints of sinusoidal motion and a fixed phase relationship with the regenerator. This enables optimal control of the P-V diagram area of the thermodynamic cycle.

- (iii) Use of the hydraulic drive eliminates the conventional piston-connecting rod-crank arrangement and the problem of side forces associated with it.

3. Power Control :

- (a) Controlling the power has always been one of the most difficult aspects of Stirling-Malone engines. Different power control methods, such as: controlling the motion of the regenerator or piston, changing the engine speed or changing the cycle pressure were investigated individually. None of these gave the desired level of control over the full range of engine power output. Some were discounted for reasons of - engine life, unacceptable torque ripple, imperfect repeatability of cycles or desired fixed shaft speed.
- (b) This led to the strategy of using both a coarse and fine method for controlling the power. The coarse-control set the engine power to one of five different levels. Changing the high pressure-level of the cycle, by offsetting the piston motion, was considered to be most suitable for this. Lower cycle pressures led to lower stresses and longer engine-life at part-loads and allowed the maintenance of nearly constant engine speed throughout the power range. Altering the regenerator motion was found to be the best method of fine-power-control within a given power range. The manipulation of the regenerator motion could be achieved in a number of ways such as: offsetting the motion, changing the stroke length or clipping the motion towards the cold-end. Offsetting the piston motion could simply be achieved by controlling the cylinder enabling in the pump-motor, while controlling the regenerator motion required additional features.
- (c) The total power control using the strategy stated above resulted in variable-pressure cycles, ie. the peak pressure levels of the cycle varied with the power demand, while the cyclic frequency remained constant. This gave two major advantages over controlling the power by changing the cyclic frequency (variable-frequency control). As the maximum cyclic pressure to which the hot-

end is subjected decreases from 400 down to 100 Bar at lower power demands, the service-life of the hot-end increases 10-20 times. Conversely, operating the engine at a fixed cyclic frequency throughout the power range, allows the engine to have a shaft (eg. at the pump-motor) running at nearly constant speed. This could be very attractive for some ancillary drives (eg. alternator), which present IC engines lack. The efficiency estimates for variable-frequency and variable-pressure levels were found to be similar (within $\pm 2\%$), through the power range.

- (d) Two other important findings came from the time domain simulation regarding the motion profiles of the regenerator and the piston. It was established, that by using the digital hydraulic drive, it was possible to achieve similar P-V diagrams using a sinusoidal regenerator motion (which is easier to achieve), rather than triangular or trapezoidal motion. The second finding was that the cylinder enabling sequence calculated by the pump-motor controller (which ultimately controlled the piston motion), following an analogue demand signal, caused a delay in piston motion, when sharp changes in motion were required. This resulted in unpredictable fluctuations in cycle pressure, especially when the cycle was operating at the high (pressure-spike) or low-levels (cavitation) of pressure. The problem was resolved by using a fixed ternary-code, where the controller executed a cyclic sequence of cylinder enabling decisions from pre-tuned look-up tables.

11.2 Recommendations for future work

In several stages of the modelling, assumptions have been used either to simplify the problem or to overcome computational complexities. Manufacturing tolerances and control imperfection are not considered in the design aspects of the engine. These may necessitate re-examination of some of the aspects of the model. These are summarised in the following list :

- (i) The mathematical model is based on the isothermal approach. Hence the cycle predictions are dependent on the control loops maintaining constant temperature conditions at the two ends. In the modelling, the conservation of mass and energy are considered (although based on some assumptions), but conservation of momentum has not been included. A more detailed approach including all three of the conservation laws as well as time domain model of the various parasitic losses may improve the model sufficiently to raise it to a third-order simulation of the engine.

- (ii) The time domain simulations were carried out for a single TD pile. For the engine with more than one TD pile, the output power predictions for each (on a cycle-by-cycle basis) were superimposed, as the investigation of multi-cylinder performance was considered beyond the scope of this thesis. In reality the instantaneous torque output from each TD pile will vary within a cycle. In the case of engines with more than one TD pile, the combined instantaneous torque variation is the result from superimposition of the models. The torque is also dependant on the phasing of the TD piles. For a two stroke engine, a likely choice may be to have half of the TD piles phased at 180 degrees relative to the others. As the high and low pressure-levels may not spread in equal proportions over a cycle, superimposition of these may result in spiky peaks and troughs in the instantaneous torque output of an engine with multiple TD piles. Conversely the inertia and presence of some hydraulic buffer (eg. an accumulator) with the pump-motor may minimise this effect. This needs further investigation.

- (iii) In modelling the heat transfer aspects of the engine, steady-states of heat flow were considered, although cyclic variations (quasi-steady) have been taken into account. Modelling of the transition between different power levels were based on isothermal considerations of the desired thermal parameters. The transient state of thermal response with varying heat flow rates have not been investigated. It would be useful to model the transient thermal response, especially of the hot-end under varying power levels and at engine starting conditions.

- (iv) An advantage of the Malone engine is that the fluid is left at low pressure level when the engine is not working. This minimises leakage problems and requirement of recharging the working fluid. Starting the engine will require pumping power from the hydraulic drive system to raise the fluid pressure. This may be retrieved from fluid energy stored in an accumulator or some other energy storage source (eg. battery). These requirements have not been detailed in the present engine design and need closer attention.

- (v) A number of engine parameters can be used to control the power of the Artemis-Malone engine. Several of these parameters (eg. regenerator and piston strokes or cycle pressure level) have been investigated in order to be used for power control. The interesting parameter of regenerator spinning speed has been used for maintaining hot-end temperature at different cycle pressure-levels. It affects the hot-end temperature by changing flow turbulence inside the regenerator which effectively changes the thermal impedance at the steam-fin interface. Higher swirling velocity can prevent the build up of large thermal impedance at the steam-fin interface, due to reduced fluid density, at lower pressures. The effectiveness of this parameter was realized at the final stage of the modelling and has not been investigated in detail yet. The spinning speed of the regenerator can be changed easily by controlling the driving-impeller speed, although this would have consequence on the regenerator drive-power requirement. The possibility of using it as a power control technique, especially for fine-power-control, may significantly simplify the power control technique.

- (vi) For the construction of the composite design of the hot-end, Inconel was chosen as the material for hot-strength and copper for its thermal conductivity. The validity of the design is based on the performance of the brazed surfaces under high internal pressure and at high temperatures for a long enough service life. The hot-end metal also needs to be protected against oxidation, for which nickel plating has been suggested. Copper creep and the permeability of the protective plating, may affect the performance of the hot-end design adversely. The availability of new materials possessing good thermal conductivity and high-

temperature strength, equivalent to the hot-end composite, may greatly increase the reliability of the hot-end.

- (vii) To reach the next stage an experimental prototype of the engine is necessary. This would test both the fabrication techniques and the performance estimates. An experimental model of the engine may reveal some effects, which may have been over or underestimated or even over-looked in the theoretical approach. Fortunately, this last point is being actively pursued at present.

References

Anon, (1979) : "Assesment of the State of Technology of Automotive Stirling Engines", NASA report CR-159631, USA 1979.

Beale et al. (1973) : Beale W, Holmes W, Lewis R.S Cheng E, "Free Piston Stirling Engines - a Progress Report", SAE paper no. 730647, 1973.

Bauwens, (1993) : Bauwens L, "Stirling Modelling on Eulerian Grids", *28th Inter-society Energy Conversion Engineering Conference*, Paper No. 93511, vol.2, pp. 725-730, Atlanta, Aug 1993.

Berchowicz (1978) : Berchowicz D.M, "A computer and Experimental Simulation of Stirling Cycle Machines", M.Sc thesis, University of Witwatersrand, South Africa, 1978.

Berchowicz (1986) : Berchowicz D.M, "Design and Optimization of Stirling Machines", Ph.D thesis, University of Witwatersrand, South Africa, 1986.

Campbell, (1986) : Campbell I.M, "Energy and the Atmosphere", John Wiley & Sons Ltd, 2nd edition p-92, Chichester 1986. ISBN 0-471-909548.

Chen and West, (1987) : Chen N.C.J. and West C.D, "Analysis of a Mechanically Simple External Engine with an Unusual Cycle", Oak Ridge National Laboratory Report ONRL/TM-10351, 1987.

Craig, (1992) : Craig T, "Mactaggart-Scott MSBV Dual Displacement Radial RHP Pump 1969", Technical Director MTS ltd, personal Communication with Rampen W.H.S.

Dunn et al. (1975) : Dunn P.D, Rice G. and Thring R.H, "Hydraulic and Rotary Drive Stirling Engines with Fluidised Bed Combustion/Heat Pipe System", *10th Inter-society Energy Conversion Engineering Conference*, Paper No. 759141, pp. 942-947, Newark NJ USA, 1975.

Ehsan, (1995) : Ehsan Md, Rampen W.H.S. and Taylor J.R.M, "Simulation and Dynamic Response of Computer Controlled Digital Hydraulic Pump/Motor System Used in Wave Energy Power Conversion", *2nd European Wave Power Conference*, pp. 305-311, Lisbon, 8-10 Nov 1995.

Ehsan, (1996) : Ehsan Md, Rampen W.H.S and Salter S.H, "Computer Simulation of the Performance of Digital-Displacement Pump-Motors" *ASME International Mechanical Engineering Congress and Exposition*, FPST Volume-3, pp.19-24, Atlanta Nov. 1996.

Finkelstein (1960) : Finkelstein T, "Generalized Thermodynamic Analysis of Stirling Engines", SAE winter annual meeting, paper No. 118B, 1960.

Finkelstein (1975) : Finkelstein T, "Computer Analysis of Stirling Engines", *10th Inter-society Energy Conversion Engineering Conference*, pp. 933-941, Newark NJ, Aug 17-22, USA 1975.

Gedeon, (1992) : Gedeon D, "A Globally-Implicit Stirling Cycle Simulation", *21th Inter-society Energy Conversion Engineering Conference*, Paper No. 869121, pp. 550-554, San Diego USA, 1986.

Geng and Tew, (1992) : Geng, S.M. and Tew R.C, "Comparison of GLIMPS and HFAST Stirling Engine Code Predictions with Experimental Data", NASA Technical Memorandum 105549, 1992.

Goodwall, (1980) : Goodwall P.M, "The Efficient Use of Steam", IPC Business press ltd, London 1980, p 45 - Noise control. ISBN 0-861-03018-4.

Greenfield, (1972) : Greenfield P, "Creep of Metals at High Temperatures", Published by Mills & Boon Ltd, London 1972. ISBN 0-263-51846-9.

Henderson et al. (1971) : Henderson J. and Snedden D, "Complex stress creep relaxation of commercially pure copper at 250 C", chapter-10 of "Advances in Creep design", Edited by Smith et al, Applied Science Publishers ltd, London 1971. ISBN 0-444-20119-X.

Hargreaves, (1991) : Hargreaves, C.M., "The Philips Stirling Engine", Elsevier Science Publishers B.V, Amsterdam, 1991.

Inco Alloy Intl, (1985) : "INCONEL alloy 625", Inco Alloys International 1985, product catalogue, England.

Incropera, (1990) : Incropera P.F. and Dewitt P.D, "Introduction to Heat Transfer", 2nd Edition, John Wiley & Sons, Singapore 1990. ISBN 0-471-51728-3.

Isshiki, (1992) : Isshiki N, "Simple Vector Analysis of Stirling Machine's Performance", *Proceedings of the 27th Inter-society Energy Conversion Engineering Conference*, paper no.929030, vol.5, Sandiago CA, Aug 3-7, USA 1992.

Kitzner (1980) : Kitzner E.W, "Automotive Stirling Engine Development Program", NASA report CR-159836, USA 1980.

Lee, (1976) : Lee K, "The Stirling Cycle with Adiabatic Compression and Expansion", M.Sc thesis, University of Calgary, Canada 1976.

Malone, (1931) : Malone J.F.J, "A New Prime Mover", *Journal of Royal society of Arts*, Volume 79, pp. 679-709, London 1931.

Mathcad : Mathcad, Version 6.0, 1995, MathSoft Inc. Boston USA.

MATRIXx : System Build (MatrixX), Dynamic simulation package, Version 4.1, 1994, Integrated Systems Inc, CA, USA.

Martini, (1983): Martini W, "Stirling Engine Design Manual", Martini Associates, 3636E, Oaks Drive, Salt lake City, UT 84121, USA 1983.

Mattavi et al. (1969) : Mattavi J.N, Heffner F.E. and Miklos A.A, "The Stirling Engine for Underwater Vehicle Applications", SAE paper no. 690731, pp. 2376-2400, 1969.

Meijer, (1959) : Meijer R.J, "The Philips Hot-Gas Engine with Rhombic Drive", Philips Technical Review, vol. 20, pp. 245-276, 1959.

Miller, (1987) : Miller, J.E, "The Reciprocating Pump - Theory, Design and Use", John Wiley and Sons, pp. 261-262, New York, 1987.

Moller, (1957) : Moller C.B, Force Pump for Slurries (with solenoid valves), US Patent no. - 2,785,638.

Organ, (1991) : Organ A.J, "Stirling Engine Thermodynamic Design", Cambridge: MRT publications 1991. ISBN 0-951-80870-2.

Organ, (1992) : Organ A.J, "Thermodynamic Analysis of the Stirling Cycle Machine - A Review of the Literature", *Proceedings of Institution of Mechanical Engineers (IMEchE)*, vol. 201, No.C6, pp. 381-402, 1987.

Petzold, (1983) : Petzold L.R, "A Description of DASSL: A Differential/Algebraic System Solver", *Scientific Computing*, eds. R.S. Stepleman et al. pp 65-68, North Holland, Amsterdam, 1983.

Qvale and Smith, (1969) : Qvale E.B. and Smith J.L, "A Mathematical Model for Steady Operation of Stirling Type Engine", *Journal of Energy and Power (ASME)*, vol.90, pp. 45-50, 1969.

Rampen et al. (1990) : Rampen W.H.S. and Salter S.H, "The Digital Displacement Hydraulic Piston Pump", *Proc. 9th International Symposium on Fluid Power*, BHR Group, Cambridge, STI, pp. 33-46, April 1990.

Rampen et al. (1991) : Rampen W.H.S, Salter S.H. and Fussey A, "Constant Pressure Control of the Digital Displacement Pump", 4th Bath Intn'l Fluid Power Workshop, *Fluid Power Systems and Modelling*, RSP, pp. 45-62, Bath, Sept. 1991.

Rampen, (1992) : "The Digital Displacement Hydraulic Piston Pump", Ph.D thesis, University of Edinburgh, Scotland, 1992.

Rampen and Salter, (1992) : Rampen W.H.S. and Salter S.H, "Measuring and Predicting the Frequency Response of the Digital Hydraulic Pump", *5th Bath Intn'l Fluid Power Workshop, Circuit, Component and Systems Design*, Bath, RSP, pp. 155-166, Sept. 1992.

Rampen et al. (1994) : Rampen W.H.S, Almond J.P, and Salter S.H, "The Digital Displacement Pump/Motor Operating Cycle: Experimental Results Demonstrating the Fundamental Characteristics". *International Fluid Power Workshop*, Bath 1994.

Rampen et al. (1995) : Rampen W.H.S, Almond J.P, Taylor J.R.M, Ehsan Md. and Salter S.H, "Progress on the Development of the Wedding-cake Digital Hydraulic Pump/Motor", *2nd European Wave Power Conference*, pp.289-296, Lisbon, 8-10 Nov 1995.

Reader and Barnes, (1988) : Reader G.T. and Barnes C, "The Effect of Bottom End Temperature on the Performance of a Stirling Engine", *Proceedings of the 23rd Inter-society Energy Conversion Engineering Conference* (by ASME), Paper no. 889350, Denver USA, 1988.

Reader and Hooper, (1983) : Reader G.T. and Hooper C, "Stirling Engines" E & F N Spon, London and New York 1983, ISBN 0-419-12400-4.

Rix, (1988) : Rix D.H, "A Thermodynamic design simulation for Stirling Cycle Machines Using a Lagrangian Formulation", *Proceedings of Institution of Mechanical Engineers (IMEchE)*, vol. 202, No.C2, pp. 85-93, 1988.

Ross, (1979) : Ross M.A, "Balanced Crankshaft Mechanism for the Two-piston Stirling Engine", US Patent no. - 4,138,897.

Salter and Rampen, (1993) : Salter S.H. and Rampen W.H.S, "The Wedding Cake Multi-Eccentric Radial Piston Hydraulic Machine with Direct Computer Control of Displacement", *Proc. 10th International Conference on Fluid Power*, BHR Group, Brugge, MEP, pp. 47-64, April 1993.

Schimdt, (1861) : Schimdt G, "Theore der Geschlossen Calorischen Maschine Laubroy und Schwatskopff in Berlin. Z. ver Oster Ing. p.79, 1861.

Schwartz, (1995) : "Brazing for the Engineering Technologist", Chapman & Hall, London, 1995. ISBN 0-412-60480-9.

Srinivasan et al. (1985) : Srinivasan V, Walker G, Fauvel R, Senft J.R, "Ringbom-Stirling Engine Simulation and Parametric Study", ASME 85-DGP-21, 1985.

Swift, (1989) : Swift G.W, "Simple Theory of a Malone Engine", *24th Inter-society Energy Conversion Engineering Conference*, paper no. 899055, pp2355-2361, 1989.

Taylor, (1984) : Taylor D.R, "Comparison and Selection of Computer Simulation Codes for Stirling Engines", *Proceedings of the 2nd International Conference on Stirling Engines*, June 21-24, Shanghai, China 1984.

Urieli and Berchowitz (1984) : Urieli I. and Berchowitz D.M, "Stirling Cycle Engine Analysis", Adam Hilger, Bristol 1984.

Urieli, (1977) : Urieli I, "A Computer Simulation of Stirling Cycle Machines", Ph.D thesis, University of Witwatersrand, South Africa, 1977.

Walker, (1980) : "Stirling Engines", Clarendon press, Oxford, 1980.
ISBN 0-19-856209-8.

Walker and Khan, (1965) : Walker G. and Khan M, "The Theoretical Performance of Stirling Cycle Engines", SAE paper no. 949A, *International Automotive Engine Conference*, Detroit, Jan 1965.

Walker et al. (1990) : Walker G, Weiss M, Reader G, Fauvel O.R, "Adventures with MARWEISS : A Summary of Experience with Stirling Simulation", *Proceedings of the 25th Inter-society Energy Conversion Engineering Conference*, pp. 342-345, Reno NV, USA 1990.

Walker et al. (1992) : Walker G, weiss M, Reader G, Fauvel R. and Bingham E.R, "The Stirling Alternative", *Proceedings of the 27th Inter-society Energy Conversion Engineering Conference*, vol.5, pp.97-100, Aug 3-7, San Diego CA, 1992.

Walker et al. (1994) : Walker G, Reader G, Fauvel O.R. and Bingham E.R, "The Stirling Alternative", Gordon & Breach Science Publishers, Switzerland, 1994. ISBN 2-88124-600-1.

Weiss and Fauvel (1986) : Weiss M. and Fauvel R, "A User-friendly, Graphics Oriented, Martini Stirling Engine Simulation Program", *Proceedings of the 3rd International Conference on Stirling Engines*, June 25-27, vol. 1, pp. 209-213, Rome 1986.

West, (1982) : West C.D, "Liquid Piston Stirling Engines", Van Nostrand Reinhold Co. New York, 1982.

West, (1986) : West C.D, "Principles and Applications of Stirling Engines", Van Nostrand Reinhold Co, New York, 1986.

Wetelets et al. (1976) : Wetelets R.P, Ruggles A.E, Hagen K.G. and Torti V, "Status of the Tidal Regenerator Engine for Nuclear Circulatory Support System", *Proceedings of the 11th Inter-society Energy Conversion Engineering Conference*, pp. 136 - 142, Lake Tahoe, Nevada USA, Sept 1976.

Wood, (1987) : Wood J.G, "A New Mechanical Linkage for Stirling Cycle Machines", *Proceedings of the 22nd Inter-society Energy Conversion Engineering Conference*, paper no. 879422, Philadelphia USA, Aug 1987.

Appendix A : The static simulation model

The static modelling is developed using the mathematical package Mathcad (version 6.0). The principle in which the model works have been described in chapter four. Advantage of using Mathcad is that all the design equations can be described with text accompanying it. Hence the programme is readable to any one just like normal text. Most of the symbols used in the Mathcad model is self-explanatory, but it is important to understand the various value-assigning symbols used for variables. These include the following :

- (≡) This symbol defines a global variable. The value assigned is valid from the beginning of the programme, irrespective of the placement of the definition in the program. The validity is maintained throughout the programme, unless the variable is redefined any where else. Global variables can only be defined in terms of constant numbers. Example, $PH \equiv 400.10^5$.
- (:=) This symbol also defines a variable. But unlike the previous one the variable is only effective in the following lines (ie. after it's placement) of the programme. Variables can be defined as constant values or in terms of other already defined variables (using any of the symbols \equiv or $:=$). Example: $kwex := 1.92$ or $Aex:=2.lex.Wex$.
- (=) This symbol is used to restate the numerical value of already defined variables. Hence it can not be used for redefining a value. Example $Aex:=2.lex.Wex \quad Aex = 8.96$.
- (=) This symbol is used in conjunction with the functions *Given* and *Find*, for solving closed-loop values of a variable. A starting value needs to be provided (initialization) for the variable to be evaluated. Example,

$$\begin{array}{l} \text{Starting guess} \quad \text{Dioa} := .08 \\ \\ \text{Given} \quad \sigma_i = PH \cdot \frac{t_{cu} + t_{inc}}{t_{inc}} \cdot \frac{Dioa^2 + Dii^2}{Dioa^2 - Dii^2} \\ \\ \text{Dioa} := \text{Find}(Dioa) \end{array}$$

In the last three pages of the programme, values of important variables are listed and the control panel is placed. This contains main engine parameters, defined as global variables and allows checking of the closed-loop solutions. Placing them at the end provides a very useful and fast way of investigating the effect of parameter changes on the resulting cycle, without needing to move to the respective parts of the programme.

Malone Module Performance Calculations

S H Salter,

Md. Ehsan, Department of Mechanical Engineering, University of Edinburgh, Scotland

We want to calculate the performance of a crankless Stirling-Malone module using water as the working fluid connected to a high-pressure oil hydraulic machine. A number, NM, of separate thermal modules are coupled to a pair of isolator sections which separate the cold end water from the hydraulic oil. The two isolator sections work alternately giving power at all times.

This paper starts by defining sufficient dimensions for the estimation of thermal impedances. Steam properties are taken from initial guesses of temperature values which are later refined. We then imagine that an input quantity of heat is flowing through the chain of thermal impedances and calculate the various temperature drops. In the middle of the chain the heat goes through an ideal heat engine with a thermal efficiency depending on the calculated temperatures. This gives a notional work output from which the ancillary losses and stray heat flows can be subtracted to give the net useful output. The dimensions are then used to calculate the total engine weight.

The reader should refer to general arrangement drawings and a more extended description of the design philosophy. The design can be optimised for different life, weight, volume and efficiency requirements by a few identified factors.

Design parameters can be set in a control panel at the end of the document together with the more important results. All values are MKS unless stated.

The overall length of the engine is set by the spacing of the thermal modules **mod**. The bore of a thermal module **D** is then set by the design factor **kb**. Most of the other dimensions are then set by design factors relative to the bore, safe stresses and the design pressure **PH**. Most of the thermal properties are driven by the value of **Q**, the amount of heat flowing into a single thermal module and the temperature **Tmw** at the middle of the wall of a hot chamber which is the metalurgical limit of the wall material.

Key starting dimensions

Present choice of thermal module spacing		mod = 0.084
Present choice of bore factor		kb = 0.476
Thermal module bore	$D := kb \cdot mod$	D = 0.04
Present choice of heat flow per module		Q = 27000
Present choice of middle wall temperature C		Tmw = 658
Present choice of module number		NM = 4
Present choice of upper pressure		PH = $4 \cdot 10^7$

Initial Thermal Estimates

Steam tables show that the pressures corresponding to the highest temperatures would not be safe for any economic design. However by controlling the stroke of the regenerator so as to keep within the safe pressure limit we achieve a desirably rectangular pressure-volume diagram and make best use of the material creep life.

The present guesses for high and sink temperatures **TH** and **TS** are needed to calculate fluid properties. Run the programme for a given **Q** value, check the resulting temperatures at steam fin and condensing fin and reset the initial guesses to converge on a more accurate value. Present choices are

$$TH = 548 \quad TS = 95 \text{ C}$$

The first guess for the Carnot efficiency is

$$\eta_{th} := \frac{TH - TS}{TH + 273} \quad \eta_{th} = 0.552$$

The hot end cylinder is a laminated stack of washers of two materials. The heat from the flame is brought in by the larger washers acting as fins. The flame fin material is chosen for its thermal conductivity, not hot strength. It will almost certainly be copper which melts at 1083 C. Its tensile strength falls to zero at about 900C. The copper thickness is **tcu**. The flow of heat out of the hot end will be dictated by power delivered to the hydraulics. The flow of fuel and air must therefore be regulated to maintain a steady, safe temperature in the tips of the copper fins despite power variation.

The internal pressure stress of the hot-end cylinder is taken entirely by the smaller slices of Inconel of thickness **tlnc**. This is chosen for hot strength rather than thermal conductivity. Inconel 625 is available in 0.5, 0.7, and 0.9 mm sheet at £22 /kilogram in small quantities. The stack will be vacuum-brazed under a large compressive load.

The Inconel slices are subject to both creep and high cycle fatigue and will require careful design. Data published by International Nickel show that creep is more serious than fatigue. For 0.2% creep in 2000 hours at 650 C we can stress to 250 E6 N/m². The thermal expansion coefficient of copper is 16.7 ppm C. Inconel 625 has an expansion coefficient of 13.8 ppm C over the working range.

The inner diameter of the Inconel disc is greater than D so that the inner diameters of the copper sheets form fins in contact with the steam. The length of the steam fins set by factor k_{sf} relative to the copper thickness t_{cu} .

Present choice of copper fin thickness		$t_{cu} = 0.0007$
Steam fin length	$L_{sf} := t_{cu} \cdot k_{sf}$	$L_{sf} = 0.004$
Inner diameter of Inconel	$D_{ii} := D + 2 \cdot L_{sf}$	$D_{ii} = 0.048$
Inconel thickness is set by	$k_{ic} = 1.5$	$t_{inc} := t_{cu} \cdot k_{ic}$ $t_{inc} = 0.001$

Hot-End Stress

The Inconel outer diameter, also the flame fin root diameter, is set so that the stress of the inner material is not exceeded. It is necessary to solve the thickwall stress equation given in Shigley section 2-11

Choose inner stress $\sigma_i = 3 \cdot 10^8$ Starting guess for outer, $D_{ioa} := .08$

Given
$$\sigma_i = PH \cdot \frac{t_{cu} + t_{inc}}{t_{inc}} \cdot \frac{D_{ioa}^2 + D_{ii}^2}{D_{ioa}^2 - D_{ii}^2}$$

$D_{ioa} := \text{Find}(D_{ioa})$ $D_{ioa} = 0.06$

It may be useful to modify this from the control panel $D_{io} = 0.06$

$$\sigma_{ir} := PH \cdot \frac{t_{cu} + t_{inc}}{t_{inc}} \cdot \frac{D_{io}^2 + D_{ii}^2}{D_{io}^2 - D_{ii}^2} \quad \sigma_{ir} = 2.957 \cdot 10^8$$

The tangential stress in a thick wall under internal pressure falls with increasing radius. At the outside of the Inconel it is

$$\sigma_o := PH \cdot \frac{t_{cu} + t_{inc}}{t_{inc}} \cdot \frac{D_{ii}^2}{D_{io}^2 - D_{ii}^2} \cdot 2 \quad \sigma_o = 2.29 \cdot 10^8$$

The ratio of these stresses is $\frac{\sigma_o}{\sigma_{ir}} = 0.775$

The mean value is
$$\sigma_m := \frac{\sigma_{ir} + \sigma_o}{2} \quad \sigma_m = 2.624 \cdot 10^8$$

If an over stressed part of the Inconel starts to creep it will relieve its own stress and increase that of the rest with a trend towards the mean value. This provides a considerable advantage and safety factor.

The force extruding the copper is the result of maximum pressure

$PH = 4 \cdot 10^7$

$F_{ex} := PH \cdot \pi \cdot D_{ii} \cdot t_{cu}$

$F_{ex} = 4196$

The mean shear stress in the copper needed to oppose the pressure would be

$$\sigma_{scu} := \frac{F_{ex}}{0.25 \cdot \pi \cdot (D_{io}^2 - D_{ii}^2) \cdot 2} \quad \sigma_{scu} = 2.017 \cdot 10^6$$

Note that in pounds per square inch this is only $\frac{\sigma_{scu}}{6895} = 292.472$

The radial length of the Inconel disk is

$$r_{inc} := \frac{D_{io} - D_{ii}}{2} \quad r_{inc} = 0.006$$

The expansion difference from cold along the length of the Inconel is

$$ex := (T_{mw} - 20) \cdot (16.7 - 13.8) \cdot 10^{-6} \cdot r_{inc} \quad ex \cdot 10^6 = 11.378$$

The differential thermal strain is

$$\epsilon_{th} := \frac{ex}{r_{inc}} \quad \epsilon_{th} \cdot 10^6 = 1850.2$$

The materials should be unstressed at the temperature of the vacuum brazing which will be above normal working temperature. Thermal creep at the working temperature will also tend to relieve the interfacial stress. This means that the worst thermal difference stress will occur when the engine is cold. Fortunately this is when the materials have their greatest strength. The tendency will be to expand the copper and contract the Inconel on cooling.

Hot end Temperature Calculations

Next we can check temperature drops across the heat transfer surfaces starting at the the hot gas input.

Axial length L_{fb} of fin blocks is set by the travel of the regenerator which is set as a multiple of D by the factor k_R .

$k_R = 2.9$ $L_{fb} := D \cdot k_R$ $L_{fb} = 0.116$

Number of flame fins
$$N_{ff} := \text{floor}\left(\frac{L_{fb}}{t_{cu} + t_{inc}}\right)$$
 $N_{ff} = 66$

The nominal outside diameter of round flame fins D_f is the same as the module spacing mod along the line of the modules but the dimension can be increased perpendicular to it. An extension toward the down stream end would help heat transfer from the cooler out-going gases.

$$D_f := mod$$

$$D_f = 0.084$$

The surface area of the flame-fins can be largely reduced by joining adjacent fins (eg. by brazing). This also can be used for control

No. of fins joined, $nf = 2$

Flat area of the flame fins $A_{ff} := \frac{\pi}{4} \cdot (D_f^2 - D_{io}^2) \cdot \frac{2}{nf} \cdot N_{ff}$ $A_{ff} = 0.179$

Although circular fins are convenient for mathematical analysis, rectangular or hexagonal-shaped ones may be packed more closely and use the full area of sheet material. The side of a square with the same area and central block diameter.

$$S_{ff} := \sqrt{A_{ff} + \frac{\pi \cdot D_{io}^2}{4}}$$

$$S_{ff} = 0.427$$

The width of the engine allows a 30% increase of fin dimension perpendicular to the line of modules. The actual flame fin area of the proposed rectangular fins is

$$A_{fa} := \left(mod \cdot 1.3 \cdot mod - \frac{\pi}{4} \cdot D_{io}^2 \right) \cdot \frac{2}{nf} \cdot N_{ff}$$

$$A_{fa} = 0.419$$

To allow later analysis with symbolic expressions for the efficiency of circular fins we will take a mean value so that

$$A_{ff} := \frac{A_{ff} + A_{fa}}{2}$$

$$A_{ff} = 0.299$$

A more exact calculation will require finite element analysis.

The heat transfer coefficient from gas to fin depends on the velocity and physical properties of the hot gases, the geometry of the flow path and the radiated heat flux. We must first estimate the volume consumption of fuel and air. Assume that we are burning natural gas which we can take as methane CH_4 . One kg will provide $45E6$ joules so that the mass of methane per second M_m giving Q joules to one thermal module is

$$M_m := \frac{Q \cdot LF}{45 \cdot 10^6}$$

$$Q_h := Q \cdot LF$$

$$Q_h = 27891$$

$$M_m \cdot 10^3 = 0.62$$

The combustion equation $CH_4 + 2O_2 + 8N_2 > CO_2 + 2H_2O + 8N_2$ shows that 16 kg of methane burn with $2 \cdot 32$ kg of oxygen accompanied by $8 \cdot 28$ kg of nitrogen with an extra AR of air to make certain of complete combustion. The mass flow of all gases per thermal module will be

$$\text{Air Ratio, } AR = 2.052$$

$$MG := M_m \cdot \frac{16 + (2 \cdot 32 + 8 \cdot 28) \cdot AR}{16}$$

$$MG = 0.0235$$

As there is such a large proportion of nitrogen we can use data on air for the gas properties. The specific heat of air at one atmosphere changes only slightly over the temperature range. Take the value of 1286 from Incropera page A15.

We make an initial guess of the temperature T_{ih} to which the incoming air is preheated and then refine the guess later

$$T_{ih} = 738$$

The initial flame temperature will be (in degree C) $TF1 := T_{ih} + \frac{M_m \cdot 45 \cdot 10^6}{MG \cdot 1220}$ $TF1 = 1710$
 $TF1C := TF1$

The average absolute flame temperature through the copper fin volume is about

$$TF := \frac{TF1 + T_{oh}}{2} + 273$$

$$TFC := TF - 273$$

$$TF = 1513 \text{ K}$$

The density of an ideal gas falls with absolute temperature. Interpolate from values at 1800 K.

Density $\rho_a := 0.2488 \cdot \frac{1400}{TF}$ $\rho_a = 0.23$

The volume flow of all gases going through the copper fin section is

$$VGC := \frac{MG}{\rho_a}$$

$$VGC = 0.102$$

At the inlet to the engine the volume of cold air flow (density 1.25 kg/m³) is

$$V_{cld} := \frac{MG}{1.25}$$

$$V_{cld} = 0.019$$

The gases will pass once through the gaps between the fins. At the narrowest this has a cross sectional area of

$$A_p := t_{inc} \cdot nf \cdot (D_f - D_{io})$$

$$A_p \cdot 10^6 = 50.4$$

The gas velocity in each passage is

$$\text{vel} := \frac{\text{VGC}}{\text{Ap} \cdot \frac{\text{Nff}}{\text{nf}}} \quad \text{vel} = 61.413$$

$$\text{velg} := \text{vel}$$

Check the speed of sound at this temperature.

$$\text{Mach} := \frac{\text{vel}}{\sqrt{\frac{101300}{\rho a}}} \quad \text{Mach} = 0.093$$

The viscosity of an ideal gas rises with the square root of absolute temperature.

Viscosity of the gas is $\mu_g := 53 \cdot 10^{-6} \cdot \sqrt{\frac{\text{TF}}{1400}}$ $\mu_g \cdot 10^6 = 55.1$

Flame fin length $L_{ff} := \frac{D_f - D_{io}}{2}$ $L_{ff} = 0.012$

The hydraulic mean diameter of the gap between fins is

$$D_{hmf} := \frac{4 \cdot L_{ff} \cdot t_{inc} \cdot n_f}{2 \cdot L_{ff} + n_f \cdot t_{inc}} \quad D_{hmf} = 0.0039$$

$$D_{hmf} := D_{hmf}$$

Reynolds number for the gases referred to the hydraulic mean diameter

$$R_{nog} := \frac{\text{vel} \cdot D_{hmf} \cdot \rho_a}{\mu_g} \quad R_{nog} = 991 \quad \text{This is very definitely laminar flow.}$$

The pressure drop through through the fin block is

$$\Delta P_p := \frac{\text{VGC}}{\left(\frac{\text{Nff}}{\text{nf}}\right)} \cdot \frac{12 \cdot \mu_g \cdot D_f}{\left(D_f - \frac{D_{io}}{2}\right) \cdot (t_{inc} \cdot n_f)^3} \quad \Delta P_p = 344$$

Thermal conductivity of hot air as a function of temperature is given in table A15 of Incropera. We interpolate from values close to 1800 K

$$k_a := 0.120 + (\text{TF} - 1800) \cdot \frac{.120 - .113}{100} \quad k_a = 0.1$$

The appropriate expression for heat transfer between close parallel plates in laminar flow is given in Incropera page 461.

$$H_{tff} := \frac{6.49 \cdot k_a}{D_{hmf}} \quad \text{choice} := \frac{L_{ff}}{t_{inc} \cdot n_f}$$

Choice for constant, based on aspect ratio of flow, as in Incropera, $\text{choice} = 5.714$ hence, $H_{tff} = 168$

Fin conductivity (copper) $\lambda_1 := 380$

The flame fin efficiency is $\eta_{ff} := \frac{\tanh\left[\sqrt{\frac{2 \cdot H_{tff}}{\lambda_1 \cdot n_f \cdot t_{cu}}} \cdot \left(L_{ff} + \frac{t_{cu} \cdot n_f}{2}\right)\right]}{\sqrt{\frac{2 \cdot H_{tff}}{\lambda_1 \cdot n_f \cdot t_{cu}}} \cdot \left(L_{ff} + \frac{n_f \cdot t_{cu}}{2}\right)}$ $\eta_{ff} = 0.967$

Temperature drop gas-to-fin root assuming full fin efficiency

$$\Delta T_{1a} := \frac{Q}{A_{ff} \cdot H_{tff}} \quad \Delta T_{1a} = 537.8$$

Temperature drop including fin efficiency

$$\Delta T_{ff} := \frac{\Delta T_{1a}}{\eta_{ff}} \quad \Delta T_{ff} = 556$$

It is convenient to calculate a series of thermal resistances Z in watts per degree C.

Resistance flame to fin root $Z_{ff} := \frac{1}{A_{ff} \cdot H_{tff} \cdot \eta_{ff}}$ $Z_{ff} = 0.0206$

Temperature at flame-fin base $T_{ffb} := \text{TF} - 273 - Q \cdot Z_{ff}$ $T_{ffb} = 684.176$

$$m := \sqrt{\frac{2 \cdot H_{tff}}{\lambda_1 \cdot n_f \cdot t_{cu}}} \quad T_{fo} := \text{TF} - (\text{TF} - T_{ffb}) \cdot \left[\frac{1}{\cosh(m \cdot L_{ff})} + \left(\frac{H_{tff}}{m \cdot \lambda_1}\right) \cdot \sinh(m \cdot L_{ff}) \right]$$

Temperature at the outer edge of flame fins $T_{fo} = 716.014$

Temperature of gases leaving the hot-end $T_{oh} := \text{TF} - \left(\frac{Q}{\text{MG} \cdot 1220}\right)$ $T_{oh} = 769.061$

By way of comparison if we take the case of a liquid metal with heat transfer 3000 W/m²K feeding an unfinned cylinder of the full length L_{fb}

$$Z_{1b} := \frac{1}{\pi \cdot D_{io} \cdot L_{fb} \cdot 3000}$$

$$Z_{1b} = 0.015$$

Note the ratio of unfinned liquid metal to the laminated fin design

$$\frac{Z_{1b}}{Z_{ff}} = 0.74$$

The thermal resistance through the copper parts of the wall of the hot pressure chamber from Incropera page 98 equation 3.27 is

$$\lambda_1 = 380$$

$$Z_{w1} := \frac{\ln\left(\frac{D_{io}}{D_{ii}}\right)}{2 \cdot \pi \cdot \lambda_1 \cdot N_{ff} \cdot t_{cu}}$$

$$Z_{w1} = 2.07961 \cdot 10^{-3}$$

The thermal resistance through the Inconel parts of the wall of the hot pressure chamber is

$$\lambda_2 := 15$$

$$Z_{w2} := \frac{\ln\left(\frac{D_{io}}{D_{ii}}\right)}{2 \cdot \pi \cdot \lambda_2 \cdot N_{ff} \cdot t_{inc}}$$

$$Z_{w2} = 0.03512$$

The thermal resistance of the parallel combination making up the hot wall is

$$Z_{hw} := \frac{1}{\left(\frac{1}{Z_{w1}} + \frac{1}{Z_{w2}}\right)}$$

$$Z_{hw} = 1.96336 \cdot 10^{-3}$$

Heat can also pass from flame to fin as radiation. The surface of the copper can be plated with nickel and then oxidised to give an efficient black with emissivity 0.59 to 0.86 (Hottel and Sarofim page 163). There is more uncertainty about the emissivity of the flame especially as the flame layer is very thin and the fuel source yet to be chosen. The problem is discussed in Hottel section 6.9.

Choice of gas emissivity

$$em_g := 0.005$$

The Stefan-Boltzman constant is 5.678 E-8 W/m²K

The radiation heat transfer coefficient from Goodall page 287 is

$$H_{tfr} := em_g \cdot 5.678 \cdot 10^{-8} \cdot \frac{TF^4 - (650 + 273)^4}{TF - (650 + 273)}$$

$$H_{tfr} = 2.173$$

This is not much help. A large increase in gas emissivity caused, say, by the presence of carbon particles would improve heat transfer but we are trying to keep combustion as clean as possible. For the time being it seems reasonable to ignore radiation from the gas. However radiation from over-heated copper to cooler copper may be useful.

Take the value of copper emissivity

$$em_{cu} := 0.6$$

Take a hot spot temperature in Kelvin

$$T_{hs} := 900 + 273$$

The radiation heat transfer coefficient from blackened copper is more useful.

$$H_{tcur} := em_{cu} \cdot 5.678 \cdot 10^{-8} \cdot \frac{T_{hs}^4 - (650 + 273)^4}{T_{hs} - (650 + 273)}$$

$$H_{tcur} = 159.084$$

Sealing Tube Heat Transfer

The inner tube is a composite member of a outer inconel tube and an inner copper tube.

Seal-tube thickness, $t_{seal} = 0$

$$t_{tbinc} := \frac{t_{seal}}{2}$$

$$t_{tbcu} := \frac{t_{seal}}{2}$$

$$Z_{tinc} := \frac{\ln\left(\frac{D_{ii}}{D_{ii} - 2 \cdot t_{tbinc}}\right)}{2 \cdot \pi \cdot \lambda_2 \cdot L_{fb}}$$

$$Z_{tcu} := \frac{\ln\left[\frac{D_{ii} - 2 \cdot t_{tbinc}}{D_{ii} - 2 \cdot (t_{tbinc} + t_{tbcu})}\right]}{2 \cdot \pi \cdot \lambda_1 \cdot L_{fb}}$$

$$Z_{tinc} = 0$$

$$Z_{tcu} = 0$$

$$Z_{tube} := Z_{tinc} + Z_{tcu} \quad \Delta T_{tb} := Q \cdot Z_{tube}$$

Temperature drop across seal-tube, $\Delta T_{tb} = 0$

In case of a sealing tube the steam-fin length is recalculated as,

$$L_{sfr} := L_{sf} - t_{tbinc} - t_{tbcu}$$

$$L_{sf} = 0.004$$

$$L_{sfr} = 0.004$$

Incase of any alrgap present,

For an air-gap of thickness, $t_{air} = 0$

$$\lambda_{air} := .064$$

$$Z_{air} := \frac{\ln\left(\frac{D_{ii}}{D_{ii} - 2 \cdot t_{air}}\right)}{2 \cdot \pi \cdot \lambda_{air} \cdot L_{fb}}$$

$$D_{ii} = 0.048$$

$$Z_{air} = 0$$

$$\Delta T_{ag} := Q \cdot Z_{air}$$

Temperature drop across seal-tube, $\Delta T_{ag} = 0$

Steam Fin to Steam Transfer

Exposed inside area of steam fins (with recalculated outer diameters, for seal-tube)

$$D_{osf} := D_{ii} - 2 \cdot (t_{binc} + t_{bcu})$$

$$A_{sf} := \frac{\pi}{4} \cdot (D_{osf}^2 - D^2) \cdot N_{fs} \cdot 2 + \pi \cdot D \cdot t_{cu} \cdot N_{fs}$$

$$A_{sf} = 0.076$$

$$D_{osf} = 0.048$$

The heat transfer from steam fins to steam can be greatly increased by forcing a swirl by the rotation of the body of the regenerator. This could be done using tangential jets near the cold end of the separator section impinging on the outer wall of the regenerator. The swirl velocity can be increased at high values of Q .

The present choice of minimum circumferential swirl velocity is

$$V_{sw} = 3$$

With the extra the velocity is $V_{swe} := V_{sw} + \frac{k_{sw}}{10000} \cdot Q$

$$V_{swe} = 4.89$$

The rotation speed would be

$$\omega := \frac{V_{swe}}{0.5 \cdot D}$$

$$\omega = 244.495$$

$$rpm := \omega \cdot \frac{60}{2 \cdot \pi}$$

$$rpm = 2334.756$$

Heat transfer to steam depends on its physical properties. We obtain them from Incropera page A 19. We use data for 800 K and linearly interpolate to TH and PH. Note that pressure does not affect viscosity of a gas or of steam away from the critical point.

$$\text{Density} \quad \rho_{sld} := 0.2739 \cdot \frac{800}{TH + 273} \cdot \frac{PH}{10^5}$$

$$\rho_s = 143.2$$

$$\text{Viscosity} \quad \mu_s := 27.86 \cdot 10^{-6} \cdot \sqrt{\frac{TH + 273}{800}}$$

$$\mu_s \cdot 10^6 = 28.223$$

Prandtl number for steam from page A19 of Incropera

$$Pr := 1.02$$

Incropera page 461 says that, in calculations of heat transfer coefficient, the expression for circular pipes can be used for other sections such as parallel fins by replacing pipe diameter by hydraulic mean diameter D_{hm} . This is 4 area / perimeter.

$$D_{hms} := \frac{4 \cdot L_{sfr} \cdot \left(\frac{L_{fb}}{N_{fs}} - t_{cu}\right)}{t_{inc} + 2 \cdot L_{sfr}}$$

$$D_{hms} = 1.86 \cdot 10^{-3}$$

Reynolds number for steam referred to the hydraulic mean diameter of the fin gap is

$$R_{nos} := \frac{V_{swe} \cdot D_{hms} \cdot \rho_s}{\mu_s}$$

$$R_{nos} = 46183$$

This is turbulent. The flow round the inside of the steam fins will behave as if there were very long parallel walls and so will be fully developed.

Flow in rectangular bends is discussed by Ward-Smith in section E2.4.2. Even in laminar flow there are internal circulations. In turbulent flow there is a large rise in friction coefficient which implies better heat transfer. The straight flow friction coefficient from page 166 is

$$f_{cs} := \left(4 \cdot \log\left(\frac{R_{nos}}{4.53 \cdot \log(R_{nos}) - 3.82}\right)\right)^{-2}$$

$$f_{cs} = 0.005$$

The radius of curvature of the bend is

$$R_c := \frac{D}{2}$$

$$R_c = 0.02$$

The correction for curves involves Deans number

$$D_r := R_{nos} \cdot \left(\frac{D_{hms}}{R_c}\right)^{0.5}$$

$$D_r = 14089$$

The new friction coefficient from equation E107 on page 277 is

$$f_{ccs} := f_{cs} \cdot 0.0805 \cdot D_r^{0.5} \cdot \left(1 + -5.218 \cdot D_r^{-0.5} + 104.4 \cdot D_r^{-1} + -202.8 \cdot D_r^{-1.5}\right)$$

$$f_{ccs} = 0.049$$

The ratio of curved to straight is

$$\frac{f_{ccs}}{f_{cs}} = 9.205$$

The shear torque for the hot end of one module is given by

$$\tau := \frac{1}{2} \cdot \rho_s \cdot V_{swe}^2 \cdot A_{sf} \cdot \frac{D}{2} \cdot f_{ccs}$$

$$\tau = 0.127$$

This is equivalent to a pair of forces at the circumference of the rotor

$$f_c R := \tau \cdot \frac{2}{D} \quad f_c R = 6.362$$

The power to spin the rotor for one module is

$$P_{\text{owswH}} := \tau \cdot \omega \cdot N M \quad P_{\text{owswH}} = 124.4$$

We can apply a temperature correction for the conductivity of steam by linear interpolation from the 800 K value from the data on page A 19 of Incropera. (Pressure does not affect conductivity, see Kaye and Laby page 70.)

$$k_s := 0.0592 + (T_H + 273 - 800) \cdot \frac{0.0637 - 0.0592}{50} \quad k_s = 0.061$$

The relevant heat transfer expression for straight flow is from Incropera page 456.

$$\text{The Nusselt number is} \quad N_{\text{us}} := 0.023 \cdot R_{\text{nos}}^{\frac{4}{5}} \cdot Pr^{\frac{1}{3}} \quad N_{\text{us}} = 124.8$$

$$\text{The heat transfer coefficient} \quad H_{\text{tfs1}} := \frac{N_{\text{us}} \cdot k_s}{D_{\text{hms}}} \quad H_{\text{tfs1}} = 4096$$

If we calculate the Nusselt number from the enhanced friction coefficient using the Gnielinski equation as suggested by Incropera on page 457 equation 8.63a we get

$$N_{\text{us2}} := \frac{\frac{f_{\text{ccs}}}{8} \cdot (R_{\text{nos}} - 1000) \cdot Pr}{1 + 12.7 \cdot \left(\frac{f_{\text{ccs}}}{8}\right)^{0.5} \cdot (Pr^{0.667} - 1)} \quad N_{\text{us2}} = 279$$

This would raise the heat transfer coefficient to

$$H_{\text{tfs}} := \frac{N_{\text{us2}} \cdot k_s}{D_{\text{hms}}} \quad H_{\text{tfs}} = 9145$$

Unfortunately heat will be transferred only during the fraction f_{Rhc} of the cycle when the regenerator is moving from hot to cold. The correction is

$$H_{\text{tfs}} := H_{\text{tfs}} \cdot f_{\text{Rhc}} \quad H_{\text{tfs}} = 5268$$

The heat transfer coefficient without spin would be the laminar flow value for a parallel plates (page 461 Incropera) of

$$H_{\text{tfsL}} := \frac{8.23 \cdot k_s}{D_{\text{hms}}} \quad H_{\text{tfsL}} = 270$$

$$\text{The ratio of spin to non-spin coefficients is} \quad R_{\text{sns}} := \frac{H_{\text{tfs}}}{H_{\text{tfsL}}} \quad R_{\text{sns}} = 19.5$$

The addition of swirl is very valuable. The experimental check of these predictions is the first stage of the development of the engine.

$$\text{Fin efficiency of steam fins} \quad \eta_{\text{sf}} := \frac{\tanh\left[\frac{2 \cdot H_{\text{tfs}} \cdot \left(L_{\text{sf}} + \frac{t_{\text{cu}}}{2}\right)}{\sqrt{\lambda_1 \cdot t_{\text{cu}}}}\right]}{\frac{2 \cdot H_{\text{tfs}} \cdot \left(L_{\text{sf}} + \frac{t_{\text{cu}}}{2}\right)}{\sqrt{\lambda_1 \cdot t_{\text{cu}}}}} \quad \eta_{\text{sf}} = 0.818$$

$$\text{Thermal resistance fin to steam} \quad Z_{\text{sf}} := \frac{1}{A_{\text{sf}} \cdot H_{\text{tfs}} \cdot \eta_{\text{sf}}} \quad Z_{\text{sf}} = 3.0616 \cdot 10^{-3}$$

$$\text{Temperature drop fin to steam} \quad \Delta T_{\text{sf}} := Q \cdot Z_{\text{sf}} \quad \Delta T_{\text{sf}} = 82.7$$

$$\text{The heat flux density at the boiling surface in Watts/m}^2 \text{ is} \quad H_{\text{fd}} := \frac{Q}{A_{\text{sf}}} \quad H_{\text{fd}} = 3.56 \cdot 10^5$$

At very high values of Q this may be a limiting factor. Goodall page 287 suggests an upper limit of 1.1E6.

Cold-end Temperature Calculations

We use the same length L_{fb} and inside diameter D for the cold chamber but make the whole of solid copper with fins inside and out. The length of the condensing fins is set as a function of their thickness by the factor k_{cf} .

$$\text{Condensing fin length} \quad L_{\text{fc}} := t_{\text{cf}} \cdot k_{\text{cf}} \quad t_{\text{cf}} = 0.001 \quad L_{\text{fc}} = 0.004$$

$$\text{Inner water wall diameter} \quad D_{\text{ci}} := D + 2 \cdot L_{\text{fc}} \quad D_{\text{ci}} = 0.048$$

$$\text{Number of condensing fins} \quad N_{\text{fc}} := \text{floor}\left(\frac{L_{\text{fb}}}{2 \cdot t_{\text{cf}}}\right) \quad N_{\text{fc}} = 58$$

$$\text{Area of condensing fins} \quad A_{\text{cf}} := \frac{\pi}{4} \cdot (D_{\text{ci}}^2 - D^2) \cdot 2 \cdot N_{\text{fc}} + \pi \cdot D \cdot N_{\text{fc}} \cdot t_{\text{cf}} \quad A_{\text{cf}} = 0.067$$

All sources say that the condensing heat transfer coefficients are always above the other parts of the steam cycle and Goodall quotes the range 20 000 to 45 000 W/m²K. Swirl may improve on these numbers. It should be conservative to calculate heat transfer for swirled liquid. If steam from the cold end of the regenerator is vented directly into liquid water as fine bubbles of the diameter of the shim gap the heat transfer should be good.

We can repeat the earlier calculation for flow in rectangular bends discussed by Ward-Smith in section E2.4.2.

The hydraulic mean diameter for the condensing fin channel is

$$D_{hmc} := \frac{4 \cdot L_{fc} \cdot t_{cf}}{2 \cdot L_{fc} + t_{cf}}$$

Reynolds number for water at 100 C referred to the hydraulic mean diameter is

$$R_{now} := \frac{V_{swe} \cdot D_{hmc} \cdot 958}{279 \cdot 10^{-6}} \quad R_{now} = 29631$$

Prandtl number for water from Incropera A22 is

$$Pr_w := 1.7$$

The friction coefficient for a straight pipe flow for this Reynolds number is

$$f_{cw} := \left(4 \cdot \log \left(\frac{R_{now}}{4.53 \cdot \log(R_{now}) - 3.82} \right) \right)^{-2} \quad f_{cw} = 0.006$$

The radius of curvature of the bend is

$$R_c := \frac{D_{ci}}{2} \quad R_c = 0.024$$

The correction for curves involves Deans number

$$D_r := R_{now} \cdot \left(\frac{D_{hmc}}{R_c} \right)^{0.5} \quad D_r = 8077$$

The new friction coefficient from equation E107 on page 277 is

$$f_{ccw} := f_{cw} \cdot 0.0805 \cdot D_r^{0.5} \cdot \left(1 + -5.218 \cdot D_r^{-0.5} + 104.4 \cdot D_r^{-1} + -202.8 \cdot D_r^{-1.5} \right) \quad f_{ccw} = 0.041$$

The ratio of curved to straight friction coefficients is

$$\frac{f_{ccw}}{f_{cw}} = 6.906$$

We now use the friction coefficient to predict a Nusselt number using the Gnielinski equation from page 457 of Incropera.

$$Nuc := \frac{\frac{f_{ccw}}{8} \cdot (R_{now} - 1000) \cdot Pr_w}{1 + 12.7 \cdot \left(\frac{f_{ccw}}{8} \right)^{0.5} \cdot (Pr_w^{0.666} - 1)} \quad Nuc = 179$$

The thermal conductivity of water is

$$k_w := 0.68$$

The heat transfer coefficient is

$$H_{tfc} := \frac{Nuc \cdot k_w}{D_{hmc}} \quad H_{tfc} = 68966$$

Correcting for the cycle fraction

$$H_{tfc} := H_{tfc} \cdot (1 - f_{tRhc}) \quad H_{tfc} = 29242$$

This seems in line with Goodall for moderate swirl velocities but rather high for the highest ones. Careful measurements will be needed to confirm the assumptions. However the exit flow from the swirl-inducing jets will be going directly into the cold chamber there should be even greater enhancement. The heat transfer coefficient for non-condensing water without swirl would be the laminar value for parallel plates.

$$H_{tfcL} := \frac{8.23 \cdot k_w}{D_{hmc}} \quad H_{tfcL} = 3171.29$$

The ratio of swirl to non-swirl is

$$\frac{H_{tfc}}{H_{tfcL}} = 9.221$$

Condensing fin efficiency

$$\eta_{cf} := \frac{\tanh \left[\sqrt{\frac{2 \cdot H_{tfc}}{\lambda_1 \cdot t_{cf}} \cdot \left(L_{fc} + \frac{t_{cf}}{2} \right)} \right]}{\sqrt{\frac{2 \cdot H_{tfc}}{\lambda_1 \cdot t_{cf}} \cdot \left(L_{fc} + \frac{t_{cf}}{2} \right)}} \quad \eta_{cf} = 0.559$$

Thermal resistance of condensing

$$Z_{cf} := \frac{1}{A_{cf} \cdot H_{tfc} \cdot \eta_{cf}} \quad Z_{cf} = 9.128 \cdot 10^{-4}$$

The amount of heat that must flow out of the cold end to the cooling water Q_w is the incoming heat minus the useful work.

We can use the guessed efficiency

$$Q_w := Q \cdot (1 - \eta_{th}) \quad Q_w = 12102$$

Condensing temperature drop

$$\Delta T_{cf} := Q_w \cdot Z_{cf} \quad \Delta T_{cf} = 11.047$$

Now we can estimate the power needed to drive the rotor swirl at the cold end. The torque for the cold end of one module when the regenerator is fully in the cold end is given by

$$\tau := \frac{1}{2} \cdot 980 \cdot V_{swe}^2 \cdot A_{cf} \cdot \frac{D}{2} \cdot f_{ccw} \quad \tau = 0.64$$

This is equivalent to a pair of forces at the circumference of the rotor

$$f_{cR} := \tau \cdot \frac{1}{D} \quad f_{cR} = 16$$

The mean power to spin the cold end rotor for one thermal module is

$$p_{owswC} := \tau \cdot \omega \cdot \frac{1}{2} \quad p_{owswC} = 78.2$$

At high values of swirl velocity this can rise to several kilowatts .

Assume that the jet velocity is 2.5 times the regenerator peripheral speed. Assume 12 slit jets which are k_{je} of the value of D in width and k_{hj} high

$$k_{je} := .025$$

$$k_{hj} := 0.5$$

$$\text{Jet width } k_{je} \cdot D = 0.001$$

$$\text{Jet height } k_{hj} \cdot D = 0.02$$

$$\text{Jet flow rate } q_j := 12 \cdot k_{je} \cdot D \cdot k_{hj} \cdot D \cdot 2.5 \cdot V_{swe}$$

$$q_j \cdot 10^6 = 2934.117$$

$$\text{Jet stagnation pressure } P_j := \frac{1}{2} \cdot 985 \cdot (2.5 \cdot V_{swe})^2$$

$$P_j = 73604.433$$

$$\text{Jet force } F_j := P_j \cdot 12 \cdot k_{je} \cdot D \cdot k_{hj} \cdot D$$

$$F_j = 17.666$$

$$\text{Jet power } P_{owj} := q_j \cdot P_j$$

$$P_{owj} = 215.964$$

$$\text{Jet approach channel width } W_j := 12 \cdot k_{je} \cdot D$$

$$W_j = 0.012$$

The time for the jet flow to refill the internal volume of the cold end is

$$T_j := \frac{q_j}{0.25 \cdot \pi \cdot [D^2 \cdot L_{fb} + (D_{ci}^2 - D^2) \cdot N_{fc}]}$$

$$T_j = 0.098$$

The space between adjacent modules is

$$SM := D_f - D$$

$$SM = 0.044$$

The mean power to swirl the cold ends of the whole engine is

$$P_{owswC} := p_{owswC} \cdot NM$$

$$P_{owswC} = 312.967$$

The 0.1% yield stress of Hidurel 64H high strength copper alloy is given as 270 E6 N/M2. Taking 50 % of this for a fatigue margin gives 135 E6. Assume conservatively that there is no strength contribution from the cooling fins.

Present choice of cold copper working stress

$$\sigma_{cc} := 1.35 \cdot 10^8$$

Wall thickness of cooling section

$$tw := \frac{PH \cdot D_{ci}}{2 \cdot \sigma_{cc}}$$

$$tw = 0.007$$

This can be reduced by providing support for the outer water fins from a strong water jacket so that the conducting material is not stressed.

Set a new value for the wall thickness

$$tw := \frac{tw}{2}$$

$$tw = 0.0035$$

The thermal resistance of the cold wall is

$$Z_{cw} := \frac{\ln\left(\frac{D_{ci} + 2 \cdot tw}{D_{ci}}\right)}{2 \cdot \pi \cdot L_{fb} \cdot \lambda_1}$$

$$Z_{cw} = 4.9879 \cdot 10^{-4}$$

Cold wall temperature drop

$$\Delta T_{cw} := Q_w \cdot Z_{cw}$$

$$\Delta T_{cw} = 6$$

Transfer to the Cooling Water

Outer water fin length

$$L_{wf} := t_{cf} \cdot k_{wf}$$

$$L_{wf} = 0.0037$$

Outer water fin diameter

$$D_{co} := D_{ci} + 2 \cdot tw + 2 \cdot L_{wf}$$

$$D_{co} = 0.062$$

Outer water fin area

$$A_{wf} := \frac{\pi}{4} \cdot [D_{co}^2 - (D_{ci} + 2 \cdot tw)^2] \cdot 2 \cdot N_{fc}$$

$$A_{wf} = 0.08$$

The hydraulic mean diameter of channel between the water fins is

$$D_{hmw} := \frac{4 \cdot L_{wf} \cdot t_{cf}}{2 \cdot L_{wf} + t_{cf}}$$

$$D_{hmw} \cdot 10^6 = 1764.706$$

Note that a lost wax casting could use hyperbolic rather than rectangular fin sections for improved performance and lower wall stress.

Now we calculate the heat transfer to the cooling water. An empirical expression for fin to cold water heat transfer coefficient in pipes is given in Goodall page 282. Assume that the water jacket flow velocity tracks the hot end rotor swirl with a factor k_{wfv} . The water fin velocity will be

$$k_{wfv} = 0.5$$

$$V_{wf} := V_{swe} \cdot k_{wfv}$$

$$V_{wf} = 2.445$$

$$H_{tfw} := 1063 \cdot \left[1 + 0.00293 \cdot (TCW + 273) \cdot V_{wf}^{0.8} \cdot \frac{1}{D_{hmw}^{0.2}} \right]$$

$$H_{tfw} = 8486$$

Cooling water fin efficiency

$$\eta_{wf} := \frac{\tanh\left[\sqrt{\frac{2 \cdot H_{tfw}}{\lambda_1 \cdot t_{cf}}} \cdot \left(L_{wf} + \frac{t_{cf}}{2}\right)\right]}{\sqrt{\frac{2 \cdot H_{tfw}}{\lambda_1 \cdot t_{cf}}} \cdot \left(L_{wf} + \frac{t_{cf}}{2}\right)}$$

$$\eta_{wf} = 0.797$$

Thermal resistance to water

$$Z_{wf} := \frac{1}{A_{wf} \cdot H_{tfw} \cdot \eta_{wf}}$$

$$Z_{wf} = 1.86 \cdot 10^{-3}$$

Temperature drop to water

$$\Delta T_{wf} := Q_w \cdot Z_{wf}$$

$$\Delta T_{wf} = 22.478$$

If we stress the outer water jacket at 200 E6 its wall thickness will be

$$t_j := \frac{PH \cdot D_{co}}{2 \cdot 200 \cdot 10^6} \quad t_j = 0.006$$

The outside diameter of the outer jacket is

$$D_{oj} := D_{co} + 2 \cdot t_j \quad D_{oj} = 0.074$$

Now we calculate temperatures upwards from the cooling water at

Water fin temperature	$T_{wf} := TCW + \Delta T_{wf}$	TCW = 55
Condensing fin root	$T_{cf} := T_{wf} + \Delta T_{cf}$	T _{wf} = 77.5
Condensing fins	$T_{cs} := T_{cf} + \Delta T_{cf}$	T _{cf} = 83.5
		T _{cs} = 94.6

Volume of cooling water/sec for the whole engine

$$VW := \frac{Q_w}{(T_{wf} - TCW) \cdot 4185000} \cdot NM \quad VW \cdot 10^3 = 0.5146$$

Water velocity in a 25mm hose

$$Vel_w := \frac{VW}{0.25 \cdot \pi \cdot 0.025^2} \quad Vel_w = 1.048$$

We need to calculate the power to drive the cooling water through the fins of the cold end jacket. Adjacent modules share a common steel casing for the copper cooling block. The flow for two adjacent modules enters at a point 25% up from the bottom of the casing and is fed to the bottom half of the fins on each module. It flows 180 degrees round each of the two copper blocks to a drill way which connects to the top half of the fins. It then flows 180 degrees back to a second drill way and leaves the steel jacket at a point 75% up from the bottom.

The cold water pump must force water round the corners and between the fins of the cold-end block. The cross section of the flow passage and the flow velocity vary at points round the loop.

We increase the minimum volume of cooling water **VW** calculated above

$$VW := VW \cdot 3 \quad VW = 0.002$$

The flow through a hose into one jacket pair is

$$V_h := \frac{VW \cdot 2}{NM} \quad V_h \cdot 10^6 = 772$$

Hose length $L_h := 1$ Hose diameter $D_h := .025$

Water velocity

$$Vel_h := \frac{V_h}{0.25 \cdot \pi \cdot D_h^2} \quad Vel_h = 1.572$$

Reynolds number

$$R_{nh} := \frac{Vel_h \cdot D_h \cdot 980}{.0005} \quad R_{nh} = 77052$$

The friction coefficient for a straight pipe flow for this Reynolds number is

$$f_{ch} := \left(4 \cdot \log \left(\frac{R_{nh}}{4.53 \cdot \log(R_{nh}) - 3.82} \right) \right)^{-2} \quad f_{ch} = 0.005$$

The pressure drop along two hoses is

$$\Delta Ph_1 := \frac{4 \cdot f_{ch}}{D_h} \cdot \frac{1}{2} \cdot 980 \cdot Vel_h^2 \cdot 2 \quad \Delta Ph_1 = 1845$$

The flow goes divided into two paths round three corners each with a loss coefficient of 0.5. Pressure drop for the double journey is

$$\Delta Ph_2 := \frac{1}{2} \cdot 980 \cdot Vel_h^2 \cdot 0.5 \cdot 3 \cdot 2 \quad \Delta Ph_2 = 3635$$

The flow splits into many paths between the fins of the bottom half of the fin block. Flow goes both sides. The volume flow between each fin is

$$V_f := \frac{VW}{NM \cdot 2 \cdot 0.5 \cdot N_{fc}} \quad V_f \cdot 10^6 = 6.654$$

The velocity of the water is

$$V_{elf} := \frac{V_f}{L_{wf} \cdot t_{cf}} \quad V_{elf} = 1.774$$

The hydraulic mean diameter of the passage is

$$D_{hmw} = 0.002$$

Reynolds number referred to the hydraulic mean diameter is

$$R_{nf} := \frac{V_{elf} \cdot D_{hmw} \cdot 980}{.0005} \quad R_{nf} = 6138$$

The friction coefficient is

$$f_{cf} := \left(4 \cdot \log \left(\frac{R_{nf}}{4.53 \cdot \log(R_{nf}) - 3.82} \right) \right)^{-2} \quad f_{cf} = 0.009$$

The pressure drop along both upper and lower halves of the block is

$$\Delta Ph_3 := \frac{4 \cdot f_{cf}}{D_{hmw}} \cdot \frac{1}{2} \cdot 980 \cdot Vel_h^2 \cdot \frac{\pi \cdot D_{co}}{2} \quad \Delta Ph_3 = 2359$$

The pressure drop of the entire cooling water path is

$$\sum \Delta Ph = 7839$$

The power to pump the cooling water is

$$Pow_c := VW \cdot \sum \Delta Ph \quad Pow_c = 12.1$$

Creep life Calculations

Now we can calculate temperatures either side of the preset choice for the middle of the Inconel slices.

The mid Inconel temperature is **defined** as

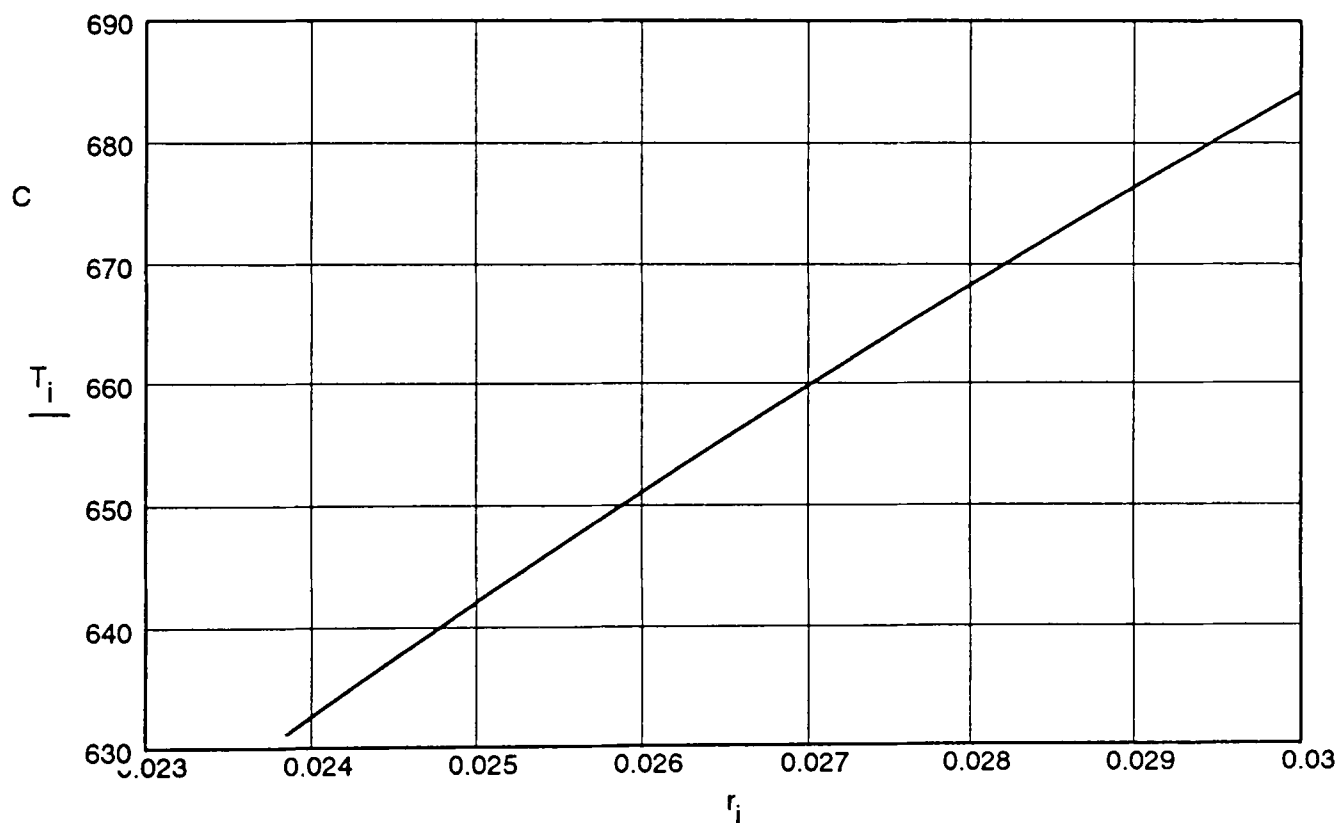
The temperature drop across the wall is	$\Delta T_{hw} := Q \cdot Z_{hw}$	$\Delta T_{hw} = 53.011$
Flame fin root	$T_{fr} := T_{ffb}$	$T_{fr} = 684$
Flame fin hottest spot	$T_{ft} := T_{fo}$	$T_{ft} = 716$
The inside Inconel temperature	$T_{iinc} := T_{fr} - Q \cdot Z_{hw}$	$T_{iinc} = 631$
The inside temp of sealing tube	$T_{sr} := T_{iinc} - Q \cdot (Z_{tube} + Z_{air})$	$T_{sr} = 631.2$
The steam temperature	$T_{st} := T_{sr} - \Delta T_{sf}$	$T_{st} = 549$

The stress and temperature pattern of the Inconel slices is of crucial importance. We plot the values at **N** points through the wall thickness using the stress expression 2-55 given in Shigley page 76 and the temperature gradient expression from Incropera table 3.3 page 107

$$N := 10 \quad i := 0..N \quad r_i := \frac{D_{ii}}{2} + r_{inc} \cdot \frac{i}{N}$$

The temperature at the *i*th point is

$$T_i := T_{fr} + \Delta T_{hw} \cdot \frac{\ln\left(\frac{r_i}{0.5 \cdot D_{io}}\right)}{\ln\left(\frac{D_{io}}{D_{ii}}\right)}$$



The radial stress at the *l*th point is

$$\sigma_{r_i} := \frac{PH \cdot \frac{t_{inc} + t_{cu}}{t_{inc}} \cdot \left(\frac{D_{ii}}{2}\right)^2}{\left(\frac{D_{io}}{2}\right)^2 - \left(\frac{D_{ii}}{2}\right)^2} \left[1 - \frac{\left(\frac{D_{io}}{2}\right)^2}{\left(r_i\right)^2} \right]$$

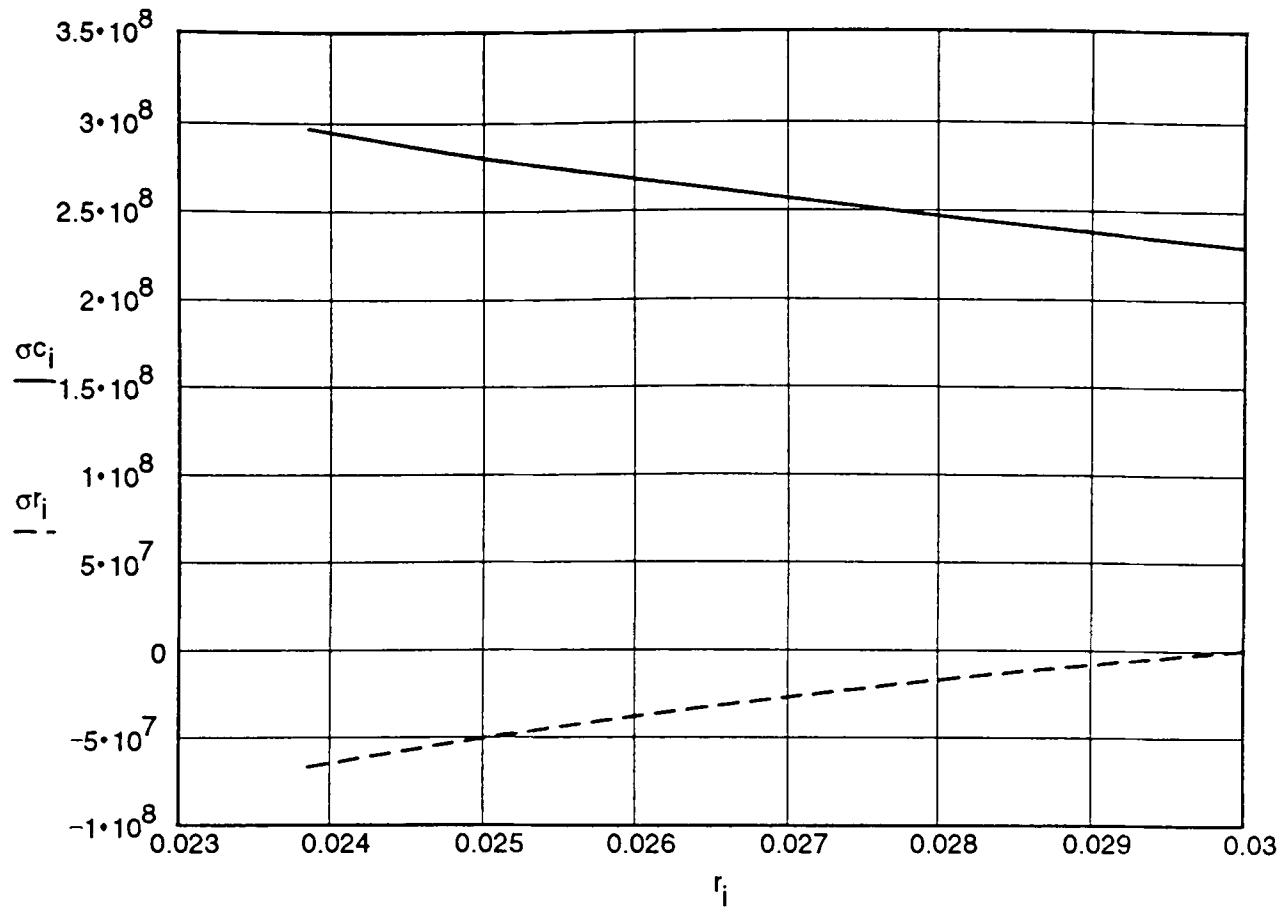
The tangential stress at the *l*th point is

$$\sigma_{t_i} := \frac{PH \cdot \frac{t_{inc} + t_{cu}}{t_{inc}} \cdot \left(\frac{D_{ii}}{2}\right)^2}{\left(\frac{D_{io}}{2}\right)^2 - \left(\frac{D_{ii}}{2}\right)^2} \left[1 + \frac{\left(\frac{D_{io}}{2}\right)^2}{\left(r_i\right)^2} \right]$$

The maximum combined stress at the *l*th point is

$$\sigma_{c_i} := \frac{1}{2} \cdot (\sigma_{t_i} + \sigma_{r_i}) + \sqrt{\frac{1}{4} \cdot (\sigma_{t_i} - \sigma_{r_i})^2}$$

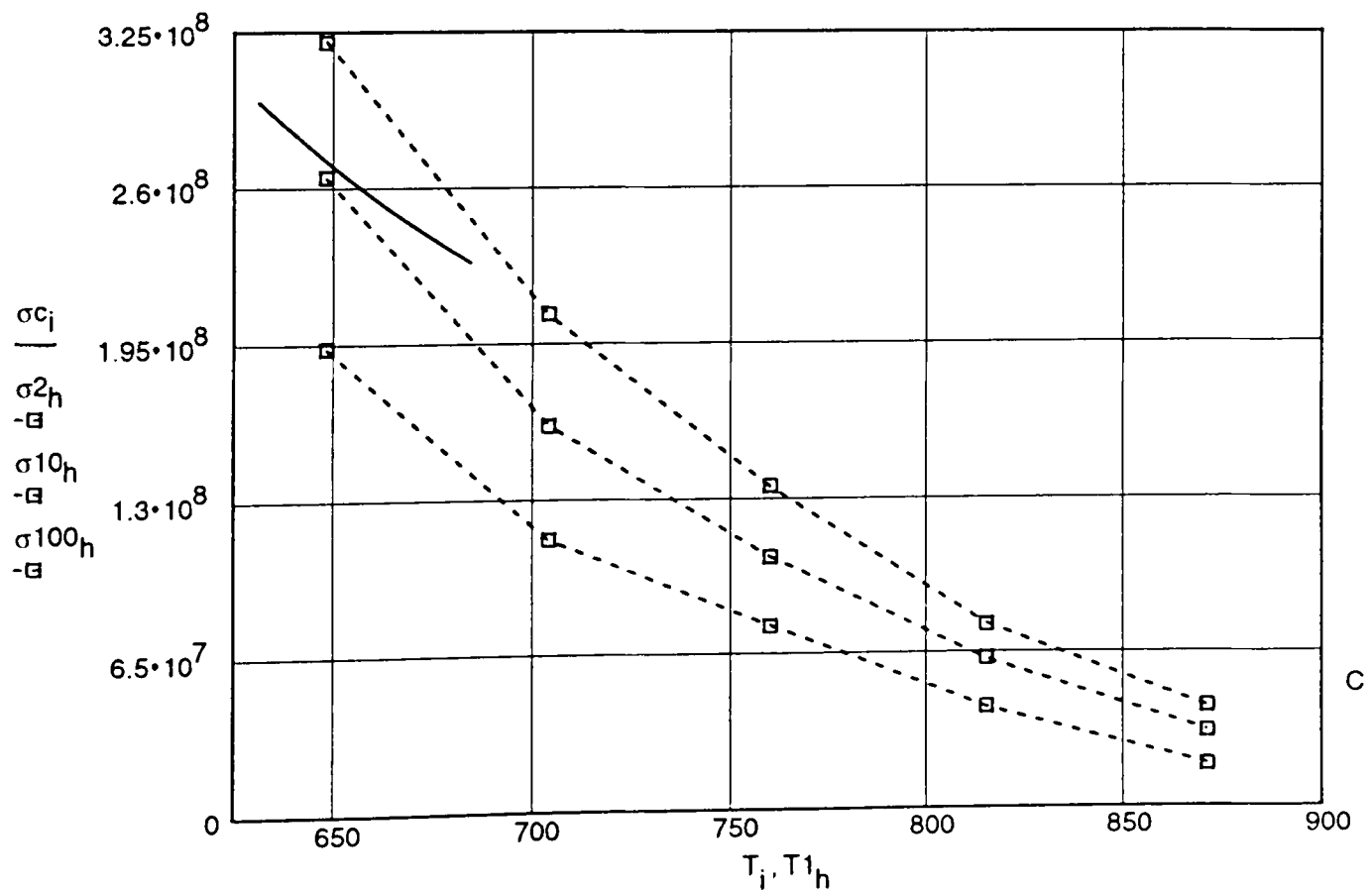
Plotting the three against radius:



We can also plot temperature against combined stress along the radial thickness of the Inconel disks and compare the values with data for 2000 and 10,000 and 100,000 hour rupture life for Inconel 625.

$h := 1..5$

$\sigma_{2h} :=$	$\sigma_{10h} :=$	$\sigma_{100h} :=$	$T_{1h} :=$
$321 \cdot 10^6$	$264 \cdot 10^6$	$193 \cdot 10^6$	648
$207 \cdot 10^6$	$161 \cdot 10^6$	$113 \cdot 10^6$	704
$135 \cdot 10^6$	$105.5 \cdot 10^6$	$76.7 \cdot 10^6$	760
$76.7 \cdot 10^6$	$62 \cdot 10^6$	$42 \cdot 10^6$	815
$42 \cdot 10^6$	$32 \cdot 10^6$	$18 \cdot 10^6$	871



Heat flux	$Q = 27000$	Inconel stress	$\sigma_{ir} = 2.957 \cdot 10^8$
Pressure max	$PH = 4 \cdot 10^7$	Mid Inc temp	$T_{mw} = 658$

It is useful to move the top left section of the control panel to this screen and adjust values for heat flux Q , maximum pressure PH , Inner Inconel stress σ_i and mid Inconel temperature T_{mw} . The heat flow Q tilts the curve of the stress temperature line. It is parallel to the material lines at about half maximum heat flux. At low heat flux the inner radius of the disk is in trouble but, at high flux, the problem is the outer radius. Values suitable for the required life and load pattern are easily identified. Values for pressure and temperature can be adjusted on an instant by instant basis by the engine management system.

Note that the flame fins have only their own weight to support. An external cage can help them. The Copper Development Association publish data for the hot strength of tough pitch arsenical copper. This falls more or less linearly from 230 E6 at 0 C to zero at 900 C. The strength at temperature T can be expressed as

$$\sigma_{cuH}(T) := \frac{-230 \cdot 10^6}{900} \cdot T + 230 \cdot 10^6$$

The copper strength at the hottest spot is

$$\sigma_{cuH}(T_{ft}) = 4.702 \cdot 10^7$$

We now have the temperature range for an ideal heat engine working between the two calculated temperatures. Its thermal efficiency, ignoring ancillary losses, will be

$$\eta_{th2} := \frac{T_{st} - T_{cs}}{T_{st} + 273}$$

$$\eta_{th2} = 0.553$$

The power out before ancillary losses is

$$Pow := Q \cdot NM \cdot \eta_{th2}$$

$$Pow = 59677.836$$

Mid-wall metal temperature at the hot-end

$$T_{mw} := \frac{T_{fr} + T_{iinc}}{2}$$

$$T_{mw} = 657.671$$

Maximum allowable heat-flow considering 800 C at the fin-base

$$Q_{max} := \frac{800 - T_{iinc}}{Z_{hw}}$$

$$Q_{max} = 85992.678$$

Exhaust Heat Recovery

The heat in the combustion gases is too precious to throw away. We can recover much of it with a heat exchanger warming up the incoming air. In this analysis the terms in and out refer to the engine rather than the heat exchanger. We take in cold air at temperature T_{ic} . It reaches the combustion chamber at T_{ih} . The outgoing combustion gases leave the flame fins at temperature T_{oh} . We reject heat to the atmosphere at temperature T_{oc} . The specific heat of air at this temperature is 1.063 kJ/kgK very little different from the low temperature value. (Incropera page A150. The heat exchanger will have counter-flow conditions with equations given in Incropera section 11.3.2.

Present choices of temperatures cold in and hot out are

$$T_{ic} = 25$$

$$T_{oh} = 769.061$$

The heat exchanger can be made from a scroll of two interleaved sheets of material of width kw_{ex} times L_{fb} . The gap between the sheets is defined by dimples or a zig-zag separating spring.

Width of heat exchanger scroll is set relative to fin block length by

$$W_{ex} := L_{fb} \cdot kw_{ex}$$

$$kw_{ex} := 1.929$$

$$W_{ex} = 0.224$$

Present choice of exhaust heat exchanger gap

$$g_{ex} = 0.014$$

Present choice of number of double wraps

$$N_{lex} = 10$$

Count up

$$i := 0..N_{lex}$$

The length of the inner layer is

$$L_{inex} := (NM \cdot mod + .05) \cdot 2 + 2.2 \cdot mod$$

$$L_{inex} = 0.957$$

The length of each successive layer increases by $2 \pi g_{ex}$ so that the total length

$$L_{ex} := N_{lex} \cdot L_{inex} + \sum_{i=0}^{N_{lex}} i \cdot 2 \cdot \pi \cdot 2 \cdot g_{ex}$$

$$L_{ex} = 19.417$$

The extra thickness round the outside of the engine block will be

$$y_{ex} := N_{lex} \cdot g_{ex}$$

$$y_{ex} = 0.143$$

The area of both sheets of the heat exchanger material is

$$A_{ex} := 2 \cdot L_{ex} \cdot W_{ex}$$

$$A_{ex} = 8.69$$

The cross-sectional area of the heat exchanger passage is

$$A_{pex} := W_{ex} \cdot g_{ex}$$

$$A_{pex} = 0.003$$

The hydraulic mean diameter is

$$D_{hmex} := \frac{4 \cdot W_{ex} \cdot g_{ex}}{2 \cdot (W_{ex} + g_{ex})}$$

$$D_{hmex} = 0.027$$

With a thickness of 0.25 mm and 10% extra for ends the mass of the exchanger surfaces will be

$$M_{12} := A_{ex} \cdot 0.00025 \cdot 8000 \cdot 1.1$$

$$M_{12} = 19.118$$

The fluid properties midway (450 C) from Incropera page A15 are

$$\rho_{ex} := 0.77$$

$$k_{ex} := 0.0373$$

$$\mu_{ex} := 25 \cdot 10^{-6}$$

$$Pr_{ex} := 0.686$$

The midway volume of gas per engine is

$$VG := \frac{MG \cdot NM}{\rho_{ex}}$$

$$VG = 0.122$$

The midway velocity is

$$V_{ex} := \frac{VG}{A_{pex}}$$

$$V_{ex} = 38.305$$

Reynolds number is

$$R_{noex} := \frac{V_{ex} \cdot D_{hmex} \cdot \rho_{ex}}{\mu_{ex}}$$

$$R_{noex} = 31611.304$$

The Nusselt number is
$$Nu_{ex} := 0.023 \cdot R_{noex}^{\frac{4}{5}} \cdot Pr^{\frac{1}{3}}$$
 $Nu_{ex} = 92.144$

For turbulent flow the heat transfer coefficient is
$$H_{tfex} := \frac{Nu_{ex} \cdot k_{ex}}{D_{hmex}}$$
 $H_{tfex} = 128.276$

For a 0.25 mm stainless steel sheet with thermal conductivity 20 W/mK the heat transfer coefficient of the bulk material is very much higher:

$$H_{tfss} := \frac{20}{0.00025} \quad H_{tfss} = 80000$$

Refer to Incropera page 618 for explanation of the NTU method used for heat exchanger calculations when only two of the temperatures are known.

The heat capacity rates (mass flow times specific heat) are close so

$$C_r := 0.9 \quad C_{min} := MG \cdot NM \cdot 1030 \quad C_{min} = 96.872$$

The NTU value (page 618 equation 11.25)
$$NTU := \frac{H_{tfex} \cdot A_{ex}}{C_{min}} \quad NTU = 12$$

The effectiveness (equ 11.30a)
$$\epsilon := \frac{1 - \exp(-NTU \cdot (1 - C_r))}{1 - C_r \cdot \exp(-NTU \cdot (1 - C_r))} \quad \epsilon = 0.956$$

From equ 11.39 the ideal
$$q_{max} := C_{min} \cdot (T_{oh} - T_{ic}) \quad q_{max} = 72079$$

The actual heat transferred is
$$q_{tr} := q_{max} \cdot \epsilon \quad q_{tr} = 68890$$

The heat lost to the outside air is
$$W_{ha} := q_{max} - q_{tr} \quad W_{ha} = 3189$$

The output temperature is
$$T_{oc} := T_{ic} + \frac{W_{ha}}{MG \cdot NM \cdot 1030} \quad T_{oc} = 57.918$$

The feed temperature to the combustion chamber is
$$MG = 0.024$$

$$T_{ih} := T_{ic} + \frac{q_{tr}}{MG \cdot NM \cdot 1030} \quad T_{ih} = 736.143$$

Heat Exchanger Pressure Drop

Calculation of the pressure drop in non-circular passages is explained in Ward-Smith section C4 using a friction coefficient f_c calculated from section C3 equation C117 and the hydraulic mean diameter of the passage D_{hmex} calculated above.

$$f_c := \left(4 \cdot \log \left(\frac{R_{noex}}{4.53 \cdot \log(R_{noex}) - 3.82} \right) \right)^{-2} \quad f_c = 0.006$$

$$VGC = 0.102$$

$$V_{cld} = 0.019$$

The pressure drop for a one-way trip through the heat exchanger is

$$\Delta P_{ex} := \frac{4 \cdot f_c}{D_{hmex}} \cdot \frac{1}{2} \cdot \rho_{ex} \cdot V_{ex}^2 \cdot L_{ex} \quad \Delta P_{ex} = 9509.104$$

If this is too high it may affect the assumptions on gas density of the flame and risk distortion of the heat exchanger materials.

The double-trip pumping power including the pressure drop through the fin block is

$$W_{expu} := (2 \cdot V_{cld} \cdot \Delta P_{ex} + VGC \cdot \Delta P_p) \cdot NM \quad W_{expu} = 1571$$

Small values of gap improve heat transfer at the expense of pumping power. A larger number of wraps combined with bigger gaps can help both at the expense of bulk. The ratio of pumping loss to heat loss should be chosen to reflect the lower value of thermal energy.

The ratio of heat loss to pumping power is
$$\frac{W_{expu}}{W_{ha}} = 0.493$$

The combined heat loss and pumping power is
$$W_{extot} := W_{expu} + W_{ha} \quad W_{extot} = 4760.273$$

The density at T_{ih} is
$$\rho_a := 0.3482 \cdot \frac{1000}{T_{ih} + 273} \quad \rho_a = 0.23$$

The stream velocity in the input flow at temperature T_{ih} is

$$V_{st} := MG \cdot \frac{1}{\rho_a} \cdot \frac{1}{A_{pex}} \quad V_{st} = 21.37$$

The transit time for the exhaust is

$$T_{tex} := \frac{L_{ex}}{V_{st}} \quad T_{tex} = 0.909$$

Increasing this time, perhaps with a enlargement in the outlet passage part way through the heat exchanger, will reduce NOX production by giving longer time for the reverse dissociation.

Noise Prediction

Goodall page 45 reports the work of Erskine on the sound level of an escaping jet in terms of velocity, exit area and density difference. Converting the area of the exhaust outlet to a diameter d_{ex} gives

$$d_{ex} := \sqrt{\frac{4 \cdot W_{ex} \cdot g_{ex}}{\pi}} \quad d_{ex} = 0.064$$

$$dB := 60 \cdot \log(V_{ex}) + 20 \cdot \log(d_{ex}) + 20 \cdot \log\left(\frac{T_{oc} + 273}{T_{ic} + 273}\right) - 4 \quad dB = 67.991$$

$$si_{ex} = 4.5$$

If the exit area is increased by a silencer with area ratio

This will change the diameter and velocity to
$$d_{ex} := si_{ex} \cdot d_{ex} \quad d_{ex} = 0.287$$

$$\text{Velex} := \frac{\text{Velex}}{\text{siex}}$$

$$\text{Velex} = 8.512$$

The modified noise prediction is

$$\text{dB} := 60 \cdot \log(\text{Velex}) + 20 \cdot \log(\text{dex}) + 20 \cdot \log\left(\frac{\text{ToC} + 273}{\text{Tic} + 273}\right) - 4 \quad \text{dB} = 41.9$$

Regenerator

Now we can consider the regenerator-displacer. Its diameter is **DR**. Its length is set by the factor **kLR**. Its solidity is set by the factor **ksR**. Its core diameter is set by **kdR**. Its density is γ_R . It must travel the full length of the fin block **Lfb**.

$$\begin{aligned} D = 0.04 & \quad \text{kLR} = 6 & \quad \text{ksR} = 0.6 & \quad \text{kdR} = 0.29 & \quad \gamma_R := 8000 \\ \text{The diameter} & & \text{DR} := D \cdot 0.956 & & \text{DR} = 0.038 \\ \text{The body length} & & \text{LR} := D \cdot \text{kLR} & & \text{LR} = 0.24 \\ \text{The flow area} & \quad \text{Aro} := \frac{\pi}{4} \cdot \left[\text{DR}^2 - (\text{kdR} \cdot \text{DR})^2 \right] \cdot (1 - \text{ksR}) & & & \text{Aro} \cdot 10^6 = 421 \end{aligned}$$

$$\begin{aligned} \text{The blocked area} & \quad \text{Arb} := \frac{\pi}{4} \cdot \left[\text{DR}^2 - (\text{kdR} \cdot \text{DR})^2 \right] \cdot \text{ksR} & & & \text{Arb} \cdot 10^6 = 631 \end{aligned}$$

$$\begin{aligned} \text{Regenerator mass} & \quad \text{MR} := \frac{\pi}{4} \cdot \left(\text{DR}^2 - \text{kdR} \cdot \text{DR}^2 \right) \cdot \text{ksR} \cdot \text{LR} \cdot \gamma_R & & & \text{MR} = 0.939 \end{aligned}$$

$$\begin{aligned} \text{The present choice of regenerator shim thickness is} & & & & \text{tsR} \cdot 10^6 = 100 \end{aligned}$$

$$\begin{aligned} \text{The gap between layers will be defined by dimples and will be} & & & & \\ \text{tRg} := \text{tsR} \cdot (1 - \text{ksR}) & & & & \text{tRg} \cdot 10^6 = 40 \end{aligned}$$

The surface area of **both sides** of the regenerator shim is

$$\text{AsR} := \frac{\text{MR}}{\gamma_R \cdot \text{tsR}} \cdot 2 \quad \text{AsR} = 2.349$$

$$\begin{aligned} \text{The unwrapped length of the shim is} & \quad \text{LuwR} := \frac{\text{AsR}}{\text{LR}} & & & \text{LuwR} = 9.785 \end{aligned}$$

$$\begin{aligned} \text{The open volume inside the regenerator} & \quad \text{VoR} := \text{Aro} \cdot \text{LR} & & & \text{VoR} \cdot 10^6 = 100.988 \end{aligned}$$

The hot chamber volume increases from its starting value by the regenerator stroke times the cross-sectional area of the regenerator. The total volume change is

$$\Delta V := \text{Lfb} \cdot \left(1 - \text{kdR}^2 \right) \cdot \frac{\pi}{4} \cdot \text{DR}^2 \quad \Delta V \cdot 10^6 = 122.028 \text{ ml}$$

Assume that because of slow movement, the pressure and temperature of the hot chamber stay constant. The increase in mass of working fluid in the hot chamber is this volume times the steam density calculated above

$$\rho_s = 143.2 \quad \Delta \text{MH} := \Delta V \cdot \rho_s \quad \Delta \text{MH} = 0.017$$

The increase in mass must have flowed through the regenerator from the cold end. But movement of the regenerator reduced the cold chamber volume by the same amount ΔV . This would have had a mass depending on the cold density of the fluid. If the cooling system reduces this to 125 C and the pressure is still **PH** the cold density from steam tables will be

$$\begin{aligned} \text{The mass moving out of the cold end is} & \quad \Delta \text{MC} := \Delta V \cdot \rho_{\text{chp}} & & & \rho_{\text{chp}} := 976 \\ & & & & \Delta \text{MC} = 0.119 \end{aligned}$$

$$\begin{aligned} \text{The difference in masses is} & & & & \Delta \Delta \text{M} = 0.102 \\ \Delta \Delta \text{M} := \Delta \text{MC} - \Delta \text{MH} & & & & \end{aligned}$$

This mass difference must flow out to the isolator at constant pressure of **PH**. Its volume will be

$$\text{VL2} := \Delta \Delta \text{M} \cdot \frac{1}{\rho_{\text{chp}}} \quad \text{VL2} \cdot 10^6 = 104.1$$

This equivalent to the piston motion for a piston assisted pressure-rise and regenerator assisted pressure-fall cycle. For a piston assisted pressure-rise and pressure-fall cycle the piston motion is divided into two parts :

$$\text{Part of isolator-piston motion which maintains high-level of cycle pressure :} \quad \text{PstnA} = 0.073$$

$$\text{Part of isolator-piston motion which reduces cycle pressure to } \mathbf{P_{\text{expand}}} : \quad \text{PstnB} = 0.071$$

(These values are calculated from the time-domain model)

The initial work done by one thermal module in one stroke in piston assisted pressure-rise and pressure-fall cycle is :

$$\text{W1} := \left(\frac{\Delta V}{\text{Lfb}} \right) \cdot \left[\text{PstnA} \cdot \text{PH} + \text{PstnB} \cdot \left(\frac{\text{PH} + \text{P}_{\text{expand}}}{2} \right) \right] \quad \text{W1} = 4864.172$$

[In a piston assisted pressure-rise and regenerator assisted pressure-fall cycle this would be, $\text{W1} = \text{VL2} \cdot \text{PH}$]

We now move the regenerator back to the hot chamber so as to send the remaining working fluid to the cold end. The temperature at the hot end stays the same because heat can still flow from the steam fins. The pressure falls to **PL**. The density in the hot end is therefore

$$\rho_{\text{slp}} := 2.65$$

The dead volume of the hot end consists of the gaps between the steam fins. It is

$$VH2 := \frac{\pi}{4} \cdot (Dii^2 - D^2) \cdot tinc \cdot Nff \quad VH2 \cdot 10^6 = 36.755$$

The mass at the hot end is

$$MH2 := VH2 \cdot \rho slp \quad MH2 = 9.74019 \cdot 10^{-5}$$

We draw energy from the hydraulic machine to raise the pressure to PH. The hot end density will be

$$\rho shp := \rho s \quad \rho shp = 143.2$$

The mass at the hot end will be

$$MH3 := VH2 \cdot \rho shp \quad MH3 = 0.005$$

Some extra mass had to be pumped into the regenerator defined as $\Delta Mreg$ (Value may be supplied from MxX. The cold volume needed will be

$$VC3 := \frac{MH3 - MH2 + \Delta Mreg}{950} \quad VC3 \cdot 10^6 = 52.49$$

The work to do this is about $PL := 1 \cdot 10^6$ $W2 := \frac{(PH + PL)}{2} \cdot VC3$ $W2 = 1076.055$

This is very small compared with the value of the main work stroke **W1**. Large amounts of energy flow into and out of the regenerator but if it ends at the state as it began then it can be ignored.

The work from one cycle of the whole engine is

$$Weng := (W1 - W2) \cdot \frac{NM}{Fnp} \quad \text{For, } Fnp = 0.98 \quad Weng = 15462$$

Where Fnp is a correction factor, compensating non-linearity of pressure variation present in real cycles.

The vale of this correction factor is estimated from the results of the time-domain model.

The engine speed to produce the calculated power output is

$$cps := \frac{Pow}{Weng} \quad cps = 3.86$$

Hence the engine speed in revs/min $Engrpm := cps \cdot 60$ $Engrpm = 231.583$

The isolator will consist of an elastomeric tube fitting round two round bars of diameter **dib** inside a long hole of diameter **di** bored in the base block. The overall length will be

$$Li := NM \cdot mod - .05 \quad Li = 0.286$$

The available area is reduced by the presence of the bars and bladder by a factor

$$kbr := 0.95$$

Choose a bar diameter $dib := D \cdot \frac{10}{45}$ $dib = 0.009$

The hole diameter is set by the need to accept all the liquid from one stroke of half the thermal modules with a margin of 20% leaving room for the bars.

$$di := \sqrt{\left(\frac{NM \cdot 0.5 \cdot VI2}{kbr \cdot Li} \cdot \frac{4}{\pi} + 2 \cdot \frac{\pi}{4} \cdot dib^2 \right) \cdot 1.2} \quad di = 0.036$$

We will now construct an instant-by-instant analysis of pressures and movement of regenerator and isolator. First we establish controls for the times of movement.

Working period $per := \frac{1}{cps}$ $per = 0.259$

Chosen fraction of time for regenerator is moving in either direction $ftRm = 0.924$

Chosen fraction time moving the regenerator from cold to hot $ftRhc = 0.576$

Define the starting point of the cycle as the beginning of the movement of the regenerator towards the cold chamber. The acceleration forces are small compared to drag forces so we can assume instantaneous change to constant velocity.

Time regenerator going hot to cold $tRhc := per \cdot ftRm \cdot ftRhc$ $tRhc = 0.138$

Time regenerator going cold to hot $tRch := per \cdot ftRm \cdot (1 - ftRhc)$ $tRch = 0.102$

Calculations relating to the fluid in the regenerator are difficult because of the large temperature gradient and consequent change of conditions along the length. However many can be avoided if the conditions at the end of a cycle are the same as those at the start. We also ignore the passage from the cold chamber to the isolator.

We now want to calculate the forces on the regenerator. But there is the problem that the temperature of the working fluid changes by a large amount as it moves through the regenerator. This will change both its density and viscosity. Assume that the temperature change is linear and that the pressure drop through the passage is small compared to the standing pressure. Assume that the cold pressure has been raised to **PH** by work from the hydraulic machine. Split the length of the regenerator into **NLR** layers number by the range **i**.

$$NLR := 10 \quad i := 1..NLR \quad \text{From the Cold-end}$$

The temperature at the centre of the **ith** layer is

$$TL_i := TS + \frac{i - 0.5}{NLR} \cdot (TH - TS)$$

Check some values over the range TH down to TS

$$TH = 548$$

$$TL_{NLR} = 525.35$$

$$TL_1 = 117.65$$

$$TS = 95$$

Estimates of viscosity depend on whether the fluid is liquid water, saturated steam or supercritical steam. The viscosity of a liquids fall rapidly with temperature but with an ideal gas, viscosity rises with the square root of absolute temperature. O'Connor page 5-7 gives viscosity data for water and steam at various pressures up to 200 bar. The trend suggests strongly that as pressure increases the behaviour becomes more like that of the liquid. See also page 5-78 for the lower pressure temperature behaviour. The worst case is the high pressure one. We will assume that water behaviour applies to the lower temperatures and that trends continue above 650 K as if the steam were behaving like a gas with viscosity rising with the square root of temperature. Viscosity values up to 647 K are taken from Incropera page A 23.

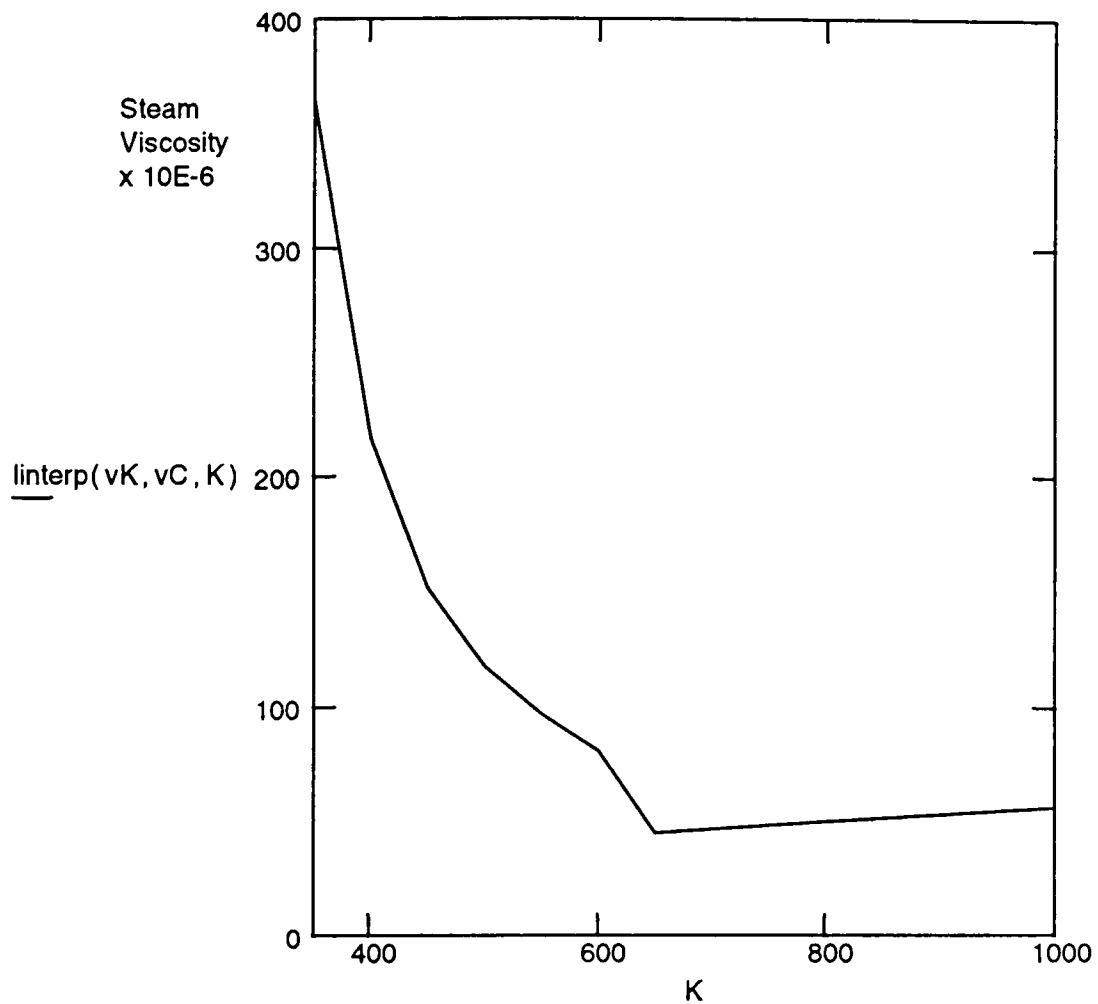
$$vK_j :=$$

$$vC_j :=$$

$$K := 300, 350 .. 1000$$

$$j := 0 .. 30$$

350	365
375	274
400	217
430	173
450	152
470	136
500	118
530	104
550	97
570	91
600	81
620	72
640	59
645	54
647	45
725	47.6
750	48.45
775	49.25
800	50
825	51
850	51.6
875	52.3
900	53
1000	56



$$\mu(T) := \text{linterp}(vK, vC, T) \cdot 10^{-6}$$

$$\mu(320) \cdot 10^6 = 474.2$$

We now need to convert back to centigrade from absolute and define an interpolated value for the ith layer as follows.

$$\mu_i := \mu(TL_i + 273)$$

Maximum and minimum values are

$$\mu_{NLR} \cdot 10^6 = 49.95$$

$$\mu_1 \cdot 10^6 = 238.318$$

A spot test value is

$$\mu_5 \cdot 10^6 = 90.383$$

The length of each layer

$$LL := \frac{LR}{NLR}$$

$$LL = 0.024$$

The specific volume (m³/kg) at each layer is proportional to the absolute temperature at the layer. Interpolate the values at 600 bar and 450 C from Rogers and Mayhew page 9.

$$vol_i := 0.209 \cdot 10^{-2} \cdot \left(\frac{TL_i + 273}{450 + 273} \right)$$

$$vol_{NLR} = 0.00231$$

$$vol_1 = 0.00113$$

The densities are

$$\rho_i := \frac{1}{vol_i}$$

$$\rho_{NLR} = 433.31$$

$$\rho_1 = 885.532$$

We make the initial assumption that the mass flow into the regenerator is the same at each layer and depends on its velocity, the cold density and the blocked area of the regenerator. (The actual conditions may be more complicated.)

$$\dot{m} := \frac{Lfb}{tRhc} \cdot \rho_1 \cdot A_{rb}$$

$$\dot{m} = 0.47$$

The volume flow at each layer is mdot times the specific volume

$$qdot_i := mdot \cdot vol_i$$

$$qdot_{NLR} \cdot 10^6 = 1085$$

$$qdot_1 \cdot 10^6 = 531$$

The velocity at each layer is volume divided by the open area

$$vel_i := \frac{qdot_i}{Aro}$$

$$vel_{NLR} = 2.579$$

$$vel_1 = 1.262$$

The Reynolds number at each layer is

$$Rno_i := \frac{vel_i \cdot \rho_i \cdot tRg}{\mu_i}$$

$$Rno_{NLR} = 894.836$$

$$Rno_1 = 187.554$$

We can use the laminar flow equations. The pressure drop across the ith layer is.

$$\Delta Phc_i := \frac{qdot_i \cdot 12 \cdot \mu_i \cdot LL}{LuwR \cdot tRg^3}$$

$$\Delta Phc_{NLR} = 24926.098$$

$$\Delta Phc_1 = 58192.337$$

$$\sum \Delta Phc = 3.253 \cdot 10^5$$

The total pressure drop

The drive force is

$$FRhc := \sum \Delta Phc \cdot (Aro + Arb)$$

$$FRhc = 342.168$$

We now want to move the regenerator back from cold to the hot end. The excess mass from the hot end will be cooled on its way through the generator. We can repeat the force calculation for the movement of the regenerator in the other direction by changing the input specific volume to the hot-end value and using the cold to hot time. The mass flow into the regenerator as it moves from **cold** end to **hot** end must be the same at each layer and depends on its velocity, the **hot** density and the blocked area of the regenerator.

Some the properties must be recalculated for the lower pressure which will be present for most of the return stroke.

$$mdot := \frac{Lfb}{tRch} \cdot \frac{1}{vol_{NLR}} \cdot Arb$$

$$mdot = 0.313$$

The volume flow at each layer is mdot times the specific volume

$$qdot_i := mdot \cdot vol_i$$

$$qdot_{NLR} \cdot 10^6 = 1085.115$$

The pressure drop across the ith layer using the laminar flow equation is

$$\Delta Pch_i := \frac{qdot_i \cdot 12 \cdot \mu_i \cdot LL}{LuwR \cdot tRg^3}$$

$$\Delta Pch_{NLR} = 16569.348$$

$$qdot_1 \cdot 10^6 = 352.957$$

$$\Delta Pch_1 = 38682.713$$

The total pressure drop

The pressure acts only on the ends of the shim coil so that the force to drive the regenerator is

$$FRch := \sum \Delta Pch \cdot (Arb + Aro)$$

$$FRch = 227.452$$

The force for the other direction was

$$FRhc = 342.168$$

If the drive pressure is 100 bar the piston area for the larger force is

$$Api := \frac{FRhc}{100 \cdot 10^5}$$

$$Api \cdot 10^6 = 34.217$$

The necessary diameter is

$$dpi := \sqrt{\frac{4 \cdot Api}{\pi}}$$

$$dpi \cdot 10^3 = 6.6$$

The volume needed is

$$qpi := Api \cdot Lfb$$

$$qpi \cdot 10^6 = 3.969$$

The regenerator drive powers for the whole engine are

$$PowRhc := FRhc \cdot \frac{Lfb}{tRhc} \cdot NM$$

$$PowRhc = 1151.402$$

$$PowRch := FRch \cdot \frac{Lfb}{tRch} \cdot NM$$

$$PowRch = 1039.764$$

Mean regenerator drive power is

$$PowRM := \frac{PowRhc \cdot ftRm \cdot ftRhc + PowRch \cdot ftRm \cdot (1 - ftRhc)}{2}$$

$$PowRM = 510.079$$

We have the option to adjust the balance between the fraction of time taken ftRhc in the two directions to minimise the mean power.

Now we can consider the thermal behaviour of the regenerator.

We want to find how much heat has to flow from the regenerator to the working fluid as it arrives in the hot chamber. We can look up values for the properties of steam at the nearby points of 400 bar and 550 C and then make linear interpolations to our chosen values of TH and PH. At present these are

$$TH = 548$$

$$PH = 4 \cdot 10^7$$

The slope of the temperature density curve at the hot end is

$$spT := \frac{143.2 - 392.1}{125} \quad spT = -1.991$$

Assume that on arrival the steam is cooler than TH by (estimated from time-domain model)

$$\Delta TH := 125$$

The working density at the chosen value of TH will be

$$\rho_s := 143.2 + (TH - \Delta TH - 550) \cdot spT \quad \rho_s = 396.082$$

The slope of the pressure density curve is

$$spP := \frac{143.2 - 98.4}{10^7}$$

The density at PH will be

$$\rho_s := \rho_s + (PH - 500 \cdot 10^5) \cdot spP \quad \rho_s = 351.282$$

We can now do the same for the slope of the internal energy - temperature curve.

$$stE := \frac{2872 \cdot 10^3 - 2107 \cdot 10^3}{125} \quad stE = 6120$$

The temperature-corrected internal energy in J per kg will be

$$Enw := 2872 \cdot 10^3 + (TH - \Delta TH - 550) \cdot stE \quad Enw = 2.095 \cdot 10^6$$

The pressure energy slope is

$$spE := \frac{2872 \cdot 10^3 - 2972 \cdot 10^3}{10^7} \quad spE = -0.01$$

The change in pressure-corrected internal energy of the hot end in J per kg will be

$$Enw := [Enw + (PH - 500 \cdot 10^5) \cdot spE] \quad Enw = 2.195 \cdot 10^6$$

The internal energy gain in the ΔMH kilograms of steam per working stroke will be

$$EnwH := Enw \cdot \Delta MH \quad EnwH = 38351.982$$

The internal energy of the cold fluid before the move is very little affected by pressure. The value for 125 C and 10 bar is 524.5 kJ/kg while at 500 bar it is only 508.1. The slope down to 100 C of the enthalpy temperature curve at 10 bar is

$$stE := \frac{(524.5 - 418.7) \cdot 10^3}{25} \quad stE = 4232$$

The temperature-corrected internal energy in joules of the cold steam before the move is

$$EnwL := [521.2 \cdot 10^3 + (TS - 125) \cdot stE] \cdot \Delta MH \quad EnwL = 6889$$

The change in internal energy per stroke is

$$\Delta E := (EnwH - EnwL) \quad \Delta E = 31463$$

If the internal energy is evenly shared and if the specific heat of the stainless steel regenerator material is 550 J/ kg K (Kaye and Laby page 60) the temperature change of each part will be

$$\Delta TR := \frac{\Delta E}{MR \cdot 550} \quad \Delta TR = 60.89$$

The heat flux density rate is

$$Hf := \frac{\Delta E}{AsR \cdot tRh} \quad Hf = 1 \cdot 10^5$$

The flow is laminar so that the heat transfer coefficient is

$$Htfrh := \frac{8.23 \cdot ks}{1 \cdot tRg} \quad Htfrh = 12569$$

This is high because of the very small gap

The temperature drop from steam to regenerator surface at the conditions of the hot end is

$$\Delta Trh := \frac{\Delta E}{Htfrh} \quad \Delta Trh = 2.503$$

At the cold end of the regenerator the properties will be close to those of condensing steam at TS. The thermal conductivity of steam at 100 C is given on page A22 of Incropera as

$$ksc := 0.0248$$

The heat transfer coefficient is

$$Htfrc := \frac{8.23 \cdot ksc}{1 \cdot tRg} \quad Htfrc = 5102.6$$

The temperature drop from steam to regenerator surface at the cold end is

$$\Delta Trc := \frac{\Delta E}{Htfrc} \quad \Delta Trc = 6.166$$

Regenerator Bearings

Now we can study the regenerator swirl bearings. First we see if we can achieve hydrodynamic separation using the analysis from O'Connor page 5-39. There will be a pair of bearings, one at each end of the separator tube. But because the load on each bearing depends on the position of the regenerator we assume that a force equivalent to 1 g on the regenerator mass is taken by a single bearing of diameter

$$dbc := DR \quad dbc = 0.038$$

The length to diameter ratio is

$$kbe := 0.5$$

The 'pressure' is

$$Pbe := \frac{MR \cdot 9.81}{dbc^2 \cdot kbe} \quad Pbe = 12604$$

This is so low that we can use equations for incompressible flow even in steam.

The radial clearance is must be large enough to accomodate a 100 C temperature difference.

$$cbe := \frac{dbc}{2} \cdot 100 \cdot 17 \cdot 10^{-6} \quad cbe \cdot 10^6 = 32.505$$

The revs per second $Nbe := \frac{\omega}{2 \cdot \pi} \quad Nbe = 38.913$

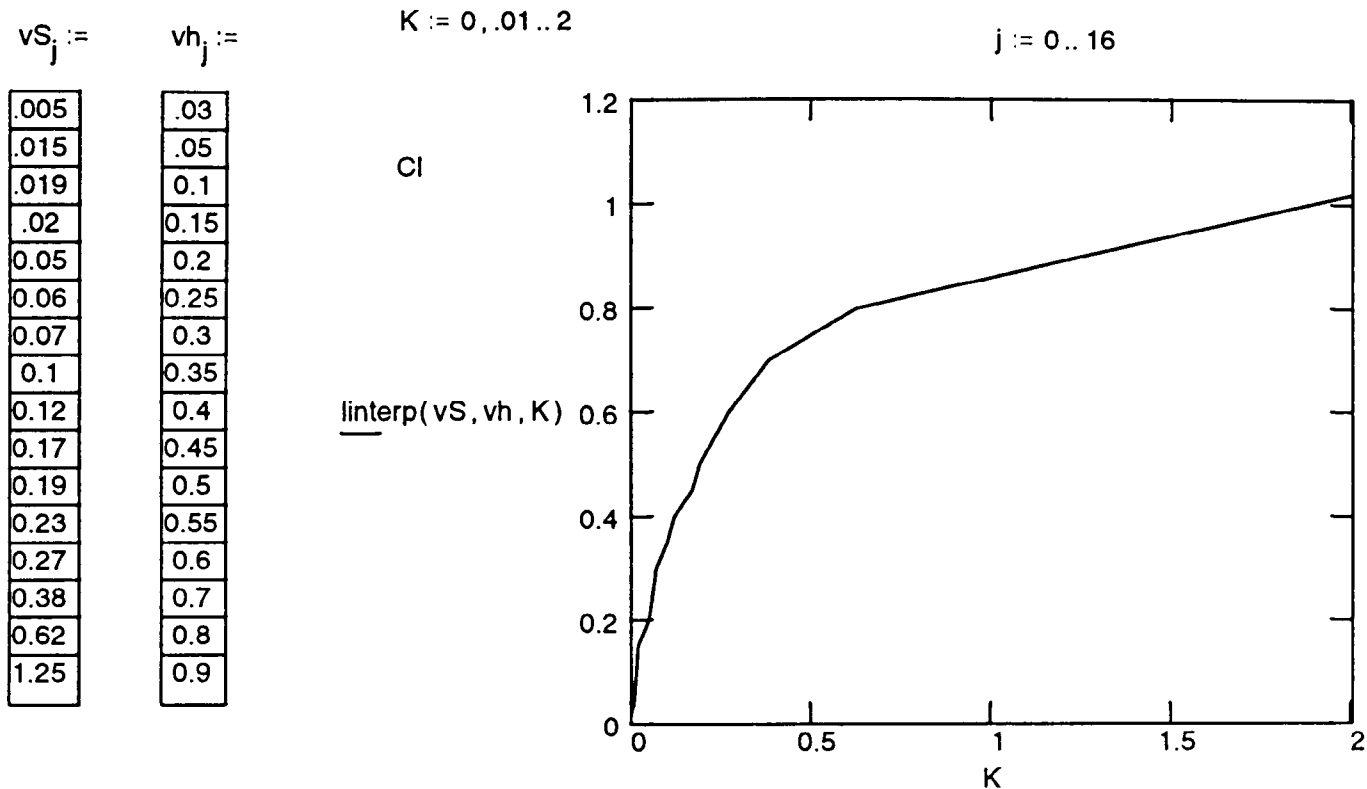
The viscosity of steam is undesirably low and temperature dependent. We will use the lowest value which occurs at the critical temperature and is

$$\mu_{be} := 45 \cdot 10^{-6}$$

The characteristic Sommerfeld bearing number is

$$Sbe := \left(\frac{dbc}{2 \cdot cbe} \right)^2 \cdot \frac{\mu_{be} \cdot Nbe}{Pbe} \quad Sbe = 0.048$$

From figure 62 page 5-52 in O'Connor we can construct the curve giving the minimum gap-to-clearance ratio against Sommerfeld number for the fully flooded bearing.



The fractional minimum clearance is

$$hc(S) := \text{interp}(vS, vh, S) \quad hc(Sbe) = 0.197$$

The actual minimum clearance is

$$hbe := hc(Sbe) \cdot cbe \quad hbe \cdot 10^6 = 6.397$$

We can conclude that full separation is possible even with the very poor lubricity of steam and even at the lowest rotation speeds. We should also see what happens if the lower bearing gets filled with water at 100 C having viscosity

$$\mu_w := 279 \cdot 10^{-6}$$

The Sommerfeld number is

$$Sbe := \left(\frac{dbc}{2 \cdot cbe} \right)^2 \cdot \frac{\mu_w \cdot Nbe}{Pbe} \quad Sbe = 0.298$$

The actual minimum clearance with water is

$$hbe := hc(Sbe) \cdot cbe \quad hbe \cdot 10^6 = 20.332$$

An alternative approach to the bearing analysis can use the analytical expression from equation 10.57 in Hamrock and calculating the load for a given bearing eccentricity. Converting to the Hamrock notation:

Choose the ratio of offset to radial clearance

$$\epsilon := 0.82$$

$$Fb := \frac{\mu_{be} \cdot \omega \cdot 0.5 \cdot DR \cdot (kbe \cdot DR)^3}{4 \cdot cbe^2} \cdot \frac{\epsilon}{(1 - \epsilon^2)^2} \left[16 \cdot \epsilon^2 + \pi^2 \cdot (1 - \epsilon^2) \right]^{0.5}$$

$$Fb = 9.944$$

The equivalent side g is

$$sg := \frac{Fb}{MR \cdot 9.81} \quad sg = 1.079$$

The actual clearance is

$$hbe := cbe - cbe \cdot \epsilon \quad hbe \cdot 10^6 = 5.851$$

It is useful to adjust the choice of ϵ . A value of 0.82 brings the two estimates into good agreement.

Swirl Bars

If there are large friction coefficients as a result of swirl there is the problem of keeping swirl going when the regenerator has moved out of a compartment. One very powerful way of doing this is to have a pair of bars running the full length of the inside of engine passing through the body of the regenerator. The bars would rotate with the regenerator but would not slid with it so that swirl would be induced in both hot and cold chambers. The centrifugal bending of the bars and friction in the bearings which locate them to the body of the regenerator are problems.

Bar wall	$tbar := 0.0005$	Bar length	$Lbar := Lfb + LR$	$Lbar = 0.356$
Bar diameter	$dbar := D \cdot 0.3$			$dbar = 0.012$
Section moment	$Ibar := \frac{\pi}{64} \cdot [dbar^4 - (dbar - 2 \cdot tbar)^4]$			
Bar radius from axis	$rbar := 0.4 \cdot D$			$rbar = 0.016$
Bar mass	$Mbar := \frac{\pi}{4} \cdot dbar \cdot tbar \cdot 8000$			$Mbar = 0.038$
Centrifugal force	$Fbar := Mbar \cdot rbar \cdot \omega^2$			$Fbar = 36.059$

Firstly we treat the bar as a simply supported beam. The deflection is

$$ybar := \frac{Fbar \cdot Lbar^3}{76.8 \cdot 2 \cdot 10^{11} \cdot Ibar} \quad ybar \cdot 10^3 = 0.354$$

The maximum stress is $\sigma bar := \frac{Fbar \cdot Lbar}{8} \cdot \frac{dbar}{2} \cdot \frac{1}{Ibar} \quad \sigma bar = 3.218 \cdot 10^7$

If the centrifugal force was taken by plain bearing with $\mu = 0.1$ the power per engine would be

$$Powf := 2 \cdot NM \cdot Fbar \cdot 0.1 \cdot kR \cdot D \cdot 2 \cdot cps \quad Powf = 25.832$$

A seal with side float and spherical freedom would suffer no load. A web between bars would need a more complicated seal but would be even more effective. It may also be possible to design a collapsing lazy-tongs mechanism which can erect itself as the regenerator moves out of a compartment.

Waste Heat Flows

Total thermal impedance of the useful thermal flow

$$Ztot := Zff + Zhw + Ztube + Zair + Zsf + Zcf + Zcw + Zwf \quad Ztot = 0.029$$

We can now calculate the thermal resistances opposing the flow of waste heat. Assume that the hot head including the exhaust heat exchanger is covered by an insulating blanket. Assume that the air inlet is closed. Assume that the water in the cold block is an infinite heat sink but is not convecting.

Blanket thickness	$tbl := 0.05$		
Blanket area	$Abl := NM \cdot Df \cdot Df \cdot 3.5$		
Blanket conductivity of multilayer evacuated silica powder			$kbl := 0.0017$

Blanket resistance $zbl := \frac{tbl}{Abl \cdot kbl} \quad zbl = 297.738$

The conductivity of the stainless steel of the separator block is $ksep := 15$
The wall thickness of the separator must be $twsep := \frac{PH \cdot D}{2 \cdot 150 \cdot 10^6} \quad twsep = 0.005$

Separator resistance $zsep := \frac{LR - Lfb}{\pi \cdot D \cdot twsep \cdot ksep} \cdot \frac{1}{NM} \quad zsep = 3.084$

This could be increased by wall-thickness taper towards the cold end, by making the separator from a stack of rings with reduced contact area or by using a ceramic material strengthened by outer bands of tensile material.

The conductivity of the vertical block of water in the separator block is higher at the critical point (0.238) than at the superheated temperatures (.046 at 600 C). Use the worst case for now.

The thermal resistance of the shim of the regenerator material is $kwa := 0.238$

$$zreg := \frac{LR}{0.25 \cdot D^2 \cdot 15 \cdot ksR \cdot NM} \quad zreg = 16.666$$

Water resistance $zwa := \frac{LR}{0.25 \cdot \pi \cdot D^2 \cdot kwa \cdot (1 - ksR) \cdot NM} \quad zwa = 501.5$

Heat will flow to the side plates through the 20 mm heat shield round the combustion volume. However if we make the side plates out of Cr Mo V steel we can allow its temperature to rise to 75% of the range between ambient and TH. This means that the apparent thermal impedance of the heat shield material will rise by a factor of 4. Its value is.

$$zsp := \frac{0.02}{2 \cdot NM \cdot Lfb \cdot 0.4 \cdot 0.0017} \cdot 4 \quad zsp = 126.772$$

If we assume the unwanted convective flow paths are blocked with effective lagging material the total thermal resistance in parallel with the useful heat path is

$$ztot := \frac{1}{\left(\frac{1}{zbl} + \frac{1}{zsep} + \frac{1}{zreg} + \frac{1}{zwa} + \frac{1}{zsp} \right)} \quad ztot = 2.515$$

Total waste heat including exhaust $QW := \frac{TH}{ztot} + Wha \quad QW = 3407$

Weight Estimates

Now we can make initial estimates of weight of an entire engine consisting of NM thermal sections. Weights so far are

Copper fins $M_1 := \text{Affa} \cdot \text{tcu} \cdot 0.5 \cdot 8500 \cdot \text{nf} \cdot \text{NM}$ $M_1 = 9.967$

$$M1 := \left(1 \cdot \text{mod}^2 - \frac{\pi}{4} \cdot D^2 \right) \cdot 8500 \cdot \text{tcu} \cdot \text{Nff} \cdot \text{NM} \quad (\text{Both estimations give similar values}) \quad M1 = 9.11$$

Inconel slices $M_2 := \frac{\pi}{4} \cdot (D_{io}^2 - D_{ii}^2) \cdot \text{tinc} \cdot \text{Nff} \cdot 8000 \cdot \text{NM}$ $M_2 = 2.307$

Regenerators $M_3 := \text{NM} \cdot \text{MR}$ $M_3 = 3.758$

The enclosing side plates must also resist the pressure on the cylinder head. The force per module is

$$F_{ax} := \text{PH} \cdot \frac{\pi}{4} \cdot D_{ii}^2 \quad F_{ax} = 71483$$

The effective length of the side plates is 0.4 mod at the widest point of the flame port. Their safe stress is 300E6. Because of the favourable shape of the elliptical flame port we allow a stress concentration factor of only 1.5 (See Peterson figure 128). The thickness is

$$t_p := \frac{F_{ax}}{300 \cdot 10^6 \cdot 2 \cdot 0.4 \cdot \text{mod}} \cdot 1.5 \quad t_p = 0.005$$

We should check the stress in the area above the flame ports where the whole width is available but where there are round holes with stress concentration factors of 3.

$$\sigma_p := \frac{F_{ax}}{2 \cdot \text{mod} \cdot t_p} \cdot 3 \quad \sigma_p = 2.4 \cdot 10^8$$

The side plates are attached at each end of the engine by short socket head shoulder screws fitting into accurately bored holes. We use four screws per module. The safe shear stress is 450E6. The minimum dowel diameter is

$$d_d := \sqrt{\left(\frac{F_{ax}}{4 \cdot 450 \cdot 10^6} \right) \cdot \frac{4}{\pi}} \quad d_d = 0.007$$

The Unbrako M8 shoulder screw has a 10 mm dowel diameter. The M10 has 12 mm.

The length of the separators is the difference between the regenerator and fin block. The weight of separators is

$$M_4 := \pi \cdot D \cdot t_{wsep} \cdot (LR - Lfb) \cdot \text{NM} \cdot 2 \cdot 7860 \quad M_4 = 5.226$$

The base block is a Meehanite casting. The width 1.5 * mod. Its height must allow a safe wall round the isolator bores. Its solid outline weight will be

$$M_{SO} := \text{NM} \cdot \text{mod} \cdot 1.5 \cdot \text{mod} \cdot 1.2 \cdot d_i \cdot 7860 \quad M_{SO} = 14.508$$

The weight removed for the isolator holes will be

$$M_{RW2} := \text{NM} \cdot \text{mod} \cdot \frac{\pi}{4} \cdot d_i^2 \cdot 2 \cdot 7860 \quad M_{RW2} = 5.476$$

The final base weight is $M_5 := M_{SO} - M_{RW2}$ $M_5 = 9.032$

The force trying to lift a cylinder head must be passed to the tie side plates by a top plate. We can analyse this as a simply-supported beam with a central point load. The depth is Yb. The stress is 200E6. The beam length is 1.5 times mod. The beam width for one module is mod.

The beam moment is $Mom := \frac{F_{ax}}{2} \cdot \frac{1.5 \cdot \text{mod}}{2}$ $Mom = 2252$

The beam depth must be $Y_b := \sqrt{\frac{6 \cdot Mom}{200 \cdot 10^6 \cdot \text{mod}}}$ $Y_b = 0.028$

The weight of the top plate is $M_6 := (\text{NM} \cdot \text{mod} + .05) \cdot 1.5 \cdot \text{mod} \cdot Y_b \cdot 7860$ $M_6 = 10.841$

The total height of the engine will be $Ho_a := 1.2 \cdot d_i + Lfb + LR + Lfb + 0.2 \cdot D + Y_b$ $Ho_a = 0.552$

The weight of side plates will be $M_7 := \text{NM} \cdot \text{mod} \cdot t_p \cdot 7860 \cdot Ho_a \cdot 2$ $M_7 = 15.5$

The mass of the finned copper block at the cold end is

$$M_8 := \left[\frac{\pi \cdot Lfb}{4} \cdot (D_{co}^2 - D^2) - \pi \cdot D \cdot t_{cf} \cdot Lfc - \pi \cdot t_{cf} \cdot Lwf \cdot (D_{ci} + tw) \right] \cdot \text{NM} \cdot 8500 \quad M_8 = 6.9$$

The mass of the steel water jacket is

$$M_9 := \left(\text{mod}^2 - \frac{\pi}{4} \cdot D_{co}^2 \right) \cdot Lfb \cdot 7860 \cdot \text{NM} \quad M_9 = 14.71$$

Provisional estimate for wedding cake motor weight $M_{11} := 10$

Total engine weight so far $\sum M = 107.393$

The total length of the engine is $Lo_a := \text{NM} \cdot \text{mod} + 2 \cdot y_{ex}$ $Lo_a = 0.621$

Further Minor Calculations

The joules per stroke for the engine

$$J := \frac{Q \cdot NM}{\text{cps}} \quad J = 27981$$

If the specific heat of the hot copper is 384 J/kg K and 506 for Inconel the temperature drop from the fin block to supply one full stroke would be

$$\Delta TB1 := \frac{J}{384 \cdot M_1 + 545 \cdot M_2} \quad \Delta TB1 = 5.503$$

Small drops suggest no problem about pulsed heat flow.

A Stirling engine can easily be used in reverse as a heat pump so that regenerative braking is possible with useful energy saving for a subsequent acceleration. If we reckon that a common driving event is the slowdown of a 1000 kg car from 25 to 10 m/sec (about 50 to 20 mph) the change in kinetic energy is

$$\Delta KE := \frac{1}{2} \cdot 1000 \cdot (25^2 - 10^2) \quad \Delta KE = 2.625 \cdot 10^5$$

The temperature rise of the hot-end block would be

$$\Delta TB2 := \frac{\Delta KE}{384 \cdot M_1 + 545 \cdot M_2} \quad \Delta TB2 = 51.6$$

This could be a useful feature for braking after a burst of high power working when the inner of the hot end hat been cooled but should be used with caution if the creep life of the Inconel is not to be reduced.

To warm the entire engine from dead cold will require an amount of heat

$$Q_c := (650 - 20) \cdot (M_1 \cdot 384 + M_2 \cdot 506) \quad Q_c = 3.147 \cdot 10^6$$

If the heat flux is 10E5 J/sec per thermal module) the warm up time will be

$$T_w := \frac{Q_c}{10^5 \cdot NM} \quad T_w = 7.867$$

At 1996 costs for petrol (£2.3 for 4.5 * x 0.8 x 45 MJ) this would cost in pence

$$p_wu := \frac{Q_c \cdot 2.3}{4.54 \cdot 0.8 \cdot 45 \cdot 10^6} \cdot 100 \quad p_wu = 4.428$$

The thermal capacity of the hot copper and Inconel parts of a whole engine is

$$C_{th} := M_1 \cdot 385 + M_2 \cdot 506 \quad C_{th} = 5005$$

After an elapsed time tel of 8 hours

$$tel := 8 \cdot 3600$$

The block temperature will be

$$T_{bl} := 600 \cdot e^{-\left(\frac{tel}{z_{tot} \cdot C_{th}}\right)} \quad T_{bl} = 60.903$$

After an 8 hour stand the rewarm cost is

$$\frac{p_wu \cdot (650 - T_{bl})}{650} = 4.013$$

Rewarm costs with off-peak electricity would be about half the above. A reduction of stray heat loss is important for intermitent users.

Recall that the vehicle can be driven with energy taken from the pressure accumulator system so that a longer warm up time with a gentler heat flux can be accepted. However a well lagged engine will retain a large fraction of its stored heat over night.

Now we can add all the losses with a 25% allowance for ancillary drive conversion

$$PowL := (PowRM + W_{expu} + PowswH + PowswC + Powc) \cdot 1.25 \quad PowL = 3164$$

The actual power out is

$$Powact := Pow - PowL \quad Powact = 56514.12$$

The final efficiency is

$$\eta_f := \frac{Powact}{Q \cdot NM + QW} \quad \eta_f = 0.507$$

The power-to-weight ratio including 20% for items not yet calculated

$$PWR := \frac{Powact}{\sum M \cdot 1.2} \quad PWR = 439$$

$$BHP := \frac{Powact}{746}$$

$$BHP = 75.756$$

$$Masslb := \sum M \cdot 2.205$$

$$Masslb = 237$$

Displacement

$$\Delta := \frac{\pi}{4} \cdot DR^2 \cdot Lfb \cdot NM \cdot 10^6$$

$$\Delta = 532.929 \text{ cc}$$

Heat flux	$Q = 27000$	Power gross	$Pow = 59677.84$
Max heat	$Q_{max} = 85993$	- losses	$Powact = 56514.12$
Pressure max	$PH = 4 \cdot 10^7$	Thermal efficiency	$\eta_{th} = 0.552$
Inconel stress	$\sigma_i \approx 300 \cdot 10^6$		$\eta_{th2} = 0.553$
Mid Inc temp	$T_{mw} = 657.671$	Final efficiency	$\eta_f = 0.507$
Thermal module #	$NM = 4$	Speed	$cps = 3.86$ $Engrpm = 231.583$
Module spacing	$mod = 0.084$	Inconel rad. thick	$rinc = 0.006$
Bore factor	$kb \approx 0.4762$	Inconel outer auto	$Dioa = 0.06$
Bore	$D = 0.04$	Inconel od override	$Dio \approx 0.060$
Inconel inner	$D_{ii} = 0.048$	No. of flame-fin Nff = 66	steam-fin Nfs ≈ 66 water-fins Nfc = 58
Copper fin thickness	$t_{cu} \approx .0007$	Flame and steam fin lengths	$L_{ff} = 0.012$ $L_{sfr} = 0.004$
Inconel/copper ratio	$kic \approx 1.5$	Condensing inner	$D_{ci} = 0.048$
Inconel thickness	$t_{inc} = 0.001$	Condensing fin	$L_{fc} = 0.00375$
Sealing tube	$t_{seal} \approx .000$	Condensing wall	$tw = 0.00352$
Air gap	$t_{air} \approx 0 \cdot 10^{-6}$	Water outer	$D_{co} = 0.062$
Inconel Stresses	$\sigma_o = 2.29 \cdot 10^8$ $\sigma_{ir} = 2.96 \cdot 10^8$	Jacket	$D_{oj} = 0.074$
	$\sigma_m = 2.624 \cdot 10^8$	Fin block length	$L_{fb} = 0.116$
Copper shear σ	$\sigma_{scu} = 2 \cdot 10^6$	Side plate thick	$tp = 0.005$
Hot strength	$\sigma_{cuH}(T_{fo}) = 4.7 \cdot 10^7$	Copper mass	$M_1 = 9.967$
Steam fin length	$k_{sf} \approx 5.5$	Inconel mass	$M_2 = 2.307$
Condensing fin	$k_{cf} \approx 3.75$	Total mass	$\sum M = 107$ $Mass_{lb} = 236.802$
Water fin length	$k_{wf} \approx 3.75$	Height	$H_{oa} = 0.552$
Cold fin thickness	$t_{cf} \approx .001$	Length	$L_{oa} = 0.621$
Swirl actual vel	$V_{swe} = 4.89$ $rpm = 2335$	Flame fin η	$\eta_{ff} = 0.967$
Swirl base vel	$V_{sw} = 3$	Steam fin η	$\eta_{sf} = 0.818$
Swirl increase	$k_{sw} \approx 0.7$	Condense fin η	$\eta_{cf} = 0.559$
Swirl powers	$Pow_{swH} = 124$ $Pow_{swC} = 313$	Water fin η	$\eta_{wf} = 0.797$
Swirl benefit	$R_{sns} = 19.5$	Flame to fin	$Z_{ff} = 0.02059$ $A_{ff} = 0.299$
Swirl ratio steam/cond	$k_{cs} \approx 1$	Hot wall	$Z_{hw} = 1.96336 \cdot 10^{-3}$
HTFC gas to fin	$H_{tff} = 168$	Seal-tube	$Z_{tube} = 0$
HTFC fin to steam	$H_{tfs} = 5268$	Airgap	$Z_{air} = 0$
HTFC condensing	$H_{tfc} = 29242$	Steam fin	$Z_{sf} = 3.06164 \cdot 10^{-3}$
HTFC cooling water	$H_{tfcw} = 8486$	Condensing	$Z_{cf} = 0.00091$
HTFC hot end regen	$H_{tfrh} = 12569$	Cold wall	$Z_{cw} = 4.9879 \cdot 10^{-4}$
HTFC cold end regen	$H_{tfrc} = 5103$	Waterfin	$Z_{wf} = 1.85737 \cdot 10^{-3}$
HTFC exhaust exch	$H_{tfex} = 128$	Total Z	$Z_{tot} = 0.029$

BHP = 75.756

Power weight ratio

$$\frac{Q}{Q_{max}} = 0.314$$

Regenerator length

Regenerator solidity

Regenerator core

Regen shim thick

Regenerator stroke

Regen gap

Cycle fractions

Mass flow comb. products

Mass flow fuel

Flame temp

Flame to fin

Hot wall

Sealtube

Air-gap

Steam fin

Condensing

Cold wall

Water fin

Flame temp

* Fin tip (850mx)

Wall outer

Wall inner

Seal tube in /
Steam root

Guess steam

Steam

Guess condense

Condensing

Water fin

Water out

Cold water in temp

PWR = 439

kLR = 6

ksR = 0.6

kdR = 0.29

tsR = .0001

kR = 2.9

tRg · 10⁶ = 40

ftRm = 0.924

ftRhC = 0.576

MG = 0.024

Mm = 0.00062

TF1 = 1710.302

ΔTff = 555.975

ΔThw = 53.011

ΔTtb = 0

ΔTag = 0

ΔTsf = 82.664

ΔTcf = 11.047

ΔTcw = 6.037

ΔTwf = 22.478

TF = 1513

Tft = 716

Tfr = 684

Tiinc = 631.2

Tsr = 631

TH = 548

Tst = 549

TS = 95

Tcs = 95

Tcf = 84

Twf = 77

TCW = 55

Out vol $V_{I2} \cdot 10^6 = 104$

$$\frac{\Delta TR + \Delta Trh}{\Delta Tsf} = 0.767$$

Regenerator mass

Regen body length

Unwrapped length

Hot end change

Cold end change

Regen body change

Regenerator forces

Regen peak power

Mean power

Sommerfeld #

Min clearances

Side gee

MR = 0.939

LR = 0.24

LuwR = 9.8

ΔTrh = 2.5

ΔTrc = 6.2

ΔTR = 60.9

FRhc = 342.2

FRch = 227.5

PowRhC = 1151

PowRM = 510

Sbe = 0.298

hbe · 10⁶ = 6

sg = 1.079

Heat exchanger for air-preheating

Air in vol

Temp air in cold

Wrap number

Air exchanger gap

Temp exhaust out

NTU Effectiveness

Transit time

Exch length

Air heat exch area

Air heat exch mass

Exhaust layer thick

Exhaust ΔP

Fin block ΔP

Exhaust pump pow

Exhaust heat loss

Exhaust total loss

Vcld = 0.019

Tic = 25

Nlex = 10

gex = 0.014

Toc = 57.9

ε = 0.82

Ttex = 0.909

Lex = 19.4

Aex = 8.69

M₁₂ = 19.118

yex = 0.143

ΔPex = 9509

ΔPp = 344

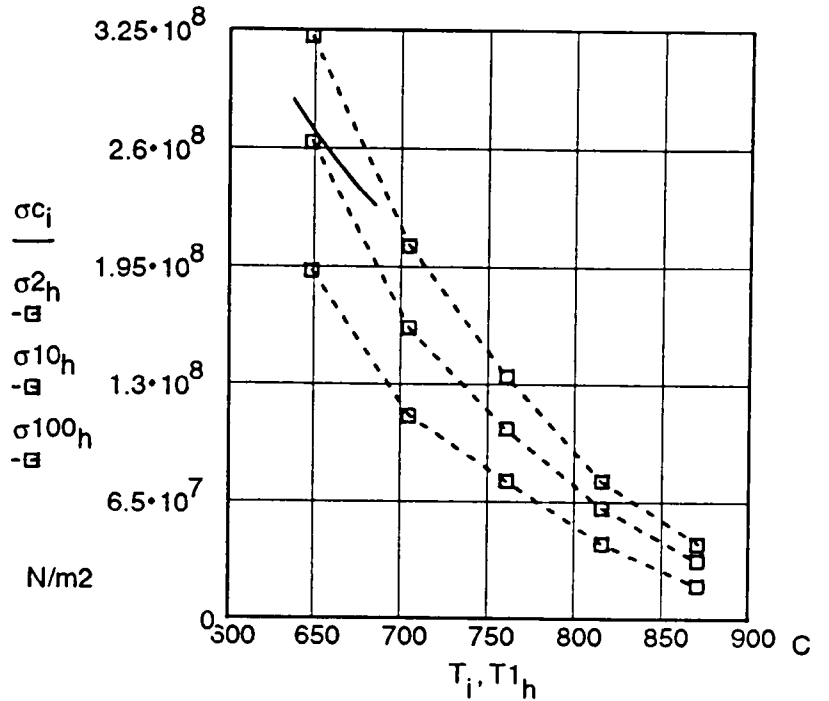
Wexpu = 1571

Wha = 3189

Wextot = 4760

Key Design Parameters for a Full-Power Application.

Heat flux	Q = 27000
Max heat	Qmax = 85992.678
Shaft power	Powact = 56514 BHP = 75.76
Indicated power	Pow = 59678
	Engrpm = 231.58
Metal limit	BHPmet = 220
Final efficiency	$\eta_f = 0.507$
Max fin tip	Tft = 716.014
Steam temp	Tst = 548.502
Condense temp	Tcs = 94.562
Exhaust noise	dB = 41.862
Fin block ΔP	$\Delta P_p = 344$
Air pump pow	Wexpu = 1571
Pressure max	PH = $4 \cdot 10^7$
Total mass	$\sum M = 107.393$
Swirl velocity	Vswe = 4.89
Copper thick	tcu = 0.0007
Inconel thick	tinc = 0.001
Module	mod = 0.084
Bore	D = 0.04
Stroke	Lfb = 0.116
Displace cc	$\Delta = 532.929$



Radial stress/Temperature and Inconel 625 rupture stresses for 4000, 20,000 and 200,000 hours of engine operation with 50% stress cycle.

Losses:	$\frac{TH}{z_{tot}} = 218$	Swirl drive	PowswH = 124
Stray heat			PowswC = 313
Regenerator	PowRM = 510	Cold water	Powc = 12.1
		Total	PowL = 3164

Checking the closed-loops :

Loop-1	Loop -2	Loop -3	Loop -4	Loop -5
Temp of hot air entering burner	Temp of hot gases leaving hot-end	Temp of steam at hot-end	Temp of water at cold-end	Heat balnce
Tih = 736.14	Toh = 769.06	Tst = 548.5	Tcs = 94.56	$Q_h = Q + QW/4$
Tih \approx 738	Toh \approx 770	TH \approx 548	TS \approx 95	$\frac{QW}{4} = 852$
				Q \approx 27000
				Qh = 27891

Other important parameters (need to be checked for variable heat flows) :

Upper cycle pressure	PH $\approx 400 \cdot 10^5$	Flame temperature at burner	TF1C = 1710.3
Air-Ratio	AR ≈ 2.052	Average flame temperature	TFC = 1240.2
Loss-factor (fuel)	LF ≈ 1.033	Temp at flame-fin base	Tffb = 684.18
No. of TD piles/modules	NM ≈ 4	Temp st flame-fin outer edge	Tfo = 716.01
Module spacing	mod ≈ 0.084	Exhaust gas temperature	Toc = 57.92
No. of adjacent flame-fins joined	nf ≈ 2	Total gas flow per module	MG = 0.024
Mid-wall temperature of hot-end	Tmw ≈ 658	Steam-density at hot-end	$\rho_s \approx 143.2$
Base velocity of regn. swirling	Vsw ≈ 3	Gas velocity passing hot-end	velg = 61.41
Regenerator spinning speed	rpm = 2335	Reynolds number of hot-gas flow	Rnog = 990.9
Air exchanger wrap number	Nlex ≈ 10	Aspect ratio of flow-section (flame-fin)	choice = 5.714
Air exchanger gap	gex ≈ 0.01425	Reynolds number at steam-fin interface	Rnos = 46183
Final efficiency	$\eta_f = 0.507$	Ratio of spin to non-spin co-efficient	Rsns = 19.5
Power-to-weight Ratio	PWR = 439		

Corrections from time-domain model (MatrixX) :

Fluid mass needed to be pumped into the regenerator to raise pressure	$\Delta M_{reg} \approx 0.0447$	Piston motions	
Correction factor for non-linearity of pressure variation in real cycle	Fnp ≈ 0.98	Part of piston motion when high cycle pressure is maintained	PstnA $\approx 73 \cdot 10^{-3}$
Reduced cycle pressure at the end of regenerator stroke towards cold-end	Pexpand $\approx 80 \cdot 10^5$	Part of piston motion when cycle pressure is decreased	PstnB $\approx 71 \cdot 10^{-3}$
Motoring work per cycle	W1 = 4864.2		
Pumping work per cycle	W2 = 1076.1		

Appendix B : Time-domain simulation models

The time-domain simulation models developed for the Artemis-Malone engine are presented in this section. The program is developed using 'System Build' (MATRIXx) graphical simulation package. The program is composed of a group of sub-programs, which are termed as super-blocks. Each of the Super-blocks could be again composed of a number of super-blocks and functional blocks. Functional blocks are like small programs itself which compute a certain task, these generally built in features but most of them are also user definable. Input -output connections make data exchanges between different Super-blocks. A structure of hierarchy is maintained between the super-blocks, which may activated at same time rates, different time frames or conditionally according the programme. The simulation results for a defined time period are plotted as graphs using Xmath graphics (part of MATRIXx) and could be transferred to other packages.

The full program is presented as follows :

B1. Theoretical engine cycle (PSEUDOTD)

B1.1 : Regenerator motion model (REGNDSPL)

B1.2 : Checking acceleration requirement of regenerator motion (Accltest)

B1.3 : Fluid mass inside regenerator (REGNmass)

B1.4 : Tracking cycle completion (CYCLEtrg)

B1.5 : Cyclic power Calculation (POWER)

B1.6 : Cyclic temperature variation of the hot-end fluid (TEMPCAL)

B1.6.1 : Thermal impedance at the steam-fin interface (Z Steamfin)

B2 : Real engine model (TDPILE)

B2.1 : Regenerator motion model (REGNDSPL)

B2.1.1 : Adjusting regenerator motion amplitude (Ampl Fraction)

B2.2 : Tracking cycle completion (CYCLEtrg)

B2.3 : Cyclic power Calculation (POWER)

B2.4 : Piston motion generated from pump-motor following ternary-code (PSTNbin)

Ten-cylinder pump-motor model (PM10)

B2.5.1 Desired flow demand from the pump-motor (Demand)

B2.5.2 Pump-motor shaft speed (RPM)

B2.5.3 Triggering pump-motor cylinders reaching TDC/BDC (VS TRIGGER)

B2.5.4 Cumulative flow error compared to demand (CUM ERR)

B2.5.5 Setting regenerator offset needed corresponding to
power demand(REGN_OFFSET)

B2.5.6 Cylinder enabling decisions, read from a ternary-table or following some
control algorithm (DECIMAKE)

B2.5.6.1 Keeps track of the load demand changes on cycle-by-cycle
basis (LOAD CHANGE)

B2.5.6.1.1 Evaluate power demand in terms of power-zones (STRATEGI)

B2.5.6.1.2 Keeping the track of transition cycles
(LOAD SHIFT / LOAD SHIFT OLD)

B2.5.7 Pump-motor cylinder-1 (CL1)

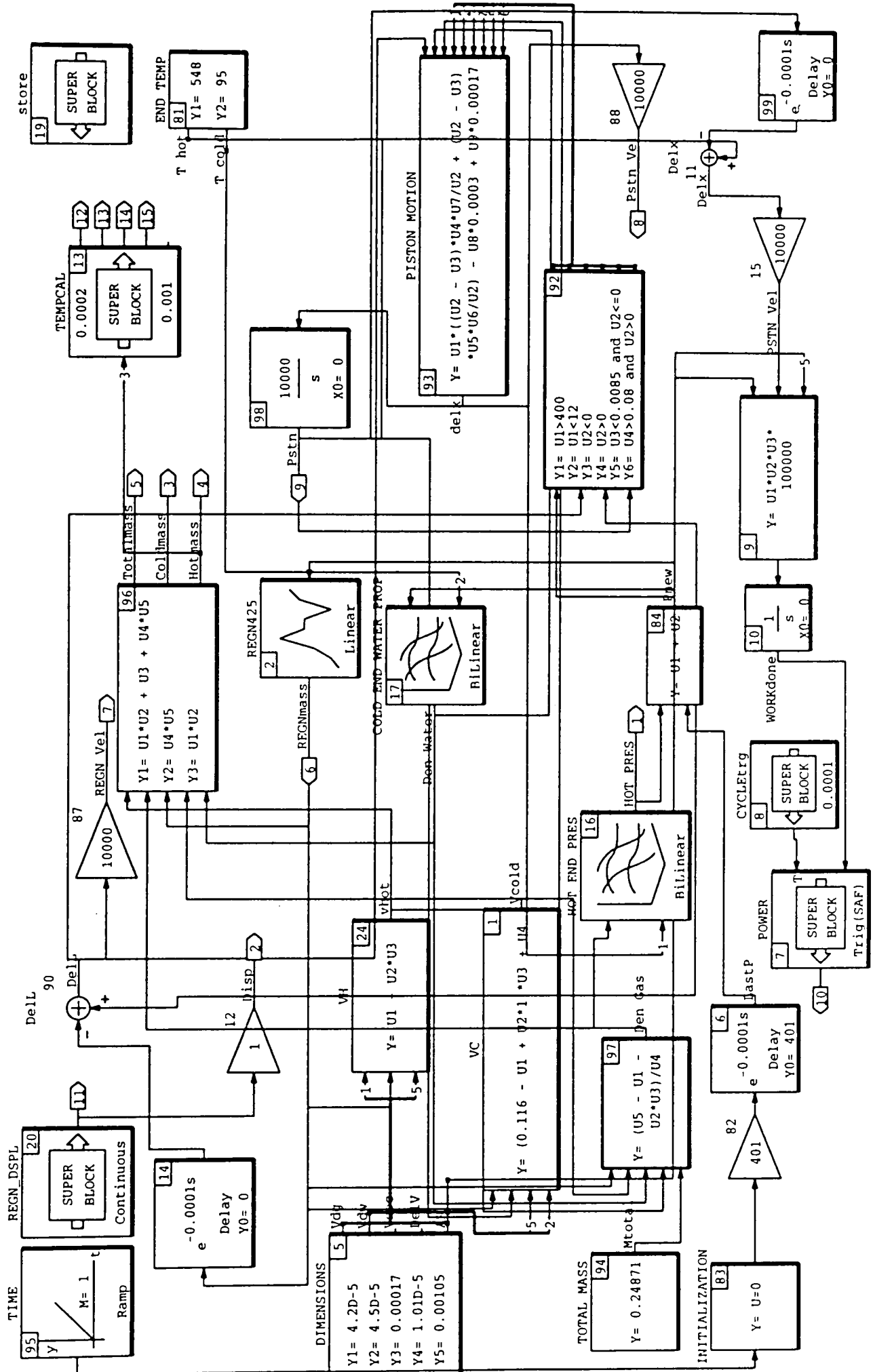
B2.5.8 Pump-motor cylinder-2 (CL2)

B2.5.9 Pump-motor cylinder-1 (CL3)

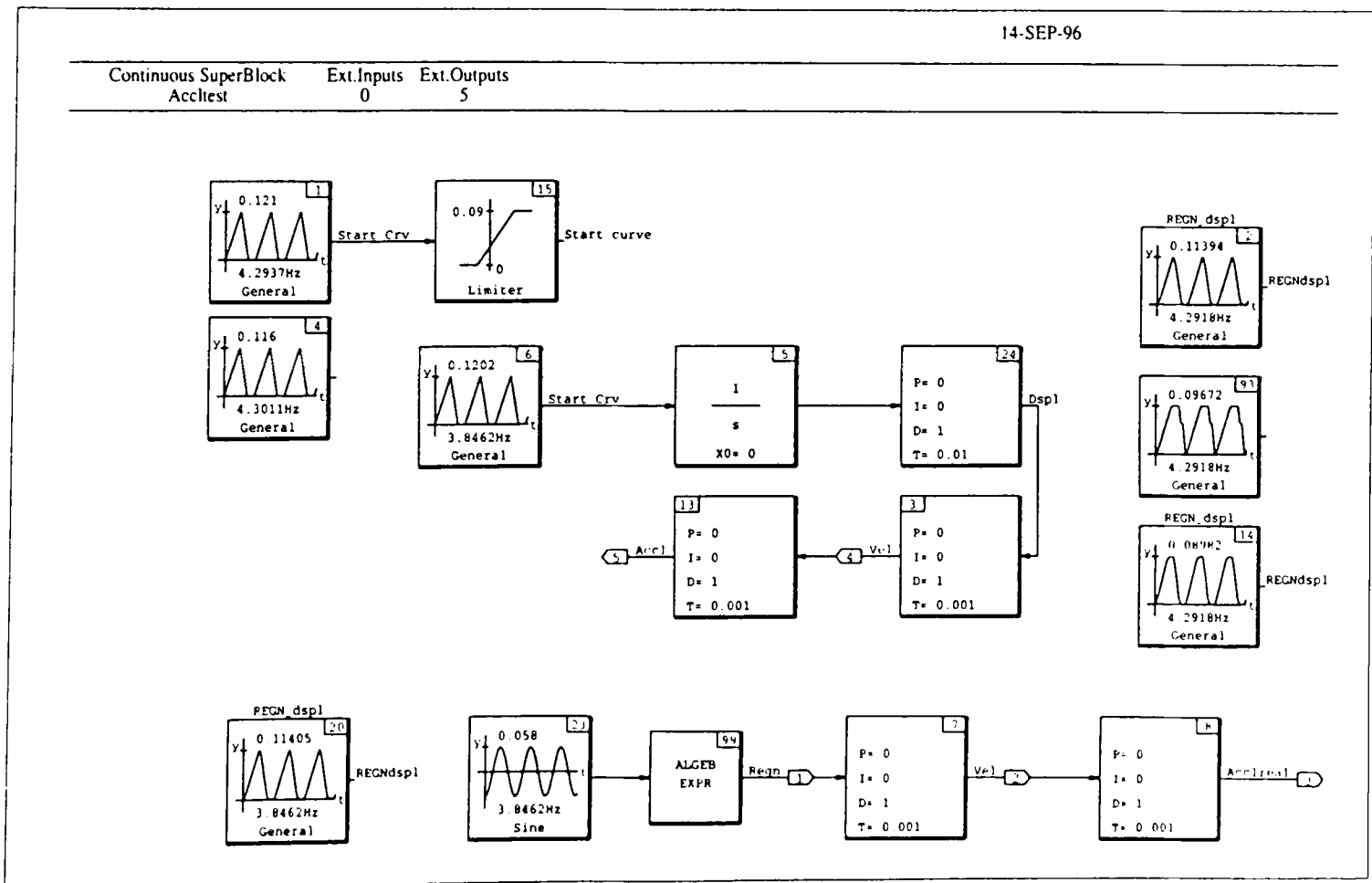
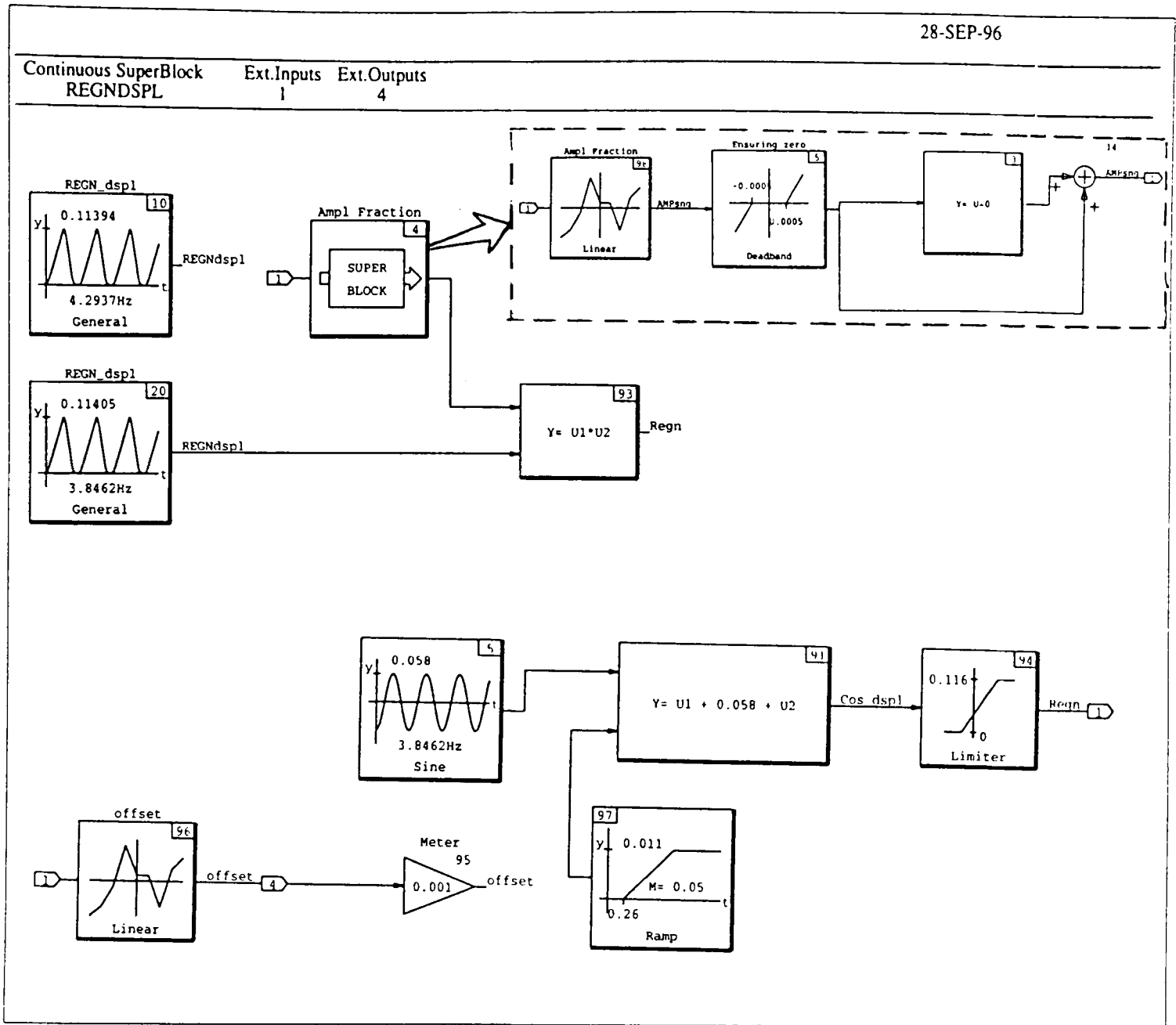
B2.5.10 Pump-motor cylinder-1 (CL10)

14-SEP-96

Continuous SuperBlock Ext.Inputs Ext.Outputs
 PSEUDOTD 0 15

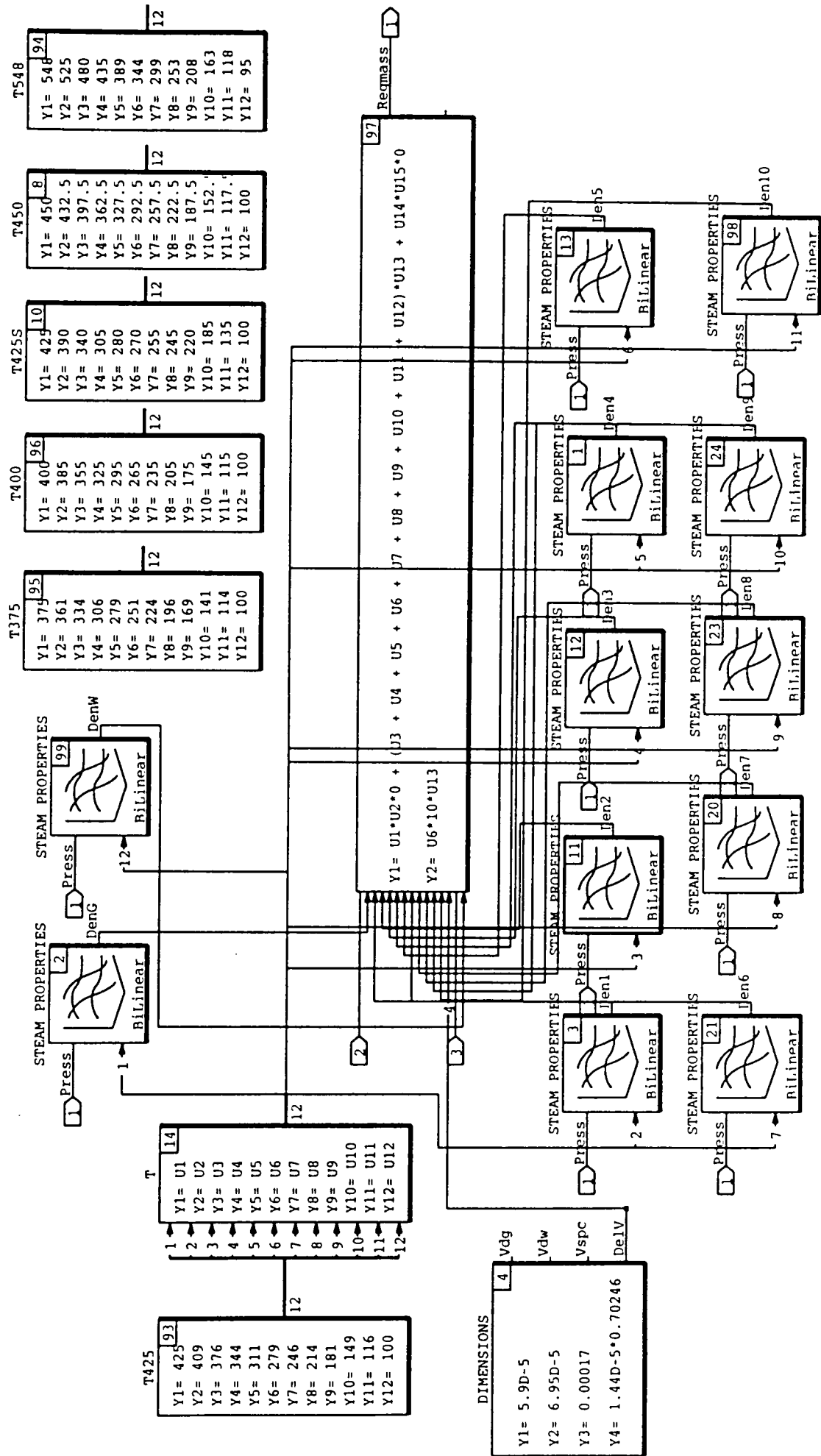


B1: Theoretical engine cycle (PSEUDOTD)



14-SEP-96

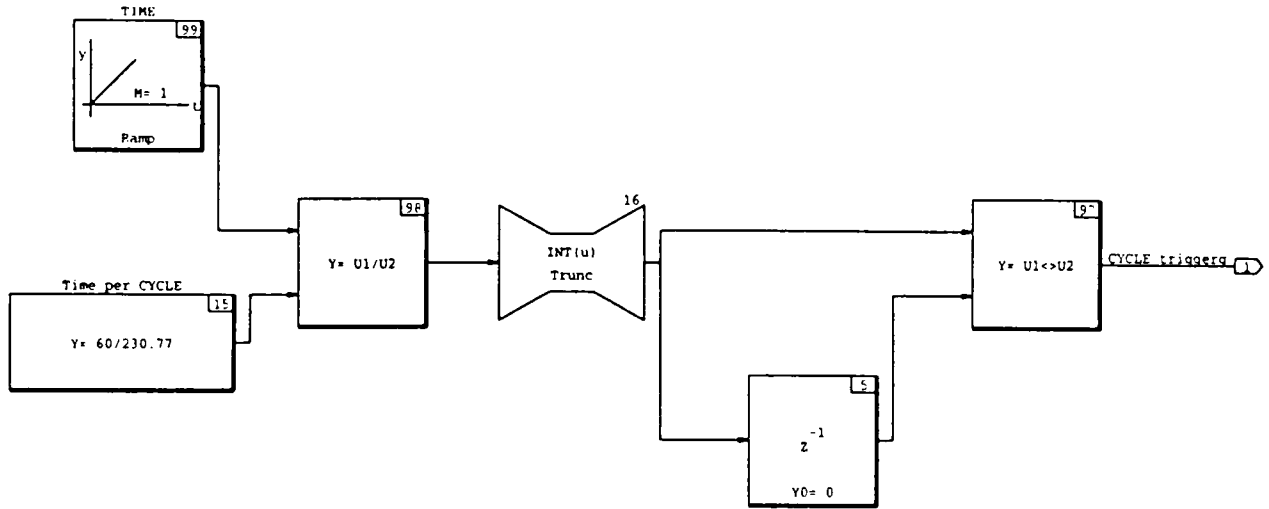
Discrete SuperBlock Sampling Interval First Sample Ext.Inputs Ext.Outputs Enable
 REGNmass 0.001 0 3 1 Parent



B1.3 : Fluid mass inside regenerator (REGNmass)

14-SEP-96

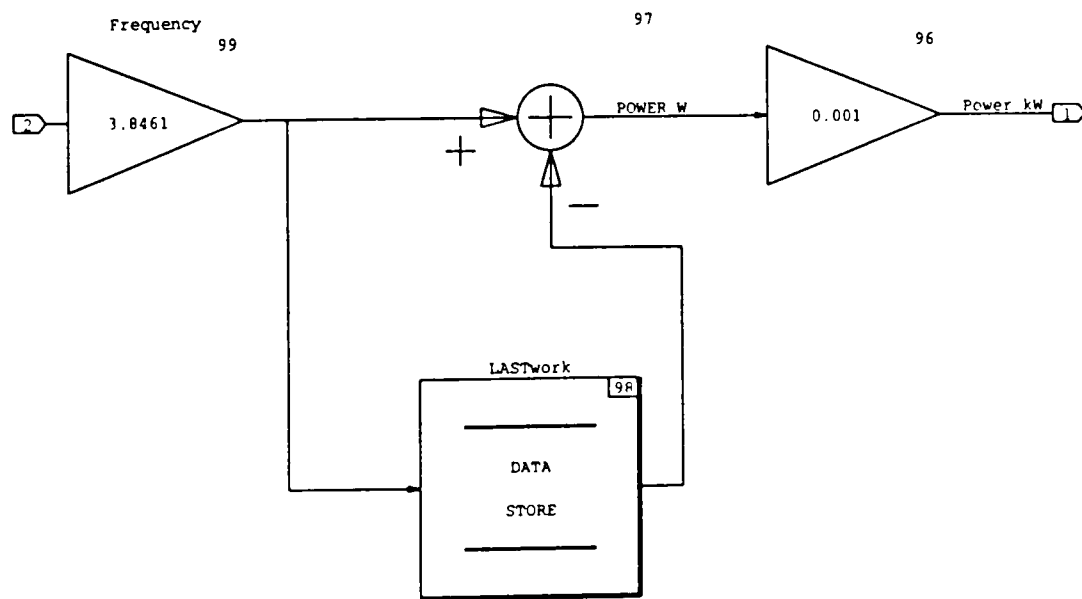
Discrete SuperBlock	Sampling Interval	First Sample	Ext.Inputs	Ext.Outputs	Enable Parent
CYCLEtrg	0.0001	0	0	1	Parent



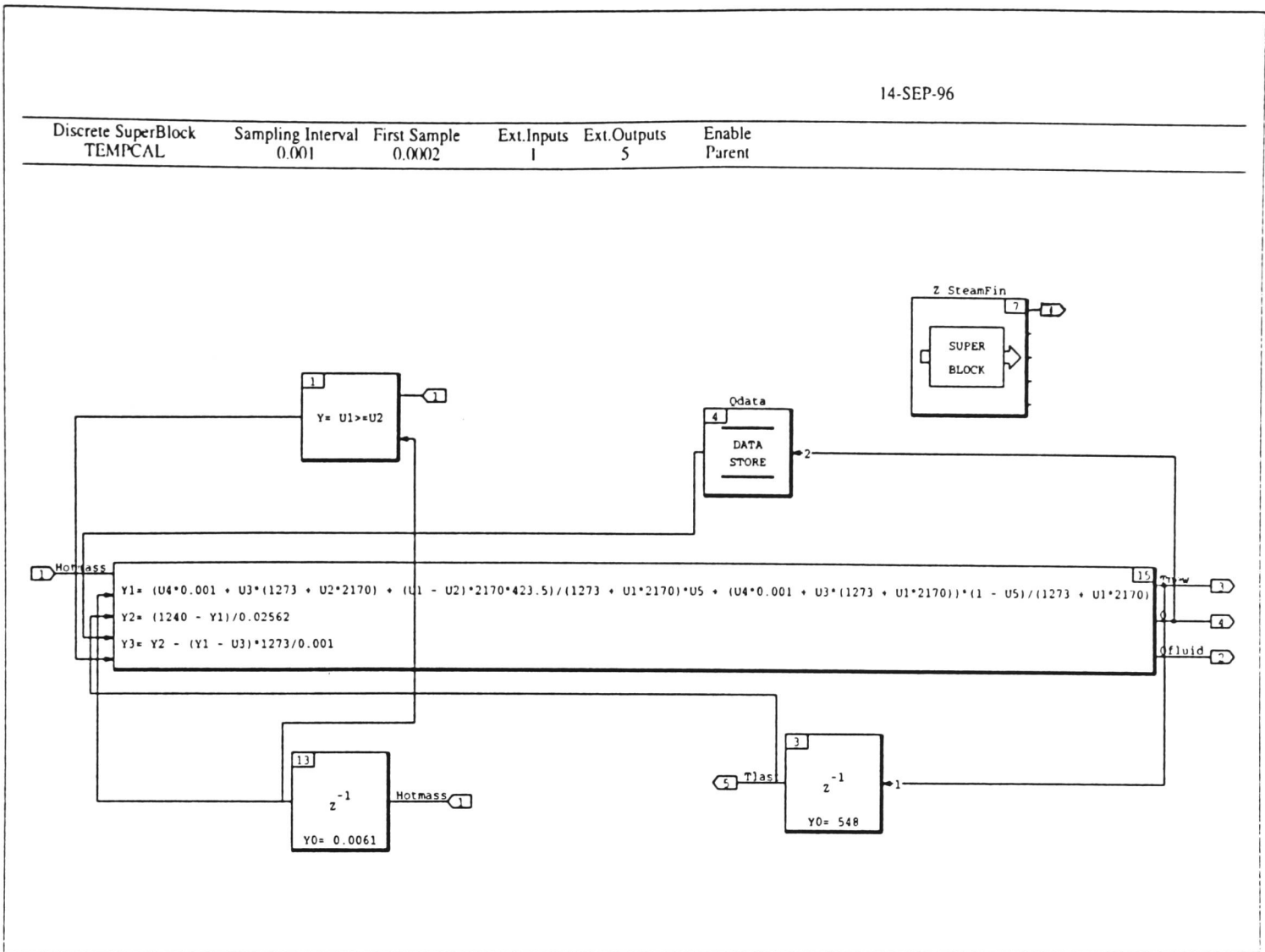
B1.4 : Tracking cycle completion (CYCLEtrg)

14-SEP-96

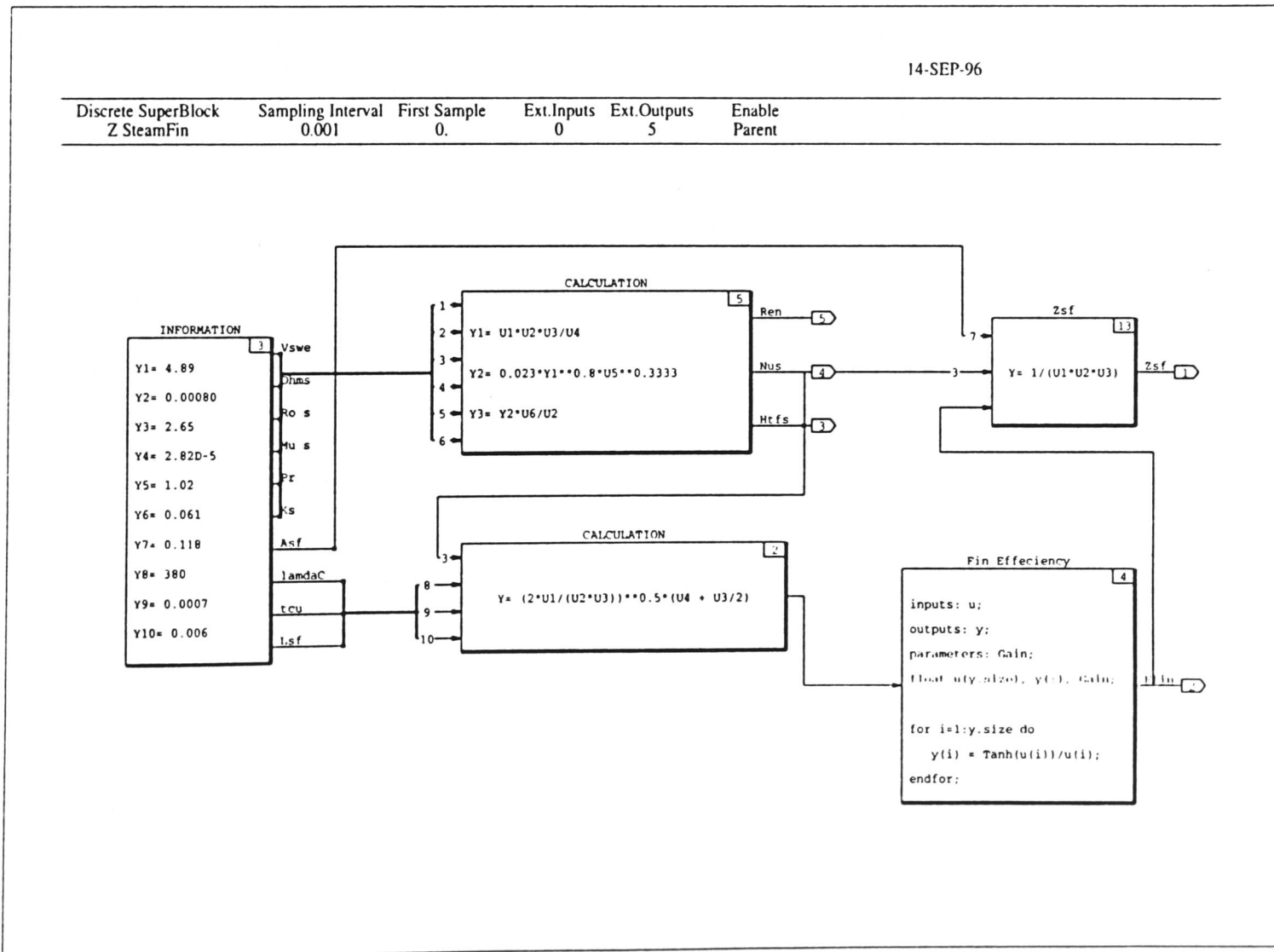
Triggered SuperBlock	Timing Requirement	Output Posting	Ext.Inputs	Ext.Outputs	Trigger
POWER	0.1	As Soon As Finished	2	1	1



B1.5 : Cyclic power Calculation (POWER)

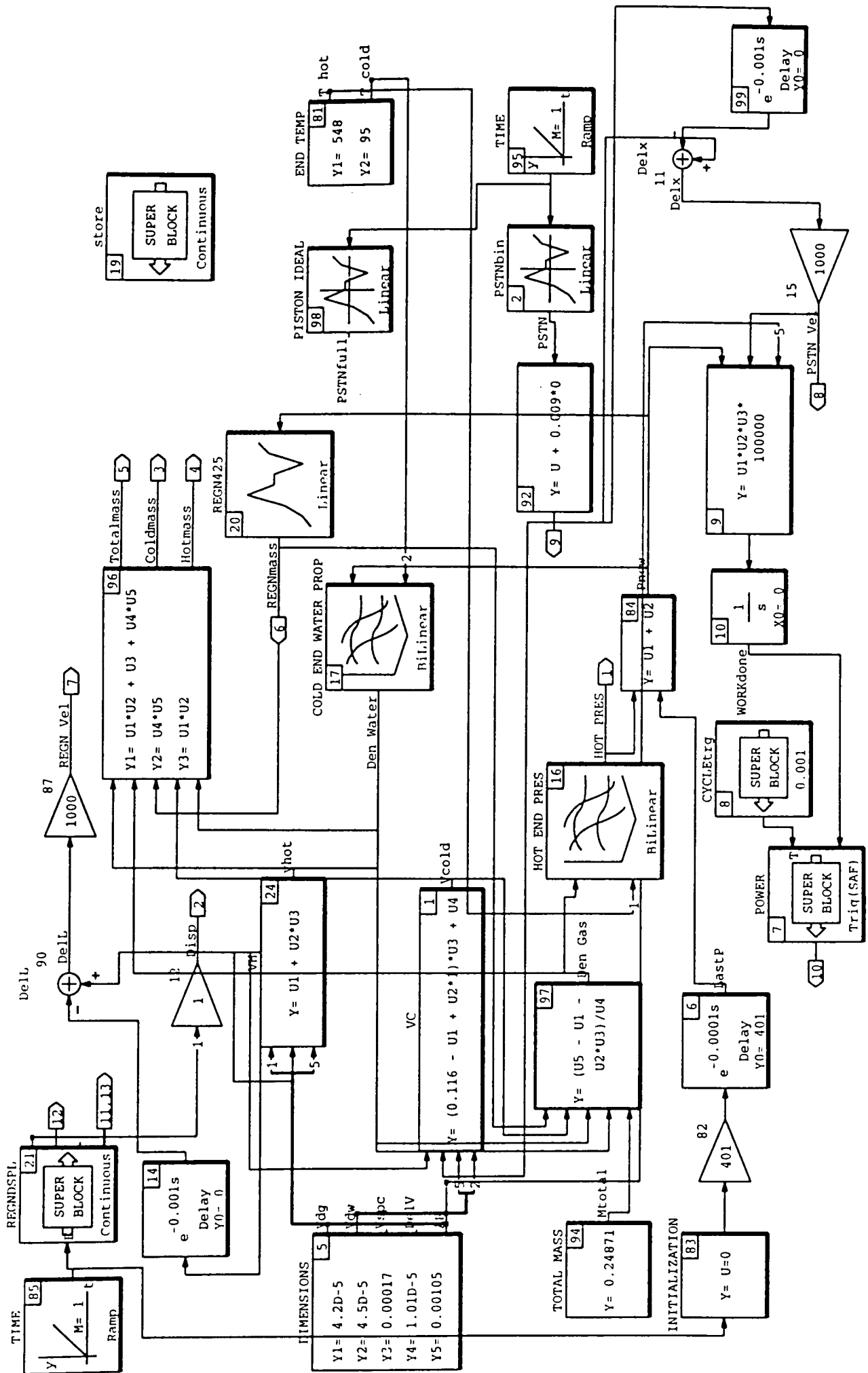


B1.6 : Cyclic temperature variation of the hot-end fluid (TEMPCAL)



B1.6.1 : Thermal impedance at the steam-fin interface (Z Steamfin)

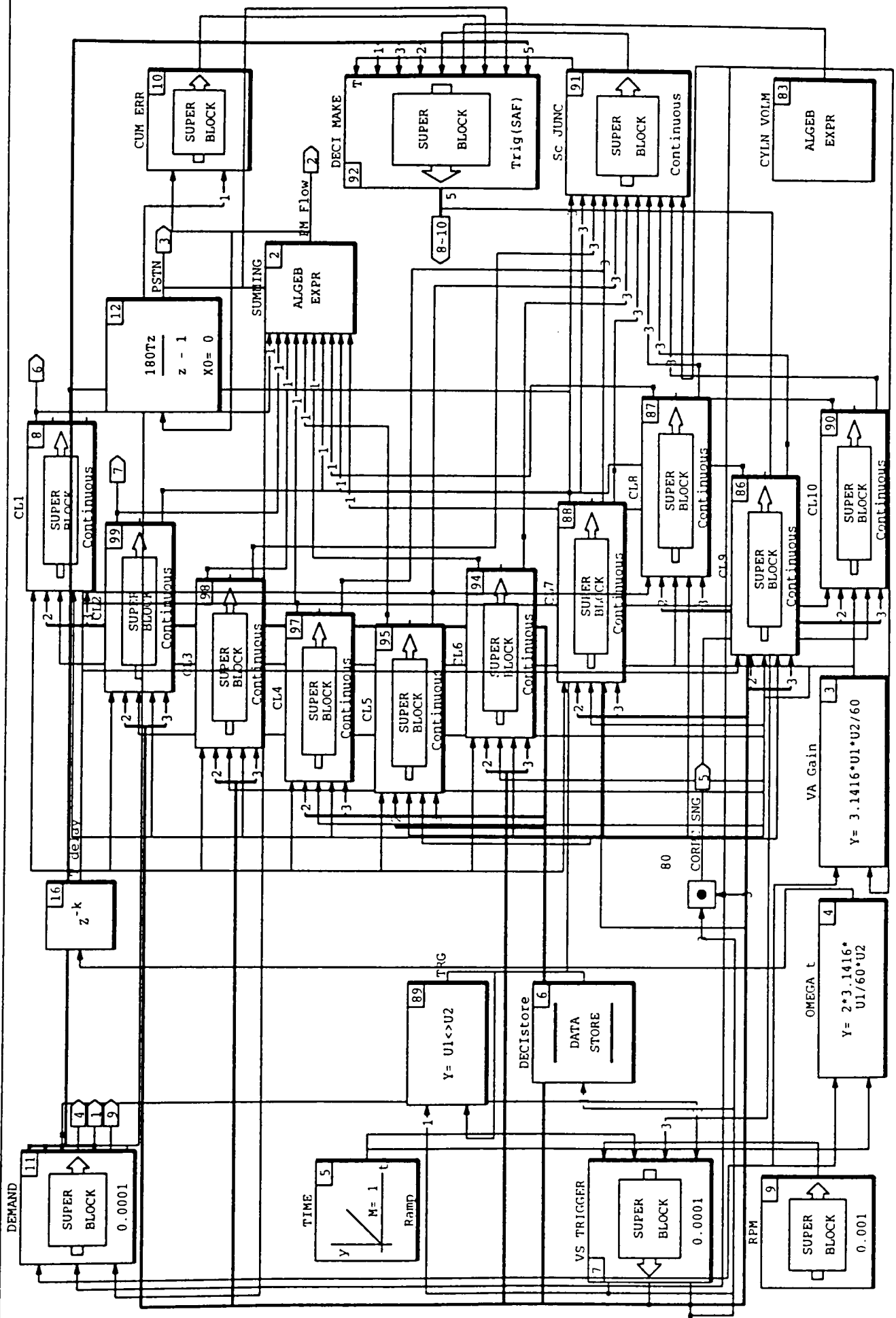
Continuous SuperBlock (TDPILE)
 Ext.Inputs 0
 Ext.Outputs 15



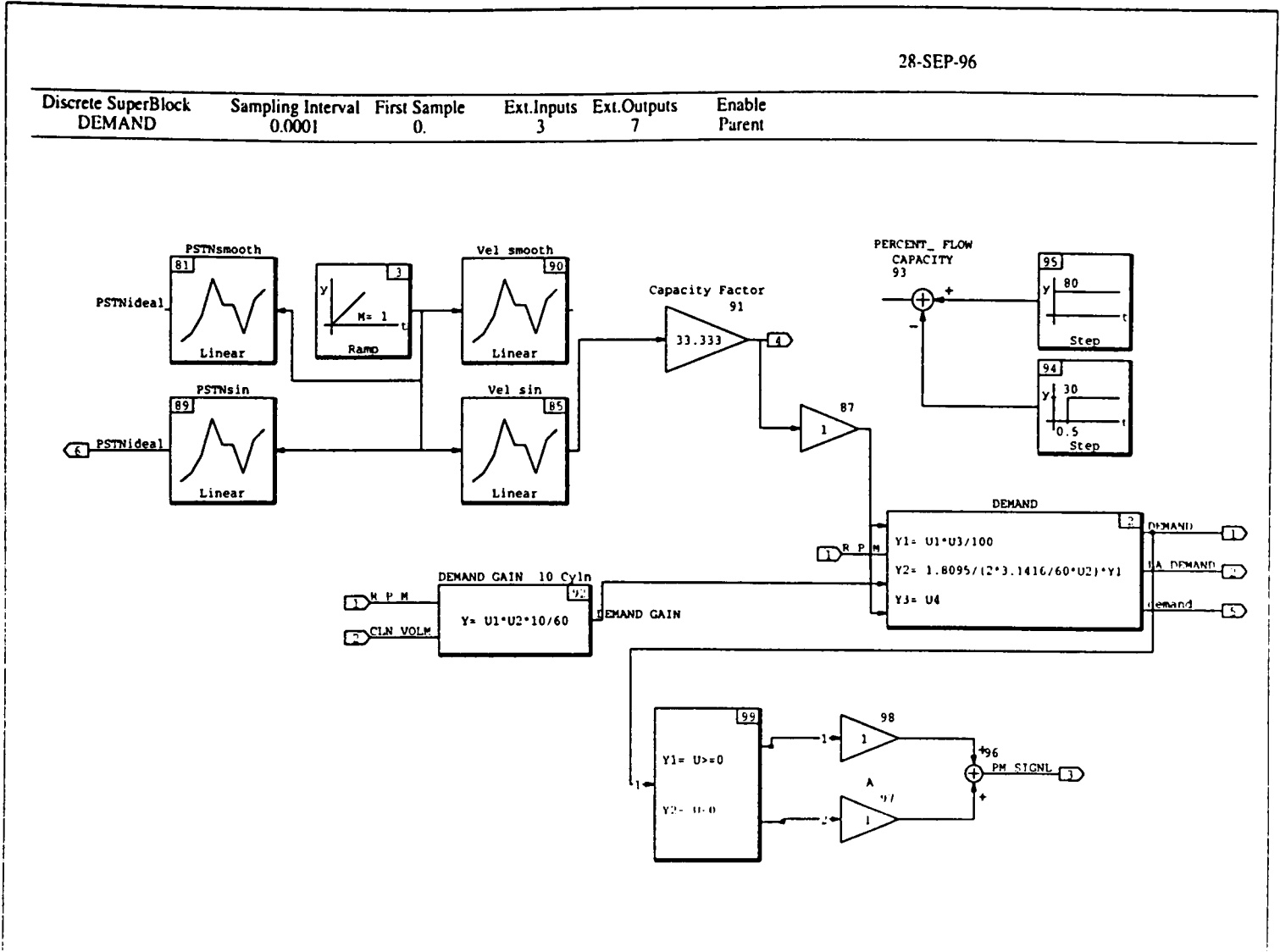
B2 : Real engine model (TDPILE)

28-SEP-96

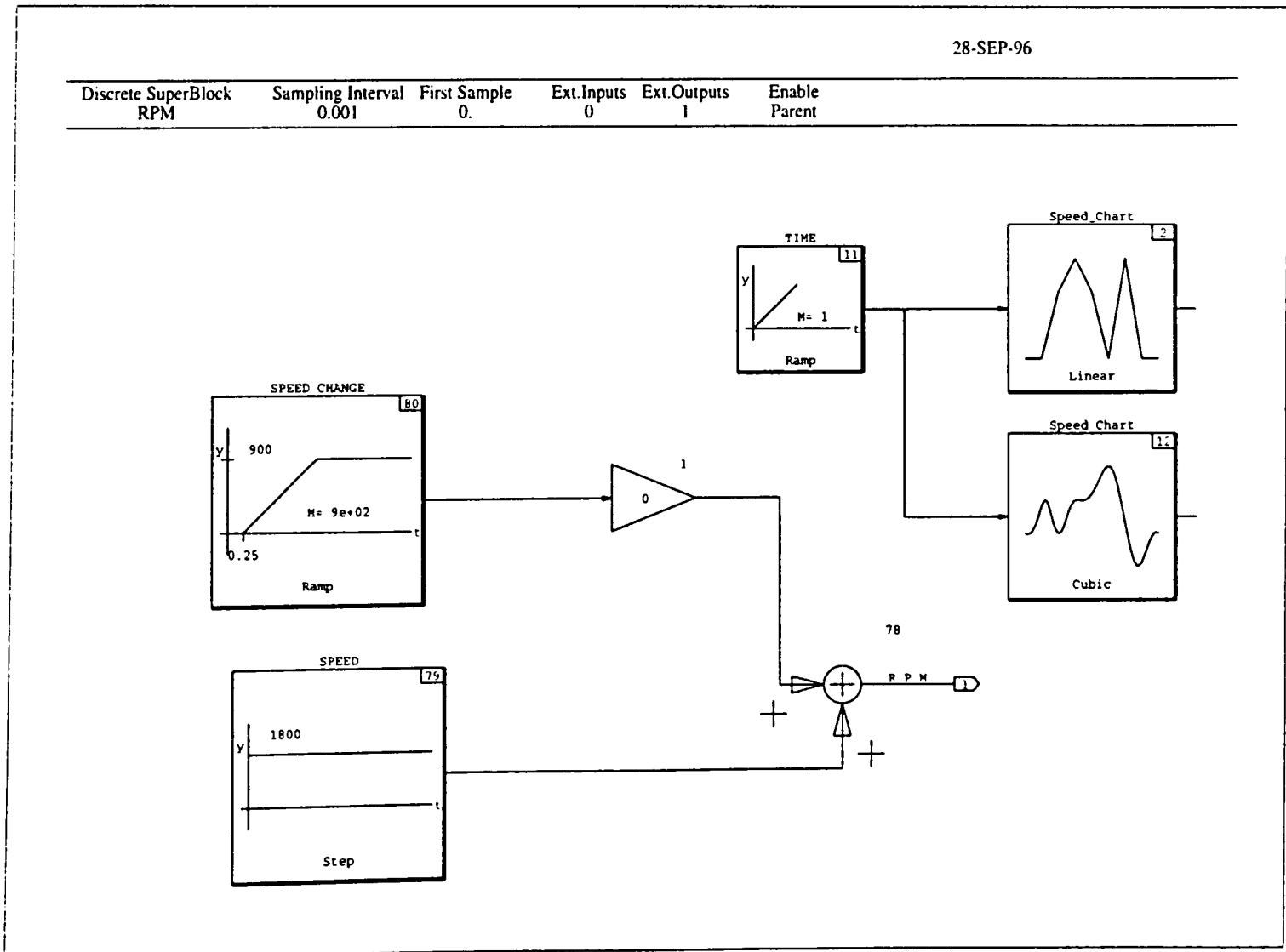
Discrete SuperBlock PM10 Sampling Interval 0.0001 First Sample 0. Ext.Inputs 0 Ext.Outputs 10 Enable Parent



B2.4 : Ten-cylinder pump-motor model (PM10)



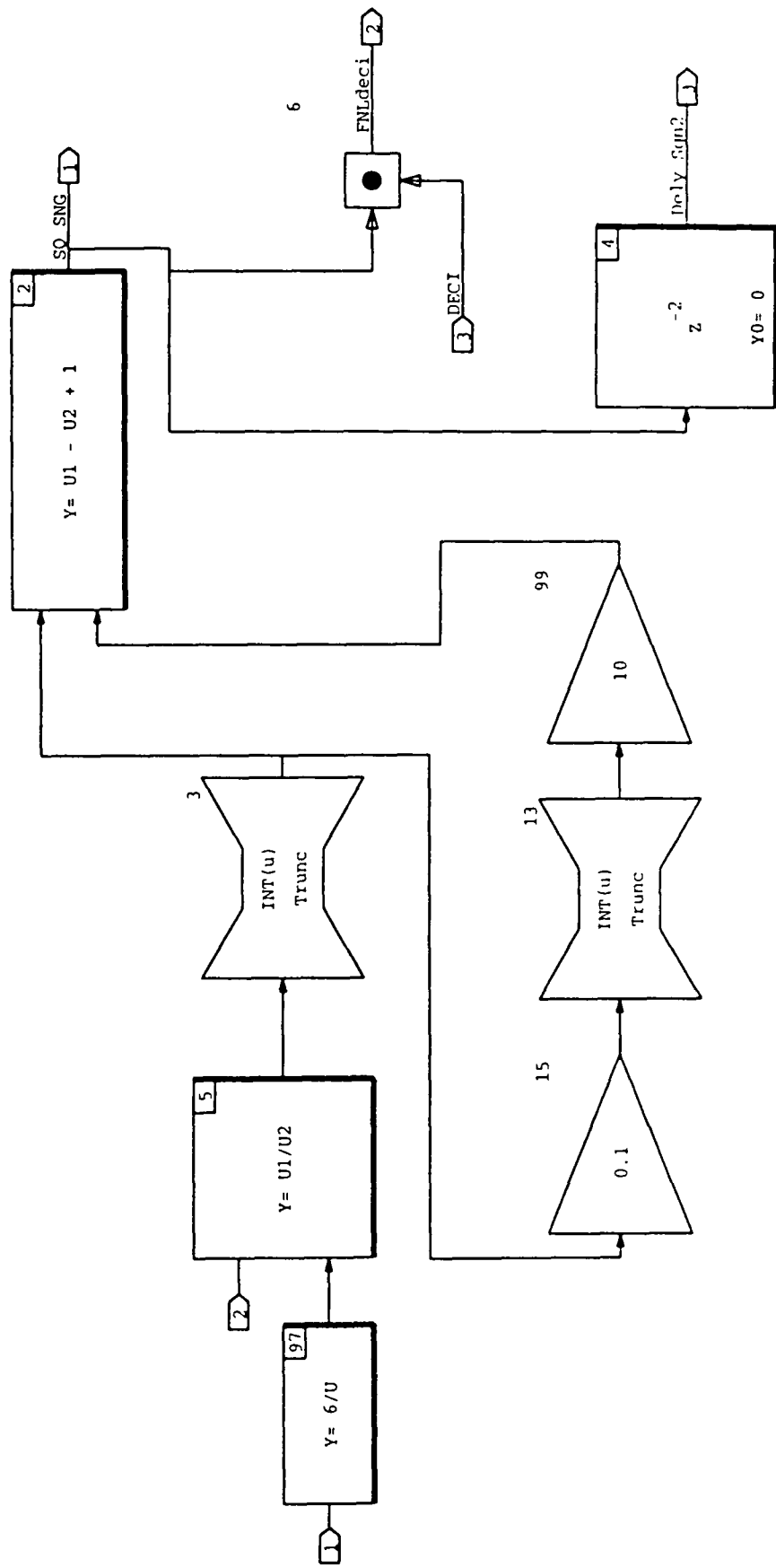
B2.5.1 : Desired flow demand from the pump-motor (Demand)



B2.5.2 : Pump-motor shaft speed (RPM)

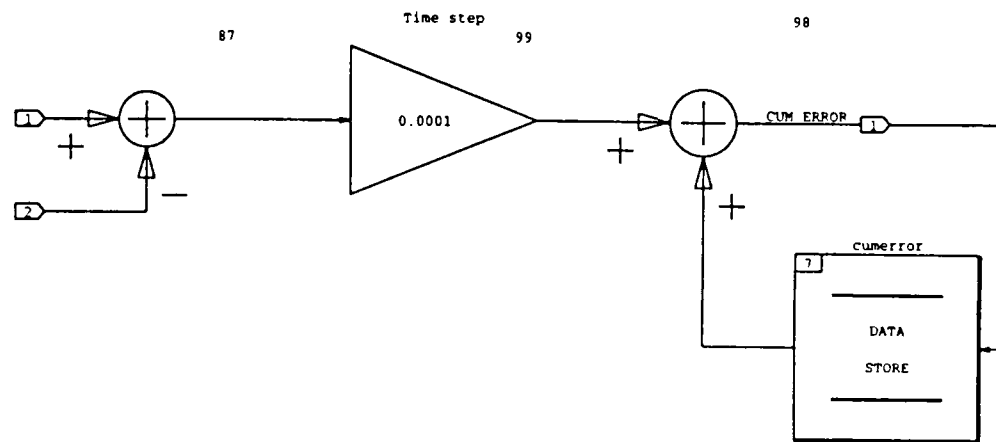
28-SEP-96

Discrete SuperBlock	VS TRIGGER	Sampling Interval	0.0001	First Sample	0.	Ext.Inputs	4	Ext.Outputs	3	Enable	Parent
---------------------	------------	-------------------	--------	--------------	----	------------	---	-------------	---	--------	--------



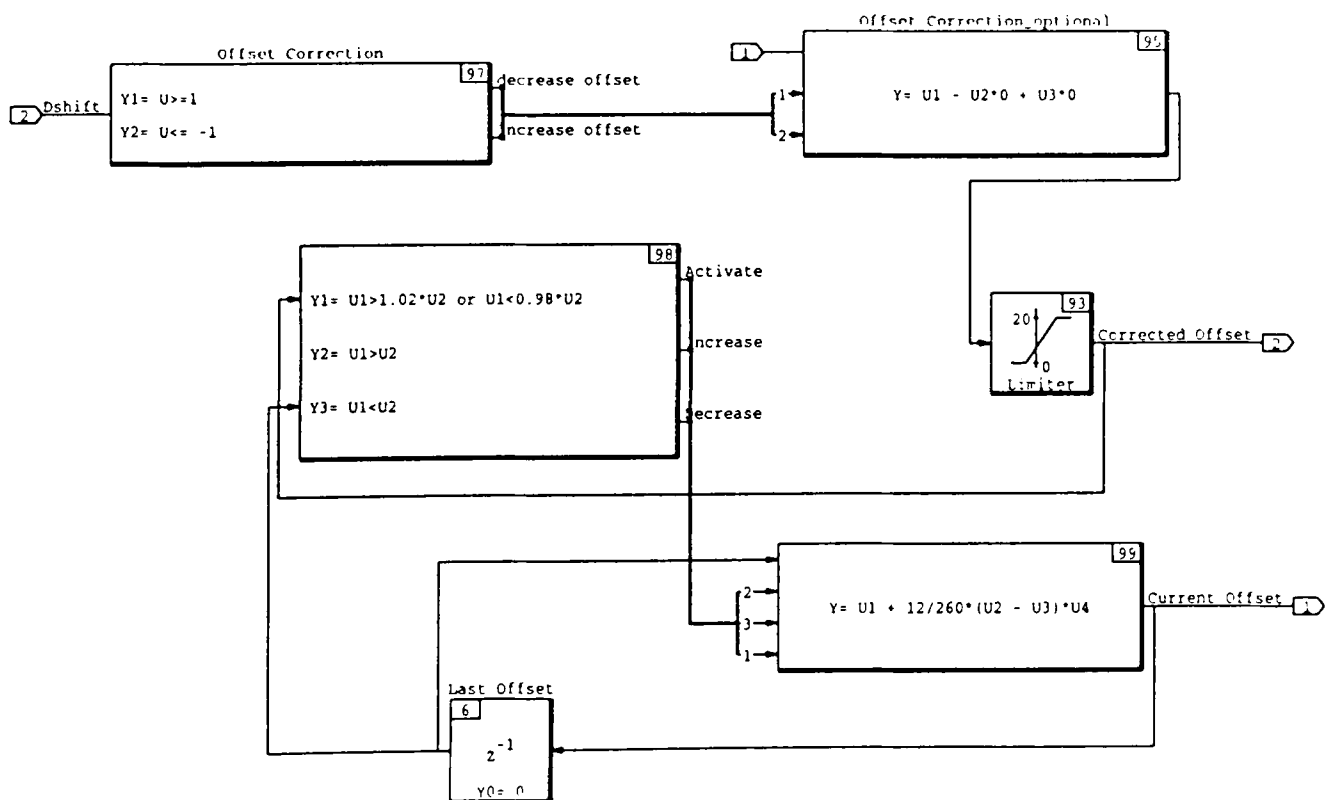
B2.5.3 : Triggering pump-motor cylinders reaching TDC/BDC (VS TRIGGER)

Discrete SuperBlock	Sampling Interval	First Sample	Ext.Inputs	Ext.Outputs	Enable Parent
CUM ERR	0.0001	0.	2	1	Parent



B2.5.4 : Cumulative flow error compared to demand (CUM ERR)

Discrete SuperBlock	Sampling Interval	First Sample	Ext.Inputs	Ext.Outputs	Enable Parent
REGN_OFFSET	0.001	0.	2	2	Parent



B2.5.5 : Setting regenerator offset needed corresponding to power demand (REGN_OFFSET)

Triggered SuperBlock
 DECI MAKE

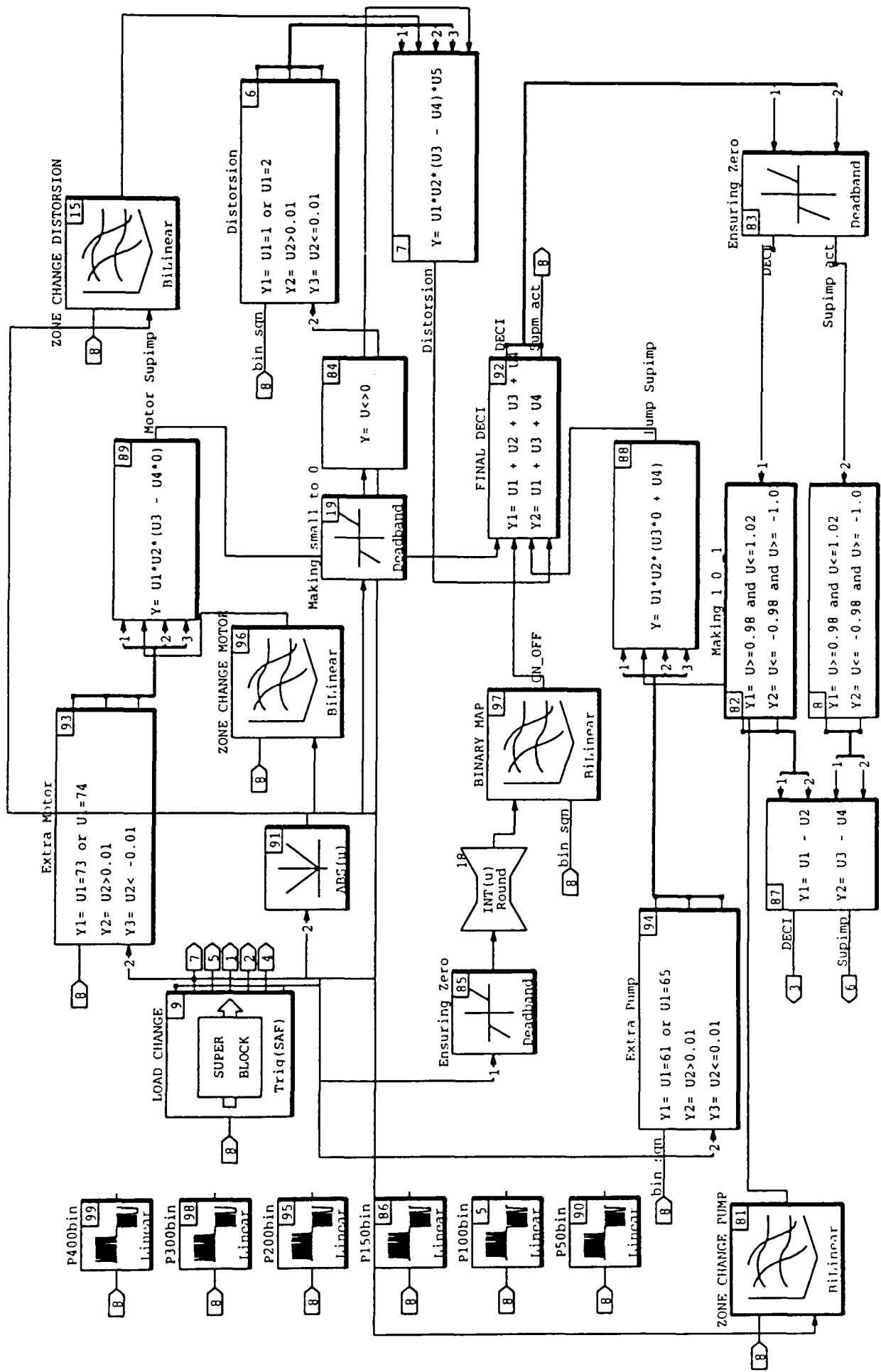
Timing Requirement
 1.0E-06

Output Posting
 As Soon As Finished

Ext.Inputs
 9

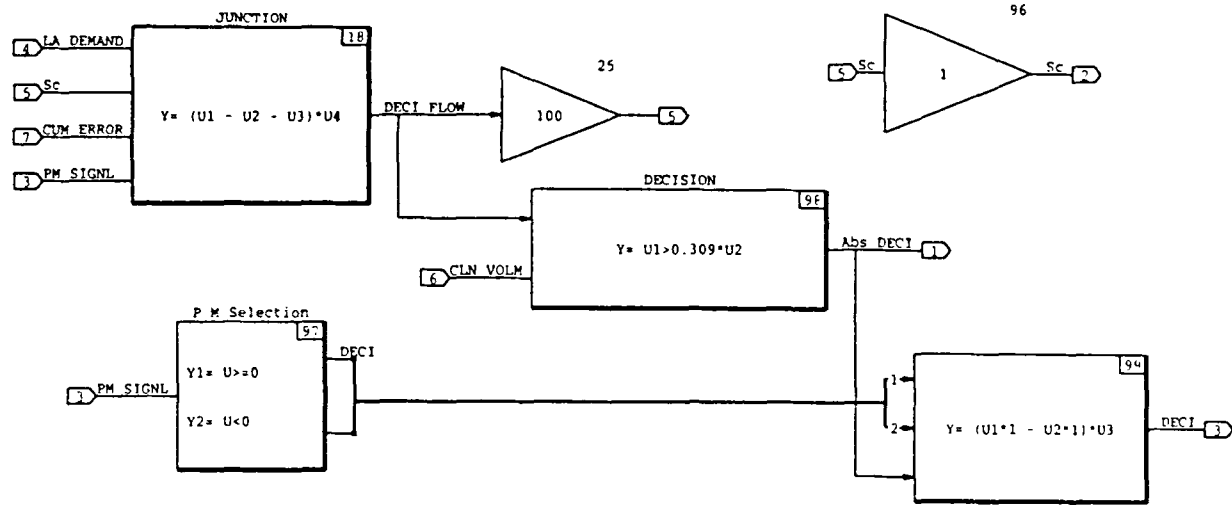
Ext.Outputs
 8

Trigger
 1



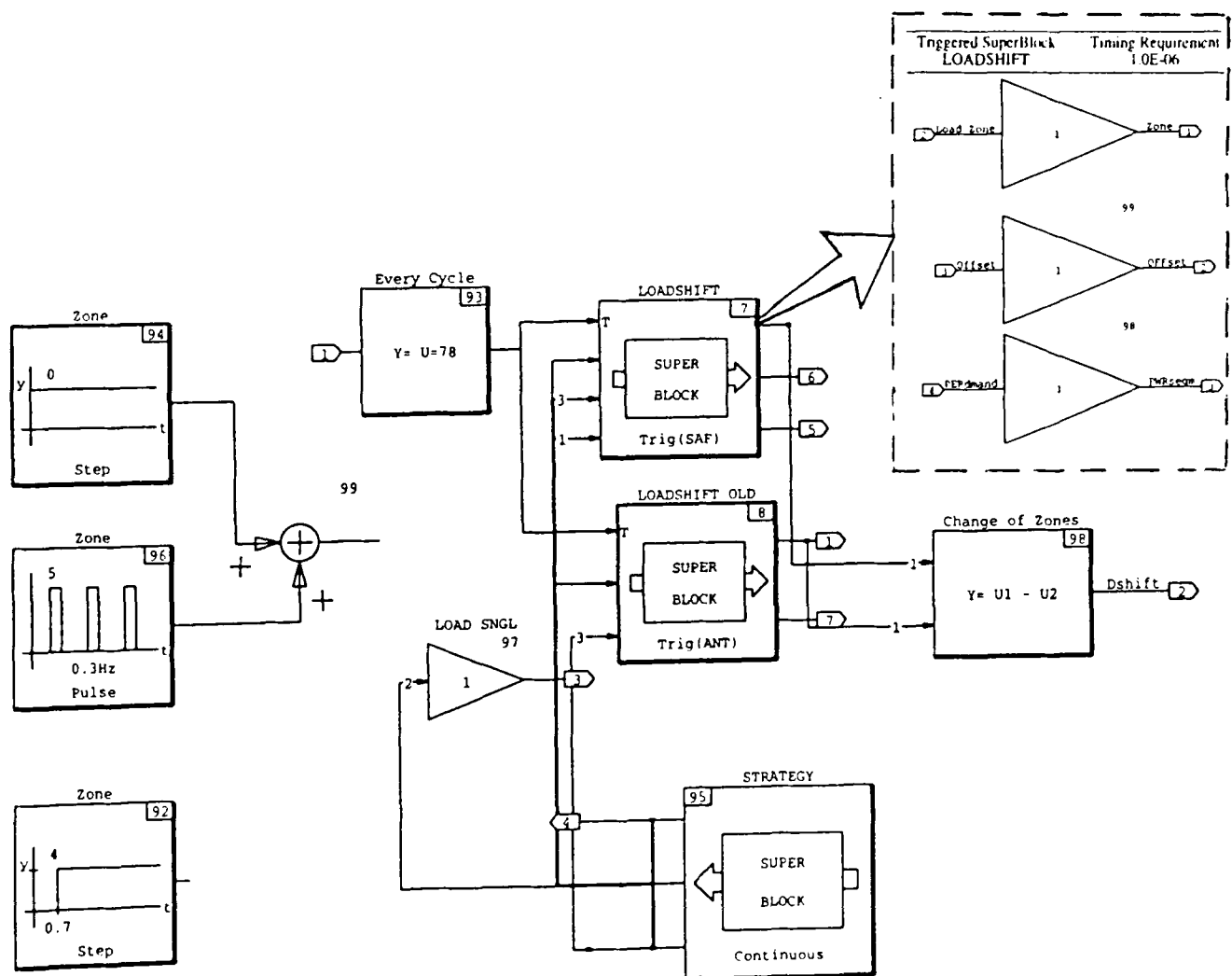
B2.5.6a: Cylinder enabling decisions read from a ternary-table (DECIMAKE)

Triggered SuperBlock	Timing Requirement	Output Posting	Ext.Inputs	Ext.Outputs	Trigger
DECI MAKE	1.0E-06	As Soon As Finished	9	5	1



B2.5.6b: Cylinder enabling decisions following flow-control algorithm (DECIMAKE)

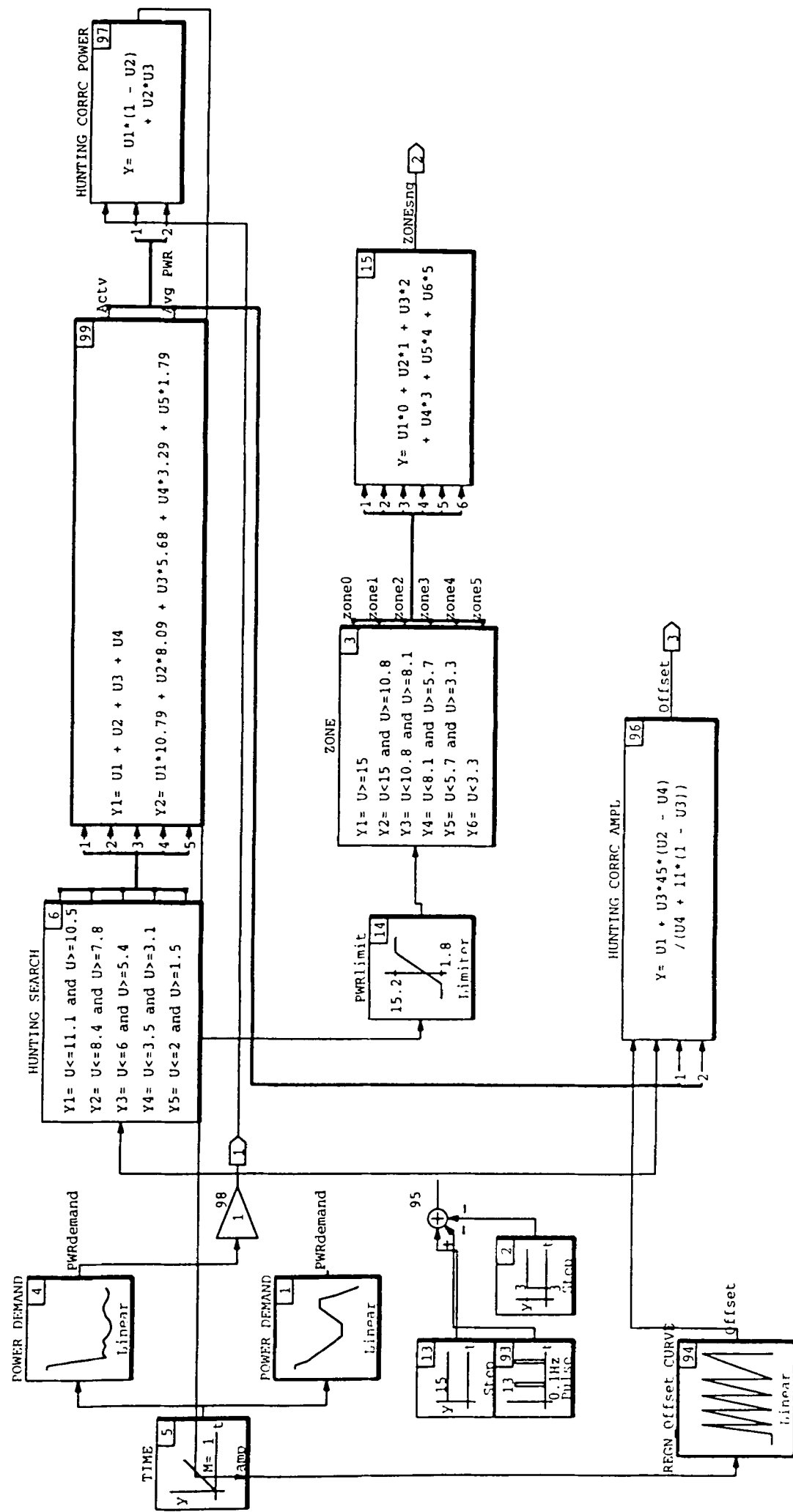
Triggered SuperBlock	Timing Requirement	Output Posting	Ext.Inputs	Ext.Outputs	Trigger
LOAD CHANGE	1.0E-06	As Soon As Finished	1	7	Parent



B2.5.6.1 : Keeps track of the load demand changes on cycle-by-cycle basis (LOAD CHANGE)

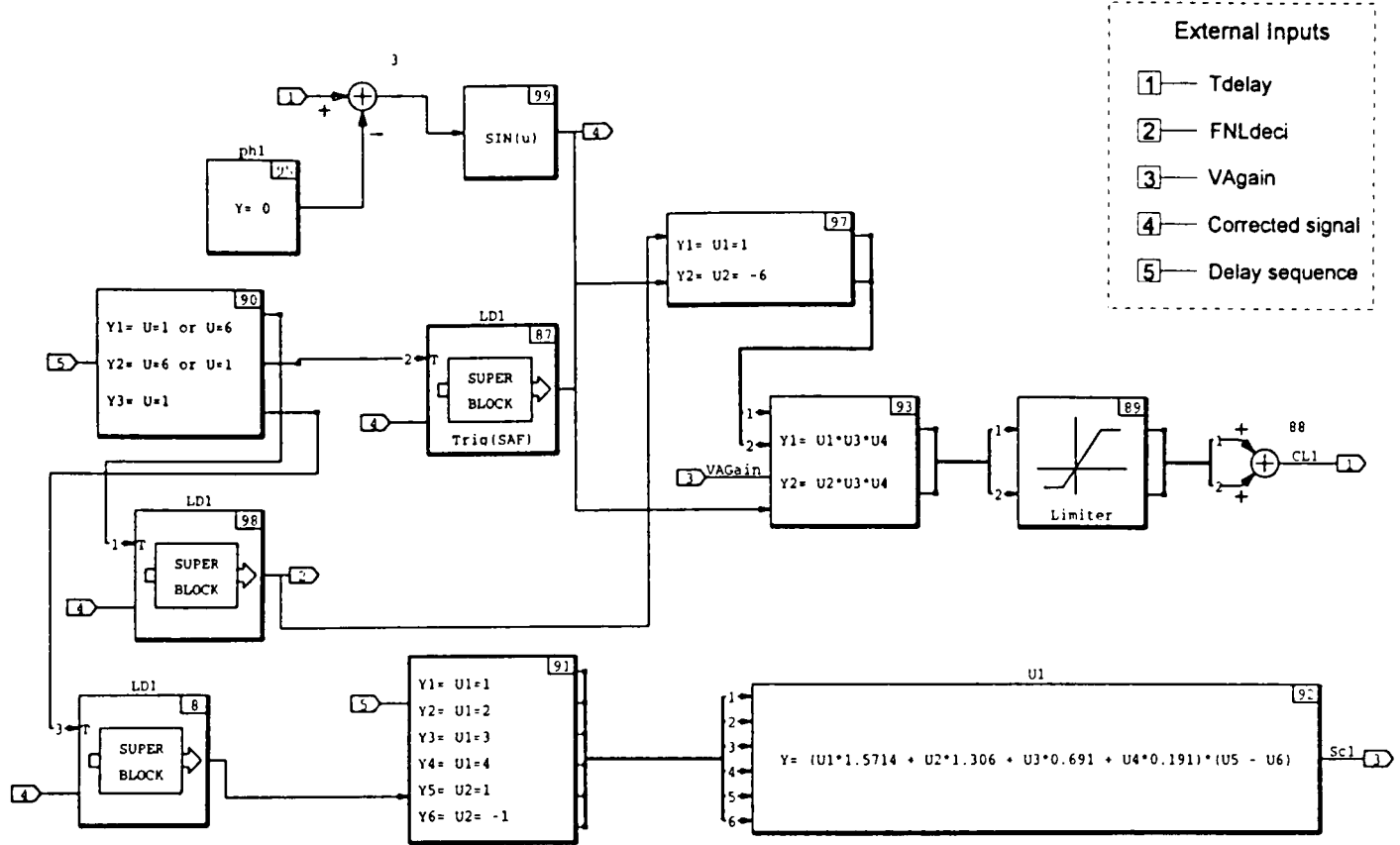
28-SEP-96

Continuous SuperBlock Ext.Inputs Ext.Outputs
 STRATEGY 0 3



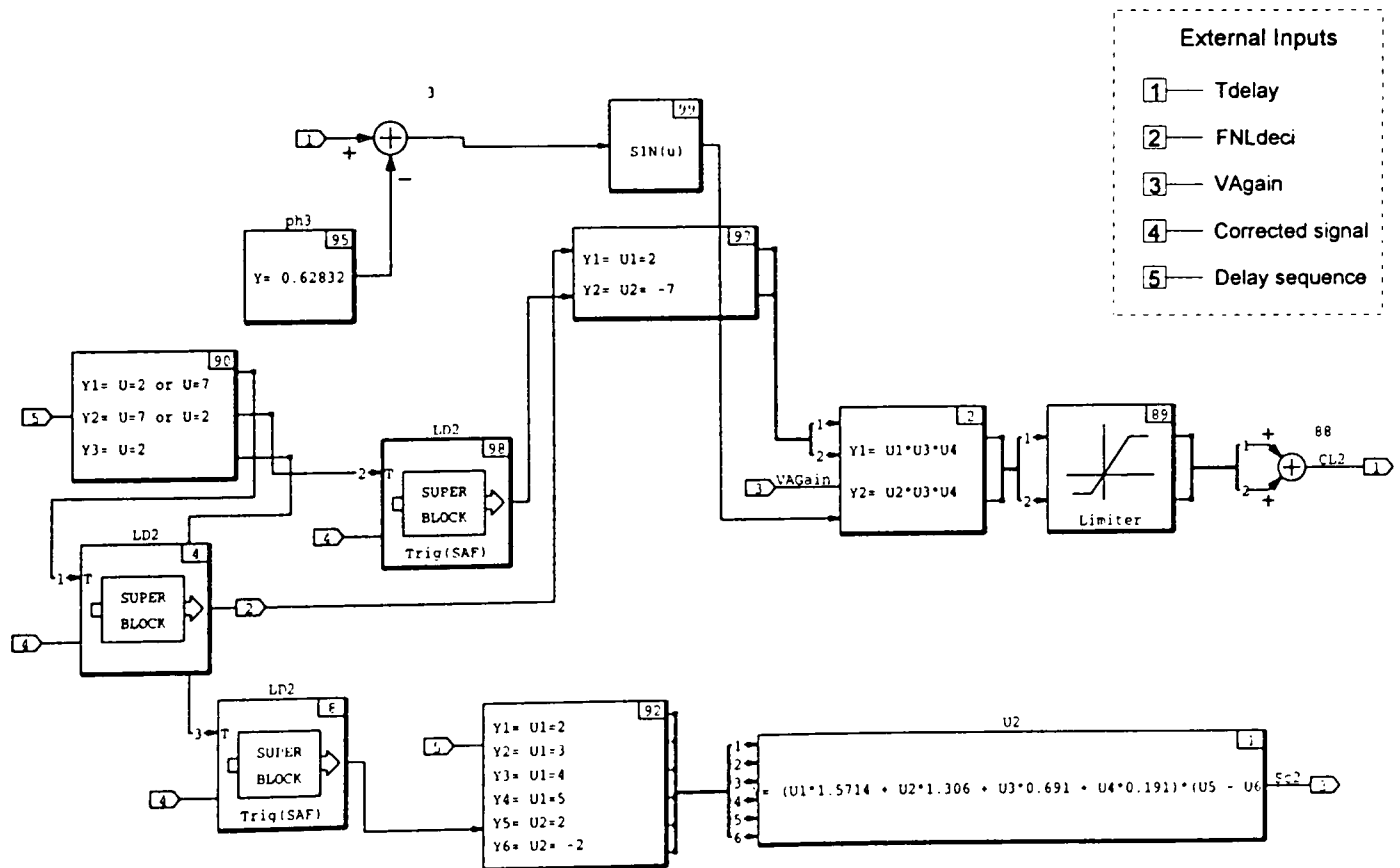
B2.5.6.1.1 : Evaluate power demand in terms of power-zones (STRATEGY)

Continuous SuperBlock
CL1 Ext.Inputs 5 Ext.Outputs 4



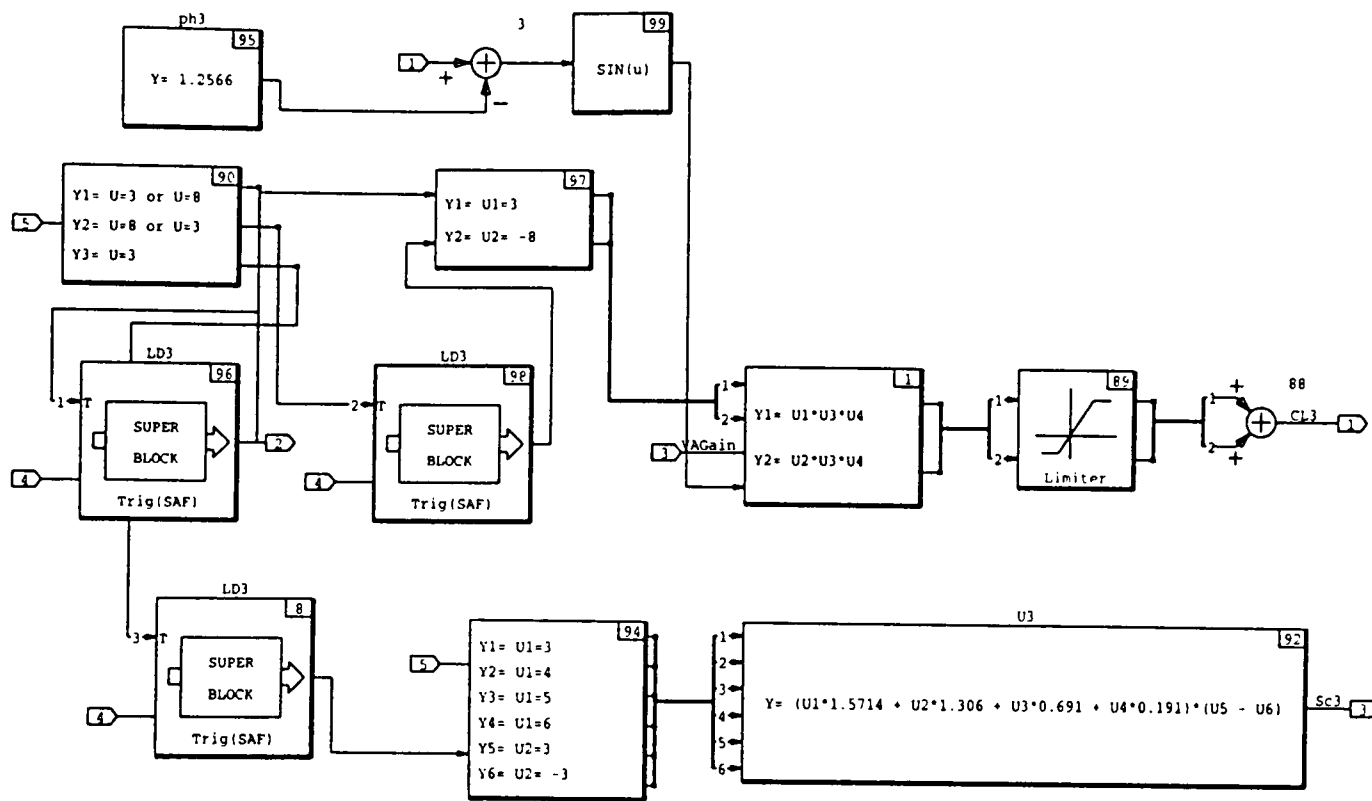
B2.5.7 : Pump-motor cylinder-1 (CL1)

Continuous SuperBlock
CL2 Ext.Inputs 5 Ext.Outputs 3



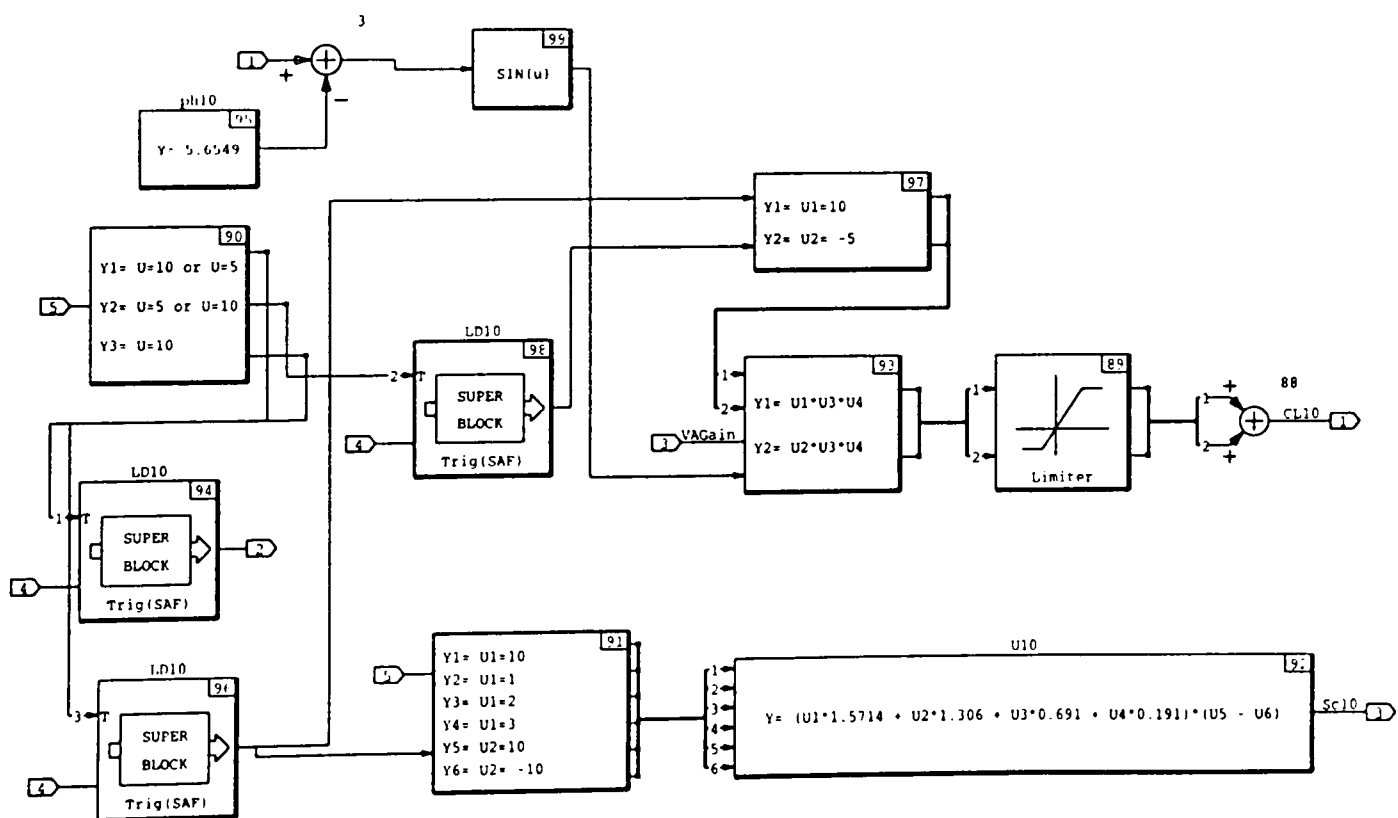
B2.5.8 : Pump-motor cylinder-2 (CL2)

Continuous SuperBlock
CL3 Ext.Inputs 5 Ext.Outputs 3



B2.5.9 : Pump-motor cylinder-1 (CL3)

Continuous SuperBlock
CL10 Ext.Inputs 5 Ext.Outputs 3



B2.5.10 : Pump-motor cylinder-1 (CL10)

APPENDIX C1 : Ternary-code for piston motion. Sinusoidal regenerator motion with fixed stroke, which may be offset for power control

DECI	Zone 0 400 bar	Zone 1 270 bar	Zone 2 200 bar	Zone 3 150 bar	Zone 4 100 bar	Zone 5 50 bar
1	0	0	0	0	0	0
2	0	0	0	0	0	0
3	0	0	0	0	0	0
4	1	1	0	0	0	0
5	0	0	1	0	0	0
6	0	0	0	1	0	1
7	0	0	0	0	1	0
8	1	1	1	0	0	0
9	0	0	0	1	1	1
10	0	0	0	0	0	0
11	1	1	1	0	0	0
12	0	0	0	1	1	1
13	1	1	1	1	1	1
14	0	0	0	0	0	0
15	0	0	0	0	0	0
16	1	1	1	1	1	1
17	0	1	1	1	1	1
18	1	0	0	0	0	0
19	0	0	0	0	0	0
20	1	1	1	1	1	1
21	0	1	1	1	1	1
22	1	0	0	0	0	0
23	0	0	0	0	0	1
24	0	1	1	1	1	0
25	1	1	1	1	1	1
26	0	0	0	0	0	0
27	1	0	0	0	0	1
28	1	0	0	0	0	0
29	1	1	1	1	1	1
30	0	1	1	1	1	0
31	0	0	0	0	0	0
32	1	0	0	0	0	0
33	1	1	1	1	1	1
34	0	1	0	0	0	0
35	1	0	0	0	0	0
36	1	1	0	0	0	0
37	0	0	1	1	1	1
38	0	1	0	0	0	0
39	0	0	1	1	1	0
40	0	0	0	0	0	0
41	0	0	0	0	0	0
42	0	0	0	0	0	0
43	0	0	0	0	0	0
44	0	0	0	0	0	0
45	0	0	0	0	0	0
46	0	0	0	0	0	0
47	0	0	0	0	0	0
48	0	0	0	0	-1	0
49	0	0	0	-1	-1	-1
50	0	0	-1	-1	-1	-1

51	0	-1	0	0	0	0
52	-1	-1	-1	-1	-1	-1
53	0	0	0	0	0	0
54	-1	-1	-1	-1	-1	-1
55	0	0	0	0	0	-1
56	-1	-1	-1	-1	-1	0
57	0	0	0	0	0	0
58	-1	-1	-1	-1	-1	-1
59	0	0	0	0	0	0
60	-1	-1	-1	-1	-1	-1
61	0	0	0	0	0	0
62	-1	-1	-1	-1	-1	-1
63	0	0	0	0	0	0
64	-1	-1	-1	-1	-1	-1
65	0	0	0	0	0	0
66	-1	-1	-1	-1	-1	-1
67	0	0	0	0	0	0
68	0	0	0	0	0	0
69	0	0	0	0	0	0
70	-1	-1	-1	-1	-1	-1
71	-1	-1	-1	-1	-1	-1
72	-1	-1	-1	-1	-1	-1
73	-1	-1	-1	-1	-1	-1
74	-1	-1	-1	-1	0	0
75	-1	-1	-1	0	0	0
76	-1	-1	0	0	0	0
77	-1	0	0	0	0	0
78	0	0	0	0	0	0

Replacing decisions for power-zone shift

	ZONE SHIFTS		(Extra Motor)			
DECI	0	1	2	3	4	5
73	0	0	0	0	0	1
74	0	0	0	0	1	1
75	0	0	0	1	1	1
76	0	0	1	1	1	1
77	0	1	1	1	1	1

Replacing decisions for power-zone shift

	ZONE SHIFTS		(Extra Pump)			
DECI	0	-1	-2	-3	-4	-5
61	0	0	0	0	0	-1
65	0	0	0	0	-1	-1
67	0	0	0	-1	-1	-1
68	0	0	-1	-1	-1	-1
69	0	-1	-1	-1	-1	-1

Replacing decisions for cycle distortion during power zone-shifts (opposite sign for negative zone shifts)

	ZONE SHIFTS		(Distortion)			
DECI	0	1	2	3	4	5
1	0	1	1	1	1	1
2	0	0	1	1	1	1
3	0	1	0	1	1	1
19	0	-1	0	-1	-1	-1
26	0	0	-1	-1	-1	-1
31	0	-1	-1	-1	-1	-1

APPENDIX C2 : Ternary-code for piston motion. Sinusoidal regenerator motion, which may be offset and clipped at the cold-end for power control

DECI	Zone 0 400 bar	Zone 1 300 bar	Zone 2 200 bar	Zone 3 150 bar	Zone 4 100 bar	Zone 5 50 bar
1	0	0	0	0	0	0
2	0	0	0	0	0	0
3	0	0	0	0	0	0
4	1	1	0	0	0	0
5	0	0	1	0	0	0
6	0	0	0	1	0	1
7	0	1	0	0	1	0
8	1	0	1	0	0	0
9	0	0	0	1	1	1
10	0	1	0	0	0	0
11	1	0	1	0	0	0
12	0	0	0	1	1	1
13	1	1	1	1	1	1
14	0	0	0	0	0	0
15	0	0	0	0	0	0
16	1	1	1	1	1	1
17	0	0	1	1	1	1
18	1	1	0	0	0	0
19	0	0	0	0	0	0
20	1	0	1	1	1	1
21	0	1	1	1	1	1
22	1	1	0	0	0	0
23	0	0	0	0	0	1
24	0	0	1	1	1	0
25	1	1	1	1	1	1
26	0	0	0	0	0	0
27	1	0	0	0	0	1
28	1	1	0	0	0	0
29	1	0	1	1	1	1
30	0	1	1	1	1	0
31	0	0	0	0	0	0
32	1	1	0	0	0	0
33	1	0	1	1	1	1
34	0	1	0	0	0	0
35	1	0	0	0	0	0
36	1	0	0	0	0	0
37	0	0	1	1	1	1
38	0	1	0	0	0	0
39	0	0	1	1	1	0
40	0	0	0	0	0	0
41	0	0	0	0	0	0
42	0	1	0	0	0	0
43	0	0	0	0	0	0
44	0	0	0	0	0	0
45	0	1	0	0	0	0
46	0	0	0	0	0	0
47	0	0	0	0	0	0
48	0	0	0	0	-1	0
49	0	0	0	-1	-1	-1
50	0	-1	-1	-1	-1	-1

51	0	0	0	0	0	0
52	-1	-1	-1	-1	-1	-1
53	0	0	0	0	0	0
54	-1	-1	-1	-1	-1	-1
55	0	0	0	0	0	-1
56	-1	-1	-1	-1	-1	0
57	0	0	0	0	0	0
58	-1	-1	-1	-1	-1	-1
59	0	0	0	0	0	0
60	-1	-1	-1	-1	-1	-1
61	0	0	0	0	0	0
62	-1	-1	-1	-1	-1	-1
63	0	0	0	0	0	0
64	-1	-1	-1	-1	-1	-1
65	0	0	0	0	0	0
66	-1	-1	-1	-1	-1	-1
67	0	0	0	0	0	0
68	0	0	0	0	0	0
69	0	0	0	0	0	0
70	-1	-1	-1	-1	-1	-1
71	-1	-1	-1	-1	-1	-1
72	-1	-1	-1	-1	-1	-1
73	-1	-1	-1	-1	-1	-1
74	-1	-1	-1	-1	0	0
75	-1	-1	-1	0	0	0
76	-1	-1	0	0	0	0
77	-1	0	0	0	0	0
78	0	0	0	0	0	0

Replacing decisions for power-zone shift

	ZONE SHIFTS (Extra Motor)					
DECI	0	1	2	3	4	5
73	0	0	0	0	0	1
74	0	0	0	0	1	1
75	0	0	0	1	1	1
76	0	0	1	1	1	1
77	0	1	1	1	1	1

Replacing decisions for power-zone shift

	ZONE SHIFTS (Extra Pump)					
DECI	0	-1	-2	-3	-4	-5
61	0	0	0	0	0	-1
65	0	0	0	0	-1	-1
67	0	0	0	-1	-1	-1
68	0	0	-1	-1	-1	-1
69	0	-1	-1	-1	-1	-1

Replacing decisions for cycle distortion during power zone-shifts (opposite sign for negative zone shifts)

	ZONE SHIFTS (Distortion)					
DECI	0	1	2	3	4	5
1	0	1	1	1	1	1
2	0	0	1	1	1	1
3	0	1	0	1	1	1
19	0	-1	0	-1	-1	-1
26	0	0	-1	-1	-1	-1
31	0	-1	-1	-1	-1	-1

APPENDIX C3 : Ternary-code for piston motion. Triangular (smooth) regenerator motion, stroke length of which may be varied for power control

DECI	Zone 0 400 bar	Zone 1 300 bar	Zone 2 200 bar	Zone 3 150 bar	Zone 4 100 bar	Zone 5 50 bar
1	0	0	0	0	0	0
2	1	0	0	0	0	0
3	0	0	0	0	0	0
4	0	1	1	1	0	0
5	0	0	0	0	1	1
6	1	0	0	0	0	0
7	0	1	1	1	0	0
8	0	0	0	0	1	1
9	0	0	0	0	0	0
10	1	0	1	0	0	0
11	0	1	0	1	1	1
12	0	0	0	0	0	0
13	1	0	1	0	0	0
14	0	1	0	1	1	1
15	0	0	0	0	0	0
16	0	0	1	0	0	0
17	1	1	0	1	1	1
18	0	0	0	0	0	0
19	0	0	1	0	0	0
20	1	0	0	1	1	1
21	0	1	0	0	0	0
22	0	0	1	0	0	0
23	0	0	0	1	1	1
24	1	1	0	0	0	0
25	0	0	0	0	0	0
26	0	0	1	1	1	1
27	1	1	0	0	0	0
28	0	0	0	0	0	0
29	0	1	1	1	1	1
30	0	1	0	0	0	0
31	1	1	0	0	0	0
32	1	1	1	1	1	1
33	1	1	0	0	0	0
34	1	0	1	0	1	0
35	1	1	1	1	0	1
36	1	0	1	1	0	0
37	1	1	1	1	1	0
38	1	1	1	1	0	1
39	0	0	1	1	0	0
40	0	0	0	0	1	1
41	0	0	0	0	1	0
42	0	0	0	0	0	0
43	0	0	0	0	0	0
44	0	0	0	0	0	0
45	0	0	0	0	0	0
46	0	0	-1	-1	-1	-1
47	0	-1	-1	-1	0	-1
48	0	-1	0	0	-1	-1
49	-1	0	-1	-1	-1	-1
50	-1	-1	-1	-1	-1	-1

51	-1	-1	0	0	-1	0
52	0	0	-1	-1	-1	-1
53	-1	-1	0	0	0	0
54	0	0	-1	-1	-1	-1
55	-1	-1	0	-1	0	0
56	0	0	-1	0	-1	-1
57	-1	-1	-1	-1	-1	0
58	0	0	0	-1	0	-1
59	-1	-1	-1	0	-1	0
60	0	0	-1	-1	-1	0
61	-1	-1	0	-1	0	-1
62	-1	0	-1	0	0	0
63	0	-1	0	0	0	0
64	0	0	0	0	0	0
65	0	0	0	0	0	0
66	-1	0	0	-1	0	-1
67	0	-1	-1	0	-1	-1
68	-1	0	0	-1	-1	-1
69	0	-1	-1	0	0	0
70	-1	-1	-1	0	0	0
71	0	-1	-1	-1	-1	0
72	-1	-1	-1	-1	0	0
73	-1	-1	0	0	0	0
74	-1	0	0	0	0	0
75	-1	0	0	0	0	0
76	0	0	0	0	0	0
77	0	0	0	0	0	0
78	0	0	0	0	0	0

Replacing decisions for power-zone shift

DECI	ZONE SHIFTS (Extra Motor)					
	0	1	2	3	4	5
71	0	0	0	0	0	1
72	0	0	0	0	1	1
73	0	0	0	1	1	1
74	0	0	1	1	1	1
75	0	1	1	1	1	1

Replacing decisions for power-zone shift

DECI	ZONE SHIFTS (Extra Pump)					
	0	1	2	3	4	5
64	0	0	0	0	0	-1
65	0	0	0	0	-1	-1
76	0	0	0	-1	-1	-1
77	0	0	-1	-1	-1	-1
78	0	-1	-1	-1	-1	-1

Replacing decisions for cycle distortion during power-zone shifts (opposite sign for negative zone shifts)

DECI	ZONE SHIFTS (Distortion)					
	0	1	2	3	4	5
1	0	1	1	1	1	1
3	0	0	1	1	1	1
9	0	1	0	1	1	1
18	0	-1	0	-1	-1	-1
25	0	0	-1	-1	-1	-1
28	0	-1	-1	-1	-1	-1

TABLE 11. DENSITY OF WATER AND STEAM

Pressure/(MN/m ²) Pressure/bar Sat. Celsius temp., °C Sat. density kg/m ³	[0.1 MN/m ² = 1 bar ≈ 14.5 lbf/in ²]																			Celsius temp., °C	
	C to bar										C to bar										
	0	0.01	0.05	0.1	0.5	1	2	4	6	8	10	15	20	22.12	25	30	40	50	100		1000
0	1000	1000	1000	1000	1000	1001	1002	1003	1004	1005	1007	1010	1011	1012	1014	1019	1024	1046		0	
0	0.1	0.1	0.1	0.1	0.1	0.1	0.1	0.1	0.1	0.1	0.1	0.1	0.1	0.1	0.1	0.1	0.1	0.1	0.1	0.1	25
45.8	81.3	99.6	151.8	179.9	212.4	250.3	275.6	295.0	311.0	342.1	365.7	374.15								50	
990	971	958	915	887	850	799	758	722	688	603	491	315								75	
0.0681	0.309	0.590	2.67	5.15	10.05	20.10	30.8	42.5	55.4	96.7	170.2	315								100	
0	1000	1000	1000	1000	1001	1002	1003	1004	1005	1007	1010	1011	1012	1014	1019	1024	1046			100	
0	0.1	0.1	0.1	0.1	0.1	0.1	0.1	0.1	0.1	0.1	0.1	0.1	0.1	0.1	0.1	0.1	0.1	0.1	0.1	200	
45.8	81.3	99.6	151.8	179.9	212.4	250.3	275.6	295.0	311.0	342.1	365.7	374.15								225	
990	971	958	915	887	850	799	758	722	688	603	491	315								250	
0.0681	0.309	0.590	2.67	5.15	10.05	20.10	30.8	42.5	55.4	96.7	170.2	315								275	
0	1000	1000	1000	1000	1001	1002	1003	1004	1005	1007	1010	1011	1012	1014	1019	1024	1046			300	
0	0.1	0.1	0.1	0.1	0.1	0.1	0.1	0.1	0.1	0.1	0.1	0.1	0.1	0.1	0.1	0.1	0.1	0.1	0.1	325	
45.8	81.3	99.6	151.8	179.9	212.4	250.3	275.6	295.0	311.0	342.1	365.7	374.15								350	
990	971	958	915	887	850	799	758	722	688	603	491	315								375	
0.0681	0.309	0.590	2.67	5.15	10.05	20.10	30.8	42.5	55.4	96.7	170.2	315								400	
0	1000	1000	1000	1000	1001	1002	1003	1004	1005	1007	1010	1011	1012	1014	1019	1024	1046			425	
0	0.1	0.1	0.1	0.1	0.1	0.1	0.1	0.1	0.1	0.1	0.1	0.1	0.1	0.1	0.1	0.1	0.1	0.1	0.1	450	
45.8	81.3	99.6	151.8	179.9	212.4	250.3	275.6	295.0	311.0	342.1	365.7	374.15								475	
990	971	958	915	887	850	799	758	722	688	603	491	315								500	
0.0681	0.309	0.590	2.67	5.15	10.05	20.10	30.8	42.5	55.4	96.7	170.2	315								550	
0	1000	1000	1000	1000	1001	1002	1003	1004	1005	1007	1010	1011	1012	1014	1019	1024	1046			600	
0	0.1	0.1	0.1	0.1	0.1	0.1	0.1	0.1	0.1	0.1	0.1	0.1	0.1	0.1	0.1	0.1	0.1	0.1	0.1	650	
45.8	81.3	99.6	151.8	179.9	212.4	250.3	275.6	295.0	311.0	342.1	365.7	374.15								700	
990	971	958	915	887	850	799	758	722	688	603	491	315								750	
0.0681	0.309	0.590	2.67	5.15	10.05	20.10	30.8	42.5	55.4	96.7	170.2	315								800	

HOT-END PRESSURE TABLE (bar)


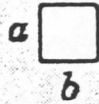
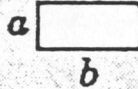
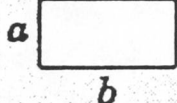
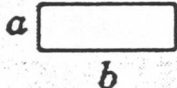
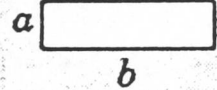
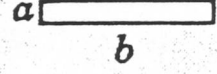


Density	0.25	1	2.5	5	10	15	23	28	43	60	68	78	100	145	200	450
Temp 475	0.863	3.438	8.567	16.98	33.40	49.36	73.95	88.57	129.1	171.1	189.6	212.0	253.5	320.4	387.4	762.3
500	0.894	3.555	8.840	17.56	34.63	51.23	76.84	92.31	135.5	180.4	200.7	223.8	270.0	347.4	427.5	855.5
550	0.951	3.789	9.436	18.77	37.08	54.97	82.71	99.66	147.8	198.8	221.2	248.4	303.6	403.4	508.8	1009
600	1.008	4.020	10.04	19.96	39.49	58.69	88.52	106.7	159.4	216.0	241.2	271.7	334.8	453.5	586.2	1178
650	1.064	4.252	10.59	21.12	41.89	62.33	94.40	113.8	170.9	232.8	260.6	294.9	366.1	503.6	657.9	1359

(this table is calculated from the data of the table above)

Note: Density is tabulated here, instead of specific volume, since interpolation between pressures is thereby facilitated.

Appendix D : Table for density of water and steam
 Source : "Thermodynamic Tables in SI Units", Haywood R.W, 3rd edition
 Cambridge University Press, Cambridge 1990. ISBN 0-521-38693-4

Nusselt numbers for fully developed
laminar flow in tubes of differing cross section

CROSS SECTION	$\frac{b}{a}$	$Nu_D \equiv \frac{hD_h}{k}$	
		(uniform q_s'')	(uniform T_s)
	—	4.36	3.66
	1.0	3.61	2.98
	1.43	3.73	3.08
	2.0	4.12	3.39
	3.0	4.79	3.96
	4.0	5.33	4.44
	8.0	6.49	5.60
	∞	8.23	7.54
	—	3.11	2.47

D_h = Hydraulic diameter = $(4 \times \text{Cross-sectional Area}) / (\text{Wetted perimeter})$.

Uniform q_s'' = Uniform surface heat flux.

Uniform T_s = Uniform surface temperature.

This table is used to evaluate convective heat transfer co-efficient at gas-flamefin interface.

Appendix E : Nusselt numbers for fully developed laminar flow
Source : "Introduction to Heat Transfer", Incropera P.F. and Dewitt P.D, 2nd Edition,
page 461, John Wiley & Sons, Singapore 1990. ISBN 0-471-51728-3.

Appendix F : Information about J. F. Malone and his work

John Fox Jennings Malone was born in England in 1880. His formal education ended by 1898 and then he served the merchant marine for 14 years. During that time he was wounded seventeen times in different Arab and Latin-American wars. Leaving the merchant marine, Malone found the Sentinel Instrument company and later, the Fox instrument company which mainly made tank-level indicators for ships. He began experimenting with liquid engines in the 1920s, in Newcastle - Upon - Tyne. Malone built and tested three liquid engines between 1924-1931. In 1925 he completed the first liquid-based engine. It burned coal and used high-pressure liquid water as working fluid. Malone referred the first engine as crude and cumbersome. In 1927 Malone completed

a much smaller and more versatile 50 horse-power engine and began an extensive programme of experimentation with it. Malone also made another small horizontal engine. So far as is known, Malone presented only one account of his work to the Royal Society of Arts in 1931. Malone in his paper claimed 27% indicated efficiency (compared to about 13% efficiency of contemporary steam engines). The paper contained photographs of two large two-cylinder vertical machines and a smaller single-cylinder horizontal engine. They operated at low speeds of 24 - 250 rpm. High pressures were used, which varied from a low value of nearly 70 bar to a maximum of 275 bars. The original intent of the engines was to power ships and to double their range on a load of coal. Although Malone's engines used supercritical water as the working fluid, he also experimented with oils, liquid carbon-dioxide and mercury and concluded that he had found water to be best (Malone, 1931). Malone also worked on a air based Stirling variant but this produced disappointing performance. Dr. G.Walker, then at Newcastle, got involved and pointed out much of the poor performance was due to long un-insulated pipes. Some improvement resulted from modifications but not enough to continue.

Malone published little of his work and presumably faced adverse treatment from contemporary researchers. In a 1939 letter to Selwyn Anderson the bitterness was evident. Malone wrote about his measurement and calculations (which he haven't detailed in his paper), "I refused to publish this information because it costed me a lot to learn it and I may yet obtain some reward if it is not known. Also because to my amazement I found my enemies were alleged centres of learning, Universities and the like. A study of liquids as mediums in thermodynamics will teach an engineer more



J.F.J Malone

about the art of thermodynamics than all the universities on earth, or the memory men who infest them, and knowledge for knowledge's sake is better than their parasitical life."

It is still not clear why Malone's promising work came to an end. In his article "John Malone and the Invention of liquid-based Engines", Gregory W. Swift (Condensed Matter and Thermal Physics Group, Los Alamos, USA) indicated several possible reasons. The worldwide economic depression of the 1930s must have made venture capital scarce. Some may have dismissed the idea of liquid working fluid because it contradicted conventional wisdom. Use of large coal-powered steam turbines with 20% efficiency were becoming dominant for large power applications (above 10,000 horse power). The internal combustion engines (both petrol and diesel) were already more advanced and their quick start-up and incomparable power-to-weight ratio made it seem the only practical choice for automobiles and aeroplanes. By the end of the depression and World War II - steam engines were disappearing, internal-combustion engines and turbines were used everywhere and Malone's work had been forgotten. Malone died in 1959. After his death, his son Ray wrote, "Now, as patent rights have long expired, I can see no advantage in publishing any of the information which Malone accumulated while developing his liquid-engine". As far as is known nothing remains of his experimental works, test results etc.

Source: "John Malone and the Invention of liquid-based Engines", G. W. Swift, Los Alamos Science, vol. 21, page 117, USA 1993.

Visit paid to Malone's son, Ray Malone, by W.H.S Rampen at Coldstream, Scotland 1995.